Department of Civil and Structural Engineering

University of Sheffield

THE INFLUENCE OF HUMAN OCCUPANTS ON THE DYNAMIC PROPERTIES OF SLENDER STRUCTURES

by

REGINA SACHSE

A thesis submitted for the Degree of Doctor of Philosophy in Engineering

April 2002

Deeply indebted to my parents

GISELA AND GERHARD SACHSE

and in loving memory of

PETER WEINROTHER, HILDE SACHSE,

AND LUTZ LEHMANN.

ABSTRACT

This thesis describes a combined analytical and experimental investigation into the influence of human occupants on the dynamic properties of civil engineering structures. This is an increasingly important issue in the design of assembly structures against human-induced vibrations.

An analytical parametric study demonstrated that a damped single degree of freedom (SDOF) model of one or more human occupants can explain (1) natural frequency increases and decreases, (2) additional natural frequencies, and (3) response reductions, reported in the literature.

Experimental investigations employed a lightly damped simply supported prestressed concrete beam spanning 11 m and weighing 15 tonnes. The influence of up to five stationary humans on the modal properties of this laboratory based, but realistic, full-scale test structure was quantified. For this purpose, natural frequencies, damping ratios, mode shapes, and modal masses were estimated by curve-fitting of measured frequency response functions. It was shown that the occupants affected the three investigated vertical bending modes of the test structure (at about 4.5 Hz, 17 Hz, and 38 Hz). The occupants most significantly increased damping and it was established that the location, the posture and the number of occupants were important. Within the range of low-level vibrations studied, the level of vibration of the structure had only little effect.

The combined analytical studies and experiments demonstrated that the presence of groups of stationary humans can be modelled by a damped 'human' SDOF system attached to the 'structural' SDOF system representing a well separated mode of an empty assembly structure. Based on the obtained experimental data, the mass, frequency and damping properties (m_H, f_H and ζ_H) of a damped SDOF model of groups of sitting occupants were derived. It was established that these properties varied with the natural frequency of the structural system. It was found that m_H decreases while f_H and ζ_H increase with increasing natural frequency of the empty structural system. Based on these findings, m_H should be assumed to be greater than 60% of the total mass of occupants, f_H smaller than approximately 9 Hz and ζ_H less than 40% in the case of empty structures with natural frequencies below about 17 Hz.

The derived damped SDOF human model was used to quantify the influence of occupants on the dynamic response of a range of structures modelled as SDOF systems. These data are provided in the form of design charts. They can, until further information becomes available, be used to estimate dynamic responses of civil engineering structures occupied by sitting humans to sinusoidal excitations.

ACKNOWLEDGEMENTS

Since October 1998, I have enjoyed being a member of the Vibration Engineering Section of the Department of Civil and Structural Engineering at the University of Sheffield. I am grateful for the friendly and productive working atmosphere. I particularly appreciate the willing participation of Cheah Hung Yu (Brian), Taufik Widjaja, Nino Pesic, and Drs Paul Reynolds and Aleksandar Pavic in experiments.

I want to express my sincere gratitude to Dr Aleksandar Pavic for his continuously challenging supervision.

I am also obliged to all scientists and friends who provided many interesting publications, other useful material and advice. Explicitly, I want to thank Stefan Witte and Associate Professor James Brownjohn.

TABLE OF CONTENTS

LIST OF TABLES

LIST OF FIGURES

ABBREVIATIONS

AISC	American Institute of Steel Construction, Chicago, USA
ASA	American Standards Association
ASCE	American Society of Civil Engineers, Reston, USA
ASD	auto-spectral density
BRE	Building Research Establishment, UK
BSI	British Standards Institution, UK
CBD	Canadian Building Digest
DATS	Data Acquisition, Signal Processing and Display Software of Prosig Ltd., Fareham, UK
DFT	discrete Fourier transformation
DLF	dynamic load factor
DOF	degree of freedom
DTA	Dynamic Testing Agency, Cranfield, UK
DTLR	Department for Transport, Local Government and the Regions, London, UK
EPSRC	Engineering and Physical Sciences Research Council, Swindon, UK
FE	finite element
FFT	Fast Fourier transformation
FRF	frequency response function
FT	Fourier transformation
IABSE	International Association for Bridge and Structural Engineering, Zürich, Switzerland
ICATS	Imperial College Analysis and Testing Software, London, UK
ICE	Institution of Civil Engineers, London, UK
ID	identification
IMAC	International Modal Analysis Conference
IRF	impulse response function
ISO	International Organization for Standardization, Geneva, Switzerland
IStructE	Institution of Structural Engineers, London, UK

MDOF	multi degree of freedom
MIMO	multi-input multi-output
NRCC	National Research Council of Canada, Ottawa, Canada
PARF	Peak Amplitude Reduction Factor
r.m.s	root-mean-square
SBA	Staatliche Bauaufsicht, Berlin, GDR
SCOSS	The Standing Committee on Structural Safety, London, UK
SDOF	single degree of freedom
SEM	Society for Experimental Mechanics, Bethel, Connecticut, USA
SIA	Swiss Society of Engineers and Architects, Zürich, Switzerland
SIMO	single-input multi-output
SISO	single-input single-output
TP	test point
TS	test subject

2-DOF system	dynamic system with two DOFs, one attached to the other
2-SDOF system	dynamic system with two independent single DOFs

NOTATION

LATIN SYMBOLS

a_r	complex term in the state-space
a_s	magnitude of $A_s(f_s)$
$a_{r.m.s.}$	weighted root-mean-square (r.m.s.) acceleration
$A(f)$, $A(\omega)$	accelerance: FRF relating acceleration responses to force excitations
$A_s(f)$, $A_s(\omega)$	accelerance of a SDOF system (structural accelerance)
$A_{ss}(f)$, $A_{ss}(\omega)$	accelerance of the grounded DOF of a 2-DOF system (structural accelerance)
$A_{77}(f)$	experimental point-accelerance at TP 7
$[A]$	state-space matrix combining matrixes $[C]$ and $[M]$
${}_rA_{jk}$	residue of mode r corresponding to points j and k
b_r	complex term in the state-space
$[B]$	state-space matrix combining matrixes $[K]$ and $[M]$
c	viscous damping
c_n; c_r	viscous damping of DOF n; viscous damping of mode r
c_H	viscous damping of a human model
c_s	viscous damping of a SDOF structure model
$[C]$	viscous damping matrix
d	complex term
f	frequency ($f = \omega/(2 \cdot \pi)$) in Hz (cycles per second)
f_r	natural frequency of mode r
$f_{e,r}$	natural frequency of mode r effected by an exponential window
f_H	natural frequency of a human model

f_s	natural frequency of a SDOF structure model
f_{max}	upper frequency limit defined by the characteristics of an anti-aliasing filter
$f_{samp.}$	sampling frequency
$f^{(MM)}$	natural frequency of a mass-only human-structure model
$f_r^{(DM)}$	natural frequency of mode r of a damped 2-DOF human-structure model
$f_r^{(UM)}$	natural frequency of mode r of an undamped 2-DOF human-structure model
$F(t)$	time dependent force
$F(f)$, $F(\omega)$	frequency spectrum of the force time history $F(t)$
$F^{DP}(f)$	discrete spectrum of a windowed excitation $F(t)$ provided by the spectrum analyser DP 430
$g(t)$	modal force defined by excitation $\{F(t)\}$ and mode shape $\{\psi\}_r$
$g'(t)$	modal force defined by state-space excitation $\{Q(t)\}$ and mode shape $\{\psi'\}_r$
$G(f)$	single-sided auto- or cross-spectrum ($0 \leq f \leq f_{max}$)
$\overline{G}(f)$	averaged single-sided auto- or cross-spectrum
$G_w(f)$	single-sided auto-spectrum of $v(t)$
$G_{vw}(f)$	single-sided cross-spectrum of $v(t)$ and $w(t)$
$G^p(f)$	single-sided auto- or cross-spectrum of periodic signals
$G^r(f)$	single-sided spectral density of (stationary ergodic) random signals
$G^t(f)$	single-sided spectral density of transient signals
$G^{DP}(f)$	discrete auto- or cross-spectrum provided by the spectrum analyser DP 430
h	height
$h_{jk}(t)$	impulse response function (IRF), inverse FT of $H_{jk}(f)$
$^{AN}h(t)$	IRF regenerated from modal or spatial properties
$^{EX}h(t)$	IRF calculated from an experimental FRF by inverse FT
$h^{corr}(t)$	IRF without the effect of an exponential window
$H(\omega)$	frequency response function (FRF)
$^{AN}H(f)$	FRF regenerated from modal or spatial properties

${}^{EX}H(f)$	experimentally estimated FRF
$H^{corr}(f)$	FRF without the effect of an exponential window
$H_{jk}(f)$, $H_{jk}(\omega)$	FRF (displacement, velocity or acceleration response at point j to a force excitation at point k)
$[H(\omega)]$	Matrix of FRFs
H_1, H_2	experimental FRF estimators
$I(f)$, $I(\omega)$	mechanical impedance: FRF relating force excitations to displacement responses, inverse of $Y(\omega)$
k	stiffness
k_n; k_r	stiffness corresponding to DOF n; modal stiffness of mode r
k_H	spring stiffness of a human model
k_s	stiffness of a SDOF structure model
$[K]$	stiffness matrix
L	number of elements of a discrete signal
m	mass
m_n; m_r	mass of DOF n; modal mass corresponding to mode r
m_H	lumped mass of a DOF of a human model
m_s	mass of a SDOF structure model
m_T	total mass of a person or a group of people
$M(f)$, $M(\omega)$	apparent mass: FRF relating force excitations to acceleration responses, inverse of $\alpha(\omega)$
$[M]$	mass matrix
N	total number of DOFs or modes
$p(t)$	modal (generalised or principal) coordinate
$p'(t)$	modal (generalised or principal) coordinate of a system in the state-space
P	factor defining the time constant RC of an exponential window $w_E(t)$
$Q(t)$	force excitation in the state-space
RC	time constant defining an exponential window $w_E(t)$

$R(\tau)$	correlation as function of time shift τ
$R(r)$	discrete correlation function
R_w	auto-correlation function of time history $v(t)$
R_{vw}	cross-correlation function of time histories $v(t)$ and $w(t)$
R^p	correlation function of periodic signals
R^r	correlation function of (stationary ergodic) random signals
R^t	correlation function of transient signals
$S(f)$, $S(\omega)$	double-sided auto- or cross-spectrum
$S(j)$	discrete auto- or cross-spectrum
S_w	auto-spectrum of time history $v(t)$
S_{vw}	cross-spectrum of time histories $v(t)$ and $w(t)$
S^p	auto- or cross-spectrum of periodic signals
S^r	auto- or cross-spectral density of (stationary ergodic) random signals
S^t	auto- or cross-spectral density of transient signals
T	period
t	time
$u(t)$	state-space variable
$v(t)$	time dependent signal
$v(k)$	discrete description of the time history $v(t)$
$V(f)$, $V(\omega)$	frequency spectrum of $v(t)$
$V(j)$	discrete frequency spectrum of $v(k)$
$V^{DP}(f)$	discrete spectrum of a windowed response $v(t)$ provided by the spectrum analyser DP 430
VDV	vibration dose value
$w(t)$	time dependent signal
$w(k)$	discrete description of the time history $w(t)$
$w_H(t)$	Hanning window
$w_E(t)$	exponential window

$w_{E+}(t)$	time function similar to $w_E(t)$ but with an exponent of opposite sign
$W(\omega)$	frequency spectrum of $w(t)$
$W(j)$	discrete frequency spectrum of $w(k)$
$x(t)$	displacement as function of time
$x(t)_{trans}$	transient displacement response of a SDOF system
$x(t)_{forced}$	forced displacement response of a SDOF system
$\ddot{x}_w(t)$	frequency weighted acceleration
$X(\omega)$	spectrum of $x(t)$, FT of $x(t)$
$Y(\omega)$	mobility: FRF relating velocity responses to force excitations
$Z_{jk}(\omega)$	inverse (reciprocal) of the general FRF $H_{jk}(\omega)$

GREEK SYMBOLS

α	mass ratio (ratio of m_H to m_s)
$\alpha(\omega)$	receptance: FRF that relates displacement responses to force excitations
β	frequency ratio (ratio of f_H to f_s)
$\gamma^2(f)$, $\gamma^2(\omega)$	coherence
ζ	damping ratio
ζ_r	damping ratio of mode r
$\zeta_{e,r}$	damping ratio ζ_r affected by an exponential window $w_E(t)$
ζ_H	damping ratio of a human model
ζ_s	damping ratio of a SDOF structure model
Δ	difference of an experimental and an analytical accelerance
Δf	frequency spacing
Δt	time step
$[\Theta]$	modal matrix: matrix of mode shapes $\{\psi\}_r$
$[\Theta']$	modal state-space matrix: matrix of mode shapes (eigenvectors) $\{\psi'\}_r$
λ	eigenvalue

λ'	eigenvalue of a state-space eigenproblem
τ	time, time shift
ψ_{nr}	mode shape at DOF n in mode r
$\{\psi\}_r$	mode shape (eigenvector) of mode r of a viscously damped system
$\{\psi'\}_r$	mode shape of mode r in the state-space
ω	circular frequency ($\omega = 2 \cdot \pi \cdot f$) in rad/s (radians per second)
ω_r	circular natural frequency of mode r
ω_{rd}	damped circular natural frequency of mode r
$\omega_{e,r}$	circular natural frequency of mode r affected by an exponential window $w_E(t)$
ω_S	circular natural frequency of a SDOF structure model
ω_H	circular natural frequency of a SDOF human model
ω_O	circular frequency with a period T

MATHEMATICS

e	2.71828... ($e^{i\cdot\omega t} = cos(\omega \cdot t) + i \cdot sin(\omega \cdot t)$)
i	imaginary ($\sqrt{-1}$)
j	variable integer: DOF, discrete frequency
k	variable integer: DOF, discrete time, number of averages
n	variable integer: DOF, number of samples
r	variable integer: discrete time shift, mode
π	3.14159...
a^T	transpose of a
a^*	complex conjugate of a
$Imag(a)$	imaginary part of the complex number a
$Re(a)$	real part of the complex number a
a_j	element j of a column vector $\{a\}$
a_{jk}	element j of column vector k of matrix $[a]$

$\{a\}$	column vector
$\{a\}_k$	column k of matrix $[a]$
$[a]$	matrix
$[I]$	identity matrix (matrix elements are unity at diagonal and otherwise zero)
$a(t)$	function of t
$\dot{a}(t)$	first derivative of $a(t)$
$\ddot{a}(t)$	second derivative of $a(t)$

1. INTRODUCTION

Live entertainment is a very popular pastime. It attracts large crowds to civil engineering structures such as concert halls and stadia. Often, the spectators are actively involved and their motion induces significant dynamic forces into the occupied structure. These dynamic forces result in human-induced vibrations that are an issue of increasing concern (Thorburn 1999).

It is important to realise that large groups of human occupants do not only induce significant dynamic forces but also change the dynamic properties of the structure they occupy. Although the former issue is much more researched, its latter counterpart is equally important for design against human-induced vibrations. Therefore, this thesis concentrates on the influence of human occupants on the dynamic properties of structures. Human-induced forces are not investigated here. Nevertheless, publications relevant to this topic are included in the bibliography.

According to Littler (1998, p. 124), the influence of human occupants on civil engineering structures "is extremely difficult if not impossible to predict". This is because spectators should be modelled as dynamic system and not as simple mass (Ellis and Ji 1997) as previously assumed. This fact is not widely appreciated in the civil engineering community in the UK and elsewhere. Therefore, this thesis summarises the existing knowledge and extends it to enhance the understanding of the influence of humans on slender structures they occupy.

The research presented in this thesis investigated the influence of human occupants on dynamic properties of civil engineering structures by adopting a dual analytical and experimental approach. The thesis is presented in eight chapters. The introduction, the literature review, and the theoretical background presented in the first three chapters are the basis for all further investigations (Figure 1.1). The main body of this work is the analysis of human-structure systems from an analytical (chapter 4) and an experimental point (chapter 5) of view. Based on the experimental data, a dynamic human occupant model was derived (chapter 6). Also in chapter 6, the human occupant model is verified. Furthermore, it is used to provide some preliminary guidelines to assess the influence of human occupants on slender civil engineering structures. Finally, chapters 7 and 8 present conclusions and recommendations for further work.

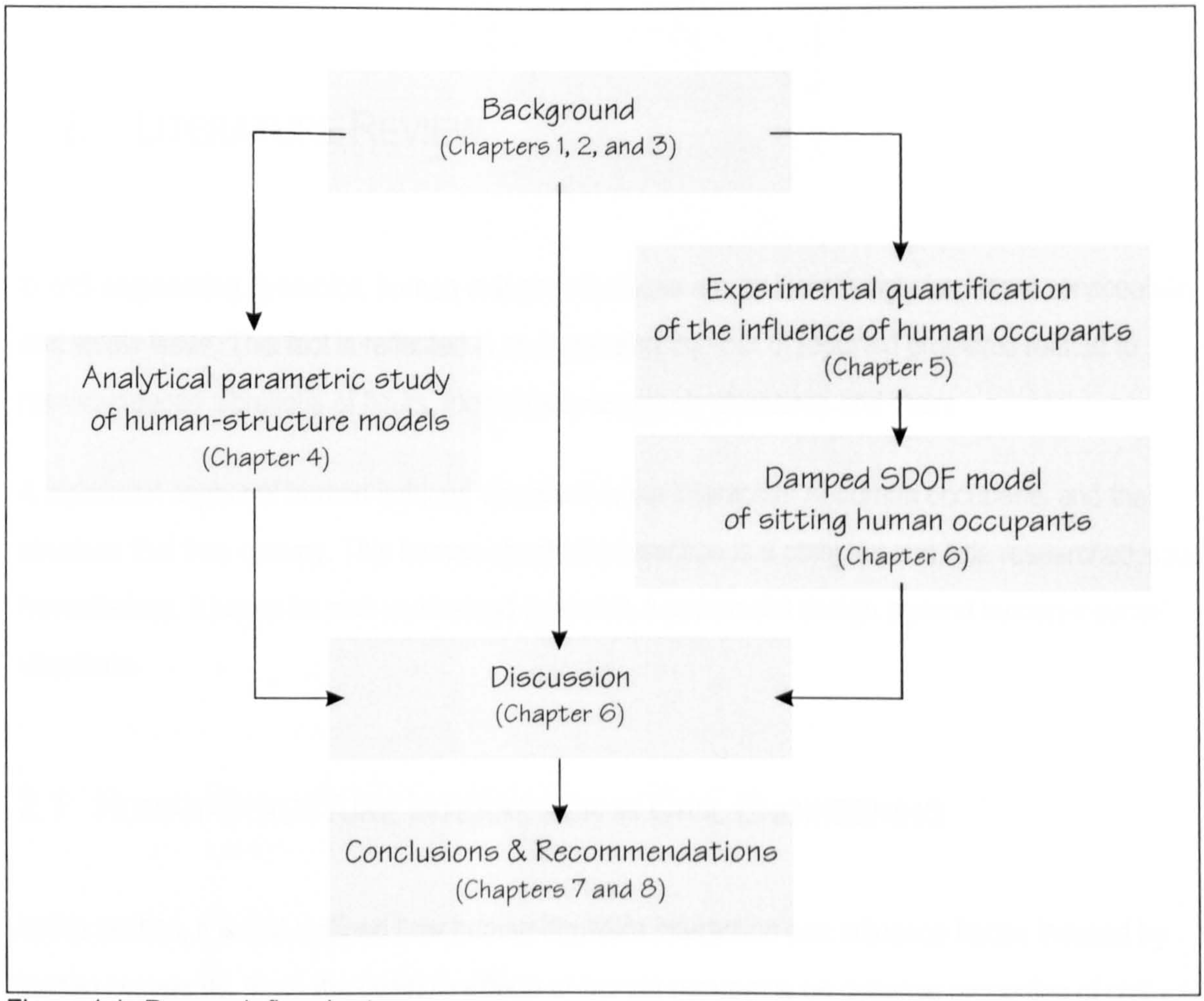

Figure 1.1: Research flowchart.

To aid the reader, references to books or other voluminous publications often include the relevant page number. If the information cannot only be found on this but also on the following or several following pages, this is indicated by 'f' or 'ff' after the page number respectively.

2. LITERATURE REVIEW

In civil engineering dynamics, human-induced vibrations are an increasingly important serviceability and safety issue. This fact is reflected in an increasing number of reported problems related to human-induced vibrations of floors, footbridges, assembly structures and stairs.

A significant aspect of human-induced vibrations is the interaction of human occupants and the structure that they occupy. This human-structure interaction is a complex and little researched issue. Nevertheless, it has to be well understood to enable a successful design against human-induced vibrations.

2.1 HUMAN-STRUCTURE INTERACTION IN CIVIL ENGINEERING

In this section, it is first outlined how human-structure interaction can influence forces induced by human occupants. Next, the possible effects of human occupants on dynamic properties of civil engineering structures are presented and their modelling is discussed.

Ultimately, both effects should be linked and related to psychological effects. Only then can a complete picture of human-structure interaction be obtained.

2.1.1 EFFECTS OF HUMAN-STRUCTURE INTERACTION ON HUMAN-INDUCED FORCES

Human occupants can induce dynamic forces on civil engineering structures by various activities such as walking, jumping, dancing, or hand clapping. Research into quantifying such human-induced forces has been ongoing for many decades (Tilden 1913; ASA 1932; Galbraith and Barton 1970; Nilsson 1976; Wyatt 1985).

Since about 1980, experimentally estimated human-induced force time histories have usually been approximated by Fourier series. Thereby, the common key assumption is that the human-induced forces are perfectly periodic. The factors corresponding to each sinusoidal component of this Fourier series are named dynamic load factors (DLFs) and are reported in a number of publications (Pernica

1990; Bachmann et al. 1995; Kerr 1998). An alternative approach is to define human-induced forces as auto-spectral density (ASD) functions (McConnell 1995) in the frequency domain (Ohlsson 1982; Tuan and Saul 1985; Mouring and Ellingwood 1994; Eriksson 1994).

Dynamic forces induced by crowds are an issue of great concern (Kasperski 2001), as can be seen in an increasing number of publications dealing with crowd-induced vibrations. Nevertheless, the quantification of crowd-induced forces still needs additional research. In particular, the dependency of the nature and level of induced forces on the number of test subjects is currently not clear.

Although, it has been found that dynamic loads induced by groups of people are higher than those induced by individuals, the human-induced forces do not increase linearly with the number of actors. This is so even if people are synchronised by a prompt (Ebrahimpour and Sack 1992; Kasperski and Niemann 1993) that can be provided by music, movements of other people, or perceptible movements of the occupied structure (van Staalduinen and Courage 1994; Fujino et al. 1993). Interestingly, visual and audio contact between people influences the synchronisation of individuals (Hamam 1994; Ebrahimpour and Fitts 1996).

Generally, the synchronisation of people on civil engineering structures can be deliberate or unintentional. Deliberate synchronisation, as in aerobic classes or cases of vandal loading, and thus amplification of vibrations is unquestionably an important issue (Stevenson 1821; Quast 1993; Kasperski 1996). However, the unintentional synchronisation of human occupants is similarly important. It too can lead to structural vibrations strong enough to disturb people in their movement (Dallard et al. 2000) and, therefore, structures can become unserviceable or even unsafe due to panic.

The unintentional synchronisation of pedestrians to structural movements (and therefore to each other) has been observed on several footbridges as reported by Petersen (1972), Bachmann (1992), Fujino et al. (1993), Dallard et al. (2000), Anonymous (2001), Curtis (2001), and Sample (2001). Acknowledging the potential problem posed by this phenomenon, it was included into design proposals by Schulze (1980), Vogel (1983), Slavik (1985), Grundmann and Schneider (1990), and Grundmann et al. (1993).

Research into the reasons and the extend of synchronisation between pedestrians and footbridges has been performed by Schneider (1991) and Fujino et al. (1993). Recently, new research into this known but little understood phenomenon was prompted by strong pedestrian-structure

synchronisation during the opening of the Millennium Bridge in London in June 2000 (Parker 2000; Fitzpatrick 2001).

It should be realised that human-structure synchronisation is only one aspect of human-structure interaction influencing human-induced forces. In fact, human-induced forces may depend on the stiffness of the surface on which people perform (Pimentel 1997, p. 182). Indeed, Baumann and Bachmann (1988, p. 46) found DLFs of walking to be up to 10% higher if estimated on stiff ground and not on a flexible 19 m long prestressed beam. This matter is currently being jointly investigated at the Universities of Manchester and Sheffield under a major research project (Pavic et al. 1999) funded by the Engineering and Physical Sciences Research Council (EPSRC).

In designing against human-induced vibrations, human-induced forces should always be considered in connection with the modal properties (natural frequencies, damping ratios, mode shapes, and modal masses) of the structure they are applied to. These dynamic properties could be, similarly to the human-induced forces, affected by human-structure interaction.

2.1.2 Effects of Human-Structure Interaction on Modal Properties

Human occupants present on civil engineering structures have the ability both to excite and alter the dynamic system. Therefore, strictly speaking, modal properties of the joint human-structure system should be considered in a design against human-induced vibrations. However, due to the lack of reliable information on the properties of occupied structures, the majority of civil engineering design procedures neglect the influence of human occupants on the dynamics of the vibrating system. Those which do not so, do so in different and often inconsistent ways.

The intuitive way to model human occupants of civil engineering structures is to model them as additional mass to the structure. This mass-only model has been widely accepted for a long time (Walley 1959; Allen and Rainer 1975; Ohlsson 1982, p. 6.10; Ebrahimpour et al. 1989). Naturally, such a model leads to a frequency decrease, as observed by Lenzen (1966) for a group of people occupying a floor.

However, Lenzen (1966) also reported, similarly to Polensek (1975) and Rainer and Pernica (1981), a significant increase in damping. Based on these and more similar investigations (such as Eyre and Cullington 1985; Manheim and Honeck 1987; Ebrahimpour et al. 1989; Bishop et al. 1993; Quast

1993; Pimentel and Waldron 1996; Brownjohn 1999), it is nowadays widely accepted that human occupants add damping to structures they occupy. Based on this notion, the National Building Code of Canada (NBC), published by the National Research Council of Canada (NRCC), specifies that damping ratios should be doubled (to values from 4% to 12%) when designing heavily populated structures (NRCC 1985; NRCC 1995).

The observed increases in damping due to human occupation cannot be explained by human occupants modelled as an additional mass only. Nevertheless, this mass-only model is used in the NBC guideline on human-induced vibrations of floors and footbridges (NRCC 1995), in the 'Green Guide' (Department of National Heritage, Scottish Office 1997), and by Allen et al. (1999). It is also still employed in the design of structures such as balconies (Gerasch 1990; Setareh and Hanson 1992), stadia (Eibl and Rösch 1990; Harte and Meskouris 1991; Batista and Magluta 1993; van Staalduinen and Courage 1994; Bennett and Swensson 1997; Reid et al. 1997), and footbridges (Beyer et al. 1995; Luza 1997, p. 55; Hothan 1999, p. 25).

To address this inconsistency, Ohlsson (1982, p. 2.11f) and Rainer and Pernica (1985, p. 7) indicated that damped dynamic models of human occupants could be employed. In 1987, Foschi and Gupta adopted this approach because damped dynamic models of human occupants can, contrary to the mass model, explain increased damping due to human occupation. However, generally, it was assumed that the mass-only occupant model can accurately predict frequency changes imposed by human occupants of civil engineering structures (Ohlsson 1982; Ebrahimpour et al. 1989).

In 1988, experiments by Lenzing showed that the mass-only model does not always predict the natural frequencies of human-occupied structures appropriately. Contrary to his expectations, the fundamental frequency of a small wooden plate (74 Hz) did not reduce significantly if a person more than twice as heavy as the structure (32 kg) was on it. Instead, the natural frequency of the structure increased slightly (Lenzing 1988, p. 47). This phenomenon was readily explained by the human occupant being a dynamic system with mass, stiffness, and damping properties (Lenzing 1988, p. 48).

Three years later, in 1991, response measurements at Twickenham stadium (Ellis and Ji 1997) also indicated that human occupants of a real-life civil engineering structure had been acting more as dynamic mass-spring-damper systems than as additional mass. In particular, if occupied by

spectators, the tested assembly structure clearly showed an additional mode (Figure 2.1). It was hypothesised that this additional mode was caused by human occupants adding a degree of freedom (DOF) to the structure (Ellis and Ji 1997).

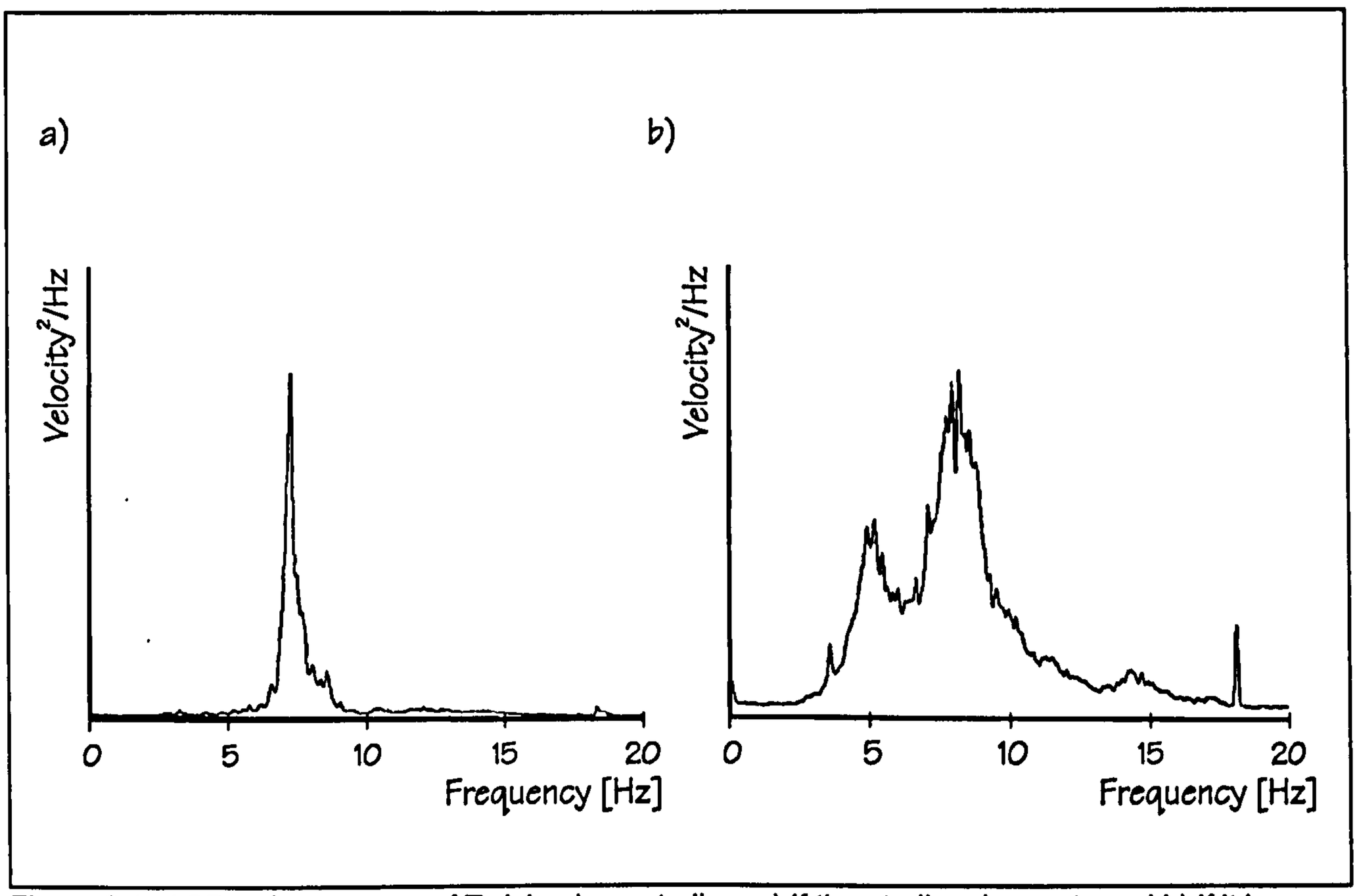

Figure 2.1: ASDs of responses of Twickenham stadium a) if the stadium is empty and b) if it is occupied by a crowd (after Ellis and Ji 1997, figure 2).

Ellis and Ji (1997) presented ASDs of the response of Twickenham stadium (Figure 2.1) without indicating the magnitude of the response. Therefore, levels of vibration of the empty and the occupied structure cannot be compared. They used the response ASDs of three different trusses of Twickenham stadium to estimate natural frequencies (Table 2.1). Natural frequencies of the empty structure were obtained by SDOF curve-fitting. In case of the human-occupied structure, curve-fitting was based on 2-DOF models. This procedure led to the identification of a fundamental frequency between 7.24 Hz and 8.55 Hz (Table 2.1). Under human occupation, two modes with natural frequencies ranging from 5.13 to 5.44 Hz and from 7.89 to 8.72 Hz, respectively, were identified (Table 2.1).

Interestingly, Ellis and Ji (1997) reported, based on peaks of response ASDs, a similar reduction of the fundamental frequency of an assembly structure to about 5 Hz, referring to a temporary grandstand with a fundamental frequency of the empty structure of 16 Hz.

Table 2.1: Natural frequencies at Twickenham stadium (Ellis and Ji 1997, table 1).

	Empty structure	Human-occupied structure
Truss 5	8.55 Hz	5.44 Hz and 8.72 Hz
Truss 9	7.32 Hz	5.41 Hz and 7.91 Hz
Truss 11	7.24 Hz	5.13 Hz and 7.89 Hz

However, structures with vertical modes with natural frequencies below 6 Hz are generally required to be designed against human-induced vibrations (Department of National Heritage, Scottish Office 1997; Institution of Structural Engineers (IStructE) 2001), where the limit of 6 Hz applies to natural frequencies of the empty structure. However, measurements by Ellis and Ji (1997) demonstrate that human occupants can reduce fundamental frequencies of empty structures as high as 16 Hz to below 6 Hz. Therefore, a limit of 6 Hz of vertical modes of empty structures might not be suitable for the design of assembly structures against human-induced vibrations.

Measurements on other assembly structures (Littler 1998; 2000) emphasised the need to model human occupants as a dynamic system and to identify reliable human occupant models. In particular, Littler estimated natural frequencies of a retractable grandstand with 99 seats (Littler 1998) by peak-picking of ASDs of responses to a small impact (Littler 2000). Based on the resulting data (Table 2.2), Littler concluded that the modes of the structure were affected differently by standing or sitting human occupants.

Table 2.2: Natural frequencies of a retractable grandstand (Littler 2000, table 2).

	Front to back mode	Sway mode	Vertical mode
Empty stand	3.05 Hz	3.66 Hz	13.6 Hz
Standing occupants	3.30 Hz	3.54 Hz	9.16 Hz
Sitting occupants	1.71 Hz	1.83 Hz	9.03 Hz

Interestingly, sitting or standing human occupants led to increase and decreases of natural frequencies of horizontal modes respectively (Table 2.2). This indicates that not only vertical, but also horizontal modes could be influenced by human occupants as additional dynamic systems.

In summary, human occupation of civil engineering structures can lead to increased damping, a change of natural frequencies, and also to additional natural frequencies, meaning additional modes of vibration. Only if appropriate dynamic models of human occupants were known, would it be possible to predict the dynamic properties of the human-occupied structures. These should be used in conjunction with human-induced loading in order to predict dynamic responses of such structures as required in their design and/or assessment.

Modelling human occupants is particularly important in the design of slender assembly structures. Such structures can be subjected to high levels of human-induced forces and their dynamic properties can be changed significantly (Figure 2.1).

To model human occupants appropriately, dynamic models of one or more human bodies corresponding to vertical, fore and aft, and lateral vibrations need to be identified (Ji 2000). Furthermore, it is necessary to analyse different postures of human occupants, as demonstrated in Table 2.2 for sitting and standing spectators.

Development of appropriate dynamic models of a human body or of a crowd is clearly the way forward. However, although a number of such models has been developed in biomechanics (mainly to be used in mechanical and aerospace engineering) their application to civil engineering problems may be limited due to substantially different design conditions. A review of this important and sometimes confusing area is clearly warranted as demonstrated in the next sections.

2.2 Biomechanic Models of the Human Body

There are a number of biomechanic models of humans (Griffin 1990). Some of them model the whole body and others only parts such as hands or arms to analyse health related issues. These models are not of interest here because this research is concerned with models of the whole human body developed to predict, say, dynamic properties of human-structure systems such as occupied vehicle seats (Suggs et al. 1969; Wei and Griffin 1995; Boileau and Rakheja 1998). This problem is similar to the influence of human occupants on civil engineering structures. Therefore, dynamic whole-body models developed in this context are evaluated in this review.

2.2.1 Whole-Body Biomechanic Models

Biomechanic researchers usually obtain dynamic characteristics of the whole human body experimentally by placing a person on a shaking table in laboratory conditions. Thereby, the applied force and the response of the human-structure system at the driving point are measured. These data are used to calculate driving-point frequency response functions (FRFs). These FRFs generally relate an acceleration or velocity response to a sinusoidal base excitation and are, therefore, provided as apparent mass $M(f)$ or mechanical impedance $I(f)$. By curve-fitting such experimental FRFs, dynamic properties of biodynamic human models are identified (Wei and Griffin 1998).

The simplest biodynamic model of the human body is a damped single degree of freedom (SDOF) system (Figure 2.2a). This type of model can lead to good approximations of experimental and analytical driving-point FRFs.

However, two peaks were often visible in the apparent mass $M(f)$ of sitting individuals (Wei and Griffin 1998; Mansfield and Griffin 2000) and generally in the apparent mass of standing people (Matsumoto 1996). Therefore, the damped SDOF model (having only one peak in the FRF) has been extended into a two DOF model, which enabled fitting of two peaks in experimental driving-point FRFs. The additional DOF was either attached to the first DOF (Allen 1978) as shown in Figure 2.3a or, more often, completely independent of the first DOF (Suggs et al. 1969; Wei and Griffin 1998) as indicated in Figure 2.3b.

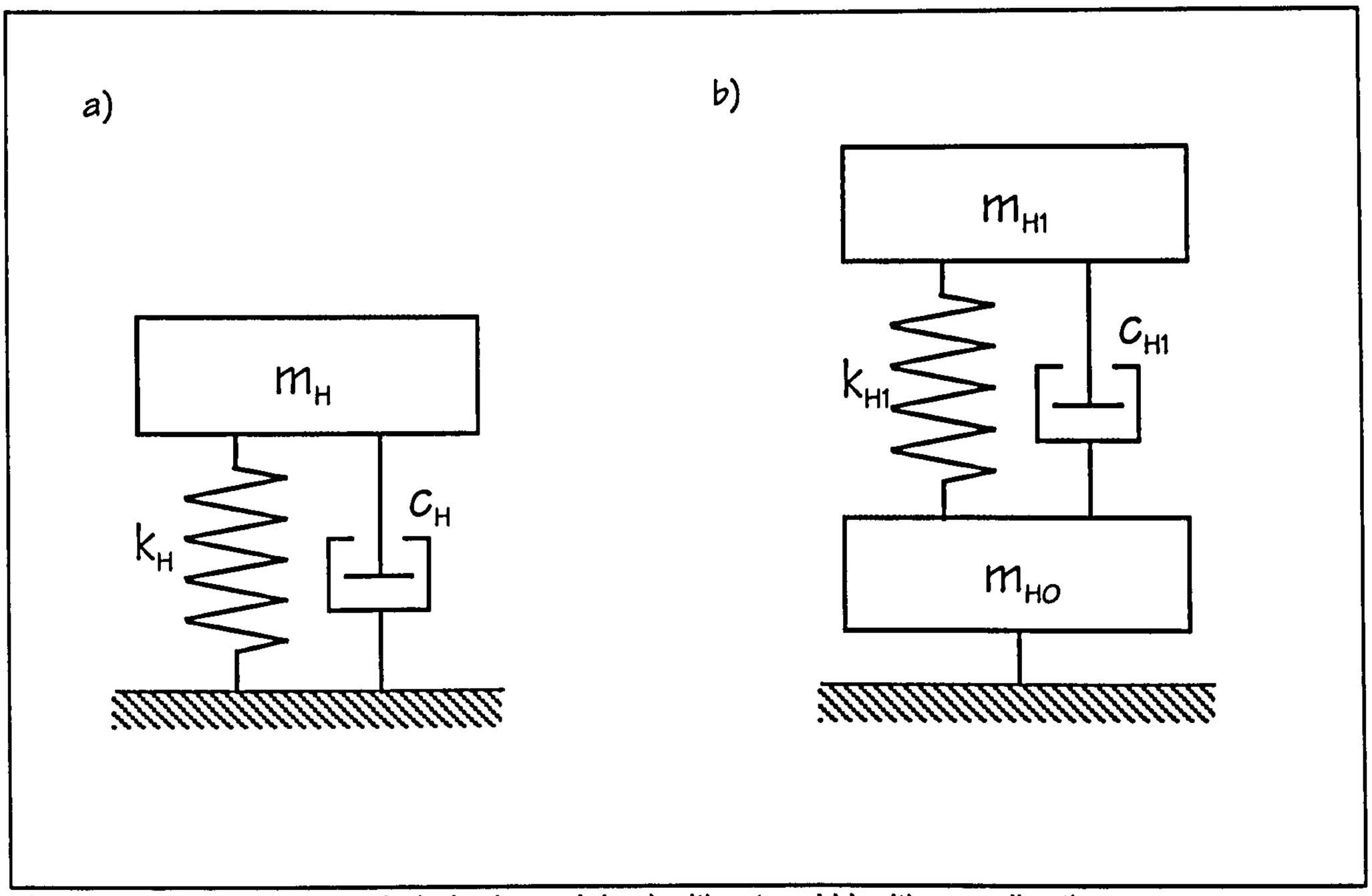

Figure 2.2: SDOF human whole-body models a) without and b) with non-vibrating mass.

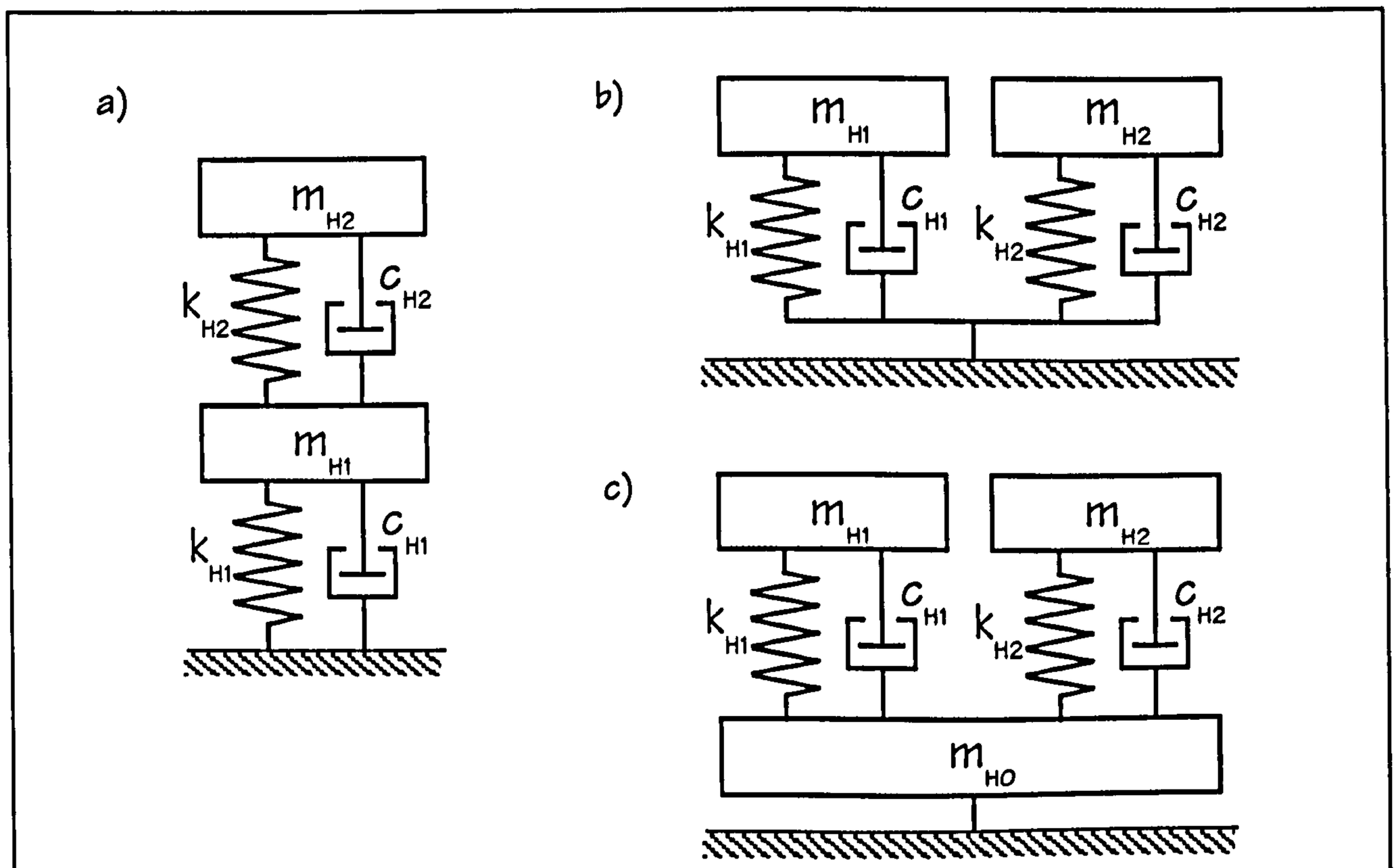

Figure 2.3: Human whole-body models using a) a 2-DOF system, b) a 2-SDOF system, and c) a 2-SDOF system with a non-vibrating mass.

Further research showed that adding a non-vibrating mass m_{HO} to a SDOF model (Figure 2.2b) or a 2-SDOF model (Figure 2.3c) led to better fits of experimental FRFs. Wei and Griffin (1998, p. 870) justified this non-vibrating mass m_{HO} as presenting "the effect of other modes that are above the frequency range of interest".

Finally, it is emphasised that models of the human body solely derived from driving-point FRFs should not be used to predict movements of particular parts of the human body (International Organization for Standardization (ISO) 1981). For this purpose, separately derived and more complex models of the human body are available (Nigam and Malik 1987; ISO 1987; Qassem et al. 1994; Boileau et al. 1996). However, these models are often unsuitable for describing driving-point FRFs (Boileau and Rakheja 1998).

2.2.2 Properties of the Human Body

Most biomechanic research determining whole-body vibrations concentrated on vertical vibrations of sitting (often male) people. Fewer investigations involved standing humans (Coermann 1962; Matsumoto 1996; Matsumoto and Griffin 1998; Matsumoto and Griffin 2000) or looked at horizontal vibrations (Fairley and Griffin 1990; Holmlund and Lundström 1998; Mansfield and Lundström 1999a; Mansfield and Lundström 1999b).

Many publications present experimental driving-point FRFs. However, only a few biodynamic models were fit into the experimental data (Wei and Griffin 1998). Four of these whole-body models related to vertical vibrations of a sitting person are presented in Table 2.3.

Each of these models is characterised by its lumped properties of mass (m_H), stiffness (k_H), and viscous damping (c_H). They define the modal properties natural frequency f and damping ratio ζ (Table 2.3). It is noteworthy that all four models feature a heavily damped mode with natural frequencies f_1 ranging from 4.5 to 5.0 Hz and damping ratios ζ_1 ranging from about 20% to about 50% (Table 2.3).

Table 2.3: Characteristics of biomechanic models of a sitting human subjected to vertical vibrations.

Model	Spatial properties	Modal Properties
Coermann (1962) [1]: Damped SDOF model	m_H = 86.2 kg (86200 dyne s²/cm) k_H = 85.25 kN/m (85.25 dyne/cm) c_H = 1.72 kNs/m (1.72·10⁶ dyne s/cm)	f_1 = 5.0 Hz ζ_1 = 32%
Suggs et al. (1969) [2]: 2-SDOF model	m_{H1} = 36.3 kg (80 lb) k_{H1} = 28.45 kN/m (1952 lb/ft) c_{H1} = 474 Ns/m (32.5 lb s/ft)	f_1 = 4.5 Hz ζ_1 = 23%
	m_{H2} = 12.5 kg (27.6 lb) k_{H2} = 15.03 kN/m (1030 lb/ft) c_{H2} = 271 Ns/m (18.6 lb s/ft)	f_2 = 5.5 Hz ζ_2 = 31%
Wei and Griffin (1998) [3]: SDOF model with non-vibrating mass	m_{HO} = 4.1 kg	-
	m_{H1} = 46.7 kg k_{H1} = 44.115 kN/m c_{H1} = 1.522 kNs/m	f_1 = 4.9 Hz ζ_1 = 53%
Wei and Griffin (1998) [3]: 2-SDOF model with non-vibrating mass	m_{HO} = 5.6 kg	-
	m_{H1} = 36.2 kg k_{H1} = 35.007 kN/m c_{H1} = 815 Ns/m	f_1 = 4.9 Hz ζ_1 = 36%
	m_{H2} = 8.9 kg k_{H2} = 33.254 kN/m c_{H2} = 484 Ns/m	f_2 = 9.7 Hz ζ_2 = 44%

Imperial units were converted into metric units employing Beranek (1988, appendix B3).
[1] Based on the mechanical impedances I(f) of eight men.
[2] Based on the mechanical impedances I(f) of 11 men.
[3] Based on the apparent masses M(f) of 60 people.

The 2-SDOF models by Suggs et al. (1969) and Wei and Griffin (1998) have an additional DOF and, therefore, a second mode. This second mode accounts for a second broad peak in the frequency range from 8 Hz to 15 Hz often apparent in driving-point FRFs (Fairley and Griffin 1989; Matsumoto 1996; Matsumoto and Griffin 1998; Mansfield and Lundström 1999b; Holmlund et al. 2000; Mansfield and Griffin 2000). However, the influence of the second mode on the apparent mass

M(f) is rather small. For instance, the apparent masses M(f) of the SDOF and the 2-SDOF model (both featuring a non-vibrating mass) based on the same experimental data by Wei and Griffin (1998) match closely, as indicated by the green lines in Figure 2.4.

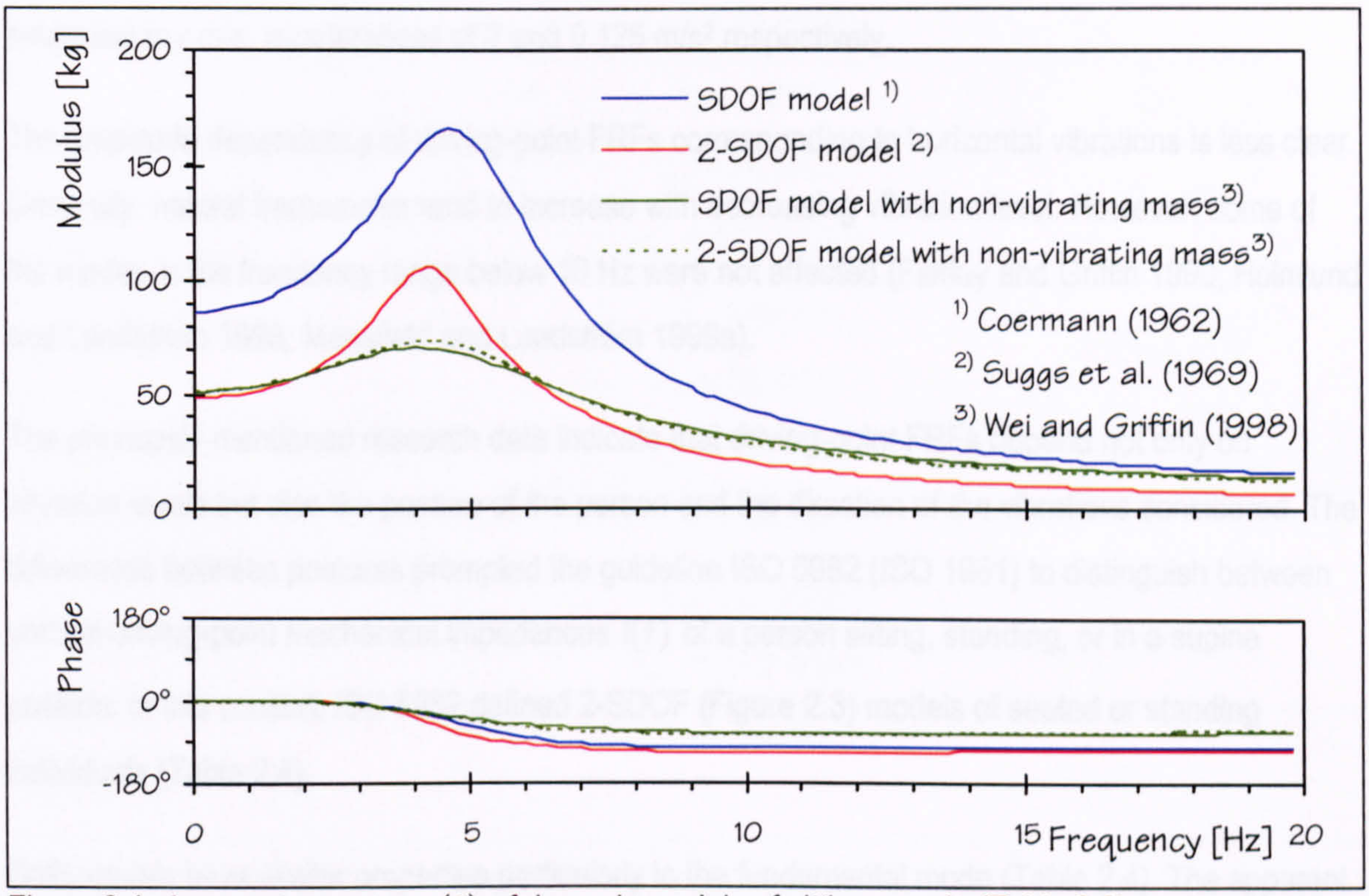

Figure 2.4: Apparent masses M(f) of dynamic models of sitting people (Table 2.3).

In contrast to models based on the same research (Wei and Griffin 1998), apparent masses M(f) of models based on different research (represented by different colours) deviate significantly (Figure 2.4). In general, driving-point FRFs presented in different publications often deviate significantly. This scatter is mainly due to employing different individuals (Hinz and Seidel 1987; Fairley and Griffin 1989; Mansfield 1996; Matsumoto 1996; Wei and Griffin 1998). Additional variability is introduced by varying test conditions (Boileau et al. 1998; Holmlund et al. 2000).

A major factor influencing the estimated driving-point FRFs is the excitation. Biomechanics usually employ sinusoidal, sine sweep, or random excitation with frequencies from below 1 Hz up to about 20 Hz. The vibration levels range from 0.1 to 2.5 m/s^2 root-mean-square (r.m.s.) accelerations, which correspond to vibration levels common in vehicles (Mansfield and Griffin 2000).

Research has shown that the frequencies corresponding to the peaks of driving-point FRFs increase with decreasing vibration levels (Hinz and Seidel 1987; Fairley and Griffin 1989; Matsumoto and

Griffin 1998; Mansfield and Griffin 2000). For example, decreasing r.m.s. accelerations eight times, from 2 to 0.25 m/s², increased the frequency of the first peak of $M(f)$ of vertical vibrations of sitting people by 50%, from 4 to 6 Hz (Fairley and Griffin 1989). Similarly, Matsumoto and Griffin (1998) found the frequency of the first peak of $M(f)$ increased from 5 to 7 Hz if standing people were subjected to r.m.s. accelerations of 2 and 0.125 m/s² respectively.

The amplitude dependency of driving-point FRFs corresponding to horizontal vibrations is less clear. Generally, natural frequencies tend to increase with decreasing vibration level. However, some of the modes in the frequency range below 10 Hz were not affected (Fairley and Griffin 1990; Holmlund and Lundström 1998; Mansfield and Lundström 1999a).

The previously mentioned research data indicate that driving-point FRFs depend not only on vibration levels but also the posture of the person and the direction of the vibrations considered. The differences between postures prompted the guideline ISO 5982 (ISO 1981) to distinguish between vertical driving-point mechanical impedances $I(f)$ of a person sitting, standing, or in a supine position. In this context, ISO 5982 defined 2-SDOF (Figure 2.3) models of seated or standing individuals (Table 2.4).

Both models have similar properties particularly in the fundamental mode (Table 2.4). The apparent masses $M(f)$ of both models (Figure 2.5) fit well within the apparent masses $M(f)$ of sitting people defined in Table 2.3 (Figure 2.4).

Nevertheless, ISO 5982 was heavily criticised because of its limited and inconsistent experimental background (Griffin 1990, p. 370f; Holmlund et al. 1995; Matsumoto 1996; Boileau et al. 1998). Recently, a revision of ISO 5982 has been published (ISO 2001). The revised standard includes a single more complex model of a human body. This model aims to represent not only the driving-point FRFs, but also the transmission of vibrations to the head of a seated person (ISO 2001). So far, the transmission of vibrations to the head of a sitting or standing person could be evaluated using the 4-DOF model in ISO 7962 (ISO 1987), which was replaced by ISO 5982 (ISO 2001).

Table 2.4: Characteristics of human models specified in ISO 5982 (ISO 1981).

Model	Spatial properties	Modal Properties
ISO 5982 (ISO 1981): 2-SDOF model of the seated human body	m_{H1} = 69 kg k_{H1} = 68 kN/m c_{H1} = 1.54 kNs/m	f_1 = 5.0 Hz ζ_1 = 36%
	m_{H2} = 6 kg k_{H2} = 24 kN/m c_{H2} = 0.19 kNs/m	f_2 = 10.1 Hz ζ_2 = 25%
ISO 5982 (ISO 1981): 2-SDOF model of the standing human body	m_{H1} = 62 kg k_{H1} = 62 kN/m c_{H1} = 1.46 kNs/m	f_1 = 5.0 Hz ζ_1 = 37%
	m_{H2} = 13 kg k_{H2} = 80 kN/m c_{H2} = 0.93 kNs/m	f_2 = 12.5 Hz ζ_2 = 46%

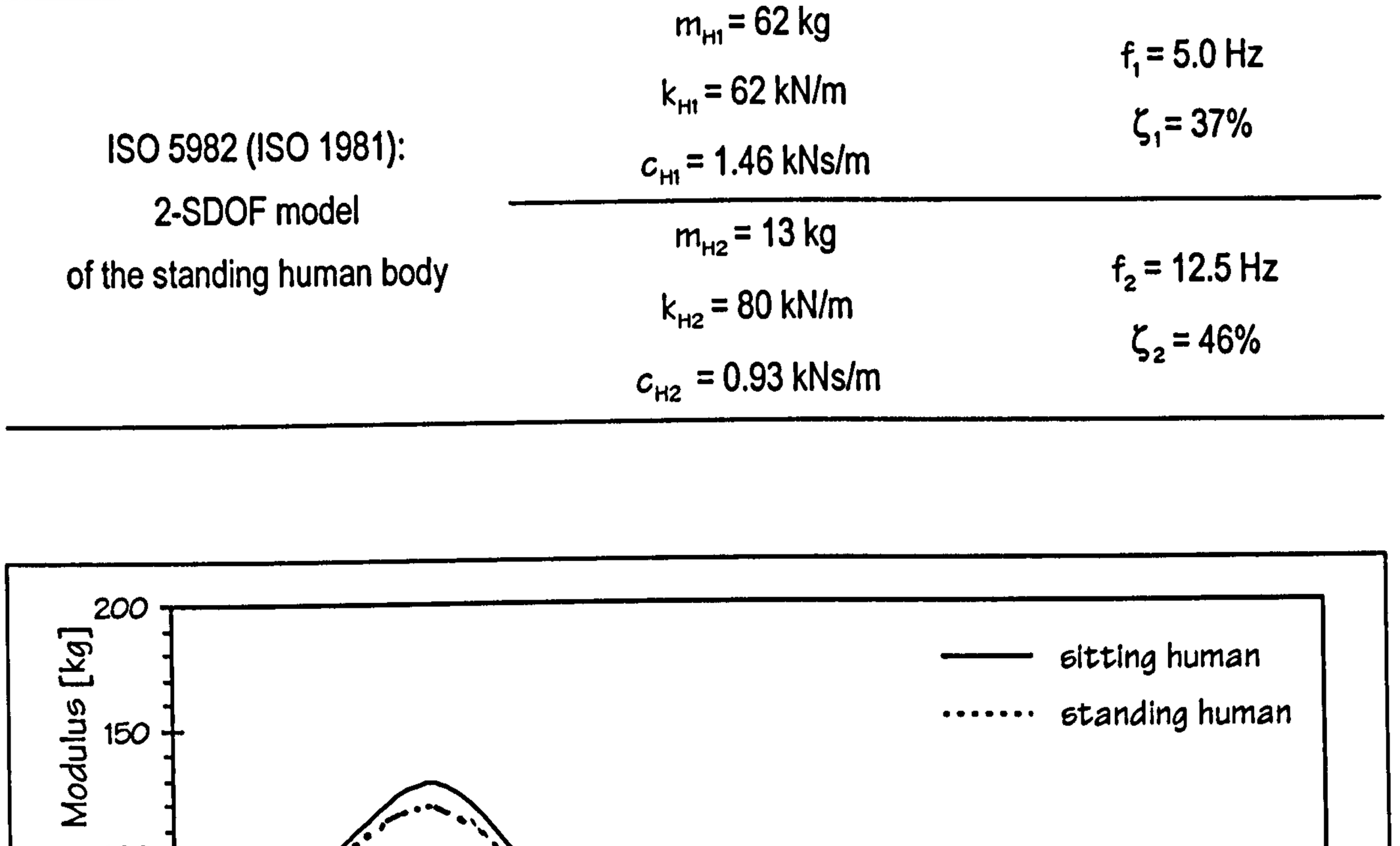

Figure 2.5: Apparent masses M(f) of sitting and standing people according to ISO 5982 (Table 2.4).

In summary, when utilising the results of biomechanic research of whole-body dynamic models in civil engineering, several important issues must be borne in mind. Firstly, the human body is a very complex non-linear dynamic system that has properties that differ between different people (inter-subject variability) and between individuals themselves (intra-subject variability) (ISO 1981; Griffin 1990). Secondly, vertical vibrations of the whole-body of sitting or standing people are dominated by a heavily damped mode. This mode has a natural frequency between 4 and 6 Hz and its damping ratio is quoted with values ranging from 20% up to 50%.

Thirdly, and most importantly, the properties of the human body strongly depend on the magnitude of vibration. However, vibration levels usually encountered in civil engineering are considerably smaller than those employed by biomechanics to derive dynamic human models (Griffin 1990, p. 39). Therefore, it is essential to verify and, possibly, update biomechanic models before they are adopted to model human occupants of civil engineering structures. Furthermore, all biomechanical models known to the writer represent single individuals only. However, modelling groups of occupants is essential in modelling the dynamic behaviour of assembly structures.

2.3 Dynamic Models of Humans in Civil Engineering

Current design guidelines assess the vibration serviceability of civil engineering structures based on their vibration response (ISO 1989; British Standard Institution (BSI) 1992; ISO 1992). However, as previously mentioned, correct prediction of structural responses to human-induced vibrations requires detailed knowledge of the dynamic properties of the joint human-structure system. With this in mind, civil engineers increasingly attempt to model human occupants as dynamic systems (Ji 1995; Falati 1999; Williams et al. 1999). Such research should lead to dynamic models of human occupants appropriate for use in civil engineering and will be reviewed in sections 2.4 and 2.5.

In this section, dynamic human models related to human impact and the energy absorbed by the human body are reviewed. Thereby, only models developed or presented by civil engineers are included.

2.3.1 Modelling Human Impactors on Flexible Structures

More than 20 years ago, civil engineers started to employ dynamic models of the human body to tackle safety and serviceability issues. In 1976, Struck developed dynamic models of humans to analyse people impacting on non-structural elements such as partition walls.

Simple mass-spring systems (Figure 2.2a with $c_H = 0$) are used to assess the impact of people on flexible structures (Struck 1976; Mann 1979; Struck and Limberger 1981; Canisius 2000).

Struck (1976) used this dynamic human model to describe people hitting partition walls with their shoulder. He estimated the mass m_H as ranging from 15 to 30 kg and stiffnesses k_H as ranging from about 10 to 50 kN/m (Struck 1976, p. 18).

Moreover, Mann (1979), Struck and Limberger (1981), and Canisius (2000) investigated the impact of a person landing on his/her feet. In doing so, they assumed that the total mass m_T of a human landing on their feet is the same as the lumped mass m_H of a spring-mass model of the human body.

Mann (1979) analysed soft landing of (probably three different) individuals from heights of 20 cm to 90 cm. He concluded that the stiffness k_H is at least 3 kN/m for soft landing. In case of hard landing, he specified an upper value of the stiffness k_H depending on the drop height h [m]:

$$k_H = 20\ \mathrm{kN/m} - h \cdot 13\ \mathrm{kN/m^2}. \tag{2.1}$$

Significantly higher stiffnesses k_H of 65 kN/m and 130 kN/m were estimated by Struck and Limberger (1981) for landing on one foot or both feet, respectively. However, these data correspond to the extreme case of a person hanging on a bar with his/her feet up to 24 cm above the ground dropping with straight knees.

Finally, recent work by Canisius et al. (1998) analysed people dropping from heights of 25 to 75 cm onto scaffold boards. This work is thought to have led to stiffnesses k_H ranging from 1 to 30 kN/m. It should be said that these values are the writer's interpretation of data presented by Canisius (2000, figure 6).

2.3.2 Energy Absorbed by Human Occupants

In 1977, Farah was prompted by prior biomechanical research (Pradko and Lee 1966; Pradko et al. 1967; Lee and Pradko 1968) to assess the serviceability of civil engineering structures using dynamic human models. Farah used the energy absorbed by the human body as a measure of vibration serviceability, whereby more energy absorbed by the human occupant corresponded to less comfort. He re-evaluated data of several biomechanic publications presenting dynamic human models and decided to employ a 2-DOF model of the human body (Figure 2.3a). Parameters of this model (Table 2.5) are based on the re-evaluation of the modulus of the mechanical impedance I(f) of one standing person reported by Coermann (1962, figure 6).

Since the work of Farah (1977), the energy absorbed by the human body has been an issue that was neglected in both biomechanics and civil engineering. However, since 1995, there has been an increase in the research into the energy absorbed by the human body (Lundström et al. 1995; Lundström and Holmlund 1998; Lundström et al. 1998; Mansfield and Griffin 1998; Holmlund 1999; Mansfield et al. 2000).

Table 2.5: Characteristics of a damped 2-DOF human whole-body model.

Human Model	Spatial properties	Modal Properties
	m_{H1} = 74.4 kg (5.1 slugs)	
	m_{H2} = 7.3 kg (0.5 slugs)	f_1 = 6.9 Hz
Farah (1977):	k_{H1} = 149.2 kN/m (10224 lb/ft)	ζ_1 = 25%
2-DOF model	k_{H2} = 15.4 kN/m (1052 lb/ft)	f_2 = 7.6 Hz
	c_{H1} = 2.85 kNs/m (195.0 lb s/ft)	ζ_2 = 31%
	c_{H2} = 0.086 kNs/m (5.9 lb s/ft)	

Units were converted into metric units employing Beranek (1988, appendix B3).

As for civil engineering applications, Brownjohn (1999; 2001) quantified the energies absorbed by a standing human occupant and the occupied prestressed concrete structure weighing 1200 kg simultaneously. This research highlights once again the potentially beneficial effect of including stationary human occupants into the dynamic modelling of occupied civil engineering structures.

2.4 EXPERIMENTAL INVESTIGATIONS

The influence of human occupants on civil engineering structures is a complex issue and the current state-of-the-art is such that this influence cannot be, according to Littler (1998), mathematically predicted. However, the 1990s saw several attempts to quantify the influence of one or two stationary occupants on dynamic behaviour of well-defined structures under laboratory conditions.

2.4.1 EXPERIMENTS BY ELLIS AND JI

Inspired by the results of the already mentioned measurements on assembly structures (section 2.1.2), Ellis and Ji performed laboratory experiments on a simple concrete beam (Figure 2.6). This particular research was published widely (Ellis et al. 1994a; Ellis et al. 1994b; Ji and Ellis 1994; Ji 1995; Ji and Ellis 1995; Ellis and Ji 1997; Ji and Ellis 1997; Ji and Ellis 1999). The most informative papers are Ji (1995), Ellis and Ji (1997), and Ji and Ellis (1999).

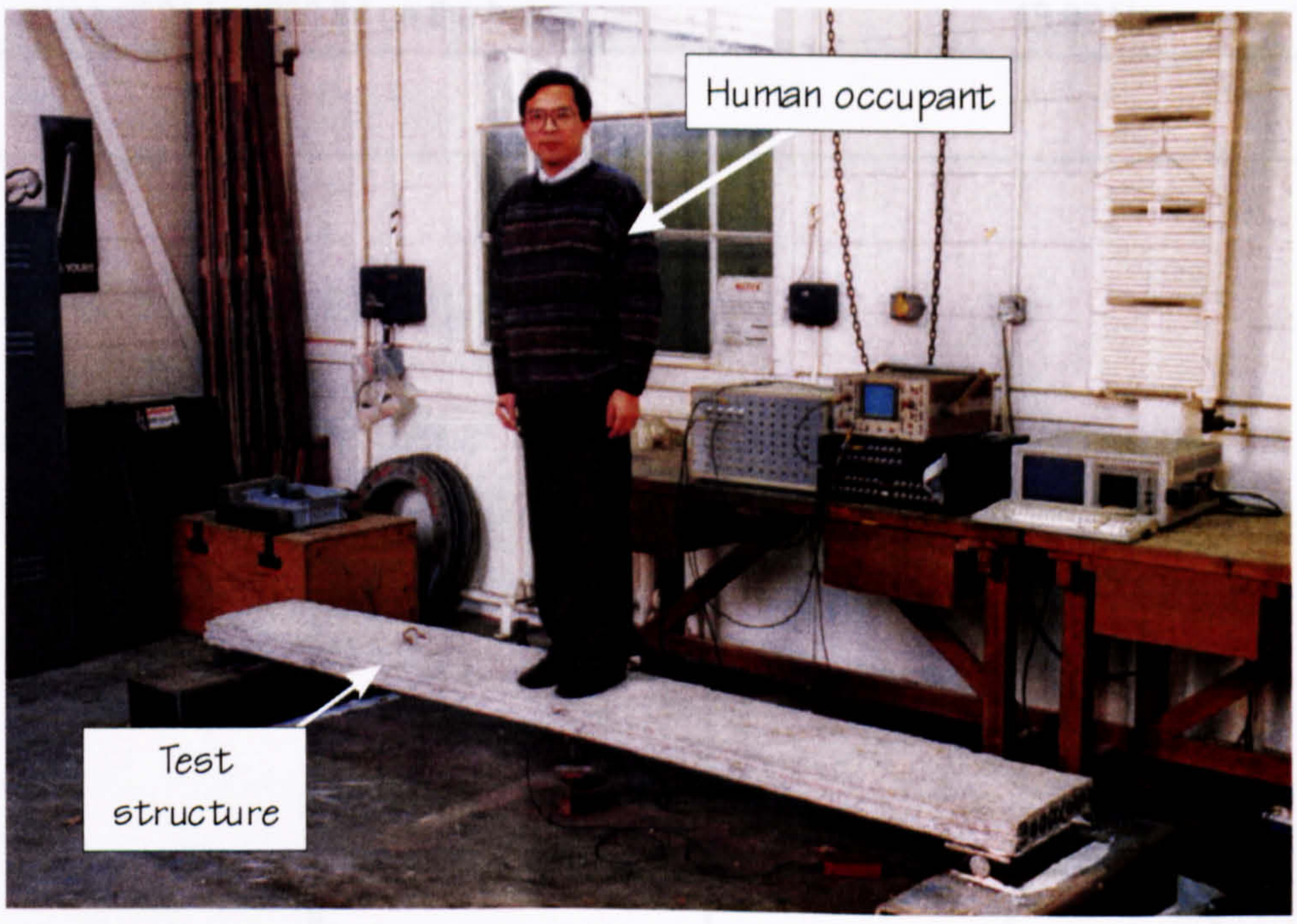

Figure 2.6: Test structure and human occupant (after Ji and Ellis 1997).

Ellis and Ji quantified the influence of four different individuals (a, b, c, and d) on a high-frequency (18.68 Hz) structure (Table 2.6) from response ASDs of the structure to impact by a hammer. The

laboratory experiments demonstrated that a human occupant can increase the natural frequency and damping of a high-frequency (18.68 Hz) structure (Figure 2.7). Additionally, the research indicated that the influence of a human occupant depends on the individual and its posture (Table 2.6). This fits well with the biomechanic observations reported by Griffin (1990) and underpins the already reported findings by Littler (2000) (Table 2.2).

Table 2.6: Influence of a single human occupant on natural frequencies of a beam (Ji 1995; Ji and Ellis 1999).

Configuration	Natural frequency
empty beam	18.68 Hz
one sitting human occupant (a)	19.04 Hz
one standing human occupant (a)	20.02 Hz
one standing human occupant (b)	20.51 Hz
one standing human occupant (c)	20.51 Hz
one standing human occupant (d)	21.00 Hz
mass of 45 kg (100 lb) on the beam	15.75 Hz
mass of 91 kg (200 lb) on the beam	13.92 Hz

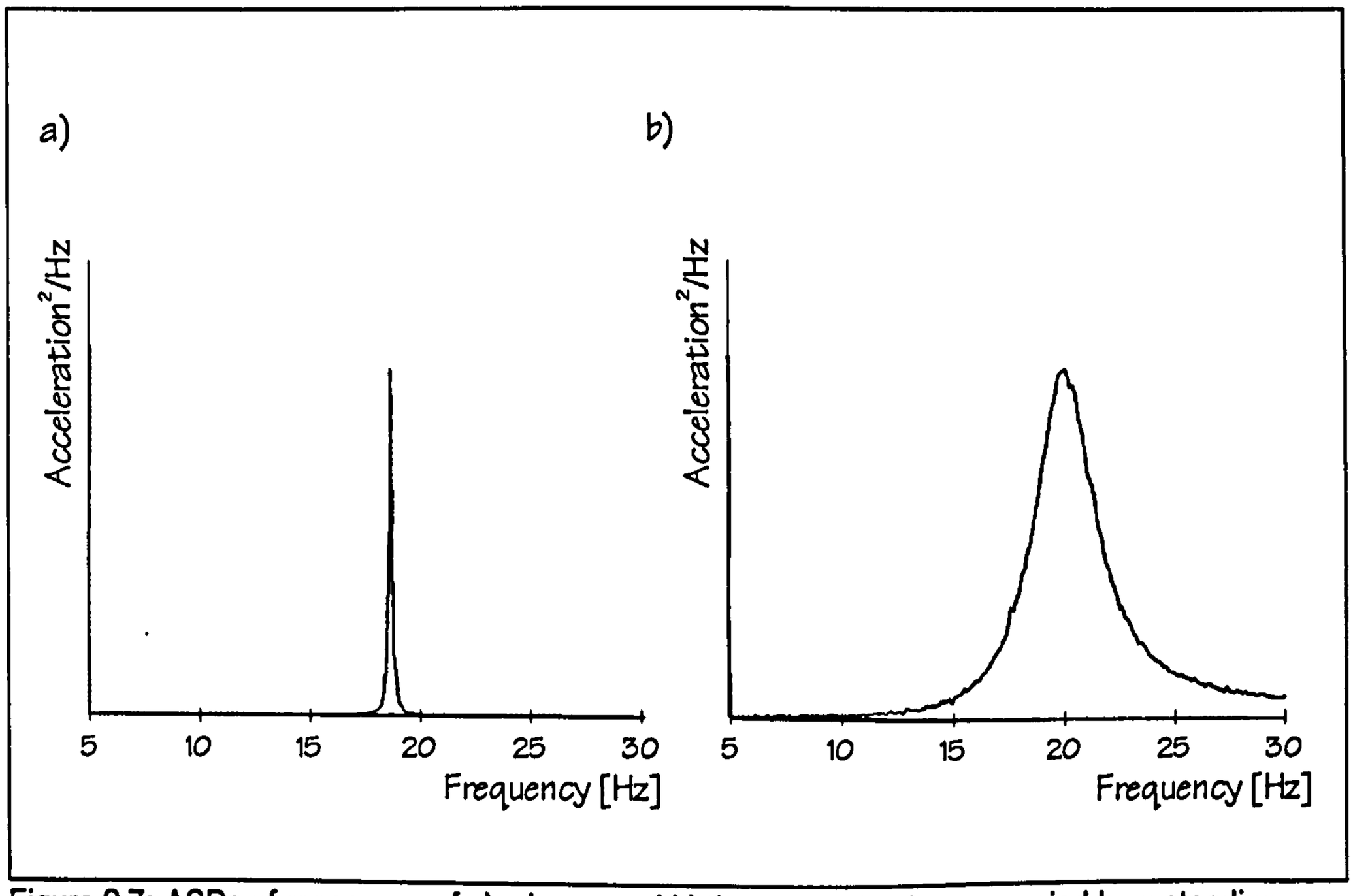

Figure 2.7: ASDs of responses of a) a beam and b) the same structure occupied by a standing person (after Ji and Ellis 1995, figure 2).

Unfortunately, Ellis and Ji did not estimate damping and the ASDs given in Figure 2.7 were reported without quantifying the response magnitude. Therefore, the effect of an occupant on the response of the light beam structure employed cannot be evaluated.

Finally, Ellis and Ji (1997) claimed that moving people are a dynamic load only because neither a jumping nor an occupant walking on the spot changed the estimated natural frequency of the beam (Figure 2.6). This statement contradicts the finding of Pimentel (1997, p. 201) that "the natural frequencies of the structure during walking remained somewhere between those obtained from pedestrians standing still (after jumping tests) and without pedestrians (following walking tests)".

Pimentel (1997, p. 139) came to his conclusion observing the reduction of natural frequencies of 2.3 Hz, 3.6 Hz, and 4.7 Hz of a footbridge. Instead of such a real-life structure, Ellis and Ji (1997) employed a small beam (Figure 2.6) with a high natural frequency of 18.68 Hz, whose fundamental frequency was increased by a stationary human occupant (Table 2.6). These differences might have led to the apparently contradictory findings and further experimental investigations are obviously required. They should quantify the effect of moving occupants not only on natural frequencies but also on damping of the occupied structure. Such an analysis might reveal structures occupied by moving (walking or jumping) occupants could be modelled as time dependent non-linear systems, as proposed by Ebrahimpour and Sack (1992).

2.4.2 Experiments by Hothan (1999)

Hothan (1999) analysed the influence of a static mass or a standing person on two similar steel structures (Figure 2.8). The first structure was 5 m long and weighted 236 kg. It was set up with seven different spans ranging from 4.8 to 2 m. The second structure was 4 m long and had a mass of 226 kg. It was employed with six spans ranging from 3.9 to 2 m.

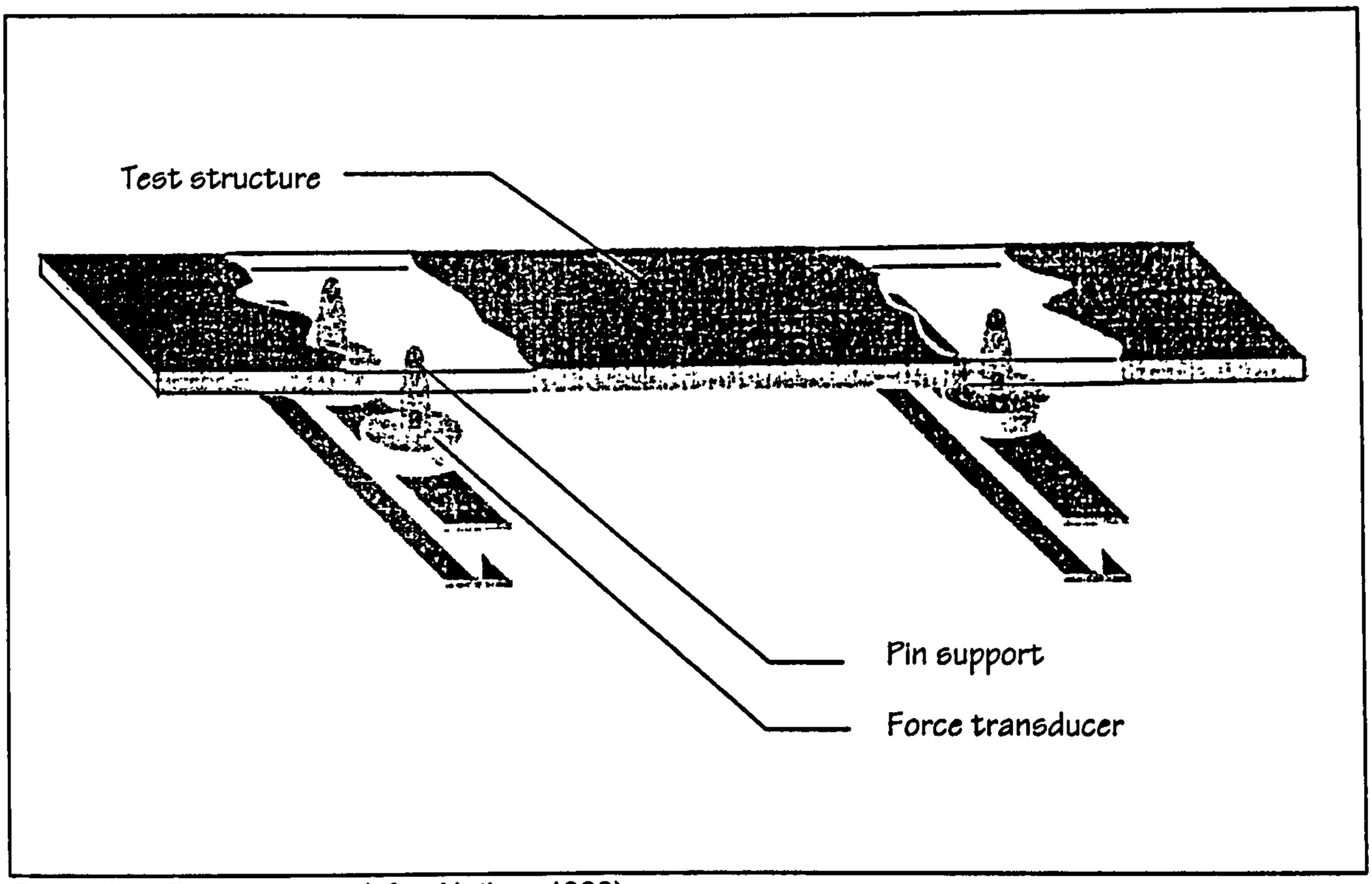

Figure 2.8: Test structure (after Hothan 1999).

Reducing the span of the first and second test structure led to 13 structural set-ups (Table 2.7). For each of them, three configurations were analysed. Firstly, the structure was empty. Secondly, a person was standing on it, and, thirdly, the structure was loaded with a static mass that equalled the total mass of the human occupant (80 kg). In this research, such a static load is going to be termed 'equivalent mass', following the suggestion of Falati (1999, p. 169).

Estimated natural frequencies and damping ratios are listed in Table 2.7. These data were determined from vibration responses of force transducers at each of the three supports (Figure 2.8) after the structure was swung by hand or impacted with a hammer. In several tests, modal properties were not determined (Table 2.7).

The failure to determine damping was most likely caused by several modes contributing to vibration responses. In such cases, decaying response time histories require sophisticated analysis for the estimation of damping. Nevertheless, damping was estimated in experiment 6 if a person was on the structure (Table 2.7), although at least two modes contributed to the vibration response (Hothan 1999, p. 15). Therefore, generally little confidence is placed into the estimated damping.

Table 2.7: Influence of a single human occupant or an equivalent mass on natural frequencies f_1 and damping ratios ζ_1 [1)] of steel structures (Hothan 1999, appendix 3).

Experiment No.	Empty structure		Human occupant		Equivalent mass	
	f_1	ζ_1	f_1	ζ_1	f_1	ζ_1
1	1.98 Hz	0.4%	1.51 Hz	1.0%	1.53 Hz	0.5%
2	2.27 Hz	0.3%	1.71 Hz	0.8%	1.72 Hz	0.3%
3	2.82 Hz	0.2%	2.05 Hz	1.0%	2.08 Hz	0.3%
4	3.49 Hz	0.1%	2.47 Hz	1.5%	2.55 Hz	0.2%
5	4.06 Hz	N/A	2.98 Hz	N/A	3.10 Hz	0.1%
6	4.12 Hz	N/A	3.31 Hz	2.5%	3.43 Hz	N/A
7	3.63 Hz	N/A	3.39 Hz	N/A	3.43 Hz	N/A
8	4.62 Hz	0.1%	3.36 Hz	2.2%	3.51 Hz	0.1%
9	5.75 Hz	0.1%	3.91 Hz	N/A	4.27 Hz	0.1%
10	6.36 Hz	0.1%	4.23 Hz	N/A	4.68 Hz	0.1%
11	8.00 Hz	0.2%	4.72 Hz	7.2%	5.80 Hz	0.1%
12	9.78 Hz	0.03%	4.73 Hz	13.6%	7.46 Hz	0.1%
13	9.84 Hz	0.03%	N/A	N/A	8.39 Hz	0.03%

[1)] Hothan (1999) provided logarithmic damping decrements δ that were evaluated and converted into damping ratios ζ_1 using $\zeta \approx \delta/2 \cdot \pi$ (Chopra 1995, p. 49).

Nevertheless, it is noteworthy that damping ratios ζ_1 for the empty and the mass loaded structure matched closely (Table 2.7). In contrast, a human occupant at least doubled the damping ratio ζ_1 of the empty structure (Table 2.7). Generally, the damping ratio ζ_1 of the human-occupied structure increased with the fundamental frequency f_1 of the empty structure (Table 2.7).

Hothan (1999) determined natural frequencies from peaks of response spectra, calculated by applying the Fast Fourier transformation (FFT) to the response signals. This methodology failed to determine a frequency of the human-occupied test structure in experiment 13. However, the influence of a human occupant on a structure is the aim of this research. Therefore, experiment 13 is excluded from the following discussion of natural frequencies f_1 (Figure 2.9).

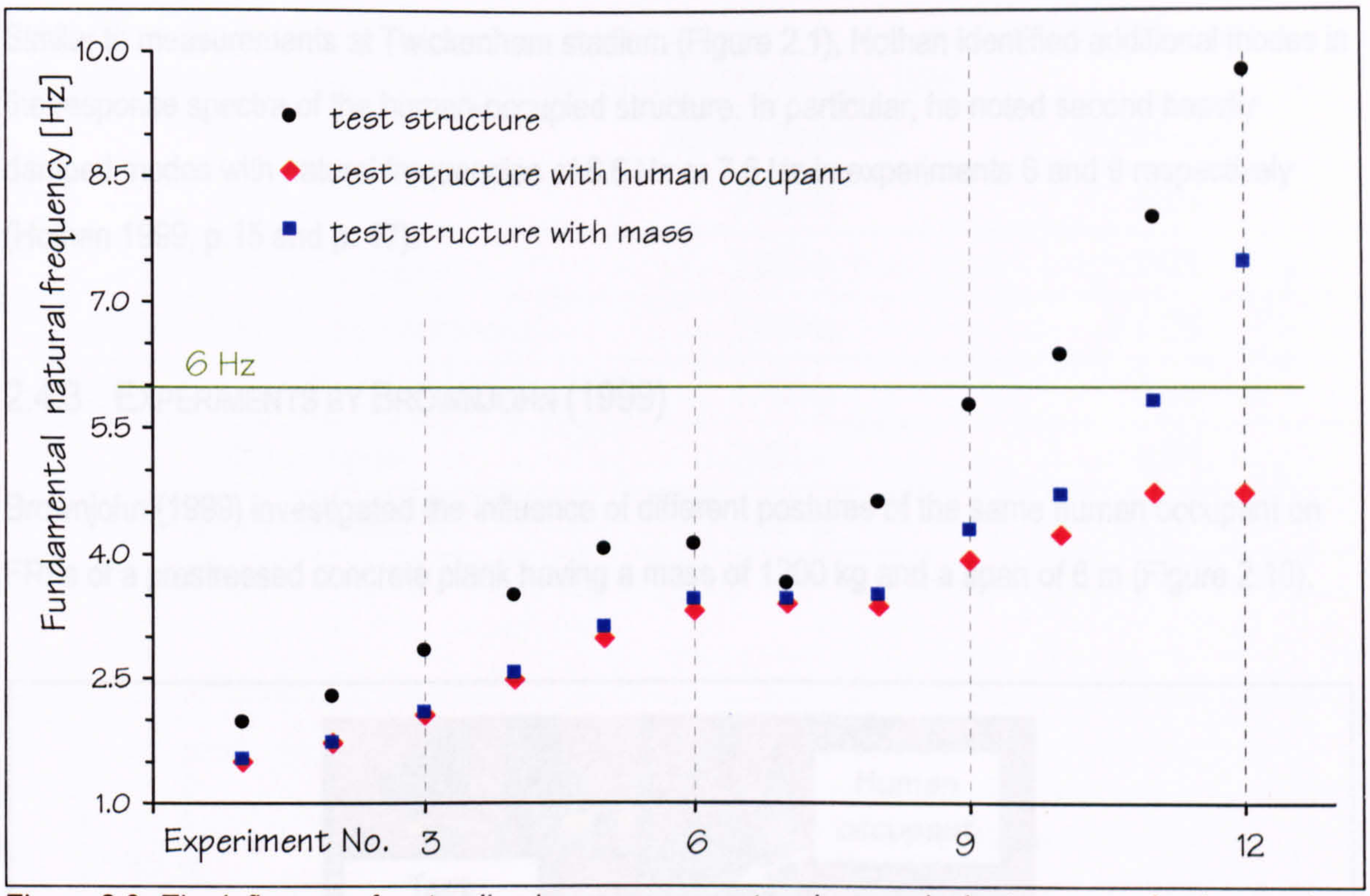

Figure 2.9: The influence of a standing human occupant and an equivalent mass on fundamental natural frequencies (after Hothan 1999).

Interestingly, the difference between natural frequencies f_1 of the structure loaded by a static mass or occupied by a person generally increases with increasing frequency of the empty structure (Table 2.7). This phenomenon is particularly pronounced for structures with fundamental frequencies above 6 Hz (Figure 2.9). It peaks with a difference of 2.7 Hz in experiment 12, where the empty structure had a natural frequency of 9.78 Hz (Table 2.7).

Hence, modelling the human occupant as a mass only would significantly overestimate the fundamental frequency f_1. This conclusion is in line with observations by Eibl and Rösch (1990) made on a full-scale stadium. The two authors analytically computed a frequency reduction of a beam-like structure from 3.9 Hz to 3.44 Hz due to the presence of 28 human occupants. However, the experimentally estimated fundamental frequency was 2.91 Hz, noticeably lower than the predicted 3.44 Hz.

Figure 2.9 shows that a human occupant can reduce the fundamental natural frequency of a three times heavier structure from above 9 Hz to below 6 Hz. In fact, the human occupant reduced natural frequencies from above 6 Hz to between 4 and 5 Hz (experiments 10, 11, and 12 in Table 2.7 and Figure 2.9). This phenomenon corresponds to measurements by Ellis and Ji (1997) on Twickenham stadium (Table 2.1) and another grandstand with a fundamental frequency of 16 Hz (section 2.1.2).

Similar to measurements at Twickenham stadium (Figure 2.1), Hothan identified additional modes in the response spectra of the human-occupied structure. In particular, he noted second heavily damped modes with natural frequencies of 6.6 Hz or 7.6 Hz in experiments 6 and 9 respectively (Hothan 1999, p.15 and p. 17).

2.4.3 EXPERIMENTS BY BROWNJOHN (1999)

Brownjohn (1999) investigated the influence of different postures of the same human occupant on FRFs of a prestressed concrete plank having a mass of 1200 kg and a span of 6 m (Figure 2.10).

Figure 2.10: Test structure and human occupant (after Brownjohn 1999).

The collected experimental data (Table 2.8 and Figure 2.11) confirm that the posture of a human occupant determines his influence on the occupied structure (Tables 2.2 and 2.6).

Remarkably, an occupant standing with bent or very bent knees (blue lines) increased damping so significantly (Figure 2.11) that the peak of the FRFs corresponding to the fundamental mode of the test structure practically disappeared.

Table 2.8: Influence of a single human occupant (80 kg) or an equivalent mass on the natural frequency and damping ratio of a beam-like structure (Brownjohn 1999).

Configuration	Natural frequency	Damping ratio
empty beam	3.16 Hz	0.8%
erect standing occupant	2.87 Hz	2.0%
occupant standing with bent knees	2.86 Hz	6.0%
occupant standing with very bent knees	3.10 Hz	9.2%
sitting occupant	2.82 Hz	2.8%
equivalent mass	2.95 Hz	1.1%

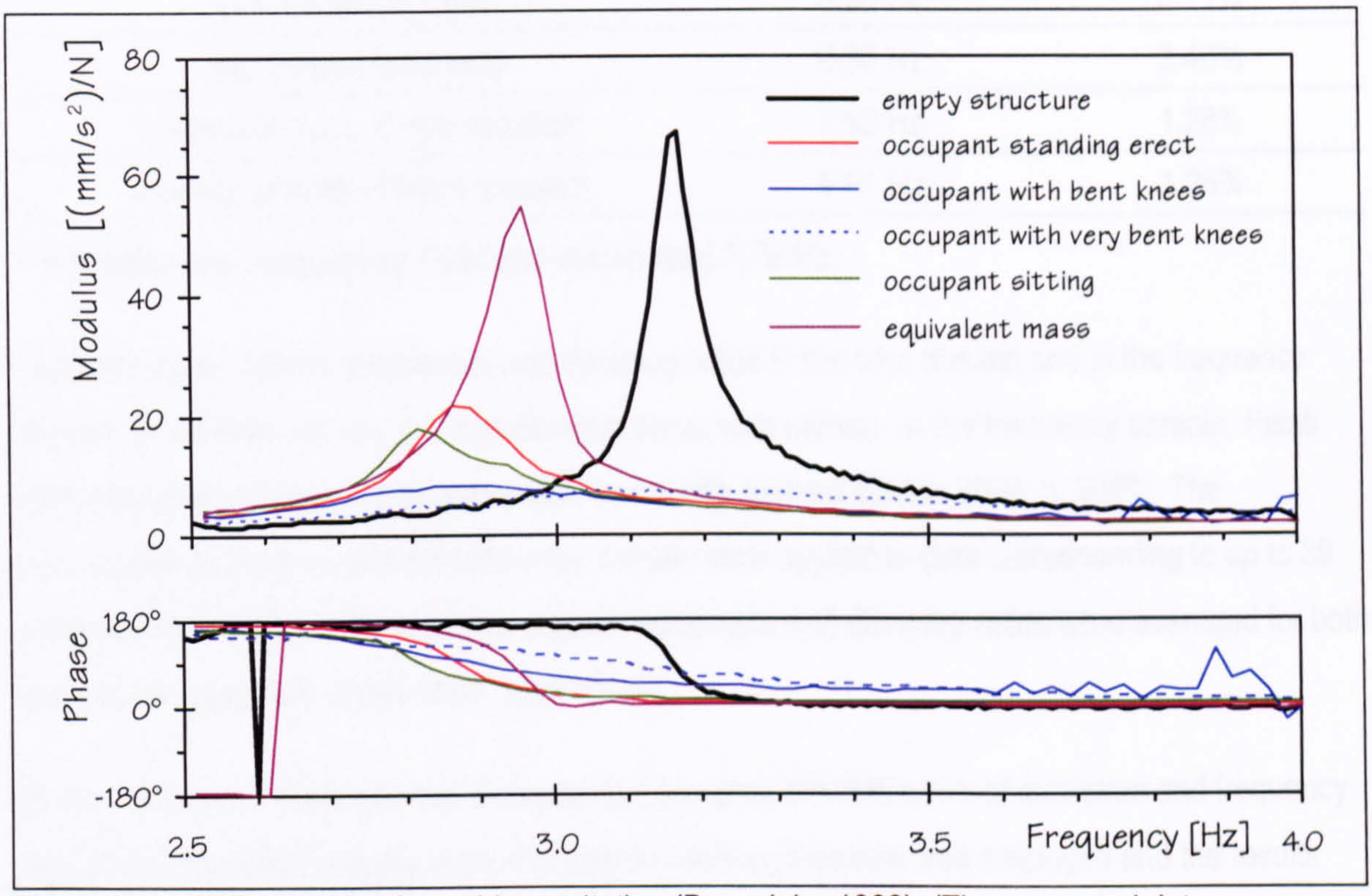

Figure 2.11: FRFs resulting from chirp excitation (Brownjohn 1999). (The presented data were provided by Brownjohn to the writer in August 2001).

2.4.4 Experiments by Falati (1999)

Falati (1999) performed investigations on a post-tensioned concrete structure having a mass of about 16,000 kg. He quantified the influence of up to two standing occupants and equivalent masses on the structure. Thereby, the structure had two different configurations: with and without

two screed layers. Discussing the influence of human occupants, Falati provided natural frequencies and damping ratios for eight configurations as listed in Table 2.9.

Table 2.9: Influence of human occupation or a mass on the natural frequency and damping ratio of a slab (Falati 1999, p. 170).

Configuration	Natural frequency	Damping ratio
empty structure (without two screed layers)	8.02 Hz	1.10%
one human occupant (75 kg)	7.76 Hz[1)]	3.84%
equivalent mass of one man (75 kg)	7.68 Hz	1.45%
empty structure with two screed layers	10.15 Hz	1.25%
one human occupant	9.96 Hz	3.11%
two human occupants	9.96 Hz	3.46%
equivalent mass of one occupant	9.93 Hz	1.28%
equivalent mass of two occupants	9.81 Hz	1.28%

[1)] This value was mistyped by Falati and should read 7.79 Hz.

Falati estimated natural frequencies and damping ratios in the time domain and in the frequency domain. In the time domain, the free vibration decay was utilised. In the frequency domain, Falati employed peak-picking and the half-power bandwidth method (Ewins 2000, p. 306ff). The identification in the time and the frequency domain were applied to data corresponding to up to 39 points on the structure. The resulting natural frequencies and damping ratios were averaged for both techniques separately (Falati 1999, appendix A).

In several cases, Falati analysed the same set-up using different levels of excitation and frequency resolutions. For each of these tests, the above outlined procedure was employed and the results were averaged for each estimation technique (time or frequency domain) separately. Finally, these averaged results corresponding to the same set-up and the time or the frequency domain analysis were averaged once more to provide the data summarised in Table 2.9.

The crude estimation technique and the wide scatter of estimates determined by Falati (1999, appendix A) do not justify an accuracy of two decimal points as giving in Table 2.9.

Nevertheless, Table 2.9 demonstrates again that one or two human occupants significantly increased the damping ratio of the test structure. Additionally, it shows that human occupation

reduced the fundamental natural frequency of the structure in both its configurations. Such a frequency reduction is consistent with observations by Hothan (1999) and Brownjohn (1999) on structures having relatively low natural frequencies. However, it is opposite to the frequency increases observed by Lenzing (1988) and Ji (1995) on structures with high fundamental frequencies (74 Hz and 18.68 Hz). This fact can be explained by the humans as additional dynamic system (Falati 1999, p. 170) and will be discussed in detail in course of this research.

Finally, it is noted that Falati (1999) reported larger frequency decreases for a static mass than for occupant(s) on the structure (Table 2.9). This is inconsistent with experiments by Hothan (1999) and Brownjohn (1999) (sections 2.4.2 and 2.4.3). However, this discrepancy might be explained by the smaller mass of occupants to the mass of the structure in experiments by Falati (1999).

2.5 HUMAN DYNAMIC MODELS OF STATIONARY HUMAN OCCUPANTS

In order to predict mathematically the influence of human occupants on civil engineering structures, a limited number of dynamic models of human occupants are available. These can be divided into damped and undamped models. The undamped models can further be separated into discrete and continuous models. Models corresponding to each of the three groups (undamped discrete, undamped continuous, and damped) are reviewed here.

2.5.1 UNDAMPED DISCRETE MODELS

Three undamped SDOF models of human occupants were found in the literature (Table 2.10). All three models of standing occupants are characterised by a mass m_H assumed to be equal to the total mass of the person m_T. However, the models have different stiffnesses k_H and, therefore, different natural frequencies f_H.

Table 2.10: Characteristics of undamped SDOF models of a standing human occupant (Lenzing 1988; Hothan 1999; Williams et al. 1999).

Human Model	Spatial properties	Modal Properties
Lenzing (1988)	$m_H = m_T$ (76 kg) k_H = 50 kN/m	f_H = 4.1 Hz
Hothan (1999)	$m_H = m_T$ (80 kg) k_H = 113.7 kN/m	f_H = 6 Hz
Williams et al. (1999)	$m_H = m_T$ (75 kg) k_H = 66 kN/m	f_H = 4.7 Hz

Lenzing (1988; p. 47f) defined the stiffness k_H by 50 kN/m probably based on research of Struck and Limberger (1981) into human impact (see section 2.3.1).

Hothan (1999, p. 19) (section 2.4.2) specified the SDOF human model by a natural frequency f_H of 6 Hz because this value was quoted by Schneider (1991, p. 25) as possibly corresponding to an upper body movement. By employing the resulting undamped SDOF model (Table 2.10), he

computed natural frequencies of a finite element (FE) human-structure model. The fundamental frequencies of this human-structure model match his experimental data closely (Figure 2.12).

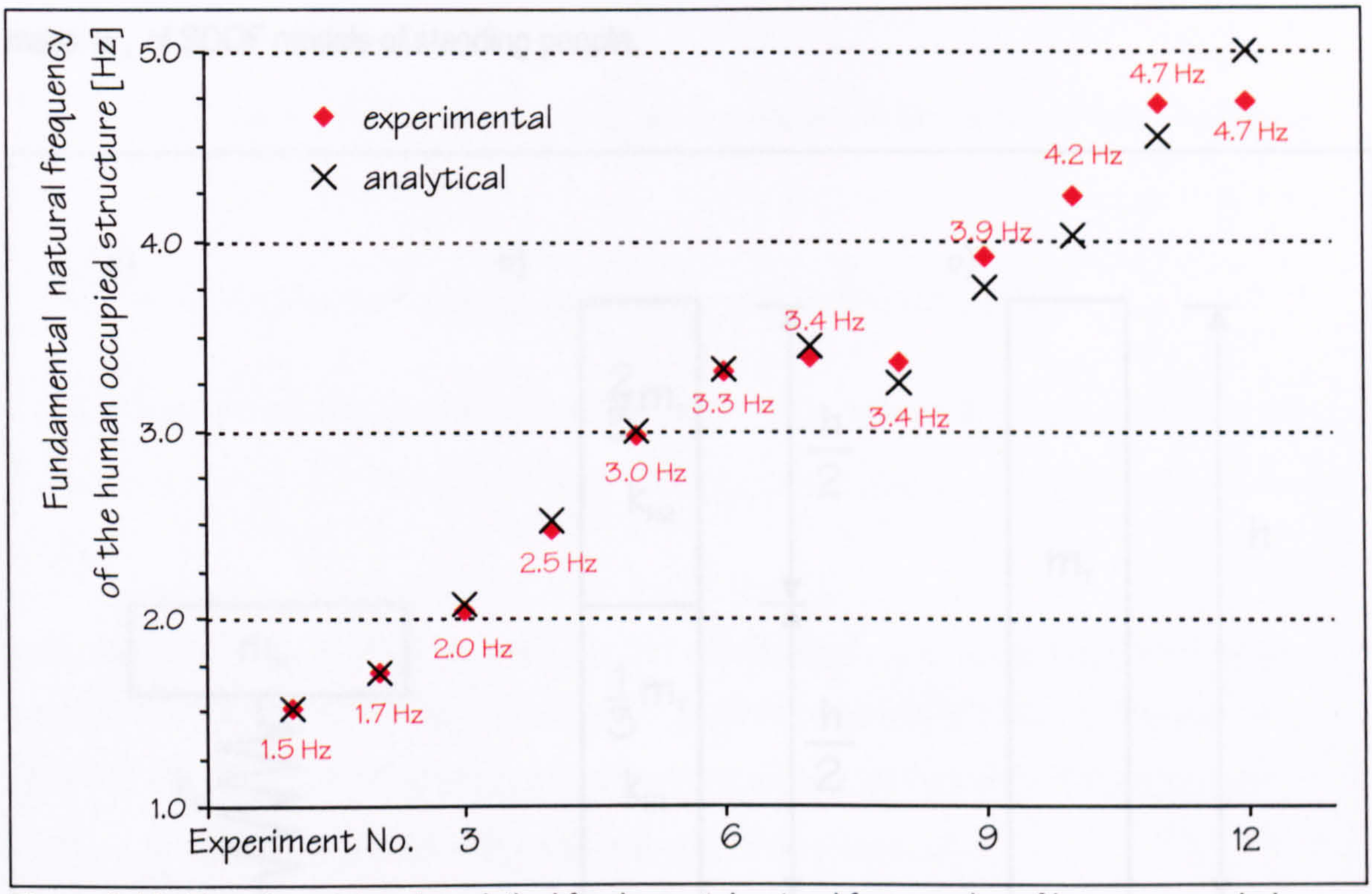

Figure 2.12: Experimental and analytical fundamental natural frequencies of human-occupied structures (after Hothan 1999).

The third undamped SDOF model of a standing occupant listed in Table 2.10 was presented by Williams et al. (1999). The numerical background of this model is not clear.

Moreover, Williams et al. (1999) extended this undamped SDOF model (Table 2.10) to an undamped 13-DOF model, which was probably based on a model proposed by Nigam and Malik (1987). The motivation for deriving a complex multi degree of freedom (MDOF) model of the human body to model human occupants of civil engineering structures is not clear to the writer. It is also not clear from the article how this was done or what the parameters of the MDOF model are.

2.5.2 Undamped Continuous Models

As previously mentioned, the undamped SDOF models (Figure 2.13a) presented by Lenzing (1988), Hothan (1999), and Williams et al. (1999) (Table 2.10) all have a lumped mass m_H assumed to be equal to the total mass m_T of the human occupant. Although this might be a valid simplification, the

mass of a SDOF model (Figures 2.2 a and 2.13a) of a continuous structure such as the human body is "different from the total mass of the structure" (Ji 2000, p. 185). Therefore, Ji (1995) and Falati (1999) developed and analysed continuous models of the standing human body to estimate the mass m_H of SDOF models of standing people.

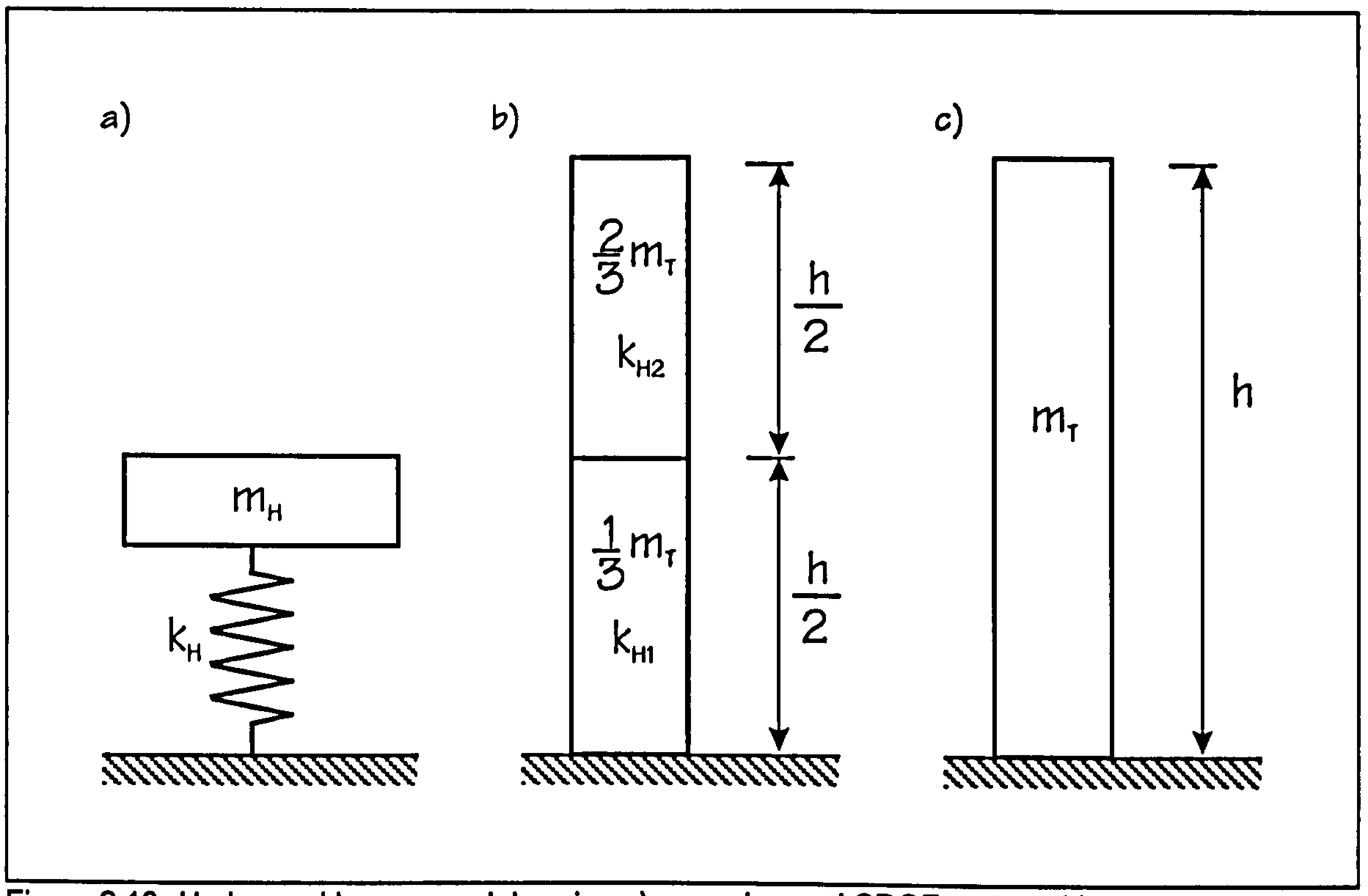

Figure 2.13: Undamped human models using a) an undamped SDOF system, b) a two-part continuous model (after Ji 1995), and c) a uniform continuous model (after Falati 1999).

Ji (1995) employed a continuous bar with two segments of different masses and stiffnesses (Figure 2.13b). He assumed that the stiffness k_H ranges from 0.5 k_{H1} to 2 k_{H1}. Based on this assumption, he concluded that the mass m_H (Figure 2.13a) of an undamped SDOF system representing one of the first four modes of a standing human ranges from 1/2 m_T to 2/3 m_T.

A significantly lower value $m_H = m_T/3$ was derived by Falati (1999, p. 177) by employing a uniform continuous model of a standing man (Figure 2.13c).

Both Ji (1995) and Falati (1999, p. 175f) then used the theoretically derived lumped mass m_H to estimate the stiffness k_H of an undamped SDOF human model (Figure 2.13a). Thereby, both researchers simplified both the human occupant and the occupied structure as undamped SDOF systems. Thus, the human-structure system is an undamped 2-DOF system, whereby the human

DOF is connected to the grounded structural DOF. This undamped human-structure model can be defined uniquely by:

(1) the natural frequency of the empty structure (f_s),

(2) one of the two natural frequencies of the undamped 2-DOF human-structure system ($f_1^{(UM)}$ or $f_2^{(UM)}$), and

(3) the lumped masses of the structure (m_s) and the human occupant (m_H).

Knowing these parameters, the natural frequency of the DOF representing the human occupant (f_H) can be estimated (Ji 1995; Randall and Peng 1995), by rearranging equation (3.83) given in section 3.1.2.3.

Applying this theory, Ji (1995) concluded that the natural frequency of a standing person ranges from 10 to 12 Hz. Falati (1999, p. 177) computed a similar frequency of 10.43 Hz. However, this value was miscalculated, as Falati employed the mistyped natural frequency of the occupied structure of 7.76 Hz and not the estimated value of 7.79 Hz (Table 2.9).

It is noted that the same procedure of assuming an undamped 2-DOF human-structure system was employed by Randall et al. (1997), who used a structure with a fundamental frequency of about 40 Hz. However, in contrast to Ji (1995) and Falati (1999), Randall et al. (1997) probably assumed the total mass of the human occupant $m_H = m_T$. They determined the natural frequencies f_H of 113 individual standing occupants to range from 9 to 16 Hz.

To summarise, Ji (1995), Randall et al. (1997), and Falati (1999) identified similar natural frequencies f_H of undamped SDOF models of standing people. Interestingly, the identified frequency range (9 to 16 Hz) corresponds to a range (8 to 15 Hz) usually associated with a second resonance of the (sitting or standing) human body (ISO 1981).

2.5.3 Damped Models

Biomechanical research established that the human body is heavily damped. This was recognised by civil engineers and led to the development and use of some damped SDOF models of human occupants (Figure 2.2a).

To the best of the writer's knowledge, Foschi and Gupta (1987) were the first to use a damped dynamic human model. This was done to predict the vibration response of wooden floors to heel-drops. It should be mentioned that heel-drop excitation is defined by "a man weighing about 170 lb (77 kg) rocking up on the balls of his feet, lifting his heels about 2.5 in. (6.4 cm) off the floor, then relaxing, allowing his heels to impact the floor" (Allen 1974).

Foschi and Gupta (1987), and also Foschi et al. (1995) and Al-Foqhaha'a (1997), modelled standing human occupants as damped SDOF systems (Figure 2.2a). They assumed the mass $m_H = m_T$.

In particular, Foschi and Gupta (1987) employed a person having a mass m_H of 91 kg (200 lb). They assumed the viscous damping c_H of a SDOF dynamic human model to be 1 kNs/m to equal the damping, probably of the fundamental mode, of the floor. However, neither the natural frequency f_H nor the stiffness k_H of this damped SDOF human model was provided.

Next, Folz and Foschi (1991) performed analytical research comparing response time histories of two human-occupied structures. They modelled a standing human occupant by either the 2-SDOF model of ISO 5982 (Table 2.4) or by an 11-DOF model. Folz and Foschi (1991) preferred the simpler 2-SDOF model to the 11-DOF model. The two authors concluded that even a simpler SDOF occupant model could be capable to sufficiently accurately predict floor responses to heel impact.

To determine the properties of a damped SDOF human model, Foschi et al. (1995) computed displacement responses of a human-structure model, using the SDOF human model, impacting the floor with a certain velocity. These responses were compared with experimental response time histories to heel-drop. Foschi et al. (1995) concluded that a SDOF human model with a stiffness k_H of 40 kN/m and viscous damping c_H between 1.25 and 1.50 kNs/m led to best approximations of the analytical and experimental response time histories. Employing the lower damping value they defined a damped SDOF human model of a man with a mass of 91 kg (Table 2.11).

The mass m_H and the stiffness k_H of the SDOF model proposed by Foschi et al. (1995) led to a natural frequency f_H of only 3.3 Hz (Table 2.11). This frequency is significantly lower than fundamental frequencies of all previously discussed biomechanic human models (Tables 2.3 and 2.4). However, the damping ratio of this model (33%) corresponds closely to the damping values reported in other models.

The human model proposed by Foschi et al. (1995) was adopted by Al-Foqhaha'a (1997). However, he employed two people with different total masses m_T than Foschi et al. (1995). Therefore, Al-Foqhaha'a (1997) obtained two damped SDOF human models (models 1 and 2) with slightly higher natural frequencies f_H and damping ratios ζ_H than the SDOF model of Foschi et al. (1995) (Table 2.11).

Table 2.11: Characteristics of damped SDOF models of a standing human occupant (after Foschi et al. 1995; Al-Foqaha'a 1997; Brownjohn 1999; Falati 1999).

Human Model	Spatial properties	Modal Properties
Foschi et al. (1995)	$m_H = m_T$ (91 kg) k_H = 40 kN/m c_H = 1.25 kNs/m	f_H = 3.3 Hz ζ_H = 33%
Al-Foqaha'a (1997) (model 1)	$m_H = m_T$ (83 kg) k_H = 40 kN/m c_H = 1.25 kNs/m	f_H = 3.5 Hz ζ_H = 34%
Al-Foqaha'a (1997) (model 2)	$m_H = m_T$ (75 kg) k_H = 40 kN/m c_H = 1.25 kNs/m	f_H = 3.7 Hz ζ_H = 36%
Brownjohn (1999)	$m_H = m_T$ (80 kg) k_H = 82 kN/m c_H = 1.946 kNs/m	f_H = 4.9 Hz ζ_H = 37%
Falati (1999)	$m_H = m_T/3$ (25 kg) k_H = 107 kN/m c_H = 1.636 kNs/m	f_H = 10.43 Hz ζ_H = 50%

Brownjohn (1999) employed a damped human model to predict the influence of a standing human occupant on his test structure. For this purpose, he defined a damped SDOF model (Table 2.11). Similar to other assumptions, this model is characterised by a mass m_H equal to the total mass m_T of the human occupant (Table 2.11). Brownjohn (1999) chose the stiffness k_H and the viscous damping c_H to lead to a natural frequency f_H and a damping ratio ζ_H corresponding to the fundamental mode of a 4-DOF human model given by ISO 7962 (ISO 1987). This ISO 7962 model

serves only for estimating the transmission of vibrations to the head of sitting or standing people. It is, in contrast to the 2-DOF models of ISO 5982 (see section 2.2.2), not aimed at modelling the influence of human occupants on the dynamic behaviour of occupied structures.

Brownjohn (1999) computed the natural frequencies and damping ratios of the human-structure system modelled as a damped 2-DOF system. He found the fundamental mode to have a frequency of 2.93 Hz and a damping ratio of 2.0%. These values correspond to the experimentally determined properties of the beam-like test structure occupied by an erect standing or a seated person (Table 2.8).

The last damped SDOF model (Figure 2.2a) of a standing person (Table 2.11) was developed by Falati (1999). He determined the mass m_H of this model as a third of the total mass m_T of an occupant from a continuous model of the standing human body. Using this value, Falati then estimated the natural frequency f_H (and consequently k_H) assuming an undamped 2-DOF human-structure system as shown in section 2.5.2.

In a next step, Falati (1999, p. 152) determined the damping ratio ζ_H of the damped SDOF human model. For this purpose, he computed responses of the structural DOF of damped 2-DOF human-structure models and compared them to experimental time histories. For this purpose, Falati probably used decaying vibrations caused by a heel-drop. He identified the damping ratio ζ_H to be within a range from 45% to 55% (Falati 1999, p. 180) and employed the median value of 50% to define a model of a standing person (Table 2.11).

2.6 Summary and Scope of Research

Human-structure interaction is an important aspect of human-induced vibrations. Nevertheless, its multiple effects are little researched and widely unknown. This research focuses on one aspect of human-structure interaction: the influence of human occupants on the dynamic properties of the structure they occupy. This issue has to be well understood to design structures, particularly assembly structures, successfully against human-induced vibrations.

To predict the influence of human occupants, a dynamic human occupant model is required. So far, several SDOF models of single people standing on civil engineering structures were proposed. However, all these SDOF occupant models were based on unwarranted assumptions in respect to damping and/or the lumped mass of the occupant model (Ji 1995; Falati 1999). Furthermore, experimental data used to derive the properties of such human models were usually incomplete and unreliable (Ji 1995; Foschi et al. 1995; Falati 1999).

The influence of human occupants was, in general, quantified using only crude estimation techniques, such as peak-picking of ASDs of response only measurements (Hothan 1999; Littler 2000). The more reliable technique of curve-fitting FRFs was used only by Brownjohn (1999). However, Brownjohn's investigations were limited to the influence of a single occupant on a rather light structure of only 1200 kg. Furthermore, only one location of the occupant and only one mode of the structure were analysed.

All of these issues will be addressed in the experimental part of this research. In fact, not only one but groups of up to five human occupants are employed. Additionally, occupant(s) will be placed at different locations on a test structure weighing about 15,000 kg. Their influence on several modes of the structure will be analysed simultaneously.

Furthermore, the influence of the level of vibration on the influence of human occupants will be investigated experimentally. The latter issue is addressed because biomechanical research identified the properties of the human body as dependent on the level of vibration.

To provide reliable and high-quality experimental data, FRFs will be estimated and modal properties will be identified by global MDOF curve-fitting. Moreover, nominally identical measurements will be repeated five times to provide increased statistical reliability of the identified modal properties.

Finally, the properties of a damped SDOF occupant model will be derived from experimental data. This human model shall represent not only single but also small groups of human occupants.

3. THEORETICAL BACKGROUND

This chapter outlines the theory employed in the experimental and analytical parts of this research. Aspects of analytical and experimental modal analysis are presented. Finally, it is outlined how analytical and experimental data are correlated in this research.

3.1 ANALYTICAL MODAL ANALYSIS

Analytical modal analysis is used to estimate response levels from response models that are derived from the spatial model of a structure, defined by mass, damping, and stiffness distributions (Ewins 2000, p. 26). In the following sections, response models of viscously damped, linear, and time-invariant systems are derived.

First, looking at the fundamentals of analytical modal analysis, responses of MDOF systems to arbitrary excitation are established in the time domain. Secondly, modal properties (natural frequencies, damping ratios, and mode shapes) of systems of particular interest in this research are derived from spatial properties. Thirdly, frequency domain response models of some dynamic systems are derived.

3.1.1 FUNDAMENTALS

The characteristics of a viscously damped SDOF system are firstly established. Then, the equation of motion of a MDOF system is used to estimate modal properties, which are used to derive response models in the time domain. These response models are established for proportionally damped systems and by employing state-space analysis for systems with general viscous damping.

The theory presented here is mainly based on Clough and Penzien (1993), Maia et al. (1997) and Ewins (2000). Also, presentations by Argyris and Mlejnek (1991), James et al. (1999), and Ginsberg (2001) were found useful.

3.1.1.1 DAMPED SDOF SYSTEM

A damped SDOF system (Figure 3.1) with a mass m, viscous damping c, and spring stiffness k is characterised by its circular natural frequency ω_r (3.1), its natural frequency f_r (3.2), and its damping ratio ζ_r (3.3).

$$\omega_r = \sqrt{\frac{k}{m}} \tag{3.1}$$

$$f_r = \frac{\omega_r}{2 \cdot \pi} = \frac{1}{2 \cdot \pi} \cdot \sqrt{\frac{k}{m}} \tag{3.2}$$

$$\zeta_r = \frac{c}{2 \cdot m \cdot \omega_r} \tag{3.3}$$

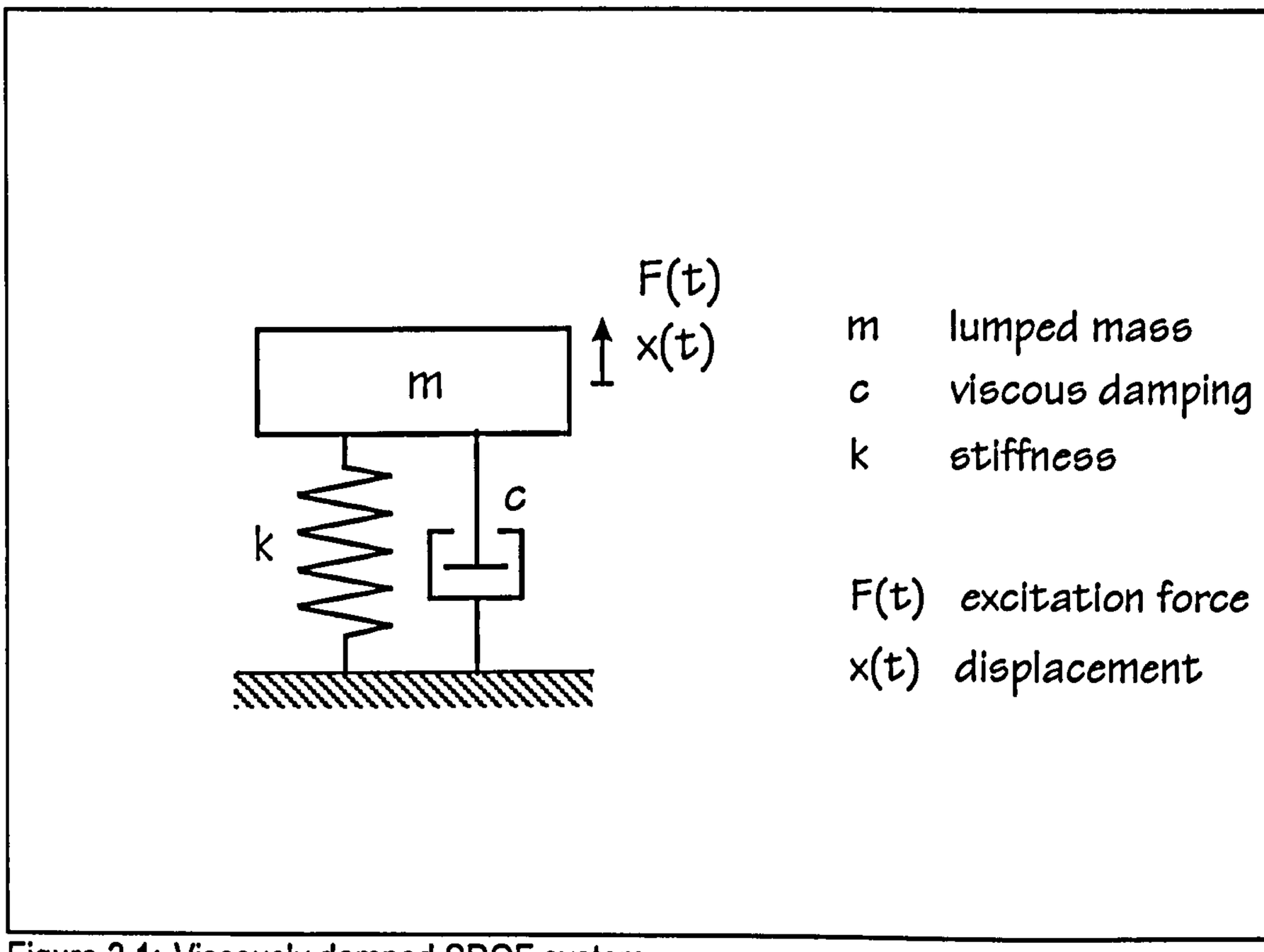

Figure 3.1: Viscously damped SDOF system.

In this research, only underdamped systems ($\zeta_r < 1$) are considered. Such damped SDOF systems can also be characterised by the natural frequency ω_{rd} of the damped system:

$$\omega_{rd} = \omega_r \cdot \sqrt{1 - \zeta_r^2} \,. \tag{3.4}$$

In this research, natural frequencies f_r of the undamped system (3.2) are used to specify damped and undamped SDOF systems.

The equation of motion of a viscously damped SDOF system (Figure 3.1) to an arbitrary excitation $F(t)$ is provided in equation (3.5).

$$m \cdot \ddot{x}(t) + c \cdot \dot{x}(t) + k \cdot x(t) = F(t) \tag{3.5}$$

The displacement response $x(t)$ of such a SDOF system can be calculated analytically from its transient response $x(t)_{trans}$ and its forced response $x(t)_{forced}$:

$$x(t) = x(t)_{trans} + x(t)_{forced}. \tag{3.6}$$

In particular, the transient response $x(t)_{trans}$ is defined by the homogeneous solution (3.7) (Clough and Penzien 1993, p. 27) of the second order differential equation of motion (3.5) and the forced response $x(t)_{forced}$ is specified by the particular solution (3.8) (Clough and Penzien 1993, p. 89).

$$x(t)_{trans} = \left(x(0) \cdot \cos(\omega_{rd} \cdot t) + \left(\frac{\dot{x}(0) + x(0) \cdot \zeta_r \cdot \omega_r}{\omega_{rd}} \right) \cdot \sin(\omega_{rd} \cdot t) \right) \cdot e^{-\zeta_r \cdot \omega_r \cdot t} \tag{3.7}$$

$$x(t)_{forced} = \frac{1}{m \cdot \omega_{rd}} \cdot \int_0^t \sin(\omega_{rd} \cdot (t - \tau)) \cdot e^{-\zeta_r \cdot \omega_r \cdot (t-\tau)} \cdot F(\tau)\, d\tau \tag{3.8}$$

The calculation of responses of a SDOF system (Figure 3.1) to an arbitrary excitation will be extended to calculate responses of MDOF systems.

3.1.1.2 Equation of Motion of MDOF Systems

Equation (3.5) established the equation of motion of a SDOF system. This equation is now expanded to the equation of motion of a viscously damped N-DOF system with spatial properties defined by the mass matrix $[M]$, the viscous damping matrix $[C]$, and the stiffness matrix $[K]$ (3.9).

$$[M] \cdot \{\ddot{x}(t)\} + [C] \cdot \{\dot{x}(t)\} + [K] \cdot \{x(t)\} = \{F(t)\} \tag{3.9}$$

The response $x(t)$ of each DOF to an arbitrary force $\{F(t)\}$ can be calculated either directly from (3.9) in the time domain or indirectly using the frequency domain as will be shown below.

The mode shapes $\{\psi\}_r$ of an undamped MDOF system can be calculated from the equation of motion (3.10) that defines its free vibrations:

$$[M]\cdot\{\ddot{x}(t)\}+[K]\cdot\{x(t)\}=\{0\}. \tag{3.10}$$

Assuming vibrations of a general form (3.11), a second order eigenproblem defined in equation (3.12) emerges from equation (3.10).

$$\{x(t)\}=\{\psi\}\cdot e^{\lambda\cdot t} \tag{3.11}$$

$$\left(\lambda^2\cdot[M]+[K]\right)\cdot\{\psi\}=\{0\} \tag{3.12}$$

Solving this eigenproblem using equation (3.13) leads to N pairs of complex conjugate eigenvalues λ_r.

$$det\left(\lambda^2\cdot[M]+[K]\right)=0 \tag{3.13}$$

Substituting these eigenvalues into equation (3.12) leads to the corresponding mode shapes $\{\psi\}_r$.

The mode shapes (eigenvectors) of undamped MDOF systems are real-valued. Thus, eigenvector elements are either in phase (same sign) or 180° out of phase (different sign).

The mode shapes $\{\psi\}_r$ of undamped MDOF systems satisfy equations (3.14) to (3.17) (Maia et al. 1997, p. 53f). These orthogonality conditions are very useful for the calculation of MDOF systems because they can be used to decouple equations as outlined in sections 3.1.1.3 and 3.1.1.4.

$$\{\psi\}_j^T\cdot[M]\cdot\{\psi\}_k=0\quad(j\neq k) \tag{3.14}$$

$$\{\psi\}_j^T\cdot[K]\cdot\{\psi\}_k=0\quad(j\neq k) \tag{3.15}$$

$$\{\psi\}_r^T\cdot[M]\cdot\{\psi\}_r=m_r\quad(j=k=r) \tag{3.16}$$

$$\{\psi\}_r^T\cdot[K]\cdot\{\psi\}_r=k_r\quad(j=k=r) \tag{3.17}$$

In real life, structures are damped. If a MDOF system is viscously damped, the free vibrations of the system can be described by equation (3.18).

$$[M]\cdot\{\ddot{x}(t)\}+[C]\cdot\{\dot{x}(t)\}+[K]\cdot\{x(t)\}=\{0\} \tag{3.18}$$

Analogous to eigenvalues and mode shapes of undamped systems, the eigenvalues λ_r and the mode shapes $\{\psi\}_r$ of damped MDOF systems can be calculated by solving the eigenproblem (3.19) and the characteristic equation (3.20).

$$\left(\lambda^2 \cdot [M] + \lambda \cdot [C] + [K]\right) \cdot \{\psi\} = \{O\} \tag{3.19}$$

$$det\left(\lambda^2 \cdot [M] + \lambda \cdot [C] + [K]\right) = O \tag{3.20}$$

However, the mode shapes $\{\psi\}_r$ of generally viscously damped MDOF systems are complex. In other words, not all phases are 0° or 180°. This means that the DOFs of such a system in free vibration do not reach their maximum values at the same instant of time. Such complex mode shapes do not satisfy equations (3.14) to (3.17).

However, mode shapes of viscously damped MDOF systems are real if the viscous damping matrix $[C]$ is a linear combination of the mass matrix $[M]$ and the stiffness matrix $[K]$ (3.21) (Ewins 2000, p. 115). In this case, the MDOF system is called proportionally damped (Maia et al. 1997, p. 57; Ginsberg 2001, p. 270f).

$$[C] = \nu \cdot [M] + \varepsilon \cdot [K] \tag{3.21}$$

The real-valued mode shapes of a proportionally damped system satisfy equation (3.14) to (3.17). Additionally, they satisfy:

$$\{\psi\}_j^T \cdot [C] \cdot \{\psi\}_k = \{\psi\}_j^T \cdot (\nu \cdot [M] + \varepsilon \cdot [K]) \cdot \{\psi\}_k = O \tag{3.22}$$

and

$$\{\psi\}_r^T \cdot [C] \cdot \{\psi\}_r = c_r . \tag{3.23}$$

These properties enable decoupling of the equation of motion (3.9). Therefore, responses associated with each mode of vibration can be calculated by solving a single and not a system of differential equations. The total response is then obtained by summing the individually calculated modal contributions as shown in section 3.1.1.3.

Generally non-proportionally damped systems do not decouple the equation of motion, which makes the computation of responses more expensive (Argyris and Mlejnek 1991). Therefore, responses of

generally damped MDOF systems are usually computed using another procedure, state-space analysis. The state-space description of MDOF systems is also often used in the identification of MDOF systems from experimental data (Ewins 2000, p. 287).

State-space analysis can handle general non-proportionally damped systems efficiently. This is achieved by simplifying the second order eigenproblem (3.12) to a first order eigenproblem that can more easily be solved numerically. This procedure is outlined in section 3.1.1.4.

3.1.1.3 Responses of Proportionally Damped Systems

To compute responses of proportionally damped systems, the equation of motion (3.9) is decoupled. For this purpose, it is transferred from the physical into modal space by substituting displacements $\{x(t)\}$ by the modal matrix $[\Theta]$:

$$[\Theta] = [\{\psi\}_1 \ldots \{\psi\}_N] \tag{3.24}$$

that summarises the mode shapes $\{\psi\}_r$ of the undamped MDOF system and the modal responses $\{p(t)\}$:

$$\{x(t)\} = [\Theta] \cdot \{p(t)\}. \tag{3.25}$$

to:

$$[M] \cdot [\Theta] \cdot \{\ddot{p}(t)\} + [C] \cdot [\Theta] \cdot \{\dot{p}(t)\} + [K] \cdot [\Theta] \cdot \{p(t)\} = \{F(t)\}. \tag{3.26}$$

Pre-multiplying the resulting equation (3.26) with the transpose of the modal matrix $[\Theta]^T$ leads to the equation of motion as presented in equation (3.27) (Argyris and Mlejnek 1991, p. 317).

$$[\Theta]^T \cdot [M] \cdot [\Theta] \cdot \{\ddot{p}(t)\} + [\Theta]^T \cdot [C] \cdot [\Theta] \cdot \{\dot{p}(t)\} + [\Theta]^T \cdot [K] \cdot [\Theta] \cdot \{p(t)\} = [\Theta]^T \cdot \{F(t)\} \tag{3.27}$$

The term on the right hand side of equation (3.27) specifies the modal force $\{g(t)\}$:

$$\{g(t)\} = [\Theta]^T \cdot \{F(t)\}. \tag{3.28}$$

Hence, forces $\{F(t)\}$ weighted by the mode shape $\{\psi\}_r$ contribute to the modal force $g_r(t)$, defined not as a vector but as a single function of time (3.29).

$$g_r(t) = \{\psi\}_r^T \cdot \{F(t)\} \tag{3.29}$$

The equation of motion (3.27) is decoupled because, in the case of proportionally damped systems, off-diagonal elements are zero (see equations (3.14), (3.15) and (3.22)). The terms on the diagonals are the modal mass m_r, modal damping c_r, and modal stiffness k_r specified in equations (3.16), (3.17), and (3.23). Using these terms, the decoupled equation (3.27) can be rewritten as N ($r = 1, 2, 3, \ldots N$) independent second order differential equations:

$$m_r \cdot \ddot{p}_r(t) + c_r \cdot \dot{p}_r(t) + k_r \cdot p_r(t) = g_r(t). \tag{3.30}$$

Modal responses $p_r(t)$ (of each of the N independent equations describing the proportionally damped MDOF system) to the modal forces $g_r(t)$ can be computed with equations (3.6), (3.7), and (3.8). These modal responses $p_r(t)$ can then be used to calculate the overall physical responses $\{x(t)\}$ of an arbitrarily excited MDOF system by adding participations from individual modes r. This becomes obvious if equation (3.25) is rewritten as (3.31), which clearly defines the physical response $x_j(t)$ at DOF j as sum of the modal responses $p_r(t)$ weighted by the mode shapes $\{\psi\}_r$.

$$x_j(t) = \sum_{r=1}^{N} \psi_{jr} \cdot p_r(t) \tag{3.31}$$

Finally, it is pointed out that the physical response $x_j(t)$ is independent of mode shape scaling. This is shown by replacing the mode shape $\{\psi\}_r$ by $\{\hat{\psi}\}_r = a \cdot \{\psi\}_r$. In this case, a different modal mass $\hat{m}_r = a^2 \cdot m_r$, different modal damping $\hat{c}_r = a^2 \cdot c_r$, and different modal stiffness $\hat{k}_r = a^2 \cdot k_r$ are obtained (equations (3.56), (3.57), and (3.58)). Furthermore, modal forces change to $\hat{g}_r(t) = a \cdot g_r(t)$ (see equation (3.29)). Using these parameters in equation (3.30), the modal response $\hat{p}_r(t) = a^{-1} \cdot p_r(t)$. At last, the modal response $\hat{p}_r(t)$ and the corresponding mode shape $\{\hat{\psi}\}_r$ are substituted into equation (3.31), which leads to the same physical responses $x_j(t)$ as if $p_r(t)$ and $\{\psi\}_r$ were employed.

Often, mode shapes are mass-normalised (Maia et al. 1997, p. 55; Ewins 2000, p. 53). However, in this research, amplitude normalisation is preferred. Therefore, the mode shape element of each mode shape with the largest translation is set to unity and its phase to zero.

3.1.1.4 State-Space Analysis of Non-Proportionally Damped Systems

As outlined above, decoupling the equation of motion (3.9) and estimating the responses $\{x(t)\}$ of a proportionally damped system is straightforward. Therefore, damping is often modelled as, or approximated with, proportional damping (Clough and Penzien 1993, p. 234ff, Ginsberg 2001, p. 271f), although this simplification can lead to significant deviations in calculated time domain responses (Argyris and Mlejnek 1991, p. 325).

Responses of non-proportionally damped MDOF systems to arbitrary excitation can be computed using an expensive procedure similar to that outlined for proportionally damped systems (Argyris and Mlejnek 1991). However, here, the more commonly used state-space method is introduced.

The state-space method decouples the equation of motion for generally (non-proportionally and proportionally) damped systems. For this purpose, orthogonality conditions of the mode shapes are employed. However, generally damped MDOF systems usually do not have real mode shapes. Therefore, they do not satisfy the orthogonality conditions (3.14), (3.15), and (3.22). However, they satisfy the orthogonality conditions (3.32) and (3.33) (Maia et al. 1997, p. 60; Ewins 2000, p. 75f).

$$\lambda_j \cdot \lambda_k \cdot \{\psi\}_j^T \cdot [M] \cdot \{\psi\}_k - \{\psi\}_j^T \cdot [K] \cdot \{\psi\}_k = 0 \quad (j \neq k) \tag{3.32}$$

$$(\lambda_j + \lambda_k) \cdot \{\psi\}_j^T \cdot [M] \cdot \{\psi\}_k + \{\psi\}_j^T \cdot [C] \cdot \{\psi\}_k = 0 \quad (j \neq k) \tag{3.33}$$

To decouple the equation of motion using these two orthogonality conditions, the equation of motion (3.9) is, for instance, expanded to equation (3.34) (Maia et al. 1997, p. 58; Ewins 2000, p. 77f).

$$\begin{bmatrix} [C] & [M] \\ [M] & [0] \end{bmatrix} \cdot \begin{Bmatrix} \{\dot{x}(t)\} \\ \{\ddot{x}(t)\} \end{Bmatrix} + \begin{bmatrix} [K] & [0] \\ [0] & [-M] \end{bmatrix} \cdot \begin{Bmatrix} \{x(t)\} \\ \{\dot{x}(t)\} \end{Bmatrix} = \begin{Bmatrix} \{F(t)\} \\ \{0\} \end{Bmatrix} \tag{3.34}$$

This equation (3.34) can be written as an equation of motion in the state-space (3.35) by defining the state-space variable $\{u(t)\}$ (3.36) and the state-space force $\{Q(t)\}$ (3.37).

$$[A] \cdot \{\dot{u}(t)\} + [B] \cdot \{u(t)\} = \{Q(t)\} \tag{3.35}$$

$$\{u(t)\} = \begin{Bmatrix} \{x(t)\} \\ \{\dot{x}(t)\} \end{Bmatrix} \tag{3.36}$$

$$\{Q(t)\} = \begin{Bmatrix} \{F(t)\} \\ \{0\} \end{Bmatrix} \tag{3.37}$$

Decoupling the state-space equation of motion (3.35) requires the modal properties of the MDOF system to be known. These modal properties can be obtained by solving the eigenproblem stated in equation (3.38) which is analogous to that provided in equation (3.12).

$$(\lambda' \cdot [A] + [B]) \cdot \{\psi'\} = \{0\} \tag{3.38}$$

The resulting $2 \cdot N$ eigenvalues λ_r' and the mode shapes $\{\psi'\}_r$ correspond to the eigensolutions of the system if analysed using equation (3.12). However, the state-space vector $\{u(t)\}$ has twice as many elements as the vector $\{x(t)\}$ (3.36). Hence, the state-space mode shapes $\{\psi'\}_r$ have twice as many elements as the mode shapes $\{\psi\}_r$ calculated from the eigenproblem (3.12). However, summarising the state-space mode shapes into the modal matrix $[\Theta']$, a relation to the mode shapes $\{\psi\}_r$ of equation (3.24) can be established as:

$$[\Theta']_{2N \times 2N} = \begin{bmatrix} \{\psi\}_1 & \cdots & \{\psi\}_N & \{\psi\}_1^* & \cdots & \{\psi\}_N^* \\ \lambda_1 \cdot \{\psi\}_1 & \cdots & \lambda_N \cdot \{\psi\}_N & \lambda_1^* \cdot \{\psi\}_1^* & \cdots & \lambda_N^* \cdot \{\psi\}_N^* \end{bmatrix}. \tag{3.39}$$

Similarly to the modal force $\{g(t)\}$ and the modal response $\{p(t)\}$ in the physical space (equations (3.28) and (3.25)), the modal force $\{g'(t)\}$ (3.40), and the modal response $\{p'(t)\}$ (3.41) are defined in the state-space.

$$\{g'(t)\} = [\Theta']^T \cdot \{Q(t)\} \tag{3.40}$$

$$\{u(t)\} = [\Theta'] \cdot \{p'(t)\} \tag{3.41}$$

Following the same procedure as for proportionally damped systems, that is substituting $\{u(t)\}$ with its state-space presentation $\{p'(t)\}$ and pre-multiplying with the transposed modal matrix $[\Theta']^T$, equation (3.35) transforms into the modal state-space equation (3.42).

$$[\Theta']^T \cdot [A] \cdot [\Theta'] \cdot \{\dot{p}'(t)\} + [\Theta']^T \cdot [B] \cdot [\Theta'] \cdot \{p'(t)\} = \{g'(t)\} \tag{3.42}$$

The equation of motion in the state-space (3.42) is decoupled because of the orthogonality conditions (3.32) and (3.33). In order to express this set of equations, equations (3.43) and (3.44) express the orthogonality conditions (equations (3.32) and (3.33)) for the case of $j = k = r$.

$$\lambda_r^2 \cdot \{\psi\}_r^T \cdot [M] \cdot \{\psi\}_r - \{\psi\}_r^T \cdot [K] \cdot \{\psi\}_r = b_r \tag{3.43}$$

$$2 \cdot \lambda_r \cdot \{\psi\}_r^T \cdot [M] \cdot \{\psi\}_r + \{\psi\}_r^T \cdot [C] \cdot \{\psi\}_r = a_r \tag{3.44}$$

Employing equations (3.43) and (3.44) that define the complex terms a_r and b_r, equation (3.42) can be expressed as a set of $2 \cdot N$ ($r = 1, 2, 3, \ldots 2 \cdot N$) first order ordinary differential equations:

$$a_r \cdot \dot{p}'_r(t) + b_r \cdot p'_r(t) = g'_r(t). \tag{3.45}$$

The equation of motion (3.45) can also be defined by equation (3.46) excluding the term b_r.

$$a_r \cdot \dot{p}'_r(t) - \lambda'_r \cdot a_r \cdot p'_r(t) = g'_r(t) \tag{3.46}$$

This is possible because the eigenproblem (3.38) can be expressed by $2 \cdot N$ equations (3.47), which lead to the eigenvalues λ'_r as defined by equation (3.48) (Maia et al. 1997, p. 68).

$$(\lambda' \cdot a_r + b_r) \cdot \{\psi'\} \cdot e^{\lambda' \cdot t} = \{0\} \tag{3.47}$$

$$\lambda'_r = -\frac{b_r}{a_r} \tag{3.48}$$

Knowing the decoupled equations of motion of a generally viscously damped MDOF system to an arbitrary excitation in the state-space (3.46), it is possible to calculate the physical responses $\{x(t)\}$ from the state-space responses $\{u(t)\}$ (3.36).

The state-space response $u_j(t)$ of any DOF j can be calculated from the modal matrix $[\Theta']$ and the modal state-space response $\{p'(t)\}$ (3.41) by superposing the responses of $2 \cdot N$ modes:

$$u_j(t) = \sum_{k=1}^{2 \cdot N} \psi'_{jk} \cdot p'_k(t). \tag{3.49}$$

It remains to estimate the state-space modal responses $p'_k(t)$. If the modal force $Q_k(t)$ and the initial conditions $p'_k(O)$ are known, the state-space modal responses $p'_k(t)$ can be calculated:

$$p'_k(t) = p'_k(O) \cdot e^{-\lambda'_k \cdot t} + \frac{1}{a_k} \int_O^t e^{-\lambda'_k \cdot (t-\tau)} \cdot Q_k(\tau)\, d\tau . \tag{3.50}$$

Equation (3.50) was derived from James et al. (1999, p. 511) by considering equation (3.48). It shows that the response $p'_k(t)$ is determined by a transient and a forced part, similarly to the response of damped SDOF systems (see equations (3.6), (3.7), and (3.8) in section 3.1.1.1).

3.1.1.5 Modal Properties

In the previous section, it was outlined how responses of damped MDOF systems can be calculated. For this purpose, eigenvalues λ_r were employed. Also, in the case of proportionally damped systems, modal masses m_r, modal damping c_r, and modal stiffnesses k_r were used. Properties of these characteristic values and their relationships are now analysed.

The eigenvalues λ_r of undamped MDOF systems correspond to the modal stiffness k_r and the modal mass m_r:

$$\lambda_r = \pm i \cdot \sqrt{\frac{k_r}{m_r}} . \tag{3.51}$$

Thus, the eigenvalues λ_r specify the circular natural frequency (3.52) and the natural frequency (3.53), which is analogous to that of a SDOF system (section 3.1.1.1), of mode r.

$$\omega_r = |\lambda_r| \tag{3.52}$$

$$f_r = \frac{1}{2 \cdot \pi} \cdot |\lambda_r| \tag{3.53}$$

If a damped MDOF system is underdamped ($\zeta_r < 1$), its eigenvalues λ_r are in the form of:

$$\lambda_r = -\omega_r \cdot \zeta_r \pm i \cdot \omega_r \cdot \sqrt{1-\zeta_r^2} . \tag{3.54}$$

Damping ratios ζ_r of each mode of vibration r of such an underdamped MDOF system can be calculated from the eigenvalues λ_r using:

$$\zeta_r = \frac{-Re(\lambda_r)}{|\lambda_r|}. \tag{3.55}$$

The circular natural frequencies ω_r and the natural frequencies f_r of mode r can be calculated using equations (3.52) and (3.53). Thereby, it is important to note that the natural frequencies f_r are different for differently damped or undamped MDOF systems.

Eigenvalues λ_r are not always complex numbers. They can also be real. This is the case if the system is overdamped and no oscillations take place. Moreover, the characteristic polynomial (3.20) can also lead to repeated eigenvalues λ_r, which can result from symmetry of the structure (Ewins 2000, p. 57). However, such solutions are not of concern in this research.

Modal masses m_r (3.16), modal stiffnesses k_r (3.17) and modal dampings c_r (3.23), of modes r of proportionally damped (or undamped) systems are real-valued. They specify the circular natural frequencies ω_r and damping ratios ζ_r of SDOF systems (equations (3.1) and (3.3)) as also specified by the eigenvalue λ_r (equations (3.52) and (3.55)).

Modal masses m_r, modal stiffnesses k_r and modal dampings c_r of non-proportionally damped systems computed by equations (3.16), (3.17), and (3.23) are complex numbers, which are not particularly meaningful. Nevertheless, if equations (3.56) to (3.58) are used (Maia et al. 1997, p. 61; Argyris and Mlejnek 1991, p. 317), modal masses m_r, modal dampings c_r and modal stiffnesses k_r are real-valued.

$$\{\psi\}_r^T \cdot [M] \cdot \{\psi\}_r^* = m_r \tag{3.56}$$

$$\{\psi\}_r^T \cdot [C] \cdot \{\psi\}_r^* = c_r \tag{3.57}$$

$$\{\psi\}_r^T \cdot [K] \cdot \{\psi\}_r^* = k_r \tag{3.58}$$

Moreover, these real-valued modal properties define the circular natural frequency ω_r (3.1) and the damping ratio ζ_r (3.3) of mode r of generally damped MDOF systems as specified by the eigenvalue λ_r (Maia et al. 1997, p. 61).

However, the modal properties defined in equations (3.56) to (3.58) do generally not decouple the equation of motion. They only decouple the equation of motion (as in (3.30) if the system is undamped or proportionally damped. In this case, mode shapes are real-valued and, therefore, equations (3.56) to (3.58) lead to the same modal mass m_r, modal damping c_r and modal stiffness k_r as equations (3.16), (3.23) and (3.17).

Finally, it should be noted that real-valued modal masses m_r as defined in equation (3.56) are used in this research to represent modal masses of non-proportionally damped systems.

3.1.2 Modal Properties of SDOF and 2-DOF Systems

In the previous section, modal properties and response models of arbitrarily excited viscously damped MDOF systems were derived. Now, focus is put on the modal properties of SDOF and 2-DOF systems that are of particular interest in this research (Figure 3.2).

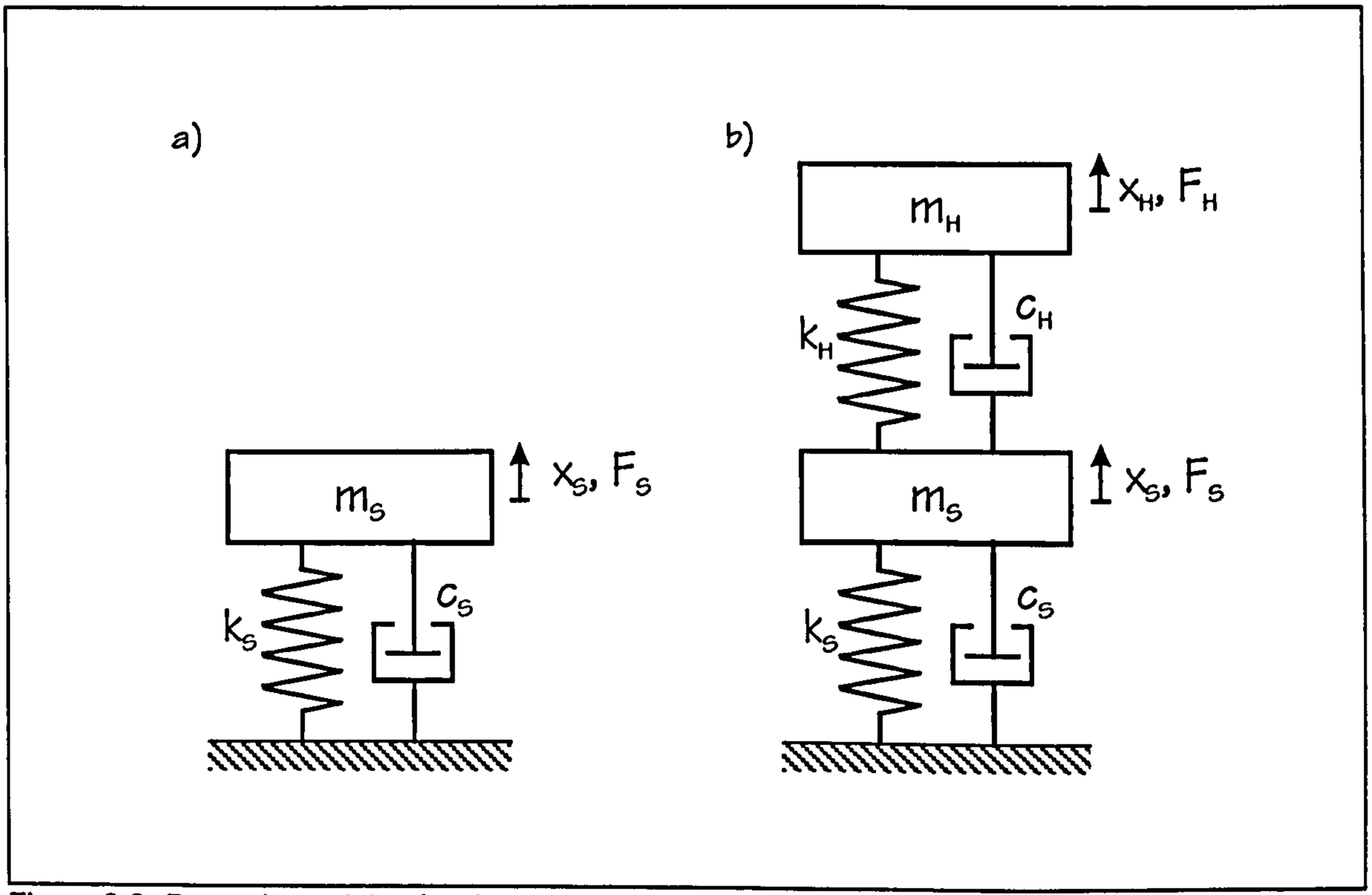

Figure 3.2: Dynamic models of a viscously damped a) structural SDOF system (m_S, c_S, k_S) and b) 2-DOF structure (m_S, c_S, k_S) and human (m_H, c_H, k_H) system.

The damped SDOF system (Figure 3.2a) is used as a simple model of a structure having lumped properties (m_S, c_S, and k_S). Similarly, human occupants are modelled as a damped SDOF system

with the properties m_H, c_H, and k_H. Combining the SDOF structure and the SDOF occupant models, the human-occupied structure is modelled as damped 2-DOF system (Figure 3.2b). This model will be used in chapters 4 and 6.

Analytical expressions for the modal properties of both systems (Figures 3.2a and 3.2b) are developed. Furthermore, the damped 2-DOF system (Figure 3.2b) is simplified to an undamped 2-DOF system, whose modal properties are derived. The undamped 2-DOF system is included here because some authors (Ellis and Ji 1997) proposed such an model of a human-occupied structure. The damped and the undamped 2-DOF human-structure system are included into an analytical parametric study of human-structure models presented in chapter 4.

3.1.2.1 Damped SDOF System

A SDOF system (Figure 3.2a) has only one mode of vibration with natural frequency and modal damping as already defined in equations (3.2) and (3.3). Similarly, the natural frequency f_s and the modal damping ratio ζ_s of the SDOF model presented in Figure 3.2a can be defined as

$$f_s = \frac{1}{2 \cdot \pi} \cdot \sqrt{\frac{k_s}{m_s}} \tag{3.59}$$

and

$$\zeta_s = \frac{c_s}{2 \cdot m_s} \cdot \sqrt{\frac{m_s}{k_s}} . \tag{3.60}$$

The mode shape of this SDOF system has only one element. Therefore, the amplitude normalised mode shape $\{\psi\}_1$ is given by equation (3.61).

$$\{\psi\}_1 = \psi_{s1} = 1 \tag{3.61}$$

In this research, SDOF systems as presented in Figure 3.2a are used to represent the empty test structure. However, SDOF systems are also used to model human occupants. In this case, the mass, viscous damping, and stiffness properties of the SDOF system are defined as m_H, c_H, and k_H. This simple SDOF model will represent not only single but also groups of human occupants.

To enable such a simplification, it is assumed that each occupant can be modelled by a damped SDOF system with a lumped mass m_H, which is a certain proportion of the total mass m_T of the individual human occupant. Furthermore, it is assumed that such a SDOF system representing any occupant has the same natural frequency f_H and the same damping ratio ζ_H. In this case, it is possible to lump several SDOF human occupant models into one.

For instance, two SDOF systems (1 and 2) be characterised by m_1, c_1, k_1 and m_2, c_2, k_2 respectively. They have identical natural frequencies f_H and damping ratios ζ_H. Both SDOF systems can be summarised into a SDOF system defined by

$$m_3 = m_1 + m_2, \tag{3.62}$$

$$c_3 = c_1 + c_2, \tag{3.63}$$

and

$$k_3 = k_1 + k_2. \tag{3.64}$$

This SDOF system has also the natural frequency f_H and the damping ratio ζ_H. This can be shown using the fact that

$$\frac{k_1}{m_1} = \frac{k_2}{m_2} \tag{3.65}$$

and

$$\frac{c_1}{m_1} = \frac{c_2}{m_2} \tag{3.66}$$

for two SDOF systems with the same natural frequency and damping ratio (see equations (3.59) and (3.60)).

Equation (3.65) can be rewritten as

$$k_1 \cdot m_2 = k_2 \cdot m_1. \tag{3.67}$$

Eliminating m_2 and k_2 from this expression by using equations (3.62) and (3.64), it becomes:

$$k_1 \cdot (m_3 - m_1) = (k_3 - k_1) \cdot m_1. \tag{3.60}$$

This equation (3.70) equals

$$k_1 \cdot m_3 = k_3 \cdot m_1 \tag{3.69}$$

and, therefore,

$$\frac{k_1}{m_1} = \frac{k_3}{m_3}. \tag{3.70}$$

This last equation (3.70) is similar to equation (3.65). It confirms that summing mass and stiffness of two SDOF systems with the same natural frequency leads to a SDOF system that also has this natural frequency.

Following a similar procedure, but starting with equation (3.66) instead of (3.67), it can be shown that

$$\frac{c_1}{m_1} = \frac{c_2}{m_2} = \frac{c_3}{m_3}. \tag{3.71}$$

This demonstrates that the damping ratio of the two SDOF systems (1 and 2) equals the damping ratio of SDOF system 3 (equation (3.60)). Thus, one SDOF model can represent an arbitrary number of SDOF human occupant models defined by a natural frequency f_H and the damping ratio ζ_H. Thereby, it is only the mass m_H that changes depending on the number of human occupants.

3.1.2.2 Damped 2-DOF System

The damped 2-DOF model (DM) presented in Figure 3.2b is used in this research as a key model for the human-structure system. Its modal properties can be calculated from its equation of motion (3.72).

$$\begin{bmatrix} m_S & O \\ O & m_H \end{bmatrix} \cdot \begin{Bmatrix} \ddot{x}_S(t) \\ \ddot{x}_H(t) \end{Bmatrix} + \begin{bmatrix} c_S + c_H & -c_H \\ -c_H & c_H \end{bmatrix} \cdot \begin{Bmatrix} \dot{x}_S(t) \\ \dot{x}_H(t) \end{Bmatrix} + \begin{bmatrix} k_S + k_H & -k_H \\ -k_H & k_H \end{bmatrix} \cdot \begin{Bmatrix} x_S(t) \\ x_H(t) \end{Bmatrix} = \begin{Bmatrix} F_S(t) \\ F_H(t) \end{Bmatrix} \tag{3.72}$$

Its natural frequencies $f_r^{(DM)}$, modal damping ratios ζ_r, and mode shapes $\{\psi\}_r$ are obtained from solving the eigenproblem:

$$\left(\lambda_r^2 \cdot \begin{bmatrix} m_S & O \\ O & m_H \end{bmatrix} + \lambda_r \cdot \begin{bmatrix} c_S + c_H & -c_H \\ -c_H & c_H \end{bmatrix} + \begin{bmatrix} k_S + k_H & -k_H \\ -k_H & k_H \end{bmatrix}\right) \cdot \begin{Bmatrix} \psi_{Sr} \\ \psi_{Hr} \end{Bmatrix} = \begin{Bmatrix} O \\ O \end{Bmatrix}, \tag{3.73}$$

which is a special case of equation (3.19). Its eigenvalues λ_r can be calculated by solving:

$$det\begin{bmatrix} m_S \cdot \lambda_r^2 + (c_S + c_H) \cdot \lambda_r + k_S + k_H & -c_H \cdot \lambda_r - k_H \\ -c_H \cdot \lambda_r - k_H & m_H \cdot \lambda_r^2 + c_H \cdot \lambda_r + k_H \end{bmatrix} = O. \tag{3.74}$$

Equation (3.74) can be rewritten as equation (3.75) and explicitly as fourth order polynomial (3.76).

$$O = (m_S \cdot \lambda_r^2 + (c_S + c_H) \cdot \lambda_r + k_S + k_H) \cdot (m_H \cdot \lambda_r^2 + c_H \cdot \lambda_r + k_H) - (-c_H \cdot \lambda_r - k_H)^2 \tag{3.75}$$

$$\begin{aligned} O = {} & m_S \cdot m_H \cdot \lambda_r^4 \\ & + (m_H \cdot c_S + m_H \cdot c_H + m_S \cdot c_H) \cdot \lambda_r^3 \\ & + (m_H \cdot k_S + m_H \cdot k_H + m_S \cdot k_H + c_H \cdot c_S) \cdot \lambda_r^2 \\ & + (c_H \cdot k_S + c_S \cdot k_H) \cdot \lambda_r \\ & + k_S \cdot k_H \end{aligned} \tag{3.76}$$

The eigenvalues λ_r (equation (3.54)) of this fourth order polynomial (3.76) can be calculated analytically (Weisstein (1999) and see Appendix A) or solved numerically by employing appropriate software. In any case, if the two eigenvalues λ_1 and λ_2 are known, the natural frequencies ($f_1^{(DM)}$ and $f_2^{(DM)}$) and the damping ratios (ζ_1 and ζ_2) can be calculated (equations (3.53) and (3.55)).

The eigenvectors $\{\psi\}_r$ of a damped 2-DOF system (Figure 3.2b) corresponding to the eigenvalues λ_r are specified by equation (3.73). Based on this equation, the ratio of mode shape elements ψ_{Hr} to ψ_{Sr} can be described by equation (3.77) or by equation (3.78) (Timoshenko et al. 1974, p. 267).

$$\frac{\lambda_r^2 \cdot m_S + \lambda_r \cdot (c_S + c_H) + k_S + k_H}{\lambda_r \cdot c_H + k_H} = \frac{\psi_{Hr}}{\psi_{Sr}} \tag{3.77}$$

$$\frac{-\lambda_r \cdot c_H - k_H}{\lambda_r^2 \cdot m_H + \lambda_r \cdot c_H + k_H} = \frac{\psi_{Hr}}{\psi_{Sr}} \tag{3.78}$$

Summarising the two mode shapes $\{\psi\}_1$ and $\{\psi\}_2$, the modal matrix $[\Theta]$ of a damped 2-DOF system (Figure 3.2b) is defined by equation (3.79).

$$[\Theta] = \begin{bmatrix} \psi_{S1} & \psi_{S2} \\ \psi_{H1} & \psi_{H2} \end{bmatrix} \tag{3.79}$$

The mode shapes $\{\psi\}_1$ and $\{\psi\}_2$ are generally complex and, therefore, there is a phase shift between the two DOFs. (Mode shapes are real if damping is proportional, meaning that the damping matrix is a linear combination of the mass and stiffness matrices.)

3.1.2.3 UNDAMPED 2-DOF SYSTEM

Following a detailed presentation of the theory of the damped 2-DOF system (Figure 3.2b), the modal properties of the undamped 2-DOF system are estimated.

The equation of motion and the eigenproblem of an undamped 2-DOF system can easily be derived from equations (3.72) and (3.73) defining the damped 2-DOF system by setting $c_s = c_H = O$. Thus, equations (3.75) and (3.76) lead to the polynomials (3.80) and (3.81) defining the eigenvalues λ_r of the undamped 2-DOF system.

$$O = (m_s \cdot \lambda_r^2 + k_s + k_H) \cdot (m_H \cdot \lambda_r^2 + k_H) - (-k_H)^2 \tag{3.80}$$

$$O = m_s \cdot m_H \cdot \lambda_r^4 + (m_H \cdot k_s + m_H \cdot k_H + m_s \cdot k_H) \cdot \lambda_r^2 + k_s \cdot k_H \tag{3.81}$$

The eigenvalues λ_r (3.54) of undamped systems ($\zeta_r = O$) contain only information on the circular natural frequency ω_r:

$$\lambda_r = \pm i \cdot \omega_r . \tag{3.82}$$

Similarly to the eigenvalues of a damped 2-DOF system (Appendix A), the eigenvalues λ_r of an undamped 2-DOF model (UM) can be calculated analytically. This fact can be used to define the natural frequencies $f_1^{(UM)}$ and $f_2^{(UM)}$ (3.83) of the undamped 2-DOF system by the modal masses (m_s and m_H) and the natural frequencies (f_s and f_H) of the two DOFs (Randall and Peng 1995) as derived in Appendix B.

$$f_{1,2}^{(UM)} = \frac{1}{2} \cdot \sqrt{(f_H + f_S)^2 + \frac{m_H}{m_S} \cdot f_H^2} \mp \frac{1}{2} \cdot \sqrt{(f_H - f_S)^2 + \frac{m_H}{m_S} \cdot f_H^2} \tag{3.83}$$

Finally, the mode shapes $\{\psi\}_1$ and $\{\psi\}_2$ of the undamped 2-DOF system are described by:

$$\frac{\omega_r^2 \cdot m_S + k_S + k_H}{k_H} = \frac{\psi_{Hr}}{\psi_{Sr}} \tag{3.84}$$

or

$$\frac{-k_H}{\omega_r^2 \cdot m_H + k_H} = \frac{\psi_{Hr}}{\psi_{Sr}}, \tag{3.85}$$

simplifications of equations (3.77) and (3.78) defining the mode shapes of damped 2-DOF systems.

It is noteworthy that the mode shapes $\{\psi\}_1$ and $\{\psi\}_2$ of undamped 2-DOF systems are real valued. Therefore, the two DOFs of undamped 2-DOF systems move in phase and 180° out of phase, respectively, in both modes.

3.1.3 Frequency Domain Response Models

In the previous section, modal properties of SDOF and two 2-DOF models were calculated from spatial properties. In this section, spatial and modal properties of the dynamic systems presented in Figures 3.2 and 3.3 will be used to define frequency domain response models analytically.

3.1.3.1 Definition of FRF and Inverse FRF

The frequency response function (FRF) and its inverse are frequency domain response models (Maia et al. 1997, p. 38; Ewins 2000, p. 36). An FRF $H_{jk}(\omega)$ defines the response $V_j(\omega)$ (displacement, velocity, or acceleration) at DOF j to a sinusoidal excitation $F_k(\omega)$ at DOF k:

$$H_{jk}(\omega) = \frac{V_j(\omega)}{F_k(\omega)}. \tag{3.86}$$

An inverse FRF $Z_{jk}(\omega)$ (3.87) is defined as the reciprocal of a FRF $H_{jk}(\omega)$ (Ewins 2000, p. 36).

$$Z_{jk}(\omega) = \frac{1}{H_{jk}(\omega)} = \frac{F_k(\omega)}{V_j(\omega)} \tag{3.87}$$

The equation of motion of MDOF systems (see equation (3.9) in section 3.1.1.2) can be used to derive analytical descriptions of FRFs. This is done by substituting a sinusoidal excitation $\{F(t)\}$

$$\{F(t)\} = \{F(\omega)\} \cdot e^{i\cdot\omega t} \tag{3.88}$$

and a sinusoidal displacement response $\{x(t)\}$ (3.89) (or its derivatives $\{\dot{x}(t)\}$ (3.90) or $\{\ddot{x}(t)\}$ (3.91)) into the equation of motion (3.9).

$$\{x(t)\} = \{X(\omega)\} \cdot e^{i\cdot\omega t} \tag{3.89}$$

$$\{\dot{x}(t)\} = i\cdot\omega\cdot\{x(t)\} \tag{3.90}$$

$$\{\ddot{x}(t)\} = (i\cdot\omega)^2\cdot\{x(t)\} = -\omega^2\cdot\{x(t)\} \tag{3.91}$$

Thereby, the equation of motion (3.9) simplifies to equation (3.92).

$$\left(-\omega^2\cdot[M] + i\cdot\omega\cdot[C] + [K]\right)\cdot\{X(\omega)\} = \{F(\omega)\} \tag{3.92}$$

Summarising the left hand term of equation (3.92), the receptance FRFs $\alpha_{jk}(\omega)$ of MDOF systems may be presented in the matrix form $[\alpha(\omega)]$ based on equation (3.93).

$$[\alpha(\omega)]^{-1}\cdot\{X(\omega)\} = \{F(\omega)\} \tag{3.93}$$

The receptance FRFs $\alpha_{jk}(\omega)$ are defined by the spatial properties ($[M]$, $[C]$, and $[K]$) of the MDOF system:

$$[\alpha(\omega)] = \left(-\omega^2\cdot[M] + i\cdot\omega\cdot[C] + [K]\right)^{-1}. \tag{3.94}$$

However, FRFs can also be defined by the modal properties of the dynamic system. Such a description is based on state-space analysis (see section 3.1.1.4). It is particularly valuable in the identification of modal properties from experimental FRFs (Ewins 2000, p. 287).

In particular, for the sinusoidal vibrations (equation (3.88) and (3.89)) described by FRFs, the state-space equation (3.46) can be simplified to equation (3.95).

$$a_r \cdot (i \cdot \omega - \lambda'_r) \cdot \{p'_r(t)\} = \{g'_r(t)\} \tag{3.95}$$

The modal responses in the state-space $\{p'_r(t)\}$ are based on the state-space variable $\{u(t)\}$, which is defined by the displacement responses $\{x(t)\}$ (see section 3.1.1.4). In case of steady-state sinusoidal vibrations, the displacement responses $\{x(t)\}$ occur at a certain frequency only (3.89). It is therefore possible to extract the frequency dependent displacements $\{X(\omega)\}$ from the state-space equation (3.95) (Maia et al. 1997, p. 69).

The receptance FRFs $\alpha_{jk}(\omega)$ can then be defined in the partial series form by equations (3.96) and (3.97), whereby ${}_rA_{jk}$ (3.98) is a complex number called the modal constant or residue (Maia et al. 1997, p. 70; Ewins 2000, p. 60).

$$\alpha_{jk}(\omega) = \sum_{r=1}^{N} \left(\frac{\psi_{jr} \cdot \psi_{kr}}{a_r \cdot (i \cdot \omega - \lambda_r)} + \frac{\psi^*_{jr} \cdot \psi^*_{kr}}{a^*_r \cdot (i \cdot \omega - \lambda^*_r)} \right) \tag{3.96}$$

$$\alpha_{jk}(\omega) = \sum_{r=1}^{N} \left(\frac{{}_rA_{jk}}{(i \cdot \omega - \lambda_r)} + \frac{{}_rA^*_{jk}}{(i \cdot \omega - \lambda^*_r)} \right) \tag{3.97}$$

$${}_rA_{jk} = \frac{\psi_{jr} \cdot \psi_{kr}}{a_r} \tag{3.98}$$

The previous paragraphs established descriptions of receptance FRFs from the displacement response $x_j(t)$ to a sinusoidal excitation $F_k(t)$. Measurements often identify response velocities $\dot{x}_j(t)$ or accelerations $\ddot{x}_j(t)$ that are related to mobility FRFs $Y_{jk}(\omega)$ or to accelerance FRFs $A_{jk}(\omega)$. In both cases, the analytical description of the FRFs $Y_{jk}(\omega)$ and $A_{jk}(\omega)$ can be derived from the receptance FRF $\alpha_{jk}(\omega)$ (equations (3.99) and (3.100)).

$$Y_{jk}(\omega) = i \cdot \omega \cdot \alpha_{jk}(\omega) \tag{3.99}$$

$$A_{jk}(\omega) = -\omega^2 \cdot \alpha_{jk}(\omega) \tag{3.100}$$

Note, multiplying by $i \cdot \omega$ or $-\omega^2$ corresponds to using the first or second derivative ($\dot{x}_j(t)$ in equation (3.90) or $\ddot{x}_j(t)$ in equation (3.91)) of the displacement $x_j(t)$.

In this research, SDOF systems (Figure 3.2a) and 2-DOF systems (Figure 3.2b) are used to model structures and corresponding human-structure systems. The accelerance FRFs $A_{jk}(\omega)$ of these dynamic systems will be used in an analytical parametric study (chapter 4). They will be established in sections 3.1.3.2 and 3.1.3.3.

This research also looks at inverse FRFs. In particular, the apparent mass $M_{jk}(\omega)$ (the reciprocal of the accelerance $A_{jk}(\omega)$):

$$M_{jk}(\omega) = \frac{1}{A_{jk}(\omega)} \tag{3.101}$$

and the mechanical impedance $I_{jk}(\omega)$ (the reciprocal of the mobility $Y_{jk}(\omega)$):

$$I_{jk}(\omega) = \frac{1}{Y_{jk}(\omega)} \tag{3.102}$$

are introduced.

The FRFs $I_{jk}(\omega)$ and $M_{jk}(\omega)$ are traditionally used in biomechanical engineering to describe dynamic properties of the human body and simple biomechanical models of the whole human body (section 2.2).

Based on recommendations by Griffin (1990, p. 360) and Wu et al. (1999), the apparent mass $M_{jk}(\omega)$ is preferred to the mechanical impedance $I_{jk}(\omega)$. The apparent mass $M_{jk}(\omega)$ of the two biomechanic models presented in Figures 2.2b and 2.3c (and thus indirectly of the models of Figures 2.2a and 2.3b) will be derived in sections 3.1.3.4 and 3.1.3.5.

3.1.3.2 Accelerance of a SDOF System

In this research, the damped SDOF system (Figure 3.2a) is used to model a structure. This SDOF system is described by one point-accelerance FRF. In the following analysis, this point-accelerance will be compared to the point-accelerance $A_{ss}(\omega)$ of the 2-DOF human-structure model (Figure 3.2b, section 3.1.3.3). Both accelerances define the response of the structure to an excitation at the DOF modelling the structure ($j = k = s$). Therefore, in this research, both accelerances are named 'structural FRFs'. However, it is necessary to distinguish between the structural FRF of the SDOF

model representing an empty structure (Figure 3.2a) and the structural FRF of the 2-DOF human-structure model (Figure 3.2b). Therefore, the structural FRF of the SDOF system is defined as $A_s(\omega)$ in contrast to the structural FRF of the 2-DOF human-structure system $A_{ss}(\omega)$.

Based on the already outlined theory (equations (3.94) and (3.96) in section 3.1.3.1), the structural FRF $A_s(\omega)$ of a SDOF system (Figure 3.2a) can be defined by modal properties in the partial series form:

$$A_s(\omega) = \frac{-\omega^2}{m_s \cdot (i \cdot \omega - \lambda_1) \cdot (i \cdot \omega - \lambda_1^*)} \tag{3.103}$$

and by spatial properties in the partial fraction form:

$$A_s(\omega) = \frac{-\omega^2}{k_s - m_s \cdot \omega^2 + i \cdot \omega \cdot c_s}. \tag{3.104}$$

In further analysis, the magnitudes of the structural FRFs of the SDOF structure model and of the 2-DOF human-structure system will be compared (see section 4.6 and chapter 6). In this comparison, the amplitude a_s (3.105) of the structural FRF $A_s(\omega)$ at the natural frequency ω_s is going to be used.

$$a_s = |A_s(\omega_s)| \tag{3.105}$$

The amplitude a_s can be derived from equations (3.103) or (3.104) and equation (3.105) and is defined by equation (3.106). Equation (3.106) demonstrates that the magnitude of the FRF $A_s(\omega_s)$ is limited only by viscous damping c_s, which is specified by the modal mass m_s and the modal damping ratio ζ_s (see equation (3.3) in section 3.1.1.1).

$$a_s = \frac{\omega_s}{c_s} = \frac{1}{2 \cdot \zeta_s \cdot m_s} \tag{3.106}$$

3.1.3.3 Accelerances of a 2-DOF System

The SDOF structure model (Figure 3.2a) is characterised by one accelerance $A_s(\omega)$. However, the 2-DOF human-structure model (Figure 3.2b) is characterised by four FRFs $A_{jk}(\omega)$ (3.107), relating excitations and responses at the two DOFs.

$$[A(\omega)] = \begin{bmatrix} A_{SS}(\omega) & A_{SH}(\omega) \\ A_{HS}(\omega) & A_{HH}(\omega) \end{bmatrix} \tag{3.107}$$

Using the theory outlined in section 3.1.3.1, the accelerances $A_{jk}(\omega)$ of the damped 2-DOF human-structure model can be defined by the contributions of two modes of vibration:

$$A_{jk}(\omega) = -\omega^2 \cdot \sum_{r=1}^{2} \left(\frac{{}_rA_{jk}}{(i\cdot\omega - \lambda_r)} + \frac{{}_rA_{jk}^*}{(i\cdot\omega - \lambda_r^*)} \right) \quad (j,k = S,H) \tag{3.108}$$

or as function of spatial properties by:

$$[A(\omega)] = \frac{-\omega^2}{d} \cdot \begin{bmatrix} -m_H\cdot\omega^2 + i\cdot\omega\cdot c_H + k_H & i\cdot\omega\cdot c_H + k_H \\ i\cdot\omega\cdot c_H + k_H & -m_S\cdot\omega^2 + i\cdot\omega\cdot(c_S + c_H) + k_S + k_H \end{bmatrix} \tag{3.109}$$

where

$$d = (k_S + k_H - m_S\cdot\omega^2 + i\cdot\omega\cdot(c_S + c_H))\cdot(k_H - m_H\cdot\omega^2 + i\cdot\omega\cdot c_H) - (-i\cdot\omega\cdot c_H - k_H)^2. \tag{3.110}$$

In this research, emphasis is put on the structural FRF $A_{SS}(\omega)$. It is therefore extracted from equations (3.109) and (3.110) and stated explicitly with equation (3.111) where d as in (3.110).

$$A_{SS}(\omega) = \frac{-\omega^2(-m_H\cdot\omega^2 + i\cdot\omega\cdot c_H + k_H)}{d} \tag{3.111}$$

Finally, it should be mentioned that attaching a SDOF system with certain properties to a structure has the potential to reduce the vibration response of a structure. Such additional SDOF systems are dynamic vibration absorbers, also called tuned mass-spring systems (Inman 2001, p. 377), and vibration dampers, which can be damped mass-spring systems or dampers only (Inman 2001, p. 384). They can be used in design as outlined in appropriate textbooks such as Hunt (1979) and Korenev and Reznikov (1993).

3.1.3.4 Apparent Mass of a SDOF System

Biomechanics use the inverse FRF apparent mass $M(\omega)$ (3.112) to describe the influence of an occupant on the sinusoidal base acceleration $\ddot{x}_o(t)$ of a supporting structure (Griffin 1990, p. 260). Hence, the apparent mass $M(\omega)$ of a SDOF system (as defined in biomechanics) is the inverse of the point-accelerance $A_{oo}(\omega)$ (Figure 3.3a).

$$M(\omega) = \frac{F_o(\omega)}{-\omega^2 \cdot X_o(\omega)} \tag{3.112}$$

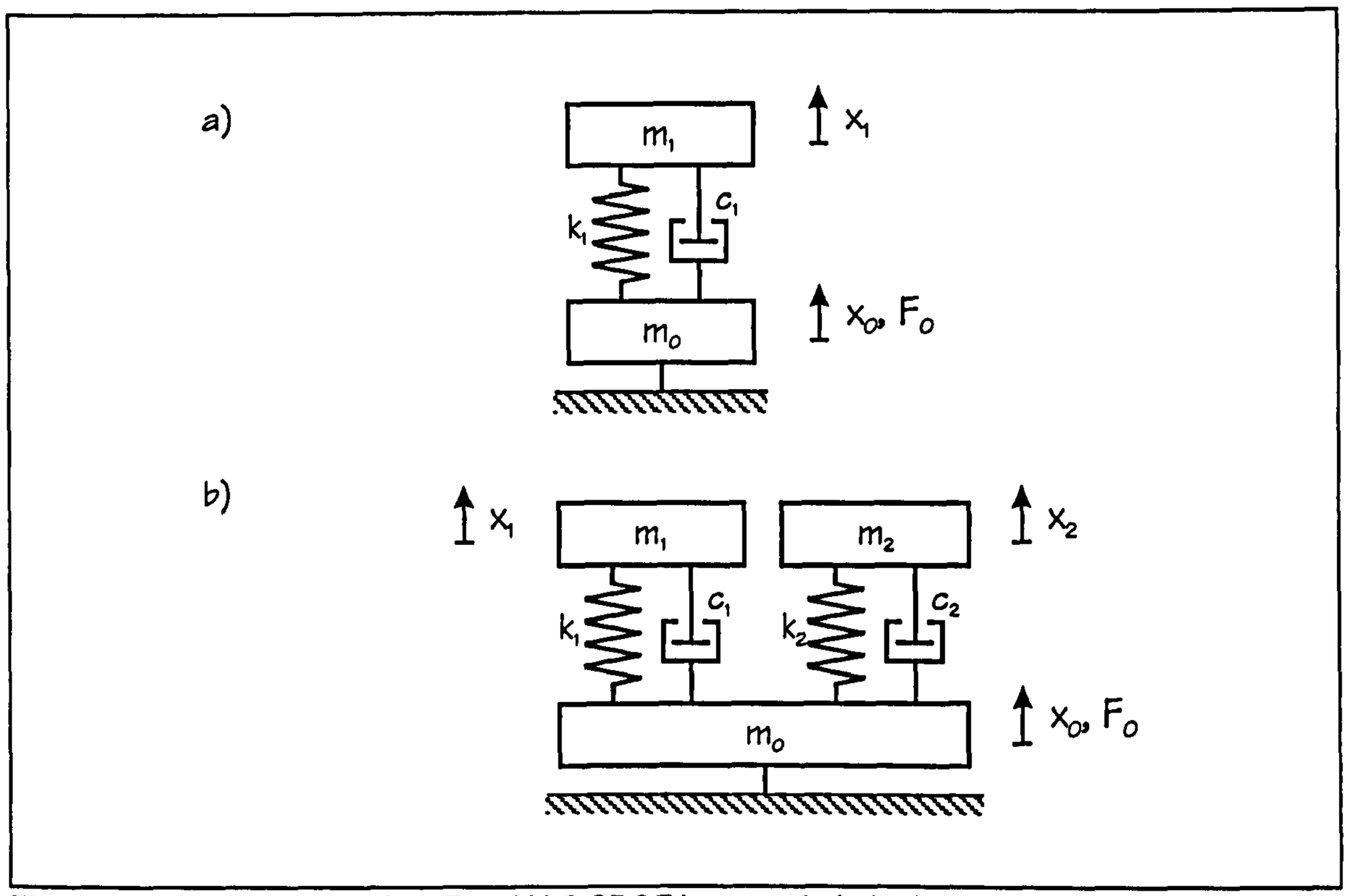

Figure 3.3: Base excited a) SDOF and b) 2-SDOF human whole-body model.

The apparent mass $M(\omega)$ can be derived from the spatial and modal properties as outlined in section 3.1.3.1. However, biomechanics usually approach the issue by combining the apparent mass (Griffin 1990, p. 378f) associated to each spatial element of a human body model (Griffin 1990, p. 361). In this research, another method, also used by biomechanical engineers, is preferred. This approach is based on the equation of motion and, therefore, is more similar to considerations common in modal analysis.

The biomechanical engineers Wei and Griffin (1998) outline that the apparent mass $M(\omega)$ of a base excited SDOF system (Figure 3.3a) can be calculated from the equations of motion (3.113) and (3.114), whereby $F_o(t)$ is a sinusoidal force on the base.

$$F_o(t) = m_o \cdot \ddot{x}_o(t) + m_1 \cdot \ddot{x}_1(t) \tag{3.113}$$

$$m_1 \cdot \ddot{x}_1(t) + c_1 \cdot (\dot{x}_1(t) - \dot{x}_o(t)) + k_1 \cdot (x_1(t) - x_o(t)) = O \tag{3.114}$$

Employing a sinusoidal base excitation $x_o(t)$:

$$x_o(t) = X_o(\omega) \cdot e^{i \cdot \omega t} \tag{3.115}$$

and a response $x_1(t)$:

$$x_1(t) = X_1(\omega) \cdot e^{i \cdot \omega t} \ , \tag{3.116}$$

equations (3.113) and (3.114) can be transferred into the frequency domain, as shown by equations (3.117) and (3.118).

$$F_o(\omega) = \omega^2 \cdot (-m_o \cdot X_o(\omega) - m_1 \cdot X_1(\omega)) \tag{3.117}$$

$$(-m_1 \cdot \omega^2 + i \cdot \omega \cdot c_1 + k_1) \cdot X_1(\omega) - (i \cdot \omega \cdot c_1 + k_1) \cdot X_o(\omega) = O \tag{3.118}$$

Substituting the force $F_o(\omega)$ (3.117) into equation (3.112) defining the apparent mass $M(\omega)$, equation (3.119) can be derived.

$$M(\omega) = m_o + m_1 \cdot \frac{X_1(\omega)}{X_o(\omega)} \tag{3.119}$$

In this definition (3.119), the masses (m_o and m_1) and the displacement $X_o(\omega)$ are known. The unknown displacement $X_1(\omega)$ results from the base displacement $X_o(\omega)$. Therefore, $X_1(\omega)$ can be defined by equation (3.120), which is obtained by rearranging equation (3.118).

$$X_1(\omega) = \frac{i \cdot \omega \cdot c_1 + k_1}{k_1 - m_1 \cdot \omega^2 + i \cdot \omega \cdot c_1} \cdot X_o(\omega) \tag{3.120}$$

Substituting equation (3.120) into equation (3.119), the apparent mass $M(\omega)$ of a damped SDOF system (Figure 3.3a) can be defined by its spatial properties:

$$M(\omega) = m_o + \frac{i \cdot \omega \cdot c_1 + k_1}{k_1 - m_1 \cdot \omega^2 + i \cdot \omega \cdot c_1} \cdot m_1. \tag{3.121}$$

3.1.3.5 Apparent Mass of a 2-SDOF System

This research focuses on simple biomechanic human body models. Therefore, the apparent mass $M(\omega)$ of just one further dynamic model of the human body is derived. This model is the 2-SDOF system with non-vibrating mass as presented in Figures 2.3b and 3.3b.

The equations of motion of this damped 2-SDOF system (Figure 3.3b) are given by equations (3.122), (3.123), and (3.124).

$$F_o(t) = m_o \cdot \ddot{x}_o(t) + m_1 \cdot \ddot{x}_1(t) + m_2 \cdot \ddot{x}_2(t) \tag{3.122}$$

$$m_1 \cdot \ddot{x}_1(t) + c_1 \cdot (\dot{x}_1(t) - \dot{x}_o(t)) + k_1 \cdot (x_1(t) - x_o(t)) = O \tag{3.123}$$

$$m_2 \cdot \ddot{x}_2(t) + c_2 \cdot (\dot{x}_2(t) - \dot{x}_o(t)) + k_2 \cdot (x_2(t) - x_o(t)) = O \tag{3.124}$$

Following a similar procedure as outlined above, the apparent mass $M(\omega)$ of a damped 2-SDOF system can be obtained as defined by equation (3.125) (Wei and Griffin 1998).

$$M(\omega) = m_o + \frac{i \cdot \omega \cdot c_1 + k_1}{k_1 - m_1 \cdot \omega^2 + i \cdot \omega \cdot c_1} \cdot m_1 + \frac{i \cdot \omega \cdot c_2 + k_2}{k_2 - m_2 \cdot \omega^2 + i \cdot \omega \cdot c_2} \cdot m_2 \tag{3.125}$$

3.2 Experimental Modal Analysis

In analytical modal analysis, modal properties are calculated from assumed mass, stiffness, and damping distributions. In contrast, in experimental modal analysis, modal properties are estimated from measured responses (Ewins 2000, p. 26). This section outlines the fundamentals of forced vibration testing, data acquisition and processing, and the identification of modal properties from experimental data. The presented material is based mainly on standard modal testing textbooks by Newland (1993), McConnell (1995), Maia et al. (1997), and Ewins (2000).

3.2.1 Fundamentals

In this research, frequency domain parameter estimation techniques based on FRFs are used to estimate experimental modal properties. The estimation of FRFs from experimental response data requires the analysis of periodic, transient, or random signals (McConnell 1995, p. 12ff; Randall 1987, p. 42ff). As is usual in vibration analysis, random signals are assumed stationary ergodic. A random signal is stationary, if its statistical properties (mean, mean square, variance, and standard deviation) are independent of time. If any sample of length T represents these properties, a stationary signal is ergodic (Newland 1993, p. 20).

3.2.1.1 Periodic and Continuous Fourier Transformation

If a continuous signal $v(t)$ is periodic, it lasts forever and can be presented by harmonic components at multiples n of the fundamental circular frequency ω_o. The frequency domain presentation of such a Fourier series:

$$v(t) = \sum_{n=-\infty}^{\infty} V(n \cdot \omega_o) \cdot e^{i \cdot n \cdot \omega_o \cdot t} \tag{3.126}$$

is a discrete frequency spectrum having values at discrete circular frequencies $\omega = n \cdot \omega_o$. This spectrum is defined by discrete Fourier coefficients $V(n \cdot \omega_o)$ (McConnell 1995, p. 24) and given by:

$$V(n \cdot \omega_o) = \frac{1}{T} \int_{-T/2}^{T/2} v(t) \cdot e^{-i \cdot n \cdot \omega_o \cdot t} dt . \tag{3.127}$$

If a signal $v(t)$ is transient, it is zero after a limited amount of time. Therefore, it cannot be described by a Fourier series. Hence, the periodic Fourier transformation (FT) pair (equations (3.116) and (3.127)) is not applicable. However, a transient signal $v(t)$ satisfies the Dirichlet condition:

$$\int_{-\infty}^{\infty} |v(t)|\,dt < \infty . \tag{3.128}$$

Therefore, it can be understood as periodic but with a period T of infinity ($T \to \infty$). In this case, the fundamental circular frequency ω_o becomes infinitesimal (Maia et al. 1997, p. 89f) and the sum of equation (3.116) becomes an integral (3.129).

$$v(t) = \int_{-\infty}^{\infty} V(\omega) \cdot e^{i \cdot \omega t}\, d\omega \tag{3.129}$$

A signal $v(t)$ that satisfies the Dirichlet condition (3.128) can be transferred into a continuous frequency spectrum $V(\omega)$ by the continuous FT:

$$V(\omega) = \frac{1}{2 \cdot \pi} \cdot \int_{-\infty}^{\infty} v(t) \cdot e^{-i \cdot \omega t}\, dt . \tag{3.130}$$

Equations (3.129) and (3.130) constitute the continuous FT pair (Newland 1993, p. 39; Ewins 2000, p. 139). The continuous FT pair can equally be defined by equations (3.131) and (3.132) (McConnell 1995, p. 32; Maia et al. 1997, p. 90; James et al. 1999, p. 368).

$$v(t) = \frac{1}{2 \cdot \pi} \cdot \int_{-\infty}^{\infty} V(\omega) \cdot e^{i \cdot \omega t}\, d\omega \tag{3.131}$$

$$V(\omega) = \int_{-\infty}^{\infty} v(t) \cdot e^{-i \cdot \omega t}\, dt \tag{3.132}$$

It is also possible to split the factor $1/(2 \cdot \pi)$ between both equations (Newland 1993, p. 39; James et al. 1999, p. 368).

Here, the definition of the continuous FT pair defined by equations (3.131) and (3.132) is used. In this form, usually as function of the frequency f (Maia et al. 1997, p. 14):

$$v(t) = \int_{-\infty}^{\infty} V(f) \cdot e^{i \cdot 2 \cdot \pi \cdot f \cdot t} \, df \tag{3.133}$$

and

$$V(f) = \int_{-\infty}^{\infty} v(t) \cdot e^{-i \cdot 2 \cdot \pi \cdot f \cdot t} \, dt, \tag{3.134}$$

it is commonly implemented into modern spectrum analysers (McConnell 1995, p. 50).

A random signal $v(t)$, similar to its periodic counterpart, does not satisfy the Dirichlet condition (3.128). Therefore, another approach is required to present random signals in the frequency domain. This approach is based on the statistical properties of signals (Argyris and Mlejnek 1991; Clough and Penzien 1993; McConnell 1995). It employs auto- and cross-correlation functions and auto- and cross-spectral densities.

3.2.1.2 Correlation Functions and Spectral Densities

The cross-correlation function $R_{vw}^{r}(\tau)$ of two random signals $v(t)$ and $w(t)$ is defined by (3.135).

$$R_{vw}^{r}(\tau) = \lim_{T \to \infty} \frac{1}{T} \int_{-T/2}^{T/2} v(t) \cdot w(t+\tau) \, dt \tag{3.135}$$

This cross-correlation function $R_{vw}^{r}(\tau)$ and its counterpart $R_{wv}^{r}(\tau)$ preserve information on the identical frequency content of both random signals $v(t)$ and $w(t)$. Therefore, if a signal $v(t)$ has periodic components, information about the frequencies and amplitudes is preserved in its auto-correlation function $R_{w}^{r}(\tau)$ (Figure 3.4).

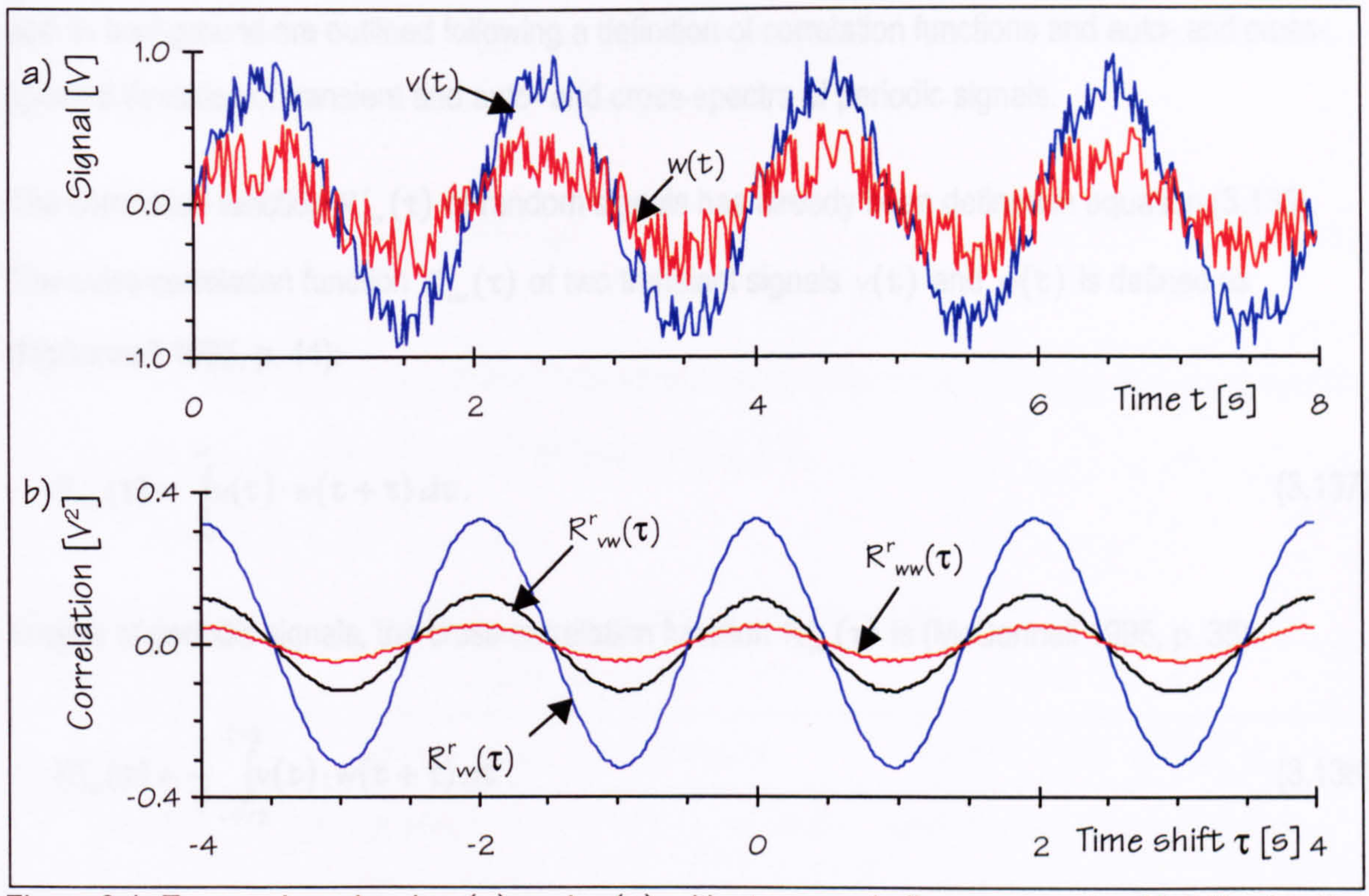

Figure 3.4: Two random signals $v(t)$ and $w(t)$ with strong periodic components of 0.5 Hz a) in the time domain and b) characterised by auto- and cross-correlation functions.

In practical random vibration analysis, random signals do not contain periodic components. In this case, auto- and cross-correlation functions $R^r_{vw}(\tau)$ are transient in the shift domain τ (Newland 1993, p. 31 and p. 41). In this case, they satisfy the Dirichlet condition (3.128) and, therefore, the continuous FT can be applied (Newland 1993, p. 36; McConnell 1995, p. 48). The resulting random signal cross-spectral density $S^r_{vw}(\omega)$:

$$S^r_{vw}(\omega) = \int_{-\infty}^{\infty} R^r_{vw}(\tau) \cdot e^{-i\cdot\omega\cdot\tau}\, d\tau \tag{3.136}$$

describes the properties of the correlation function $R^r_{vw}(\tau)$ (and thus that of the random signals $v(t)$ and $w(t)$) in the frequency domain (McConnell 1995, p. 54).

Spectral densities are usually employed to compute experimental FRFs as will be outlined later. This is because auto- and cross-correlation functions and thus auto- and cross-spectra can be defined for periodic or transient signals as well. Therefore, it is possible to employ the same algorithm for the computation of FRFs based on digitised random, transient, or periodic vibrations. This procedure

and its background are outlined following a definition of correlation functions and auto- and cross-spectral densities of transient and auto- and cross-spectra of periodic signals.

The correlation function $R^r_{vw}(\tau)$ of random signals has already been defined in equation (3.135). The cross-correlation function $R^t_{vw}(\tau)$ of two transient signals $v(t)$ and $w(t)$ is defined as (McConnell 1995, p. 44):

$$R^t_{vw}(\tau) = \int_{-\infty}^{\infty} v(t) \cdot w(t+\tau)\, dt. \tag{3.137}$$

In case of periodic signals, the cross-correlation function $R^p_{vw}(\tau)$ is (McConnell 1995, p. 38):

$$R^p_{vw}(\tau) = \frac{1}{T} \int_{-T/2}^{T/2} v(t) \cdot w(t+\tau)\, dt. \tag{3.138}$$

It is important to note the differences in the integration interval and averaging of the correlation functions $R^r_{vw}(\tau)$, $R^p_{vw}(\tau)$, and $R^t_{vw}(\tau)$ (equations (3.135), (3.137), and (3.138)). They lead to different units (Table 3.1) and require separate definitions of auto- and cross-spectra $S_{vw}(\omega)$ related to each of the three signal types.

Table 3.1: Units of $R_{vw}(\tau)$ for different types of signals.

Type of signals	Unit of $R_{vw}(\tau)$
Periodic	(unit of $v(t)$) · (unit of $w(t)$)
Transient	(unit of $v(t)$) · (unit of $w(t)$)/Hz
Random	(unit of $v(t)$) · (unit of $w(t)$)

The continuous cross-spectral density $S^r_{vw}(\omega)$ of random signals was defined by equation (3.136). Similarly, the cross-spectral density $S^t_{vw}(\omega)$ of transient signals is defined as a continuous function (McConnell 1995, p. 45):

$$S^t_{vw}(\omega) = \int_{-\infty}^{\infty} R^t_{vw}(\tau) \cdot e^{-i\cdot\omega\tau}\, d\tau. \tag{3.139}$$

In contrast, the cross-spectrum $S^p_{vw}(n \cdot \omega_o)$ of periodic signals $v(t)$ and $w(t)$ is a discrete function (McConnell 1995, p. 41):

$$S^p_{vw}(n \cdot \omega_o) = \frac{1}{T} \int_t^{t+T} R^p_{vw}(\tau) \cdot e^{-i \cdot n \cdot \omega_o \cdot \tau} \, d\tau . \tag{3.140}$$

Finally, it is pointed out that the different definitions lead to different units of auto- and cross-spectra $S_{vw}(\omega)$ (and $S_{vw}(f)$) for all three signal types (Table 3.2).

Table 3.2: Units of $S_{vw}(\omega)$ and $S_{vw}(f)$ for different types of signals.

Type of signals	Unit of $S_{vw}(\omega)$	Unit of $S_{vw}(f)$
Periodic	(unit of $v(t)$) · (unit of $w(t)$)	(unit of $v(t)$) · (unit of $w(t)$)
Transient	(unit of $v(t)$) · (unit of $w(t)$)/$(rad/s)^2$	(unit of $v(t)$) · (unit of $w(t)$)/Hz^2
Random	(unit of $v(t)$) · (unit of $w(t)$)/(rad/s)	(unit of $v(t)$) · (unit of $w(t)$)/Hz

3.2.1.3 Discrete Correlation Functions and Discrete Spectral Densities

Spectral densities of periodic, transient, and random vibrations were defined in equations (3.136), (3.139), and (3.140). These definitions are based on continuous time histories and continuous correlation functions. In practice, time domain signals $v(t)$ are usually available in discrete form. Separated by the time interval Δt, they are defined by L samples over an acquisition time T (3.141) and annotated as $v(k)$ with $k = 0, 1, 2, \ldots L-1$.

$$T = L \cdot \Delta t \tag{3.141}$$

Based on discrete time signals $v(k)$ and $w(k)$, discrete correlation functions $R_{vw}(r)$ and discrete spectral densities $S_{vw}(j)$ can be defined. This is done using the discrete sample shift r ($r = 0, 1, 2, \ldots L-1$) and discrete frequency values j ($j = 0, 1, 2, \ldots L-1$).

In case of periodic signals $v(t)$ and $w(t)$, the continuous cross-correlation function $R^p_{vw}(\tau)$ (3.138) and the discrete cross-spectra $S^p_{vw}(n \cdot \omega_o)$ (3.140) become (Newland 1993, p. 121f):

$$R_{vw}^{p}(r) = \frac{1}{T} \cdot \sum_{k=0}^{L-1} v(k) \cdot w(k+r) \cdot \Delta t = \frac{1}{L} \cdot \sum_{k=0}^{L-1} v(k) \cdot w(k+r) \tag{3.142}$$

and

$$S_{vw}^{p}(j) = \frac{1}{T} \cdot \sum_{r=0}^{L-1} R_{vw}^{p}(r) \cdot e^{-i \cdot j \cdot r \cdot 2 \cdot \pi / L} \cdot \Delta t = \frac{1}{L} \cdot \sum_{r=0}^{L-1} R_{vw}^{p}(r) \cdot e^{-i \cdot j \cdot r \cdot 2 \cdot \pi / L} \,. \tag{3.143}$$

The continuous correlation function $R_{vw}^{t}(\tau)$ (3.137) and the spectral density $S_{vw}^{t}(\omega)$ (3.139) of two transient signals $v(t)$ and $w(t)$ give:

$$R_{vw}^{t}(r) = \sum_{k=0}^{L-1} v(k) \cdot w(k+r) \cdot \Delta t = \frac{T}{L} \cdot \sum_{k=0}^{L-1} v(k) \cdot w(k+r) \tag{3.144}$$

and

$$S_{vw}^{t}(j) = T \cdot \sum_{r=0}^{L-1} R_{vw}^{t}(r) \cdot e^{-i \cdot j \cdot r \cdot 2 \cdot \pi / L} \cdot \Delta t = \frac{T^2}{L} \cdot \sum_{r=0}^{L-1} R_{vw}^{t}(r) \cdot e^{-i \cdot j \cdot r \cdot 2 \cdot \pi / L} \,. \tag{3.145}$$

Similarly, the discrete forms of the continuous functions $R_{vw}^{r}(\tau)$ (3.135) and $S_{vw}^{r}(\omega)$ (3.136) are:

$$R_{vw}^{r}(r) = \frac{1}{T} \cdot \sum_{k=0}^{L-1} v(k) \cdot w(k+r) \cdot \Delta t = \frac{1}{L} \cdot \sum_{k=0}^{L-1} v(k) \cdot w(k+r) \tag{3.146}$$

and

$$S_{vw}^{r}(j) = \sum_{r=0}^{L-1} R_{vw}^{r}(r) \cdot e^{-i \cdot j \cdot r \cdot 2 \cdot \pi / L} \cdot \Delta t = \frac{T}{L} \cdot \sum_{r=0}^{L-1} R_{vw}^{r}(r) \cdot e^{-i \cdot j \cdot r \cdot 2 \cdot \pi / L} \,. \tag{3.147}$$

In practice, only a limited number of data points L can be acquired. These data have to include a whole cycle (or its integer multiple) of a periodic signal. In case of transient signals, the acquired number of time samples L has to include the complete transient signal.

Random signals theoretically require the acquisition of an unlimited number of data points. This is not possible. However, it is possible to acquire several data blocks and average the frequency spectra of the blocks. This is permissible because only stationary ergodic random signals are considered and, therefore, "both ensemble (averaging across many time history records at a given instant in time) and temporal (averaging over time using one time history) calculations give the same

mean, mean square and statistical distributions" (McConnell 1995, p. 48). The more data blocks are employed, the closer the results of the analysis are to the assumption of infinite data acquisition time.

In general, the procedure of averaging is also used for periodic and transient signals. This is done because averaging reduces the influence of uncorrelated noise that is superimposed on and always present in real-life digitised signals (Maia et al. 1997, p. 90; Ewins 2000, p. 226).

3.2.1.4 Discrete Fourier Transformation

The only difference between the discrete formulations of $R_{vw}(\tau)$ and $S_{vw}(\omega)$ for periodic, transient, or random signals $v(t)$ and $w(t)$ is a constant factor (equations (3.142) to (3.147)). This similarity enables the computation of discrete versions of auto- and cross-spectra $S_v(\omega)$ and $S_{vw}(\omega)$ (and finally FRFs), of all three types of time signals with the same algorithm. This algorithm employs the discrete Fourier transformation (DFT).

The DFT uses discrete time domain signals $v(k)$ $(k = 0, 1, 2, \ldots L-1)$. The length of the signal, the data acquisition time, is T (3.141). The sampling frequency $f_{samp.}$ of such a signal is defined by the time steps Δt between the L samples:

$$f_{samp.} = \frac{1}{\Delta t} = \frac{L}{T}. \tag{3.148}$$

The discrete time history $v(k)$ is assumed to be periodic with the period T. It can then be described by a Fourier series (3.116) with a fundamental circular frequency:

$$\omega_0 = \frac{2 \cdot \pi}{T}. \tag{3.149}$$

The corresponding discrete spectrum $V(j)$ (3.127) has a frequency resolution:

$$\Delta f = \frac{\omega_0}{2 \cdot \pi} = \frac{1}{T} = \frac{1}{L \cdot \Delta t} = \frac{f_{samp.}}{L}. \tag{3.150}$$

Employing the parameters L, Δt, and ω_o, equations (3.116) and (3.127) of the periodic Fourier transformation can be transferred into a discrete FT pair (3.151) and (3.152) (Ewins 2000, p. 542f; Randall 1987, p. 28; James et al. 1999, p. 407).

$$v(k) = \sum_{j=0}^{L-1} V(j) \cdot e^{i \cdot j \cdot \omega_o \cdot k \cdot \Delta t} \tag{3.151}$$

$$V(j) = \frac{1}{T} \cdot \sum_{k=0}^{L-1} v(k) \cdot e^{-i \cdot j \cdot \omega_o \cdot k \cdot \Delta t} \cdot \Delta t = \frac{1}{L} \cdot \sum_{k=0}^{L-1} v(k) \cdot e^{-i \cdot j \cdot \omega_o \cdot k \cdot \Delta t} \tag{3.152}$$

The discrete spectrum $V(j)$ is defined for $j = 0, 1, 2, \ldots L-1$ at circular frequencies $\omega = j \cdot \omega_o$ (and frequencies $f = j \cdot \Delta f$). It contains redundant information in a way that:

$$V(L-j) = V(j)^* \tag{3.153}$$

for $j = 1, 2, 3, \ldots L-1$ (Ewins 2000, p. 543).

This feature corresponds to the characteristic:

$$V(\omega) = V(-\omega)^* \tag{3.154}$$

of frequency spectra defined by the periodic or the continuous FT (equations (3.127) and (3.132)).

Finally, it is remarked that the DFT pair is sometimes defined with the factor $1/L$ associated to the inverse DFT (3.151) and not to the DFT (3.152). In this case, the DFT pair corresponds more closely to the continuous FT pair of equations (3.132) and (3.131) than to the discrete Fourier series as defined in equations (3.116) and (3.127). This definition is used in the software MATLAB (1999) for example. However, in this research, the DFT is used as defined by equations (3.151) and (3.152) because it is implemented in this form by the spectrum analyser employed.

3.2.1.5 Data Processing

Stationary random signals $v(t)$ and $w(t)$ can only be described in the frequency domain by spectral densities $S_{vw}(\omega)$. Therefore, an algorithm analysing periodic, transient, and stationary random vibrations has to compute cross-spectra $S_{vw}(\omega)$ for all three types of signal.

If the discrete time signals $v(k)$ and $w(k)$ are periodic, their discrete cross-spectra $S_{vw}(j)$ can be computed from the discrete spectra $V(j)$ and $W(j)$ (McConnell 1995, p. 344):

$$S^{p}_{vw}(j) = V(j)^{*} \cdot W(j). \tag{3.155}$$

Equation (3.155) can be obtained by substituting the correlation function $R^{p}_{vw}(r)$ (3.142) into the cross-spectrum $S^{p}_{vw}(j)$ defined by equation (3.143) (Newland 1993, p. 122f):

$$S^{p}_{vw}(j) = \frac{1}{L^2} \cdot \sum_{r=0}^{L-1} \sum_{k=0}^{L-1} v(k) \cdot w(k+r) \cdot e^{-i \cdot j \cdot r \cdot 2 \cdot \pi / L}. \tag{3.156}$$

Rewriting the last factor of this equation (3.156):

$$e^{-i \cdot j \cdot r \cdot 2 \cdot \pi / L} = e^{-i \cdot j \cdot r \cdot \omega_0 \cdot \Delta t} = e^{-i \cdot j \cdot (r+k-k) \cdot \omega_0 \cdot \Delta t} = e^{-i \cdot j \cdot (r+k) \cdot \omega_0 \cdot \Delta t} \cdot e^{i \cdot j \cdot k \cdot \omega_0 \cdot \Delta t}, \tag{3.157}$$

the cross-spectrum $S^{p}_{vw}(j)$ of periodic signals $v(k)$ and $w(k)$ becomes:

$$S^{p}_{vw}(j) = \left(\frac{1}{L} \cdot \sum_{k=0}^{L-1} v(k) \cdot e^{-i \cdot j \cdot k \cdot \omega_0 \cdot \Delta t} \right) \cdot \left(\frac{1}{L} \cdot \sum_{r=0}^{L-1} w(k+r) \cdot e^{-i \cdot j \cdot (r+k) \cdot \omega_0 \cdot \Delta t} \right). \tag{3.158}$$

Considering equation (3.152), equation (3.158) is the same as equation (3.155).

Equation (3.155) is usually implemented in commercial software. It is true if the signals $v(k)$ and $w(k)$ are periodic and, therefore, the DFT can be applied. Assuming that transient or random signals are also periodic, the same algorithm defining $S^{p}_{vw}(j)$ can still be used to compute $S^{t}_{vw}(j)$ and $S^{r}_{vw}(j)$ of transient and random signals. However, in addition to the calculation of equation (3.155), a factor has to be applied:

$$S^{t}_{vw}(j) = T^2 \cdot S^{p}_{vw}(j) = T^2 \cdot V(j)^{*} \cdot W(j) \tag{3.159}$$

and

$$S^{r}_{vw}(j) = T \cdot S^{p}_{vw}(j) = T \cdot V(j)^{*} \cdot W(j). \tag{3.160}$$

because of the slightly different definitions of the correlation functions and the auto- and cross-spectra.

Finally, it should be stressed that the units of the correlation functions $R_{vw}(\tau)$ and the auto- and cross-spectra $S_{vw}(\omega)$ depend on the type of signal (Tables 3.1 and 3.2). Similarly, the units of spectra $V(\omega)$ or $V(f)$ of a signal $v(t)$ depend on the signal type (Table 3.3).

Table 3.3: Units of $V(\omega)$ and $V(f)$ for different types of signals.

Type of signals	Unit of $V(\omega)$	Unit of $V(f)$
Periodic	unit of $v(t)$	unit of $v(t)$
Transient	(unit of $v(t)$)/(rad/s)	(unit of $v(t)$)/Hz
Random	(unit of $v(t)$) $/\sqrt{(rad/s)}$	(unit of $v(t)$) $/\sqrt{Hz}$

3.2.1.6 Calculation of FRFs

Employing auto- and cross-spectra ($S^p_{vw}(\omega)$, $S^t_{vw}(\omega)$ or $S^r_{vw}(\omega)$), FRFs can be computed from periodic, transient, and random excitations $F(t)$ and the corresponding responses $v(t)$.

Analytical descriptions of FRFs $H_{jk}(\omega)$ relating the response at DOF j to a steady-state sinusoidal excitation at DOF k were derived in section 3.1.3. Experimentally, FRFs $H_{jk}(\omega)$ can be estimated as (Ewins 2000, p. 237; McConnell 1995, p. 337):

$$H_1(\omega) = \frac{S_{Fv}(\omega)}{S_{FF}(\omega)} \tag{3.161}$$

or

$$H_2(\omega) = \frac{S_w(\omega)}{S_{vF}(\omega)}. \tag{3.162}$$

In principle, the two FRF estimators $H_1(\omega)$ and $H_2(\omega)$ should result in the same function. However, $H_1(\omega)$ and $H_2(\omega)$ are affected differently by instrumentation noise (McConnell 1995, p. 345ff; Maia et al. 1997, p. 10ff), which is always present in measurements. Additionally, it is important to note that extraneous excitation (McConnell 1995, p. 352ff), which can (involuntarily) be induced by people on a structure, always affects $H_2(\omega)$. This is because this unmeasured additional excitation

influences the response and thus the response auto-spectrum $S_w(\omega)$ that is used to calculate $H_2(\omega)$ (equation (3.162)). However, if the unmeasured additional excitation is uncorrelated to the measured excitation, it has no effect on the FRF estimator $H_1(\omega)$ (3.161) because it does not affect the cross-spectrum $S_{Fv}(\omega)$. Therefore, the FRF estimator $H_1(\omega)$ is used throughout this research to define FRFs.

To assess the deviation of the two FRF estimators $H_1(\omega)$ and $H_2(\omega)$, the coherence $\gamma^2(\omega)$ is generally computed:

$$\gamma^2(\omega) = \frac{S_{Fv}(\omega) \cdot S_{vF}(\omega)}{S_{FF}(\omega) \cdot S_w(\omega)}. \tag{3.163}$$

The coherence $\gamma^2(\omega)$ can have values ranging from zero to unity. Unity coherence indicates that the FRF estimator $H_1(\omega)$ equals $H_2(\omega)$ because:

$$\gamma^2(\omega) = \frac{H_1(\omega)}{H_2(\omega)}, \tag{3.164}$$

considering equation (3.163) in conjunction with (3.161) and (3.162).

Coherence values lower than unity indicate the influence of instrumentation noise, structural non-linearities, extraneous excitation, and leakage (McConnell 1995, p. 341; Maia et al. 1997, p. 103; Ewins 2000, p. 241 and p. 238). The issue of leakage is introduced in section 3.2.3, which considers issues of signal processing.

3.2.2 Data Acquisition

Forced vibrations investigated in this research are described by excitations and responses. Employing transducers, these excitations and responses can be measured and represented as analogue electrical signals. In order to be processed digitally, the analogue electrical signals are quantized and sampled in the time domain by a digital signal analyser. Issues of quantisation and sampling are outlined below.

3.2.2.1 Parameters of Digitisation

The quantisation capabilities of a digital signal analyser are specified by its dynamic range. The signal analyser used in this research (SignalCalc430) has a dynamic range of 108 dB. This dynamic range is a consequence of the 18-bit resolution of the input converter (3.165), which can quantize an analogue signal by 2^{18} (262,144) numbers (Maia et al. 1997, p. 94).

$$20 \cdot \log_{10}\left(2^{18}\right) = 108\ dB \tag{3.165}$$

The time sampling of an analogue signal is specified by the sampling frequency $f_{samp.}$. The signal analyser SignalCalc430 can sample in time intervals Δt ranging from 0.012 ms to 49.152 ms and has sampling frequencies $f_{samp.}$ ranging from 20 Hz to 83 kHz (Data Physics 1998, p. 140).

Most spectrum analysers are limited to L of about 2000 samples limiting the computational effort in the DFT. Therefore, choosing a high sampling frequency $f_{samp.}$ (small time steps Δt) restricts the data acquisition time T (3.141) and the frequency resolution Δf (3.150). Hence, an optimal choice of the sampling parameters has to be made. Additionally, it has to be noted that the quantisation and sampling of analogue signals can introduce significant errors (Maia et al. 1997, p. 95f).

3.2.2.2 Quantisation and Sampling Errors

Common signal quantisation errors are overranging (overloading, clipping) and underranging (Maia et al. 1997, p. 96). Overranging occurs if the analogue signal exceeds the voltage range of the signal analyser. On the other hand, underranging results from using only a small fraction of the dynamic range. Both errors can be avoided by carefully selecting the voltage range.

Another serious error is aliasing. It is introduced if the sampling is too slow. It results in analogue signals containing high frequency components that cannot be separated from lower frequency components.

Aliasing occurs if the analogue signal has components above half the sampling frequency (McConnell 1995, p. 271; Wright 1995, p. 275; Maia et al. 1997 p. 94; Ewins 2000, p. 213). To make sure that no such higher components exist, commercial signal analysers apply a low-pass anti-aliasing filter before sampling the analogue signal (McConnell 1995, p. 269). However, filtering also modifies the signal in the passing frequency range (McConnell 1995, p. 269f; Wright 1995, p. 292).

Therefore, the signal analyser SignalCalc430 used here has, for example, a useful frequency range f_{max} of only 24% of the sampling frequency $f_{samp.}$ (Data Physics 1998, p. 140).

3.2.3 Signal Processing by a Spectrum Analyser

Sampled signals are usually processed by a spectrum analyser that is combined with a signal analyser digitising the data in one unit. Digitisation and sources of error were outlined in the previous section 3.2.2. In this section, the process of estimating FRFs and coherences from digitised excitations $F(t)$ and corresponding digitised responses $v(t)$ is outlined.

A spectrum analyser uses the same algorithm to process data of periodic, transient, or random time histories (Randall 1987, p. 227; McConnell 1995, p. 344). This process can be divided into four steps (Figure 3.5). Step 1 is windowing (McConnell 1995, p. 288ff; Maia et al. 1997, p. 91ff; Ewins 2000, p. 216ff) of time histories ($F(t)$ and $v(t)$) and transforming them into the frequency domain ($F(f)$ and $V(f)$). Step 2 is the computation of auto-spectra and cross-spectra $G(f)$. Step 3 is averaging of these spectra to $\overline{G}(f)$, and, finally, Step 4 is the calculation of the FRF estimator $H_1(f)$ and the coherence $\gamma^2(f)$.

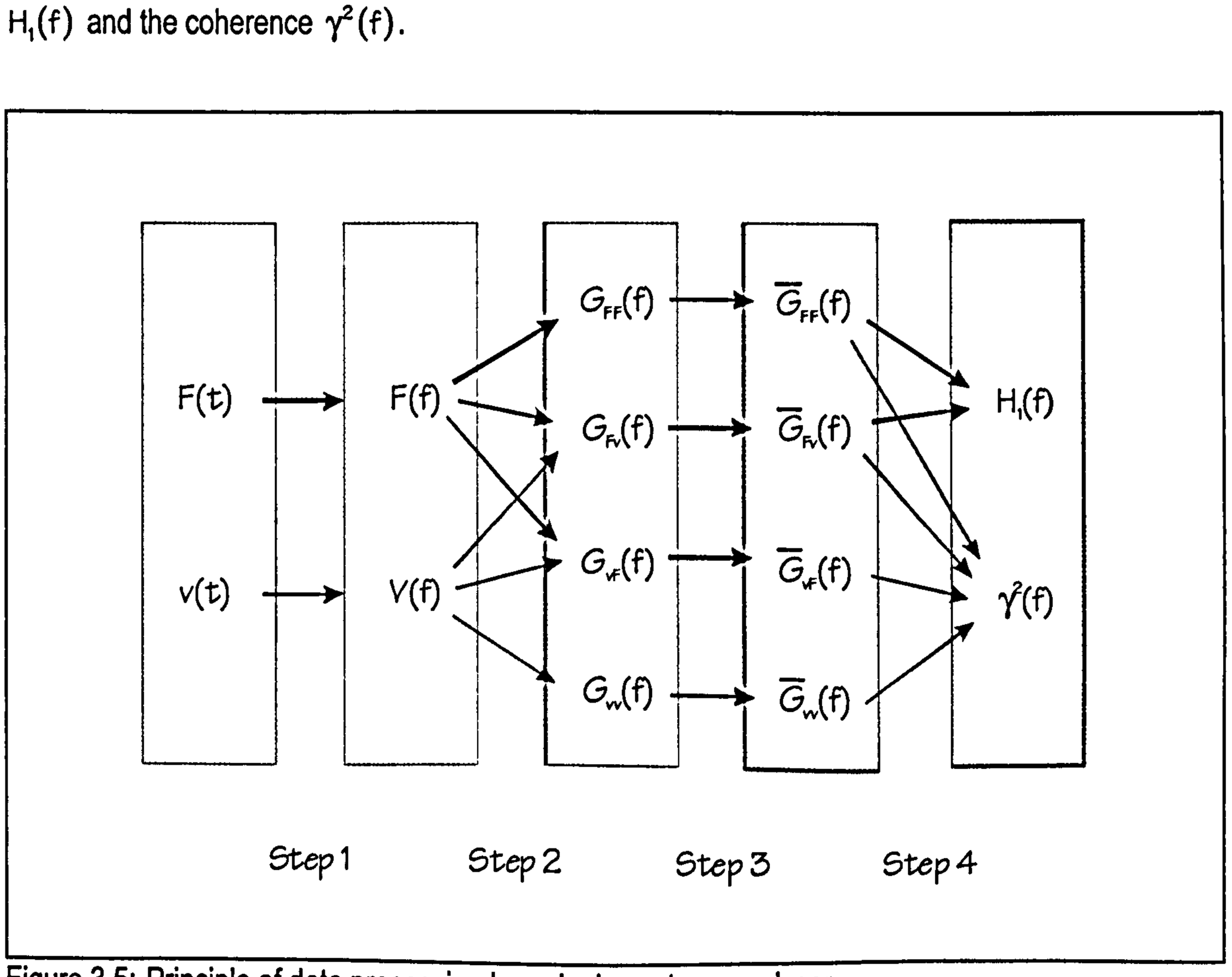

Figure 3.5: Principle of data processing by a dual spectrum analyser.

Following, each step is outlined in more detail and their implementation by the spectrum analyser DP430 (Data Physics 1998; Data Physics 1999) is outlined. This is important because formulae and parameters employed by this spectrum analyser are incompletely and contradictorily presented in the manual.

3.2.3.1 STEP 1

In experimental modal analysis, discrete time domain signals are acquired in data blocks, each limited to a duration T. These data blocks are transferred into the frequency domain using the DFT (section 3.2.1.4). The DFT is usually implemented by the fast Fourier transform (FFT) algorithm, which significantly reduces the computational effort (Maia et al. 1997, p. 97ff).

Using the DFT requires the signals to be periodic within the data acquisition time T. However, that is generally not the case and results in a resolution error called leakage (McConnell 1995, p. 73ff; Maia et al. 1997, p. 91; Ewins 2000, p. 215ff). In order to reduce leakage, time domain signals are forced to be periodic by multiplication with a window function. Several window functions are used in experimental modal analysis (McConnell 1995, 302ff; Maia et al. 1997, p. 92f; Ewins 2000, p. 216ff). In this research, the Hanning window (Maia et al. 1997, p. 92; Ewins 2000, p. 218) and the exponential window (Taber et al. 1985) are employed.

The Hanning window $w_H(t)$ (3.166) forces the signal to zero at the beginning and the end of the data acquisition time T. It is often used in connection with continuous random vibrations.

$$w_H(t) = 0.5 \cdot \left(1 - \cos\left(\frac{2 \cdot \pi \cdot t}{T}\right)\right) \quad (0 \le t \le T) \tag{3.166}$$

This research employs random and more often transient signals. Transient signals contain relevant information especially at the beginning of the data acquisition time T. Therefore, an exponential window $w_E(t)$ (equations (3.167) and (3.168)) is used for transient signals instead of the Hanning window $w_H(t)$.

$$w_E(t) = e^{-\frac{t}{RC}} \quad (0 \le t \le T) \tag{3.167}$$

$$RC = -\frac{T}{\log_e P} \tag{3.168}$$

Assuming, that the transient signal is zero at the beginning of the data acquisition time T, an exponential window makes the signal periodic artificially. This is done by reducing the already transient signal to smaller values towards the end of the data acquisition time T. In particular, the time constant RC (3.168) specifies to which percentage P the original signal is reduced to at the end of the data acquisition time T (Dynamic Testing Agency (DTA) 1993, Module 10, p. 19).

The spectrum analyser DP 430 used in this research specifies the exponential window via the parameter $(-log_e(P))^{-1}$. Other spectrum analysers are likely to use a different definition such as $-log_e(P)$ for instance.

Using digitised and windowed time histories of $F(t)$ and $v(t)$, the discrete spectra $F(j)$ and $V(j)$ can be computed (equation (3.152) in section 3.2.1.4). The spectrum analyser used in this research presents the spectra $F(j)$ and $V(j)$ as function of the frequency f and not of the circular frequency ω.

In equation (3.152) in section 3.2.1.4, discrete spectra $V(j)$ were defined at L discrete frequencies ($f = j \cdot \Delta f$). Half the values of $V(j)$ ($j = 0, 1, 2, \ldots L$) determine the spectrum uniquely (equation (3.153)). In practice, less values of the spectra are available because of the anti-aliasing filter (section 3.2.2). That is, the discrete frequency spectrum $V(j)$ covers frequencies from zero to f_{max} ($f_{max} < L/2 \cdot \Delta f$) only.

Such discrete spectra $V(j)$ ($f = 0, \Delta f, 2 \cdot \Delta f, \ldots f_{max}$) are provided by the spectrum analyser DP 430 as single-sided spectra $V^{DP}(f)$. A discrete single-sided spectrum $V^{DP}(f)$ ($f_{max} < 0.5 \cdot (L-1) \cdot \Delta f$) can be computed from a discrete (double-sided) spectrum $V(f)$ ($0 \le f \le (L-1) \cdot \Delta f$) as outlined in equations (3.169) and (3.170) (McConnell 1995, p. 284).

$$V^{DP}(0) = V(0) \tag{3.169}$$

$$V^{DP}(f) = 2 \cdot V(f) \quad (f = \Delta f, 2 \cdot \Delta f, \ldots f_{max}) \tag{3.170}$$

Internally, the spectrum analyser DP 430 denotes the spectrum of the windowed signal $v(t)$ acquired at channel 1 as $S1$.

3.2.3.2 STEP 2

Assuming signals always to be periodic, the spectrum analyser DP 430 computes cross-spectra $G_{Fv}^{DP}(f)$ in a way analogous to equation (3.155). However, equation (3.155) employs double-sided spectra $V(j)$ and $W(j)$ to define double-sided auto- or cross-spectra $S(j)$. In contrast, DP 430 computes single-sided cross-spectra $G_{Fv}^{DP}(f)$ from single-sided spectra $F^{DP}(f)$ and $V^{DP}(f)$ of the windowed excitation and response respectively. Therefore, equation (3.155) changes to:

$$G_{Fv}^{DP}(f) = \frac{1}{2} \cdot \left(F^{DP}(f)\right)^{*} \cdot V^{DP}(f). \tag{3.171}$$

The spectrum analyser DP 430 denotes a single-sided cross-spectrum $G_{Fv}^{DP}(f)$ of two signals acquired at channels 1 ($F(t)$) and 2 ($v(t)$) as $S1\_2$.

Unexpectedly, DP 430 does not employ equation (3.171) to compute auto-spectra $G_{FF}^{DP}(f)$ or $G_{w}^{DP}(f)$. In contrast, equation (3.172) is employed.

$$G_{w}^{DP}(f) = \sqrt{\left(V^{DP}(f)\right)^{*} \cdot V^{DP}(f)}\,. \tag{3.172}$$

Consequently, cross-spectra of periodic signals $G_{Fv}^{DP}(f)$ can be taken directly from the spectrum analyser (3.173). In contrast, auto-spectra $G_{FF}^{p}(f)$ and $G_{w}^{p}(f)$ have to be corrected (3.174).

$$G_{Fv}^{p}(f) = G_{Fv}^{DP}(f) \tag{3.173}$$

$$G_{w}^{p}(f) = \frac{1}{2}\left(G_{w}^{DP}(f)\right)^{2} \tag{3.174}$$

As outlined in section 3.2.1.5, auto- and cross-spectra of transient, random, and periodic signals differ by a factor (equations (3.159) and (3.160)). Therefore, auto- or cross-spectral densities of transient $G^{t}(f)$ or random $G^{r}(f)$ signals can only be obtained by further manipulation of the auto- or cross-spectra $G^{p}(f)$ (equations (3.175) and (3.176)).

$$G^{t}(f) = T^{2} \cdot G^{p}(f) \tag{3.175}$$

$$G^{r}(f) = T \cdot G^{p}(f) \tag{3.176}$$

3.2.3.3 STEP 3

FRFs are generally computed from averaged auto- or cross-spectra to reduce the influence of random noise (Clough and Penzien 1993, p. 485; Maia et al. 1997, p. 90; Ewins 2000, p. 226). Averaged single-sided auto- or cross-spectra $\overline{G}_{vw}(f)$ are obtained by acquiring a number k of data blocks and averaging of the corresponding k single-sided auto- or cross-spectra $G_{vw}(f)$ (3.177).

$$\overline{G}_{vw}(f) = \frac{1}{k}\sum_{k} G_{vw}(f) \tag{3.177}$$

Thereby, the spectrum analyser DP 430 employs $G_{vw}^{DP}(f)$ and $G_{v}^{DP}(f)$ as defined in equations (3.171) and (3.172). The resulting averaged auto- and cross-spectra $\overline{G}_{v}^{DP}(f)$ and $\overline{G}_{vw}^{DP}(f)$ are annotated by DP 430 with the letter G in contrast to S defining single-sided auto- and cross-spectra $G_{v}^{DP}(f)$ and $G_{vw}^{DP}(f)$.

It is noted that averaging can increase the overall data acquisition time significantly. This can be counteracted to some extend by overlapping of data blocks. A detailed account of this issue is provided by McConnell (1995, p. 304ff).

3.2.3.4 STEP 4

In the last step of data processing performed by a spectrum analyser, the FRF estimator $H_1(f)$ is computed from averaged single-sided spectra $\overline{G}_{Fv}(f)$ and $\overline{G}_{FF}(f)$ (McConnell 1995, p. 336):

$$H_1(f) = \frac{\overline{G}_{Fv}(f)}{\overline{G}_{FF}(f)}. \tag{3.178}$$

If the auto- and cross-spectra $\overline{G}_{FF}^{DP}(f)$ and $\overline{G}_{Fv}^{DP}(f)$ of the spectrum analyzer DP 430 are employed to compute the FRF estimator $H_1(f)$, equation (3.178) transforms into:

$$H_1(f) = \frac{2 \cdot \overline{G}_{Fv}^{DP}(f)}{\left(\overline{G}_{FF}^{DP}(f)\right)^2}. \tag{3.179}$$

Spectrum analysers generally also provide the coherence $\gamma^2(f)$. It can, analogous to equation (3.163), be estimated using single-sided spectra (McConnell 1995, p. 338):

$$\gamma^2(f) = \frac{\overline{G}_{Fv}(f) \cdot \overline{G}_{vF}(f)}{\overline{G}_{FF}(f) \cdot \overline{G}_{w}(f)}. \tag{3.180}$$

The computation of the coherence $\gamma^2(f)$ from auto- and cross-spectra provided by DP 430 (3.181) requires adaptation because of the definition of auto-spectra $\overline{G}_{FF}^{DP}(f)$ and $\overline{G}_{w}^{DP}(f)$ (equation (3.171)). Additionally, DP 430 computes only $\overline{G}_{Fv}(f)$ and not $\overline{G}_{vF}(f)$, which is employed in equation (3.180). However, $\overline{G}_{vF}(f)$ equals the complex conjugate of $\overline{G}_{Fv}(f)$ (McConnell 1995, p. 41). Consequently, equation (3.179) can be expressed as equation (3.181).

$$\gamma^2(f) = \frac{4 \cdot \overline{G}_{Fv}^{DP}(f) \cdot \left(\overline{G}_{Fv}^{DP}(f)\right)^*}{\left(\overline{G}_{FF}^{DP}(f)\right)^2 \cdot \left(\overline{G}_{w}^{DP}(f)\right)^2}. \tag{3.181}$$

FRFs resulting from the analysis of experimental data by a spectrum analyzer can be curve-fitted to extract the modal properties of the system under investigation. This issue is outlined briefly in the next section.

3.2.4 Modal Parameter Extraction

This section outlines some relevant issues related to the identification of modal parameters.

3.2.4.1 Methods

This research concentrates on the estimation of modal properties from experimentally estimated FRFs. Several frequency domain curve-fitting procedures are available for this type of analysis (Maia et al. 1997; Ewins 2000).

Of particular interest are indirect methods (Maia et al. 1997, p. 188) that estimate modal properties (in contrast to direct methods that estimate spatial properties). Indirect methods can be grouped in two different ways. On one hand, they are divided according to the number of modes present in the experimental data into single-mode (SDOF) and multi-mode (MDOF) methods. On the other hand, they are distinguished by the number of simultaneous input and output signals into single-input single-output (SISO), single-input multi-output (SIMO), and multi-input multi-output (MIMO) methods (Maia et al. 1997, p. 218).

In this research, SIMO measurements were made. Hence, SDOF and MDOF SISO and SIMO procedures can be used to determine modal properties. In particular, the SISO FRF curve-fitting procedures such as circle-fit (Maia et al. 1997, p. 219ff; Ewins 2000, p. 309ff; ICATS 2000b, p. 19f) and line-fit (Maia et al. 1997 p. 227ff; Ewins 2000, p. 318ff; ICATS 2000b, p. 21f) were used in preliminary investigations. Final estimates were made with the MDOF SIMO non-linear least squares algorithms NLLS1 and NLLS2 (ICATS 2000b, p. 27ff). They were based on prior estimates obtained by the MDOF SISO method MDOF Ident (ICATS 2000b, p. 25f).

3.2.4.2 Correction of Estimated Modal Properties

Modal properties estimated with any curve-fitting procedure have to be used carefully considering the parameters of data acquisition. This is because applying a window function to the experimental time histories to reduce leakage distorts the time histories. Therefore, the window influences estimated FRFs and thus the modal properties identified from these FRFs.

The effect of a Hanning window cannot be removed from the modal properties and it is necessary to use FRF estimates that are more or less distorted. However, the effect of an exponential window can be removed. This is because the exponential window applies a factor in the time domain that leads to specific changes in the frequency domain. This effect on the eigenvalue (that is the natural frequency and the damping ratio) can be removed (Fladung and Rost 1997).

In particular, the correct circular natural frequency ω_r (3.182) and the damping ratio ζ_r (3.183) can be calculated using the time constant RC of the exponential window, the circular natural frequency $\omega_{e,r}$, and the damping ratio $\zeta_{e,r}$ estimated by curve-fitting of the 'windowed' FRF (Fladung and Rost 1997).

$$\omega_r = \sqrt{\omega_{e,r}^2 \cdot \left(1-\zeta_{e,r}^2\right)+\left(\zeta_{e,r}\cdot\omega_{e,r}-\frac{1}{RC}\right)^2} \tag{3.182}$$

$$\zeta_r = \zeta_{e,r}\cdot\frac{\omega_{e,r}}{\omega_r}-\frac{1}{RC\cdot\omega_r} \tag{3.183}$$

It should also be mentioned that the effect of the exponential window on the natural frequency is often ignored. That is, it is assumed that $\omega_r \approx \omega_{e,r}$. In this case, the correct damping ratio ζ_r is (Clark et al. 1989; Fladung and Rost 1997):

$$\zeta_r = \zeta_{e,r} - \frac{1}{RC \cdot \omega_{e,r}}. \tag{3.184}$$

In this research, both methods lead to practically identical frequencies and damping ratios.

3.3 Analysis of Experimental and Analytical Data

The theory of analytical and experimental modal analysis was outlined in the previous sections. In this section, some additional theoretical background is provided. It is used particularly in the identification and verification of a dynamic model of human occupants.

3.3.1 Statistics

Introducing some fundamental statistics, the sample mean value $\bar{x}$:

$$\bar{x} = \frac{1}{n} \cdot \sum_{j=1}^{n} x_j \tag{3.185}$$

and the standard deviation s_x:

$$s_x = \sqrt{\frac{1}{n-1} \cdot \sum_{j=1}^{n} (x_j - \bar{x})^2} \,. \tag{3.186}$$

of n samples x_j of the value x are defined (Dally 1993, p. 1033). Additionally, a confidence interval is defined.

A confidence interval specifies the range of the true mean value μ of the analysed value x with a particular confidence (Rees 1995, p. 93ff). Assuming that the samples x_j follow a normal (Gaussian) distribution, the confidence interval is defined by the n samples of x and the chosen confidence level. In case of a small number of samples n (less than 20), the confidence interval is (Dally 1993, p. 1034ff):

$$(\bar{x} - \delta) < \mu < (\bar{x} + \delta) \tag{3.187}$$

with

$$\delta = \frac{t(\alpha, \nu)}{\sqrt{n}} \cdot s_x \,. \tag{3.188}$$

The term $t(\alpha,\nu)$ (Student's t) is specified by the ascertained confidence level and the degrees of freedom ν ($\nu = n-1$) (Dally 1993, p. 1041).

In civil engineering, a confidence level (confidence coefficient) of 95% ($\alpha = 0.05$) is usually applied. Using this value and setting the number of samples n to 5, the value of t ($\alpha = 0.05$, $\nu = 4$) is 2.776 (Montgomery and Runger 1999, p. A-6). Thus, equation (3.187) becomes equation (3.189), which defines the 95%-confidence interval of five samples of x.

$$(\bar{x} - 1.24 \cdot S_x) < \mu < (\bar{x} + 1.24 \cdot S_x) \tag{3.189}$$

This confidence interval will be used in chapter 6 to characterise the parameters of a damped SDOF model of human occupants.

Finally, it is noted that in this research, the confidence interval has an upper and a lower limit. Therefore, $t(\alpha/2,\nu)$ has to be used in a table specifying $t(\alpha,\nu)$ of a confidence interval with either an upper or a lower limit.

3.3.2 Compatibility of Modal Masses

The modal masses m_r of generally damped MDOF systems were defined in equation (3.56) in section 3.1.1.5 by the mass matrix $[M]$ and the mode shapes $\{\psi\}_r$. The mass matrix is defined by spatial properties. However, the mode shapes can be scaled arbitrarily (see section 3.1.1.3). Therefore, the value of modal mass m_r depends on the scaling of the mode shape $\{\psi\}_r$. In chapter 4 and 5 of this research, modal masses are calculated from mode shapes normalised to unity. That is, the complex mode shape element with the maximum amplitude (the antinode of the mode) is unity.

In case of modal masses m_r estimated from the (complex) mass-normalised mode shapes $\{\psi\}_r$ estimated by the modal analysis software ICATS (2000b, appendix F1), this means:

$$m_r = \frac{1}{\psi_{nr} \cdot \psi_{nr}^*}. \tag{3.190}$$

Thereby, point n is the antinode of mode r, thus, it corresponds to TP 5 or 7 (chapter 5, Figure 5.5).

In chapter 6, experimental and analytical data shall be correlated. This requires the normalisation of mode shapes to a common reference. This reference point is TP 5 or TP 7, which corresponds to the structural DOF of damped 2-DOF human-structure models (Figure 3.2b).

3.3.3 Calculating Response Time Histories using Impulse Response Functions

In chapter 6, the quality of the identified human-structure systems is evaluated using response time histories. This can be done by using the theory outlined in section 3.1.1.4. However, it is possible to use a simpler approach because the system is excited at only one DOF. This approach employs the inverse FT of the FRF, the impulse response function (IRF), and convolution as outlined next (Ewins 2000, p. 135ff).

The IRFs $h_{jk}(t)$ of a N-DOF system (3.191) relate the response $x_j(t)$ at point j to an impulse $F_k(t=O)$ at point k (Ewins 2000, p. 137).

$$h_{jk}(t) = \sum_{r=1}^{N} \left({}_rA_{jk} \cdot e^{-\lambda_r \cdot t} + {}_rA^*_{jk} \cdot e^{-\lambda^*_r \cdot t} \right) \tag{3.191}$$

This form of expressing the IRF (3.191) corresponds to the presentation of the FRF $H_{jk}(t)$ as given by equation (3.97) in section 3.1.3.1.

Using the IRF, the response of a system can be estimated not only to an impulse at $F_k(t=O)$ but to a continuous excitation $F_k(t)$. This is done by splitting the continuous excitation $F_k(t)$ into a series of impulses $F_k(t=\tau)$. The responses $x_j(t>\tau)$ to each of these impulses are added up to the overall response $x_j(t)$:

$$x_j(t) = \int_{-\infty}^{\infty} F_k(\tau) \cdot h_{jk}(t-\tau)\, d\tau. \tag{3.192}$$

This equation (3.192) is called time domain convolution or Duhamel integral. It is often expressed in form of equation (3.193) (McConnell 1995, p. 94; Inman 2001, p. 118).

$$x_j(t) = F_k(t) * h_{jk}(t) \tag{3.193}$$

In this research, response time histories are calculated using the convolution function provided in MATLAB (1999).

3.3.4 Removing the Effect of an Exponential Window from FRFs

Finally, it has to be analysed how an exponential window $w_E(t)$ (which is applied to reduce leakage) affects an entire FRF and not only extracted modal properties (section 3.2.4.2). This issue is addressed in updating of damped SDOF human models (chapter 6).

The effect of an exponential window $w_E(t)$ on any FRF $H_{jk}(\omega)$ can be removed. This is done by applying an exponential window $w_{E+}(t)$ (3.194).

$$w_{E+}(t) = e^{+\frac{t}{RC}} \quad 0 \le t \le T \tag{3.194}$$

This window $w_{E+}(t)$ cancels the effect of the exponential window $w_E(t)$ (equation (3.164) in section 3.2.3). It has to be applied in the time domain. Therefore, the IRF $h_{jk}(t)$ of the FRF $H_{jk}(t)$ has to be computed using the inverse FT (see section 3.2.1). Then, the window $w_{E+}(t)$ can be applied in the time domain to the IRF $h_{jk}(t)$ and leads to the corrected IRF $h_{jk}^{corr}(t)$:

$$h_{jk}^{corr}(t) = w_{E+}(t) \cdot h_{jk}(t). \tag{3.195}$$

Transferring the corrected IRF $h_{jk}^{corr}(t)$ back into the frequency domain leads to an FRF $H_{jk}^{corr}(\omega)$ that is not distorted by the exponential window.

It is important to note that the IRF $h_{jk}^{corr}(t)$ is characterised by a high amplification of small (noise) values as t approaches T. That results in large values and the IRF is not transient (and thus periodic with an infinite period T) anymore. This effect can deny a successful application of the discrete FT.

4. Analytical Parametric Study

This parametric study discusses the possible influence of human occupants on the modal properties of lightly damped and slender civil engineering structures from a theoretical point of view.

4.1 Introduction

The dynamic influence of human occupants on modal properties of a structure is a very complex and not well-understood issue (IStructE 2001, p. 8). To obtain insight into this phenomenon, an analytical parametric study of the human-structure dynamic system is performed.

4.1.1 Modelling the Human-Structure System

The human-structure system is difficult to comprehend if the distribution of people over the structure, individual dynamic properties of each person, and the movement of people have to be included.

Therefore, some simplifications are made in this parametric study. In particular, the human-structure system is simplified by assuming:

(1) The modal properties of the human and structure are linear and time-invariant.

(2) An arbitrary number of occupants can be modelled with a single human model.

(3) Occupants are stationary and in continuous contact with the structure.

(4) The structure itself can be modelled as a SDOF system.

Assumption (1) is an essential simplification that enables the use of linear modal analysis. Linearity and time-invariance of civil engineering structures can often be assumed. Linearity and time-invariance of the modal properties of humans are justified by the small degree of non-linearity observed in biomechanic research (Griffin 1990), which considers significantly higher levels of vibration than commonly encountered in civil engineering. Furthermore, probable changes of modal

properties of individual bodies are likely to be insignificant compared to differences between people (Griffin 1990).

Assumptions (2), (3), and (4) are used to simplify the human-structure system considered. Assumption (2) is made to enable easy handling of crowds. The simplification of assumption (3) is valid if occupants are sitting or standing. These are activities performed most of the time by occupants on assembly structures, such as floors and stadia. However, occupants of gymnasia and footbridges are more likely to jump or walk and are not in continuous contact with the structure. In this case, assumption (3) is not satisfied. Assumption (4) is satisfied if the modes of the empty structure are not closely spaced. That is often, but not always, the case.

Based on these limits set by assumptions (2), (3) and (4), further parametric studies into human-structure systems without these simplifications should be performed in the future.

4.1.1.1 Human-Structure Models

Employing the four assumptions outlined above, three human-structure models are used. In all three cases, the structure is modelled as a SDOF system (assumption (4)). Stationary human occupants are in the civil engineering commonly modelled as an additional mass to the structure (section 2.1.2). Taking this mass-only model of human occupants, the human-structure system is a damped SDOF system (Figure 4.1a).

Nevertheless, a need has emerged to model human occupants not just as mass but as a complete SDOF dynamic system (chapter 2). Prompted by this insight, Ellis and Ji (1997) proposed to model the human-structure system as an undamped 2-DOF system (Figure 4.1b).

However, this undamped model ignores the high damping of the human body (Tables 2.3 and 2.4), which may affect the damping of the joint 2-DOF human-structure dynamic system. Therefore, a third human-structure model has been developed (Figure 4.1c). This damped 2-DOF model includes the damping capabilities of both the empty structure and the human occupants.

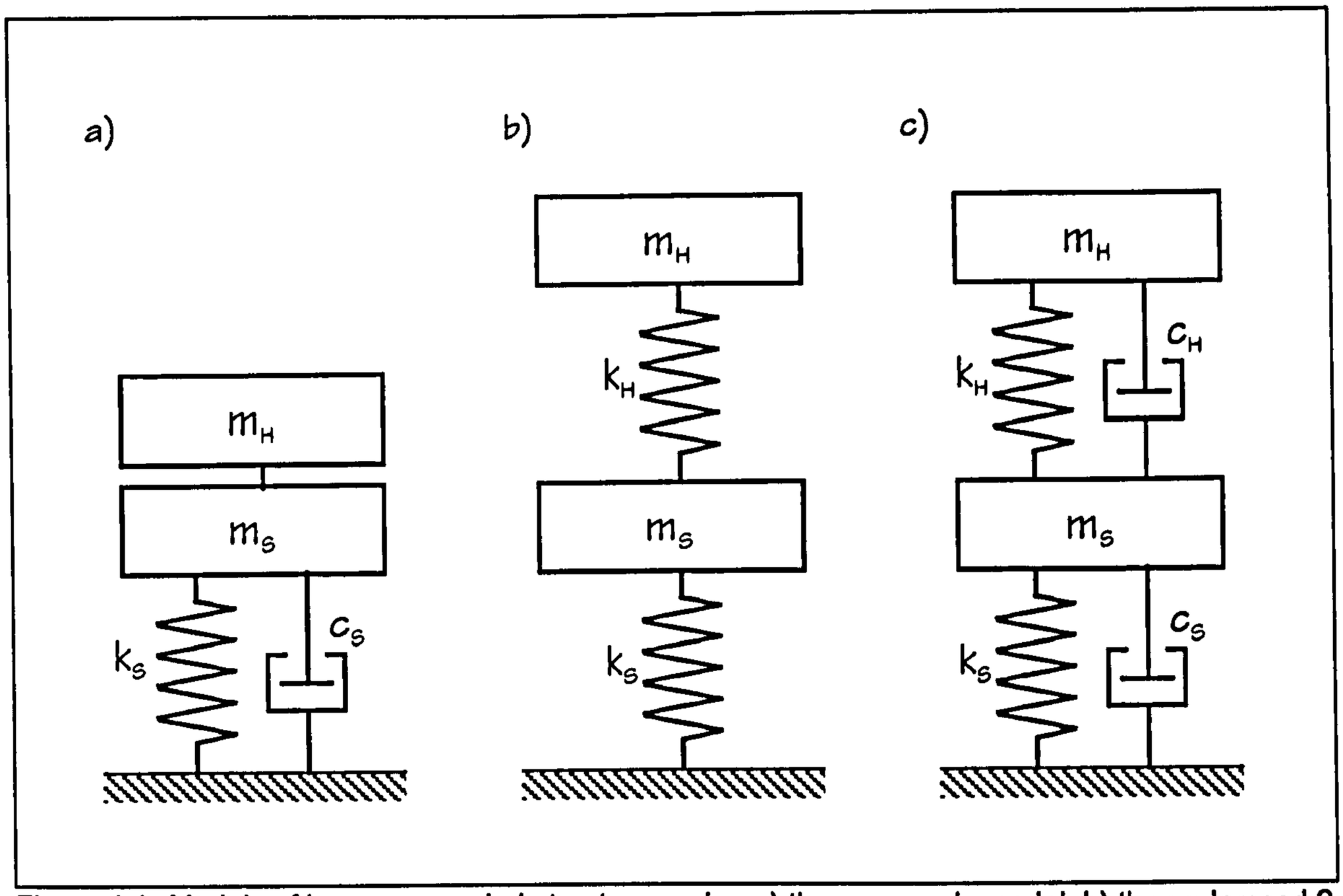

Figure 4.1: Models of human occupied structures using a) the mass-only model, b) the undamped 2-DOF model, and c) the damped 2-DOF model.

More complex human body models than the damped SDOF are nowadays used in biomechanics and have also been applied by civil engineers (chapter 2). However, vibrations of the whole human body are dominated by its fundamental mode. Therefore, it is unlikely that more than one mode of the human body is needed to model the influence of human occupants on the modal properties of structures with sufficient accuracy. Hence, such models are excluded from this study.

4.1.1.2 Parameters

Six parameters are needed to describe the three human-structure models in Figure 4.1 completely. These parameters are the lumped masses (m_s and m_H), the modal stiffnesses (k_s and k_H), and the viscous damping (c_s and c_H) of the structure and the human occupant(s), respectively. In order to simplify the analysis and presentation of the human-structure systems, the number of parameters is reduced to four.

First, the masses of the occupant m_H and the structure m_s are combined to a single parameter, the mass ratio α (Ellis and Ji 1997).

$$\alpha = \frac{m_H}{m_s} \tag{4.1}$$

In this parametric study, the mass ratio α is set to ratios 1%, 10%, 50%, and 100%. Therefore, occupation ranging from sparsely populated office floors to densely populated assembly structures is covered.

Secondly, the relation of the natural frequency of the human SDOF f_H to that of the structural SDOF f_s is expressed as frequency ratio β (Ellis and Ji 1997):

$$\beta = \frac{f_H}{f_s}. \tag{4.2}$$

Structures with low natural frequencies f_s are likely to have problems with human-induced vibrations. This is because they can easily be excited by walking, jumping etc. (IStructE 2001, p. 9). Therefore, structures with frequencies f_s up to 8 Hz are of primary interest in this study.

Natural frequencies of the human body f_H have been reported in the literature as ranging from 3 Hz to 16 Hz (chapter 2). Employing this frequency range and taking 1 Hz as the lower limit of the fundamental frequency of a structure f_s, frequency ratios β ranging from 0.4 to 16 can be expected. Having these boundaries in mind, the presentation focuses on frequency ratios β from 0 to 15.

Finally, the viscous damping (c_s and c_H) has to be specified. This is done using the damping ratios ζ_s and ζ_H of the structural and the human DOF (Figure 4.1c). The damping ratio of the structural DOF is set to a realistic value of ζ_s = 1%. The damping ratio of the SDOF model of the human body ζ_H has been set to two values: ζ_H = 30% and ζ_H = 50%. These high damping values are based on biomechanic research (ISO 1981).

4.1.2 Outline of the Parametric Study

This parametric study covers the three human-structure models presented in Figure 4.1 using the parameters defined in the previous paragraph. Each of these three simple human-structure models is characterised by natural frequencies, damping ratios, mode shapes and modal masses. However,

only natural frequencies are presented and discussed for all three models. Nevertheless, mode shapes, modal masses, and damping ratios of the most realistic damped 2-DOF human-structure model (Figure 4.1c) are presented. This damped model is also used to analyse the influence of occupants on structural FRFs. (The structural FRFs $A_s(f)$ and $A_{ss}(f)$ are defined in sections 3.1.3.2 and 3.1.3.3 by excitation and response at the SDOF modelling the structure.)

4.2 NATURAL FREQUENCIES OF DYNAMIC HUMAN-STRUCTURE SYSTEMS

In this chapter, natural frequencies of human-structure dynamic systems are investigated. This is done for three models of the human-structure system: the mass-only model (Figure 4.1a), the undamped 2-DOF model (Figure 4.1b) and the damped 2-DOF model (Figure 4.1c).

4.2.1 NATURAL FREQUENCIES OF THE MASS-ONLY MODEL

The natural frequency $f^{(MM)}$ of the human-structure system modelled with the mass-only model (Figure 4.1a) is defined by equation (4.3). This natural frequency $f^{(MM)}$ can also be expressed in terms of the mass ratio α (4.1) and the frequency of the structure f_s only (4.4).

$$f^{(MM)} = \frac{1}{2 \cdot \pi} \cdot \sqrt{\frac{k_s}{m_s + m_H}} \tag{4.3}$$

$$f^{(MM)} = \sqrt{\frac{1}{1+\alpha}} \cdot f_s \tag{4.4}$$

The dependence of the natural frequency $f^{(MM)}$, on the mass ratio α and the frequency ratio β is shown in Figure 4.2. In particular, the natural frequency $f^{(MM)}$ is presented as a function of the frequency ratio β for mass ratios α of 1%, 10%, 50%, and 100%. These natural frequencies $f^{(MM)}$ are related to the frequency of the structure f_s plotted on the vertical axis (Figure 4.2).

Figure 4.2 shows that the frequency $f^{(MM)}$ does not depend on the frequency ratio β (equation (4.4)). Nevertheless, this presentation is chosen for consistency with the following presentation of natural frequencies of undamped and damped 2-DOF human-structure systems.

Figure 4.2 also demonstrates that the ratio of the frequency of the human-structure system and the frequency of the empty structure ($f^{(MM)} / f_s$) is a constant having ordinates defined by the mass ratio α. This can be confirmed by equation (4.4), which states that the natural frequency $f^{(MM)}$ decreases with increasing mass of occupants. Hence, the ratio $f^{(MM)} / f_s$ decreases with increasing mass ratio α (Figure 4.2).

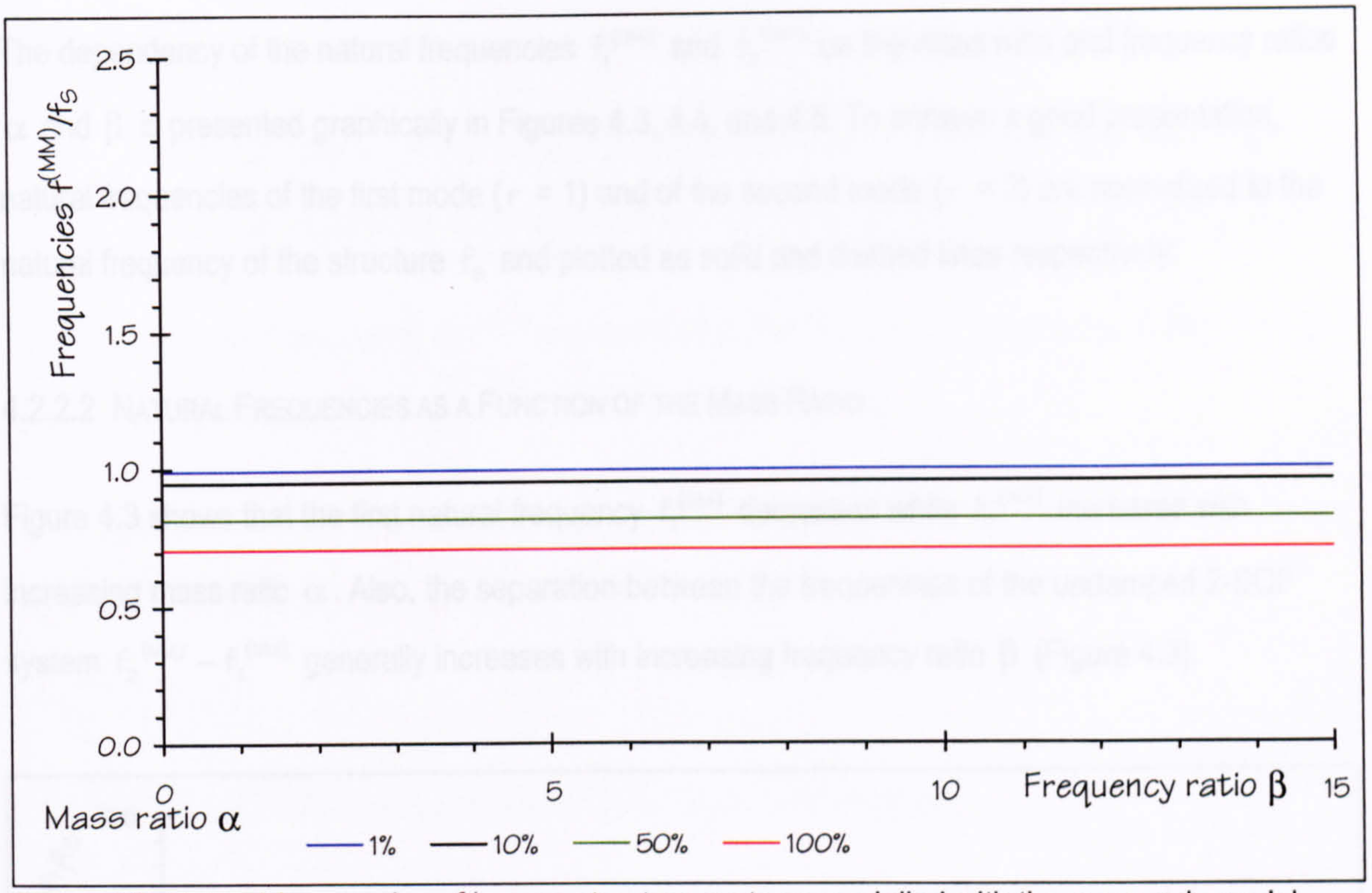

Figure 4.2: Natural frequencies of human-structure systems modelled with the mass-only model.

4.2.2 Natural Frequencies of the Undamped 2-DOF Model

The second human-structure model considered in this research is the undamped 2-DOF model (Figure 4.1b). It serves mainly as a prerequisite for a better understanding of the damped 2-DOF human-structure model.

4.2.2.1 Calculation of Natural Frequencies

The natural frequencies of the undamped 2-DOF human-structure system $f_1^{(UM)}$ and $f_2^{(UM)}$ can be expressed as a function of mass and frequency ratio α and β (equations (4.1) and (4.2)), and the natural frequency of the empty structure f_S, as specified by equations (4.5) and (4.6) (see also section 3.1.2.3 and Appendix B).

$$f_1^{(UM)} = \left(\sqrt{(\beta+1)^2+\alpha\cdot\beta^2} - \sqrt{(\beta-1)^2+\alpha\cdot\beta^2}\right)\cdot\frac{f_S}{2} \tag{4.5}$$

$$f_2^{(UM)} = \left(\sqrt{(\beta+1)^2+\alpha\cdot\beta^2} + \sqrt{(\beta-1)^2+\alpha\cdot\beta^2}\right)\cdot\frac{f_S}{2} \tag{4.6}$$

The dependency of the natural frequencies $f_1^{(UM)}$ and $f_2^{(UM)}$ on the mass ratio and frequency ratios α and β is presented graphically in Figures 4.3, 4.4, and 4.5. To achieve a good presentation, natural frequencies of the first mode ($r = 1$) and of the second mode ($r = 2$) are normalised to the natural frequency of the structure f_S and plotted as solid and dashed lines respectively.

4.2.2.2 Natural Frequencies as a Function of the Mass Ratio

Figure 4.3 shows that the first natural frequency $f_1^{(UM)}$ decreases while $f_2^{(UM)}$ increases with increasing mass ratio α. Also, the separation between the frequencies of the undamped 2-DOF system $f_2^{(UM)} - f_1^{(UM)}$ generally increases with increasing frequency ratio β (Figure 4.3).

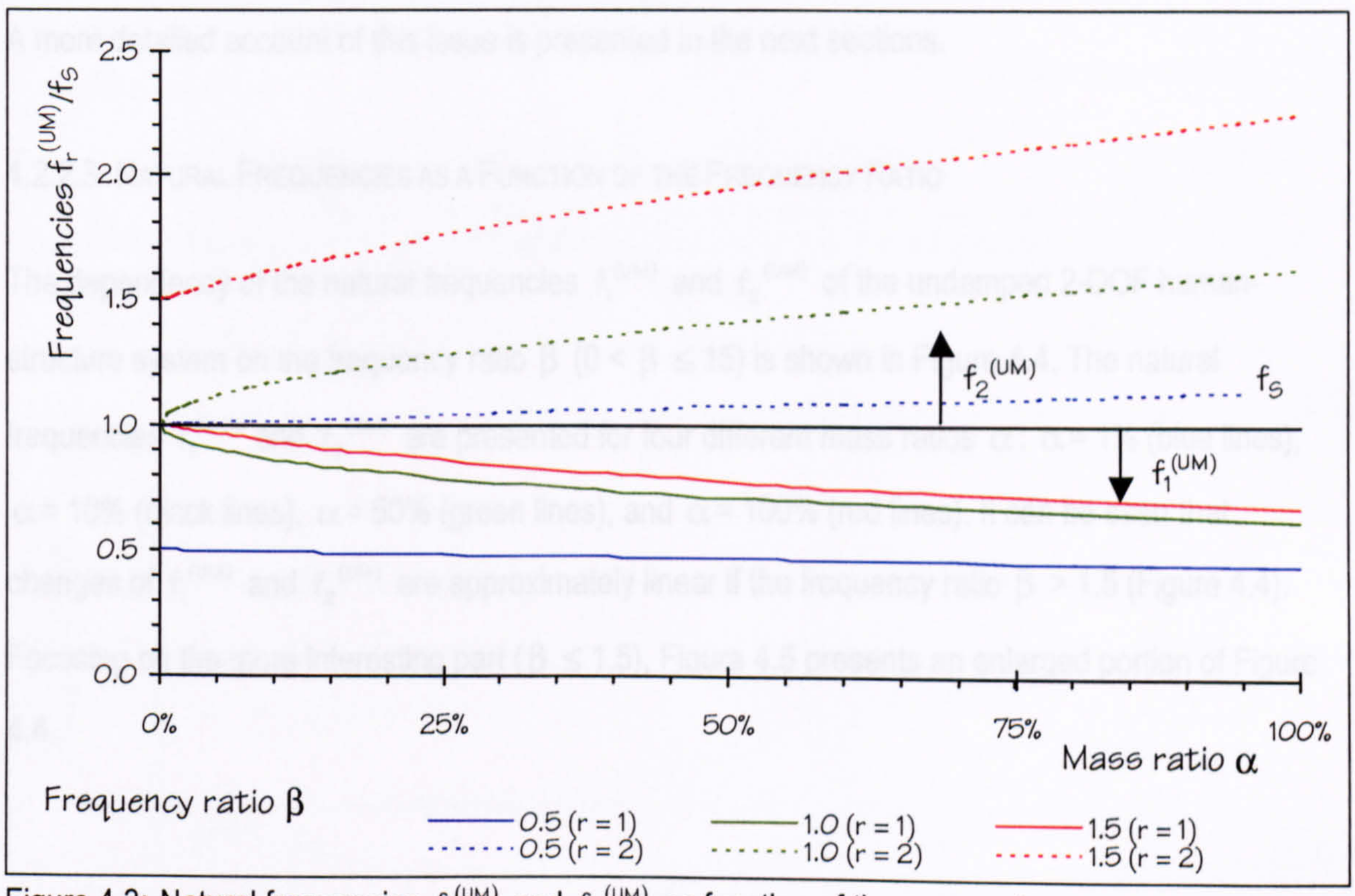

Figure 4.3: Natural frequencies $f_1^{(UM)}$ and $f_2^{(UM)}$ as function of the mass ratio α.

The frequency separation $f_2^{(UM)} - f_1^{(UM)}$ is a particularly important aspect of the human-structure dynamic system behaviour, as will be shown later. It is smallest for a human-structure system with a certain frequency ratio β if the mass ratio α is zero (see equations (4.5) and (4.6)). In this case, the natural frequencies of the undamped human-structure system $f_1^{(UM)}$ and $f_2^{(UM)}$ are equal to the frequencies of human f_H and structure f_S.

Based on these observations, it is concluded that:

(1) the first frequency $f_1^{(UM)}$ of the undamped 2-DOF system is always smaller than both of the natural frequencies of the structure and human SDOF subsystems (f_H and f_S) and

(2) the second frequency $f_2^{(UM)}$ is always higher than the natural frequencies of the subsystems (f_H and f_S).

These significant features of undamped 2-DOF systems, summarised in equation (4.7), were proven by Ellis and Ji (1997).

$$f_1^{(UM)} < (f_S, f_H) < f_2^{(UM)} \tag{4.7}$$

A more detailed account of this issue is presented in the next sections.

4.2.2.3 Natural Frequencies as a Function of the Frequency Ratio

The dependency of the natural frequencies $f_1^{(UM)}$ and $f_2^{(UM)}$ of the undamped 2-DOF human-structure system on the frequency ratio β ($0 < \beta \leq 15$) is shown in Figure 4.4. The natural frequencies $f_1^{(UM)}$ and $f_2^{(UM)}$ are presented for four different mass ratios α: $\alpha = 1\%$ (blue lines), $\alpha = 10\%$ (black lines), $\alpha = 50\%$ (green lines), and $\alpha = 100\%$ (red lines). It can be seen that changes of $f_1^{(UM)}$ and $f_2^{(UM)}$ are approximately linear if the frequency ratio $\beta > 1.5$ (Figure 4.4). Focusing on the more interesting part ($\beta \leq 1.5$), Figure 4.5 presents an enlarged portion of Figure 4.4.

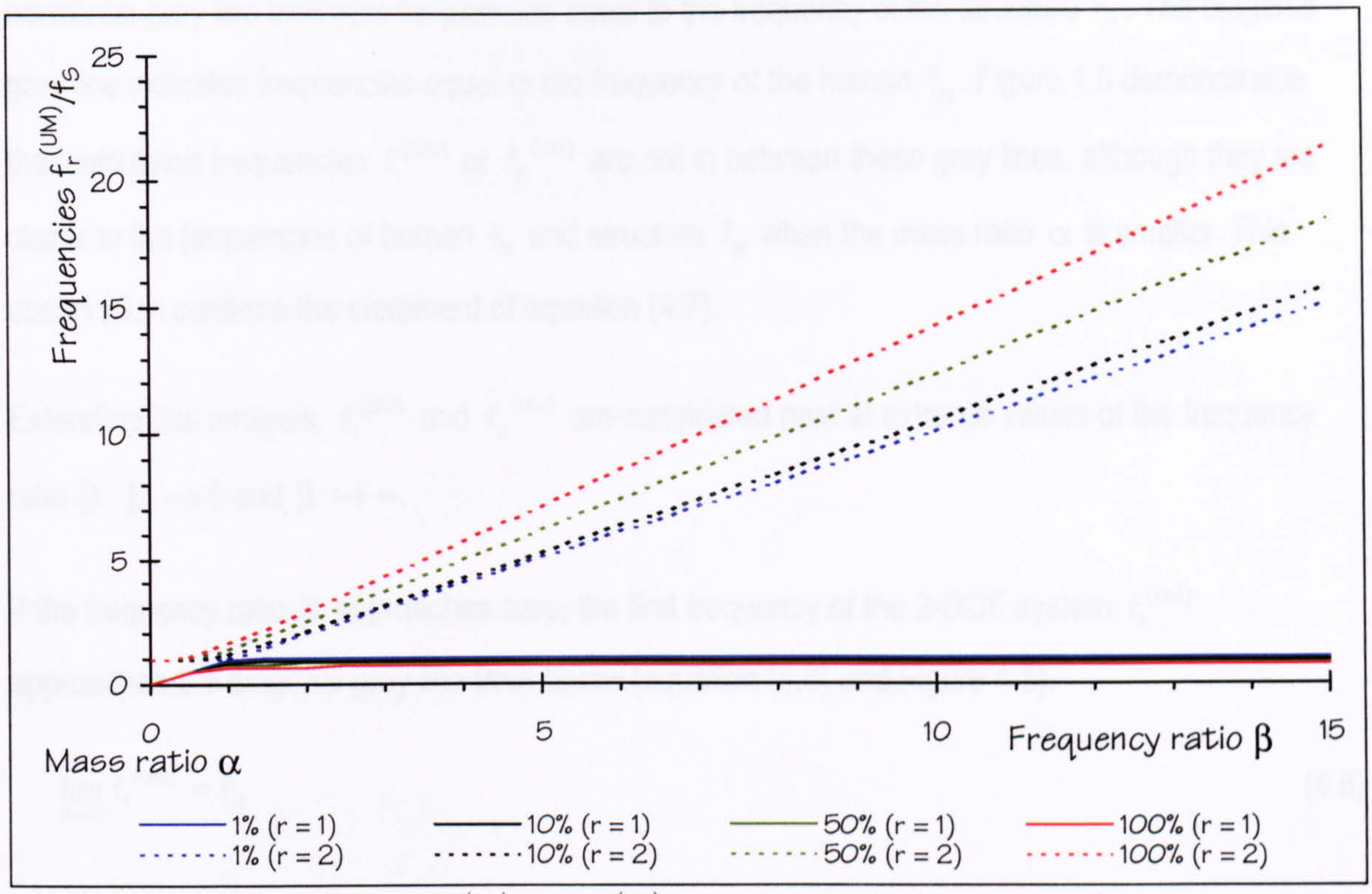

Figure 4.4: Natural frequencies $f_1^{(UM)}$ and $f_2^{(UM)}$ as function of the frequency ratio β.

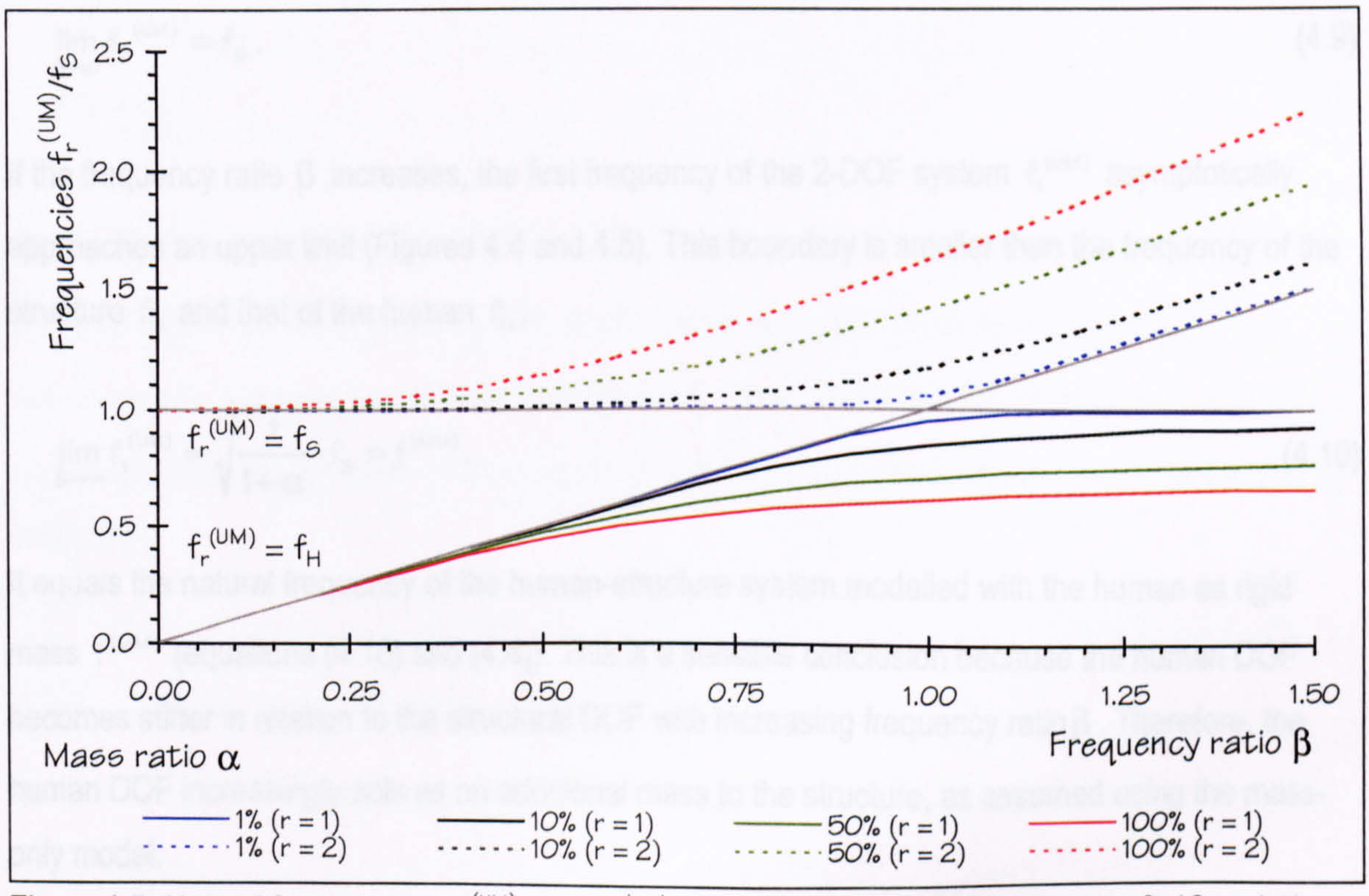

Figure 4.5: Natural frequencies $f_1^{(UM)}$ and $f_2^{(UM)}$ as function of the frequency ratio β ($\beta \leq 1.5$).

In addition to the information provided in Figure 4.4, Figure 4.5 contains two grey lines. The horizontal grey line indicates frequencies equal to the frequency of the structure f_s. The diagonal grey line indicates frequencies equal to the frequency of the human f_H. Figure 4.5 demonstrates that calculated frequencies $f_1^{(UM)}$ or $f_2^{(UM)}$ are not in between these grey lines, although they are closer to the frequencies of human f_H and structure f_s when the mass ratio α is smaller. This observation confirms the statement of equation (4.7).

Extending this analysis, $f_1^{(UM)}$ and $f_2^{(UM)}$ are considered next at extreme values of the frequency ratio β: $\beta \to 0$ and $\beta \to \infty$.

If the frequency ratio β approaches zero, the first frequency of the 2-DOF system $f_1^{(UM)}$ approaches the diagonal grey line from below (equation (4.8) and Figure 4.5).

$$\lim_{\beta \to 0} f_1^{(UM)} = f_H \tag{4.8}$$

In contrast to $f_1^{(UM)}$, the second natural frequency $f_2^{(UM)}$ has no upper limit (Figure 4.4). However, $f_2^{(UM)}$ has a lower limit equal to the frequency of the structure f_s:

$$\lim_{\beta \to 0} f_2^{(UM)} = f_s . \tag{4.9}$$

If the frequency ratio β increases, the first frequency of the 2-DOF system $f_1^{(UM)}$ asymptotically approaches an upper limit (Figures 4.4 and 4.5). This boundary is smaller than the frequency of the structure f_s and that of the human f_H:

$$\lim_{\beta \to \infty} f_1^{(UM)} = \sqrt{\frac{1}{1+\alpha}} \cdot f_s = f^{(MM)} . \tag{4.10}$$

It equals the natural frequency of the human-structure system modelled with the human as rigid mass $f^{(MM)}$ (equations (4.10) and (4.4)). This is a sensible conclusion because the human DOF becomes stiffer in relation to the structural DOF with increasing frequency ratio β. Therefore, the human DOF increasingly acts as an additional mass to the structure, as assumed using the mass-only model.

4.2.2.4 Minimum Frequency Separation

It will be shown later that the minimum frequency separation between the frequencies of the damped 2-DOF system are of particular interest. For comparison, the minimum frequency separation of the frequencies of the undamped 2-DOF human-structure system $f_2^{(UM)} - f_1^{(UM)}$ is analysed here.

The frequency separation $f_2^{(UM)} - f_1^{(UM)}$ is specified by the second term of equation (4.5) and of equation (4.6). It is a function $f(\alpha,\beta)$ of the mass ratio α and the frequency ratio β (4.11).

$$f(\alpha,\beta) = f_2^{(UM)} - f_1^{(UM)} = \sqrt{(\beta-1)^2 + \alpha\cdot\beta^2}\cdot f_s \tag{4.11}$$

This function $f(\alpha,\beta)$ and its derivative $\partial f(\alpha,\beta)/\partial\beta$ (4.12) can be used to estimate the frequency ratio β at which the frequency separation $f_2^{(UM)} - f_1^{(UM)}$ is minimal.

$$\frac{\partial f(\alpha,\beta)}{\partial\beta} = \frac{(\beta-1)+\alpha\cdot\beta}{\sqrt{(\beta-1)^2+\alpha\cdot\beta^2}}\cdot f_s \tag{4.12}$$

In particular, $f(\alpha,\beta)$ has a minimum if the first derivative $\partial f(\alpha,\beta)/\partial\beta = 0$. This is the case, if the mass and frequency ratios α and β satisfy equation (4.13).

$$\beta = \frac{1}{1+\alpha} \tag{4.13}$$

Hence, the frequency separation $f_2^{(UM)} - f_1^{(UM)}$ is minimal at certain frequency ratios $\beta \leq 1$ as shown in Figure 4.6. The frequency ratio β of minimal frequency separation $f_2^{(UM)} - f_1^{(UM)}$ decreases with increasing mass ratio α (Figure 4.6). That means that the frequency f_s of a human-structure system at which the frequency separation is minimal increases with the number of occupants.

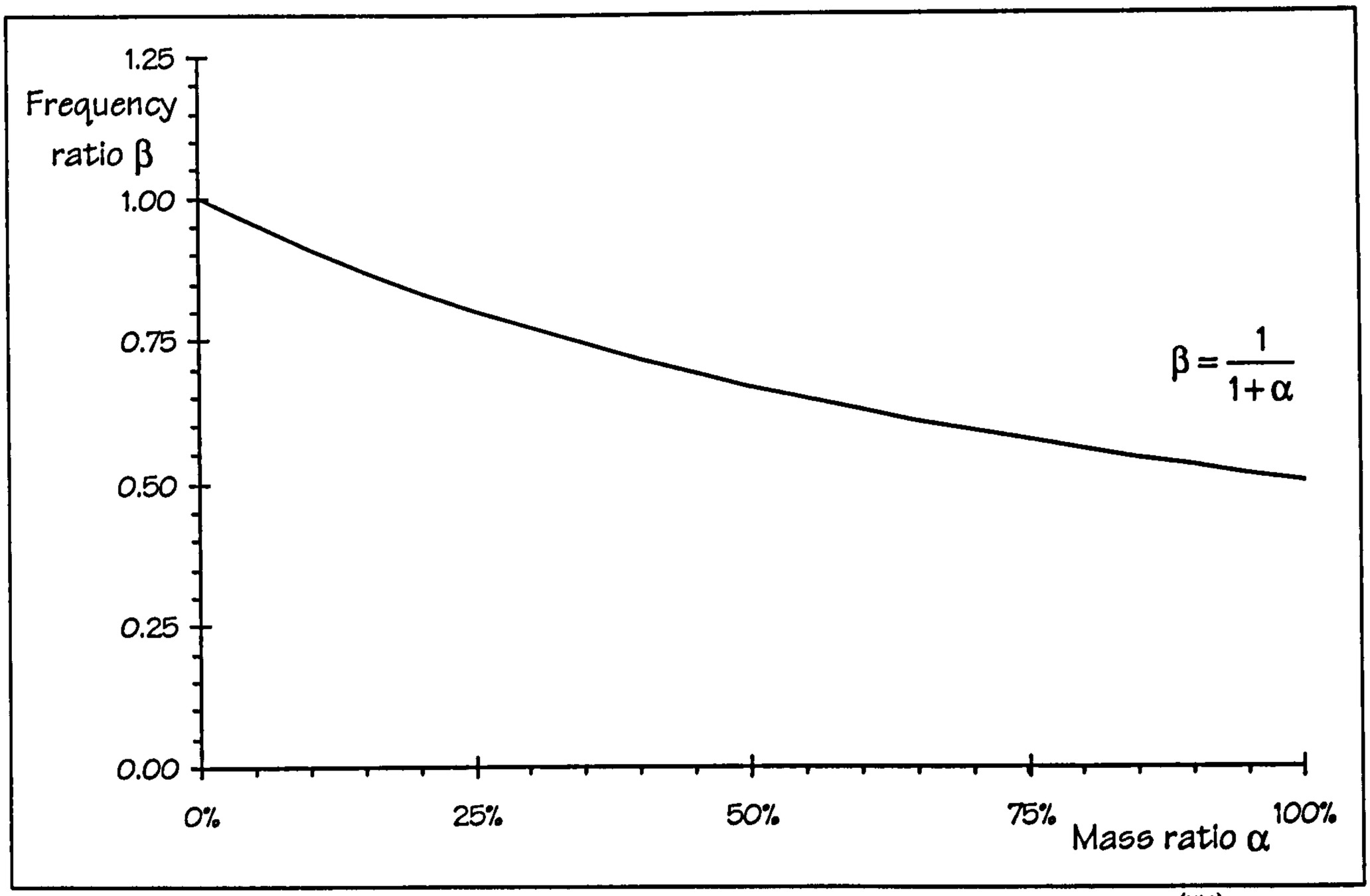

Figure 4.6: Mass and frequency ratios α and β leading to a minimum separation of $f_1^{(UM)}$ and $f_2^{(UM)}$ of the undamped 2-DOF human-structure system.

4.2.2.5 SUMMARY

The most important findings of the analysis of the natural frequencies of the undamped 2-DOF system are that the frequencies $f_1^{(UM)}$ and $f_2^{(UM)}$ are:

(1) always higher and lower, respectively, than the frequencies of the subsystems (4.7), and

(2) least separated if the mass ratio α and the frequency ratio β satisfy equation (4.13).

4.2.3 NATURAL FREQUENCIES OF THE DAMPED HUMAN-STRUCTURE SYSTEM

In this section, the natural frequencies $f_1^{(DM)}$ and $f_2^{(DM)}$ of the damped 2-DOF human-structure system (Figure 4.1c) are analysed.

4.2.3.1 Calculation of Natural Frequencies

Estimating the frequencies of the damped 2-DOF human-structure system $f_1^{(DM)}$ and $f_2^{(DM)}$ is not as straight forward as the calculation of the natural frequencies of the undamped 2-DOF system $f_1^{(UM)}$ and $f_2^{(UM)}$ (equations (4.5) and (4.6)). Instead, it is necessary to extract the natural frequencies from the complex solutions of a fourth order polynomial (see section 3.1.2.2):

$$x^4 + a \cdot x^3 + b \cdot x^2 + c \cdot x + d = 0 \tag{4.14}$$

with

$$a = 4 \cdot \pi \cdot ((1+\alpha) \cdot \beta \cdot \zeta_H + \zeta_S) \cdot f_S, \tag{4.15}$$

$$b = 4 \cdot \pi^2 \cdot (1 + 4 \cdot \beta \cdot \zeta_H \cdot \zeta_S + (1+\alpha) \cdot \beta^2) \cdot f_S^2, \tag{4.16}$$

$$c = 16 \cdot \pi^3 \cdot (\zeta_H + \zeta_S \cdot \beta) \cdot \beta \cdot f_S^3, \tag{4.17}$$

and

$$d = 16 \cdot \pi^4 \cdot \beta^2 \cdot f_S^4. \tag{4.18}$$

Appendix A outlines how this equation (4.14) can be solved analytically. However, it can also be solved numerically by software capable of eigenanalysis such as MATLAB (1999).

4.2.3.2 Natural Frequencies as a Function of α, β and ζ_H

In contrast to the calculation of natural frequencies of the undamped 2-DOF human-structure system (Figure 4.1b), the analysis of natural frequencies of the damped 2-DOF system requires the specification of damping. In this parametric study, the damping ratio of the structure ζ_S is set to a realistic value of 1%. Reported viscous damping ratios ζ_H of the human spread widely (chapter 2). Therefore, two reasonable values ζ_H = 30% and ζ_H = 50% are used.

Analysing the natural frequencies $f_1^{(DM)}$ and $f_2^{(DM)}$ of the damped 2-DOF human-structure system, their dependency on the mass and frequency ratios α and β is visualised in Figures 4.7 and 4.8 for ζ_H = 30% and ζ_H = 50%. These figures are similar to Figure 4.4, as frequency ratios β range from 0 to 15 and mass ratios α of 1%, 10%, 50%, and 100% are used.

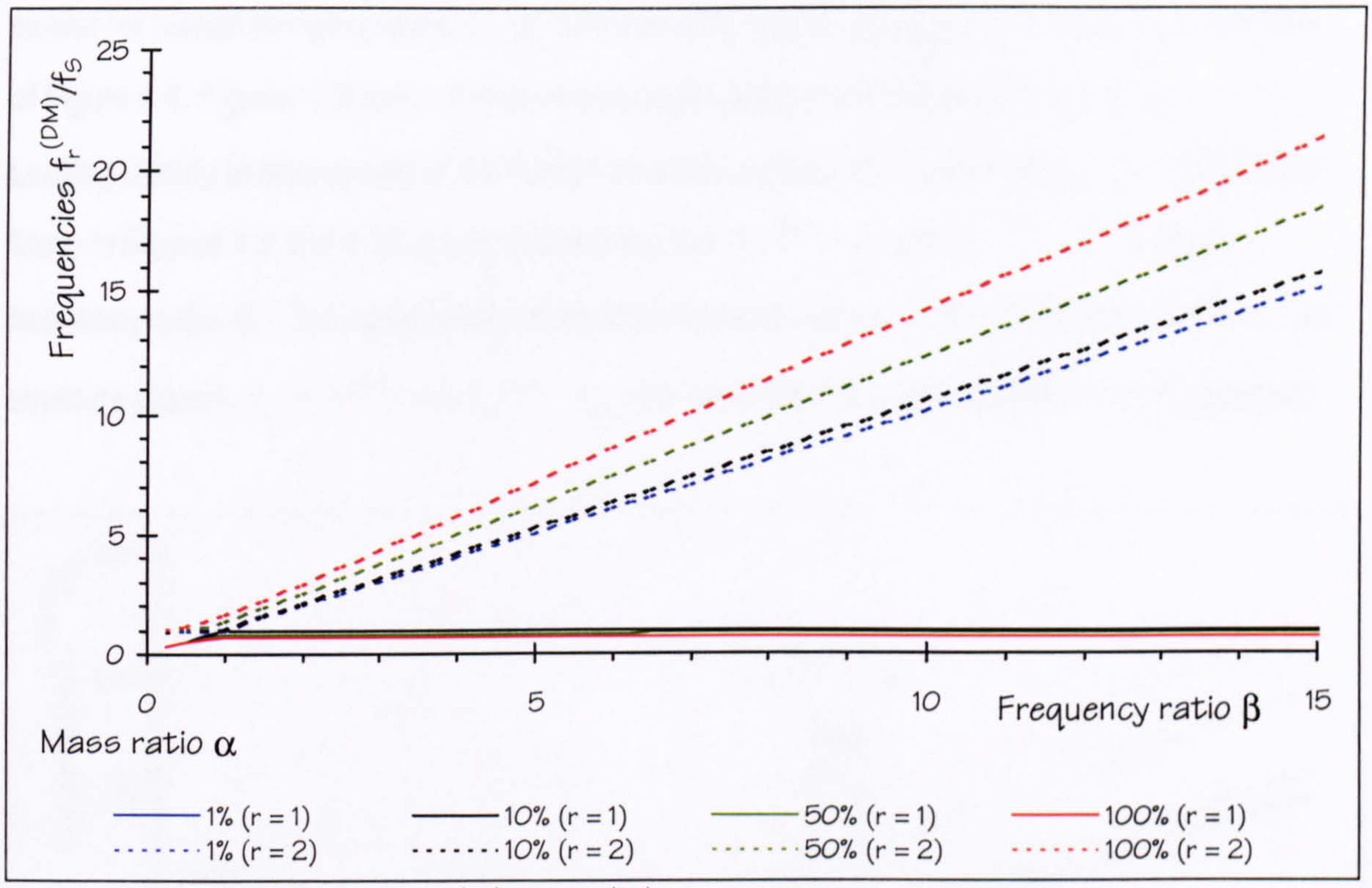

Figure 4.7: Natural frequencies $f_1^{(DM)}$ and $f_2^{(DM)}$ of a damped 2-DOF human-structure model (ζ_S = 1% and ζ_H = 30%).

Figure 4.8: Natural frequencies $f_1^{(DM)}$ and $f_2^{(DM)}$ of damped 2-DOF human-structure models (ζ_S = 1% and ζ_H = 50%).

Comparing Figures 4.7 and 4.8, it can be seen that the frequencies $f_1^{(DM)}$ and $f_2^{(DM)}$ are very similar for human damping ratios ζ_H of 30% and 50%. Similar to Figure 4.5 that is an enlargement of Figure 4.4, Figures 4.9 and 4.10 present enlarged portions of Figures 4.7 and 4.8 for $\beta \leq 1.5$. Looking closely at frequencies of the human-structure system with mass ratios of α = 10% (black lines) in Figures 4.9 and 4.10, it can be identified that $f_2^{(DM)} < f_S$ and $f_1^{(DM)} > f_H$ for certain frequency ratios β. This observation contradicts the major feature of the undamped 2-DOF human-structure system: $f_H > f_1^{(UM)}$ and $f_2^{(UM)} > f_S$ (see section 4.2.2.2 and equation (4.7) in particular).

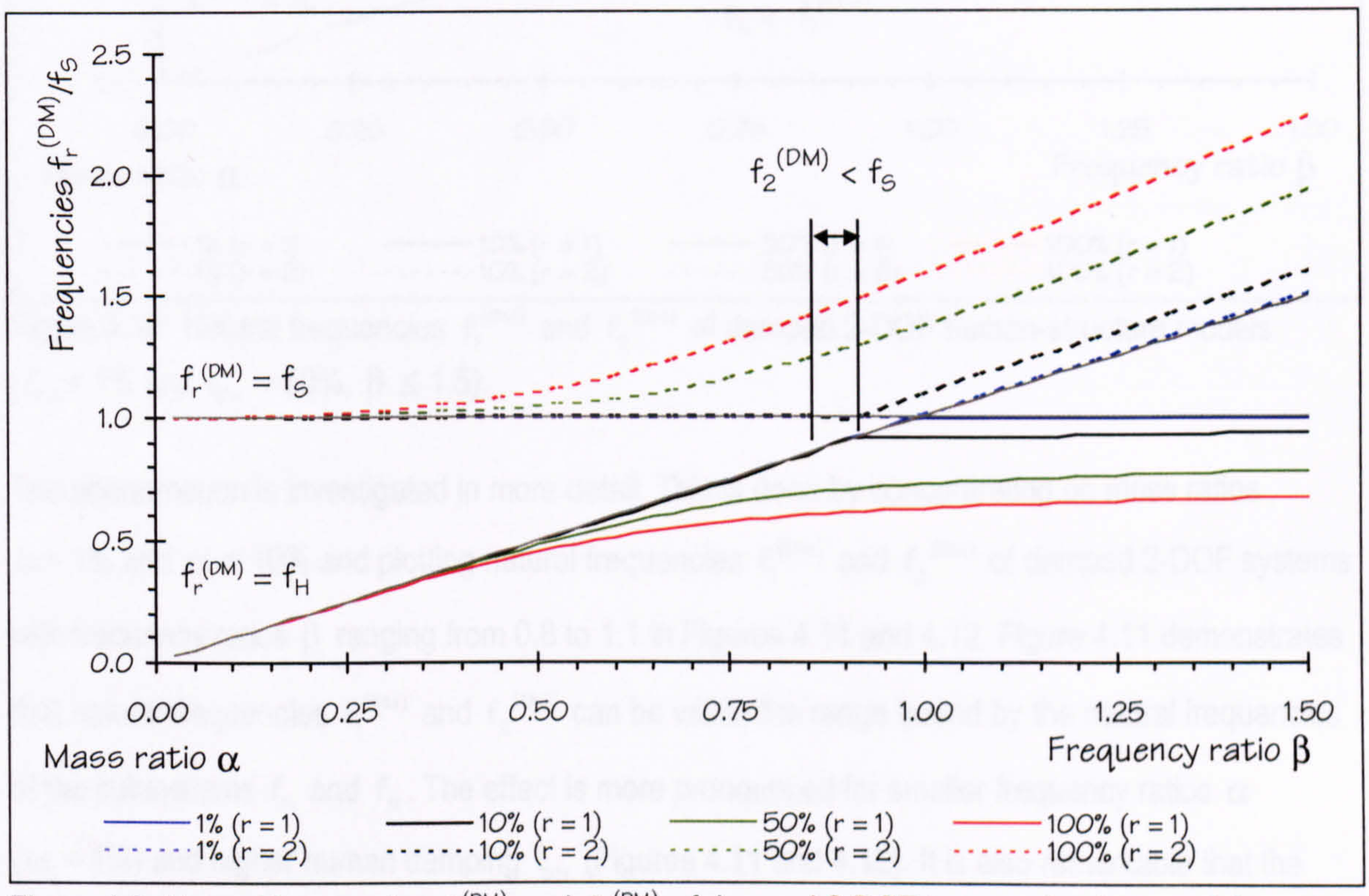

Figure 4.9: Natural frequencies $f_1^{(DM)}$ and $f_2^{(DM)}$ of damped 2-DOF human-structure models (ζ_S = 1% and ζ_H = 30%, $\beta \leq 1.5$).

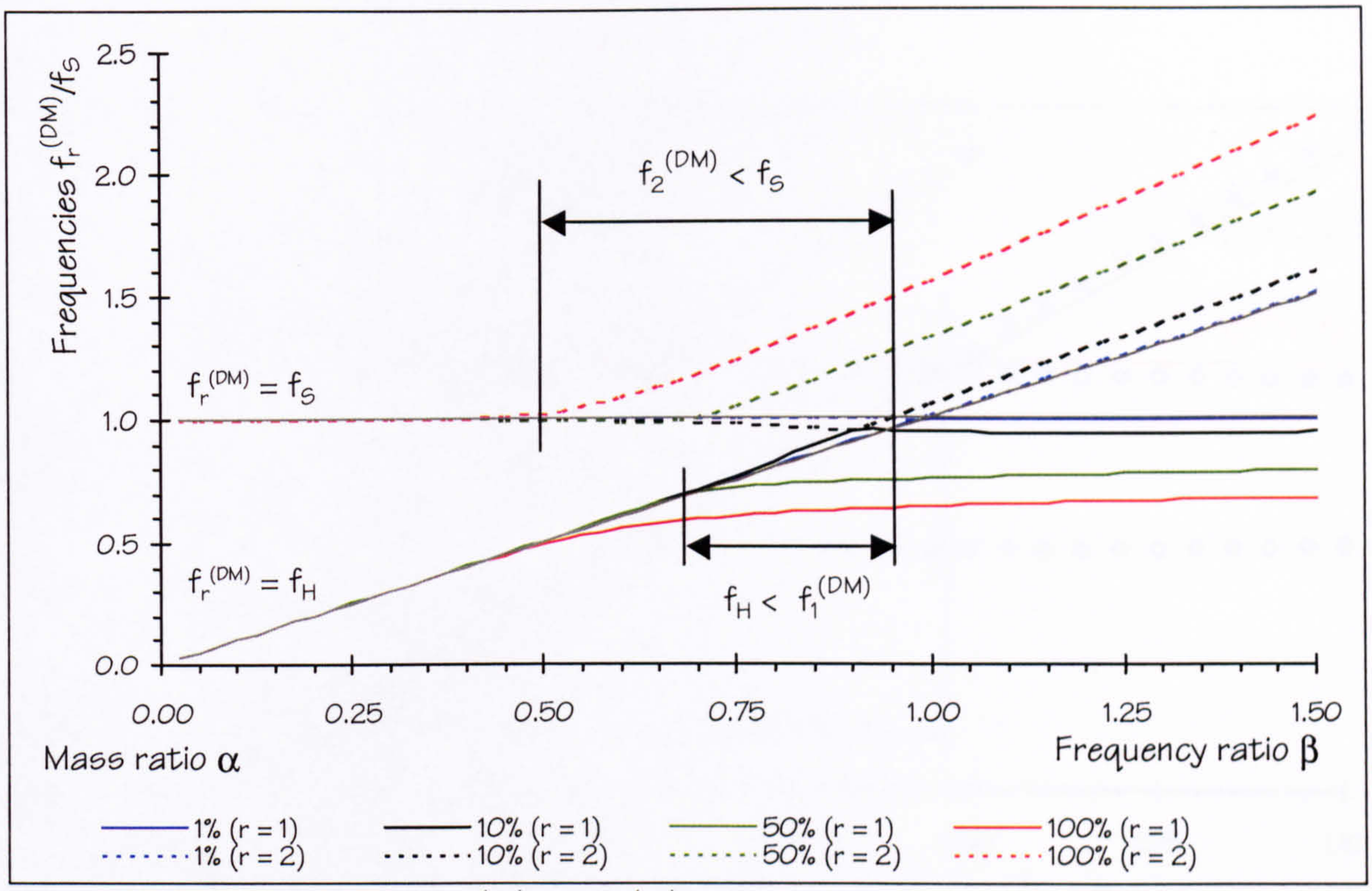

Figure 4.10: Natural frequencies $f_1^{(DM)}$ and $f_2^{(DM)}$ of damped 2-DOF human-structure models (ζ_S = 1% and ζ_H = 50%, $\beta \leq 1.5$).

The phenomenon is investigated in more detail. This is done by concentrating on mass ratios α = 1% and α = 10% and plotting natural frequencies $f_1^{(DM)}$ and $f_2^{(DM)}$ of damped 2-DOF systems with frequency ratios β ranging from 0.8 to 1.1 in Figures 4.11 and 4.12. Figure 4.11 demonstrates that natural frequencies $f_1^{(DM)}$ and $f_2^{(DM)}$ can be within the range bound by the natural frequencies of the subsystems f_H and f_S. The effect is more pronounced for smaller frequency ratios α (α = 1%) and higher human damping ζ_H (Figures 4.11 and 4.12). It is also remarkable that the frequencies $f_1^{(DM)}$ and $f_2^{(DM)}$ can even be nearly identical as indicated in Figure 4.12.

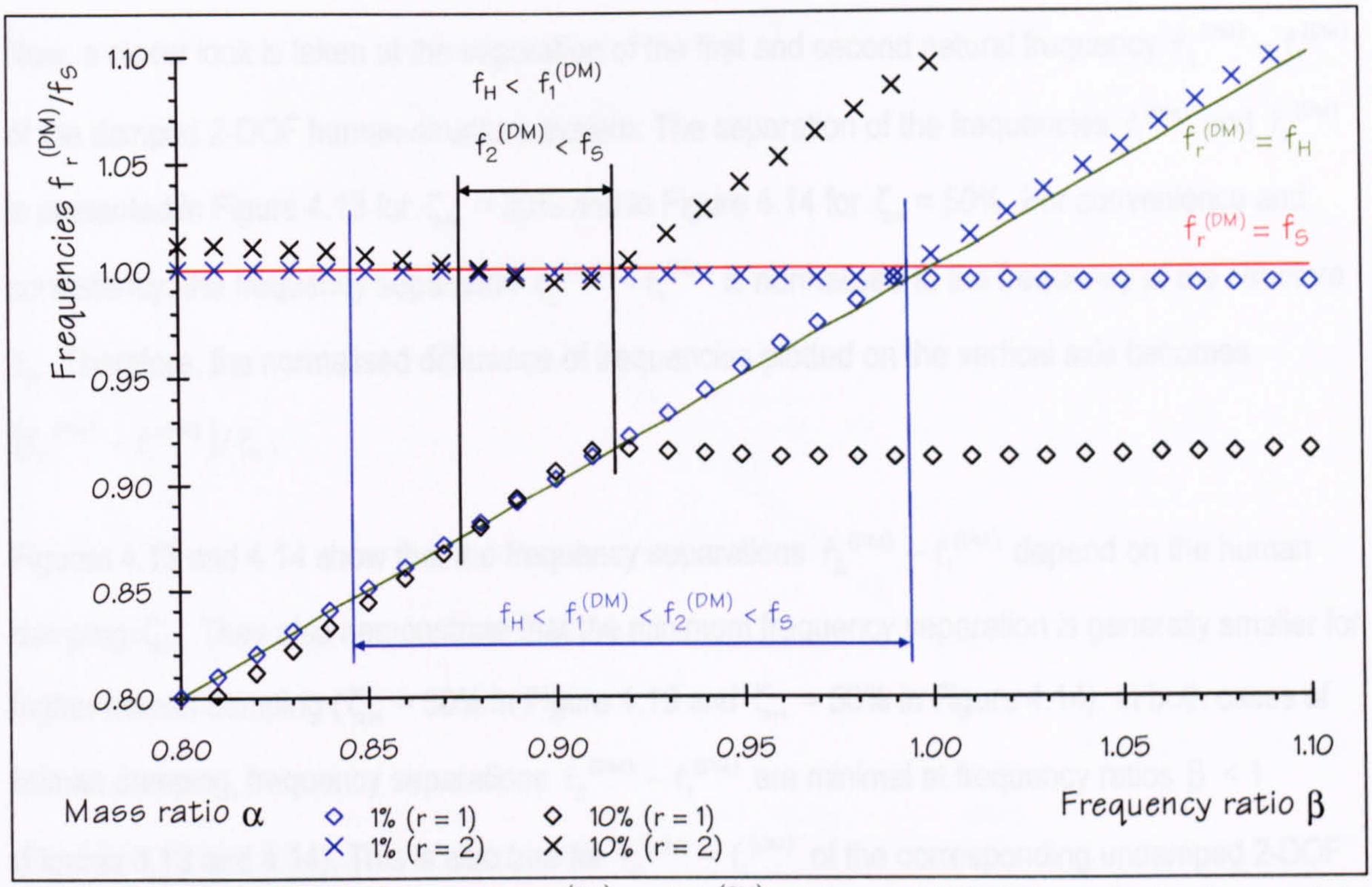

Figure 4.11: Close natural frequencies $f_1^{(DM)}$ and $f_2^{(DM)}$ of damped 2-DOF human-structure models (ζ_S = 1% and ζ_H = 30%).

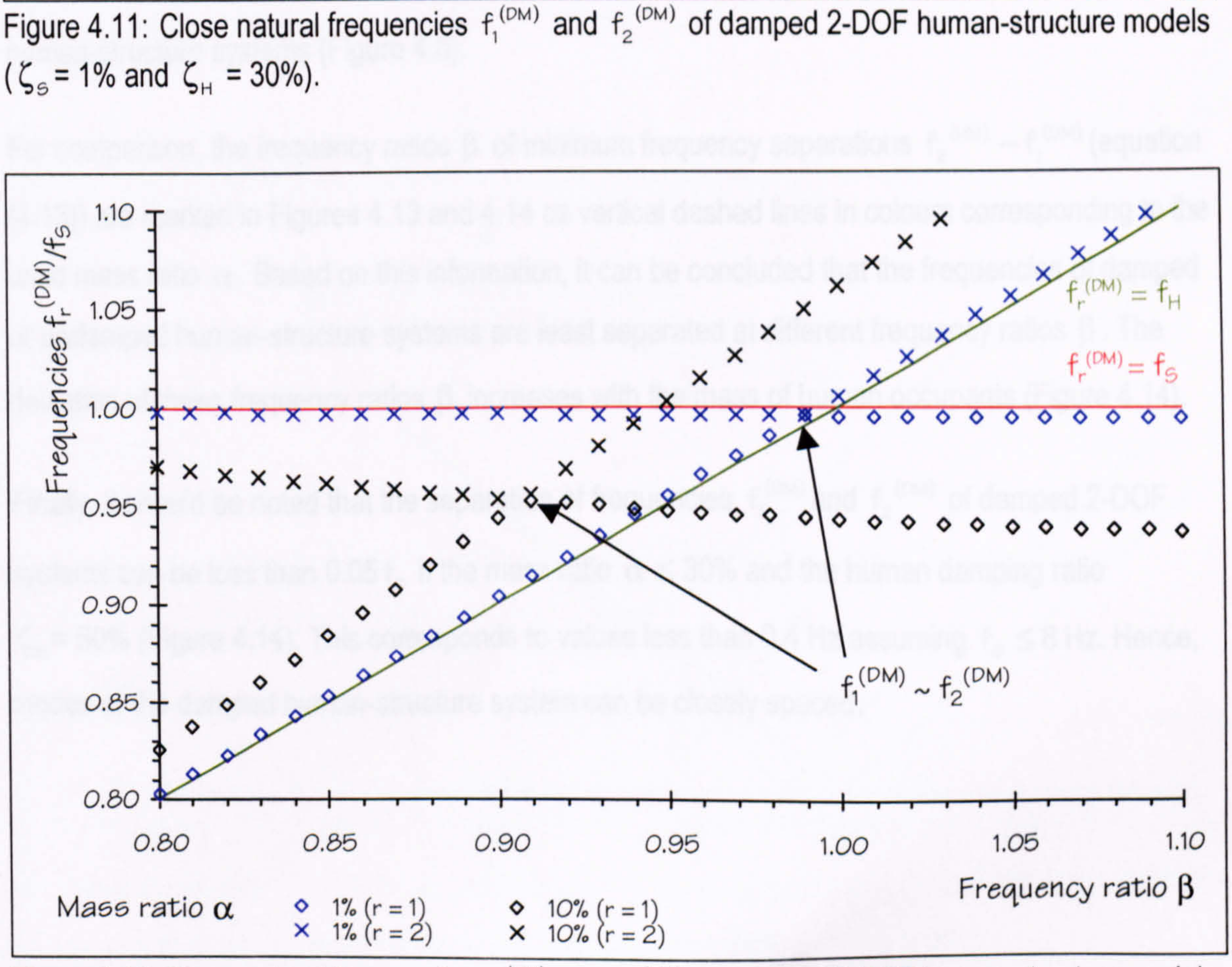

Figure 4.12: Close natural frequencies $f_1^{(DM)}$ and $f_2^{(DM)}$ of damped 2-DOF human-structure models (ζ_S = 1% and ζ_H = 50%).

4.2.3.3 Minimum Frequency Separation

Now, a closer look is taken at the separation of the first and second natural frequency $f_2^{(DM)} - f_1^{(DM)}$ of the damped 2-DOF human-structure system. The separation of the frequencies $f_1^{(DM)}$ and $f_2^{(DM)}$ is presented in Figure 4.13 for ζ_H = 30% and in Figure 4.14 for ζ_H = 50%. For convenience and consistency, the frequency separation $f_2^{(DM)} - f_1^{(DM)}$ is normalised to the frequency of the structure f_s. Therefore, the normalised difference of frequencies plotted on the vertical axis becomes $\left(f_2^{(DM)} - f_1^{(DM)}\right)/f_s$.

Figures 4.13 and 4.14 show that the frequency separations $f_2^{(DM)} - f_1^{(DM)}$ depend on the human damping ζ_H. They also demonstrate that the minimum frequency separation is generally smaller for higher human damping (ζ_H = 30% in Figure 4.13 and ζ_H = 50% in Figure 4.14). In both cases of human damping, frequency separations $f_2^{(DM)} - f_1^{(DM)}$ are minimal at frequency ratios $\beta < 1$ (Figures 4.13 and 4.14). This is also true for $f_2^{(UM)} - f_1^{(UM)}$ of the corresponding undamped 2-DOF human-structure systems (Figure 4.6).

For comparison, the frequency ratios β of minimum frequency separations $f_2^{(UM)} - f_1^{(UM)}$ (equation (4.13)) are marked in Figures 4.13 and 4.14 as vertical dashed lines in colours corresponding to the used mass ratio α. Based on this information, it can be concluded that the frequencies of damped or undamped human-structure systems are least separated at different frequency ratios β. The deviation of these frequency ratios β increases with the mass of human occupants (Figure 4.14).

Finally, it should be noted that the separation of frequencies $f_1^{(DM)}$ and $f_2^{(DM)}$ of damped 2-DOF systems can be less than $0.05\,f_s$ if the mass ratio $\alpha \leq 30\%$ and the human damping ratio ζ_H = 50% (Figure 4.14). This corresponds to values less than 0.4 Hz assuming $f_s \leq 8$ Hz. Hence, modes of the damped human-structure system can be closely spaced.

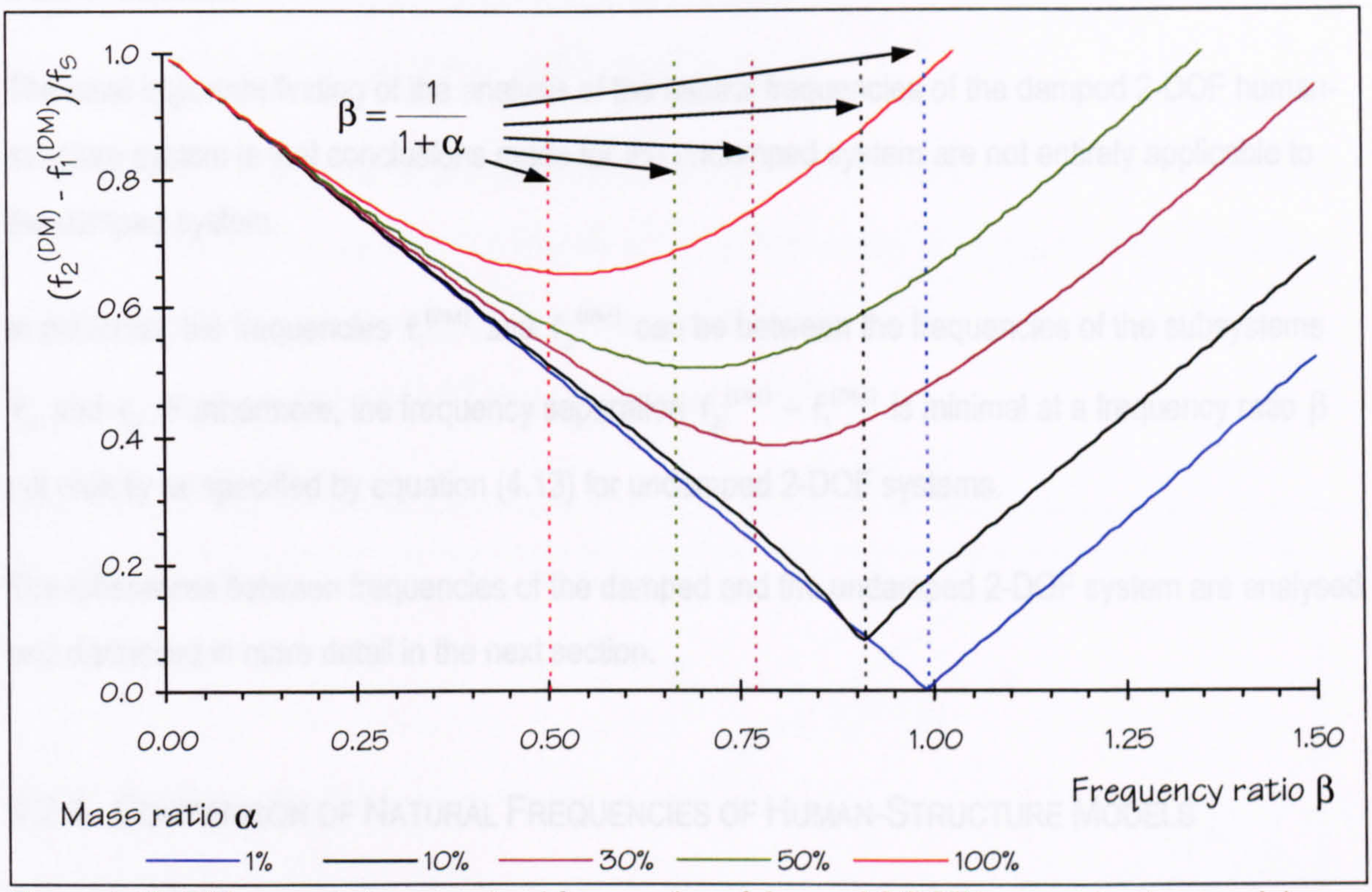

Figure 4.13: Difference between natural frequencies of damped 2-DOF human-structure models (ζ_S = 1% and ζ_H = 30%).

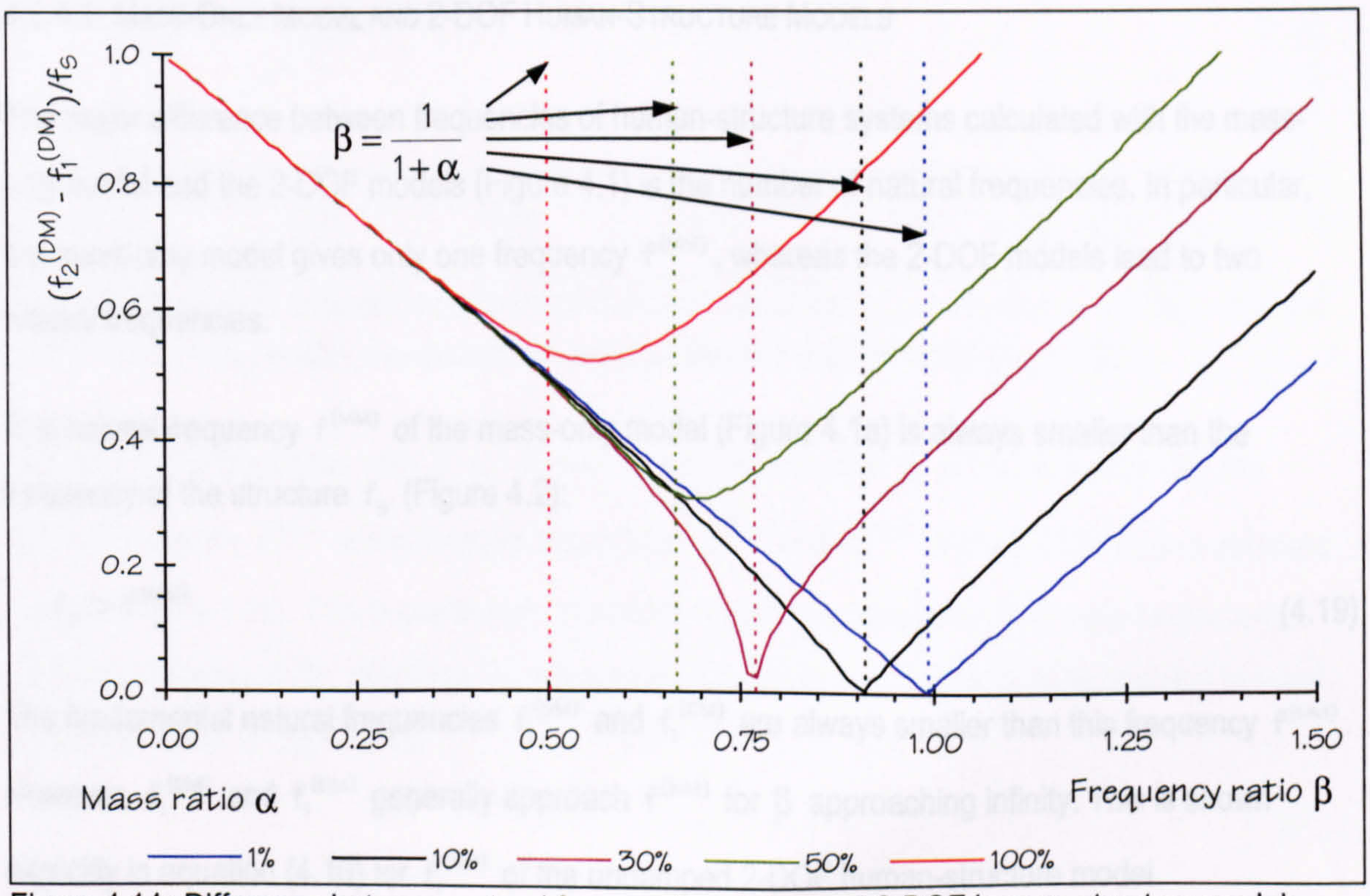

Figure 4.14: Difference between natural frequencies of damped 2-DOF human-structure models (ζ_S = 1% and ζ_H = 50%).

4.2.3.4 SUMMARY

The most important finding of the analysis of the natural frequencies of the damped 2-DOF human-structure system is that conclusions made for the undamped system are not entirely applicable to the damped system.

In particular, the frequencies $f_1^{(DM)}$ and $f_2^{(DM)}$ can be between the frequencies of the subsystems f_S and f_H. Furthermore, the frequency separation $f_2^{(DM)} - f_1^{(DM)}$ is minimal at a frequency ratio β not exactly as specified by equation (4.13) for undamped 2-DOF systems.

The differences between frequencies of the damped and the undamped 2-DOF system are analysed and discussed in more detail in the next section.

4.2.4 COMPARISON OF NATURAL FREQUENCIES OF HUMAN-STRUCTURE MODELS

In this section, the natural frequencies of all three human-structure models (Figure 4.1) are compared.

4.2.4.1 MASS-ONLY MODEL AND 2-DOF HUMAN-STRUCTURE MODELS

The major difference between frequencies of human-structure systems calculated with the mass-only model and the 2-DOF models (Figure 4.1) is the number of natural frequencies. In particular, the mass-only model gives only one frequency $f^{(MM)}$, whereas the 2-DOF models lead to two natural frequencies.

The natural frequency $f^{(MM)}$ of the mass-only model (Figure 4.1a) is always smaller than the frequency of the structure f_S (Figure 4.2):

$$f_S > f^{(MM)}. \tag{4.19}$$

The fundamental natural frequencies $f_1^{(UM)}$ and $f_1^{(DM)}$ are always smaller than this frequency $f^{(MM)}$. However, $f_1^{(UM)}$ and $f_1^{(DM)}$ generally approach $f^{(MM)}$ for β approaching infinity. This is shown explicitly in equation (4.10) for $f_1^{(UM)}$ of the undamped 2-DOF human-structure model.

The fact that $f_1^{(DM)}$ of a human-structure system is smaller than $f^{(MM)}$ is supported by the research of Eibl and Rösch (1990) and Hothan (1999) (section 2.4.2).

In general ($\alpha \leq 100\%$), the difference between the natural frequencies $f^{(MM)}$ and $f_1^{(UM)}$ is less than $0.04\, f_S$ if the frequency ratio $\beta > 1.5$ (Figure 4.15). In other words, assuming the natural frequency of the human DOF f_H as ranging from 4 to 6 Hz, the difference between $f^{(MM)}$ and $f_1^{(UM)}$ is less than 0.2 Hz for f_S smaller than 2.7 Hz or 4.0 Hz respectively.

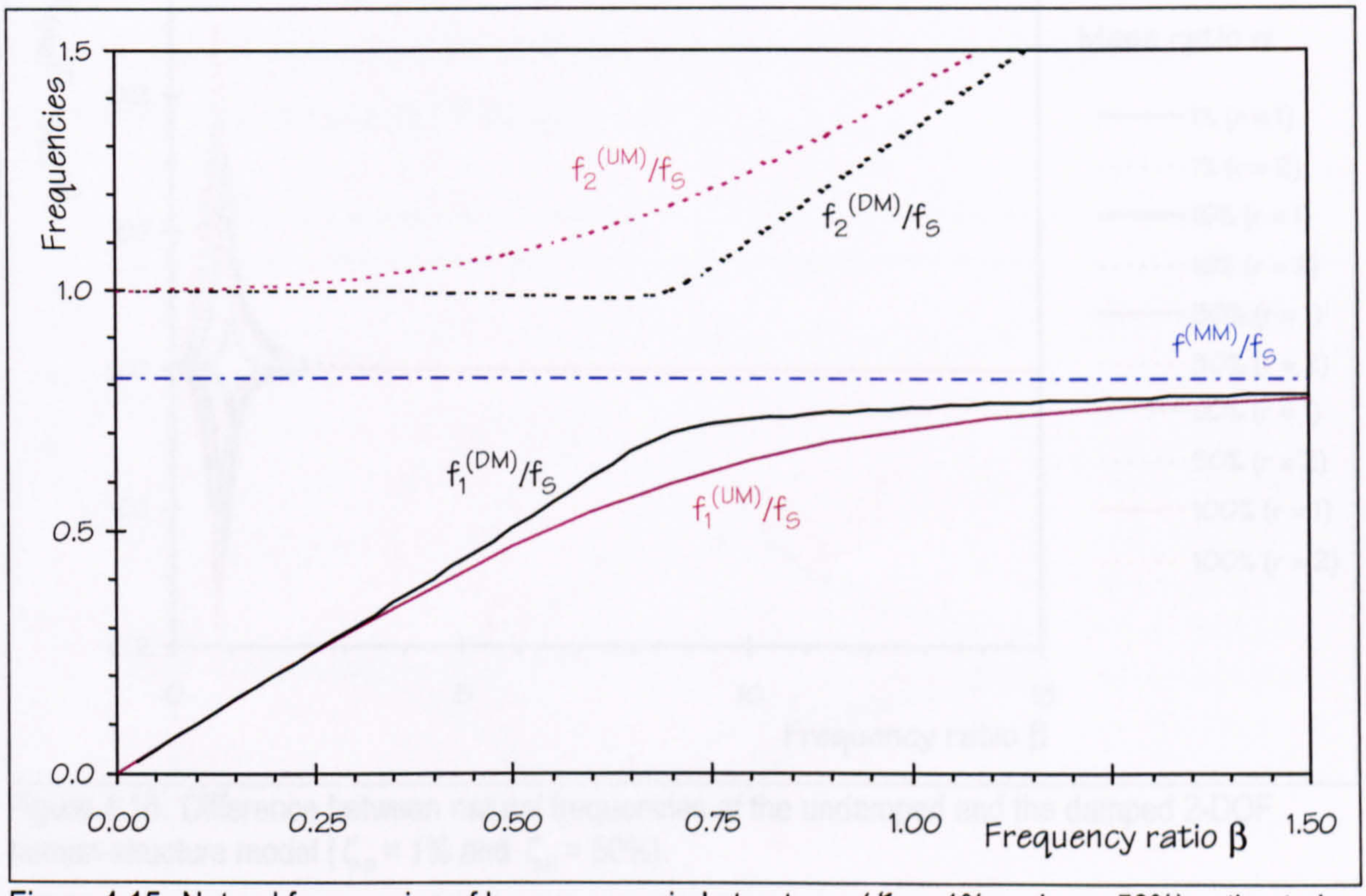

Figure 4.15: Natural frequencies of human-occupied structures ($\zeta_S = 1\%$ and $\alpha = 50\%$) estimated with the mass-only model, the undamped and the damped 2-DOF model ($\zeta_H = 50\%$).

However, if the frequency ratio $\beta \leq 1.5$ (and thus in this example f_S is higher than 4 Hz), the natural frequency $f^{(MM)}$ is significantly higher than $f_1^{(UM)}$ and $f_1^{(DM)}$ of the 2-DOF human-structure models (Figure 4.15). This is particularly important considering structures that have fundamental frequencies above 6 Hz, which are usually assumed to perform satisfactory under human-induced vibrations (IStructE 2001, p. 9).

4.2.4.2 UNDAMPED AND DAMPED 2-DOF HUMAN-STRUCTURE MODEL

Generally, the natural frequencies of the damped and the undamped 2-DOF human-structure system are relatively close (Figures 4.5 and 4.9). Analysing this issue in more detail, the difference $f_r^{(UM)} - f_r^{(DM)}$ between frequencies of the undamped (Figure 4.4) and the damped 2-DOF system (Figure 4.8) is calculated. It is normalised to f_s and presented in Figure 4.16.

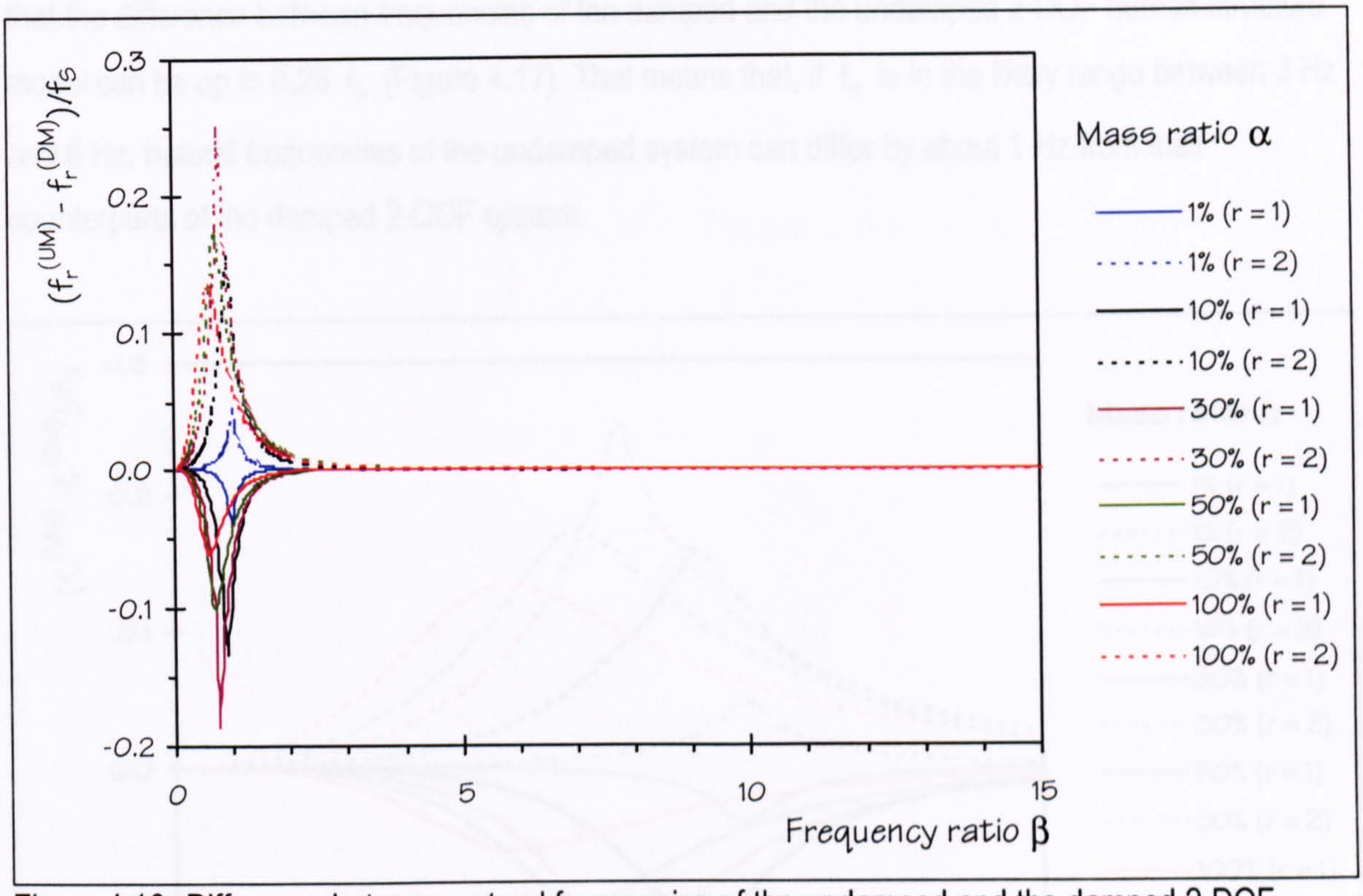

Figure 4.16: Difference between natural frequencies of the undamped and the damped 2-DOF human-structure model (ζ_S = 1% and ζ_H = 50%).

Dashed lines in Figure 4.16 reveal that the difference $f_2^{(UM)} - f_2^{(DM)}$ is positive. Hence, the second frequency of the undamped 2-DOF model is higher than that of the damped model:

$$f_2^{(UM)} > f_2^{(DM)}. \tag{4.20}$$

In contrast, fundamental frequencies of the undamped 2-DOF model are smaller than those of the damped 2-DOF human-structure system (Figure 4.16):

$$f_1^{(UM)} < f_1^{(DM)}. \tag{4.21}$$

Using previously gained knowledge, this equation (4.21) can be extended (Figure 4.15) to:

$$f_S > f^{(MM)} > f_1^{(DM)} > f_1^{(UM)}. \tag{4.22}$$

The difference between frequencies of the undamped and the damped 2-DOF model are highest for frequency ratios β around unity (Figure 4.16).

To provide better insight into this issue, a part of Figure 4.16 is enlarged by limiting the frequency ratio to $\beta \leq 1.5$. The resulting Figure 4.17 does not reveal a simple pattern. Nevertheless, it shows that the difference between frequencies of the damped and the undamped 2-DOF human-structure model can be up to 0.25 f_S (Figure 4.17). That means that, if f_S is in the likely range between 3 Hz and 6 Hz, natural frequencies of the undamped system can differ by about 1 Hz from their counterparts of the damped 2-DOF system.

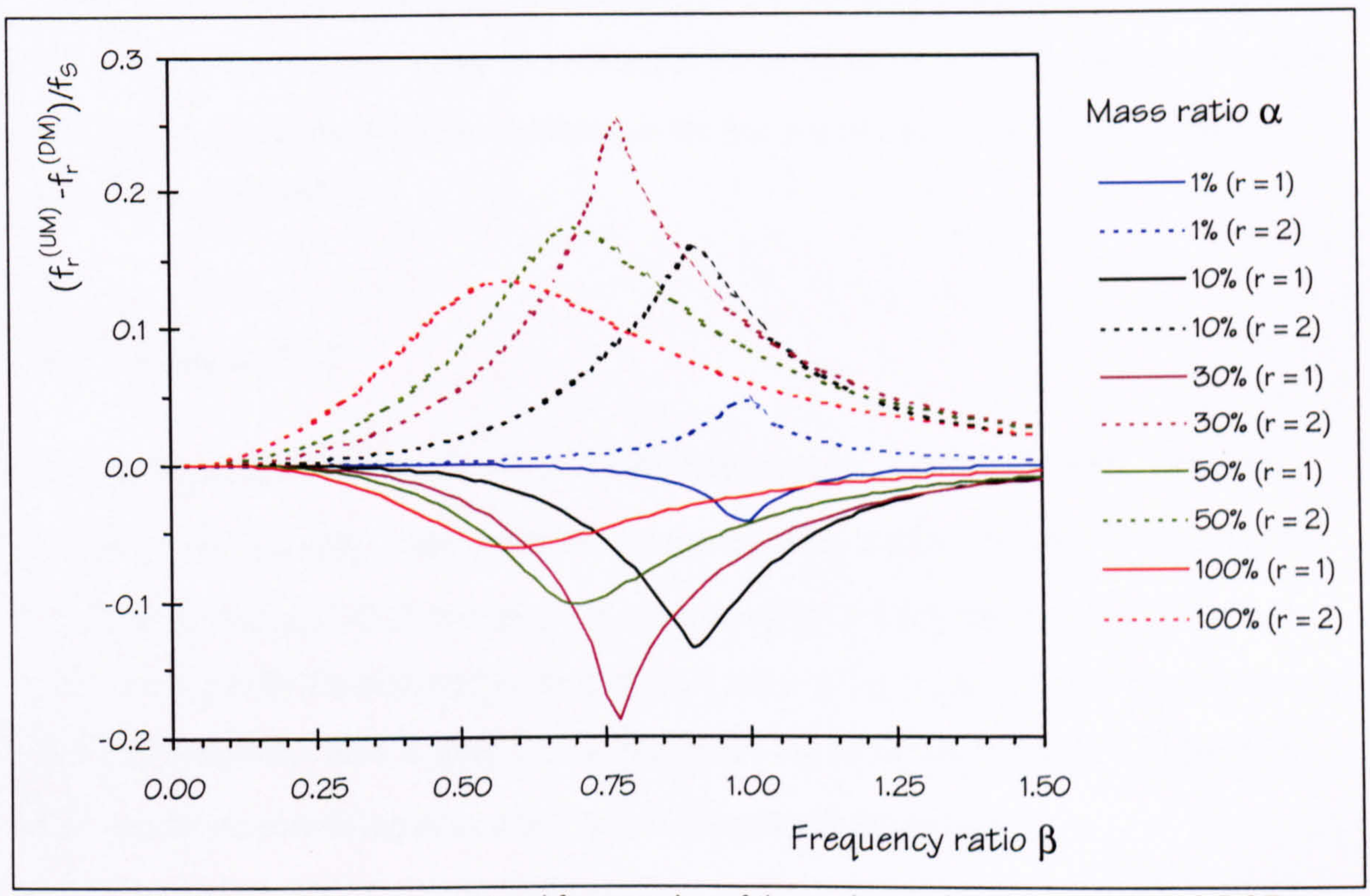

Figure 4.17: Difference between natural frequencies of the undamped and the damped 2-DOF human-structure model (ζ_S = 1% and ζ_H = 50%, $\beta \leq 1.5$).

Finally, it is noted that $f_2^{(UM)}$ and $f_2^{(DM)}$ of 2-DOF human-structure systems are close to the frequency of the structure f_S if the frequency ratio $\beta < 0.2$ (Figure 4.15). This range corresponds to structures with natural frequencies of at least 20 Hz (assuming f_H above 4 Hz), which are usually not of concern (IStructE 2001).

4.2.4.3 SUMMARY

The main conclusions drawn from the comparison of frequencies estimated with the three human-structure models are:

(1) that the fundamental frequencies of all three human-structure models $f^{(MM)}$, $f_1^{(UM)}$, and $f_1^{(DM)}$ are similar, if the frequency ratio $\beta > 1.5$ (Figure 4.15),

(2) summarised in equations (4.20) and (4.22), and

(3) the natural frequencies of the undamped $f_r^{(UM)}$ and the damped $f_r^{(DM)}$ 2-DOF human-structure system deviate by up to $0.25\, f_s$ (Figures 4.16 and 4.17).

4.3 MODE SHAPE

In the previous section, natural frequencies of the human-structure system modelled with three different human models (Figure 4.1) were analysed. In this chapter, the amplitude normalised mode shapes $\{\psi\}_r$ of the damped 2-DOF human-structure system (Figure 4.1c) are investigated.

Damping of such viscously damped 2-DOF human-structure systems is generally non-proportional. Therefore, the mode shapes $\{\psi\}_r$ are complex. To account for this complexity, mode shape magnitudes $|\{\psi\}|$ and phases $arg\{\psi\}$ are analysed separately. Thereby, it is concentrated on human-structure systems with damping ratios $\zeta_S = 1\%$ and $\zeta_H = 30\%$.

In the following sections, it is first analysed which DOF (human or structure) dominates each mode r. Secondly, it is investigated how mass and frequency ratios α and β influence the mode shape amplitude and phase differences between the first and second mode. Finally, mode complexity is discussed.

4.3.1 DOMINANT DOF

A DOF n dominates a mode r (r = 1 or 2) if the magnitude $|\psi_{nr}|$ of the amplitude normalised mode shape $\{\psi\}_r$ is unity. Investigating the dominance of the first ($n = S$) and the second DOF ($n = H$) of the damped 2-DOF human-structure system (Figure 4.1c), the dominant DOF of both modes is calculated. It is evaluated for several mass ratios α (α = 1%, 10%, and every 10% up to 100%) and frequency ratios β (from 0 to 5). The results are visualised in Figures 4.18 and 4.19, which use the mass and frequency ratios α and β as coordinate system.

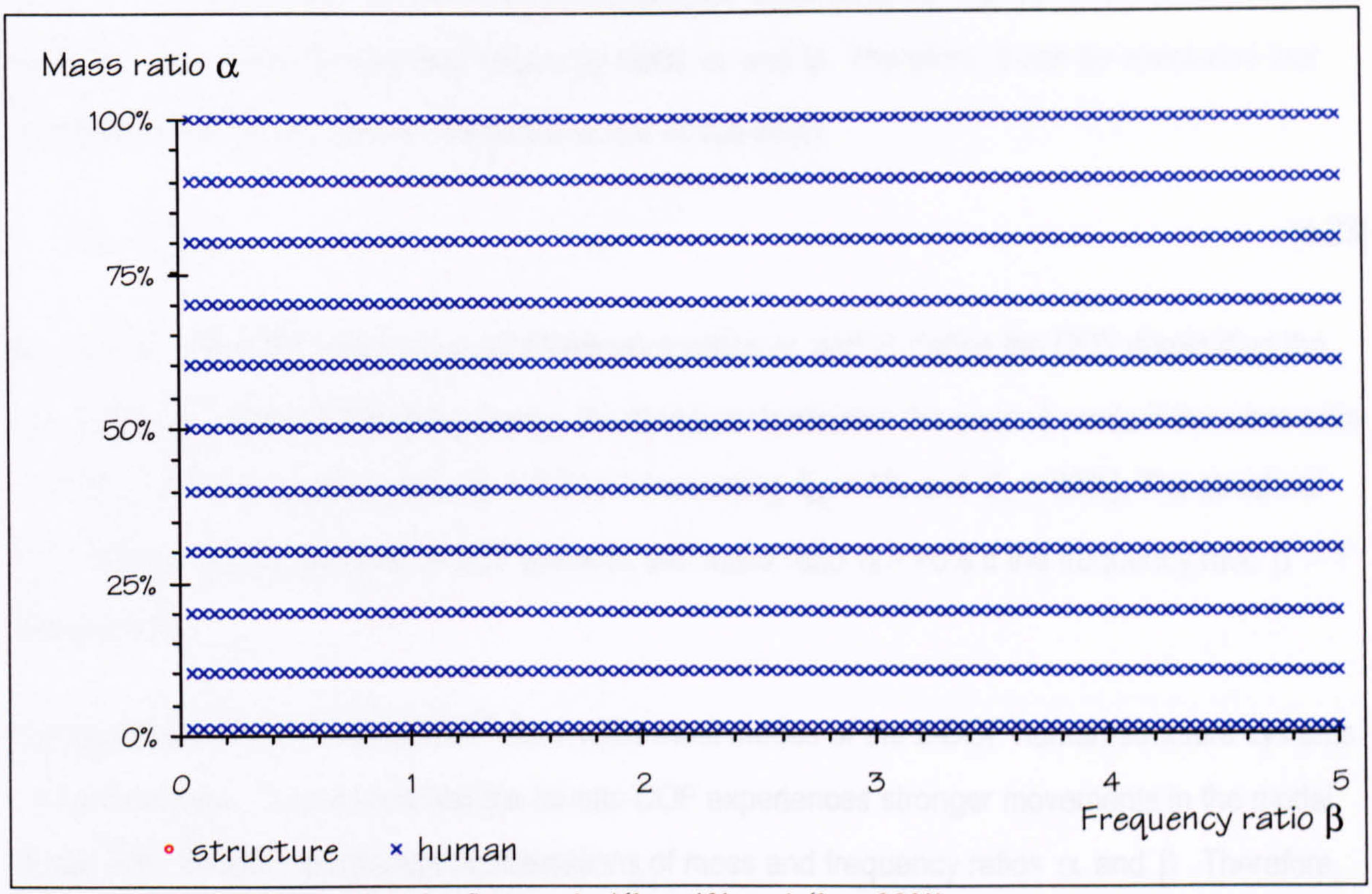

Figure 4.18: DOF dominating the first mode (ζ_S = 1% and ζ_H = 30%).

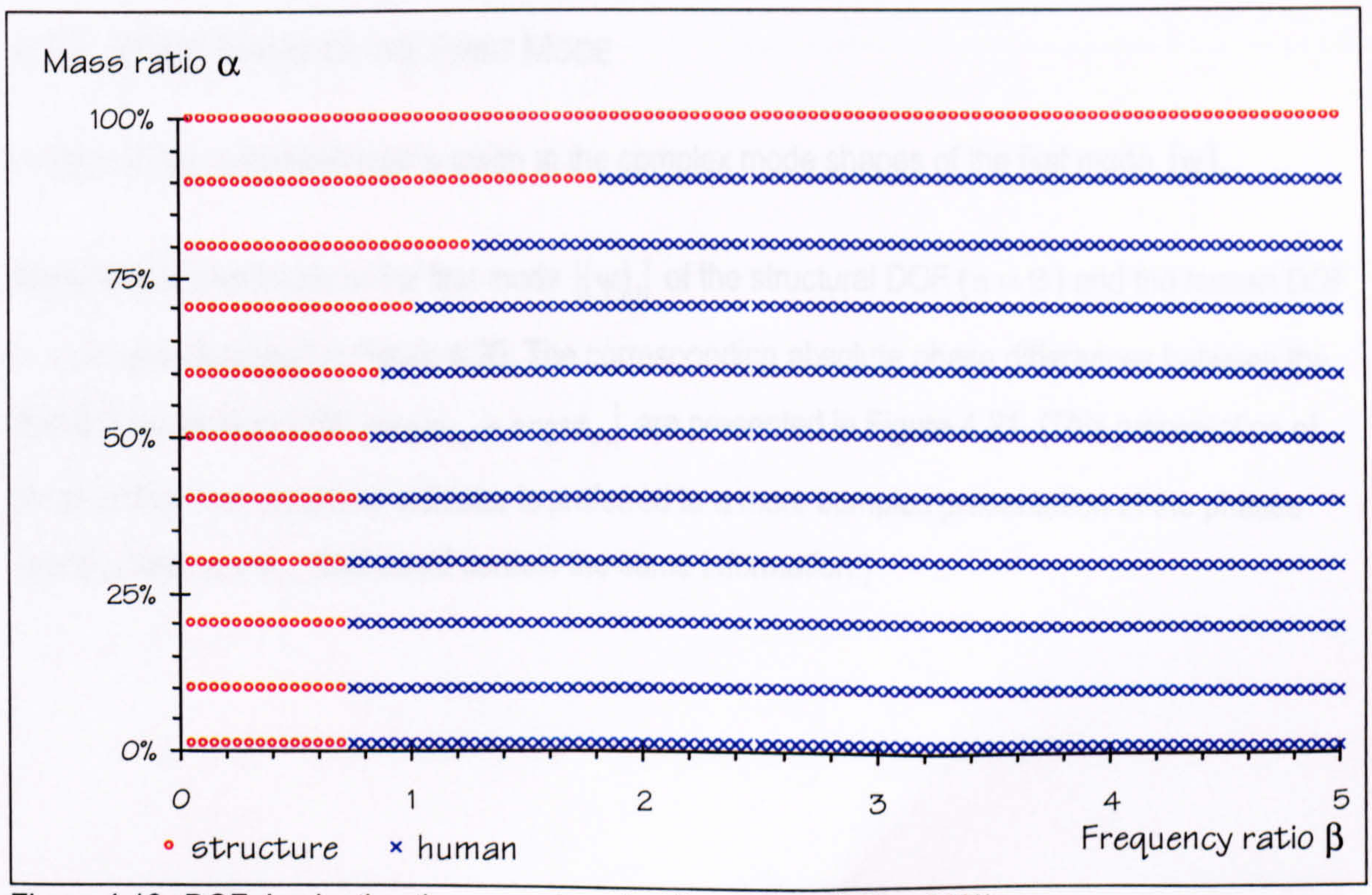

Figure 4.19: DOF dominating the second mode (ζ_S = 1% and ζ_H = 30%).

Figure 4.18 clearly demonstrates that the human DOF dominates the first mode (symbolised by blue crosses), regardless of mass and frequency ratios α and β. Therefore, it can be concluded that equation (4.23) is true, at least within the scope of this study.

$$|\psi_{S1}| < |\psi_{H1}| \tag{4.23}$$

In contrast to the first mode, mass and frequency ratios α and β define the DOF dominating the second mode (Figure 4.19). In particular, the structure dominates the second mode if the mass ratio $\alpha < 70\%$ and the frequency ratio $\beta < 0.8$ to 1 (assuming $\zeta_S = 1\%$ and $\zeta_H = 30\%$). The structural DOF also dominates damped 2-DOF systems with mass ratio $\alpha > 70\%$ if the frequency ratio $\beta > 1$ (Figure 4.19).

It is concluded that the human DOF dominates most modes of the 2-DOF human-structure systems considered here. That means that the human DOF experiences stronger movements in the modal space than the structure at most combinations of mass and frequency ratios α and β. Therefore, including the movements of the human body (the recipient of vibrations) might be a significant step forward in analysing vibration serviceability of civil engineering structures.

4.3.2 Mode Shape of the First Mode

In this section, a detailed look is taken at the complex mode shapes of the first mode $\{\psi\}_1$.

Mode shape amplitudes of the first mode $|\{\psi\}_1|$ of the structural DOF ($n = S$) and the human DOF ($n = H$) are visualised in Figure 4.20. The corresponding absolute phase differences between the first and the second DOF $|arg\,\psi_{H1} - arg\,\psi_{S1}|$ are presented in Figure 4.21. (This presentation of phase differences as phase indicator is preferred to a more complex presentation of the phases $arg\,\psi_{S1}$ and $arg\,\psi_{H1}$ that would contain the same information.)

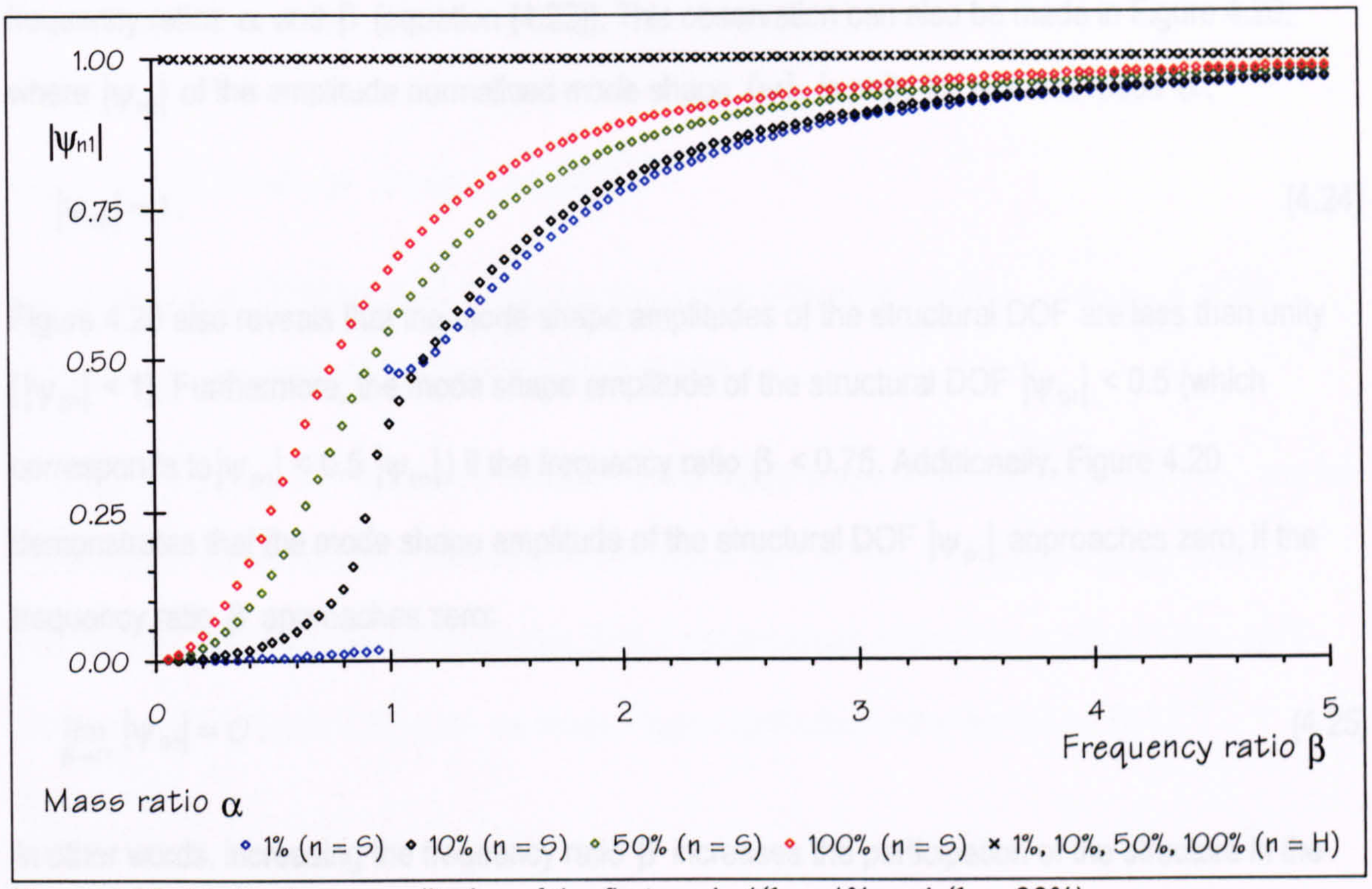

Figure 4.20: Mode shape amplitudes of the first mode (ζ_S = 1% and ζ_H = 30%).

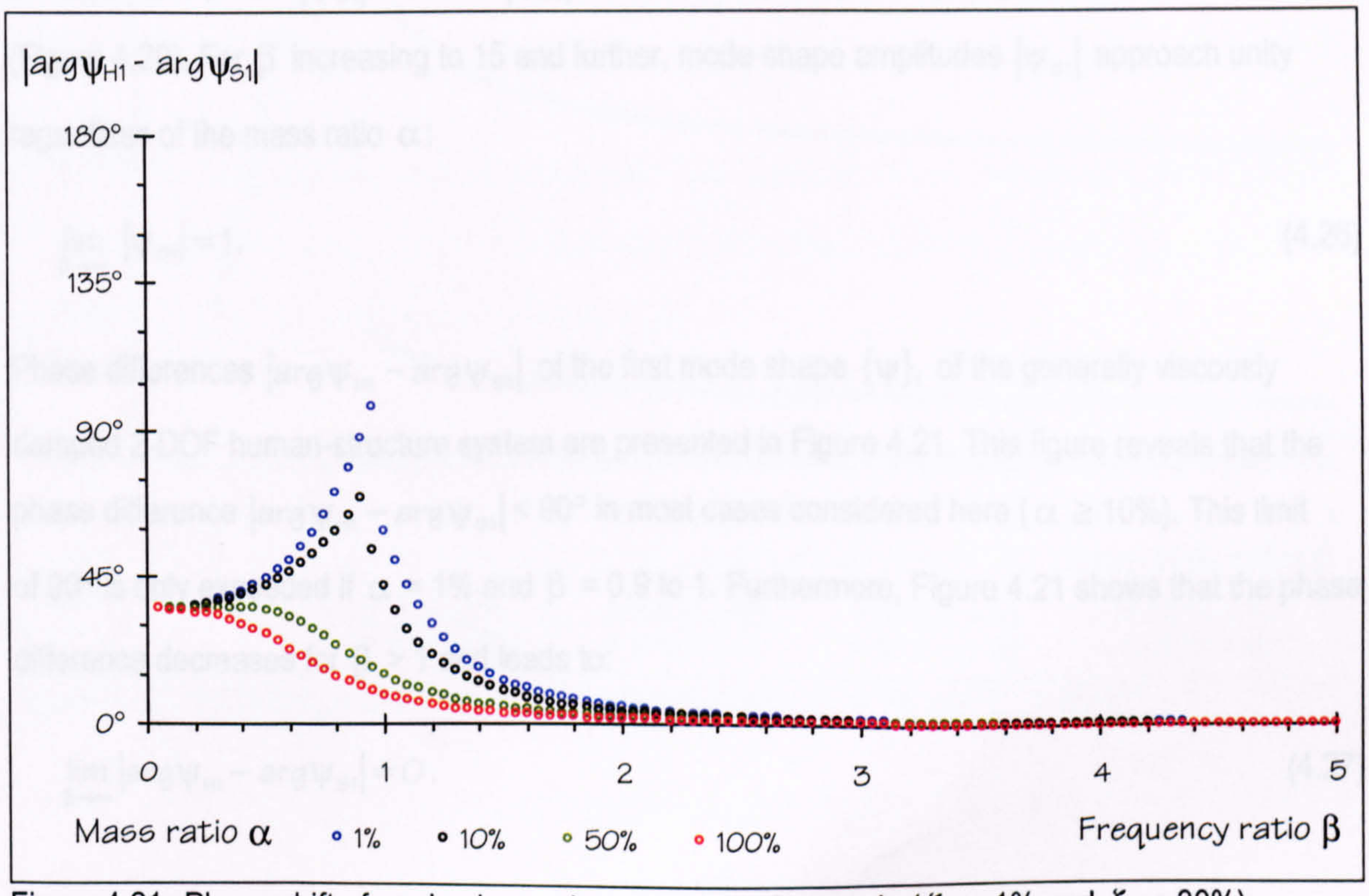

Figure 4.21: Phase shift of mode shape elements in the first mode (ζ_S = 1% and ζ_H = 30%).

It was outlined previously that the human DOF dominates the first mode regardless of mass and frequency ratios α and β (equation (4.23)). This observation can also be made in Figure 4.20, where $|\psi_{H1}|$ of the amplitude normalised mode shape $\{\psi\}$, is unity for all mass ratios α:

$$|\psi_{H1}| = 1. \tag{4.24}$$

Figure 4.20 also reveals that the mode shape amplitudes of the structural DOF are less than unity ($|\psi_{S1}| < 1$). Furthermore, the mode shape amplitude of the structural DOF $|\psi_{S1}| < 0.5$ (which corresponds to $|\psi_{S1}| < 0.5\ |\psi_{H1}|$) if the frequency ratio $\beta < 0.75$. Additionally, Figure 4.20 demonstrates that the mode shape amplitude of the structural DOF $|\psi_{S1}|$ approaches zero, if the frequency ratio β approaches zero:

$$\lim_{\beta \to O} |\psi_{S1}| = O. \tag{4.25}$$

In other words, increasing the frequency ratio β increases the participation of the structure in the first mode. In the cases considered here, the mode shape amplitude $|\psi_{S1}|$ increases steadily with increasing frequency ratio β if $\alpha \geq 10\%$. However, if α = 1%, mode shape amplitudes $|\psi_{S1}|$ increase rapidly from $|\psi_{S1}| \approx 0.05$ to $|\psi_{S1}| \approx 0.5$ at a frequency ratio β slightly smaller than unity (Figure 4.20). For β increasing to 15 and further, mode shape amplitudes $|\psi_{S1}|$ approach unity regardless of the mass ratio α:

$$\lim_{\beta \to \infty} |\psi_{S1}| = 1. \tag{4.26}$$

Phase differences $|arg\psi_{H1} - arg\psi_{S1}|$ of the first mode shape $\{\psi\}_1$ of the generally viscously damped 2-DOF human-structure system are presented in Figure 4.21. This figure reveals that the phase difference $|arg\psi_{H1} - arg\psi_{S1}| < 90°$ in most cases considered here ($\alpha \geq 10\%$). This limit of 90° is only exceeded if α = 1% and β = 0.9 to 1. Furthermore, Figure 4.21 shows that the phase difference decreases for $\beta > 1$ and leads to:

$$\lim_{\beta \to \infty} |arg\psi_{H1} - arg\psi_{S1}| = O. \tag{4.27}$$

The characteristics summarised in equations (4.24) to (4.27) will later be used to discuss mode complexity and to calculate modal masses and modal damping ratios.

4.3.3 Mode Shape of the Second Mode

The mode shape amplitude $|\{\psi\}_2|$ and absolute phase difference $|arg\,\psi_{H2} - arg\,\psi_{S2}|$ of the second mode are presented in Figures 4.22 and 4.23.

Similarly to Figure 4.19, Figure 4.22 reveals that the mode shape of the second mode $\{\psi\}_2$ can be dominated by the structural or the human DOF, that is $|\psi_{S2}| > |\psi_{H2}|$ or $|\psi_{S2}| < |\psi_{H2}|$. It also indicates that the mode shape amplitudes $|\{\psi\}_2|$ depend more strongly on mass and frequency ratios α and β (Figure 4.22) than the mode shape amplitudes of the first mode $|\{\psi\}_1|$ (Figure 4.20).

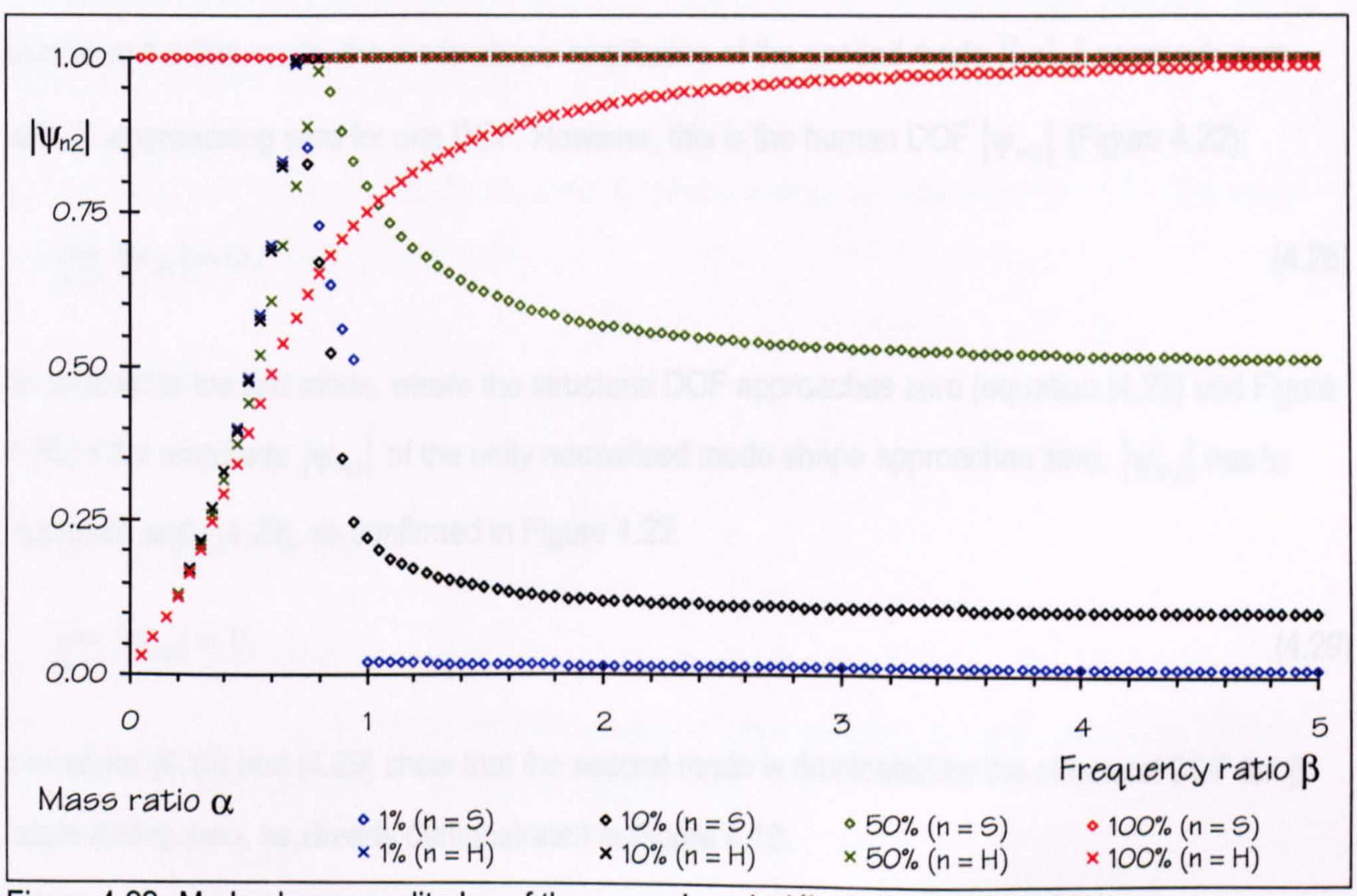

Figure 4.22: Mode shape amplitudes of the second mode (ζ_S = 1% and ζ_H = 30%).

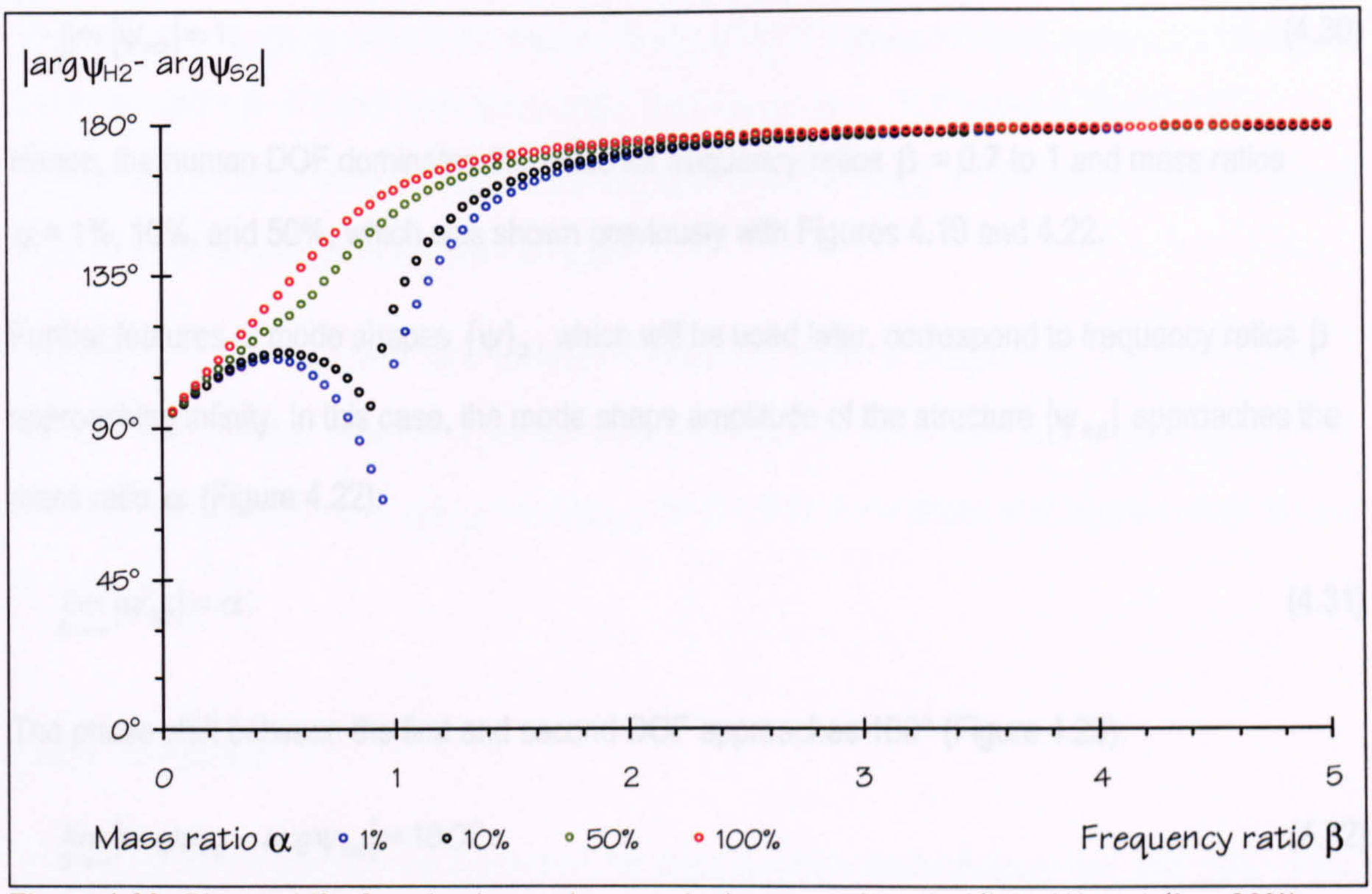

Figure 4.23: Phase shift of mode shape elements in the second mode (ζ_S = 1% and ζ_H = 30%).

Similar to the first mode, the mode shape amplitudes of the second mode $|\{\psi\}_2|$ approach zero with β approaching zero for one DOF. However, this is the human DOF $|\psi_{H2}|$ (Figure 4.22):

$$\lim_{\beta \to O} |\psi_{H2}| = O\,. \tag{4.28}$$

In contrast to the first mode, where the structural DOF approaches zero (equation (4.25) and Figure 4.20) if the amplitude $|\psi_{H2}|$ of the unity normalised mode shape approaches zero, $|\psi_{S2}|$ has to approach unity (4.29), as confirmed in Figure 4.22.

$$\lim_{\beta \to O} |\psi_{S2}| = 1 \tag{4.29}$$

Equations (4.20) and (4.29) show that the second mode is dominated by the structural DOF for β approaching zero, as already demonstrated in Figure 4.19.

With an increasing frequency ratio β, the participation of the human DOF in the mode increases (Figure 4.22). That results in $|\psi_{H2}|$ approaching unity for increasing β:

$$\lim_{\beta\to\infty} |\psi_{H2}| = 1. \tag{4.30}$$

Hence, the human DOF dominates the mode for frequency ratios β = 0.7 to 1 and mass ratios α = 1%, 10%, and 50%, which was shown previously with Figures 4.19 and 4.22.

Further features of mode shapes $\{\psi\}_2$, which will be used later, correspond to frequency ratios β approaching infinity. In this case, the mode shape amplitude of the structure $|\psi_{S2}|$ approaches the mass ratio α (Figure 4.22):

$$\lim_{\beta\to\infty} |\psi_{S2}| = \alpha. \tag{4.31}$$

The phase shift between the first and second DOF approaches 180° (Figure 4.23):

$$\lim_{\beta\to\infty} |arg\psi_{H2} - arg\psi_{S2}| = 180°. \tag{4.32}$$

It should be noted that the phase shift $|arg\psi_{H2} - arg\psi_{S2}|$ > 90° in most cases, except if α = 1% and simultaneously β = 0.8 to 1 (Figure 4.23).

Finally, it has to be mentioned that the absolute phase difference reduces to 90° if the frequency ratio β approaches zero (Figure 4.23):

$$\lim_{\beta\to 0} |arg\psi_{H2} - arg\psi_{S2}| = 90°. \tag{4.33}$$

4.3.4 Mode Complexity

Based on the discussion of mode shape amplitudes and phase differences, the complexity of the mode shapes is discussed briefly. This discussion is only qualitative because there is no agreed quantification of mode complexity (Ewins 2000, p. 113).

Mode shapes of proportionally damped systems are real valued and not complex. That is, their mode shape elements are in phase (phase shift of 0°) or out of phase (phase shift of 180°). Hence, the complexity is high if the phase shift is close to 90°. However, complexity is, regardless of phase shifts, considered small if mode shape amplitudes are small.

In the first mode, phase shifts of the heavily damped 2-DOF human-structure system are largest for frequency ratios $\beta \approx 1$ and small mass ratios, for instance $\alpha = 1\%$ (Figures 4.20 and 4.21). Simultaneously, mode shape amplitudes of the structural DOF $|\psi_{s1}| < 0.5$ (Figure 4.20). Hence, the complexity of the first mode is generally small.

Similarly, the second mode is most complex at frequency ratios β around unity (Figures 4.22 and 4.23). This is because at higher or smaller frequency ratios β either one mode shape amplitude is small compared to the other ($|\psi_{H2}| < 0.3\ |\psi_{s2}|$ for $\beta < 0.4$) or the phase shift between them is close to 180° ($\beta > 1.2$).

4.3.5 Summary

Three main conclusions can be drawn from the analysis of the mode shapes $\{\psi\}_1$ and $\{\psi\}_2$ of the damped 2-DOF human-structure system:

(1) Movement of the human DOF dominates the mode shape of the first mode $\{\psi\}_1$ (Figure 4.18).

(2) The phase shift between the first and second DOF is usually smaller than 90° in the first mode (Figure 4.21) and usually higher than 90° in the second mode (Figure 4.23).

(3) The mode complexity of the two modes of human-structure systems is highest at frequency ratios $\beta \approx 1$.

4.4 Modal Mass

Modal masses m_r are an essential tool in response calculations (see section 3.1). In this section, modal masses are calculated parametrically from amplitude normalised (that is unity scaled) mode shapes $\{\psi\}_r$. The modal masses m_1 and m_2 are analysed for 2-DOF human-structure systems with damping ratios ζ_S = 1% and ζ_H = 30% and mass ratios α = 1%, 10%, 50%, and 100%. They are presented in Figure 4.24 as solid lines (modal masses m_1) and as dashed lines (m_2) in colours corresponding to the four mass ratios α.

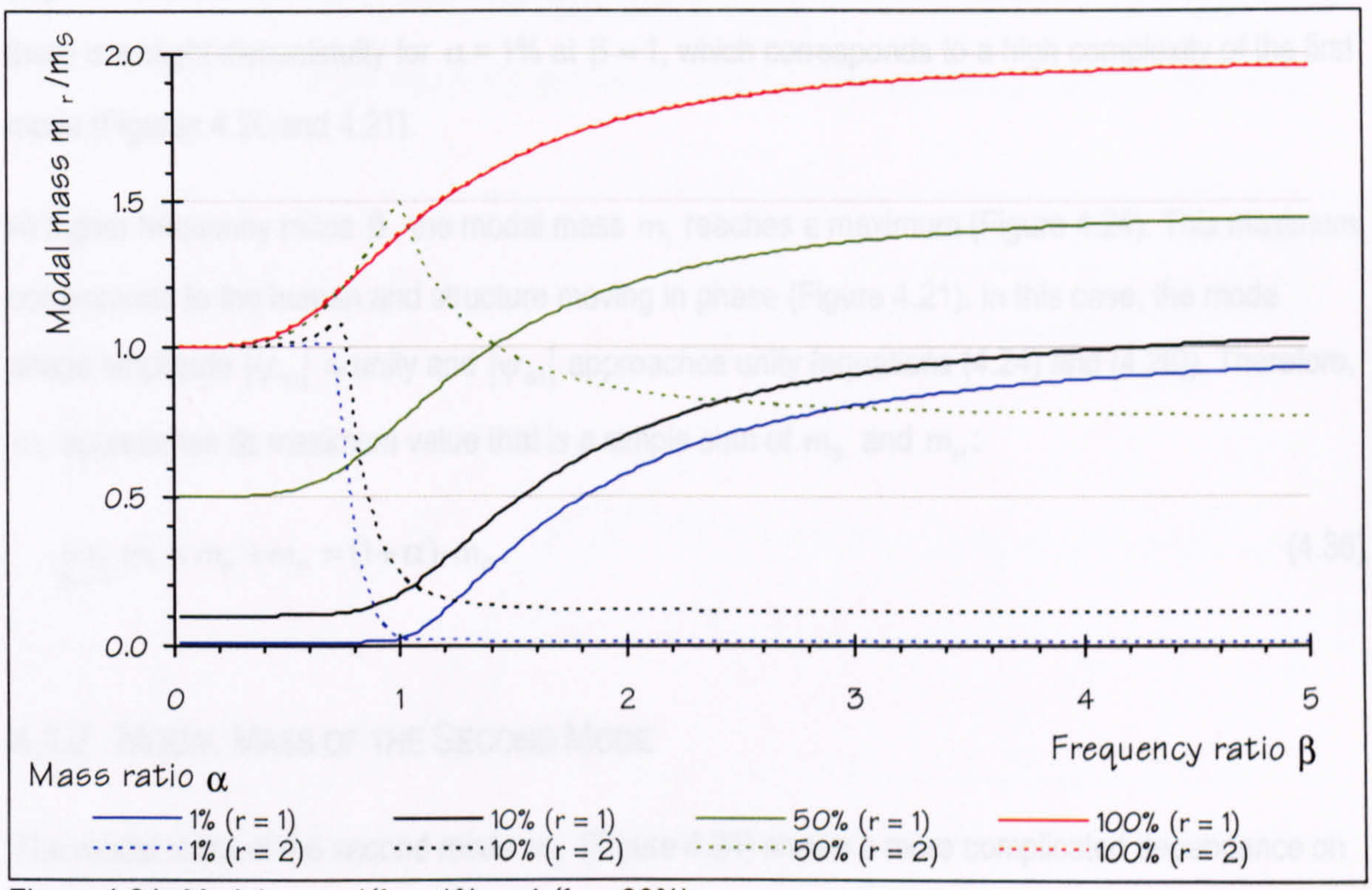

Figure 4.24: Modal mass (ζ_S = 1% and ζ_H = 30%).

4.4.1 Modal Mass of the First Mode

Figure 4.24 reveals that the unity scaled modal mass m_1 is always larger than the lumped mass of the human DOF m_H:

$$m_1 > m_H . \tag{4.34}$$

This phenomenon is due to the dominance of the human DOF in the first mode (section 4.3.1), which results in m_1 comprising the whole of m_H plus a mode shape dependent contribution of m_S. However, the participation of the structure approaches zero with decreasing β (equation (4.25)). Therefore, the modal mass m_1 approaches its lower limit m_H for the frequency ratio β approaching zero (Figure 4.24):

$$\lim_{\beta \to 0} m_1 = m_H = \alpha \cdot m_S . \tag{4.35}$$

With increasing frequency ratio β, the participation of the structural DOF in the first mode increases (Figure 4.20), so, the modal mass m_1 increases (Figure 4.24). However, Figure 4.24 shows that there is a slight discontinuity for $\alpha = 1\%$ at $\beta \approx 1$, which corresponds to a high complexity of the first mode (Figures 4.20 and 4.21).

At higher frequency ratios β, the modal mass m_1 reaches a maximum (Figure 4.24). This maximum corresponds to the human and structure moving in phase (Figure 4.21). In this case, the mode shape amplitude $|\psi_{H1}|$ is unity and $|\psi_{S1}|$ approaches unity (equations (4.24) and (4.26)). Therefore, m_1 approaches its maximum value that is a simple sum of m_S and m_H:

$$\lim_{\beta \to \infty} m_1 = m_H + m_S = (1+\alpha) \cdot m_S . \tag{4.36}$$

4.4.2 Modal Mass of the Second Mode

The modal mass of the second mode m_2 (Figure 4.24) shows a more complicated dependence on mass and frequency ratios α and β than that of the first mode. First, the two extreme cases of the frequency ratio β are considered. Next, modal masses m_2 at frequency ratios β around unity are examined.

If the frequency ratio β approaches zero, the participation of the human DOF tends to zero and the structural DOF dominates the second mode (equations (4.28) and (4.29) in section 4.3.3). Therefore, m_2 approaches its lower limit: the lumped mass of the structure m_S (4.37).

$$\lim_{\beta \to 0} m_2 = m_S \tag{4.37}$$

If the frequency ratio β approaches 15, both DOFs of the damped 2-DOF human-structure system participate in the second mode (Figures 4.23 and 4.23). With the mode shape $\{\psi\}_2$ defined by equations (4.30), (4.31), and (4.32), the modal mass m_2 can be estimated for β approaching infinity to:

$$\lim_{\beta\to\infty} m_2 = m_H + \alpha^2 \cdot m_S = \alpha \cdot (1+\alpha) \cdot m_S \tag{4.38}$$

Beside modal masses at extreme frequency ratios β, particular attention has to be paid to m_2 at frequency ratios β about unity, which is a more realistic case. This range cannot clearly be seen in Figure 4.24. Therefore, a closer look is taken at Figure 4.24 by limiting the frequency ratio to $\beta \leq 5$ and normalising the vertical axis to the sum of m_S and m_H. This procedure leads to Figure 4.25.

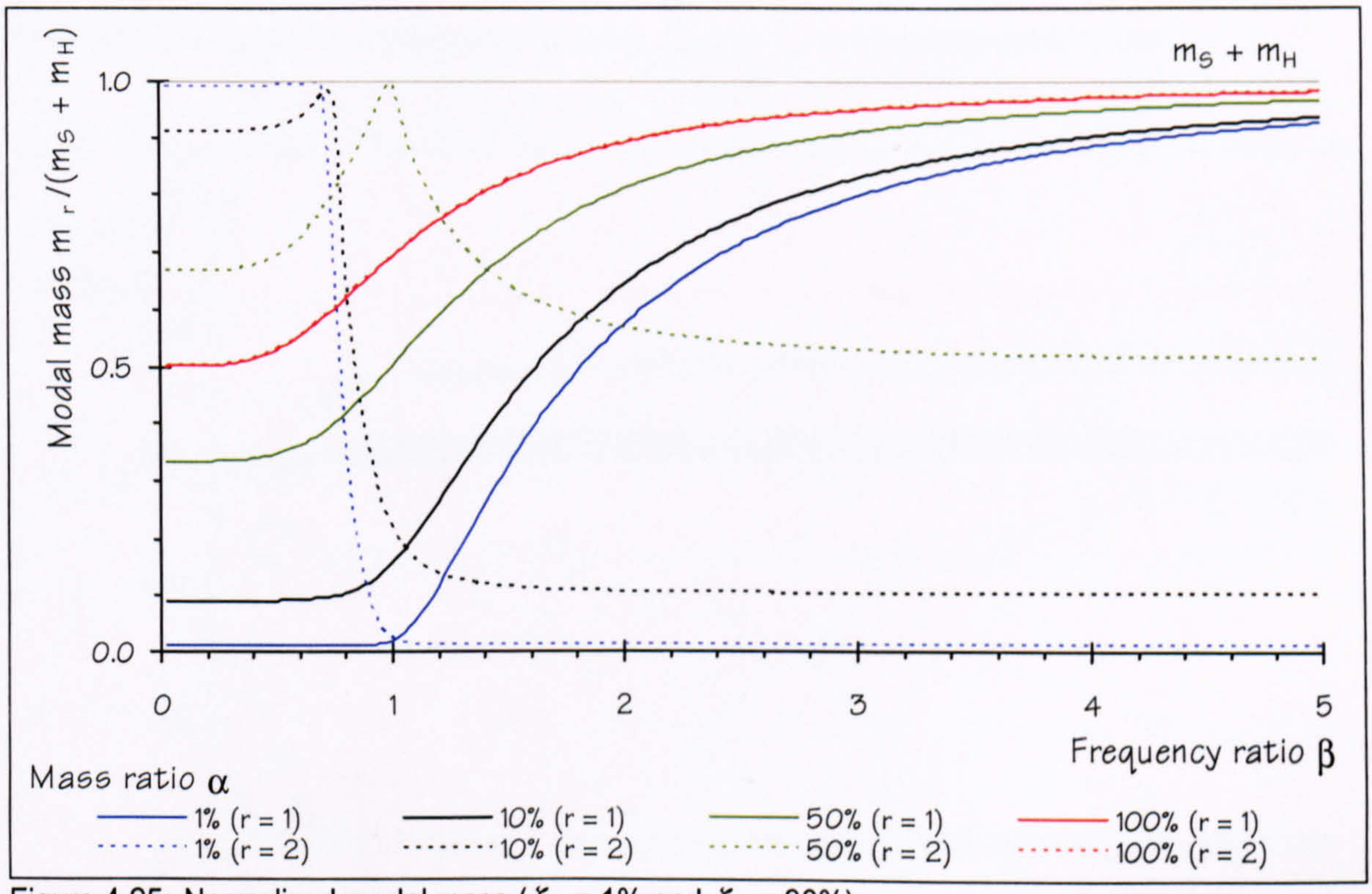

Figure 4.25: Normalised modal mass (ζ_S = 1% and ζ_H = 30%).

Figure 4.25 demonstrates that (for mass ratios $\alpha \leq 50\%$) the modal mass m_2 increases from the value m_S to the sum of m_S and m_H before dropping to the value specified by equation (4.38). With increasing mass ratio α, the local peak of m_2 widens and shifts to higher frequency ratios β (to β = 1.25 for α = 80% for example). In case of the highest investigated mass ratio α = 100%, the

modal mass m_2 of a damped 2-DOF system increases continually with the frequency ratio β and no local peak can be identified (Figure 4.25).

4.4.3 SUMMARY

It can be concluded that the modal masses m_1 and m_2 strongly depend on the mass and frequency ratios α and β, especially for frequency ratios β = 0.5 to 3. Also, the modal mass of each mode (m_1 and m_2) of the damped 2-DOF human-structure system is smaller than the sum of the masses of human m_H and structure m_S.

4.5 DAMPING RATIO

The modal damping ratios ζ_1 and ζ_2 are defined by the mode shapes and the damping matrix of the damped 2-DOF human-structure system (equation (3.57) in section 3.1.1.5). They are studied parametrically in this section for damped 2-DOF human-structure systems with assumed ζ_S = 1%. This was done by employing a range of frequency ratios β = 0 to 15 and four mass ratios: α = 1%, 10%, 50%, and 100%. The damping ratios of the human DOF ζ_H were set to 30% and 50%.

The analysis led to damping ratios presented in Figures 4.26 and 4.27 (ζ_H = 30% and ζ_H = 50%). These figures indicate that the damping ratios ζ_1 and ζ_2 strongly depend on the frequency ratio β if β < 1.5. Such frequency relations are very realistic in practical situations of crowd-occupied structures. Therefore, this frequency range was focused upon. Using Figures 4.28 and 4.29 presenting this range, the modal damping ratios ζ_1 and ζ_2 are now discussed in detail.

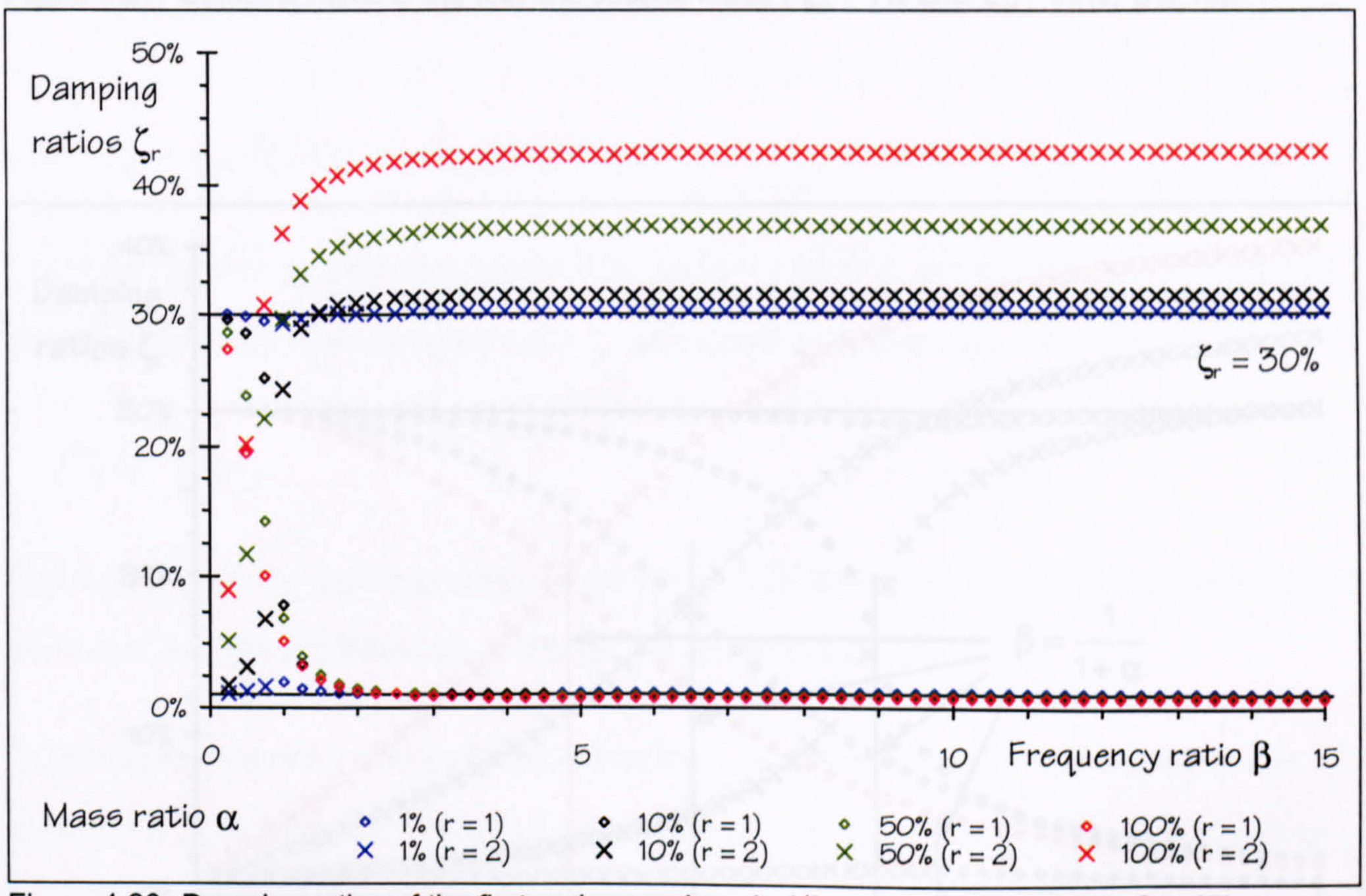

Figure 4.26: Damping ratios of the first and second mode (ζ_S = 1% and ζ_H = 30%, $\beta \leq 15$).

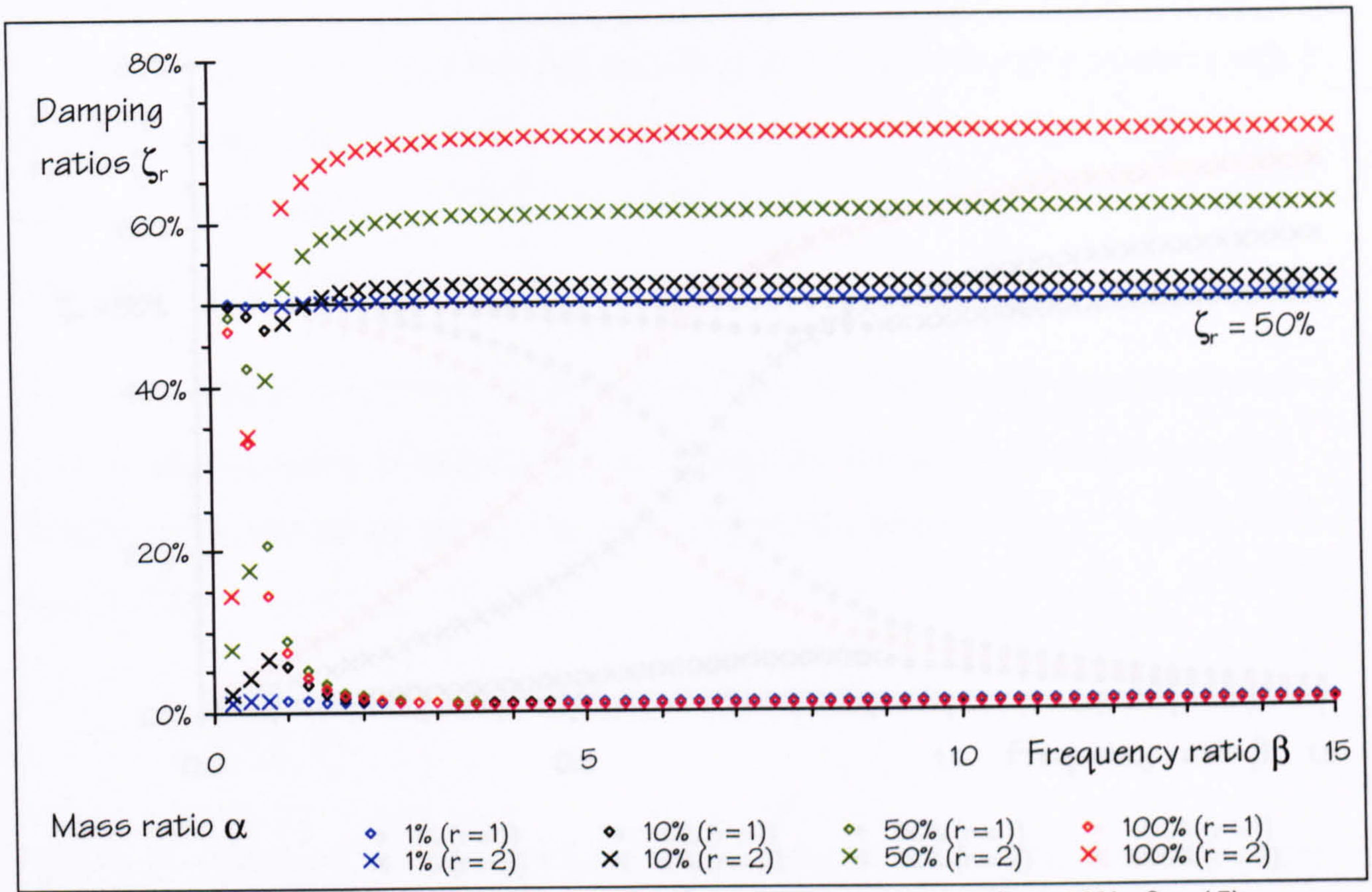

Figure 4.27: Damping ratios of the first and second mode (ζ_s = 1% and ζ_H = 50%, $\beta \leq 15$).

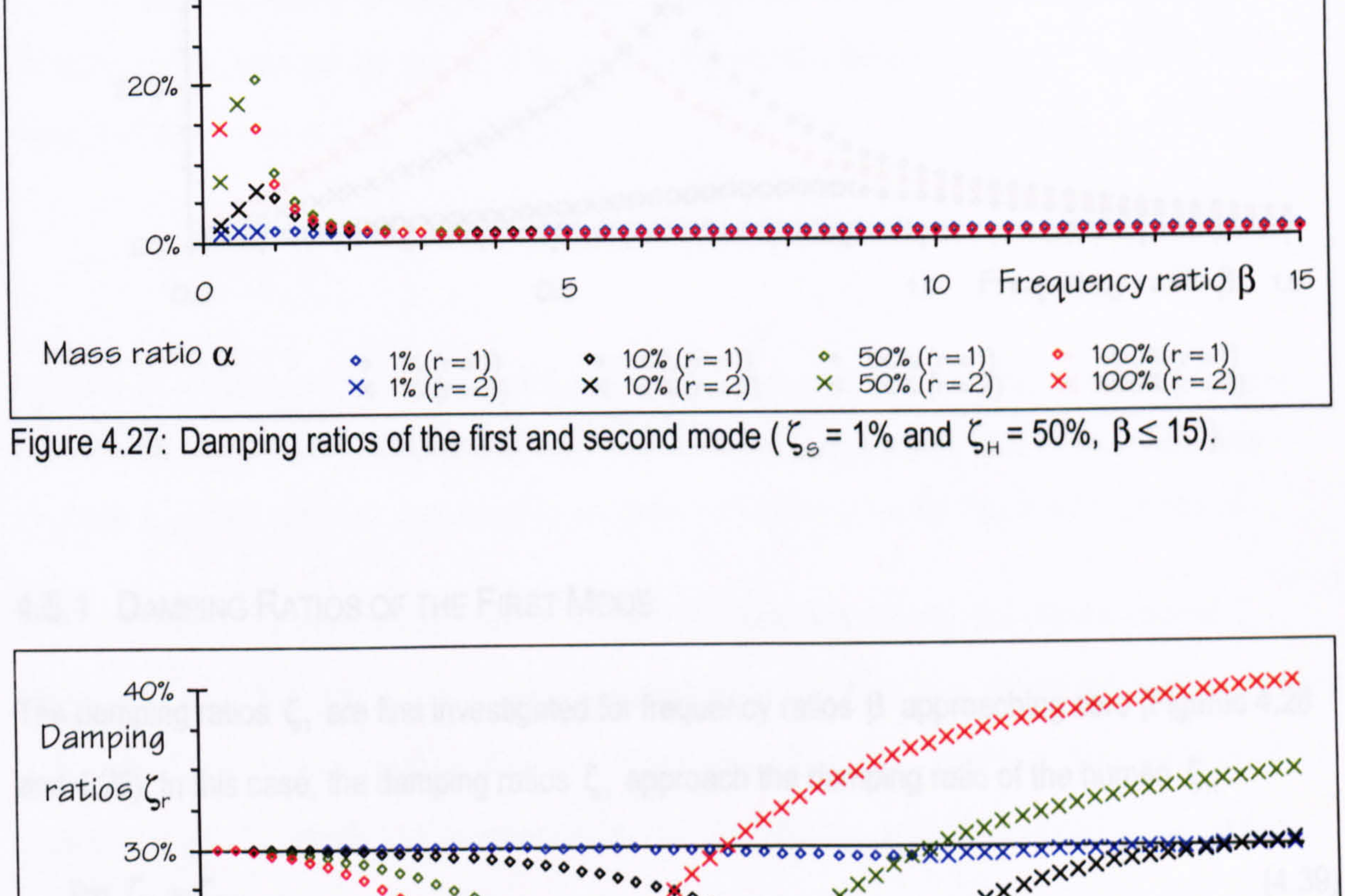

Figure 4.28: Damping ratios of the first and second mode (ζ_s = 1% and ζ_H = 30%, $\beta \leq 1.5$).

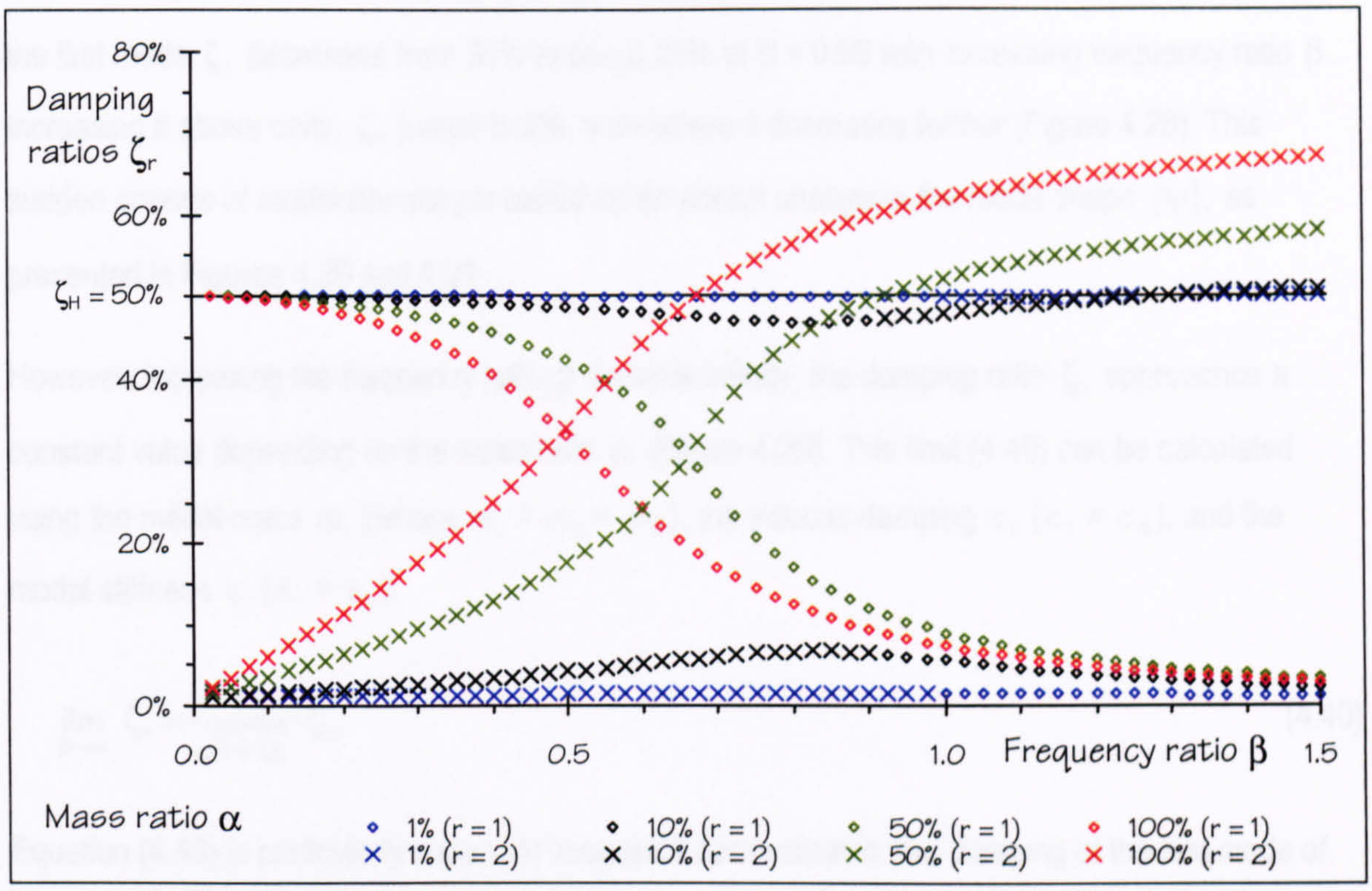

Figure 4.29: Damping ratios of the first and second mode (ζ_s = 1% and ζ_H = 50%, $\beta \leq 1.5$).

4.5.1 Damping Ratios of the First Mode

The damping ratios ζ_1 are first investigated for frequency ratios β approaching zero (Figures 4.28 and 4.29). In this case, the damping ratios ζ_1 approach the damping ratio of the human ζ_H:

$$\lim_{\beta \to 0} \zeta_1 = \zeta_H . \tag{4.39}$$

This is because in this particular case only the human DOF is engaged in the first mode as indicated by the mode shape amplitudes $|\psi_{H1}|$ and $|\psi_{S1}|$ (equations (4.24) and (4.25)).

Increasing the frequency ratio β, the damping ratio ζ_1 decreases (Figures 4.28 and 4.29). This decrease is gradual for $\alpha \geq 10\%$ if the human damping ratio ζ_H = 30% (as in Figure 4.28) and for $\alpha \geq 50\%$ if ζ_H = 50% (Figure 4.29). As long as the frequency ratio β is slightly smaller than unity, smaller mass ratios α lead to a smaller gradual decrease in ζ_1. At a certain frequency ratio β, the damping ratio ζ_1 does not decrease further gradually but rapidly (Figures 4.28 and 4.29).

For instance, if the human damping ratio ζ_H = 30% and the mass ratio α = 1%, the damping ratio of the first mode ζ_1 decreases from 30% to about 29% at β = 0.99 with increasing frequency ratio β. Increasing it above unity, ζ_1 jumps to 2%, from where it decreases further (Figure 4.28). This sudden change of modal damping is based on an abrupt change in the mode shape $\{\psi\}_1$ as presented in Figures 4.20 and 4.21.

However, increasing the frequency ratio β towards infinity, the damping ratio ζ_1 approaches a constant value depending on the mass ratio α (Figure 4.26). This limit (4.40) can be calculated using the modal mass m_1 (where $m_1 = m_S + m_H$), the viscous damping c_1 ($c_1 = c_S$), and the modal stiffness k_1 ($k_1 = k_S$).

$$\lim_{\beta \to \infty} \zeta_1 = \frac{1}{\sqrt{1+\alpha}} \cdot \zeta_S \tag{4.40}$$

Equation (4.40) is particularly important because it demonstrates that damping of the first mode of the damped 2-DOF human-structure system can actually be smaller than damping of the empty structure ζ_S. (This situation may occur in the case of structures having very low frequencies.)

To emphasise and support this somewhat surprising conclusion visually, the presentation of ζ_1 shown in Figures 4.26 and 4.27 is enlarged for low frequency ratios $\beta \leq 10$ and redrawn in Figures 4.30 and 4.31. It can now be seen that for β higher than about 3, ζ_1 is smaller than damping of the empty structure ζ_S, which was assumed to be 1%. The effect is more pronounced in the case of large mass ratios α.

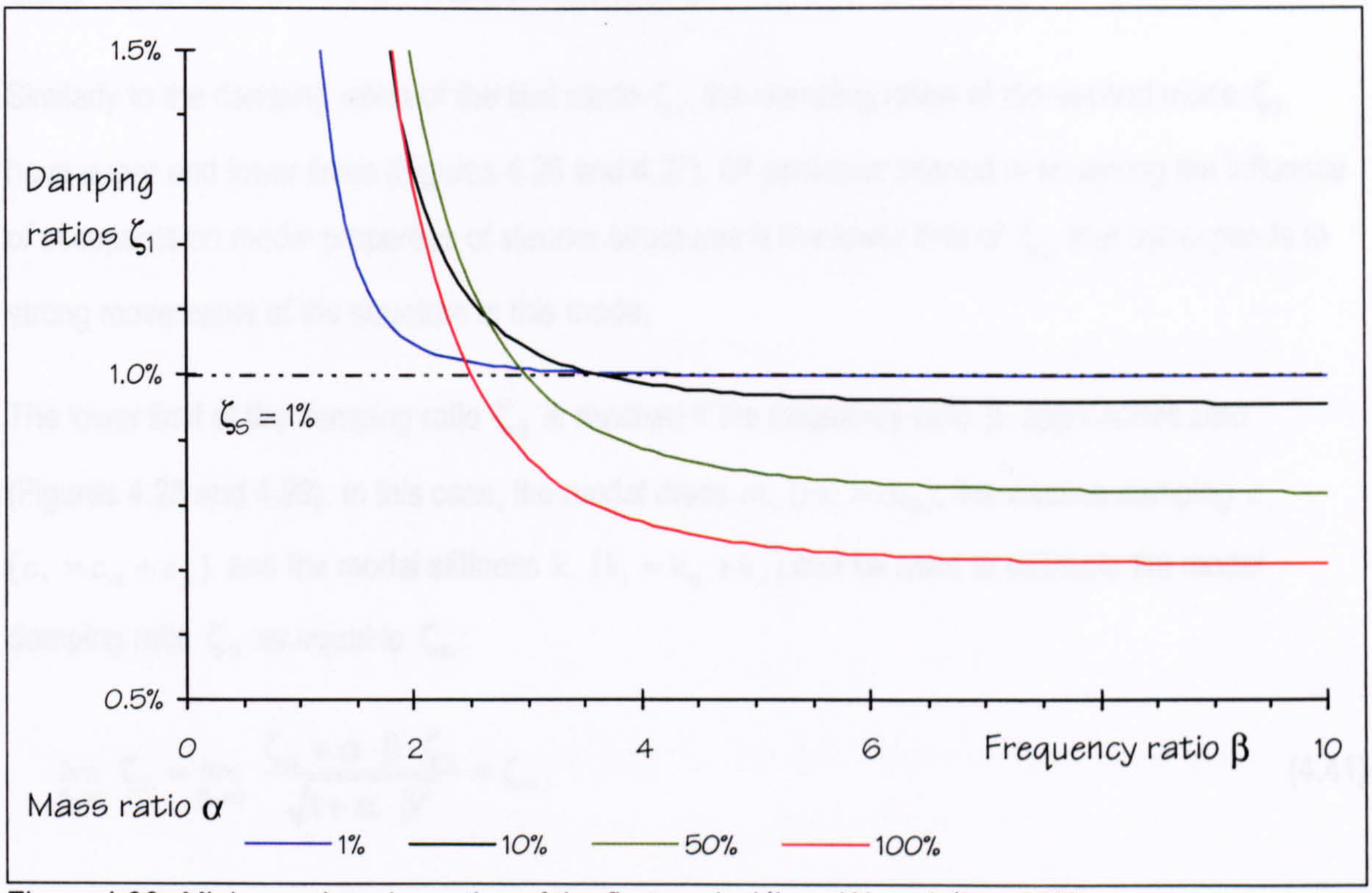

Figure 4.30: Minimum damping ratios of the first mode (ζ_S = 1% and ζ_H = 30%).

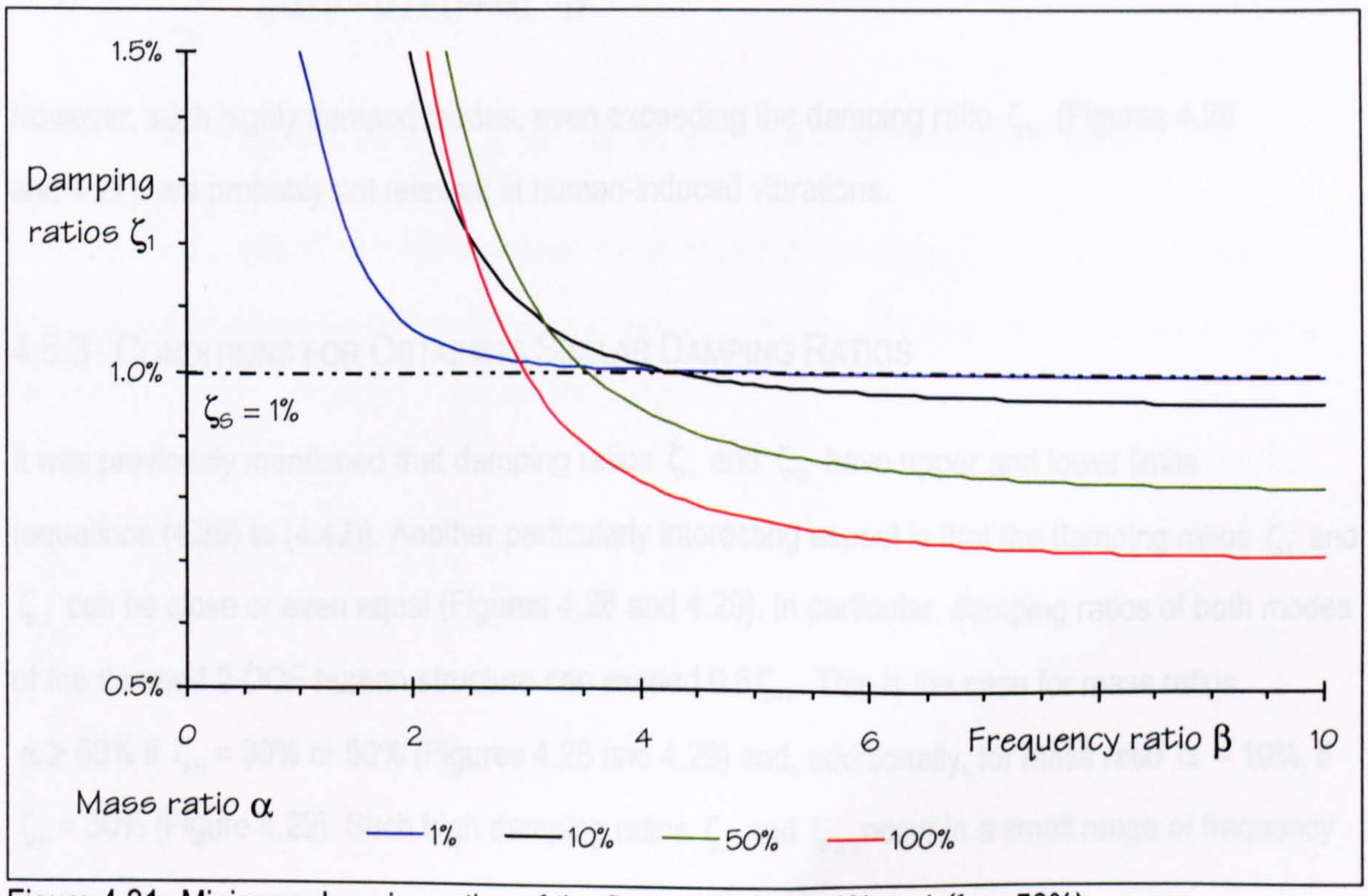

Figure 4.31: Minimum damping ratios of the first mode (ζ_S = 1% and ζ_H = 50%).

4.5.2 Damping Ratios of the Second Mode

Similarly to the damping ratios of the first mode ζ_1, the damping ratios of the second mode ζ_2 have upper and lower limits (Figures 4.26 and 4.27). Of particular interest in analysing the influence of occupants on modal properties of slender structures is the lower limit of ζ_2 that corresponds to strong movements of the structure in this mode.

The lower limit of the damping ratio ζ_2 is reached if the frequency ratio β approaches zero (Figures 4.28 and 4.29). In this case, the modal mass m_1 ($m_1 = m_s$), the viscous damping c_1 ($c_1 = c_s + c_H$), and the modal stiffness k_1 ($k_1 = k_s + k_H$) can be used to estimate the modal damping ratio ζ_2 as equal to ζ_s:

$$\lim_{\beta \to 0} \zeta_2 = \lim_{\beta \to 0} \frac{\zeta_s + \alpha \cdot \beta \cdot \zeta_H}{\sqrt{1 + \alpha \cdot \beta^2}} = \zeta_s . \tag{4.41}$$

Similarly to the lower limit (4.41), an upper limit of the damping ratio ζ_2 can be estimated. For the sake of completeness, this limit is provided in equation (4.42).

$$\lim_{\beta \to \infty} \zeta_2 = \lim_{\beta \to \infty} \frac{\alpha \cdot \zeta_s + \beta \cdot \zeta_H \cdot (1+\alpha)^2}{\sqrt{\alpha \cdot (1+\alpha) + (1+\alpha)^3 \cdot \beta^2}} \tag{4.42}$$

However, such highly damped modes, even exceeding the damping ratio ζ_H (Figures 4.26 and 4.27), are probably not relevant in human-induced vibrations.

4.5.3 Conditions for Obtaining Similar Damping Ratios

It was previously mentioned that damping ratios ζ_1 and ζ_2 have upper and lower limits (equations (4.39) to (4.42)). Another particularly interesting aspect is that the damping ratios ζ_1 and ζ_2 can be close or even equal (Figures 4.28 and 4.29). In particular, damping ratios of both modes of the damped 2-DOF human-structure can exceed $0.5\,\zeta_H$. This is the case for mass ratios $\alpha \geq 50\%$ if $\zeta_H = 30\%$ or 50% (Figures 4.28 and 4.29) and, additionally, for mass ratio α = 10%, if $\zeta_H = 30\%$ (Figure 4.29). Such high damping ratios ζ_1 and ζ_2 occur in a small range of frequency

ratios β around $\beta = \frac{1}{1+\alpha}$ (Figure 4.28). This range of frequency ratios β corresponds to close natural frequencies of the first and second mode (Figure 4.13).

Finally, it is emphasised that a considerable number of damped 2-DOF human-structure systems considered here have damping ratios ζ_1 and ζ_2 both exceeding the damping ratio ζ_s ten times (Figure 4.28). Such a significant damping increase due to human occupation can be expected particularly for structures with frequencies f_s similar and slightly higher than that of occupants (that is f_s above 4 Hz).

4.5.4 SUMMARY

Three significant conclusions can be drawn from the analytical parametric study of the damping ratios ζ_1 and ζ_2 of damped 2-DOF human-structure systems (Figure 4.1c):

(1) The damping ratio ζ_1 can be lower than the damping ratio ζ_s of the structural DOF (Figures 4.30 and 4.31).

(2) The damping ratio ζ_2 can be higher than the damping ratio ζ_H of the human DOF (Figures 4.26 and 4.27).

(3) Damping ratios ζ_1 and ζ_2 can both exceed 10% simultaneously (Figures 4.28 and 4.29).

However, responses of a structure are not only specified by damping (ζ_1 and ζ_2). They have to be calculated considering modal masses and mode superposition. These issues are combined in the discussion of FRFs presented in the following section.

4.6 STRUCTURAL FRFS

In this final section of the analytical parametric study, the influence of human occupants on the structural FRF $A_s(f)$ of a SDOF structure system (Figure 3.1) is discussed. For this purpose, six damped 2-DOF human-structure systems (Figure 4.1c) were considered.

In all six cases, the structural SDOF was defined by ζ_s = 1% and m_s = 10,000 kg. Human occupants were consistently modelled as damped SDOF system with f_H = 6.0 Hz and ζ_H = 30%. Different human-structure systems were obtained by setting mass and frequency ratios α and β differently (Table 4.1). Knowing all these parameters (ζ_s, m_s, f_H, ζ_H, α, and β), m_H and f_s were calculated (equations (4.1) and (4.2)). A following eigenanalysis led to the modal properties $f_1^{(DM)}$, $f_2^{(DM)}$, ζ_1, and ζ_2 of these human-structure models (Table 4.1).

Table 4.1: Parameters of six damped 2-DOF human-structure models.

	Mass ratio	Frequency ratio	Frequency f_s	First mode	Second mode
Case 1	α = 10%	β = 0.75[1)]	8.0 Hz	$f_1^{(DM)}$ = 5.9 Hz ζ_1 = 25.2%	$f_2^{(DM)}$ = 8.1 Hz ζ_2 = 7.0%
Case 2	α = 10%	β = 0.91[2)]	6.6 Hz	$f_1^{(DM)}$ = 6.0 Hz ζ_1 = 15.6%	$f_2^{(DM)}$ = 6.6 Hz ζ_2 = 16.8%
Case 3	α = 50%	β = 0.75[3)]	8.0 Hz	$f_1^{(DM)}$ = 5.2 Hz ζ_1 = 14.2%	$f_2^{(DM)}$ = 9.3 Hz ζ_2 = 22.1%
Case 4	α = 50%	β = 0.67[2)]	9.0 Hz	$f_1^{(DM)}$ = 5.4 Hz ζ_1 = 17.7%	$f_2^{(DM)}$ = 10.0 Hz ζ_2 = 18.4%
Case 5	α = 10%	β = 1.5[4)]	4.0 Hz	$f_1^{(DM)}$ = 3.7 Hz ζ_1 = 2.1%	$f_2^{(DM)}$ = 6.4 Hz ζ_2 = 30.2%
Case 6	α = 50%	β = 1.5[4)]	4.0 Hz	$f_1^{(DM)}$ = 3.1 Hz ζ_1 = 2.5%	$f_2^{(DM)}$ = 7.7 Hz ζ_2 = 34.4%

1) $\beta < \frac{1}{1+\alpha}$

2) $\beta = \frac{1}{1+\alpha}$

3) $\frac{1}{1+\alpha} < \beta < 1$

4) $\frac{1}{1+\alpha} < \beta$

The structural accelerance FRFs $A_{ss}(f)$ of the damped 2-DOF human-structure systems (Table 4.1) are shown in Figures 4.32 to 4.37. In these figures, lilac and blue lines present the contributions of the first and the second mode to $A_{ss}(f)$, which is outlined as thick black line. Additionally, the frequencies f_s and f_H of the subsystems and $f_1^{(DM)}$ and $f_2^{(DM)}$ of the human-structure system are presented (Figures 4.32 to 4.37).

The structural accelerance FRFs $A_{ss}(f)$ are also shown as Nyquist plots (Figure 4.38). This presentation in real and imaginary parts is rather uncommon in civil engineering. However, it enables the presence of a second mode to be observed more easily than using the conventional modulus and phase presentation (Table 4.2).

Table 4.2: The visibility of modes in the structural FRFs $A_{ss}(f)$ of the six damped 2-DOF human-structure systems defined in Table 4.1.

	Modulus of $A_{ss}(f)$	Nyquist plot of $A_{ss}(f)$
Case 1	Second mode (Figure 4.32)	Second mode (Figure 4.38)
Case 2	One mode[1)] (Figure 4.33)	Two modes (Figure 4.38)
Case 3	Two modes (Figure 4.34)	Clearly two modes (Figure 4.38)
Case 4	Second mode (Figure 4.35)	Clearly two modes (Figure 4.38)
Case 5	First mode (Figure 4.36)	First mode (Figure 4.38)
Case 6	First mode (Figure 4.37)	Clearly two modes (Figure 4.38)

1) Both modes of the damped 2-DOF human-structure system superpose and appear as one mode.

Next, each of the structural FRFs $A_{ss}(f)$ is discussed and related to the structural FRFs $A_s(f)$ of the corresponding empty structures. A visual comparison is omitted. Instead, the natural frequency f_s of the empty structure and the magnitude a_s (see section 3.1.3) are used. The natural frequencies f_s are listed in Table 4.1 for each of the six human-structure systems. The magnitude a_s is 5.0 $(mm/s^2)/N$ for all empty structures considered (equation (3.106) in section 3.1.3).

4.6.1 CASES 1 AND 2

Case 1 defines a damped 2-DOF human-structure system with a mass ratio α = 10% and a frequency ratio β = 0.75 (Table 4.1). In this case, the second natural frequency ($f_2^{(DM)}$ = 8.1 Hz) is slightly higher than the natural frequency of the empty structure (f_s = 8.0 Hz). This second mode of the 2-DOF human-structure system is the only mode visible in the structural FRF $A_{ss}(f)$ (Table 4.2, Figures 4.32 and 4.38). Thus, in this case, human occupation leads neither to a strong frequency change nor to a significant additional mode in the structural FRF.

Nevertheless, comparing the peak magnitudes of the structural FRFs $A_s(f)$ and $A_{ss}(f)$, the influence of human occupants is very clear. In Case 1, the peak magnitude of the structural FRF is reduced from 5.0 (mm/s^2)/N for the empty structure to about 0.7 (mm/s^2)/N for the human-structure system (Figure 4.32). The reduction is even stronger in Case 2 (Figure 4.33).

The human-structure dynamic system of Case 2 is characterised by two heavily damped closely spaced modes (Table 4.1). These modes superpose and, therefore, only one peak slightly below the natural frequencies f_s and $f_2^{(DM)}$ (both 6.6 Hz) is visible in the modulus of the structural FRF $A_{ss}(f)$ (Figure 4.33). It is likely that only one heavily damped mode would be identified by a less sophisticated experimental modal analysis. However, the Nyquist plot of $A_{ss}(f)$ shows the contribution of both modes (Figure 4.38).

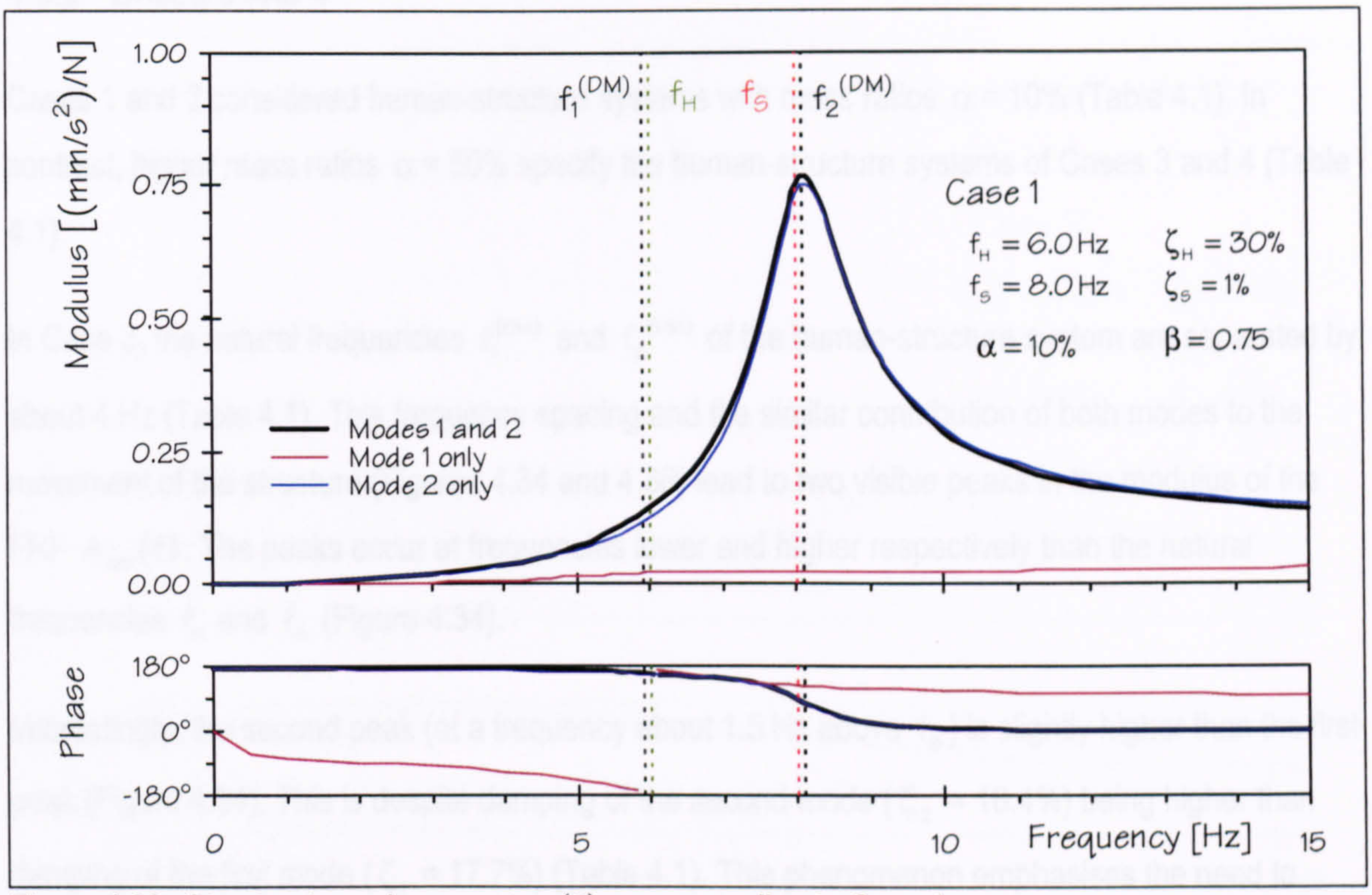

Figure 4.32: Structural accelerance $A_{ss}(f)$ corresponding to Case 1.

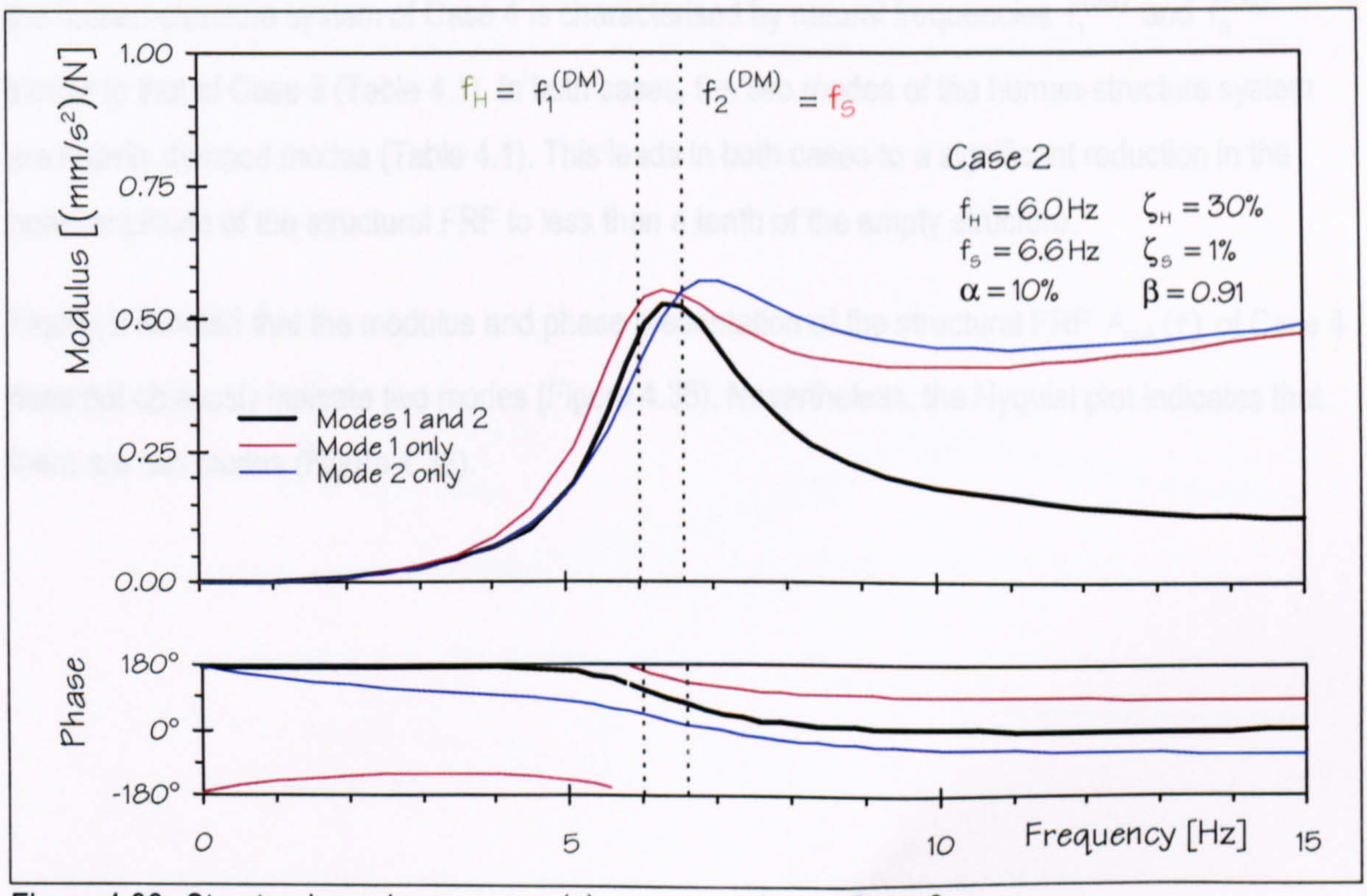

Figure 4.33: Structural accelerance $A_{ss}(f)$ corresponding to Case 2.

4.6.2 CASES 3 AND 4

Cases 1 and 2 considered human-structure systems with mass ratios $\alpha = 10\%$ (Table 4.1). In contrast, higher mass ratios $\alpha = 50\%$ specify the human-structure systems of Cases 3 and 4 (Table 4.1).

In Case 3, the natural frequencies $f_1^{(DM)}$ and $f_2^{(DM)}$ of the human-structure system are separated by about 4 Hz (Table 4.1). This frequency spacing and the similar contribution of both modes to the movement of the structure (Figures 4.34 and 4.38) lead to two visible peaks in the modulus of the FRF $A_{ss}(f)$. The peaks occur at frequencies lower and higher respectively than the natural frequencies f_H and f_S (Figure 4.34).

Interestingly, the second peak (at a frequency about 1.5 Hz above f_S) is slightly higher than the first peak (Figure 4.34). This is despite damping of the second mode (ζ_2 = 18.4%) being higher than damping of the first mode (ζ_1 = 17.7%) (Table 4.1). This phenomenon emphasises the need to consider contributions of both modes of such heavily coupled human-structure systems.

In Case 4, f_S and f_H are separated by 5 Hz in contrast to 4 Hz in Case 3 (Table 4.1). Nevertheless, the human-structure system of Case 4 is characterised by natural frequencies $f_1^{(DM)}$ and $f_2^{(DM)}$ similar to that of Case 3 (Table 4.1). In both cases, the two modes of the human-structure system are heavily damped modes (Table 4.1). This leads in both cases to a significant reduction in the peak amplitude of the structural FRF to less than a tenth of the empty structure.

Finally, it is noted that the modulus and phase presentation of the structural FRF $A_{ss}(f)$ of Case 4 does not obviously indicate two modes (Figure 4.35). Nevertheless, the Nyquist plot indicates that there are two modes (Figure 4.38).

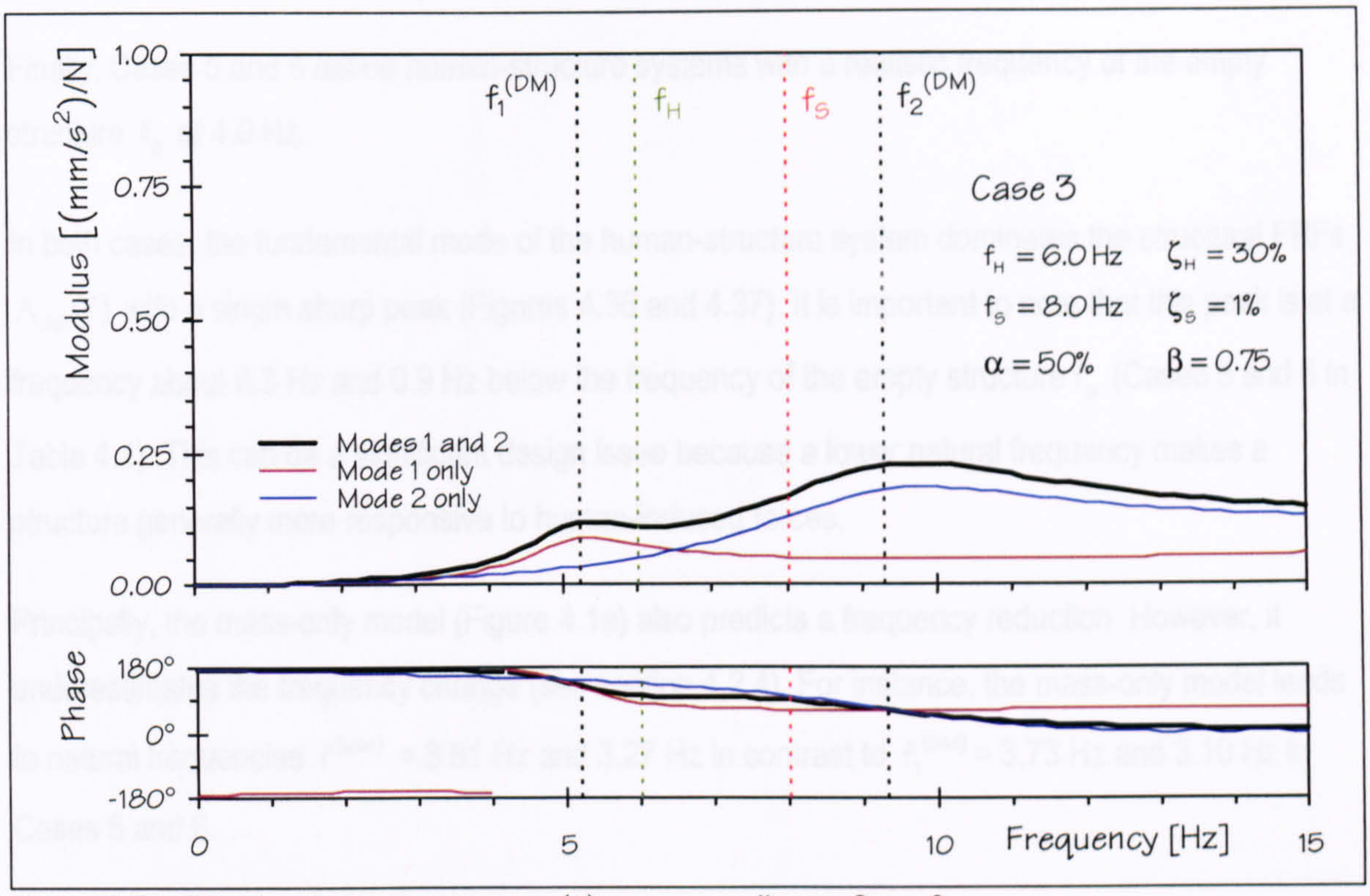

Figure 4.34: Structural accelerance $A_{ss}(f)$ corresponding to Case 3.

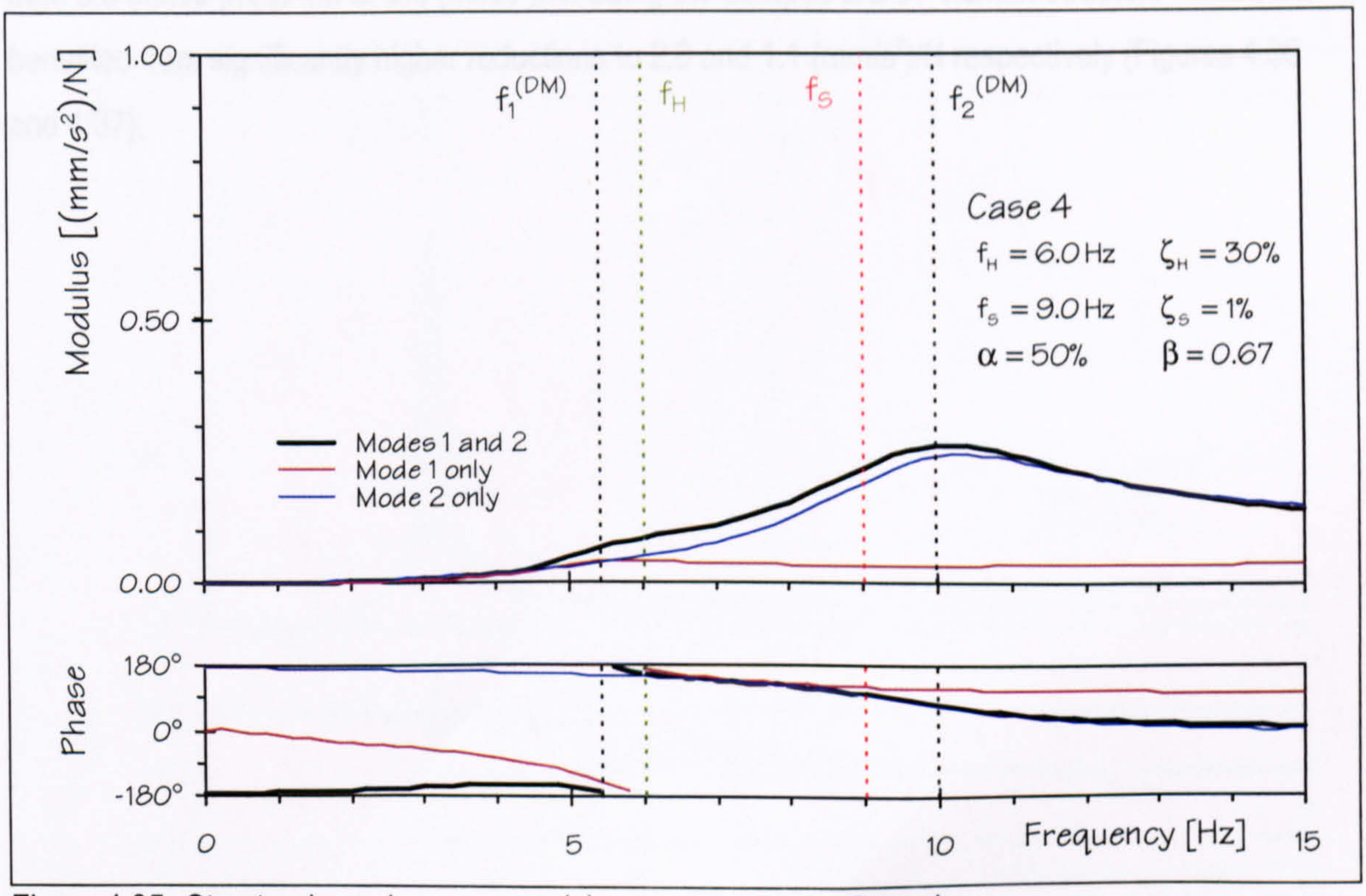

Figure 4.35: Structural accelerance $A_{ss}(f)$ corresponding to Case 4.

4.6.3 CASES 5 AND 6

Finally, Cases 5 and 6 define human-structure systems with a realistic frequency of the empty structure f_s of 4.0 Hz.

In both cases, the fundamental mode of the human-structure system dominates the structural FRFs $A_{ss}(f)$ with a single sharp peak (Figures 4.36 and 4.37). It is important to note that this peak is at a frequency about 0.3 Hz and 0.9 Hz below the frequency of the empty structure f_s (Cases 5 and 6 in Table 4.1). This can be a significant design issue because a lower natural frequency makes a structure generally more responsive to human-induced forces.

Principally, the mass-only model (Figure 4.1a) also predicts a frequency reduction. However, it underestimates the frequency change (see section 4.2.4). For instance, the mass-only model leads to natural frequencies $f^{(MM)}$ = 3.81 Hz and 3.27 Hz in contrast to $f_1^{(DM)}$ = 3.73 Hz and 3.10 Hz in Cases 5 and 6.

A further drawback of the mass-only model is the slight reduction of the peak amplitude. In Cases 5 and 6, the mass-only model of human occupants accounts for a reduction of the peak amplitude from 5.0 (mm/s^2)/N to 4.5 or 3.3 (mm/s^2)/N. Using the damped 2-DOF human-structure model, it is benefited from significantly higher reductions to 2.0 and 1.1 (mm/s^2)/N respectively (Figures 4.36 and 4.37).

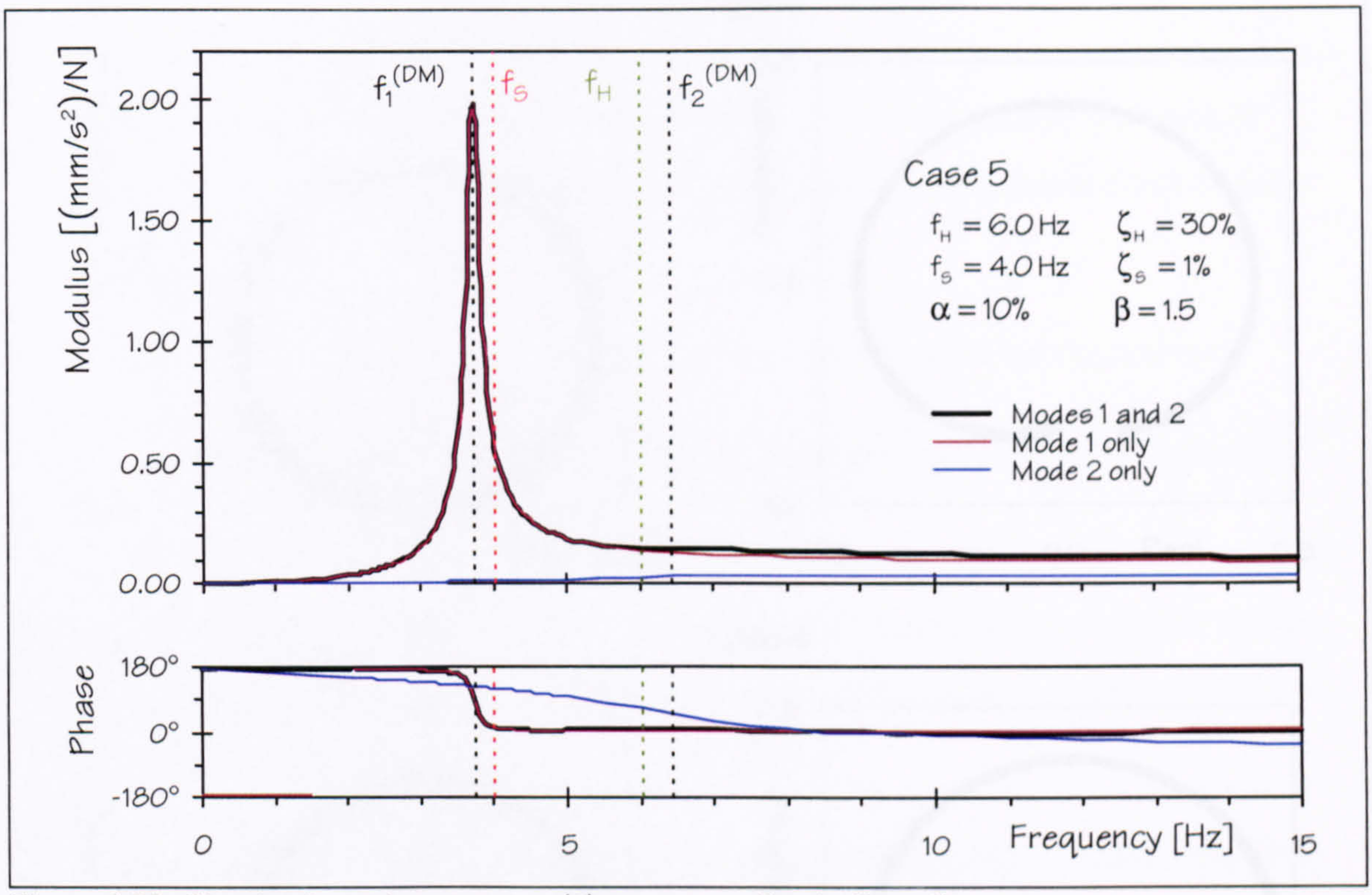

Figure 4.36: Structural accelerance $A_{ss}(f)$ corresponding to Case 5.

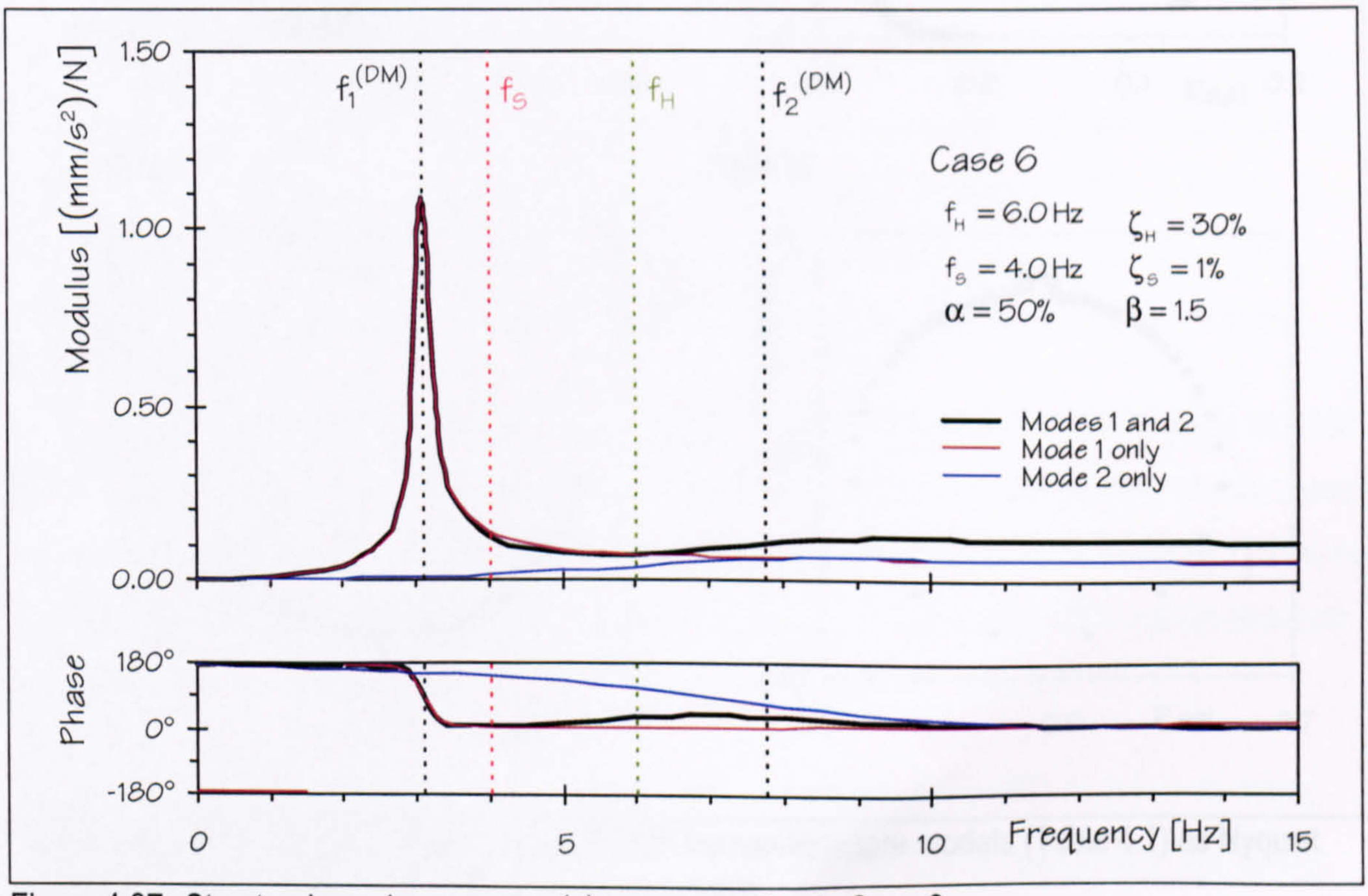

Figure 4.37: Structural accelerance $A_{ss}(f)$ corresponding to Case 6.

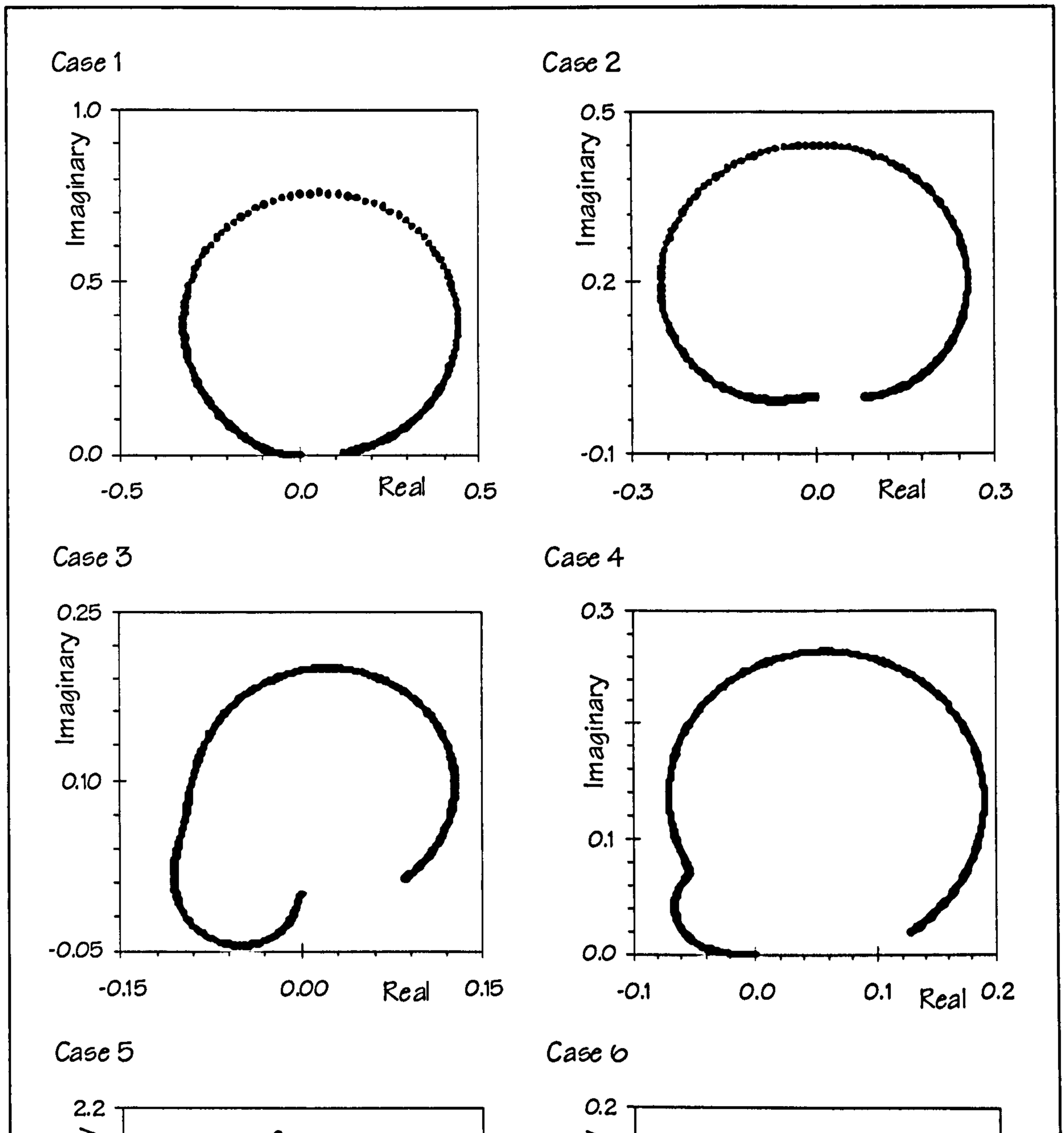

Figure 4.38: FRFs $A_{ss}(f)$ of six damped 2-DOF human-structure models (Table 4.1) as Nyquist plot (frequency spacing 0.2 Hz and units of $(mm/s^2)/N$)).

4.6.4 Discussion

As demonstrated in the literature review, human occupants add a DOF to the structure they occupy. This phenomenon results in an additional mode in the joint human-structure dynamic system compared to the structure itself. This additional mode is visible in the modulus of structural FRFs under the following two conditions:

(1) the additional mode sufficiently contributes to the movement of the structure and

(2) the natural frequencies of the modes are well separated (see example in Figure 4.34).

Both conditions have to be satisfied simultaneously. If only condition (1) is satisfied, only one peak might be visible in the modulus of the structural FRF. However, it could be spotted in the Nyquist plot (Case 2 in Figures 4.33 and 4.38). If only condition (2) is satisfied, as in Cases 1 and 5, only one mode can be identified (Figures 4.32, 4.36, and 4.38)

If the frequencies of the human and structure are well separated (condition 1), human occupants shift the peak of the structural FRF of the empty structure noticeably. This shift is positive (to higher frequencies) if $f_S > f_H$ (Figure 4.35). It is negative (to lower frequencies) if $f_S < f_H$ (Figure 4.37). Therefore, the presence of human occupants can be beneficial ($f_S > f_H$) or adverse ($f_S < f_H$) regarding human-induced forces.

In all human-structure systems considered here, human occupants reduce the peak amplitude of the structural FRF. This is also the case if neither condition (1) nor (2) is satisfied (Case 1, Table 4.2). The phenomenon leads to lower structural responses of the occupied structure than the empty structure to the same excitation. This can be particularly useful in designing assembly structures.

The influence of human occupants on the structural FRF using the damped 2-DOF human-structure model cannot easily be quantified using close form solutions. Therefore, a numerical solution based on a specially developed MATLAB script is provided in Appendix C. It enables the reader to analyse the influence of occupants on the structural FRF $A_{ss}(f)$ of other damped 2-DOF human-structure systems.

In particular, the program plots the modulus and phase of the structural FRF $A_s(f)$ of an empty structure overlaid with the structural FRF $A_{ss}(f)$ of any damped 2-DOF human-structure system.

The user has to define the structural and the human DOF via the natural frequencies f_s and f_H, modal masses m_s and m_H, and damping ratios ζ_s and ζ_H. The program outputs natural frequencies and damping ratios of the human-structure system and quantifies the frequency at which the structural FRF $A_{ss}(f)$ has its peak modulus.

4.6.5 SUMMARY

The analytical parametric study of the damped 2-DOF human-structure model (Figure 4.1c) can explain (1) a frequency increase or decrease, (2) an additional frequency, and (3) a response reduction as observed on real-life structures due to human occupation (Ellis and Ji 1997; Littler 1998). This conclusion is important because it is impossible to explain all these observations using the simpler mass-only model or the undamped 2-DOF human-structure model (Figures 4.1a and 4.1b).

Nevertheless, the mass-only model (Figure 4.1a) can be used to estimate the fundamental frequency of the human-structure system if $f_s < f_H/5$ ($\beta > 5$). Furthermore, both natural frequencies of the damped 2-DOF human-structure system can be calculated with sufficient accuracy using the undamped 2-DOF human-structure model (Figure 4.1b) if $f_s < 2/3\, f_H$ ($\beta > 1.5$).

However, in most cases of concern, the frequency of the structure is smaller than that of the human ($f_s < f_H$, $\beta < 1$). Therefore, an analysis of the damped human-structure system is required. Such an analysis is likely to result in reductions in the fundamental frequency and the peak modulus of the structural FRF.

5. EXPERIMENTAL WORK

The experimental part of this research quantified the influence of occupants (and a static mass) on the modal properties of a slender structure. The following sections describe the methodology and the experimental schedule. Additionally, they report on the performance of the experiments and present relevant experimental data. Finally, estimated mode shapes, natural frequencies, damping ratios and modal masses are presented and discussed.

5.1 METHODOLOGY OF MODAL TESTING

In this research, forced vibration testing was used. Here, the test equipment and its arrangement are presented together with information about the data acquisition and processing procedure.

5.1.1 EXPERIMENTAL SET-UP

A prestressed concrete slab of about 15,000 kg was employed as the test structure (Figure 5.1). The 2 m wide beam-like structure spanned 10.8 m between a pair of 'knife-edges' near its ends.

A key aim of this research was to obtain best quality experimental data. Therefore, FRFs were estimated to obtain modal properties. The FRFs were determined by measuring responses of the structure to excitation by an electrodynamic shaker APS Dynamics Model 113 (APS Dynamics 1996b), as shown in Figure 5.2a. This shaker was placed in a pit underneath the test structure (Figure 5.1) and attached to it by a stinger (Figure 5.2b).

Vibration responses of the test structure were measured by piezoelectric accelerometers ISOTRON Model 7754-1000 and 7754A-1000 manufactured by Endevco (Figure 5.3). These transducers were placed at nine test points (TPs) along the middle axis of the test structure (Figure 5.4).

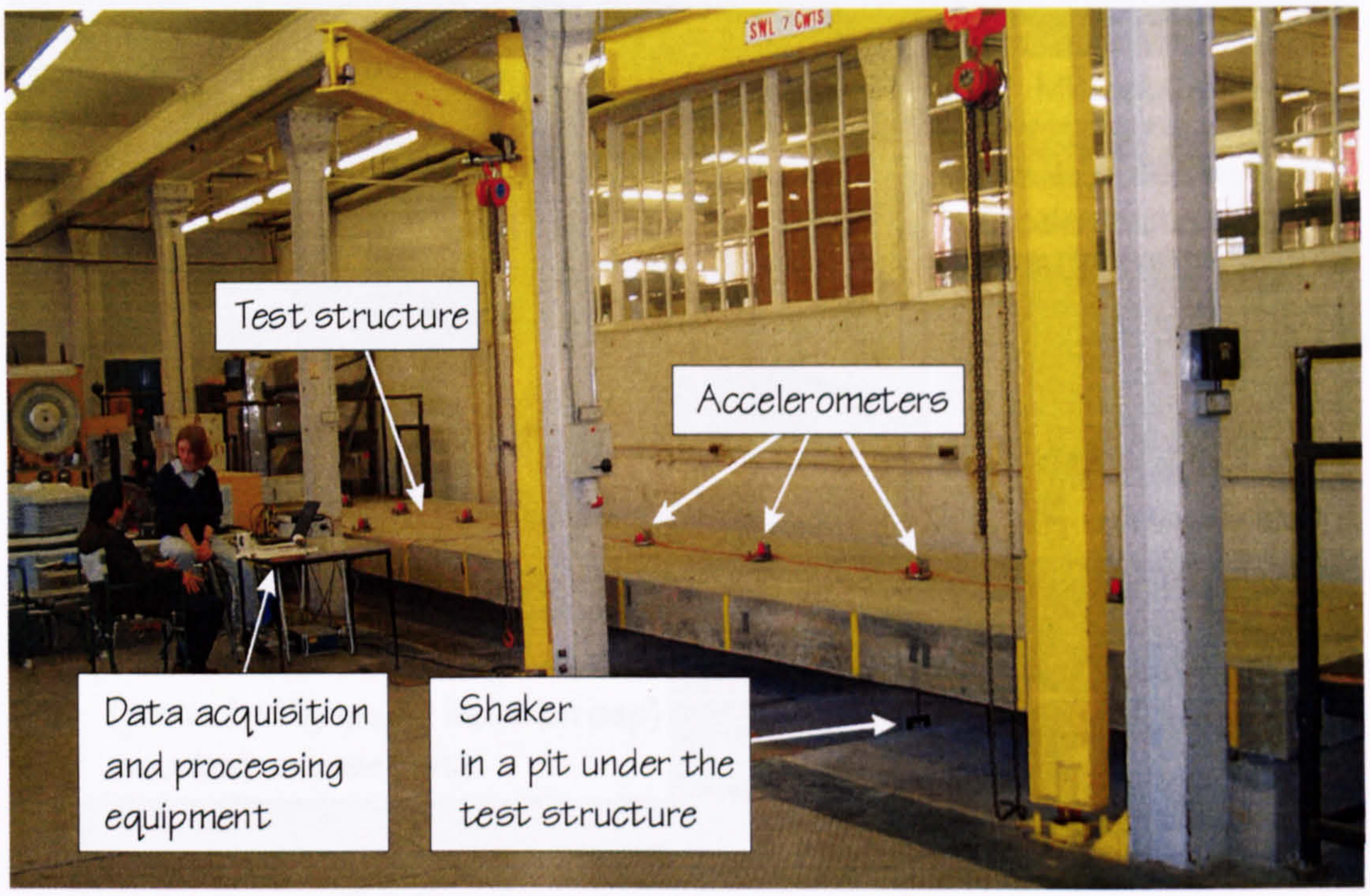

Figure 5.1: Experimental set-up in the strong floor laboratory of the University of Sheffield.

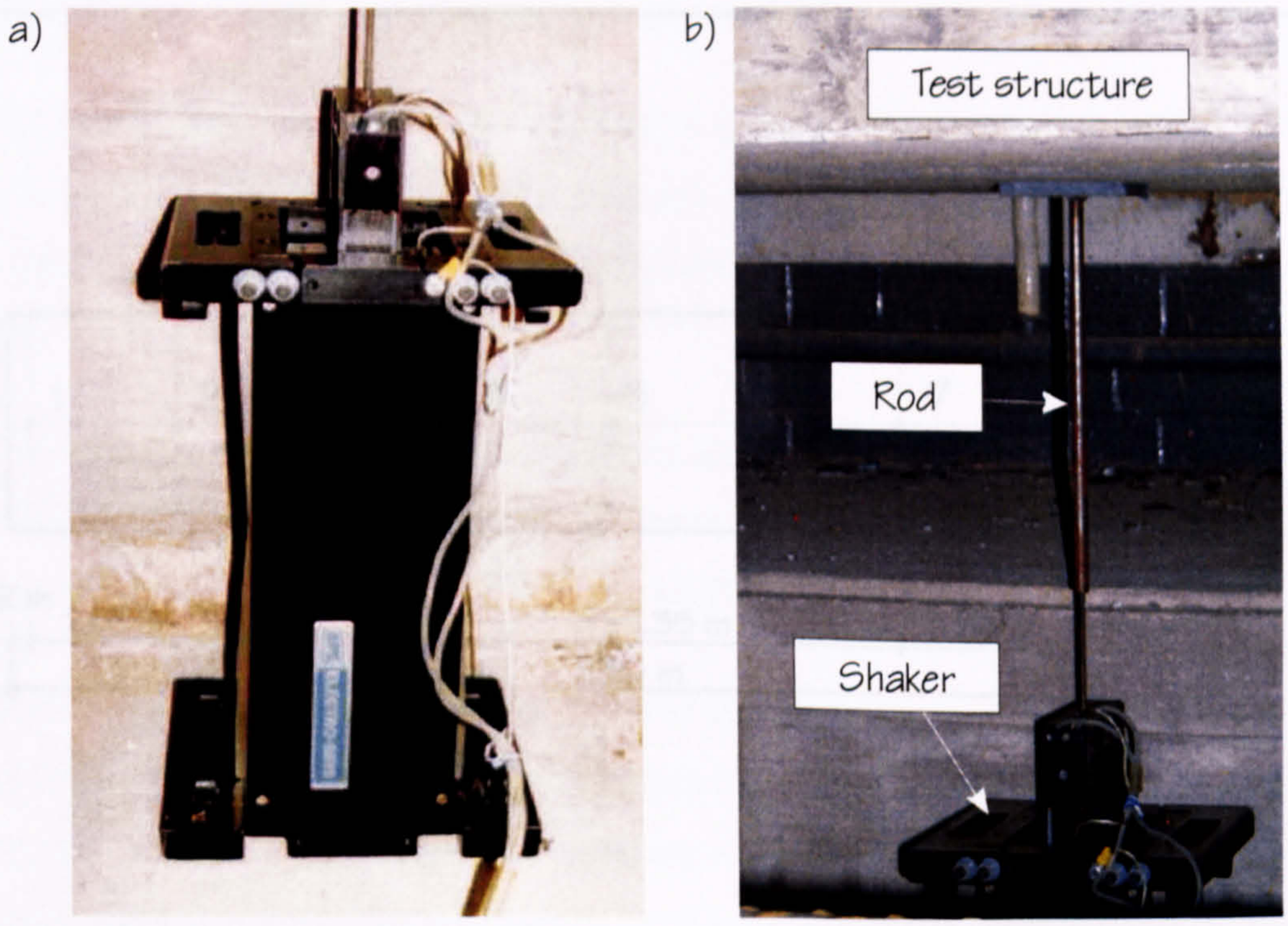

Figure 5.2: Electrodynamic shaker (a) and its attachment to the test structure (b).

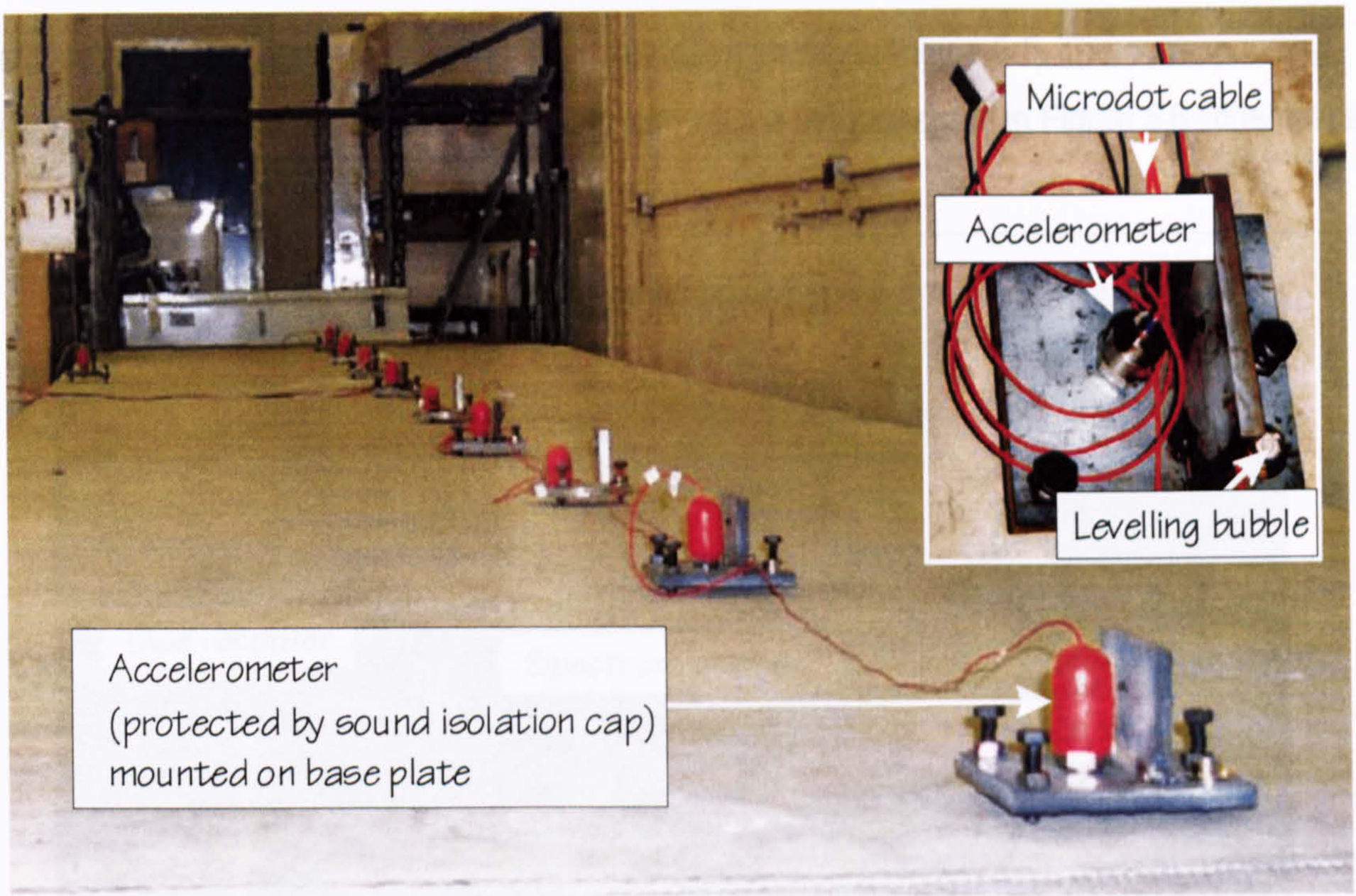

Figure 5.3: Response measurement set-up. Insert: Plan view of a base plate with an accelerometer attached.

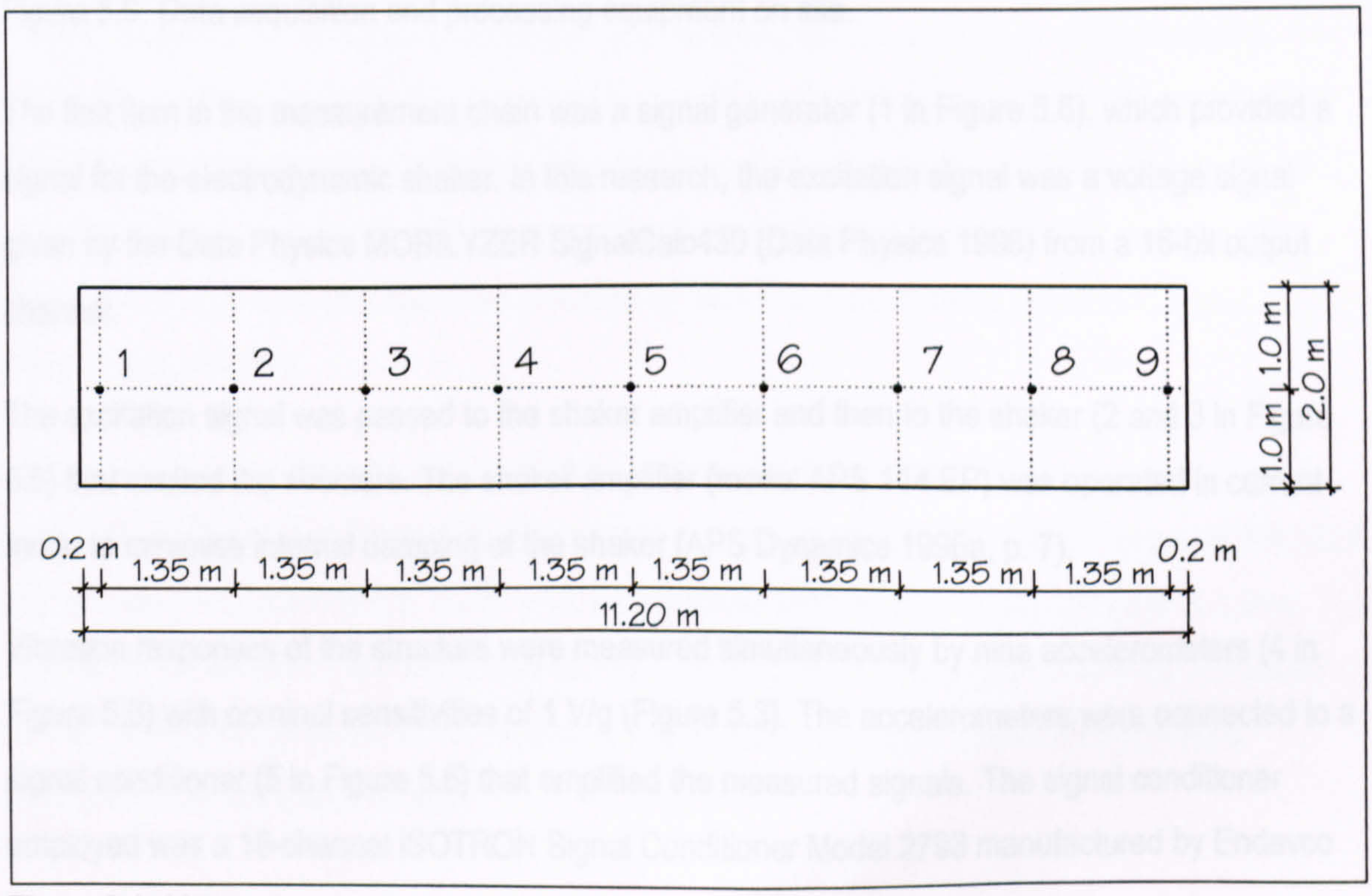

Figure 5.4: Measurement grid.

5.1.2 Instrumentation and Data Acquisition

Modal testing was performed using the instrumentation shown in Figure 5.5. The corresponding measurement chain and the procedure of data acquisition are presented in Figure 5.6 schematically.

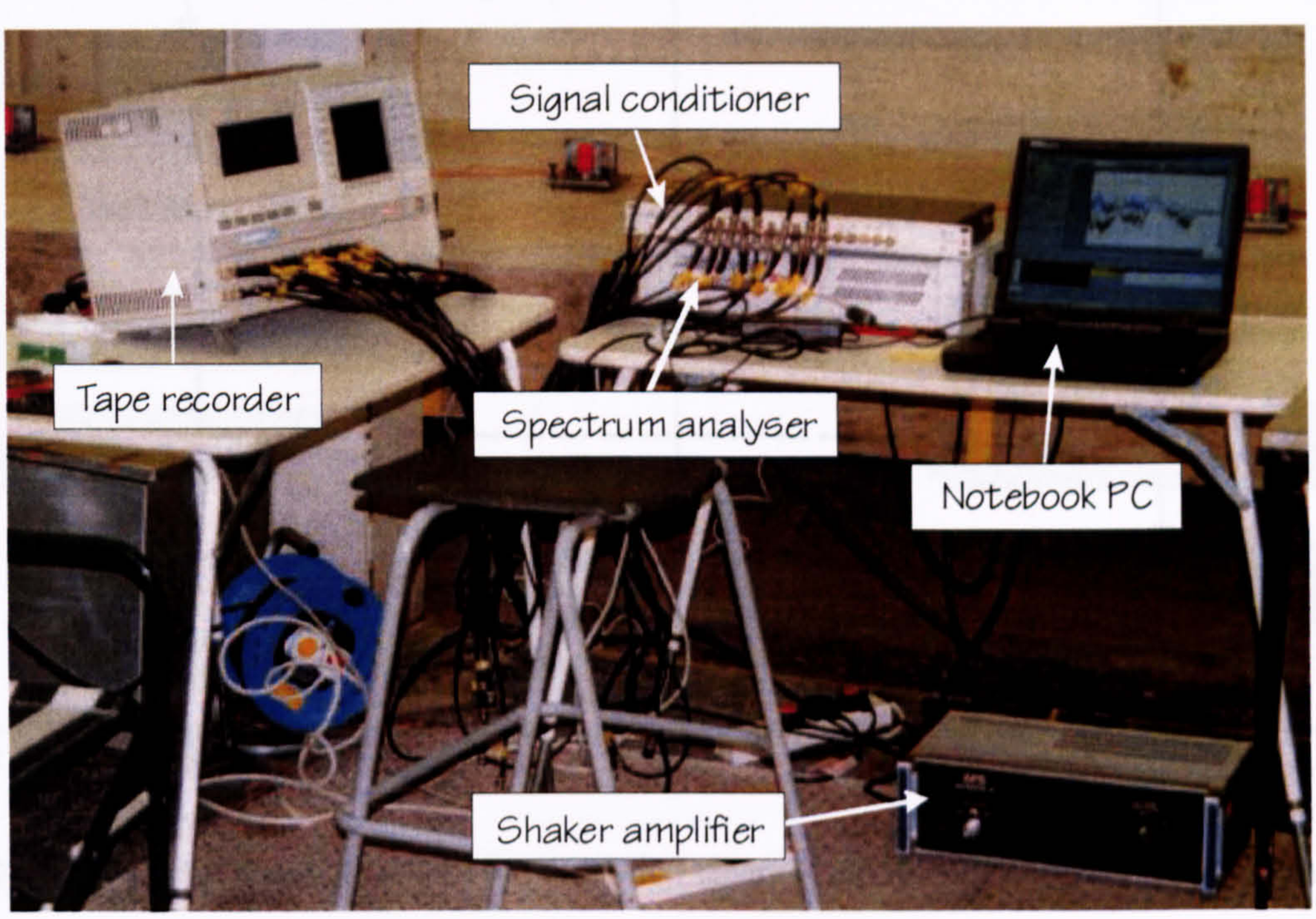

Figure 5.5: Data acquisition and processing equipment on site.

The first item in the measurement chain was a signal generator (1 in Figure 5.6), which provided a signal for the electrodynamic shaker. In this research, the excitation signal was a voltage signal given by the Data Physics MOBILYZER SignalCalc430 (Data Physics 1998) from a 16-bit output channel.

The excitation signal was passed to the shaker amplifier and then to the shaker (2 and 3 in Figure 5.6) that excited the structure. The shaker amplifier (model APS 114 EP) was operated in current mode to minimise internal damping of the shaker (APS Dynamics 1996a, p. 7).

Vibration responses of the structure were measured simultaneously by nine accelerometers (4 in Figure 5.6) with nominal sensitivities of 1 V/g (Figure 5.3). The accelerometers were connected to a signal conditioner (5 in Figure 5.6) that amplified the measured signals. The signal conditioner employed was a 16-channel ISOTRON Signal Conditioner Model 2793 manufactured by Endevco (Endevco 1996).

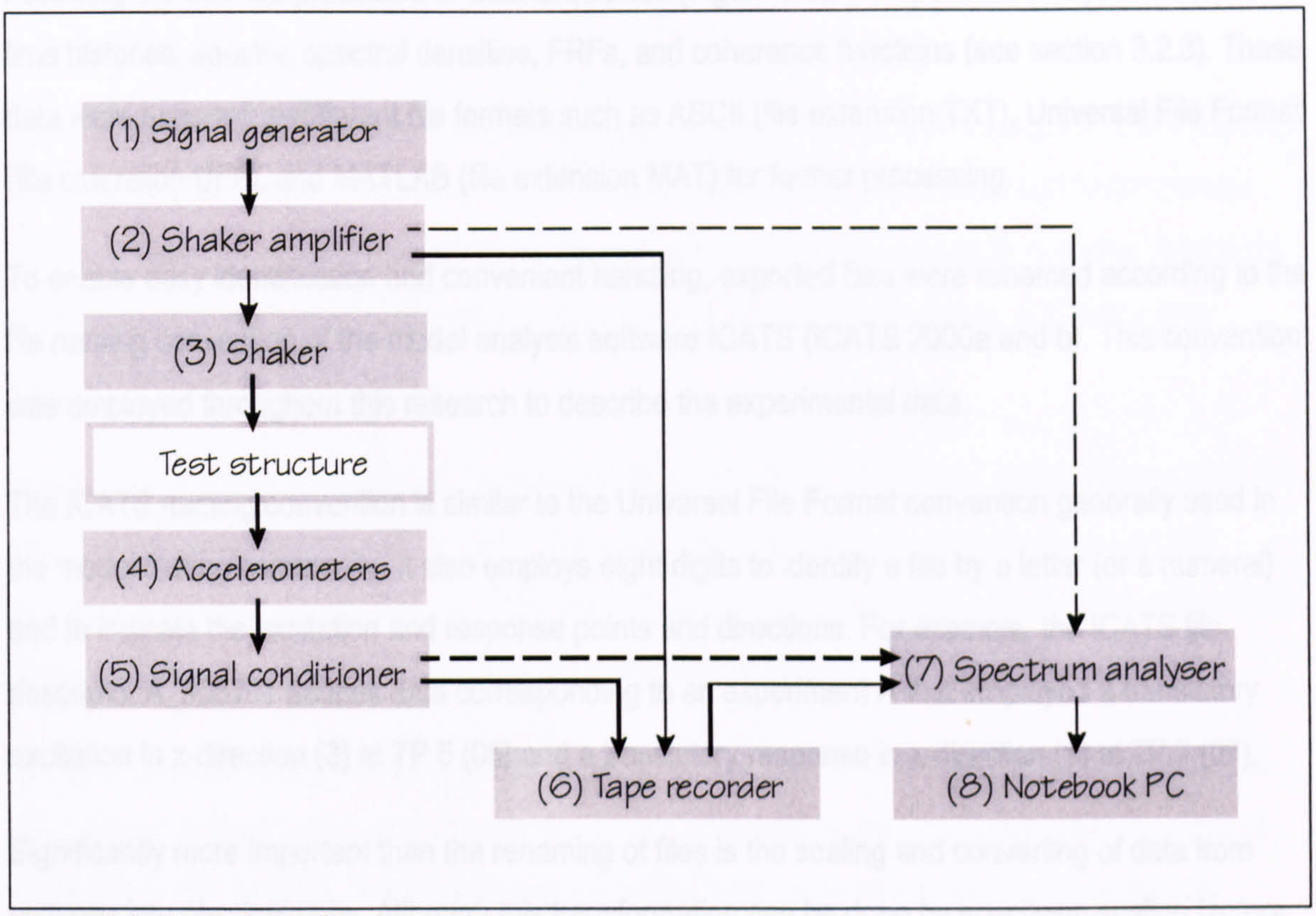

Figure 5.6: Flow chart of instrumentation.

All acceleration response signals and the excitation signal (outputs of 5 and 2 in Figure 5.6) were stored on magnetic tape (6 in Figure 5.6). The storing of analogue data on a tape recorder, a RACAL Storeplus VL 16-Channel analogue tape recorder, served as backup. It also enabled application of different digital data processing (sampling and windowing) to the same experimental data. However, processing of data by replaying a tape introduces additional noise (Morehead 1991) and immediate data processing is always preferable to monitor the quality of data during testing. Therefore, all experimental data were recorded on tape and most of them were also processed directly during testing.

Processing involved digitising and analysing the analogue data using a spectrum analyser and a notebook PC (7 and 8 in Figure 5.6). The spectrum analyser was a 18-bit Data Physics MOBILYZER SignalcCalc430 (Data Physics 1998). This system could process only seven channels at a time. Therefore, the excitation and responses at TPs 1, 3, 5, 7, and 9 only (Figure 5.4) were processed directly. Data corresponding to the remaining TPs 2, 4, 6, and 8 were obtained by replaying analogue data from magnetic tape.

Following the outlined procedure of data acquisition (Figure 5.6), the spectrum analyser provided time histories, spectra, spectral densities, FRFs, and coherence functions (see section 3.2.3). These data were exported in different file formats such as ASCII (file extension TXT), Universal File Format (file extension UFF), and MATLAB (file extension MAT) for further processing.

To enable easy identification and convenient handling, exported files were renamed according to the file naming convention of the modal analysis software ICATS (ICATS 2000a and b). This convention was employed throughout this research to describe the experimental data.

The ICATS naming convention is similar to the Universal File Format convention generally used in the modal testing community. It also employs eight digits to identify a file by a letter (or a numeral) and to indicate the excitation and response points and directions. For example, the ICATS file descriptor A_305107 defines data corresponding to an experiment A that employed a translatory excitation in z-direction (3) at TP 5 (05) and a translatory response in x-direction (1) at TP 7 (07).

Significantly more important than the renaming of files is the scaling and converting of data from voltages into physical units. Although this transformation can be done by specifying scaling factors in the spectrum analyser, it was performed during the post-processing stage at the same time as the renaming of files.

5.2 Considerations on the Performance of Experiments

The main aim of the experimental part of this research was to gather high quality FRFs that quantify the influence of human occupants on a slender test structure. The analysis of such experimental data was based on the theory of linear modal analysis presented in chapter 3. Applying this theory requires the system under investigation to (1) be linear, (2) satisfy reciprocity, and (3) be time invariant (Maia et al. 1997, p. 2).

However, slight non-linearities can be accepted (Ewins 2000, p. 270f) and are to be expected in the case of human occupation (Griffin 1990). To reduce the effect of such non-linearities, random excitation was used (Ewins 2000, p. 266). Nevertheless, reciprocity, homogeneity, and repeatability checks of the empty and the human-occupied structure were performed and will be presented.

Reciprocity was investigated by exciting the test structure at TP 5 and measuring the response at TP 7 (Figure 5.4) and vice versa. Homogeneity was analysed by applying three different levels of excitation to the structure. To determine repeatability, each experiment (except the reciprocity checks) was repeated five times under nominally identical test conditions.

Considering the novelty of the experimental investigations, modal properties of experimental data were estimated during the progress of modal testing. This approach was adopted to improve the test schedule if possible and to use limited testing resources such as time and personnel efficiently. It led to refinements of the test plan. The groups of tests finally performed are summarised in Figure 5.7.

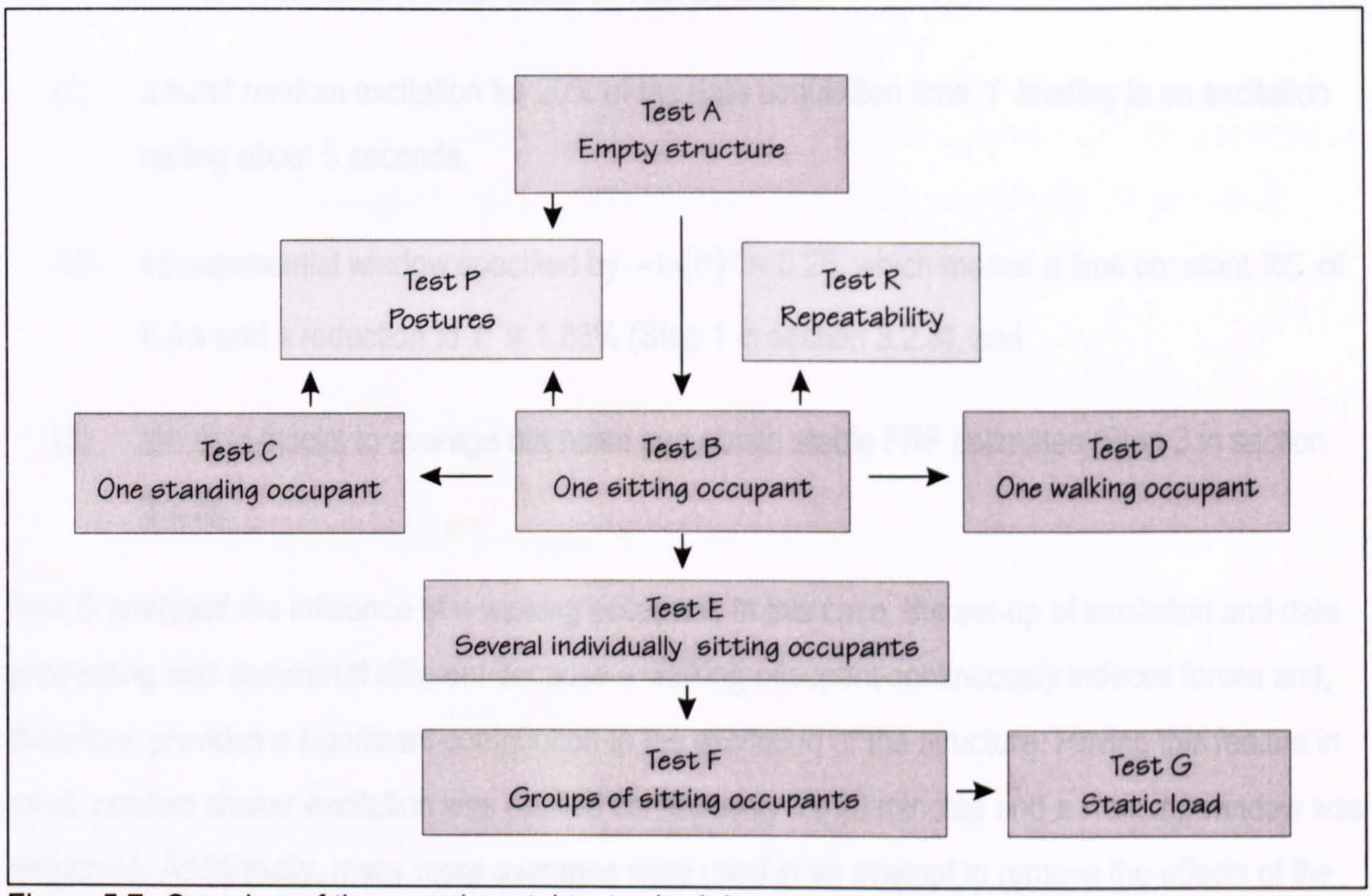

Figure 5.7: Overview of the experimental test schedule.

Modal tests of the empty test structure were performed (Test A in Figure 5.7). Also, modal tests of the structure occupied by stationary or moving occupants took place (Tests P, R, C, B, D, E, and F in Figure 5.7). Additionally, the influence of a static load with a mass equivalent to the mass of human occupants was investigated (Test G).

The data acquisition parameters listed in Table 5.1 characterise all data gathered in these experiments (A to G, P and R).

Table 5.1: Parameters of data acquisition (Data Physics 1998).

Parameter	Item	Setting
Data acquisition time T		25.2 s
Sampling parameters	Time step Δt	3.072 ms
	Sampling frequency $f_{samp.}$	325 Hz
	Number of samples L	8192
Frequency domain	Frequency range	0.0 Hz to 78.125 Hz
	Frequency resolution Δf	0.0397 Hz

Furthermore, all modal tests (except those of Test D) used

(1) a burst random excitation for 20% of the data acquisition time T leading to an excitation lasting about 5 seconds,

(2) an exponential window specified by $-\ln(P)^{-1} = 0.25$, which means a time constant RC of 6.3 s and a reduction to P = 1.83% (Step 1 in section 3.2.3), and

(3) ten data blocks to average out noise and obtain stable FRF estimates (Step 3 in section 3.2.3).

Test D analysed the influence of a walking occupant. In this case, the set-up of excitation and data processing was somewhat different because a walking occupant continuously induces forces and, therefore, provides a significant contribution to the excitation of the structure. Having this feature in mind, random shaker excitation was applied continuously for 20 minutes and a Hanning window was employed. Additionally, many more averages were used in an attempt to remove the effects of the extraneous excitation caused by the walker.

Details on the configuration of all individual experiments can be found in Appendix D. Additional and more general information is provided in the next section.

5.3 EXECUTION OF MODAL TESTS

All experiments were performed within a 30 day period (Table D.1 in Appendix D). This was possible even though work in a neighbouring laboratory imposed time restrictions because it generated vibration and noise levels that prevented successful vibration measurements.

5.3.1 TEST A: EMPTY TEST STRUCTURE

The first modal tests analysed the homogeneity of the empty test structure and served for testing the new equipment acquired in course of this particular research. In these tests, the structure was excited at TP 5 (Figure 5.4) by the shaker in a pit below the structure (A01 - A05, A06 - A09, A11, and A12 - A16 in Table D.2 in Appendix D).

Next, the shaker was relocated from the pit below TP 5 to a pit below TP 7 (Figure 5.1) to investigate the reciprocity linearity condition (A17 - A21). Exciting the structure at TP 7 enabled, in contrast to excitation at TP 5, the excitation of the second mode of the structure because TP 5 but not TP 7 is a nodal point of the second mode (Figure 5.34b in section 5.5). Including the second mode into investigations, an excitation at TP 7 was therefore used in all further experiments with the exception of the reciprocity checks B26 and C26 of the human-occupied structure (Appendix D).

Modal tests of the empty test structure with shaker excitation at TP 7 (A17 - A21) were repeated at a later date (A22 - A26) to investigate long-term repeatability (Tables D.1 and D.2). These measurements indicated slight changes in the modal properties of the empty test structure over time. Therefore, similar experiments of the empty structure (P05, P10, P15, P20, and P25) were performed after a further lapse of time (see section 5.3.6).

5.3.2 TESTS B, C, AND R: ONE SITTING OR STANDING OCCUPANT

Tests B, C, and R followed tests A17 - A21 (Appendix D). They investigated the influence of a single occupant sitting or standing (Figures 5.8a and 5.8b) on the test structure.

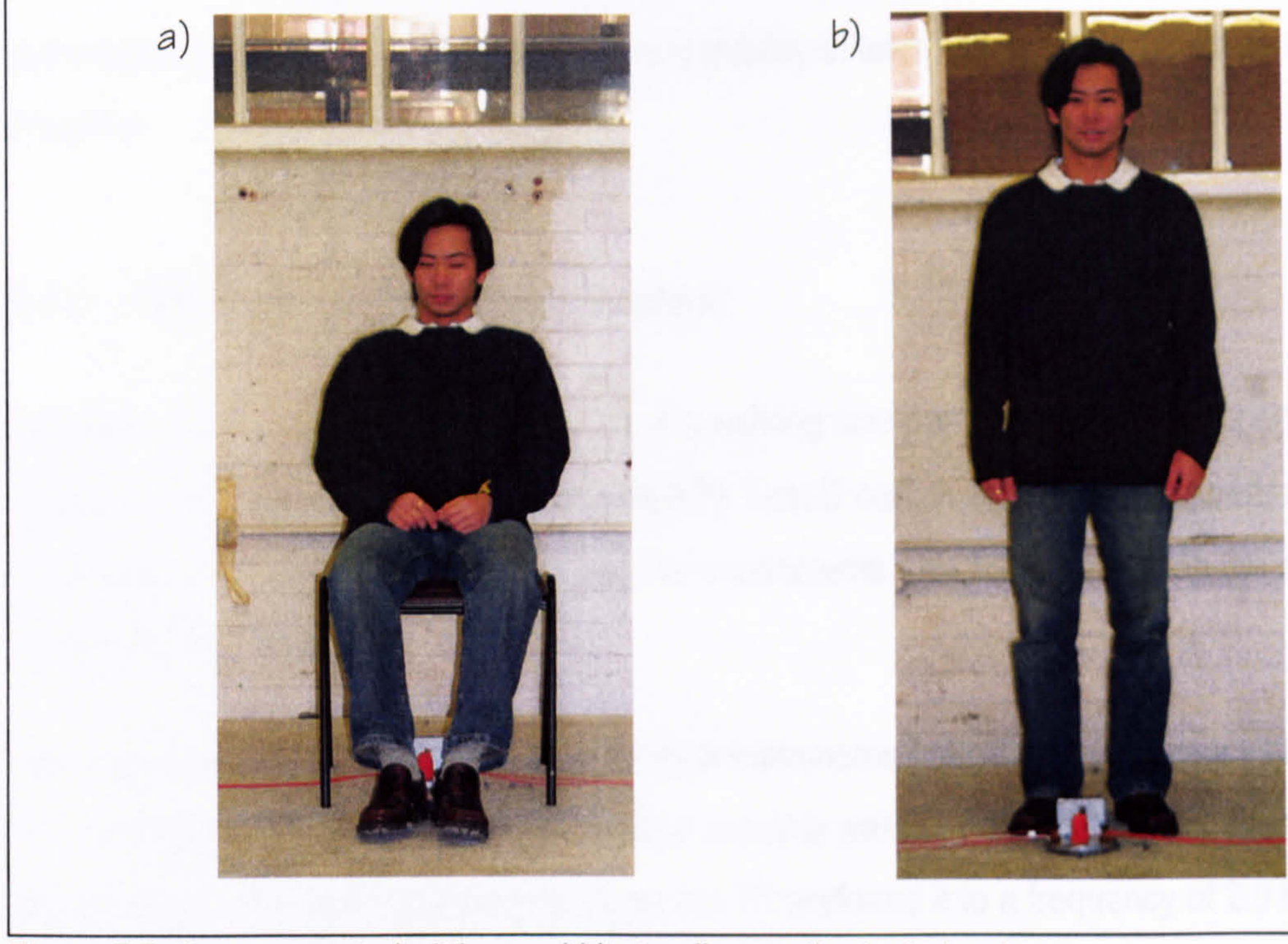

Figure 5.8: An occupant a) sitting and b) standing on the test structure.

The first of these experiments was Test B. It analysed the influence of a sitting occupant, test subject (TS) A in Table 5.2, on the modal properties of the test structure. Test B covered experiments with the same occupant at different locations on the test structure (Table D.3 in Appendix D). Additionally, three different levels of vibration were employed.

Table 5.2: Weight and height of the five males employed as TSs.

Test subject	A	B	C	D	E
Weight	59 kg	93 kg	75 kg	85 kg	90 kg
Height	1.68 m	1.72 m	1.82 m	1.80 m	1.74 m

Test B was planned to serve for comparison with similar experiments involving the same occupant standing (Test C), walking (Test D), or other individuals sitting on the test structure (Test E) as shown in Figure 5.7.

Test B was followed by Test C (Table D.4). The analysis of both tests indicated that the properties of the empty test structure changed slightly (see section 5.6.1). Therefore, additional modal tests of the empty test structure were performed (section 5.3.1). Tests B and C also revealed that damping ratios of the structure occupied by the same TS varied strongly for nominally identical and

consecutive modal tests (see section 5.6.2.2). Therefore, Test R (Table D.8) was added to the initial test schedule to investigate the long-term repeatability of tests with a single TS sitting on the structure.

5.3.3 Test D: Single Walking Occupant

Following Tests B, C, and R, the influence of a walking occupant on the modal properties of the test structure was investigated in Test D (Figure 5.7). Test D contained only three experiments: one modal test of the empty test structure and two experiments with TS A walking on the test structure (Table D.9 in Appendix D).

The walking pace of the TS was controlled by a metronome beeping at a frequency of 1.5 or 1.8 Hz. The frequency of 1.5 Hz is at the lower end of possible walking frequencies. The second walking frequency of 1.8 Hz was employed because the TS preferred it to a frequency of 2.0 Hz usually quoted in the literature as normal walking frequency.

While acquiring the data, it became obvious that FRFs did not stabilise after 50 averages if a person was walking on the test structure. This was clearly due to the high extraneous excitation induced by the walker. Additionally, it was noted that the spectrum analyser did not perform the requested overlap analysis. Only two months later, this unexpected software problem was fixed by the spectrum analyser manufacturer.

However, processing the data with more than 50 averages (by replaying analogue data from tape and increasing the overlap of data blocks) did not lead to stable estimates (see FRFs and coherences in section 5.4.2.3). Therefore, further experiments involving walking at other frequencies were abandoned. Nevertheless, similar modal testing might be successful if the occupant is walking naturally (without the prompt of a metronome) and higher magnitude shaker excitation is employed.

5.3.4 Tests E and F: Different Individuals and Groups of Sitting Occupants

Tests E investigated the structure occupied by different individuals and Test F examined crowds of two to five people sitting on the test structure (Tables D.5 and D.6 in Appendix D). Both tests were performed within two consecutive days and accompanied by a retest of the empty test structure (A22 - A26 in Table D.2).

In Test E, one of the five TSs (A, B, C, D, and E in Table 5.2) sat at TP 5 (Figure 5.4), whereas only TS A was used in the previous Tests B, C, R, and D. In Test F, two to five TSs were arranged on the structure. The occupants were close to TP 5 in experiments F01 to F20 and close to TPs 3 and 7 in experiments F21 - F25 (Figure 5.9).

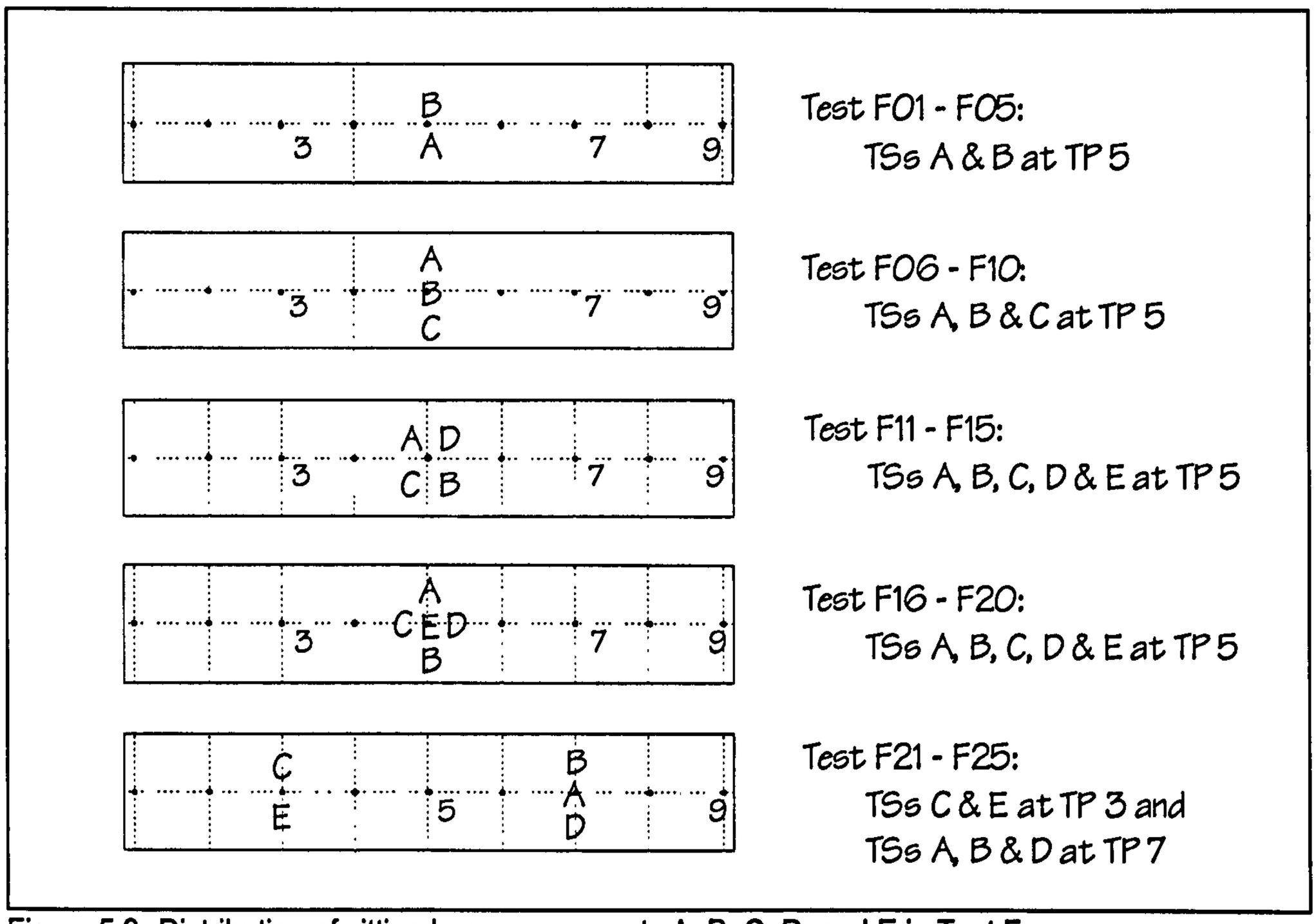

Figure 5.9: Distribution of sitting human occupants A, B, C, D, and E in Test F.

5.3.5 Test G: Equivalent Mass

Test G (Figure 5.7) investigated the influence of a static load on the test structure (Table D.7 in Appendix D). This load was applied using a stack of false floor panels (Figure 5.10). It had a mass equivalent to the overall mass of about 400 kg of the five TSs A, B, C, D, and E. Similarly to the distribution of human occupants in these tests (F16 - F20 and F21 - F25 in Figure 5.9), the equivalent mass was applied at TP 5 or distributed to TPs 3 and 7 (Table D.7).

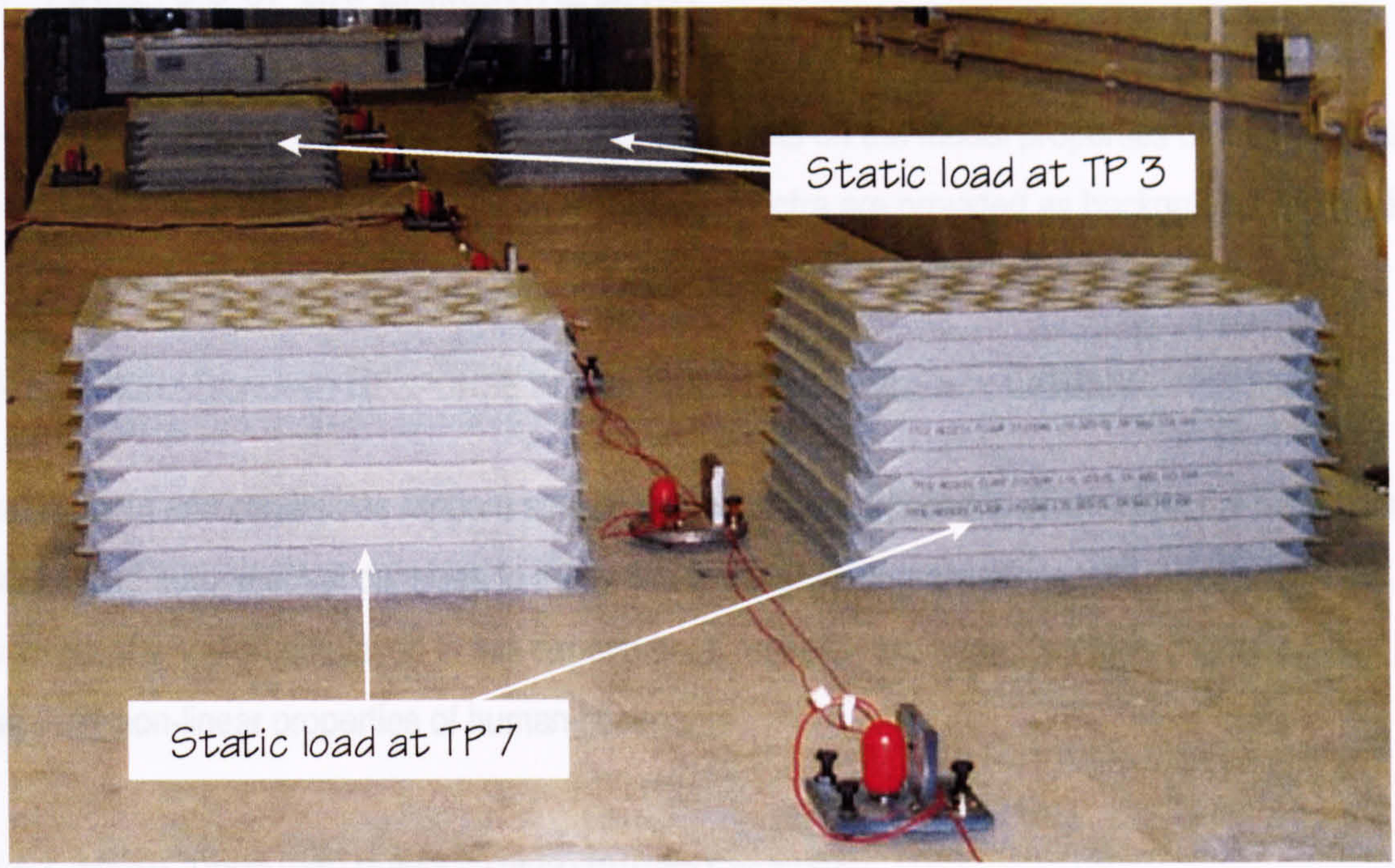

Figure 5.10: Test structure loaded with an equivalent mass.

5.3.6 Test P: Different Postures of a Single Occupant

After a detailed analysis of all previous experiments, it was decided to perform additional tests investigating the influence of the posture of a human occupant. These experiments (Test P) included a retest of the empty test structure (Table D.10 in Appendix D) to enable an analysis independent of possible changes of the empty test structure.

In Test P, TS A was standing with bent knees, standing normally, sitting, and standing with locked knees at TP 5 on the test structure. For convenience of the TS, the different postures were requested in turn and a break was given to the TS while retests of the empty structure were performed (Table D.10).

However, while acquiring modal test data with TS A standing on the structure with bent knees, it soon became clear that the occupant was not able to maintain a stable posture for the data acquisition time of 25 seconds. Instead, he was bouncing slightly and thus inducing forces. This additional excitation was (similarly to the walking excitation) not averaged out and led to unreliable damping estimates. Therefore, the analysis of these tests was abandoned and no further data on this particular test will be presented.

5.4 Analysis of Experimental Data

This research concentrated on the influence of occupants on the modal properties of the structure. Nevertheless, time domain data and corresponding spectra are provided as background information.

5.4.1 Excitation and Response in the Time and Frequency Domain

Burst random and continuous random shaker excitation were applied in different modal tests. Time histories and auto-spectral densities to these two types of testing are presented. Additionally, the low levels of vibration employed in this experimental research are quantified to account for the potentially non-linear properties of human occupants.

5.4.1.1 Modal Tests with Burst Random Shaker Excitation

Three different levels of burst random excitation were employed in this research (Figures 5.11 and 5.12). The lowest and highest excitation levels (1 and 3) were only used in homogeneity checks (Tables D.2 to D.4 in Appendix D). Usually, excitation at level 2 was employed. Sample responses to such a burst random excitation are presented in Figure 5.13.

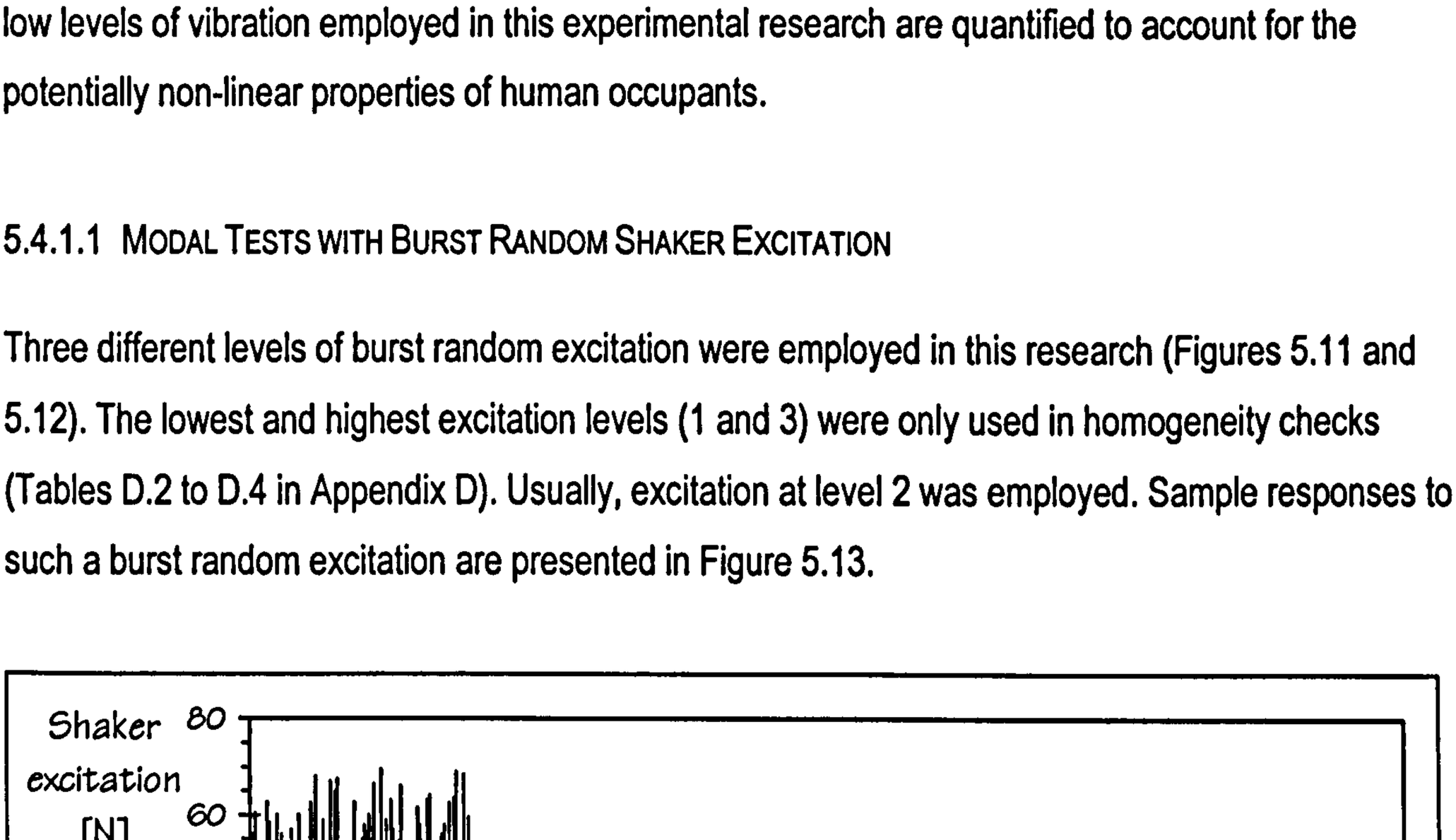

Figure 5.11: Typical burst random excitation in excitation level 2 (A06).

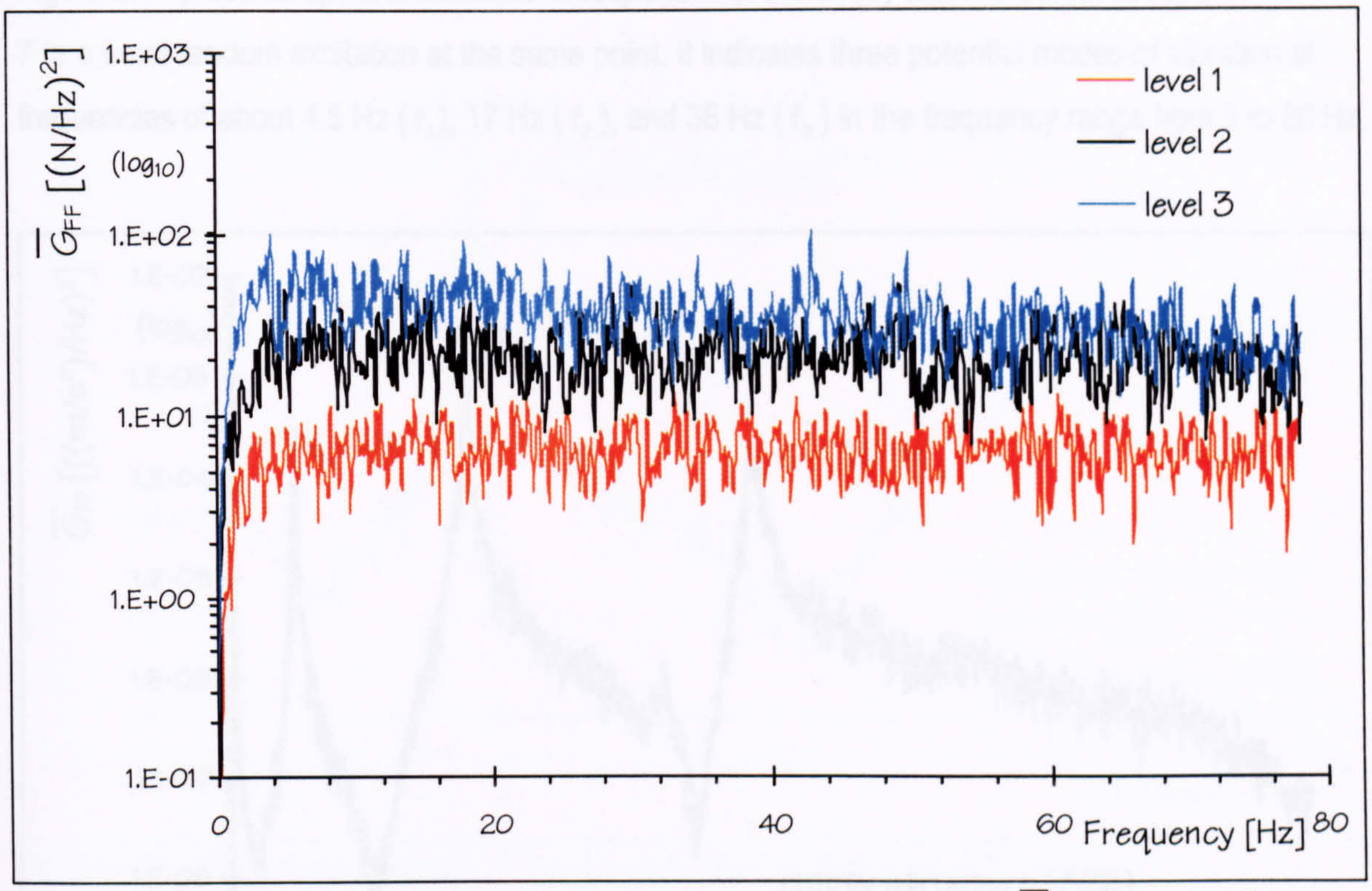

Figure 5.12: Averaged (ten averages) single-sided auto-spectral densities $\overline{G}_{FF}^{t}$ of burst random excitation for the excitation levels 1, 2, and 3 (A12, A06, and A01).

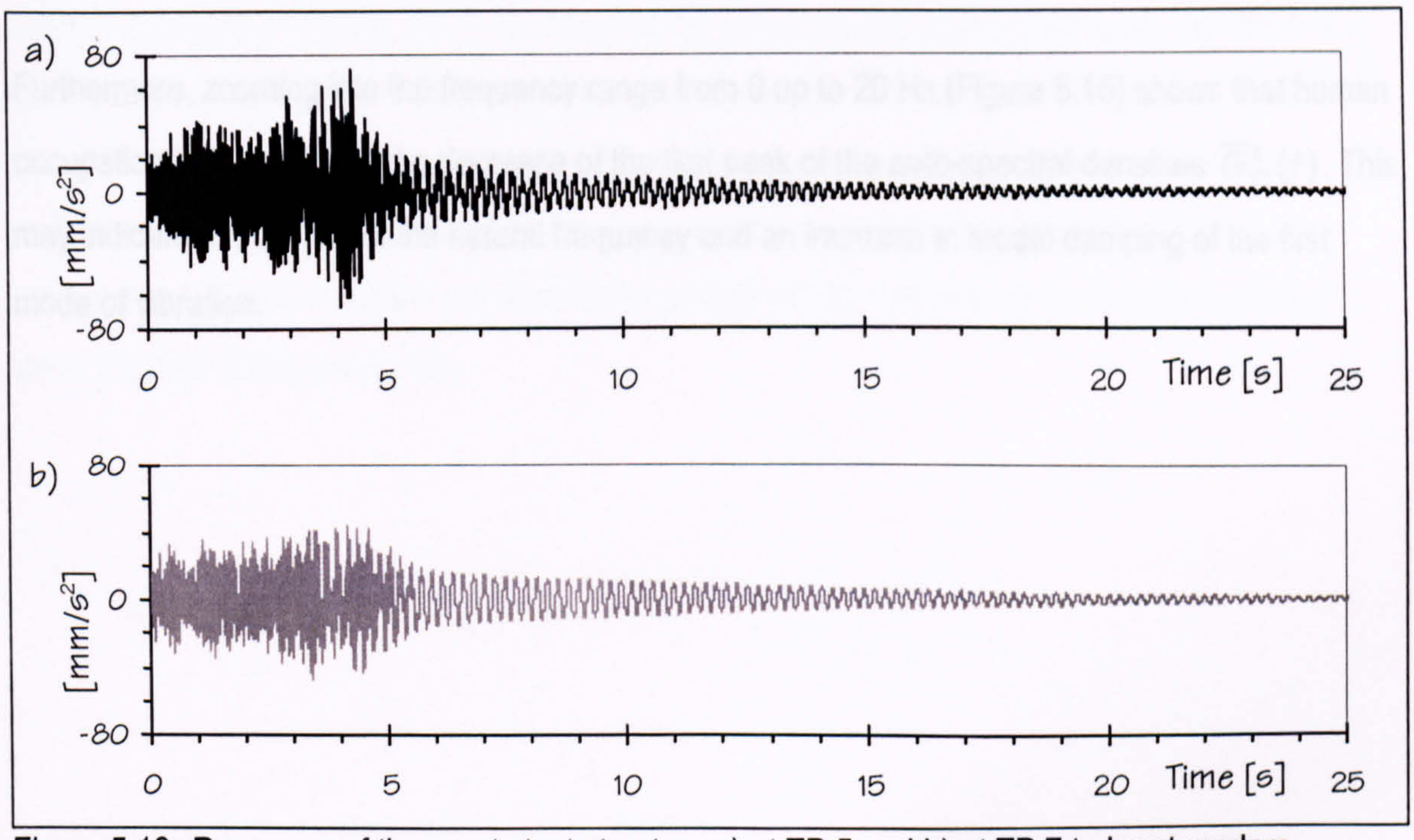

Figure 5.13: Response of the empty test structure a) at TP 5 and b) at TP 7 to burst random excitation at TP 7 (A17).

Figure 5.14 presents spectral densities of responses of the empty and the occupied structure at TP 7 to a burst random excitation at the same point. It indicates three potential modes of vibration at frequencies of about 4.5 Hz (f_1), 17 Hz (f_2), and 38 Hz (f_3) in the frequency range from 0 to 80 Hz.

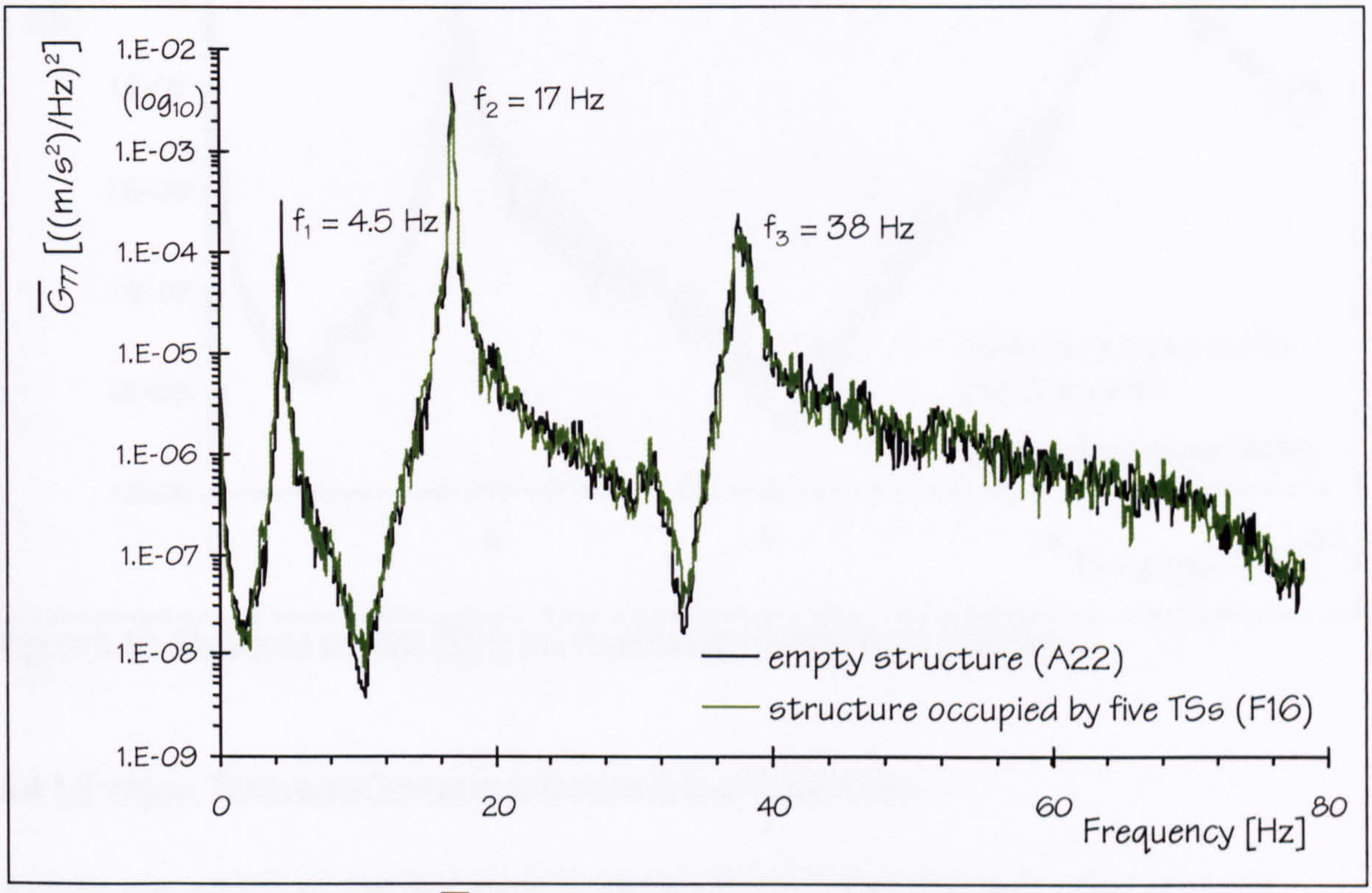

Figure 5.14: Response spectra $\overline{G}_{77}^{t}(f)$ to burst random excitation at TP 7.

Furthermore, zooming into the frequency range from 0 up to 20 Hz (Figure 5.15) shows that human occupation led to a shift and a decrease of the first peak of the auto-spectral densities $\overline{G}_{77}^{t}(f)$. This may indicate a reduction of the natural frequency and an increase in modal damping of the first mode of vibration.

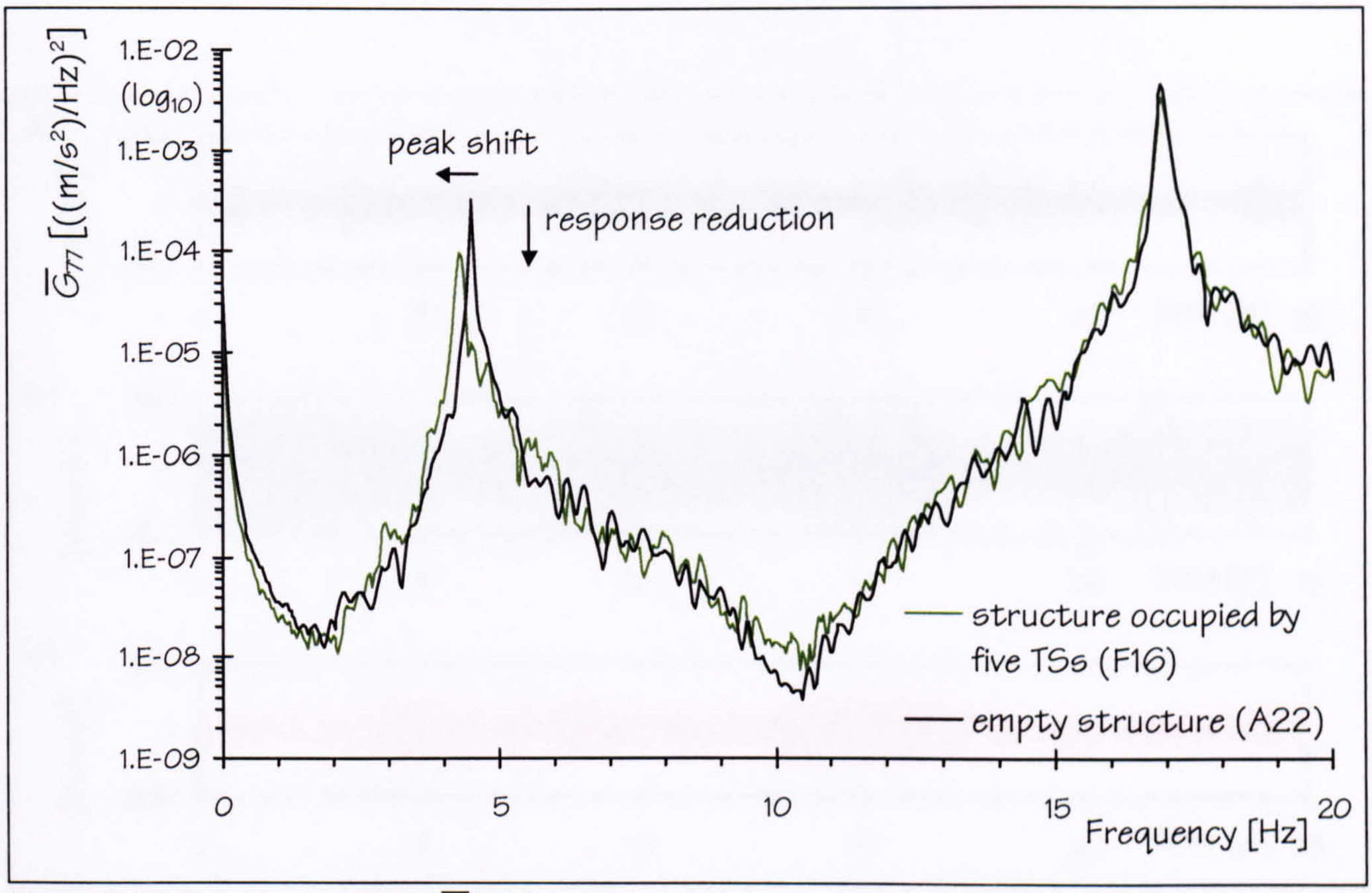

Figure 5.15: Response spectra $\overline{G}_{77}^{t}(f)$ to burst random excitation ($f \leq 20$ Hz).

5.4.1.2 Modal Tests with Continuous Random Shaker Excitation

A continuous random excitation of about 20 minutes duration was employed instead of a burst random excitation in Test D, which investigated the influence of a walking occupant (section 5.3.3). Such a continuous random excitation led to peak acceleration responses (Figure 5.16a) similar to that of burst random excitation (Figure 5.13b). However, responses of the structure to shaker excitation only were lower than in tests involving walking occupants (Figure 5.16). For instance, walking at 1.5 Hz led to responses about twice as high as the response to the shaker excitation alone (Figures 5.16a and 5.16b).

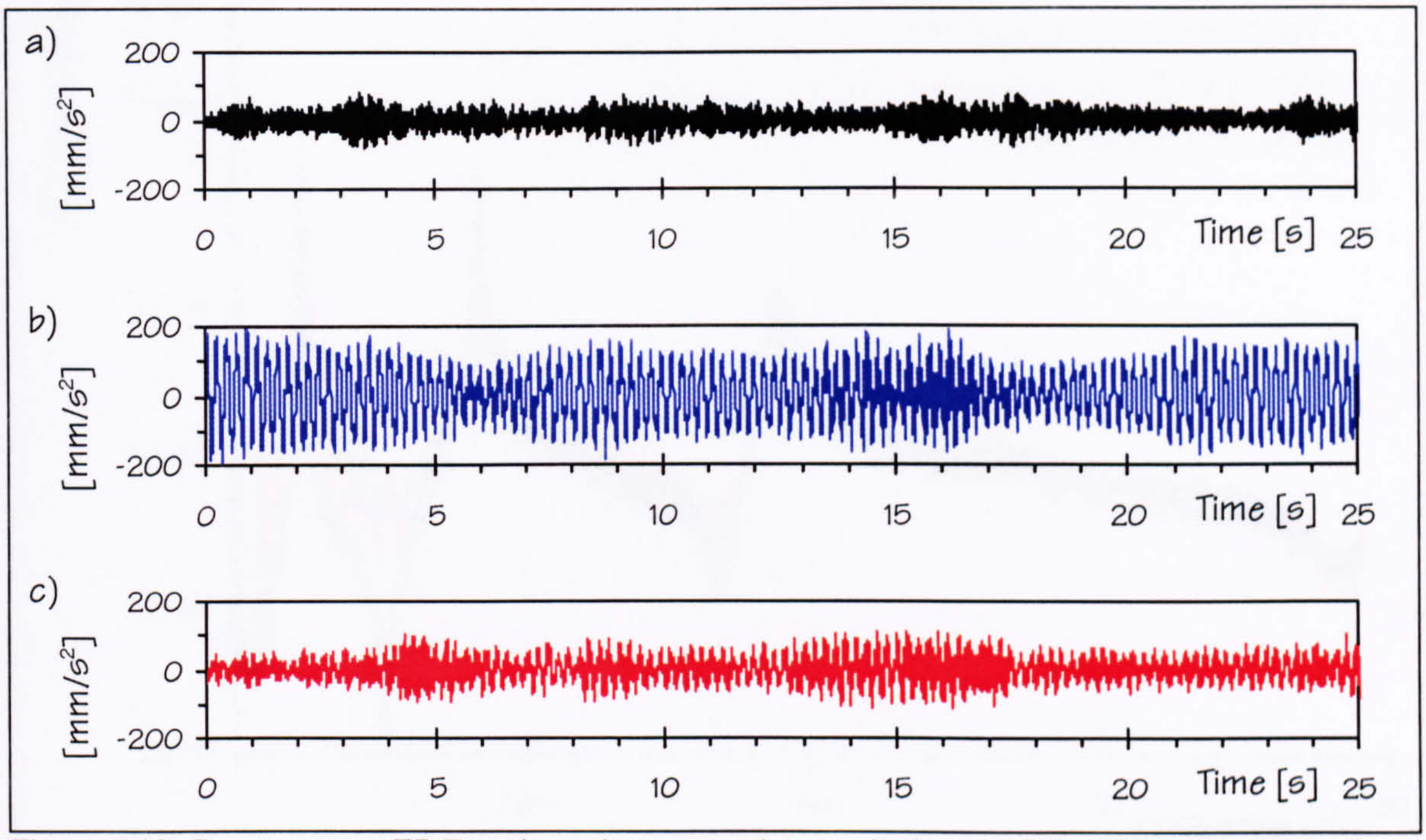

Figure 5.16: Responses at TP 7 to a) continuous random excitation at TP 7 (D03) and additional excitation by an occupant walking at b) 1.5 Hz (D01) or c) 1.8 Hz (D02).

The contribution of a walking person to the overall response of the structure is evident in the response spectra presented in Figure 5.17. Zooming into the frequency range from 0 to 20 Hz, Figure 5.18 reveals significant responses to walking at harmonics and sub-harmonics of the walking frequencies. In fact, force components up to the eighth harmonic at 12 Hz are apparent for walking at 1.5 Hz (blue line in Figure 5.18). Similarly, controlled walking at 1.8 Hz resulted in strong responses of the structure up to the sixth harmonic at 11 Hz and also at sub-harmonics such as at 2.7 Hz, 4.5 Hz, and 6.3 Hz (red line in Figure 5.18).

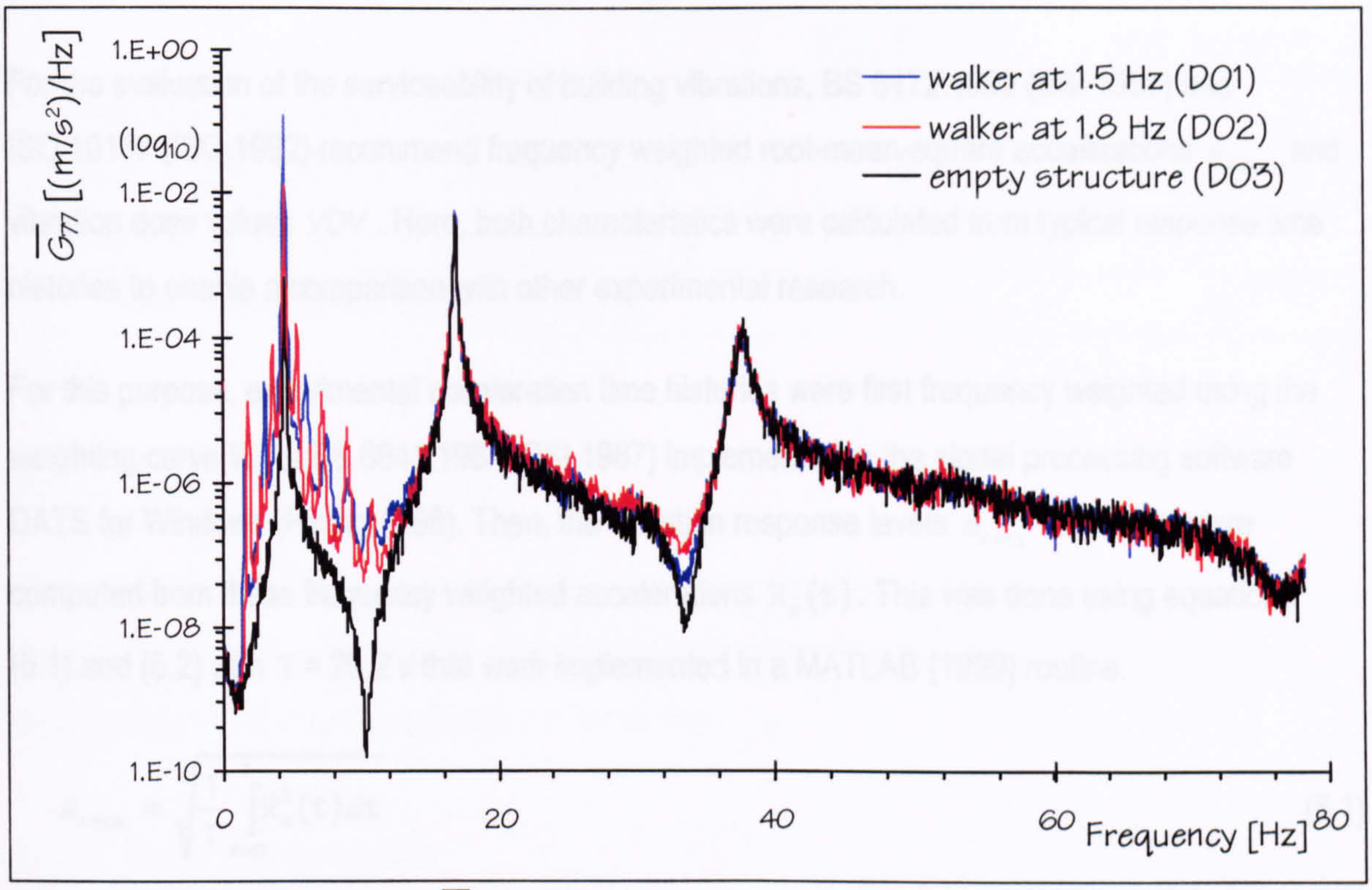

Figure 5.17: Response spectra $\overline{G}^{r}_{77}(f)$ to continuous random shaker excitation at TP 7 and an additional excitation by one occupant walking at 1.5 Hz or at 1.8 Hz.

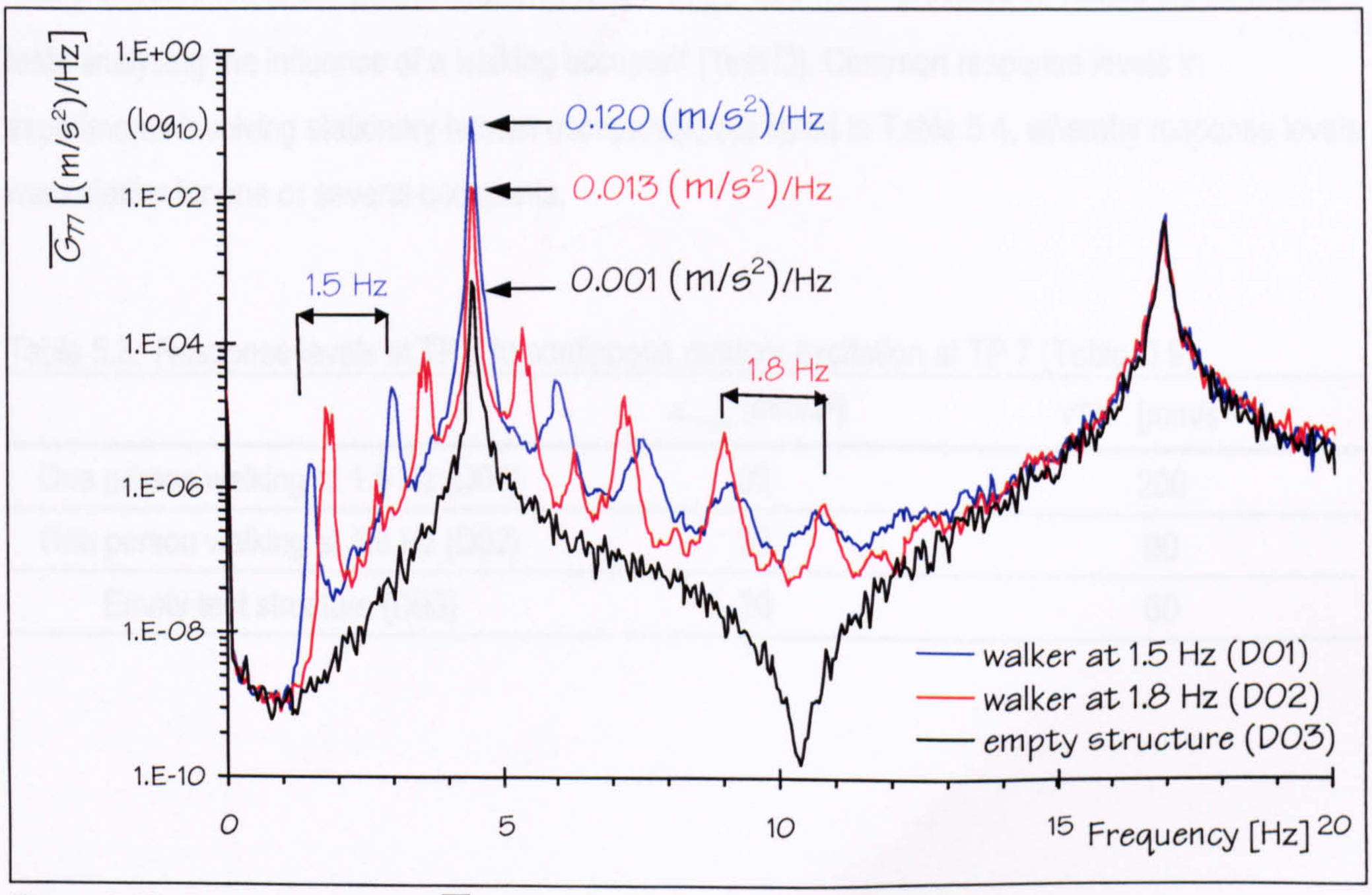

Figure 5.18: Response spectra $\overline{G}^{r}_{77}(f)$ in Test D ($f \leq 20$ Hz).

5.4.1.3 Levels of Vibration

For the evaluation of the serviceability of building vibrations, BS 6472:1992 (BSI 1992) and ISO 10137 (ISO 1992) recommend frequency weighted root-mean-square accelerations $a_{r.m.s.}$ and vibration dose values VDV. Here, both characteristics were calculated from typical response time histories to enable a comparison with other experimental research.

For this purpose, experimental acceleration time histories were first frequency weighted using the weighting curve W_b of BS 6841:1987 (BSI 1987) implemented in the signal processing software DATS for Windows (Prosig 1998). Then, the vibration response levels $a_{r.m.s.}$ and VDV were computed from these frequency weighted accelerations $\ddot{x}_w(t)$. This was done using equations (5.1) and (5.2) with $T = 25.2$ s that were implemented in a MATLAB (1999) routine.

$$a_{r.m.s.} = \sqrt{\frac{1}{T}\int_{t=0}^{T}\ddot{x}_w^2(t)dt} \tag{5.1}$$

$$VDV = \sqrt[4]{\int_{t=0}^{T}\ddot{x}_w^4(t)dt} \tag{5.2}$$

This procedure led to the typical response levels $a_{r.m.s.}$ and VDV provided in Tables 5.3 for modal tests analysing the influence of a walking occupant (Test D). Common response levels in experiments involving stationary human occupant(s) are listed in Table 5.4, whereby response levels were similar for one or several occupants.

Table 5.3: Response levels at TP 7 to continuous random excitation at TP 7 (Table D.9).

	$a_{r.m.s.}$ [mm/s^2]	VDV [mm/s$^{1.75}$]
One person walking at 1.5 Hz (D01)	80	200
One person walking at 1.8 Hz (D02)	30	90
Empty test structure (D03)	20	60

Table 5.4: Response levels at TP 5 to burst random excitation at TP 7.

	$a_{r.m.s.}$ [mm/s^2]	VDV [mm/s$^{1.75}$]
Stationary occupant at TP 5 (excitation level 1)	3	10
Stationary occupant(s) at TP 5 (excitation level 2)	4	15
Stationary occupant at TP 5 (excitation level 3)	6	21
Empty test structure (excitation level 2)	5	16

5.4.2 Quality of FRF Estimates

High quality FRF estimates were required for a reliable quantification of the influence of human occupants on modal properties. To demonstrate the quality of the modal tests performed, some representative FRFs and coherences are presented.

5.4.2.1 Empty Test Structure

Figure 5.19 demonstrates that ten averages led to stable FRFs of the empty structure. The coherences $\gamma^2(f)$ of such FRFs were satisfactory because they were close to unity at resonances of the structure (f_1, f_2, and f_3) and low only at anti-resonances (Figure 5.20). This was not only the case for directly acquired data but also if signals were replayed from magnetic tape (Figure 5.20).

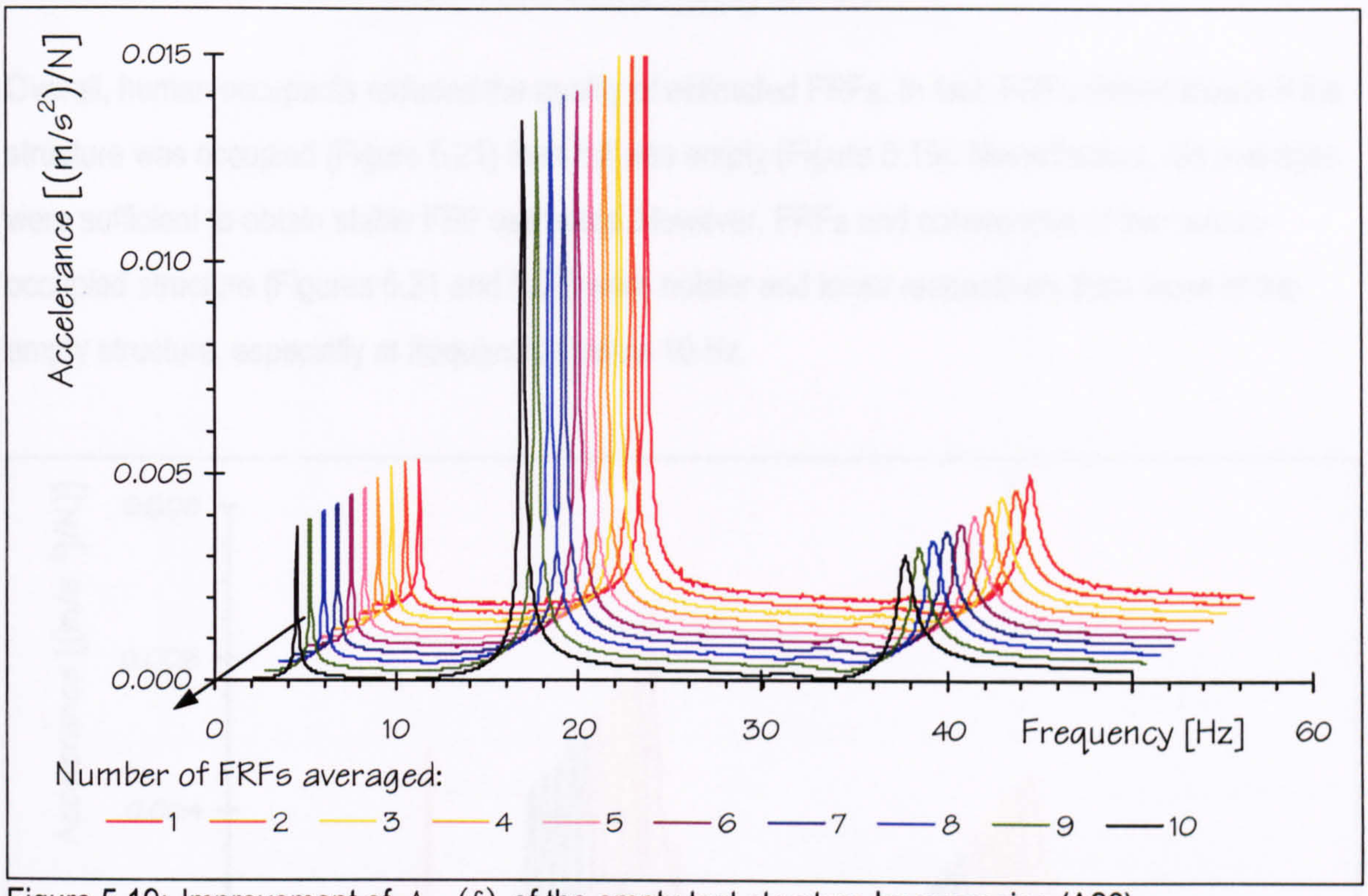

Figure 5.19: Improvement of $A_{77}(f)$ of the empty test structure by averaging (A26).

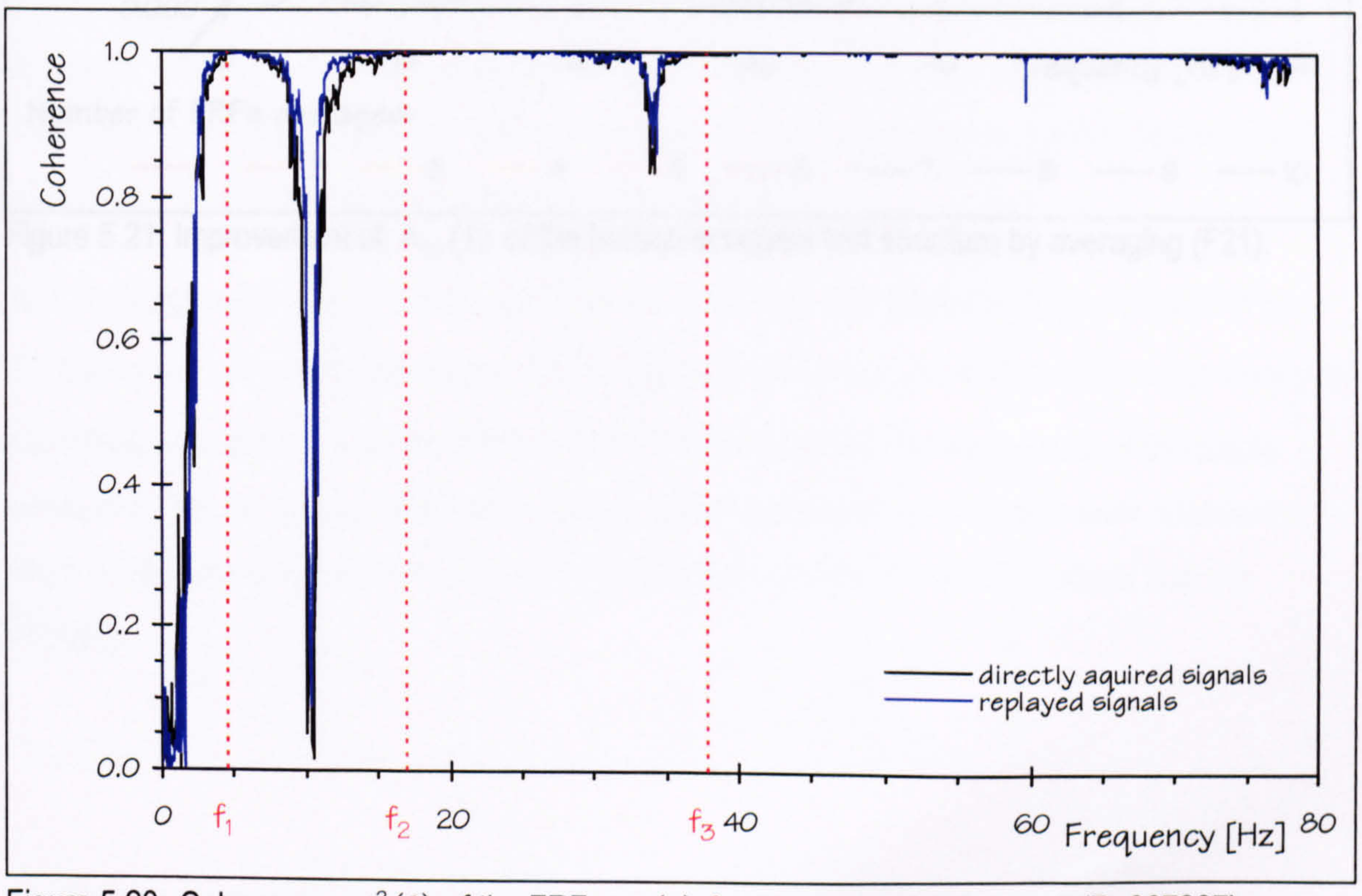

Figure 5.20: Coherences $\gamma^2(f)$ of the FRF $A_{77}(f)$ for the empty test structure (R_307307).

5.4.2.2 Stationary Human Occupant(s) on the Test Structure

Overall, human occupants reduced the quality of estimated FRFs. In fact, FRFs settled slower if the structure was occupied (Figure 5.21) than if it was empty (Figure 5.19). Nevertheless, ten averages were sufficient to obtain stable FRF estimates. However, FRFs and coherences of the human-occupied structure (Figures 5.21 and 5.22) were noisier and lower respectively than those of the empty structure, especially at frequencies below 10 Hz.

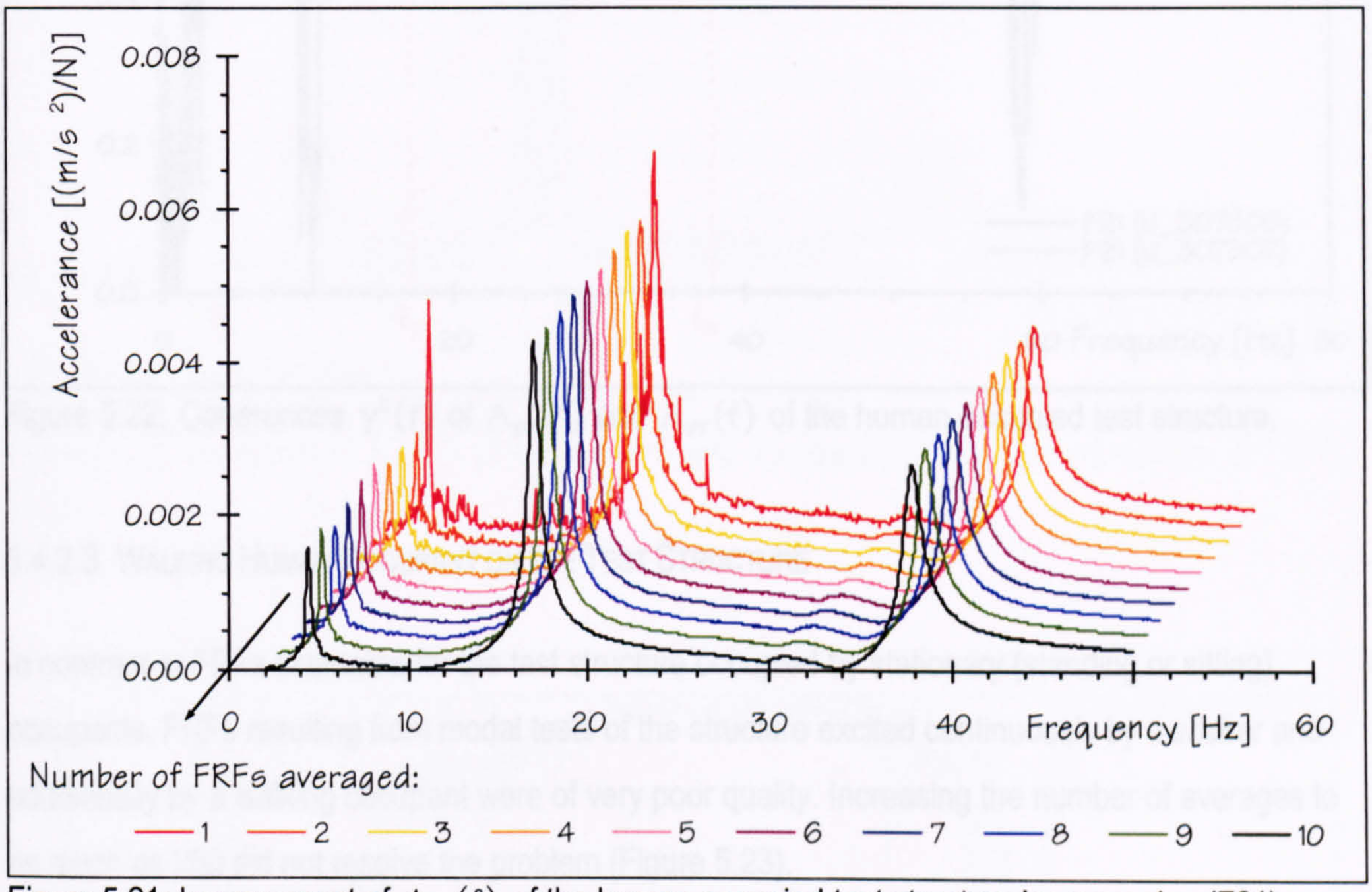

Figure 5.21: Improvement of $A_{77}(f)$ of the human-occupied test structure by averaging (F21).

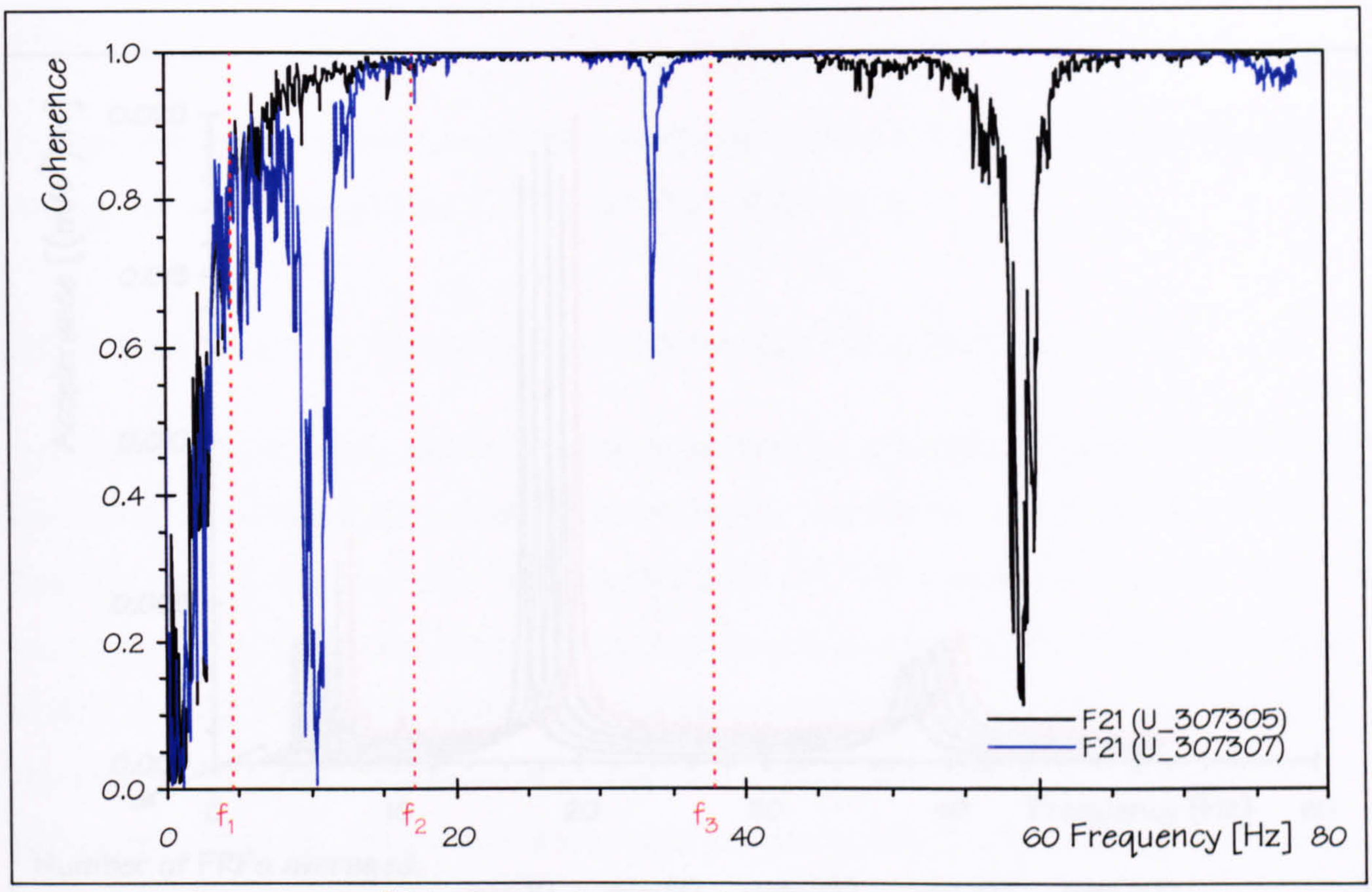

Figure 5.22: Coherences $\gamma^2(f)$ of $A_{57}(f)$ and $A_{77}(f)$ of the human-occupied test structure.

5.4.2.3 Walking Human Occupant on the Test Structure

In contrast to FRFs estimated for the test structure occupied by stationary (standing or sitting) occupants, FRFs resulting from modal tests of the structure excited continuously by a shaker and additionally by a walking occupant were of very poor quality. Increasing the number of averages to as much as 200 did not resolve the problem (Figure 5.23).

This instability was based on the strong influence of the high extraneous walking excitation (Figure 5.18) as confirmed by the coherences $\gamma^2(f)$ presented in Figure 5.24. In fact, coherences were poor if a walking occupant was on the structure (D01 and D02) but high for modal tests of the empty structure (D03). As consequence of this finding, further investigations of Test D were abandoned and the influence of a walking occupant on the modal properties of the test structure was not analysed.

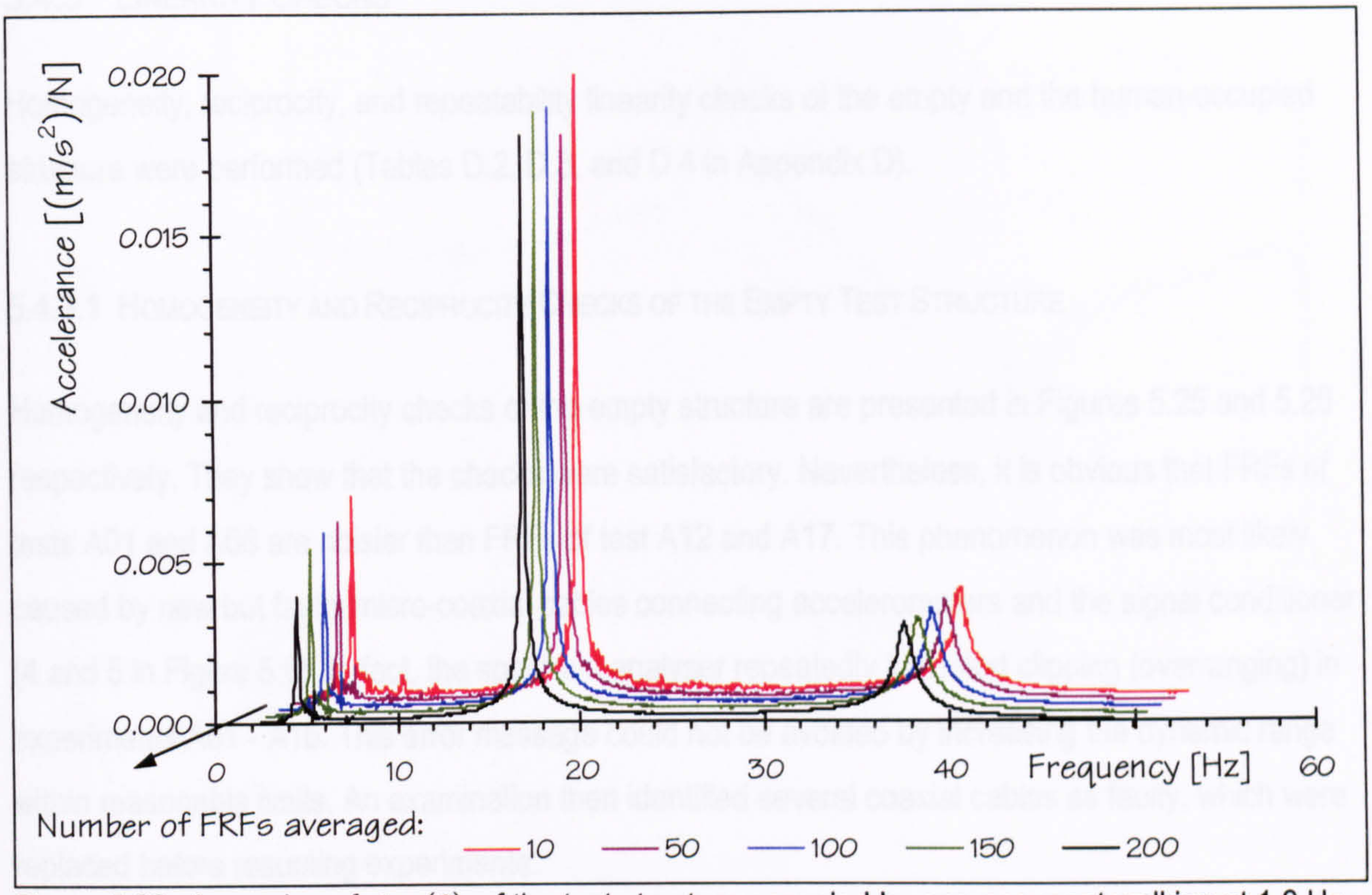

Figure 5.23: Averaging of $A_{77}(f)$ of the test structure occupied by one occupant walking at 1.8 Hz (D02).

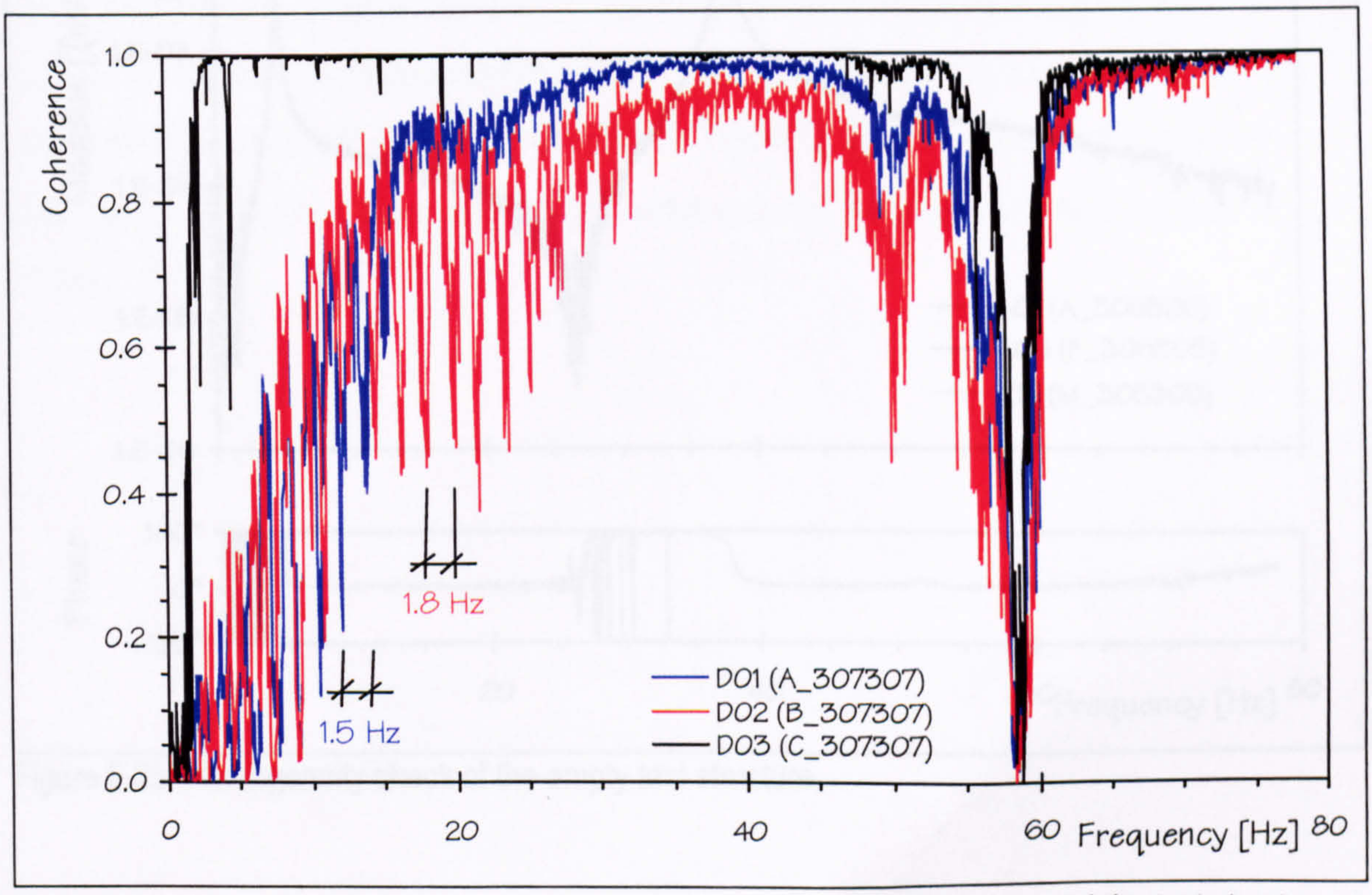

Figure 5.24: Coherences $\gamma^2(f)$ of FRFs $A_{77}(f)$ of the empty test structure and the test structure occupied by a walker.

5.4.3 Linearity Checks

Homogeneity, reciprocity, and repeatability linearity checks of the empty and the human-occupied structure were performed (Tables D.2, D.3, and D.4 in Appendix D).

5.4.3.1 Homogeneity and Reciprocity Checks of the Empty Test Structure

Homogeneity and reciprocity checks of the empty structure are presented in Figures 5.25 and 5.26 respectively. They show that the checks were satisfactory. Nevertheless, it is obvious that FRFs of tests A01 and A06 are noisier than FRFs of test A12 and A17. This phenomenon was most likely caused by new but faulty micro-coaxial cables connecting accelerometers and the signal conditioner (4 and 5 in Figure 5.6). In fact, the spectrum analyser repeatedly indicated clipping (overranging) in experiments A01 - A16. This error message could not be avoided by increasing the dynamic range within reasonable limits. An examination then identified several coaxial cables as faulty, which were replaced before resuming experiments.

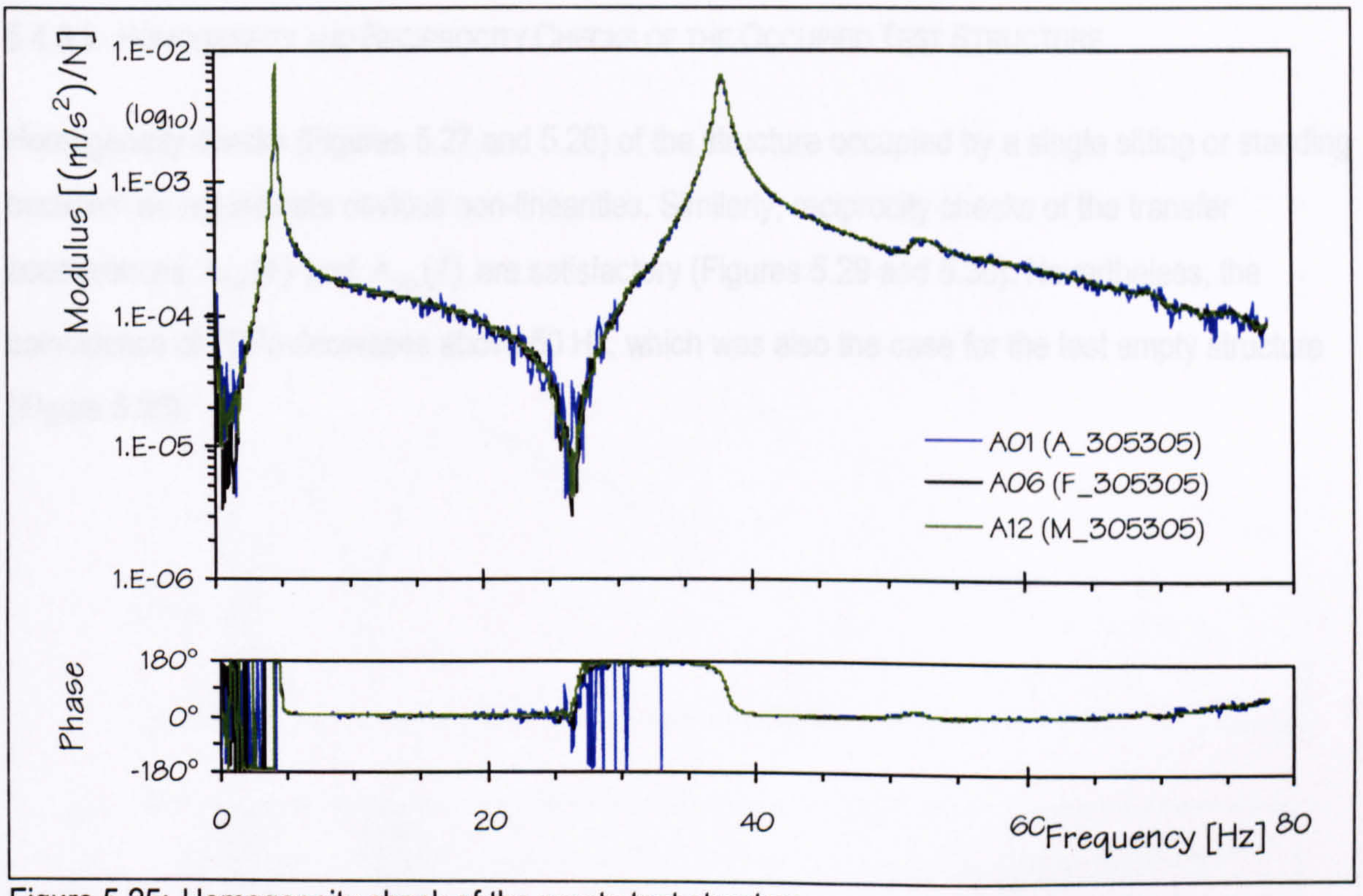

Figure 5.25: Homogeneity check of the empty test structure.

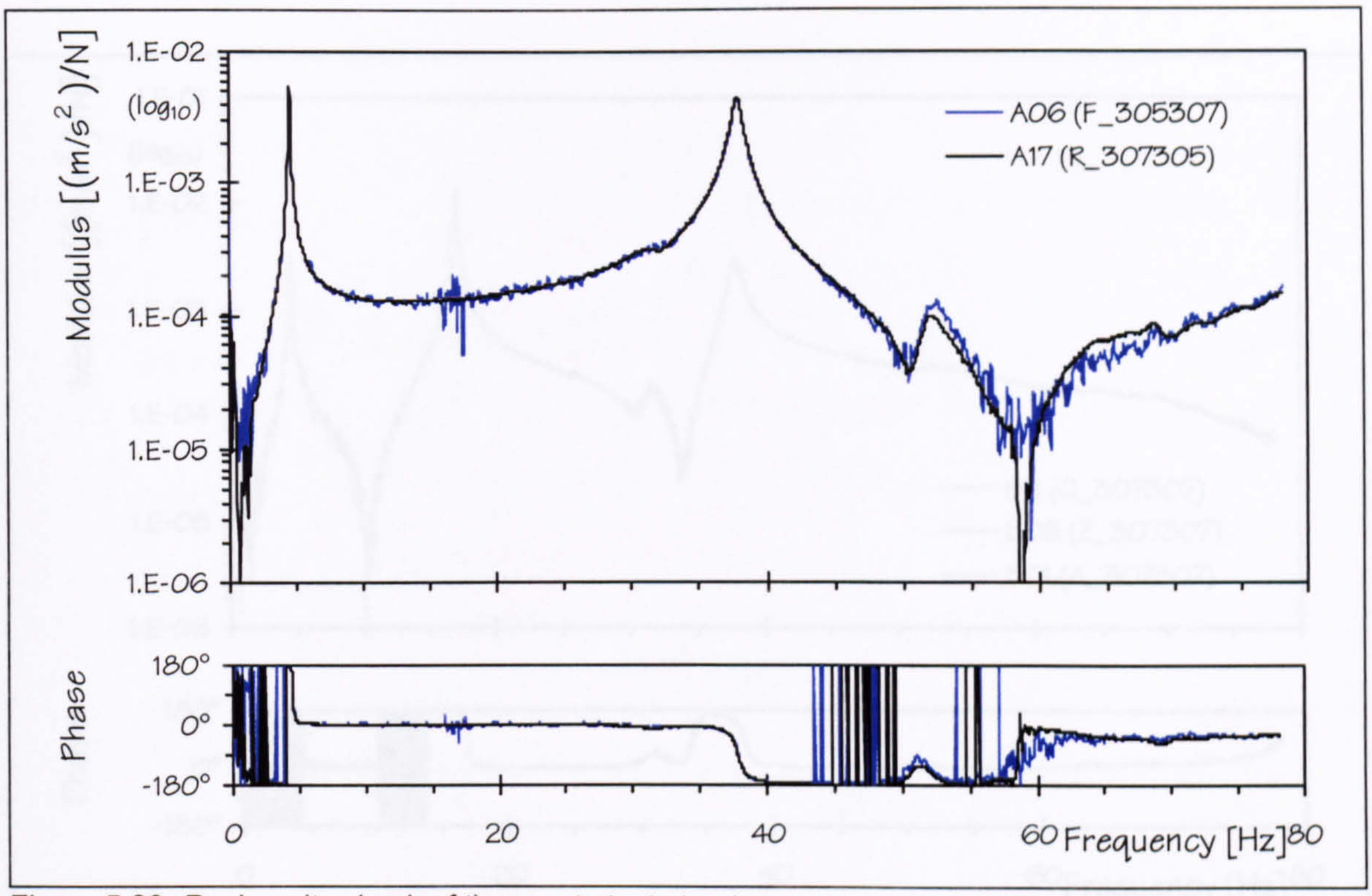

Figure 5.26: Reciprocity check of the empty test structure.

5.4.3.2 Homogeneity and Reciprocity Checks of the Occupied Test Structure

Homogeneity checks (Figures 5.27 and 5.28) of the structure occupied by a single sitting or standing occupant do not indicate obvious non-linearities. Similarly, reciprocity checks of the transfer accelerances $A_{57}(f)$ and $A_{75}(f)$ are satisfactory (Figures 5.29 and 5.30). Nevertheless, the coincidence of FRFs decreases above 50 Hz, which was also the case for the test empty structure (Figure 5.26).

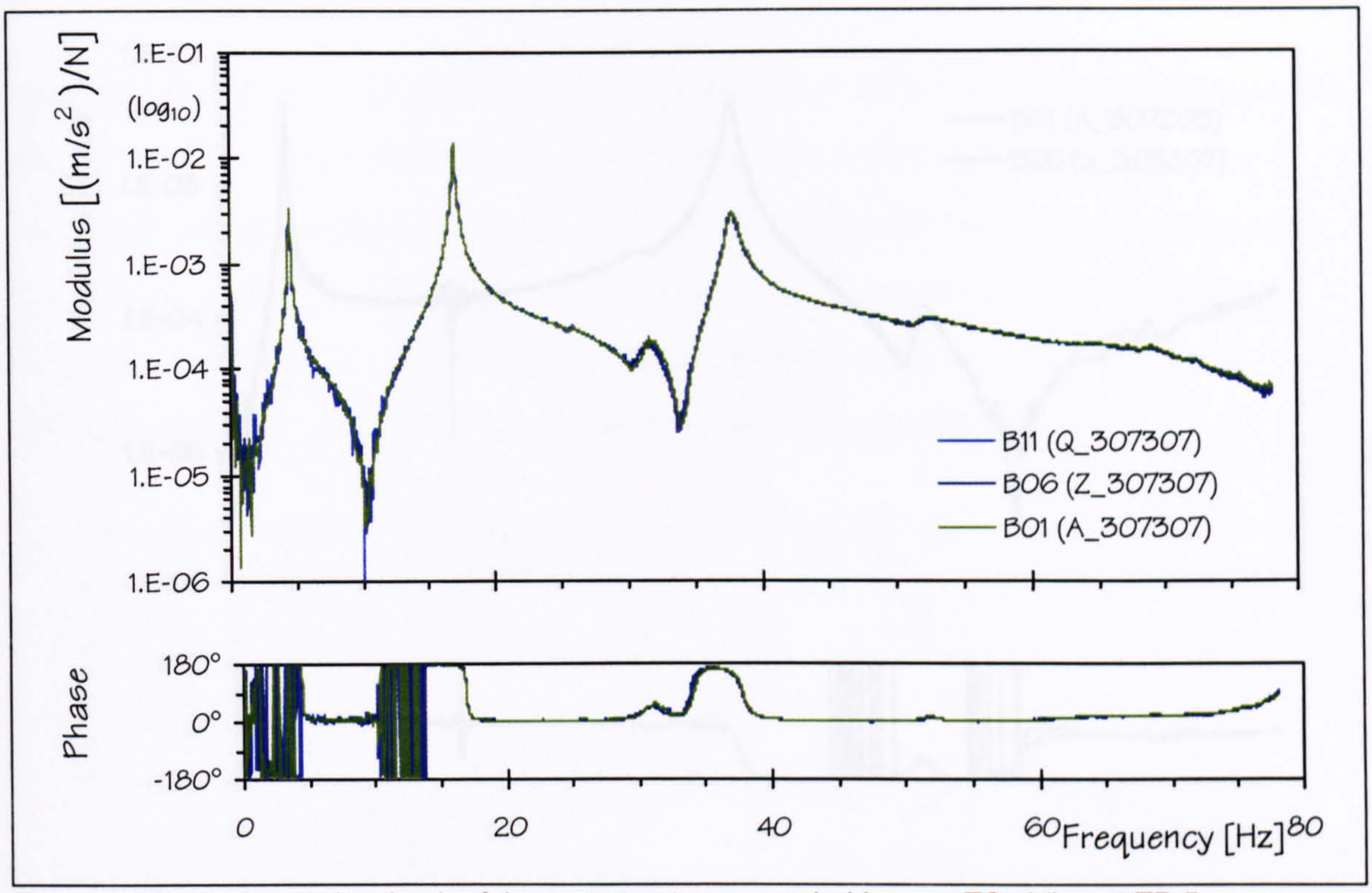

Figure 5.27: Homogeneity check of the test structure occupied by one TS sitting at TP 5.

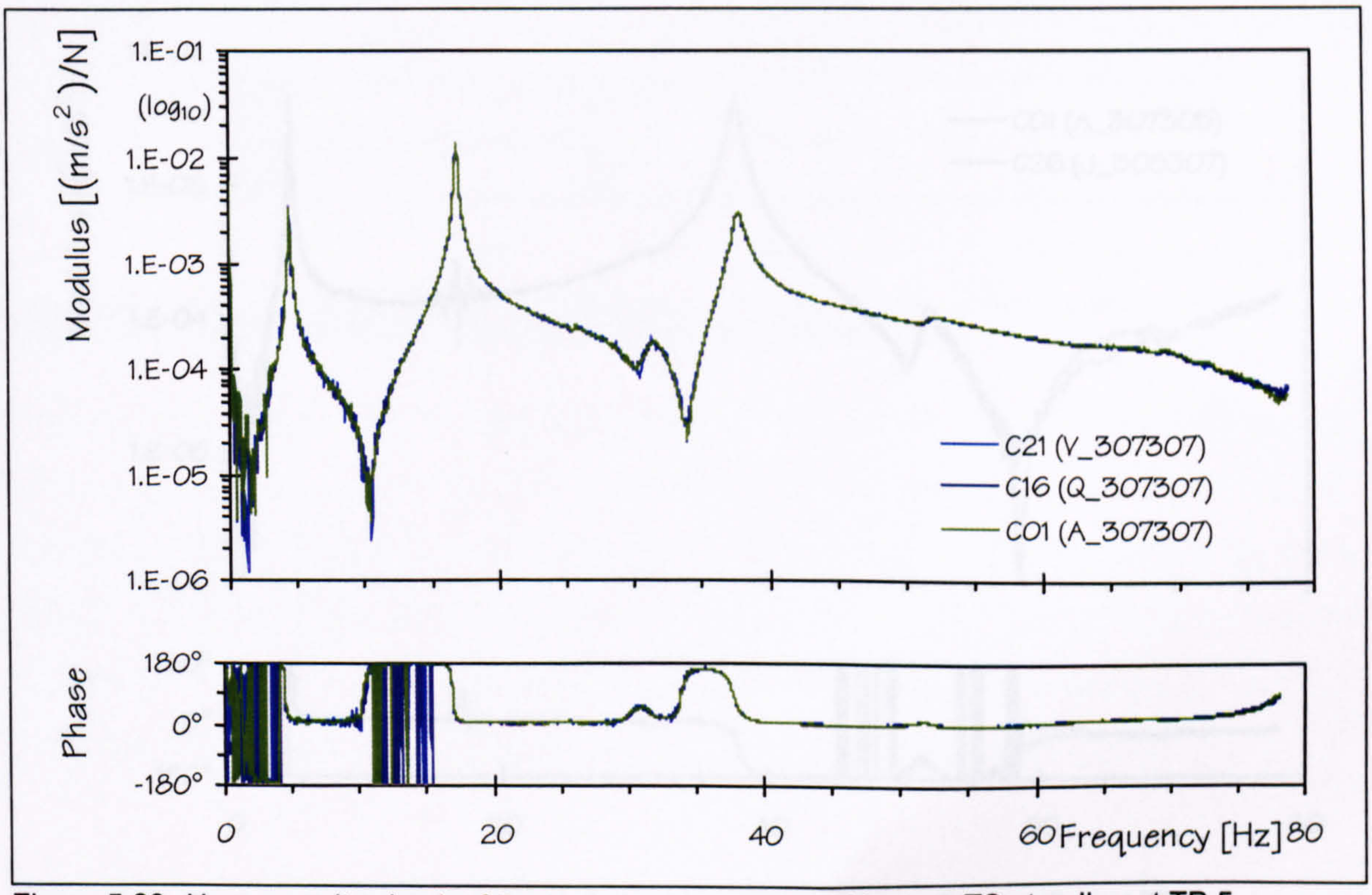

Figure 5.28: Homogeneity check of the test structure occupied by one TS standing at TP 5.

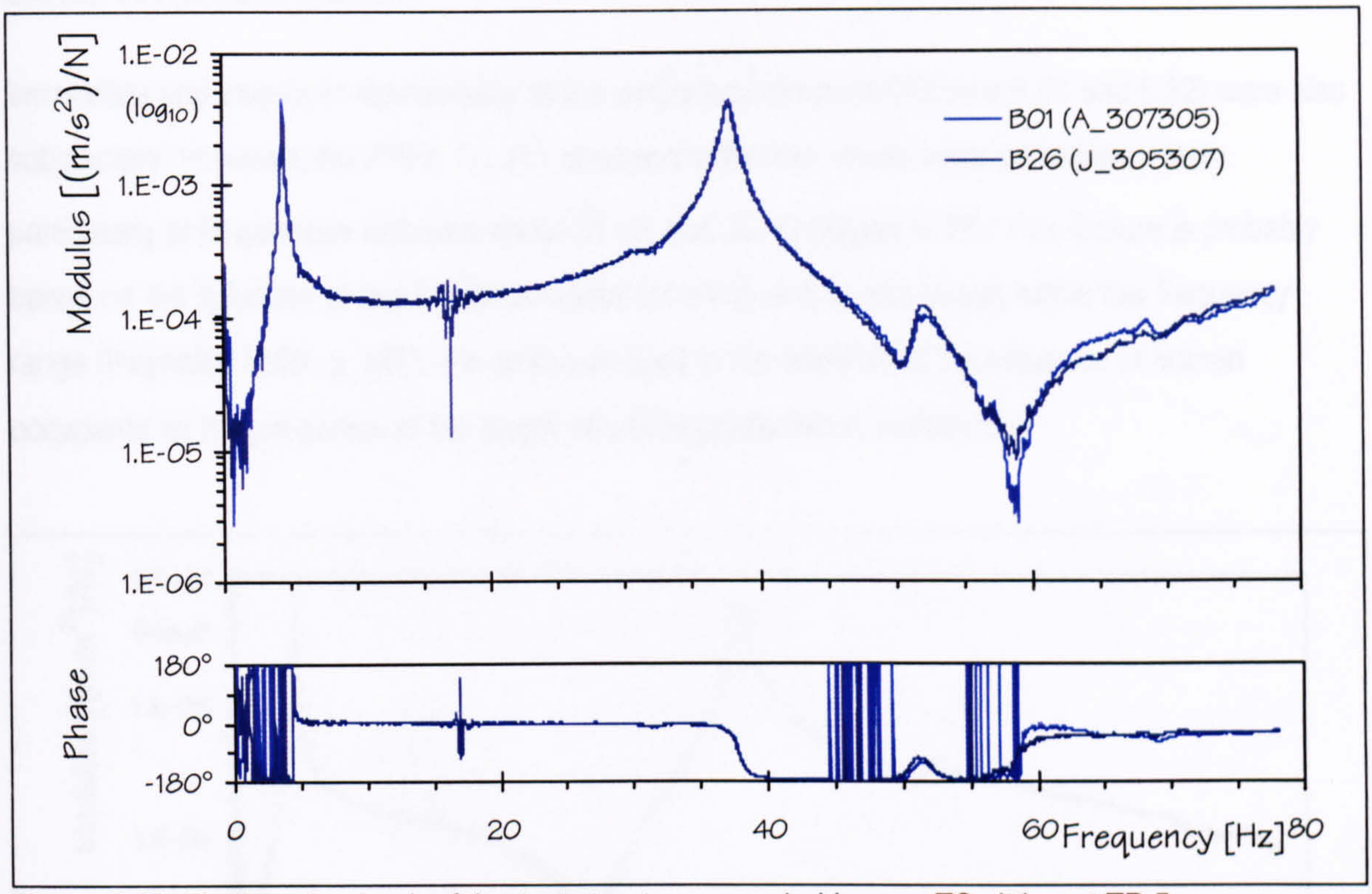

Figure 5.29: Reciprocity check of the test structure occupied by one TS sitting at TP 5.

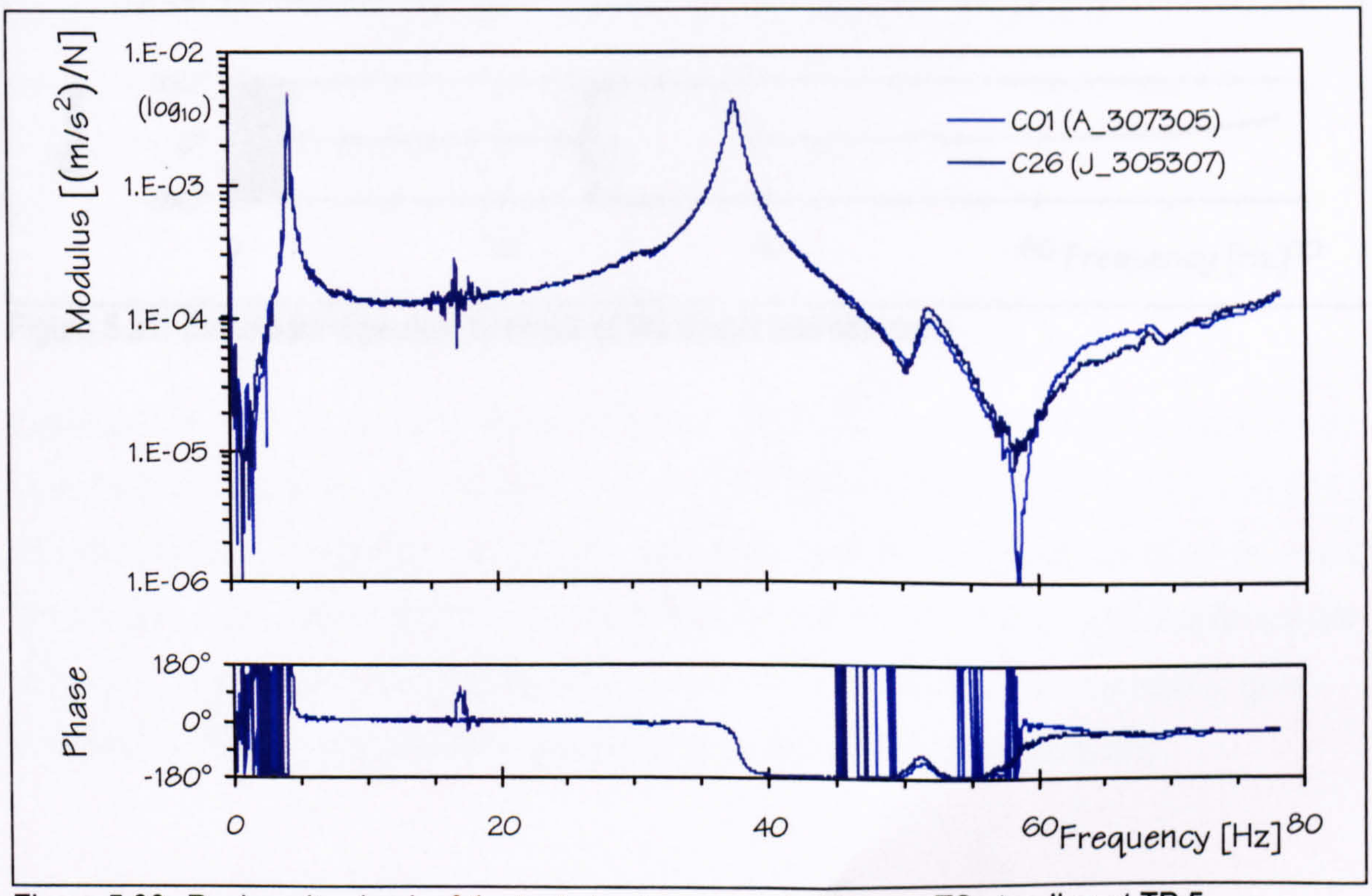

Figure 5.30: Reciprocity check of the test structure occupied by one TS standing at TP 5.

5.4.3.3 Repeatability Checks

Immediate and long-term repeatability of the empty test structure (Figures 5.31 and 5.32) were also satisfactory. However, the FRFs $A_{77}(f)$ changed within the weeks elapsed between tests particularly at frequencies between about 25 Hz and 35 Hz (Figure 5.32). This feature is probably based on the influence of two torsional modes (of which one is non-linear) within this frequency range (Reynolds 2000, p. 147). It is acknowledged in the analysis of the influence of human occupants on the properties of the empty structure presented in section 5.6.

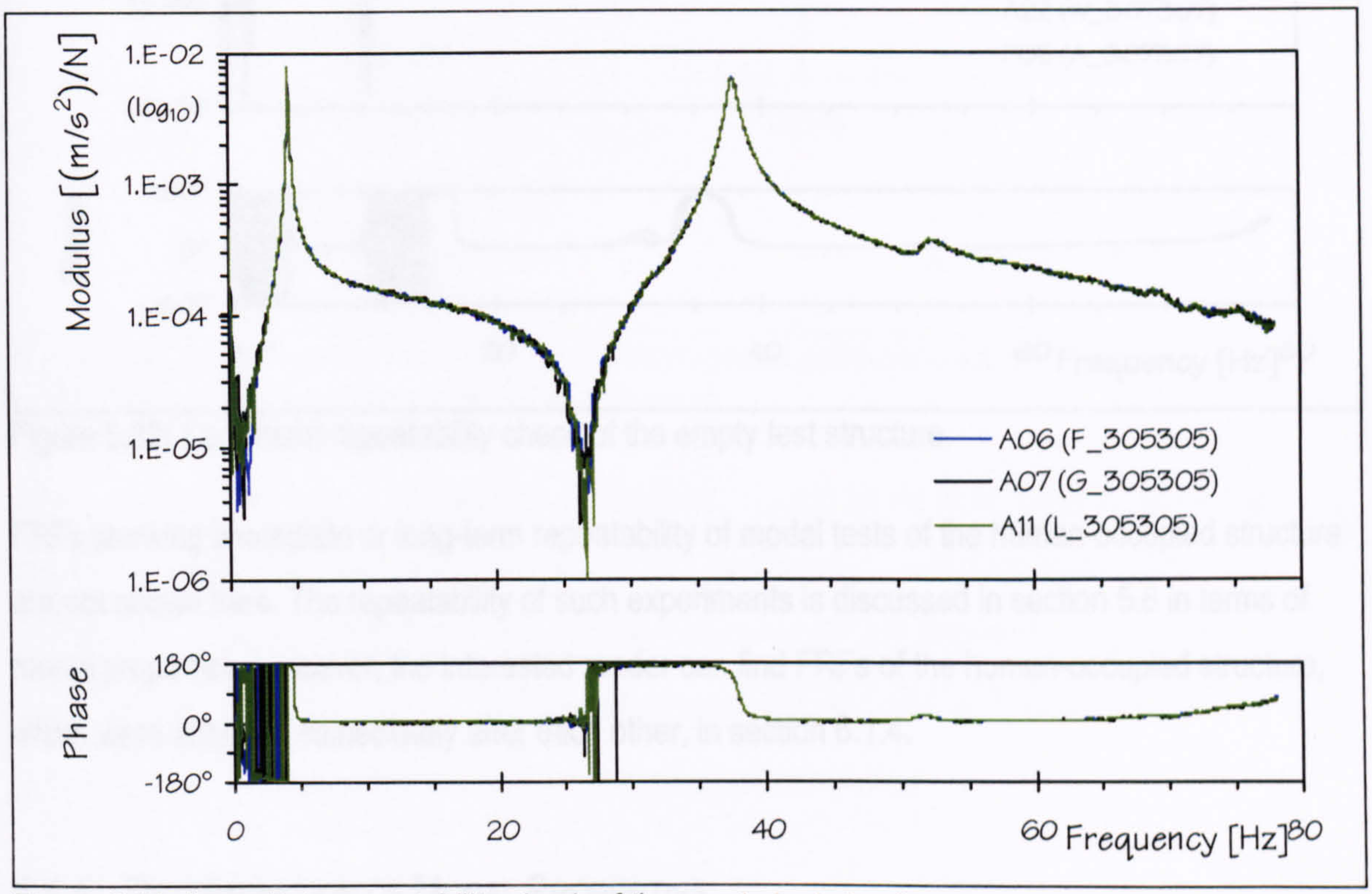

Figure 5.31: Immediate repeatability check of the empty test structure.

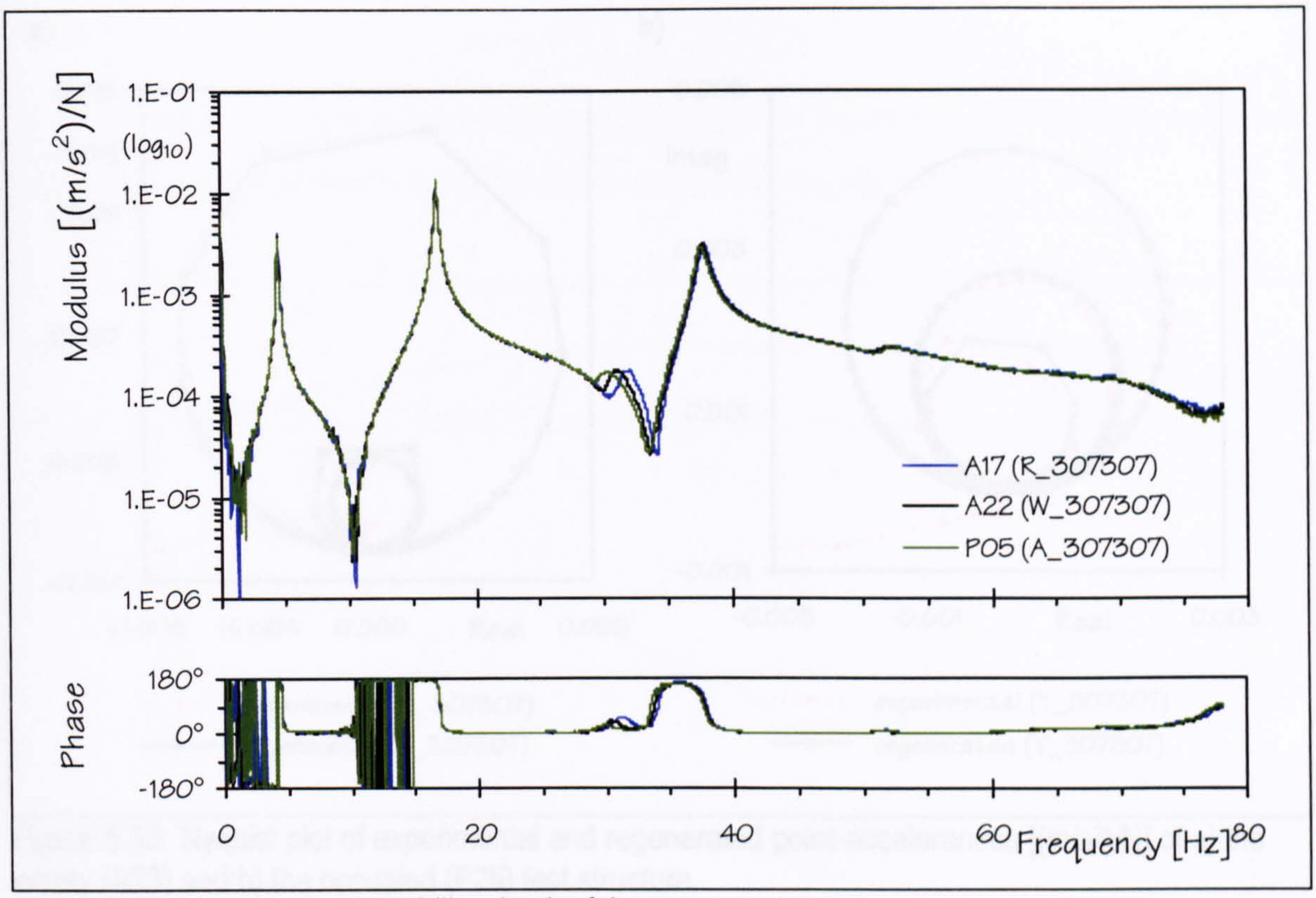

Figure 5.32: Long-term repeatability check of the empty test structure.

FRFs showing immediate or long-term repeatability of modal tests of the human-occupied structure are not shown here. The repeatability of such experiments is discussed in section 5.6 in terms of modal properties. However, the interested reader can find FRFs of the human-occupied structure, which were acquired immediately after each other, in section 6.1.4.

5.4.4 Determination of Modal Properties

It was mentioned before that the acquisition of reliable FRFs was not successful if the structure was occupied by a walking person (Test D) or by an occupant standing with bent knees (P01, P06, P11, P16, P21, and P26). Therefore, a modal analysis of these tests was not performed. However, modal properties of all other experiments were estimated by curve-fitting of FRFs using the modal analysis software ICATS (section 3.2.4). Indicating the high quality of estimated modal properties, Figure 5.33 presents two experimental FRFs and their regenerated counterparts exemplarily.

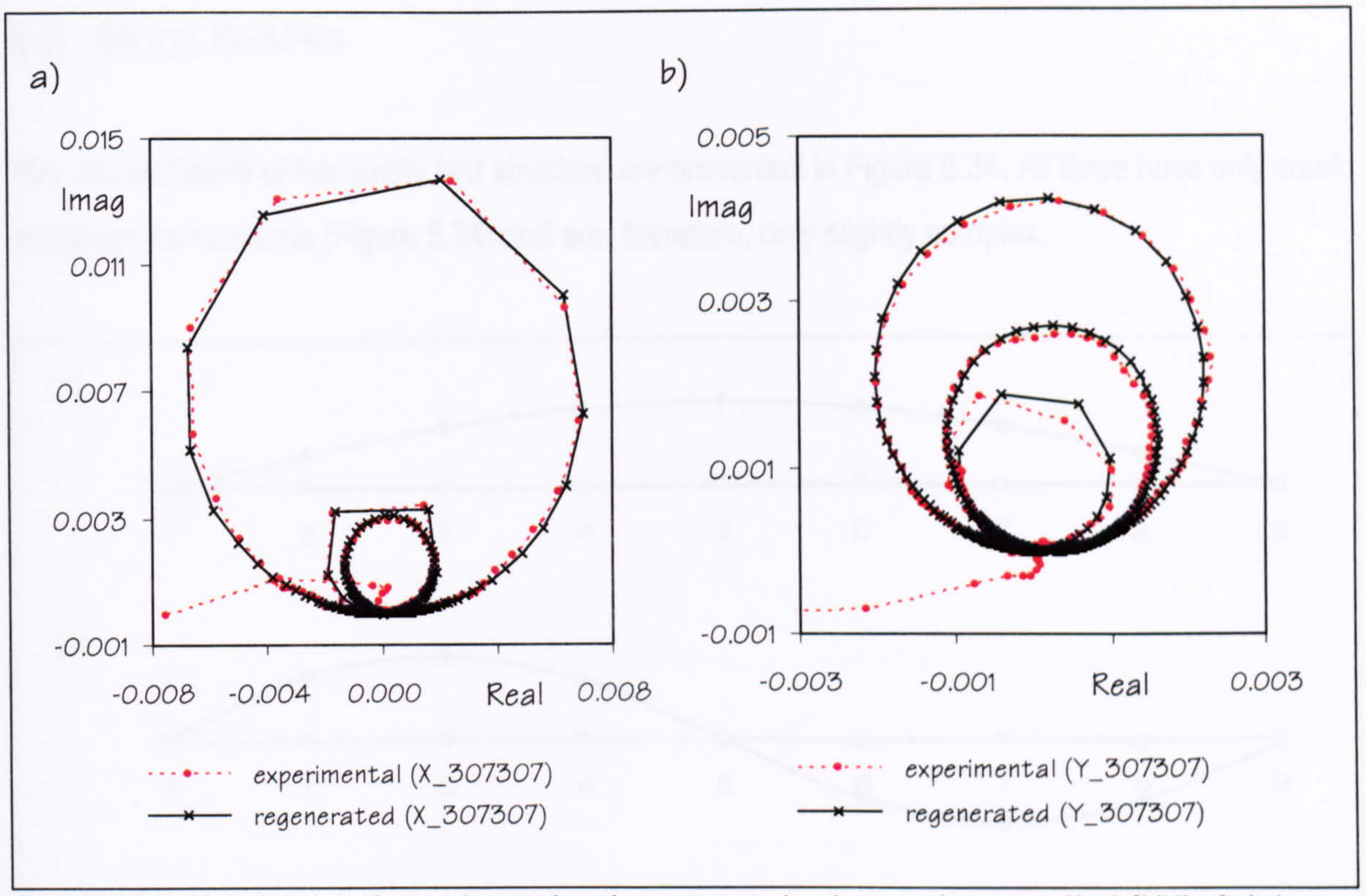

Figure 5.33: Nyquist plot of experimental and regenerated point-accelerances [(m/s²)/N] of a) the empty (A23) and b) the occupied (F25) test structure.

Three modes of vibration at frequencies of about 4.5, 17, and 38 Hz were identified within the frequency range from 0 to 80 Hz for the empty and the human-occupied structure. Their mode shapes are discussed briefly in the next section. Estimated natural frequencies (f_1, f_2, and f_3), damping ratios (ζ_1, ζ_2, and ζ_3), and modal masses (m_1, m_2, and m_3) are summarised in Appendix E. Additionally, they are discussed in sections 5.6 and 5.7.

5.5 MODE SHAPES

The mode shapes of the empty test structure are presented in Figure 5.34. All three have only small imaginary components (Figure 5.34) and are, therefore, only slightly complex.

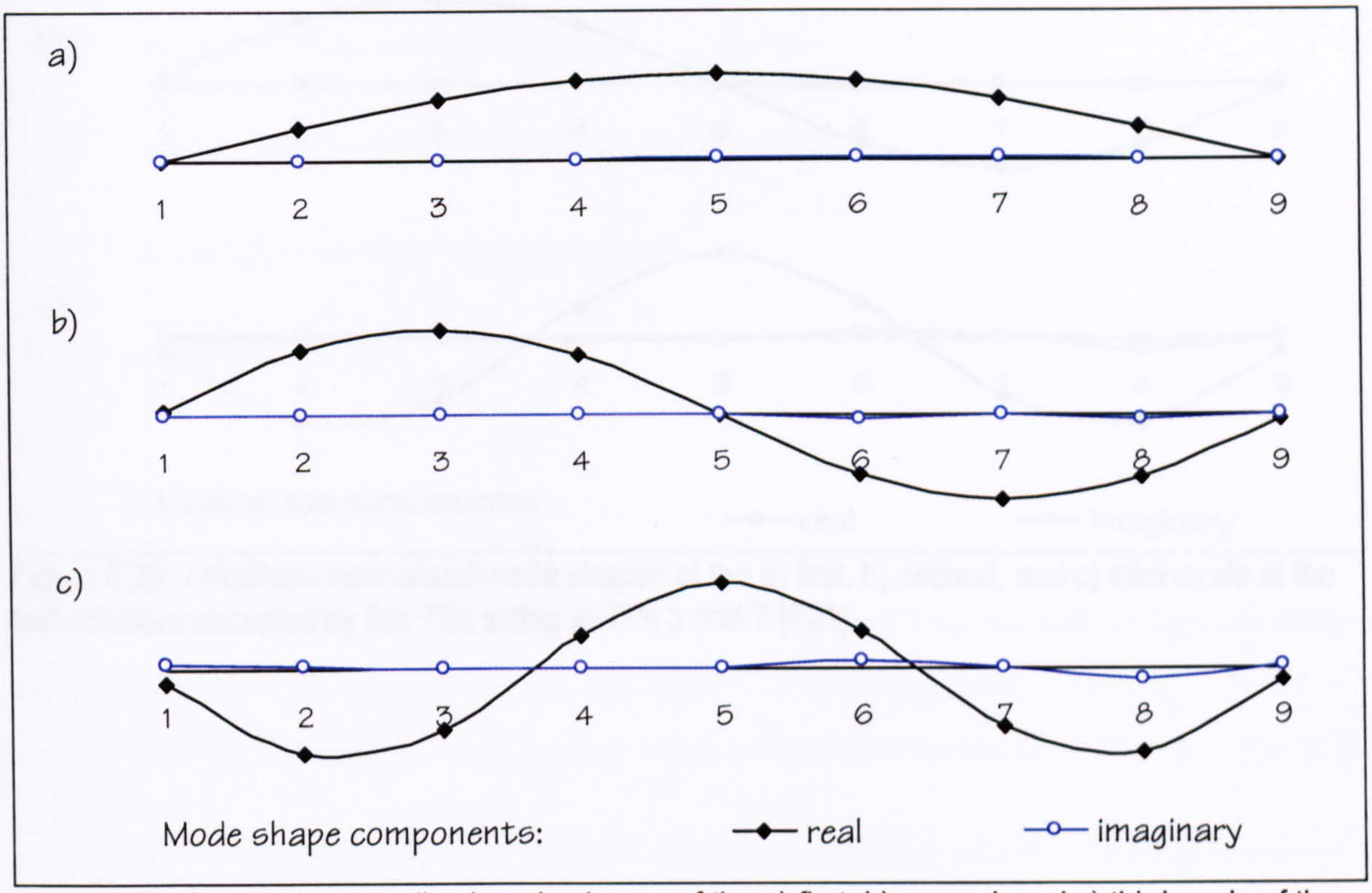

Figure 5.34: Amplitude normalised mode shapes of the a) first, b) second, and c) third mode of the empty test structure (A17).

Under different types of human occupation or mass loading, the mode shapes remained basically unchanged. To support this observation, Figure 5.35 presents mode shapes of the test structure occupied by five TS.

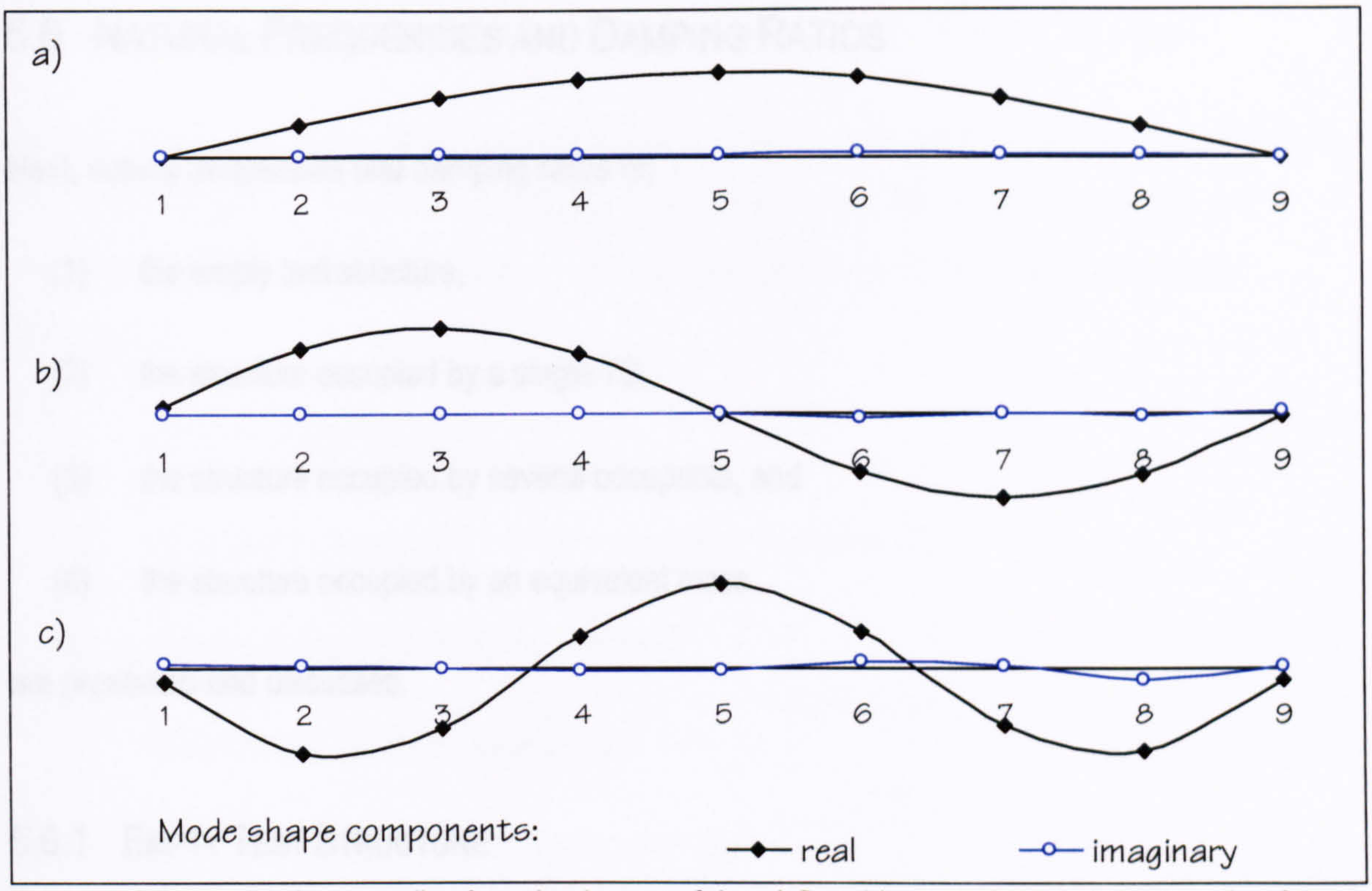

Figure 5.35: Amplitude normalised mode shapes of the a) first, b) second, and c) third mode of the test structure occupied by five TSs sitting at TPs 3 and 7 (F21).

5.6 NATURAL FREQUENCIES AND DAMPING RATIOS

Next, natural frequencies and damping ratios of:

(1) the empty test structure,

(2) the structure occupied by a single TS,

(3) the structure occupied by several occupants, and

(4) the structure occupied by an equivalent mass

are presented and discussed.

5.6.1 EMPTY TEST STRUCTURE

Natural frequencies of the three modes of the empty test structure were identified as approximately 4.5 Hz, 16.9 Hz and 37.7 Hz (Table E.1 in Appendix E). They corresponded to damping ratios of 0.3% to 0.4% for the first and second mode and about 1% for the third mode of vibration (Table E.2).

Homogeneity of the first and the third modes of vibration of the empty structure was checked using A01 - A05, A06 - A09, A11, and A12 - A16 (section 5.3.1). As already indicated by Figure 5.25, the natural frequencies and damping ratios of these two modes of the empty test structure satisfied the homogeneity linearity condition for the three excitation levels employed here (Tables E.1 and E.2). Similarly, the estimated modal properties were consistent for tests performed immediately after each other, as already indicated by Figure 5.31.

However, Figure 5.32 showed a lack of long-term repeatability. This was confirmed by a slight change of natural frequencies and damping ratios of the empty structure within the 30 days of testing (Tables E.1, E.2 and D.1). Most significantly, the fundamental frequency f_1 decreased from 4.54 Hz to 4.50 Hz (Table E.1). This phenomenon posed a potential problem for the analysis of the influence of human occupants (or a static load) on the test structure. In fact, it denied the comparison of some modal tests as shown later.

5.6.2 Test Structure Occupied by a Single Stationary Human Occupant

Several scenarios of single human occupants on the test structure were investigated in Tests B, C, E, R, and P (Tables D.3, D.4, D.5, D.8 and D.10 in Appendix D). The natural frequencies and damping ratios determined from these modal tests (see Appendix E) enabled discussing the influence of:

(1) various human occupants,

(2) the long-term repeatability of tests employing the same TS,

(3) different postures of the same occupant,

(4) three different levels of vibration, and

(5) various locations of a TS on the test structure.

5.6.2.1 Different Sitting Occupants

In Test E, several TSs (one at a time) were sitting at TP 5 (Tables D.5). The influence of each TS on the natural frequency and damping ratio of the first, second, and third mode of the test structure was analysed. The findings are now presented.

Figure 5.36 shows natural frequencies f_1 and damping ratios ζ_1 of the empty test structure and the structure occupied by a single TS. In this figure, black lines indicate the mean natural frequency f_1 and the mean damping ratio ζ_1 of (five) nominally identical tests of the empty test structure (A22 - A26 in Tables E.1 and E.2). Dots, each labelled with its test identificators (ID), indicate the properties determined from individual modal tests of the occupied structure. Finally, red and blue lines (Figures 5.36a and 5.36b) represent mean natural frequencies f_1 and damping ratios ζ_1, each corresponding to a group of five nominally identical tests of the structure occupied by the same TS (Tables E.10 and E.11). This layout was principally adopted throughout the remaining part of chapter 5.

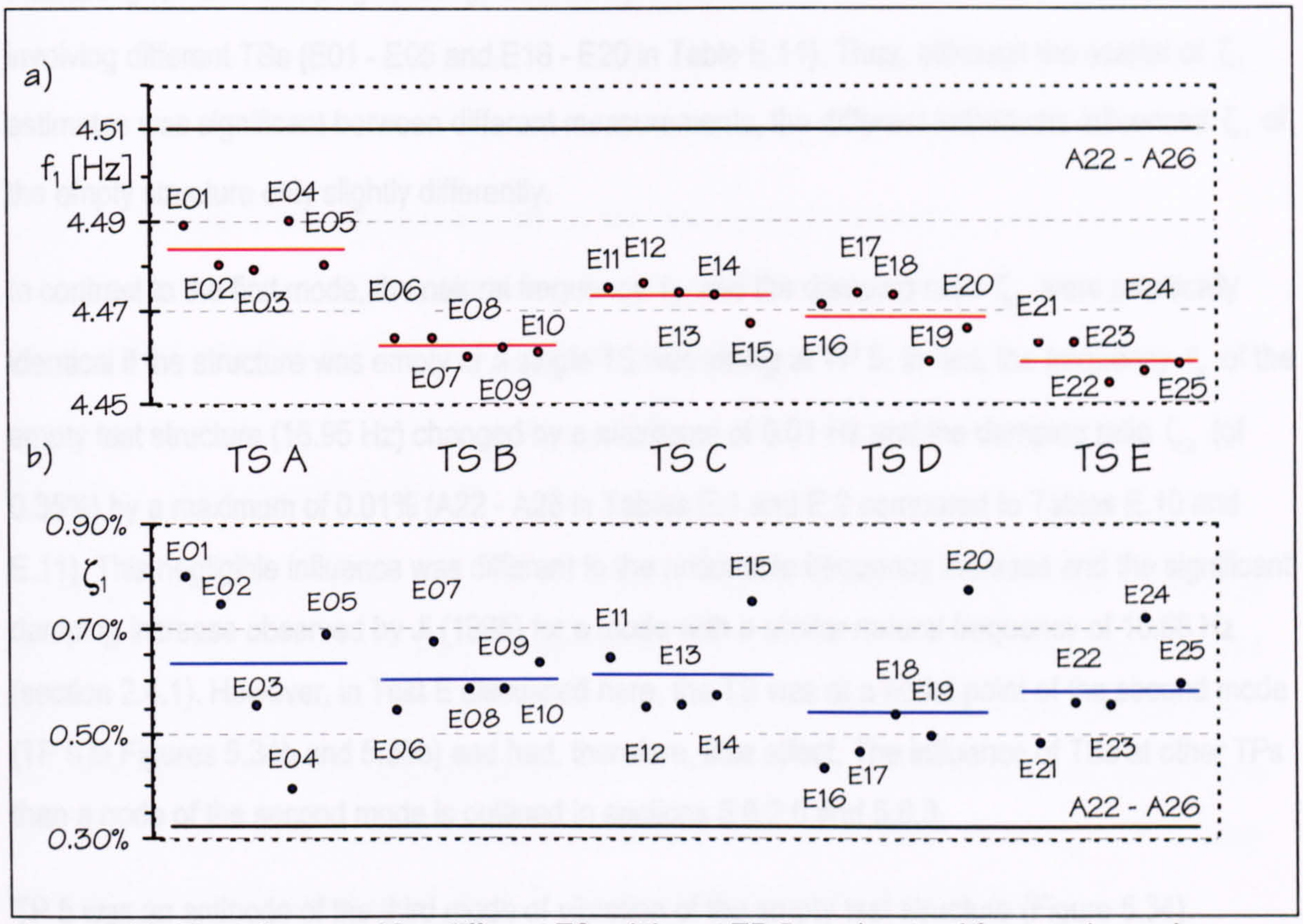

Figure 5.36: The influence of five different TSs sitting at TP 5 on a) natural frequencies and b) damping ratios of the fundamental mode of the test structure.

Figure 5.36a demonstrates that each of the five occupants reduced the fundamental natural frequency f_1 = 4.51 Hz of the test structure slightly. The strength of this reduction was consistent but different for each individual. In fact, f_1 was reduced by 0.03 Hz by TS A and as much as 0.05 Hz by TS E (E01 - E05 and E21 - E25 in Table E.10). Thereby, the standard deviations of frequencies f_1 of nominally identical tests (employing the same occupant) reached only 0.01 Hz (Table E.10).

The influence of sitting TSs on the damping ratio ζ_1 of the empty test structure was significantly more pronounced than their influence on the natural frequency f_1. In fact, TS A even doubled the damping ratio ζ_1 of the empty structure from 0.32% (A22 - A26 in Table E.1) to 0.64% (E01 - E05 in Table E.10).

Remarkably, damping values ζ_1 estimated from nominally identical tests varied significantly (Figure 5.36b). For example, they reached the extreme values of 0.40% (E04) to 0.80% (E01) if TS A sat on the structure. In this case, the standard deviation of ζ_1 reached 0.16% (E01 - E05 in Table E.11), the maximum in Test E.

Interestingly, mean damping ratios ζ_1 differed by a maximum of 0.10% between modal tests involving different TSs (E01 - E05 and E16 - E20 in Table E.11). Thus, although the scatter of ζ_1 estimates was significant between different measurements, the different individuals influenced ζ_1 of the empty structure only slightly differently.

In contrast to the first mode, the natural frequency f_2 and the damping ratio ζ_2 were practically identical if the structure was empty or a single TS was sitting at TP 5. In fact, the frequency f_2 of the empty test structure (16.95 Hz) changed by a maximum of 0.01 Hz and the damping ratio ζ_2 (of 0.35%) by a maximum of 0.01% (A22 - A26 in Tables E.1 and E.2 compared to Tables E.10 and E.11). This negligible influence was different to the noticeable frequency increase and the significant damping increase observed by Ji (1995) for a mode with a similar natural frequency of 18.68 Hz (section 2.4.1). However, in Test E discussed here, the TS was at a nodal point of the second mode (TP 5 in Figures 5.34b and 5.35b) and had, therefore, little effect. The influence of TSs at other TPs than a node of the second mode is outlined in sections 5.6.2.5 and 5.6.3.

TP 5 was an antinode of the third mode of vibration of the empty test structure (Figure 5.34). Nevertheless, a single TS sitting at this point did not affect the natural frequency f_3 or the damping ratio ζ_3 significantly (A22 - A26 in Tables E.1 and E.2, Test E in Tables E.10 ad E.11). In fact, an occupant increased (in opposite to a decrease of f_1) the natural frequency f_3 (37.73 Hz) by a maximum of 0.05 Hz and the damping ratio ζ_3 (0.94%) by less than 0.10%.

In conclusion, an analysis of the influence of five different individuals on natural frequencies and damping ratios of the test structure revealed that:

(1) The fundamental frequency f_1 of the empty test structure (4.51 Hz) was reduced by a single human occupant sitting at the antinode of this mode by values ranging from 0.03 Hz to 0.05 Hz.

(2) A single TS sitting at TP 5 approximately doubled the damping ratio ζ_1 of the empty test structure from about 0.3% to about 0.6%. Remarkably, the standard deviation of damping ratios ζ_1 reached up to 0.16% for five individual values ζ_1 estimated in nominally identical tests involving the same occupant.

(3) The natural frequency f_2 and the damping ratio ζ_2 of the empty test structure (about 17 Hz and 0.35%) were not influenced by a single human occupant at TP 5, a node of the second mode.

(4) A single occupant practically did not alter the natural frequency f_3 of the empty test structure (about 38 Hz) if he sat at the antinode of the third mode (TP 5). However, he increased the damping ratio ζ_3 of the empty structure.

5.6.2.2 LONG-TERM REPEATABILITY

The data presented in Figure 5.36 showed a relatively high scatter between estimates of individual and nominally identical modal tests involving the same TS. This was the case, even though modal tests were generally performed during the same day (Test E in Appendix D). Therefore, the long-term repeatability of such nominally identical tests was investigated. For this purpose, experiments of Tests B, R, E, and P were employed. All these tests involved the same TS sitting at TP 5. They were performed with time gaps of 18, 5, and 9 days between them (Appendix D).

Figure 5.37 illustrates the natural frequencies f_1 and damping ratios ζ_1 estimated from these modal tests of the occupied structure. As already mentioned, the properties of the empty test structure changed with time (section 5.6.1). Therefore, Figures 5.37 includes different mean natural frequencies f_1 and damping ratios ζ_1 of the empty test structure (Tables E.1 and E.2) that were employed in the discussion. Actually, only experiments A17 - A21 and Test P took place at the same day as modal tests of the occupied structure. Experiments A22 - A26 were performed seven days and one day before R01 - R06 and E01 - E05 respectively (Appendix D).

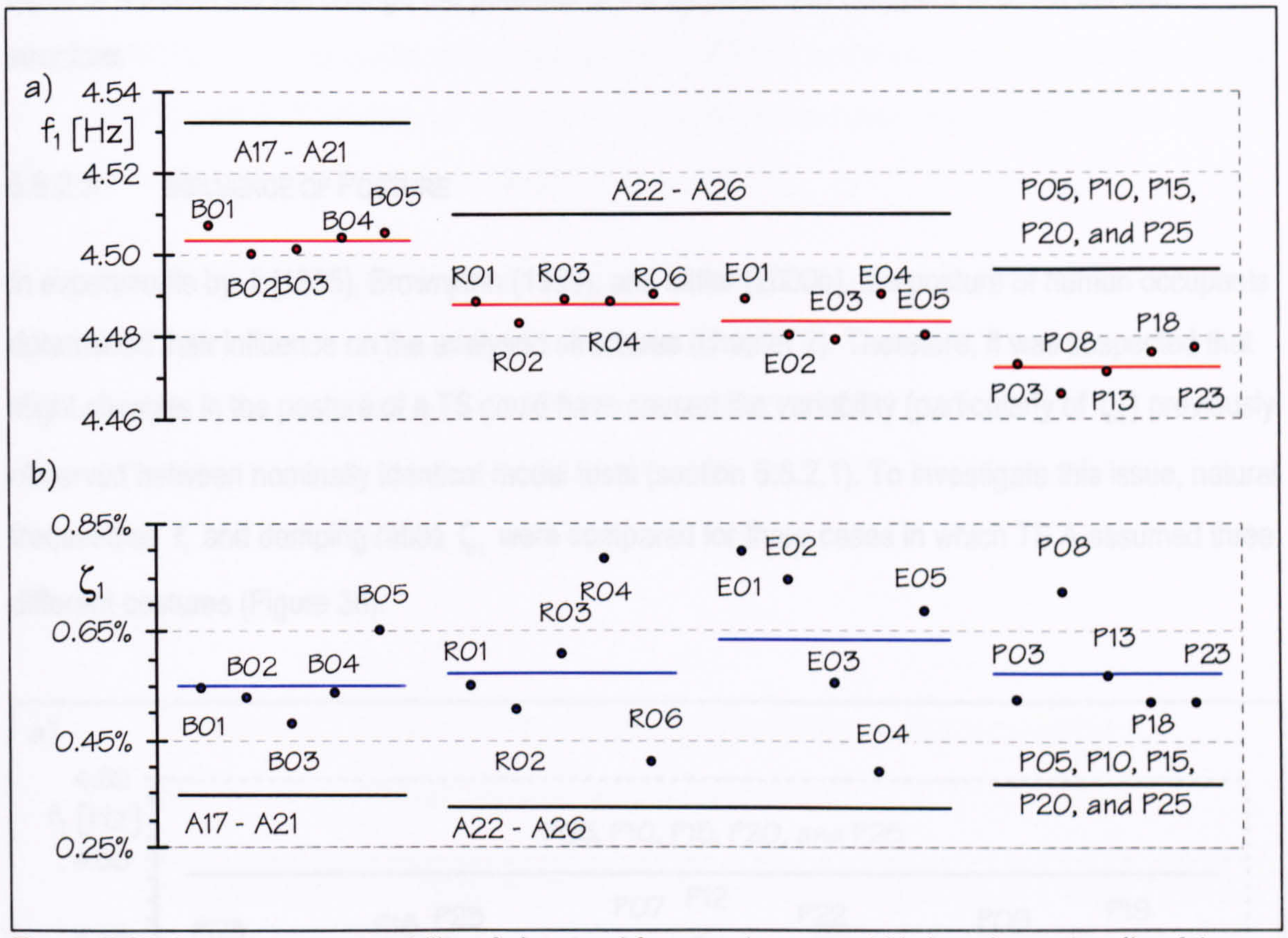

Figure 5.37: Long-term repeatability of a) natural frequencies f_1 and b) damping ratios ζ_1 of the test structure occupied by TS A sitting at TP 5.

Figure 5.37a demonstrates that TS A consistently reduced the natural frequency f_1 of the empty test structure (about 4.5 Hz) by values ranging from 0.02 Hz to 0.03 Hz. Hence, the influence of TS A on the fundamental frequency of the empty test structure remained constant during the whole period of testing. It was independent of the slight changes of the fundamental frequency of the empty test structure.

Similarly, the influence of TS A on the damping ratio ζ_1 of the empty test structure did not change with time (Figure 5.37b). Consistently, the occupant led to widely scattering damping ratios ζ_1 that, overall, approximately doubled the damping ratio ζ_1 of the empty structure (Tables E.2, E.5, E.11, and E.14).

As noted above, TS A sitting at TP 5 influenced the natural frequencies or damping ratios of the second and third mode of the test structure only marginally (section 5.6.2.1). This did not change with time (Tables E.1, E.2, E.4, E.5, E.10, E.11, E.13, and E.14). Therefore, it is concluded that a

lapse of a month did not change the potential of the same human occupant to affect the test structure.

5.6.2.3 INFLUENCE OF POSTURE

In experiments by Ji (1995), Brownjohn (1999), and Littler (2000b), the posture of human occupants determined their influence on the analysed structures (chapter 2). Therefore, it was suspected that slight changes in the posture of a TS could have caused the variability (particularly of ζ_1) previously observed between nominally identical modal tests (section 5.6.2.1). To investigate this issue, natural frequencies f_1 and damping ratios ζ_1 were compared for three cases in which TS A assumed three different postures (Figure 38).

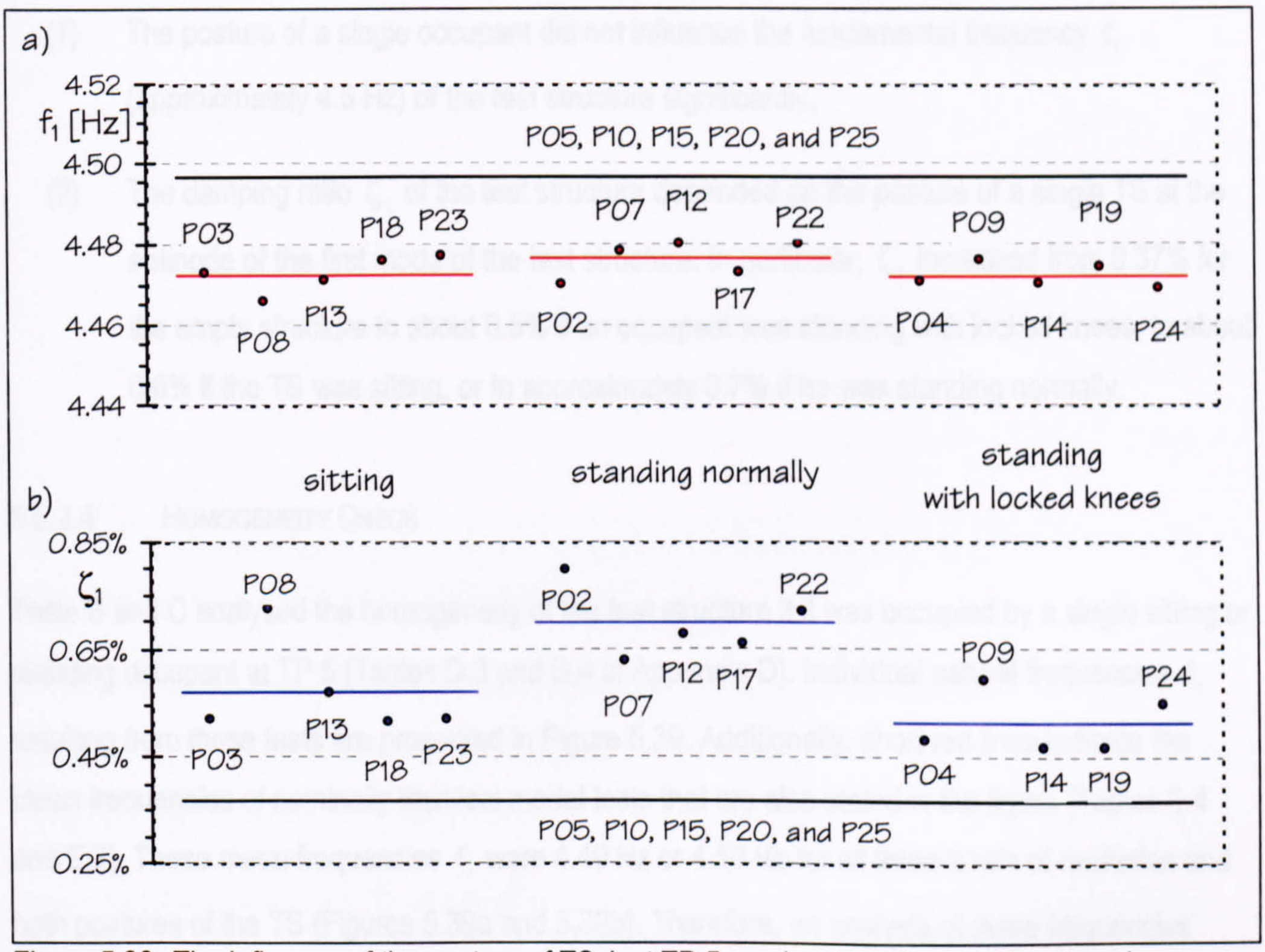

Figure 5.38: The influence of the posture of TS A at TP 5 on a) natural frequencies f_1 and b) damping ratios ζ_1.

Figure 5.38a demonstrates that the posture of a single human occupant had no significant effect on the fundamental frequency f_1 of the test structure (Tables E.1 and E.13 in Appendix E). Nevertheless, apparently, the damping ratio ζ_1 depended on the posture of the occupant (Figure

5.38b). However, in some cases, ζ_1 was very similar if the TS was sitting or standing normally (P08 and P02), sitting or standing with locked knees (P13 and P24), and standing normally or with locked knees (P07 and P09). Therefore, an analysis of only a single measurement for each posture might have led to different conclusions than given below.

In the experiments presented here, the mean damping ratio ζ_1 was highest (about 0.7%) if TS A was standing normally on the test structure (P02, P07, P12, P17, and P22 in Table E.14). It was lowest (about 0.5%) if he was standing with locked knees (P04, P09, P14, P19, and P24). A somehow medium damping ratio ζ_1 of about 0.6% was caused by the TS sitting on the structure (P03, P08, P13, P18, and P23).

In conclusion:

(1) The posture of a single occupant did not influence the fundamental frequency f_1 (approximately 4.5 Hz) of the test structure significantly.

(2) The damping ratio ζ_1 of the test structure depended on the posture of a single TS at the antinode of the first mode of the test structure. In particular, ζ_1 increased from 0.37% for the empty structure to about 0.5% if an occupant was standing with locked knees, to about 0.6% if the TS was sitting, or to approximately 0.7% if he was standing normally.

5.6.2.4 HOMOGENEITY CHECK

Tests B and C analysed the homogeneity of the test structure if it was occupied by a single sitting or standing occupant at TP 5 (Tables D.3 and D.4 in Appendix D). Individual natural frequencies f_1 resulting from these tests are presented in Figure 5.39. Additionally, short red lines indicate the mean frequencies of nominally identical modal tests that are also stated in the figure (Tables E.4 and E.7). These mean frequencies f_1 were 4.49 Hz or 4.50 Hz for all three levels of excitation and both postures of the TS (Figures 5.39a and 5.39b). Therefore, an analysis of these frequencies required particular attention to the small changes of properties of the empty structure over time (as noted in section 5.6.1).

Modal tests employing the highest and the lowest level of excitation (levels 1 and 3) were performed immediately after each other on the 26 October (B06 - B10 and B11 - B15) and on the 2 November

2000 (C16 - C20 and C21 - C25) respectively. Therefore, data resulting from tests using the extreme vibration levels (1 and 3) could be compared for a sitting TS or a standing TS separately. In doing so, it was concluded that the natural frequency f_1 was independent of the low levels of vibration employed here if it a single occupant was sitting or standing on the test structure.

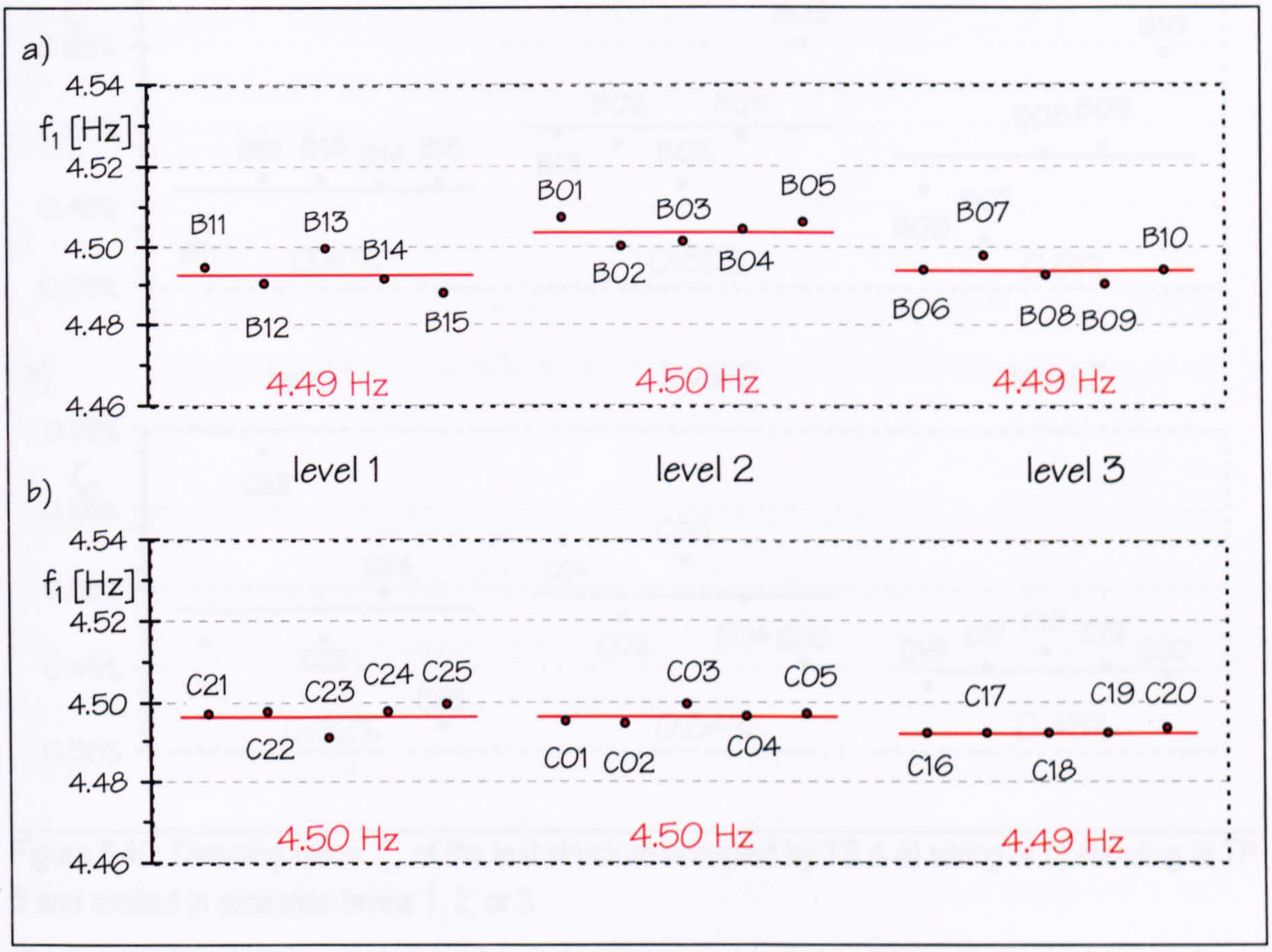

Figure 5.39: Natural frequencies f_1 of the test structure occupied by TS A a) sitting or b) standing at TP 5 and excited in one of three excitation levels.

Similarly to natural frequencies f_1, damping ratios ζ_1 of the human-occupied test structure were compared for the two extreme levels of excitation (levels 1 and 3). This analysis was supported by Figure 5.40, an analogue to Figure 5.39.

Figure 5.40a shows that the mean damping ratio ζ_1 was smallest (0.47%) for the lowest level of excitation if the TS was sitting (B11 - B15 in Figure 5.40a). Contrary, Figure 5.40b demonstrates that ζ_1 was lowest (0.45%) for the highest excitation level 3 if the occupant was standing (C16 - C20). Furthermore, if the TS was sitting, the estimated damping ratios ζ_1 scattered more widely for the higher than for lower excitation level (levels 3 and 1 in Figure 5.40a). However, if the TS was

standing (Figure 5.40b), damping ratios ζ_1 scattered more widely for the lowest level of excitation (C21 - C25).

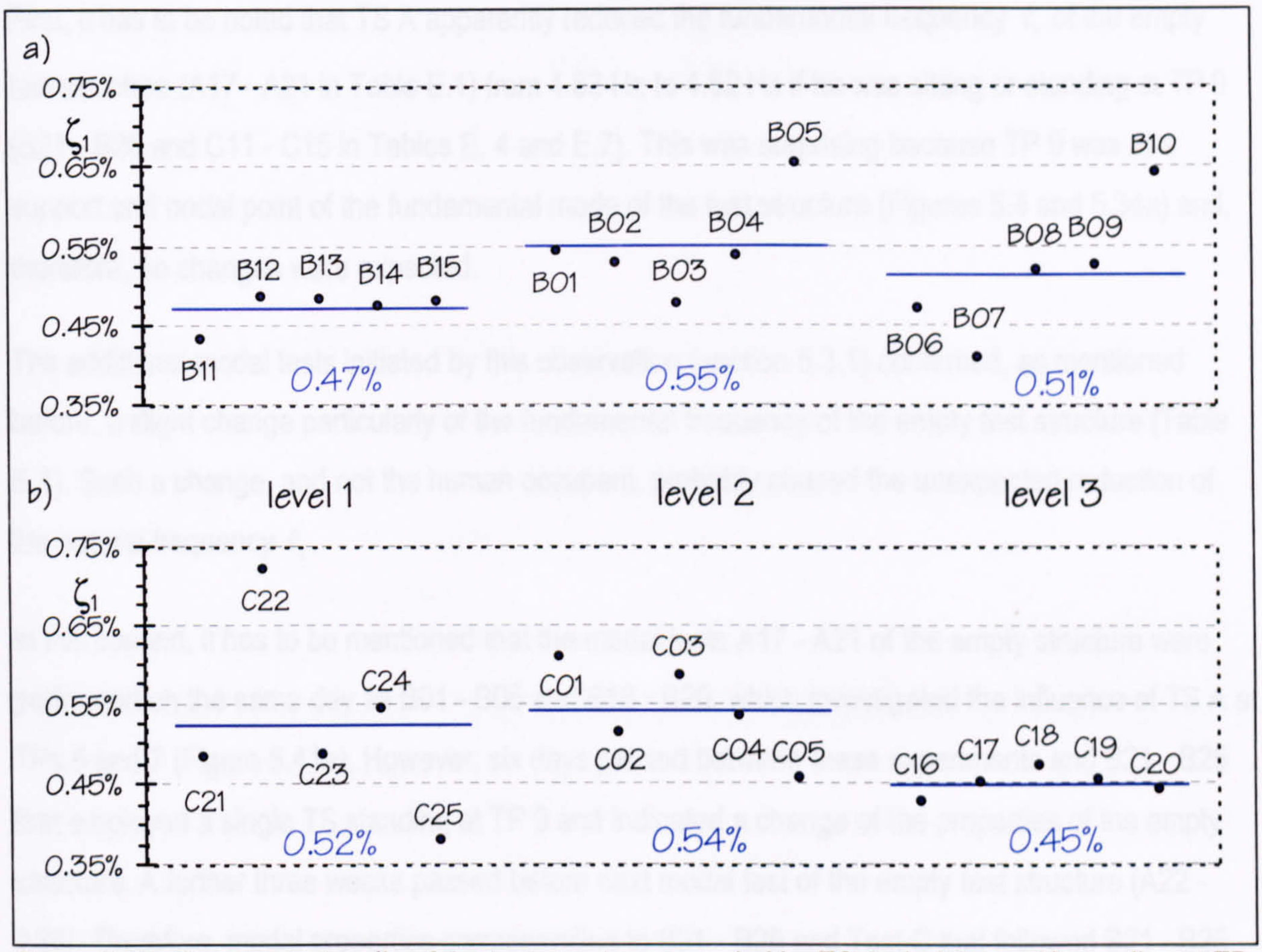

Figure 5.40: Damping ratios ζ_1 of the test structure occupied by TS A a) sitting or b) standing at TP 5 and excited in excitation levels 1, 2, or 3.

Summarising, the excitation level affected the mean values and the scatter of damping ratios ζ_1 opposite for the sitting and standing TS. This difference could be attributed to differences between the two postures. However, it could have simply been caused by the variability between individual experiments. Therefore, it was concluded that the influence of a single sitting or standing TS at TP 5 on the natural frequency f_1 and the damping ratio ζ_1 of the empty test structure was independent of the low levels of vibration employed here.

5.6.2.5 Location of an Occupant

Previously, the influence of TS A at TP 5 was analysed (sections 5.6.2.1 to 5.6.2.4). Now, this influence is compared with the influence of the same TS at two other locations (TPs 7 and 9) on the

test structure (Figure 5.4). For this purpose, natural frequencies (f_1, f_2, and f_3) and damping ratios (ζ_1, ζ_2, and ζ_3) are employed.

First, it has to be noted that TS A apparently reduced the fundamental frequency f_1 of the empty test structure (A17 - A21 in Table E.1) from 4.53 Hz to 4.52 Hz if he was sitting or standing at TP 9 (B21 - B25 and C11 - C15 in Tables E. 4 and E.7). This was surprising because TP 9 was at a support and nodal point of the fundamental mode of the test structure (Figures 5.4 and 5.34a) and, therefore, no changes were expected.

The additional modal tests initiated by this observation (section 5.3.1) confirmed, as mentioned before, a slight change particularly of the fundamental frequency of the empty test structure (Table E.1). Such a change, and not the human occupant, probably caused the unexpected reduction of the natural frequency f_1.

In this context, it has to be mentioned that the modal tests A17 - A21 of the empty structure were performed on the same day as B01 - B05 and B16 - B20, which investigated the influence of TS A at TPs 5 and 7 (Figure 5.41a). However, six days passed between these experiments and B21 - B25 that employed a single TS standing at TP 9 and indicated a change of the properties of the empty structure. A further three weeks passed before next modal test of the empty test structure (A22 - A26). Therefore, modal properties corresponding to B21 - B25 and Test C that followed B21 - B25 within a week, were not compared with properties of the empty test structure (Figures 5.41a and 5.41b). Nevertheless, C01 - C05, C06 - C10, and C11 - C15 took place on two consecutive days and, therefore, were comparable.

Considering all these aspects, the influence of TS A on the natural frequency f_1 (Figure 5.41) and the damping ratio ζ_1 (Figure 5.42) of the first mode of the empty test structure was investigated. It showed that an occupant at TP 5 had a higher influence on the frequency f_1 and the damping ratio ζ_1 than the same TS at TP 7 or TP 9 (Figures 5.41 and 5.42). In fact, f_1 and ζ_1 of the empty structure did not only change stronger but the scatter of estimates was higher the closer the TS to midspan (Figure 5.8). In other words, the influence of an occupant on the first mode increased with the mode shape amplitude at the location of the TS (Figure 5.34).

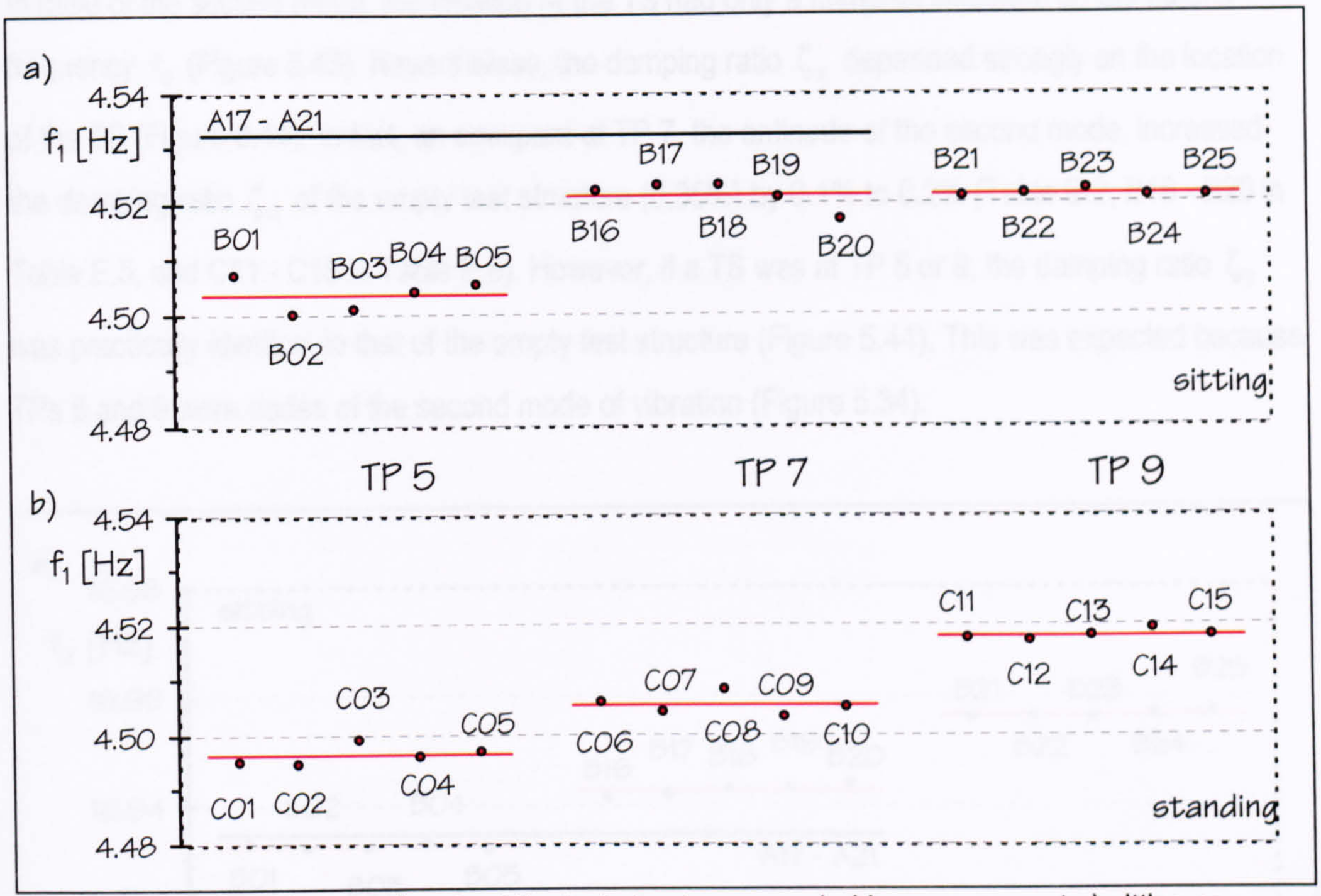

Figure 5.41: Natural frequencies f_1 of the test structure occupied by an occupant a) sitting or b) standing at various locations.

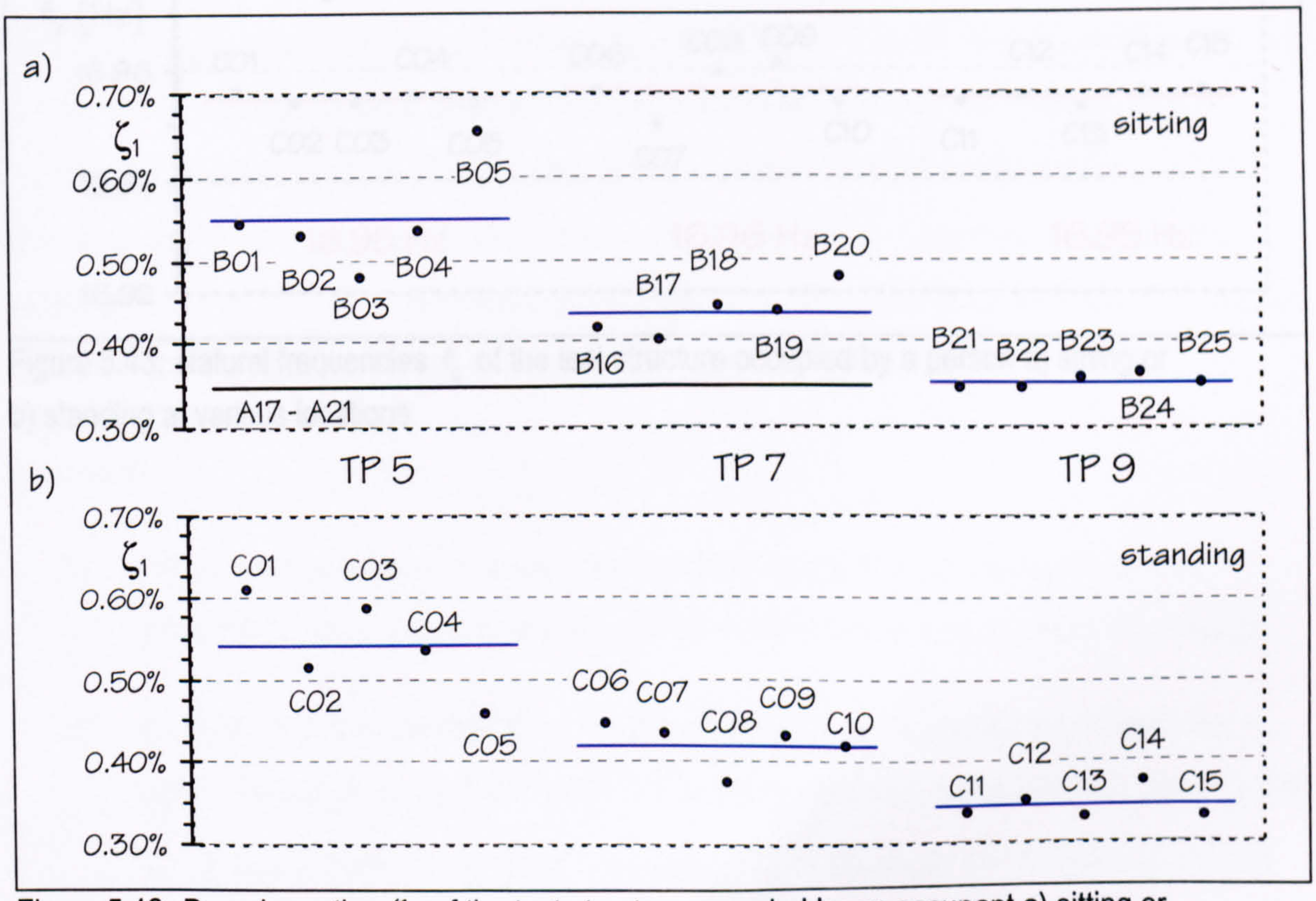

Figure 5.42: Damping ratios ζ_1 of the test structure occupied by an occupant a) sitting or b) standing at various locations.

In case of the second mode, the location of the TS had only a marginal influence on the natural frequency f_2 (Figure 5.43). Nevertheless, the damping ratio ζ_2 depended strongly on the location of the TS (Figure 5.44). In fact, an occupant at TP 7, the antinode of the second mode, increased the damping ratio ζ_2 of the empty test structure (0.35%) by 0.1% to 0.2% (Table E.2, B16 - B20 in Table E.5, and C11 - C15 in Table E.8). However, if a TS was at TP 5 or 9, the damping ratio ζ_2 was practically identical to that of the empty test structure (Figure 5.44). This was expected because TPs 5 and 9 were nodes of the second mode of vibration (Figure 5.34).

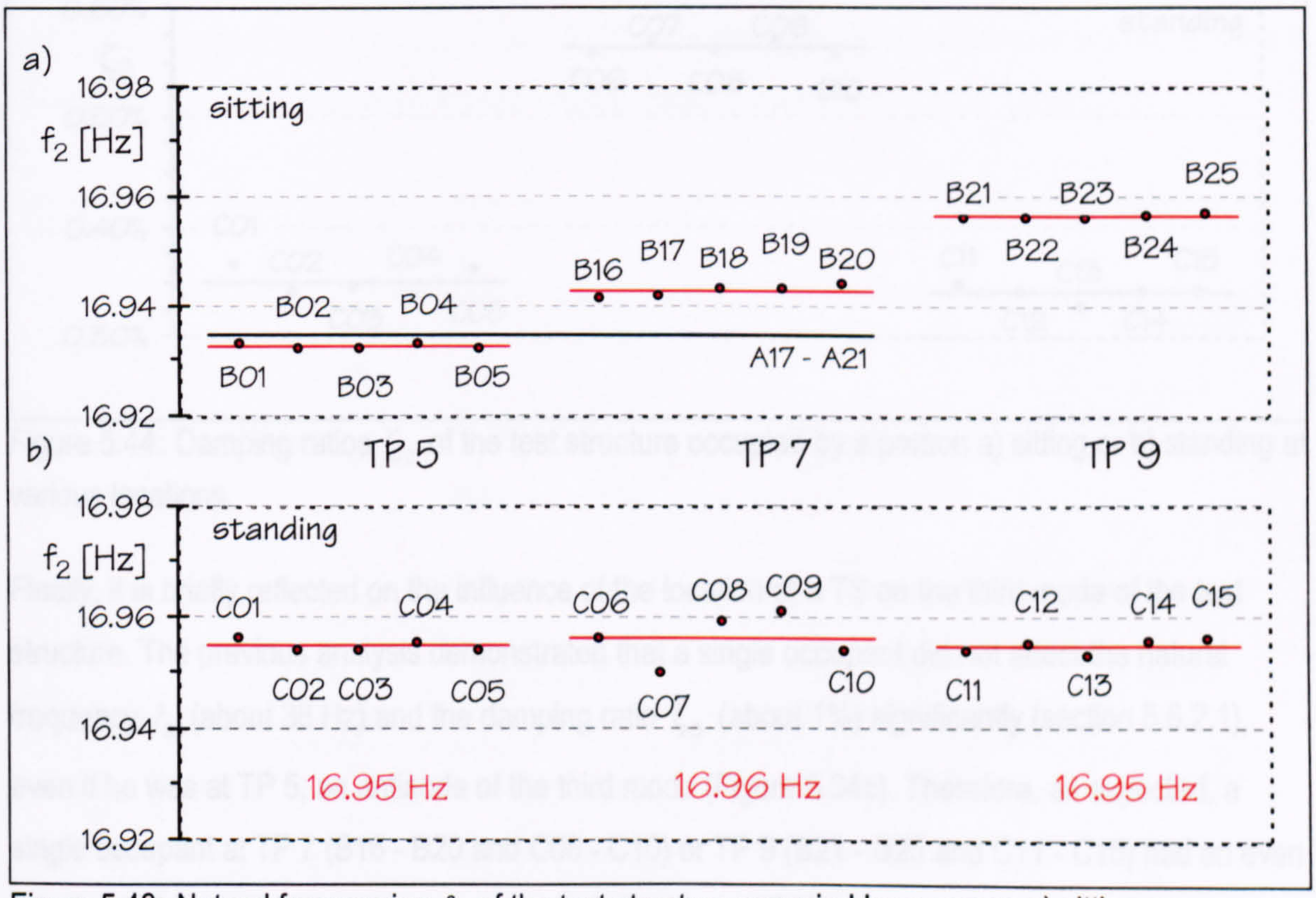

Figure 5.43: Natural frequencies f_2 of the test structure occupied by a person a) sitting or b) standing at various locations.

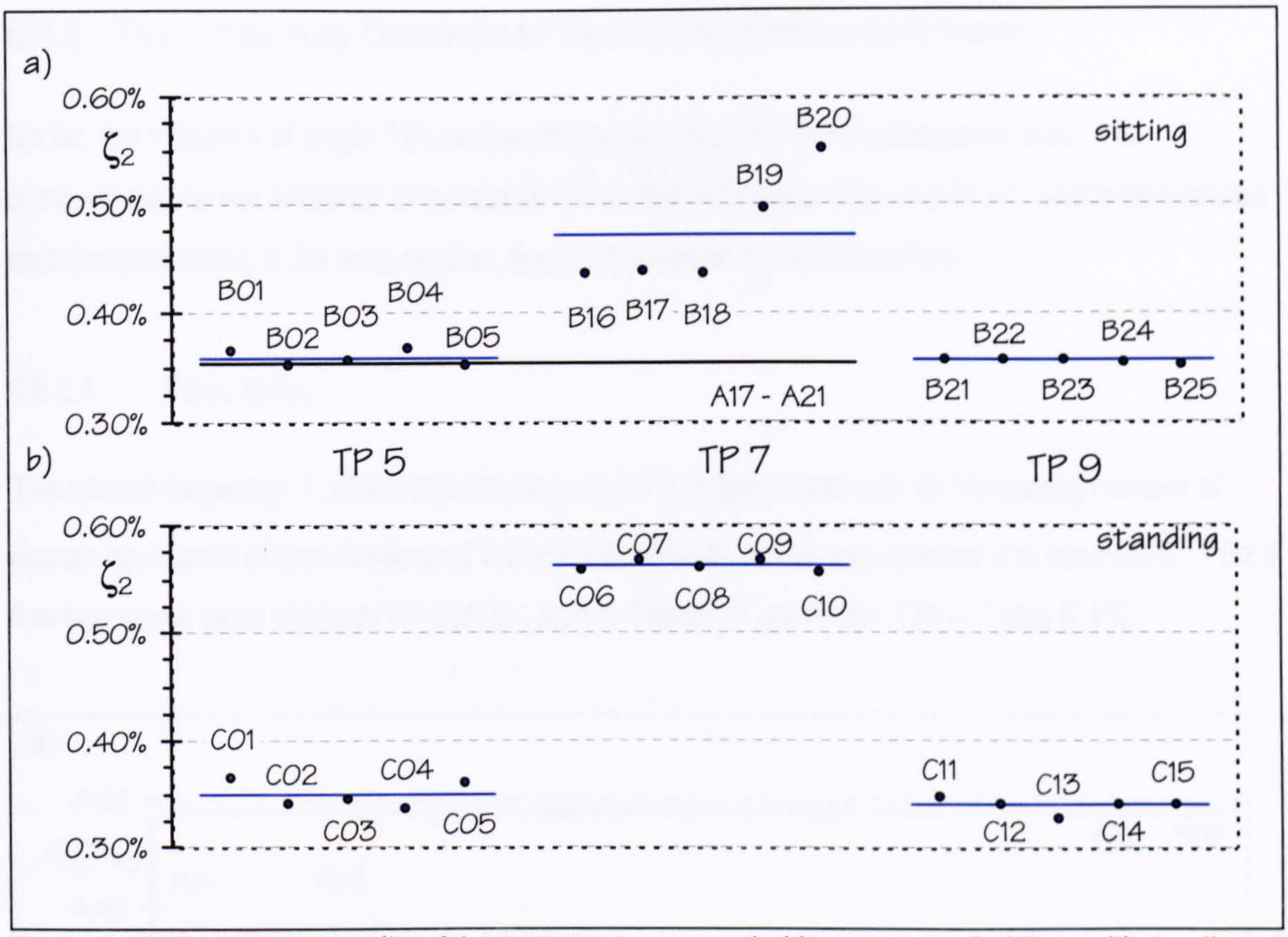

Figure 5.44: Damping ratios ζ_2 of the test structure occupied by a person a) sitting or b) standing at various locations.

Finally, it is briefly reflected on the influence of the location of a TS on the third mode of the test structure. The previous analysis demonstrated that a single occupant did not affect the natural frequency f_3 (about 38 Hz) and the damping ratio ζ_3 (about 1%) significantly (section 5.6.2.1), even if he was at TP 5, an antinode of the third mode (Figure 5.34c). Therefore, as expected, a single occupant at TP 7 (B16 - B20 and C06 - C10) or TP 9 (B21 - B25 and C11 - C15) had an even smaller, in fact negligible, influence on f_3 and ζ_3 (Appendix E).

In conclusion:

(1) The location of a human occupant affected the properties of the test structure. The influence of the occupant increased with the mode shape amplitude at the TS's location.

(2) A single TS at the antinode of the second mode (TP 7) did not affect significantly the natural frequency f_2 (approximately 17 Hz) but he did affect significantly the damping ratio ζ_2. In fact, a sitting or standing TS increased ζ_2 of the empty test structure (0.35%) by about 0.1% to 0.2%.

5.6.3 Test Structure Occupied by Two to Five Sitting Occupants

So far, the influence of single TSs on the empty test structure was investigated. Now, it is concentrated on the influence of groups of two to five occupants (Figure 5.9) on natural frequencies and damping ratios of the first, second, and third mode of the test structure.

5.6.3.1 First Mode

The natural frequency f_1 of the test structure (4.51 Hz) decreased with an increasing number of human occupants (Figure 5.45a and Table E.16). The decrease was gradual and reached 0.17 Hz if five occupants were sitting at TP 5 (A22 - A26 in Table E.1 and F16 - F20 in Table E.16).

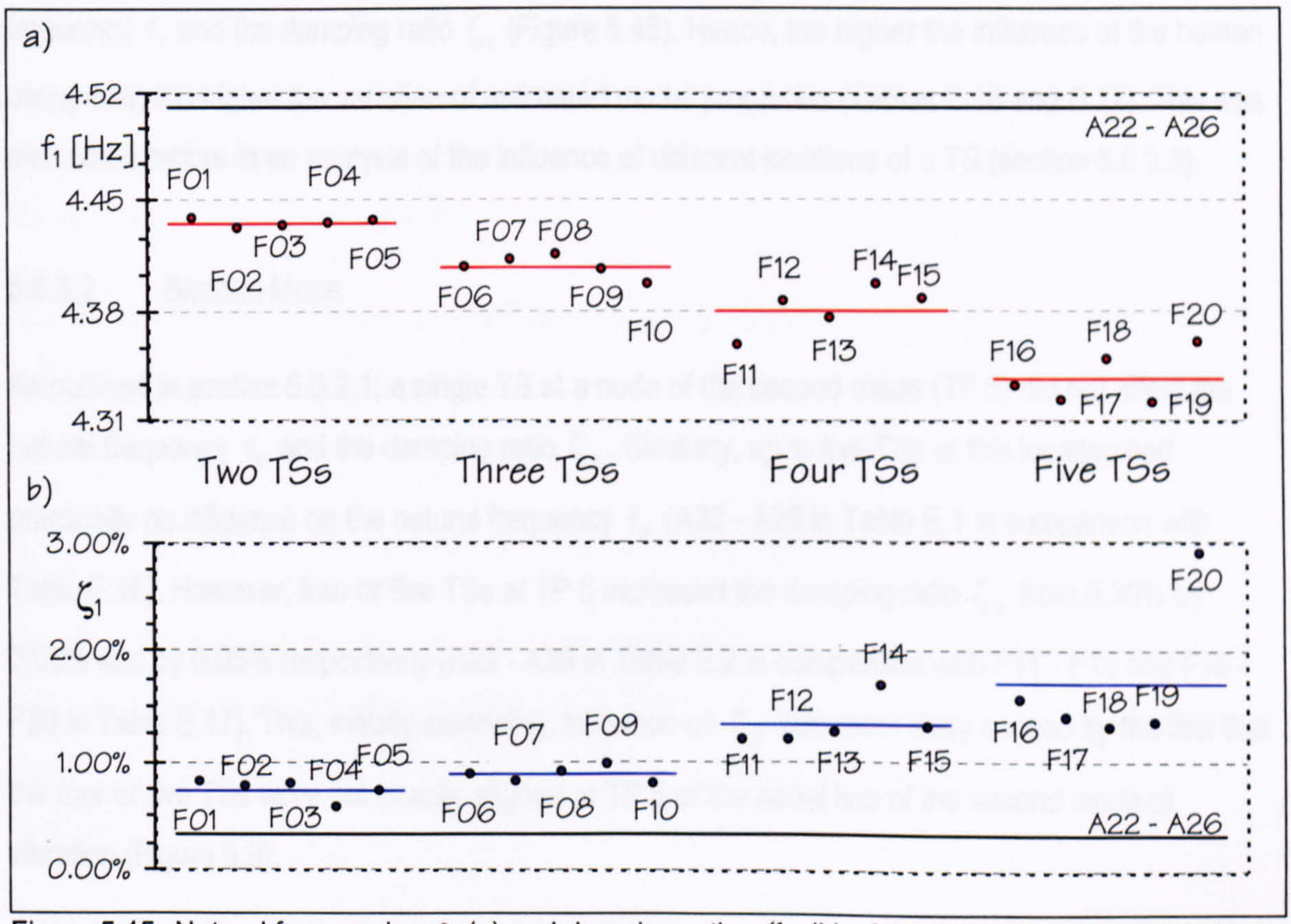

Figure 5.45: Natural frequencies f_1 (a) and damping ratios ζ_1 (b) of the test structure occupied by groups of people sitting at TP 5.

The influence of human occupants on the damping ratio ζ_1 also increased with the number of TSs (Figure 5.45b). Thus, a maximum mean damping ratio ζ_1 reached 1.69% if five TSs were on the structure. In this case, the damping ratio ζ_1 was about five times that of the empty test structure (F16 - F20 in Table E.17 and A22 - A26 in Table E.2). Generally, the damping ratio ζ_1 of the empty

test structure increased by about 0.3% per occupant at TP 5, the antinode of the first mode (A22 - A26 in Table E.2 and F01 to F20 in Table E.17).

Additionally to modal tests with groups of two to five TSs sitting at TP 5, modal tests with five TSs at TPs 3 and 7 were performed (F21 - F25). The mode shape of the first mode of vibration has lower mode shape amplitudes at these TPs 3 and 7 than at TP 5 (Figure 5.34). Therefore, as expected, the same number of occupants at TPs 3 and 7 had a smaller effect on the natural frequency f_1 and the damping ratio ζ_1 (F16 - 20 and F21 - F25 in Tables E.16 and E.17). Interestingly, five occupants at TPs 3 and 7 influenced the natural frequency f_1 as little as two people at TP 5 (F01 - F05) and the damping ratio ζ_1 similarly to four occupants at TP 5 (F11 - F15).

Generally, the more TSs were on the test structure, the less consistent were estimates of the natural frequency f_1 and the damping ratio ζ_1 (Figure 5.45). Hence, the higher the influence of the human occupants, the higher the variation of estimated modal properties (Tables E.16 and E.17). This was also noted before in an analysis of the influence of different locations of a TS (section 5.6.2.5).

5.6.3.2 SECOND MODE

As outlined in section 5.6.2.1, a single TS at a node of the second mode (TP 5) did not affect the natural frequency f_2 and the damping ratio ζ_2. Similarly, up to five TSs at this location had practically no influence on the natural frequency f_2 (A22 - A26 in Table E.1 in comparison with Table E.16). However, four or five TSs at TP 5 increased the damping ratio ζ_2 from 0.35% by 0.03% and by 0.05% respectively (A22 - A26 in Table E.2 in comparison with F11 - F15 and F16 - F20 in Table E.17). This, initially surprising, influence on ζ_2 was most likely caused by the fact that the four or five TSs were not exactly aligned at TP 5 or the nodal line of the second mode of vibration (Figure 5.9).

A single occupant sitting at TP 7 (an antinode of the second mode) practically did not alter the natural frequency f_2 of the empty structure as demonstrated by B16 - B20 in Figure 5.43. Similarly, five TSs at TPs 3 and 7 changed the natural frequency f_2 only marginally by increasing it from 16.95 Hz to 16.98 Hz (A22 - A26 in Table E.1 and F21 - F25 in Table E.16). However, they increased the damping ratio ζ_2 significantly. In fact, they quadrupled it from 0.35% for the empty

structure to 1.40% (A22 - A26 in Table E.2 and F21 - F25 in Table E.17). Thus, ζ_2 increased by approximately 0.2% per occupant at an antinode of the second mode of the test structure. Thus, human occupants were able to increase ζ_1 more (by about 0.3% per TS) than the damping ratio ζ_2 (by 0.2% per TS).

5.6.3.3 THIRD MODE

Previously analysed experiments indicated that a single human occupant changed the natural frequency f_3 and increased the damping ratio ζ_3 of the empty test structure only marginally (section 5.6.2.1). Similarly, up to five TSs did practically not affect the natural frequency f_3 (Tables E.1 and E.16) but increased the damping ratio ζ_3 (Tables E.2 and E.17). The strongest increase of the damping ratio ζ_3 occurred if five TSs were sitting at TP 5, the antinode of the third mode. In this case, ζ_3 increased by about a third from 0.94% to 1.24% (Table E.2 and F16 - F20 in Table E.17). Hence, the occupants increased not only the damping ratios of the first and second but also that of the third mode of the test structure.

Overall, the analysis showed that the influence of human occupants on f_1, ζ_1, ζ_2, and ζ_3 of the test structure increased with their number.

5.6.4 TEST STRUCTURE LOADED WITH AN EQUIVALENT MASS

Previously, it was outlined how five human occupants influenced natural frequencies and damping ratios of the empty test structure (section 5.6.3). These results are now compared with the effect of a static load (Tables E.19 and E.20 in Appendix E) with a mass equivalent to the overall mass of the five TSs.

5.6.4.1 FIRST MODE

Data in the right and left half of Figure 5.46 demonstrate that the static load influenced the natural frequency f_1 and the damping ratio ζ_1 of the empty structure (A22 - A26) more if it was at TP 5 (G01 - G05) than if it was distributed to TPs 3 and 7 (G06 - G10). In both cases, the equivalent mass

decreased the natural frequency f_1 of the empty structure and did practically not modify the damping ratio ζ_1 (Tests A and G in Figure 5.46).

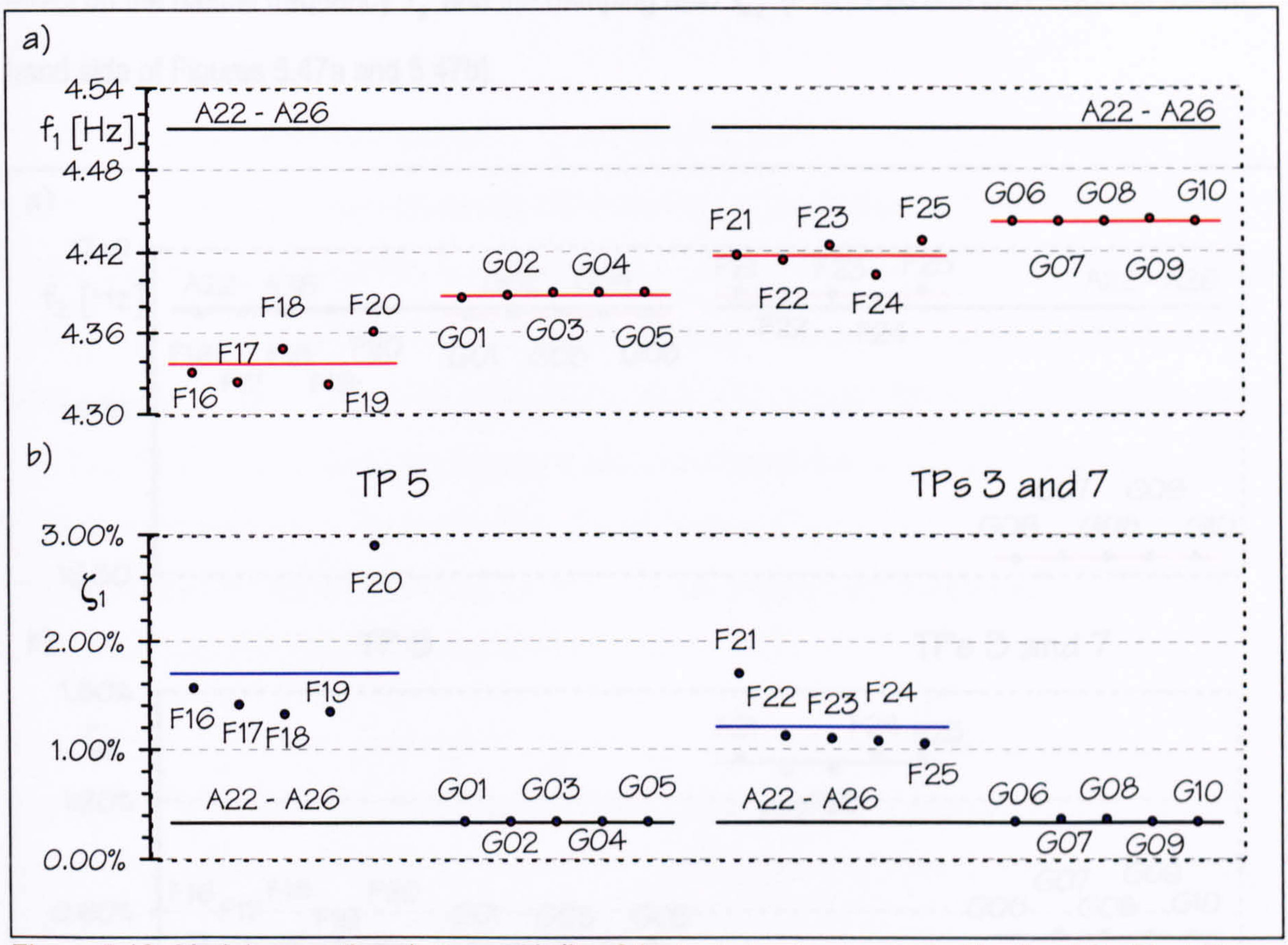

Figure 5.46: Modal properties a) f_1 and b) ζ_1 of the test structure occupied by five TSs (Test F) or an equivalent mass (Test G) at TP 3 or distributed to TPs 3 and 7.

Figures 5.46a and 5.46b demonstrate that the influence of five human occupants on f_1 and ζ_1 was higher than that of an equivalent mass. This was particularly pronounced for the damping ratio ζ_1 (Figure 5.46b). However, in this context, the reduction of the fundamental frequency f_1 by human occupants is also noteworthy (Figure 5.46a). For instance, as already noted in section 5.6.3.1, five human occupants at TP 5 (F16 - F20) reduced the fundamental frequency f_1 of the test structure (4.51 Hz) by 0.17 Hz. In contrast, the equivalent mass reduced the natural frequency by only 0.12 Hz (G01 - G05 in Table E.19 in comparison with A22 - A26 in Table E.1).

5.6.4.2 SECOND MODE

Human occupants or an equivalent mass at a node of the second mode (TP 5) had only a marginal effect on the natural frequency f_2 and the damping ratio ζ_2 (F16 - F20 and G01 - G05 on the left hand side of Figures 5.47a and 5.47b).

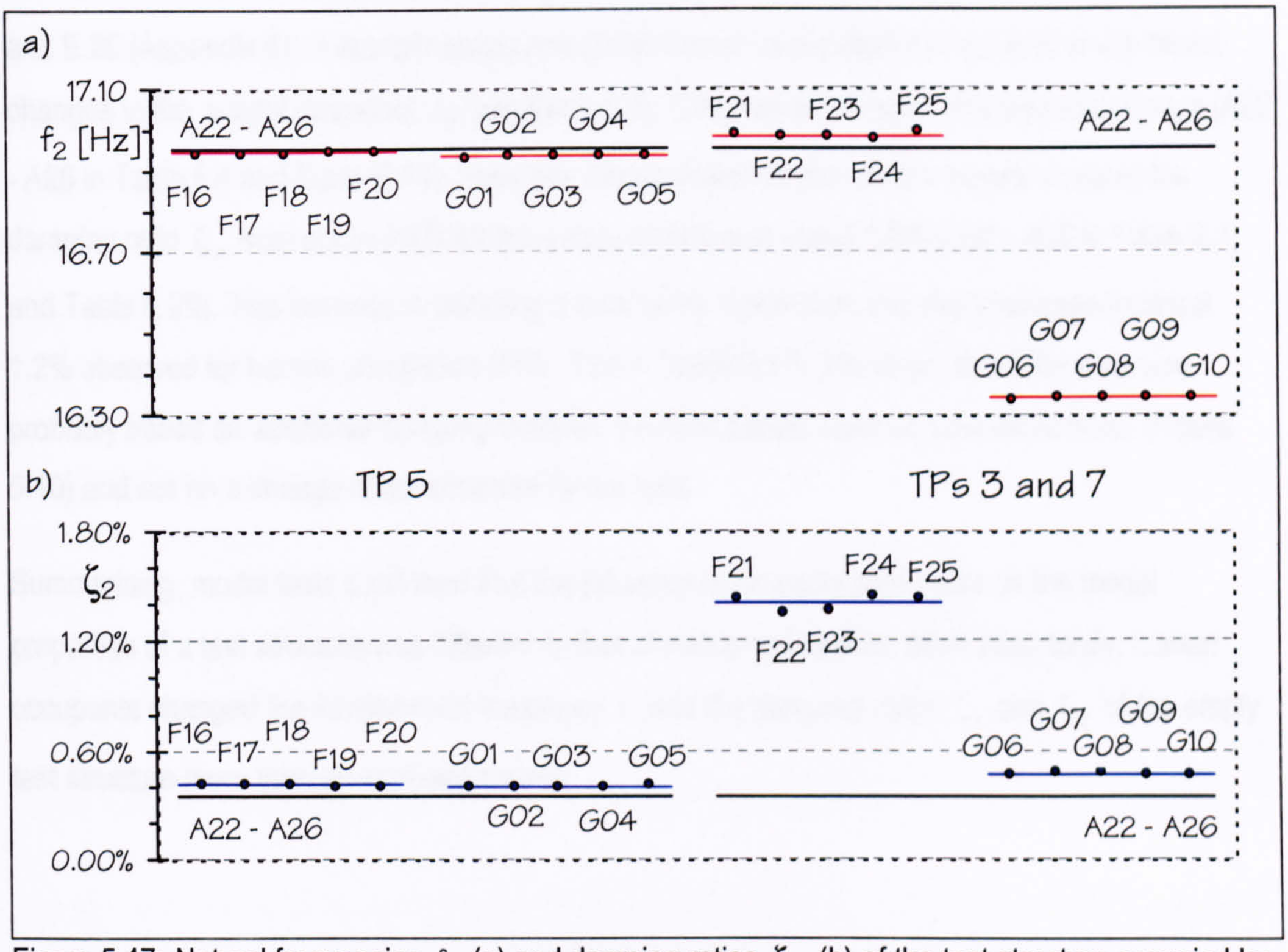

Figure 5.47: Natural frequencies f_2 (a) and damping ratios ζ_2 (b) of the test structure occupied by five TSs (Test F) or an equivalent mass (Test G).

However, if the static load was applied at the antinodes of the second mode (TPs 3 and 7), the natural frequency f_2 decreased noticeably from 16.95 Hz to 16.34 Hz (A22 - A26 and G06 - G10 in Figure 5.47a). In contrast, human occupation did not lead to a frequency reduction (F21 - F25). In fact, it led to a slight increase of f_2. This observation is consistent with the frequency increase observed by Ji (1995) (section 2.4.1). It emphasises the lack of accuracy of the mass-only model of occupants for modes with higher natural frequencies.

Remarkably, Figure 5.47b shows a strong difference between the damping ratio ζ_2 of the test structure occupied by humans or loaded with an equivalent static mass at TPs 3 and 7. However, as

noted above, ζ_2 remained practically at the low value of the empty structure (about 0.3%) if occupants were at TP 5 or if an equivalent mass was at TP 5 or TPs 3 and 7.

5.6.4.3 THIRD MODE

Finally, it is looked at natural frequencies f_3 and damping ratios ζ_3 as presented in Tables E.19 and E.20 (Appendix E). It was previously noted that human occupation did not lead to significant changes in the natural frequency f_3 (section 5.6.3). This was also true for the equivalent mass (A22 - A26 in Table 5.4 and Table E.19). However, the equivalent mass of floor panels doubled the damping ratio ζ_3 from about 0.9% for the empty structure to about 1.8% (A22 - A26 in Table E.1 and Table E.20). This increase in damping is noticeably higher than the slight increase to about 1.2% observed for human occupation (F16 - F20 in Table E.17). However, this difference was probably based on additional damping between the floor panels used as equivalent mass (Figure 5.10) and not on a change of the structure by the load.

Summarising, modal tests confirmed that the influence of an equivalent mass on the modal properties of a test structure was different to that of human occupants. Most importantly, human occupants changed the fundamental frequency f_1 and the damping ratios ζ_1 and ζ_2 of the empty test structure more than an equivalent mass.

5.7 MODAL MASSES

Modal masses m_1, m_2, and m_3 of the empty, human-occupied, and mass loaded test structure were calculated (see section 3.3.2) and summarised in Appendix E. Now, these data are discussed briefly.

The modal mass m_1 of the first mode of vibration of the 15,000 kg structure (mode shapes in Figure 5.34) was about 7,000 kg (Table E.3 in Appendix E). The modal masses m_2 of the second and m_3 of the third mode were slightly higher at 7,400 and 7,800 kg (Table E.3). The estimated values were consistent for all modal tests of the empty structure. In fact, standard deviations of m_1, m_2, and m_3 were less than 5% (up to 350 kg) of the mean values determined from groups of five tests (Table E.3).

The modal masses m_1, m_2, and m_3 of the human-occupied structure (Tables E.6, E.9, E.12, E.15, and E.18) were generally similar to estimates of the empty structure (Table E.3). However, human occupation led to a significantly higher scatter in estimated modal masses m_1. For instance, the standard deviation of m_1 reached 1100 kg (14 %) for nominally identical tests involving five sitting TSs (F16 - F20 in Table E.18). Hence, it was about three-fold the maximal standard deviation of the modal mass m_1 of the empty test structure (350 kg in P05, P10, P15, P20, and P25 in Table E.3).

A static mass placed on the test structure caused noticeable changes in modal masses (Tables E.3 and E.21). Thereby, contrary to the case of human occupation, mean values changed without increasing standard deviations. Actually, standard deviations of modal masses of the mass-loaded structure reached only 260 kg (3%). Thus, they were significantly smaller than that of the human-occupied structure (14%).

In summary, human occupant(s) increased the scatter of the estimated modal mass m_1 of the test structure. This was not the case for a static mass.

5.8 SUMMARY

In the experimental part of this research, forced vibration testing led to FRFs of the empty, the mass loaded, and human-occupied test structure. Curve-fitting of these FRFs, the influence of human occupants and an equivalent mass on modal properties of a prestressed concrete structure was quantified. This procedure was successful if one to five human occupants were sitting or standing on the structure. However, an estimation of modal properties was not possible if a human occupant was inducing forces into the structure, as was the case for walking and standing with bent knees.

The empty structure had three lightly damped vertical bending modes at approximately 4.5 Hz, 17 Hz, and 38 Hz. Up to five stationary human occupants on the structure did not lead to the identification of an additional mode. Moreover, neither human occupation nor a static mass changed the mode shapes of the test structure. Additionally, the following observations were made:

(1) Experimentally estimated natural frequencies, damping ratios, and modal masses were less consistent if human occupants were on the structure than if the structure was empty. This was an issue of immediate repeatability and not of long-term repeatability.

(2) Human occupants influenced primarily the fundamental natural frequency f_1 and the damping ratios ζ_1 and ζ_2 of the test structure. They reduced f_1 and increased the damping ratios significantly.

(3) Five sitting human occupants reduced the fundamental frequency of the test structure (about 4.5 Hz) stronger than an equivalent mass.

(4) The influence of human occupants depended on their number and location.

(5) The posture of a single occupant had only a small influence on the fundamental natural frequency f_1 of the test structure but it affected the damping ratio ζ_1 strongly.

(6) The individual properties of a single human occupant had little effect.

(7) The employed low levels of vibration did not seem to have an effect on the influence of a single human occupant.

6. HUMAN-STRUCTURE SYSTEMS: MODELLING AND DISCUSSION

It is widely agreed that a stationary human occupant, who is in continuous contact with a structure, can be modelled as a damped SDOF system, whose properties are more or less known (chapter 2). However, there is still a need for properties of a similar SDOF model representing crowds occupying civil engineering structures. Therefore, the experimental data of this research were used to identify a damped SDOF model of a group of human occupants. This model was used to provide preliminary guidance to analytically quantify the influence of human occupants on slender civil engineering structures.

The identification process is presented in section 6.1. A verification and discussion of the model are presented in section 6.2. Finally, section 6.3 provides further guidance on assessing the influence of human occupants on civil engineering structures.

6.1 DERIVATION OF A DYNAMIC HUMAN MODEL

Firstly, properties of a SDOF occupant model are identified in this section using a 2-DOF human-structure model. Next, the methodology employed in this process, its implementation and results are presented. Finally, the quality of the identified SDOF occupant model is demonstrated.

6.1.1 METHODOLOGY

Several model updating techniques (Friswell and Motthershead 1995) can principally be used to identify the properties of a damped SDOF human occupant model. In this research, the updating was based on the correlation of FRFs. The methodology employed is outlined in detail.

6.1.1.1 UPDATING BASED ON FRFS

Experimentally estimated FRFs ${}^{EX}H(f)$ and analytical FRFs ${}^{AN}H(f)$ were employed in the procedure of identifying the properties of a SDOF occupant model. In particular, a 2-DOF human-

structure model (Figure 3.2b) was searched for whose analytical FRFs ${}^{AN}H(f)$ (section 3.1.3.3) best approximated experimental FRFs ${}^{EX}H(f)$. The matching of the two FRFs ${}^{AN}H(f)$ and ${}^{EX}H(f)$ was evaluated by differences Δ (6.1). Thereby, the smallest difference indicated the best fit of analytical and experimental FRF data within a frequency range f_j to f_k.

$$\Delta = \sum_{f=f_j}^{f_k} \left| {}^{AN}H(f) - {}^{EX}H(f) \right| \tag{6.1}$$

It is important to note that an exponential window (section 3.2.3.1) was used in the acquisition of FRFs. This exponential window distorts time histories and, consequently, FRFs (Figure 6.1). Therefore, experimental FRFs ${}^{EX}H(f)$ should only be related to their analytical counterparts ${}^{AN}H(f)$ if the effects of the window were removed. This adjustment can be achieved by altering the experimental or the analytical FRFs.

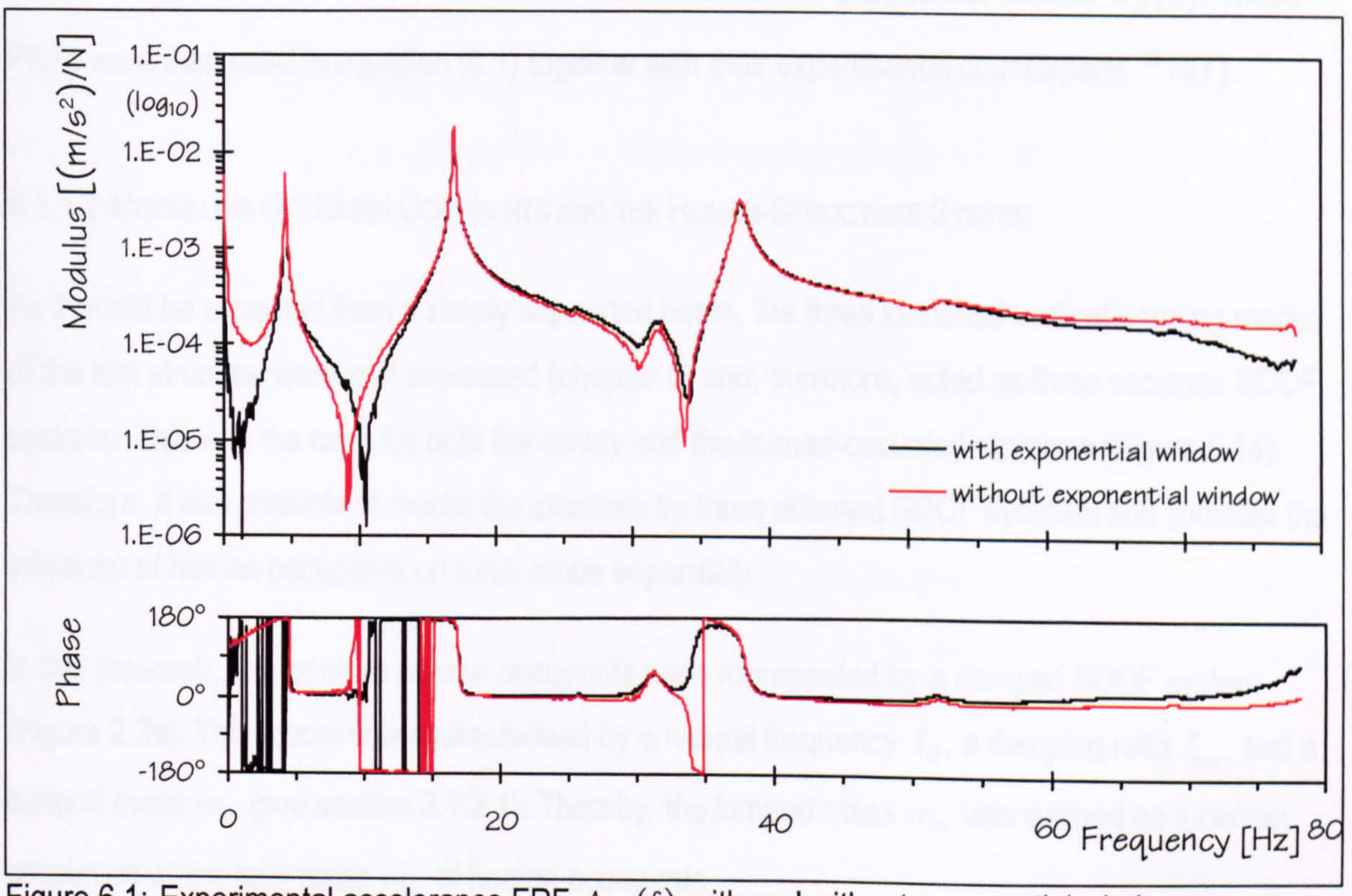

Figure 6.1: Experimental accelerance FRF $A_{77}(f)$ with and without exponential window.

Section 3.3.4 already outlined how the effect of an exponential window can be removed from an experimental FRF ${}^{EX}H(f)$. However, the IRF ${}^{EX}h^{corr}(t)$ (equation (3.195) in section 3.3.4) computed here from ${}^{EX}H(f)$ and required in this process was not transient. However, it was possible

to limit the experimental IRF ${}^{EX}h^{corr}(t)$ to the initial two-thirds of its original length T, where it decayed continuously. Using such an IRF, the effect of an exponential window was removed successfully from experimental FRF ${}^{EX}H(f)$. However, the premature cut-off of the IRF increased the frequency step Δf of the resulting experimental accelerance ${}^{EX}A^{corr}(f)$ from 0.04 to 0.07 Hz (equation (3.150) in section 3.2.1.4). Thus, removing the effect of the exponential window from experimental FRFs ${}^{EX}H(f)$ reduced the resolution of the experimental FRF data significantly.

Therefore, this approach was dismissed and, instead of altering the experimental FRFs ${}^{EX}H(f)$, the analytical FRFs ${}^{AN}H(f)$ were computed so they included the effect of an exponential window. This was done by computing analytical IRFs ${}^{AN}h(t)$ (see section 3.3.3) of interest and multiplying them with an exponential window $w_E(t)$ as used in experiments. The resulting function was, contrary to ${}^{EX}h^{corr}(t)$, transient in the time domain. Therefore, the inverse FT was performed successfully and it led to analytical FRFs ${}^{AN}H(f)$ that included the effect of the exponential window $w_E(t)$. These FRFs were then used in equation (6.1) together with their experimental counterparts ${}^{EX}H(f)$.

6.1.1.2 Modelling of Human Occupants and the Human-Structure System

As it would be expected from a simply supported beam, the three identified vertical bending modes of the test structure were well separated (chapter 5) and, therefore, acted as three separate SDOF systems. This was the case for both the empty and the human-occupied structure (Figure 5.14). Therefore, it was possible to model the structure by three different SDOF systems and consider the influence of human occupants on each mode separately.

In this research, one or more human occupants were represented by a damped SDOF system (Figure 2.2a). This model was characterised by a natural frequency f_H, a damping ratio ζ_H, and a lumped mass m_H (see section 3.1.2.1). Thereby, the lumped mass m_H was defined as a certain proportion of the total mass m_T of human occupants.

Combining a SDOF human occupant model and a SDOF structure model (Figure 3.2a), the human-occupied test structure was modelled as damped 2-DOF system (Figure 3.2b). The first (so called 'structural') DOF of a 2-DOF human-structure model represented the empty test structure. Its properties depended on the mode and test point considered. The second DOF models an arbitrary

number of human occupants. Its properties (f_H , ζ_H , and m_H as proportion of m_T) were identified by updating (sections 6.1.2 and 6.1.3).

6.1.1.3 Correlation of Experimental Data with Analytical Models

In this research, experimental FRFs of the structure and the human-occupied structure were estimated at TPs of the structure only. Vibrations of the body of human occupants were not measured. Therefore, when modelling the human-occupied structure as 2-DOF system, experimental FRFs could be related to analytical structural FRFs $A_s(f)$ or $A_{ss}(f)$ only. Thereby, the FRF $A_s(f)$ is the point-accelerance of the damped SDOF model of the empty test structure (section 3.1.3.2) whereas the FRF $A_{ss}(f)$ relates to the structural point-accelerance of the damped 2-DOF human-structure model (section 3.1.3.3).

Experimental point-accelerances of the test structure with a single TS sitting at TP 7 (B16 - B20) or of five occupants at TPs 3 and 7 (F21- F25) could have been used to estimate a SDOF human occupant model. However, the influence of five TSs was significantly higher than that of a single person. Moreover, this research aimed at modelling several occupants simultaneously. Therefore, the properties of the SDOF occupant model were derived from experiments that quantified the influence of five human occupants (F21 - F25). Nevertheless, experiments involving one to four TSs were employed in the verification of the human model (section 6.2.3).

In experiments F21 - F25, two of the five TSs were sitting at TP 3 and the other three people were sitting at TP 7 (Figure 5.9). In this case, mode shape amplitudes of the empty and the occupied test structure were similar at the locations of the TSs for all three modes investigated (TPs 3 and 7 in Figures 5.33 and 5.34). Using this feature and one SDOF human occupant model (section 3.1.2.1), the five TSs were represented by one SDOF system attached to the structure at TP 7.

Modelling human occupants and the empty test structure both as SDOF systems, the occupied structure was simplified as a 2-DOF system. The analytical accelerance $A_{ss}(f)$ of this model corresponded to experimental point-accelerances $A_{77}(f)$. Both FRFs were correlated using equation (6.1) to identify the properties of a SDOF human model.

The three structural SDOF models of the empty structure (Table 6.1) were defined by the modal properties obtained by global FRF curve-fitting (A22 - A26 in Tables E.1 to E.3 in Appendix E). This

procedure was quicker and more straightforward than an identification based on updating. Nevertheless, it led to very close fits between experimental FRFs $A_{77}(f)$ of the empty test structure and its analytical SDOF equivalents $A_s(f)$.

Table 6.1: Parameters of damped SDOF models of the three modes of the empty test structure.

	Natural frequency f_s	Damping ratio ζ_s	Mass m_s [1)]
First mode	4.51 Hz	0.32%	13910 kg
Second mode	16.95 Hz	0.35%	7370 kg
Third mode	37.73 Hz	0.94%	15980 kg

[1)] Modal masses were computed from mode shapes unity-normalised (see section 3.3.2) to TP 7.

6.1.2 Updating Procedure

Sets of parameters f_H, ζ_H, and m_H of SDOF human models (Figure 2.2a) were identified using specially written MATLAB (1999) routines. For this purpose, differences Δ (equation (6.1)) were computed between the analytical FRF $A_{ss}(f)$ of human-structure models and each of the five experimental FRFs $A_{77}(f)$ of the human-occupied structure (F21 - F25) within selected frequency ranges (f_j to f_k).

The frequency ranges (f_j to f_k) and relevant ranges of the three updating parameters f_H, ζ_H, and m_H were specified after some preliminary investigations. These preliminary investigations employed various frequency ranges and updating parameters to identify parameters leading to stable updating results.

This exploratory analysis was very helpful. In particular, it improved updating related to the first mode of the test structure. Interestingly, in this case, the frequency range (f_j to f_k) used in updating had to include frequencies corresponding to both the first and second mode of the 2-DOF human-structure model (see section 4.6). Moreover, the preliminary investigations showed that updating using the third mode of the test structure did not lead to reliable results. Consequently, identifying a human model from the influence of human occupants on the third mode of the test structure was abandoned.

Updating of 2-DOF human-structure systems corresponding to the first and second modes of the empty test structure was more successful. It led to the identification of two sets of properties of a damped SDOF human model. These are termed Human Models A and B and they were identified by incrementally varying the parameters f_H, ζ_H, and m_H within the ranges given in Table 6.2.

Table 6.2: Parameter ranges used in updating of Human Models A and B.

	Human Model A	Human Model B
f_j to f_k	about 4.0 to 7.0 Hz, Δf = 0.0397 Hz	about 15.0 to 19.0 Hz, Δf = 0.0397 Hz
f_H	5.00 to 6.50 Hz, Δf_H = 0.02 Hz	6.00 to 9.00 Hz, Δf_H = 0.02 Hz
ζ_H	20% to 60%, $\Delta \zeta_H$ = 1%	30% to 45%, $\Delta \zeta_H$ = 1%
m_H	0.80 m_T to 1.00 m_T, Δm_H = 0.01 m_T	0.70 m_T to 1.00 m_T, Δm_H = 0.01 m_T

6.1.3 Updated Human Model

The updated parameters f_H, ζ_H, and m_H (as a proportion of m_T) characterise the damped SDOF model of sitting human occupants by two sets of properties: Human Model A and Human Model B.

Human Model A represents the influence of sitting human occupants on the first mode of the test structure (4.51 Hz). Its properties were identified for each of the five experiments F21 - F25 as listed in Table 6.3.

The mean values and standard deviations of the parameters f_H, ζ_H, and m_H determined for each measurement (Table 6.3) define Human Model A. Alternatively, Human Model A is characterised by the 95% confidence intervals (section 3.3.1) of the parameters f_H, ζ_H, and m_H.

Table 6.3: Properties of Human Model A, a damped SDOF system modelling the influence of sitting human occupants on the fundamental mode (4.51 Hz) of the test structure.

Experiment	Natural frequency f_H	Damping ratio ζ_H	Lumped mass m_H
F21	5.38 Hz	34%	0.92 m_T
F22	5.78 Hz	27%	0.84 m_T
F23	6.08 Hz	36%	0.97 m_T
F24	6.12 Hz	31%	0.97 m_T
F25	6.00 Hz	35%	0.93 m_T
Mean value and standard deviation	5.87 Hz ± 0.30 Hz	33% ± 4%	0.93 m_T ± 0.05 m_T
95% confidence interval	5.49 Hz ... 6.25 Hz	28% ... 37%	0.86 m_T ... 0.99 m_T

Human Model B quantifies the influence of human occupants on the second mode (16.95 Hz) of the empty test structure. Its parameters (f_H, ζ_H, and m_H) are listed in Table 6.4 for updated 2-DOF human-structure models corresponding to each of the five experimental FRFs $A_{77}(f)$. Additionally, Table 6.4 provides the mean values and standard deviations as well as 95% confidence intervals of the parameters f_H, ζ_H, and m_H that define Human Model B.

Table 6.4: Properties of Human Model B, a damped SDOF system modelling the influence of five sitting human occupants on the second mode (16.95 Hz) of the test structure.

Experiment	Natural frequency f_H	Damping ratio ζ_H	Lumped mass m_H
F21	7.46 Hz	35%	1.00 m_T
F22	8.50 Hz	34%	0.73 m_T
F23	8.04 Hz	36%	0.80 m_T
F24	8.56 Hz	37%	0.76 m_T
F25	8.98 Hz	33%	0.75 m_T
Mean value and standard deviation	8.31 Hz ± 0.58 Hz	35% ± 2%	0.81 m_T ± 0.11 m_T
95% confidence interval	7.59 Hz ... 9.03 Hz	33% ... 37%	0.67 m_T ... 0.94 m_T

Interestingly, the parameters f_H and m_H are systematically different for Human Models A and B (Tables 6.3 and 6.4). This means that the properties of the identified damped SDOF human occupant model depend on the frequency of the mode they are related to. This feature will be analysed in the verification of the models (section 6.2) and will be included in the design considerations presented in section 6.3. It demonstrates that humans are actually not SDOF but more complex MDOF systems (Griffin 1990).

6.1.4 Quality of Updated Human-Structure Systems

The fit of experimental and analytical FRFs of the human-occupied structure was used to evaluate the identification of human models. For this purpose, two damped SDOF human models were used. These models were denoted as Human Models A* and B* (Table 6.5) and defined by the mean values of the parameters f_H, ζ_H, and m_H of Human Models A or B (Tables 6.3 and 6.4).

Table 6.5: Properties of the damped SDOF Human Models A* and B*.

	Human Model A*	Human Model B*
Natural frequency f_H	5.9 Hz	8.3 Hz
Damping ratio ζ_H	33%	35%
Lumped mass m_H	0.9 m_T	0.8 m_T

Combining Human Model A* or Human Model B* with a SDOF model of the first or second mode of the empty test structure (Table 6.1), four 2-DOF human-structure models were obtained. The structural FRFs $A_{ss}(f)$ of these four models were compared visually with the experimental FRFs $A_{77}(f)$ of the human-occupied structure (Figures 6.2 and 6.3). (Note: the analytical and experimental FRFs $A_{ss}(f)$ and $A_{77}(f)$ both included the effect of an exponential window.)

Figures 6.2 and 6.3 show that the analytical FRFs $A_{ss}(f)$ fit generally well to the experimental FRFs $A_{77}(f)$. Nevertheless, Human Model A* clearly led to a closer match of FRFs around the natural frequency of the first mode than Model B* (Figure 6.2). This is reasonable because Human Model A*, and not Human Model B*, was obtained by updating the frequency range from 4 to 7 Hz (Table 6.2). However, similarly, a human-structure model employing Human Model B* fits closer to experimental FRFs within the frequency range from 15 to 19 Hz (Figure 6.3).

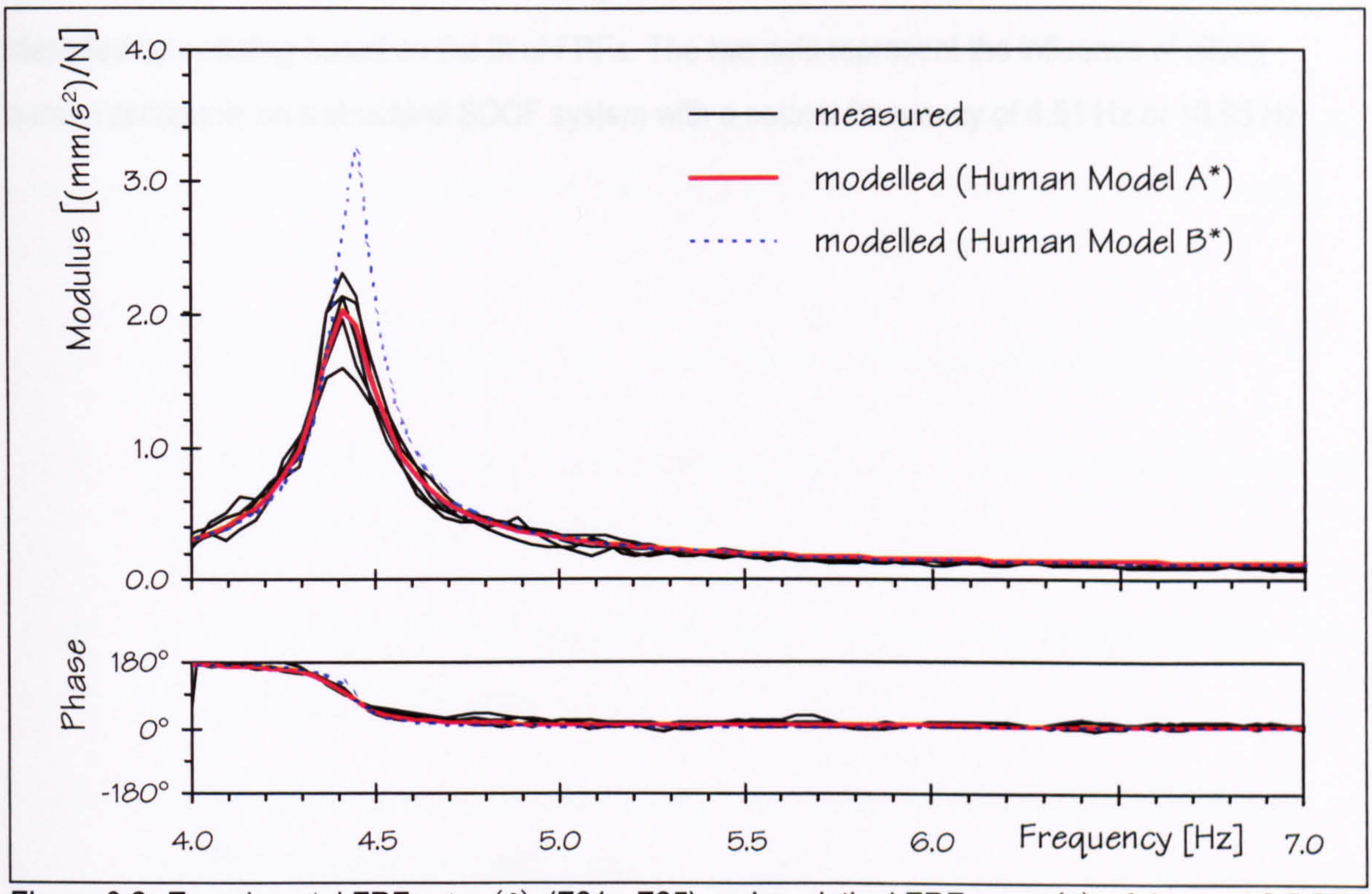

Figure 6.2: Experimental FRFs $A_{77}(f)$ (F21 - F25) and analytical FRFs $A_{ss}(f)$ of damped 2-DOF human-structure systems in the frequency range from 4 to 7 Hz.

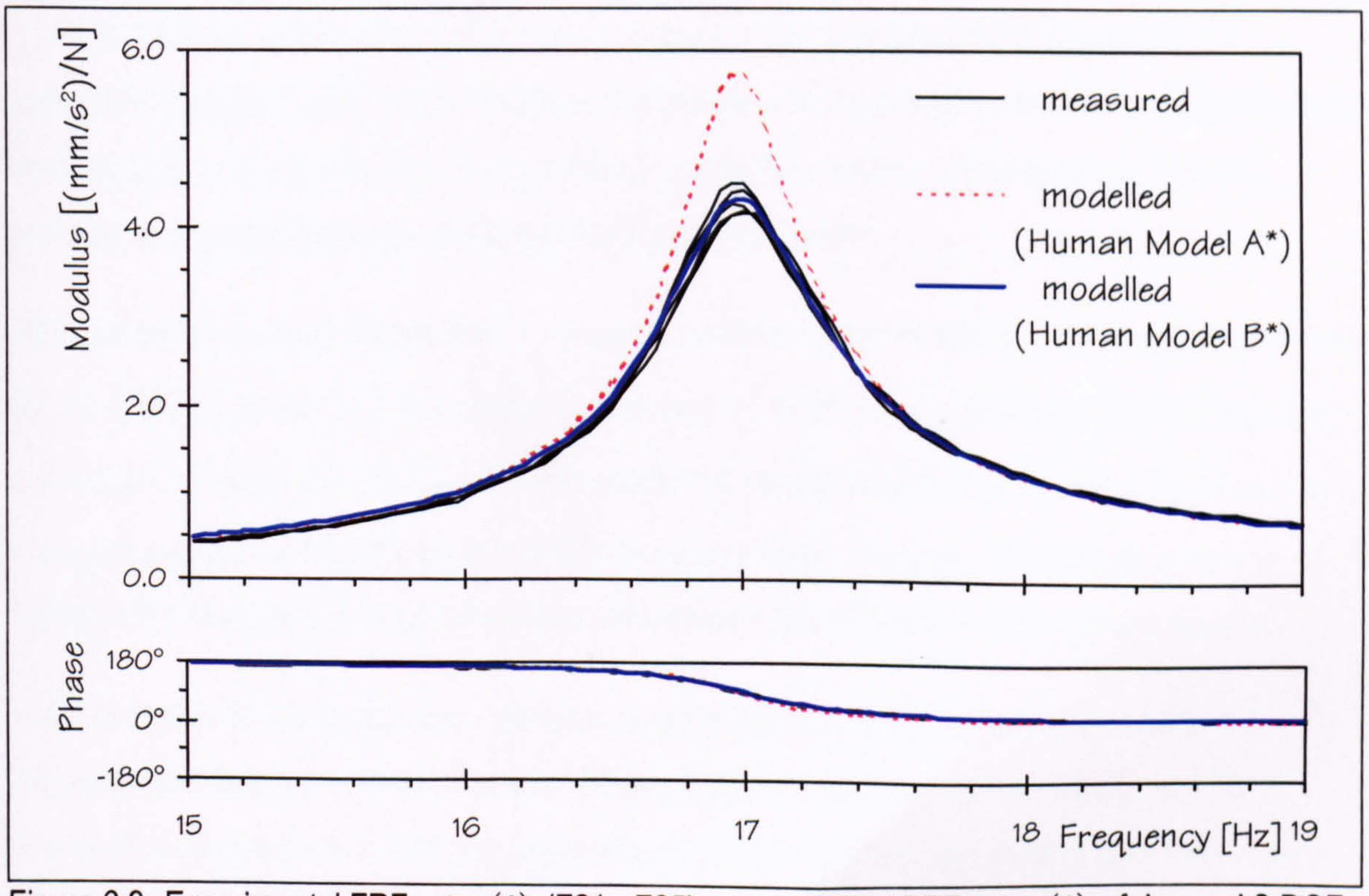

Figure 6.3: Experimental FRFs $A_{77}(f)$ (F21 - F25) and analytical FRFs $A_{ss}(f)$ of damped 2-DOF human-structure systems in the frequency range from 15 to 19 Hz.

In summary, two sets of properties of a damped SDOF model of sitting human occupants were identified by updating based on the fit of FRFs. The two sets represent the influence of sitting human occupants on a structural SDOF system with a natural frequency of 4.51 Hz or 16.95 Hz.

6.2 VERIFICATION

In the previous section, two sets of properties of a damped SDOF model of sitting human occupants were identified (Human Models A and B in Tables 6.3 and 6.4). These properties are now verified and discussed by:

(1) relating characteristics of the SDOF human model to biomechanical research,

(2) analysing the dependency of the parameters of the SDOF human model on the frequency of the related mode of the empty structure,

(3) correlating FRFs and modal properties of 2-DOF human-structure models with that of the human-occupied test structure, and

(4) comparing response time histories of the human-occupied test structure with those of corresponding human-structure models.

6.2.1 BIOMECHANIC RESEARCH

The identified properties of the SDOF Human Models A and B (Tables 6.3 and 6.4) may be explained rationally having in mind the published results of biomechanic research (section 2.2.2). This conclusion was drawn from the analysis of natural frequencies, damping ratios, lumped masses, and apparent masses of human models outlined below.

The fundamental natural frequencies f_1 of biomechanical models of sitting people range from 4.5 to 5.0 Hz (Tables 2.3 and 2.4). The natural frequencies f_H of the Human Models A and B range from 5.4 to 9.0 Hz (Tables 6.3 and 6.4). In other words, the natural frequencies f_H of the SDOF human occupant models are higher than that of biomechanic models. However, this difference can be explained by the different levels of vibration employed in the estimation of the human models.

In the experiments performed here, vibration levels lower than those usually employed in biomechanics (about 2 m/s^2) were purposely employed to create a situation realistic for civil engineering applications. In fact, the properties of Human Models A and B were determined using random vibrations with r.m.s. accelerations below 0.1 m/s^2 (section 5.4.3). Such small levels of vibration are expected to increase natural frequencies of the human body (section 2.2.2), which is

essentially an amplitude-dependent non-linear system. Fairley and Griffin (1989), for example, found the natural frequency of sitting people to be 6 Hz when using random excitation with r.m.s. accelerations of 0.25 m/s². This natural frequency is higher than the frequencies f_1 of human models (maximum of 5.0 Hz in Tables 2.3 and 2.4). However, the frequency of 6 Hz corresponds more closely to the frequencies f_H (5.4 to 9.0 Hz) identified here (Tables 6.3 and 6.4) using a completely different methodology. Therefore, the systematically higher natural frequencies of Human Models A and B are to be expected.

The identified SDOF human occupant model is characterised not only by its natural frequency f_H but also by the damping ratio ζ_H and the mass m_H. The damping ratios ζ_H range from about 30% to about 40% (Tables 6.3 and 6.4). These values correspond well to the damping ratios ζ_1 of biomechanical models of sitting people (32% to 53% in Table 2.3).

The lumped mass m_H of Human Models A and B is more than about 70% of the total mass m_T of the modelled occupant(s) (Tables 6.3 and 6.4). On the other hand, biomechanic SDOF human models often use a mass m_H equal the total mass m_T of a person (Coermann 1962; Wei and Griffin 1998a). To some extent, this assumption confirms that m_H is a relatively high percentage of the total mass m_T (which is clearly not 100%) as found in this research.

Finally, apparent masses $M(f)$ of Human Models A* and B* (Tables 6.5) and human models of ISO 5982 were compared (Figure 6.4). It was shown that apparent masses $M(f)$ fit relatively closely, which is a result of the similar properties of biomechanic human models and Human Models A and B.

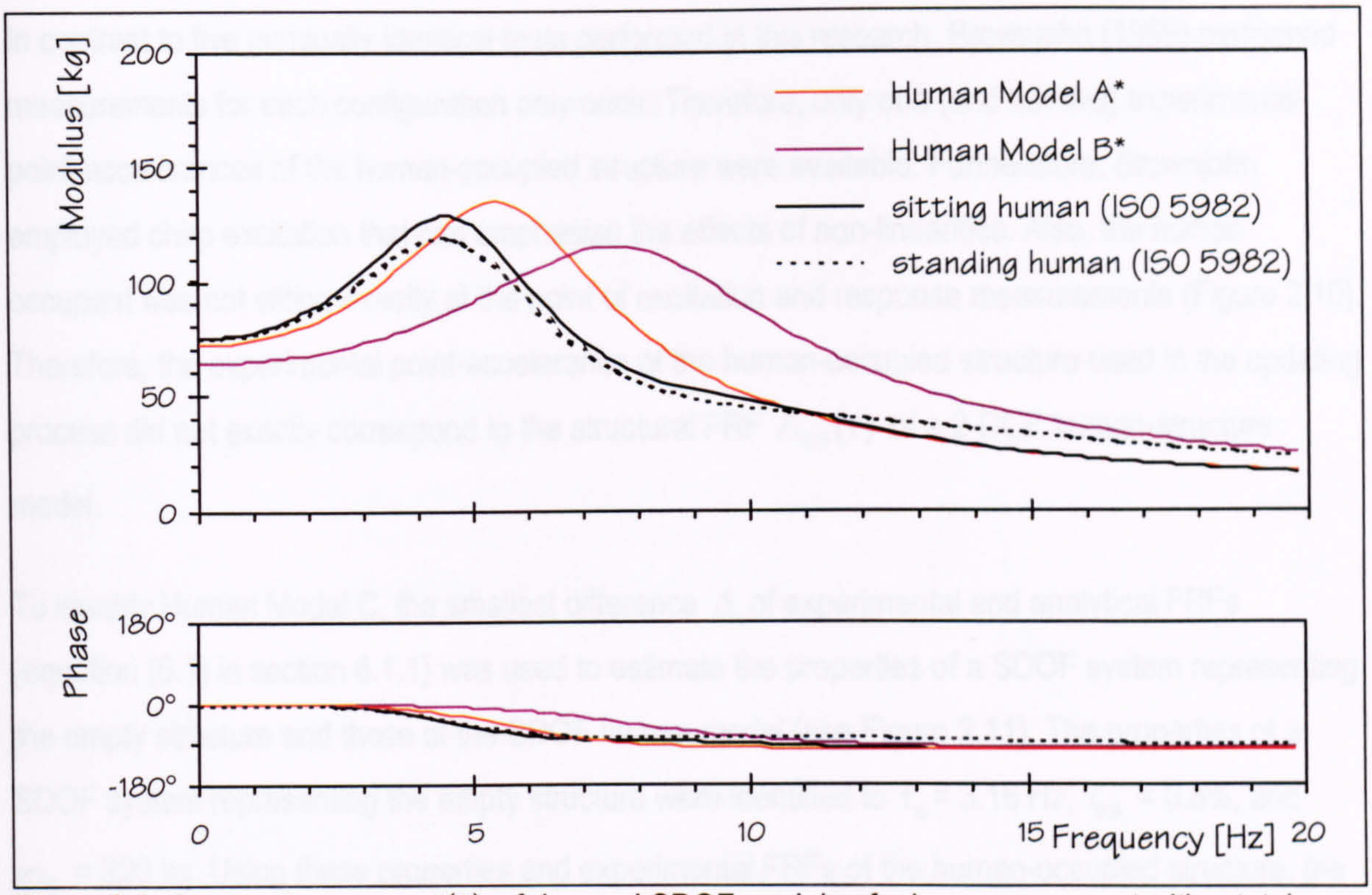

Figure 6.4: Apparent masses $M(f)$ of damped SDOF models of a human occupant with a total mass m_T of 80 kg.

6.2.2 Frequency Dependency of the Properties of the SDOF Human Model

A significant feature of the identified SDOF human occupant model is the dependency of its properties on the natural frequency of the considered mode of the empty structure (section 6.1.3). This point was confirmed using measurements performed independently by Brownjohn (1999).

Brownjohn (1999) analysed the influence of a single person on the dynamic properties of a beam-like structure with a fundamental natural frequency of 3.16 Hz (section 2.4.3). This fundamental frequency was significantly lower than the natural frequencies of 4.51 Hz and 16.95 Hz of the structural modes used to identify Human Models A and B.

Brownjohn's (1999) experimental data (auto and cross-spectral densities) were made available to the writer. FRFs computed from these data were used to identify another set of properties of the SDOF model: Human Model C. This identification principally followed the procedure of fitting FRFs (section 6.1.1) used to estimate Human Models A and B. However, using Brownjohn's FRFs, it was not necessary to remove or artificially apply a window because no window had been used in the data acquisition.

In contrast to five nominally identical tests performed in this research, Brownjohn (1999) performed measurements for each configuration only once. Therefore, only one (and not five) experimental point-accelerances of the human-occupied structure were available. Furthermore, Brownjohn employed chirp excitation that can emphasise the effects of non-linearities. Also, the human occupant was not sitting exactly at the point of excitation and response measurements (Figure 2.10). Therefore, the experimental point-accelerance of the human-occupied structure used in the updating process did not exactly correspond to the structural FRF $A_{ss}(f)$ of a 2-DOF human-structure model.

To identify Human Model C, the smallest difference Δ of experimental and analytical FRFs (equation (6.1) in section 6.1.1) was used to estimate the properties of a SDOF system representing the empty structure and those of the SDOF human model (see Figure 2.11). The properties of a SDOF system representing the empty structure were identified to f_s = 3.16 Hz, ζ_s = 0.8%, and m_s = 920 kg. Using these properties and experimental FRFs of the human-occupied structure, the properties of Human Model C were estimated to f_H = 3.8 Hz, ζ_H = 10%, and $m_H = m_T$.

Remarkably, the parameters f_H, ζ_H and m_H of the three identified sets of Human Models A, B, and C follow the same trend. That is, lowering the natural frequency f_s of the structural SDOF of the human-structure system leads to:

(1) lower natural frequency f_H,

(2) lower damping ratio ζ_H, and

(3) higher mass m_H

of the SDOF human occupant model. Considering the properties of Human Models C, A*and B* (Tables 6.3 and 6.4), it is therefore concluded that f_H < 9 Hz, ζ_H < 40% and m_H > 0.6 m_T if the natural frequency of the empty structure f_s does not exceed 16.95 Hz, the highest natural frequency f_s considered in these investigations.

Finally, computed FRFs $A_{ss}(f)$ of 2-DOF human-structure models were compared with experimentally estimated FRFs (Figure 6.5). As expected, FRFs $A_{ss}(f)$ of a 2-DOF human-structure model that uses Human Model C approximates Brownjohn's (1999) experimental data

better than a 2-DOF model based on Human Model A* or B*. Interestingly, using Human Model A* leads to a better fit than using Human Model B* (Figure 6.5). This observation further confirms the frequency dependency of the properties of the 2-DOF human occupant model.

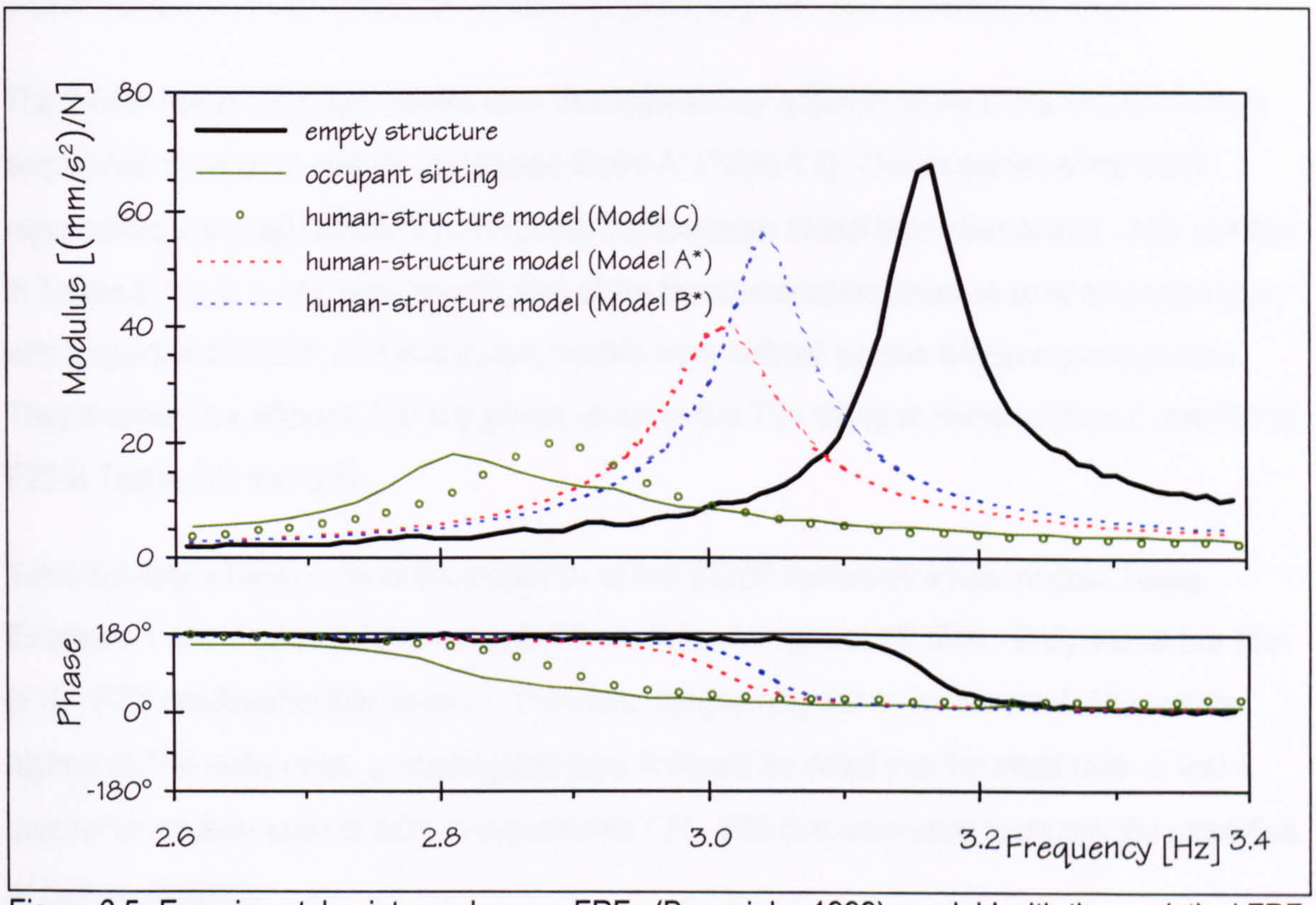

Figure 6.5: Experimental point-accelerance FRFs (Brownjohn 1999) overlaid with the analytical FRF $A_{ss}(f)$ of 2-DOF human-structure models.

6.2.3 FRFs and Modal Properties of the Human-Occupied Test Structure

Next, various experimentally estimated properties of the human-occupied test structure (which were measured but not used in developing the human model) are correlated with the analytically calculated structural FRFs and modal properties of 2-DOF human-structure models. This analysis will verify the damped SDOF occupant model and its properties further.

For this purpose, the investigation employed experimental data of tests B16 - B20, Test E, and F01 to F20 (Appendix D) that were not used in the derivation of the damped SDOF human occupant model. The analysis is presented separately for human-structure models corresponding to the first, second, and third mode of the test structure.

6.2.3.1 First Mode

To verify the properties of Human Model A (Table 6.3), the influence of one to five TSs on the fundamental mode of the test structure was investigated. In doing so, FRFs and modal properties of 2-DOF human-structure models were related to previously not used experimental data.

The 2-DOF human-structure models were characterised by a SDOF model of the empty structure and human occupants modelled by Human Model A* (Table 6.5). The properties of the SDOF representing the empty structure corresponded to the mean modal properties of A22 - A26 as listed in Tables E.1 to E.3. The experimental data of the human-occupied structure used for comparison with properties of 2-DOF human-structure models were defined by nine different configurations. They involved five different TSs and groups of two to five TSs sitting at midspan (Test E and F01 to F20 in Tables D.5 and D.6).

Table 6.6 exemplarily presents the properties of two 2-DOF human-structure models. These Examples 1 and 2 correspond to experiments involving the lightest TS (E01 - E05) and all five TSs (F16 - F20) employed in this research. Therefore, they correspond to the lowest (0.8%) and the highest (5.1%) mass ratios α investigated here. It should be noted that the mass ratio α had a somewhat medium value of 2.6% in experiments F21 - F25 that were used to identify the properties of Human Model A.

Table 6.6: Human-structure models defined by a SDOF structure model (f_s = 4.51 Hz, ζ_s = 0.32%, and m_s = 7,040 kg) and Human Model A* (f_H = 5.9 Hz, ζ_H = 33%, and m_H = 0.9 m_T).

		Example 1: One occupant	Example 2: Five occupants
Human occupant(s)		m_H = 53 kg (m_T = 59 kg)	m_H = 362 kg (m_T = 402 kg)
2-DOF human-structure system	Mass ratio	α = 0.8%	α = 5.1%
	Frequency ratio	β = 1.26	β = 1.26
	First mode	$f_1^{(DM)}$ = 4.48 Hz	$f_1^{(DM)}$ = 4.33 Hz
		ζ_1 = 0.57%	ζ_1 = 1.68%
		m_1 = 7,200 kg	m_1 = 8,080 kg
	Second mode	$f_2^{(DM)}$ = 5.94 Hz	$f_2^{(DM)}$ = 6.14 Hz
		ζ_2 = 32.87%	ζ_2 = 32.40%
		m_2 = 401,890 kg [1)]	m_2 = 66,460 kg [1)]

[1)] Mode shapes were normalised to unity at the structural DOF of the 2-DOF human-structure model. This resulted in such large modal masses m_2.

The structural accelerances $A_s(f)$ and $A_{ss}(f)$ (sections 3.1.3.2 and 3.1.3.3) of Examples 1 and 2 (Table 6.6) are presented in Figures 6.6 and 6.7. In both figures (and in the remainder of this thesis) FRFs are presented without the effect of any window. Therefore, these FRFs should not be compared with FRFs presented in the experimental chapter 5 or section 6.1.

Both FRFs $A_{ss}(f)$ presented in Figures 6.6 and 6.7 are dominated by a lightly damped fundamental mode (ζ_1 < 2% in Table 6.6). In both cases, the heavily damped second mode of both human-structure models (ζ_2 > 32%) has only a marginal influence on the structural FRF $A_{ss}(f)$. Therefore, as in Case 5 presented in Figures 4.36 and 4.38 in section 4.6, only one mode can be identified from the FRF $A_{ss}(f)$. Actually, in case of the SDOF structure model employed here, the mass ratio α would have had to exceed about 20% to enable the identification of two modes. However, in the experiments performed, the mass ratio α reached only 5.1%. This explains why the additional mode was not identified from experimental FRFs.

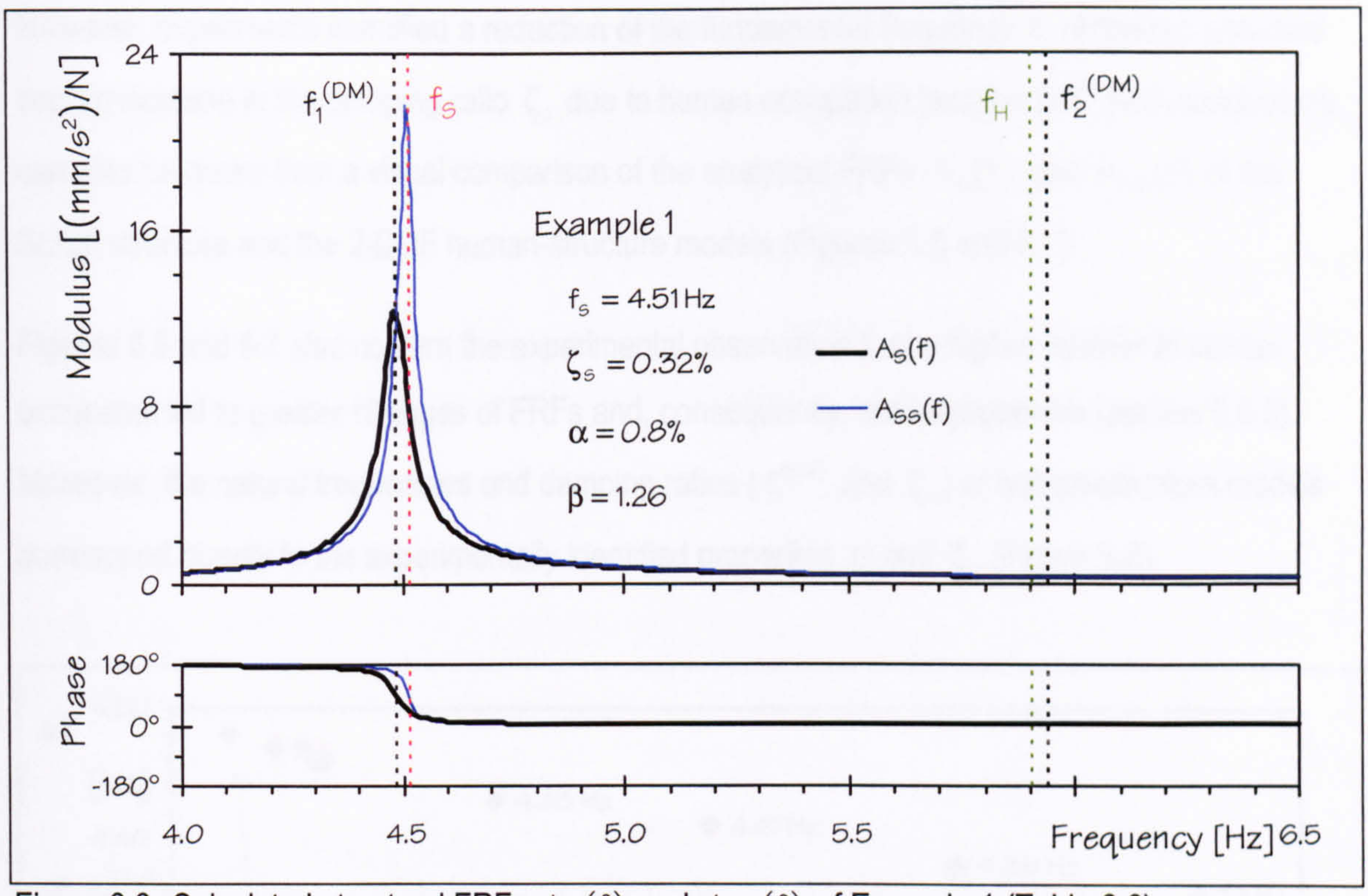

Figure 6.6: Calculated structural FRFs $A_s(f)$ and $A_{ss}(f)$ of Example 1 (Table 6.6).

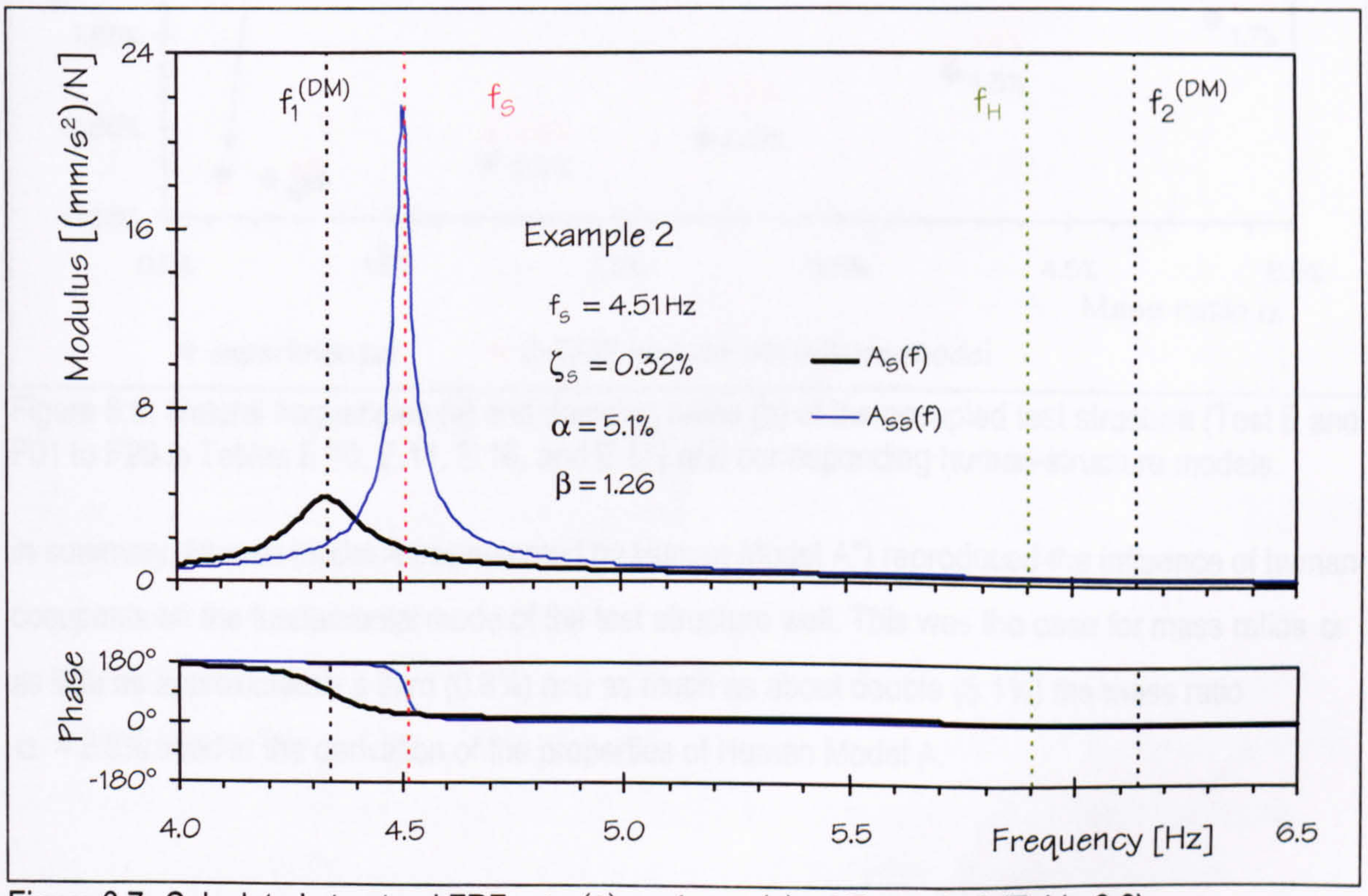

Figure 6.7: Calculated structural FRFs $A_s(f)$ and $A_{ss}(f)$ of Example 2 (Table 6.6).

However, experiments identified a reduction of the fundamental frequency f_1 of the test structure and an increase in the damping ratio ζ_1 due to human occupation (section 5.6). Both conclusions can also be drawn from a visual comparison of the analytical FRFs $A_s(f)$ and $A_{ss}(f)$ of the SDOF structure and the 2-DOF human-structure models (Figures 6.6 and 6.7).

Figures 6.6 and 6.7 also confirm the experimental observation that a higher number of human occupants led to greater changes of FRFs and, consequently, modal properties (section 5.6.3). Moreover, the natural frequencies and damping ratios ($f_1^{(DM)}$ and ζ_1) of human-structure models correspond closely to the experimentally identified properties f_1 and ζ_1 (Figure 6.8).

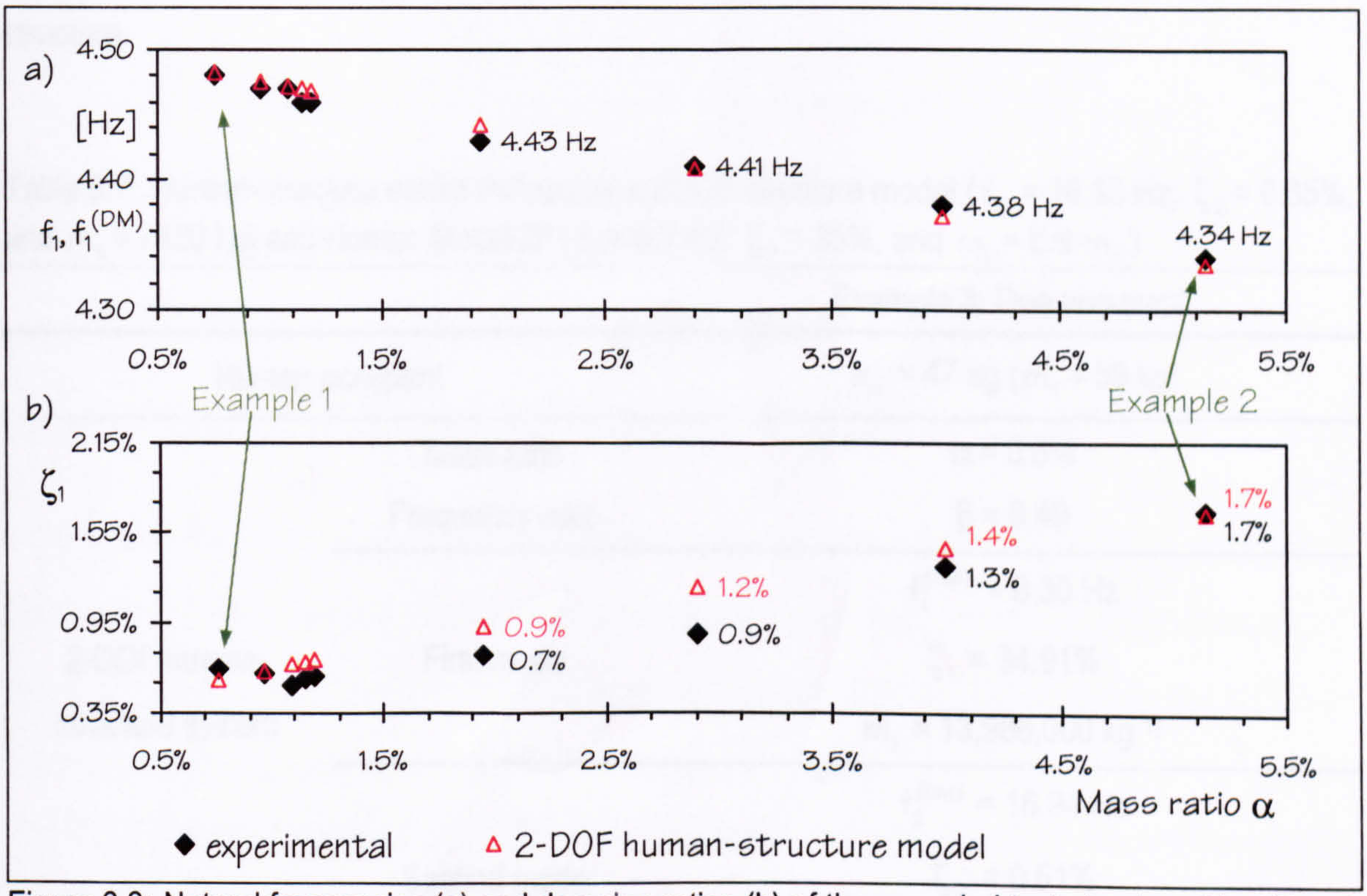

Figure 6.8: Natural frequencies (a) and damping ratios (b) of the occupied test structure (Test E and F01 to F20 in Tables E.10, E.11, E.16, and E.17) and corresponding human-structure models.

In summary, Human Model A (represented by Human Model A*) reproduced the influence of human occupants on the fundamental mode of the test structure well. This was the case for mass ratios α as little as approximately a third (0.8%) and as much as about double (5.1%) the mass ratio α = 2.6% used in the derivation of the properties of Human Model A.

6.2.3.2 Second Mode

The influence of five human occupants on the second mode of the test structure (f_2 = 16.95 Hz) was used to identify Human Model B (Table 6.4). This Human Model B is now verified using Human Model B* (Table 6.5) as its 'average' version to predict the effect of a single occupant on the second mode of the test structure. For this purpose, experiments B16 - B20 were employed. They involved TS A sitting at an antinode of the second mode of the test structure (Table D.3 in Appendix D).

The modal properties of a corresponding 2-DOF human-structure model (Example 3) were estimated (Table 6.7). In doing so, a SDOF model defined by the mean modal properties of the second mode identified in experiments A17 - A21 (Tables E.1 to E.3) represented the empty test structure.

Table 6.7: Human-structure model defined by a SDOF structure model (f_S = 16.93 Hz, ζ_S = 0.35%, and m_S = 7420 kg) and Human Model B* (f_H = 8.3 Hz, ζ_H = 35%, and m_H = 0.8 m_T).

		Example 3: One occupant
2-DOF human-structure system	Human occupant	m_H = 47 kg (m_T = 59 kg)
	Mass ratio	α = 0.6%
	Frequency ratio	β = 0.49
	First mode	$f_1^{(DM)}$ = 8.30 Hz
		ζ_1 = 34.91%
		m_1 = 13,986,000 kg [1)]
	Second mode	$f_2^{(DM)}$ = 16.94 Hz
		ζ_2 = 0.51%
		m_2 = 7,430 kg

[1)] Mode shapes were normalised to unity at the structural DOF of the 2-DOF human-structure model. This resulted in the large modal mass m_1.

Example 3 has, contrary to Examples 1 and 2 (Table 6.6), a lightly damped second mode (Table 6.7) that dominates the FRF $A_{ss}(f)$ (Figure 6.9). In contrast to the second mode, the fundamental mode of Example 3 is heavily damped (Table 6.7). This mode is, as in Case 1 of the parametric study (Table 4.1 and Figures 4.32 and 4.38 in section 4.6), not visible in the analytical FRF $A_{ss}(f)$ of the human-structure model (Figure 6.9). This explains why only modal properties corresponding

to the dominant second mode of the 2-DOF human-structure model (Figure 6.9) could be identified from experimental FRFs of the human-occupied structure.

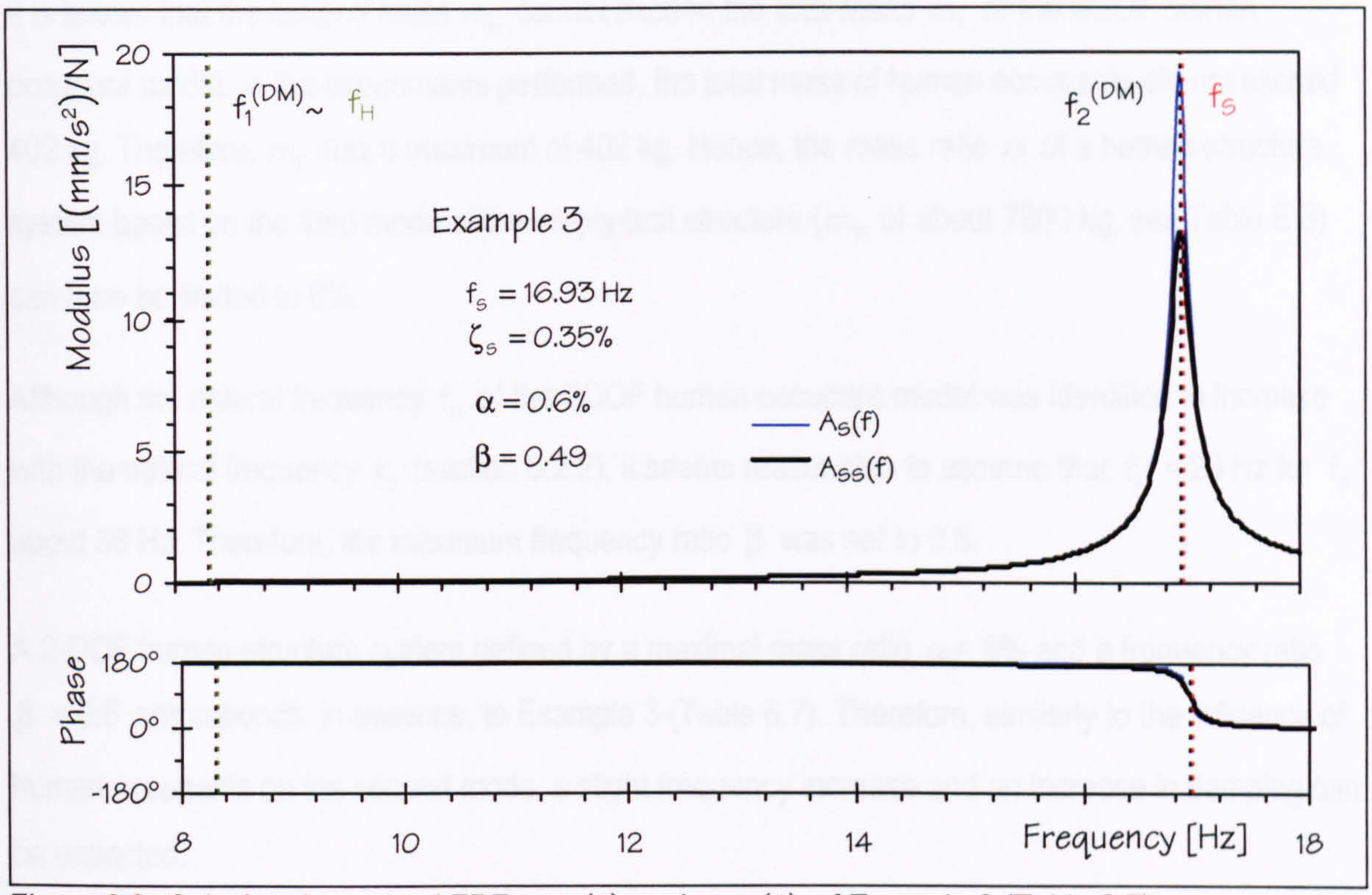

Figure 6.9: Calculated structural FRFs $A_S(f)$ and $A_{SS}(f)$ of Example 3 (Table 6.7).

Actually, the modal properties of this lightly damped second mode ($f_2^{(DM)} = 16.94$ Hz, $\zeta_2 = 0.51\%$, and $m_2 = 7430$ kg in Table 6.7) match those of the human-occupied test structure ($f_2 = 16.94$ Hz, $\zeta_2 = 0.47\%$, and $m_2 = 7420$ kg from B16 -B20 in Tables E.4 to E.6) closely. Moreover, the human-structure model accurately reproduces a small frequency increase (from 16.93 to 16.94 Hz). It also indicates a damping increase (from 0.35% to 0.47%) similar to the analytically estimated increase to 0.51%.

6.2.3.3 Third Mode

The properties of a damped SDOF human model corresponding to the third mode of the test structure (f_3 about 38 Hz) were not identified by updating (section 6.1.2). Therefore, appropriate 2-DOF human-structure models cannot be presented. Nevertheless, the influence of human occupants (modelled as damped SDOF system) on the third mode of the test structure were

discussed in general. For this purpose, appropriate mass and frequency ratios α and β had to be specified.

It is known that the lumped mass m_H cannot exceed the total mass m_T of the SDOF human occupant model. In the experiments performed, the total mass of human occupants did not exceed 402 kg. Therefore, m_H has a maximum of 402 kg. Hence, the mass ratio α of a human-structure system based on the third mode of the empty test structure (m_3 of about 7800 kg, see Table E.3) can here be limited to 6%.

Although the natural frequency f_H of the SDOF human occupant model was identified to increase with the natural frequency f_S (section 6.2.2), it seems reasonable to assume that $f_H < 20$ Hz for f_S about 38 Hz. Therefore, the maximum frequency ratio β was set to 0.5.

A 2-DOF human-structure system defined by a maximal mass ratio $\alpha = 6\%$ and a frequency ratio $\beta = 0.5$ corresponds, in essence, to Example 3 (Table 6.7). Therefore, similarly to the influence of human occupants on the second mode, a slight frequency increase and an increase in damping can be expected.

Both phenomena were found to be true for five occupants sitting at the antinode of the third mode of the test structure. In fact, the natural frequency f_3 increased slightly from 37.73 Hz to 37.83 Hz (A22 - A26 in Table E.1 and F16 - F20 in Table E.16). More clearly, the damping ratio ζ_3 increased from 0.94% to 1.24% (A22 - A26 in Table E.2 and F16 - F20 in Table E.17). Hence, the identified SDOF human occupant model also explains, at least qualitatively, the influence of human occupants on the third mode of the test structure.

6.2.4 Response Time Histories

Finally, response time histories of the human-occupied structure and corresponding 2-DOF human-structure models were compared. For this purpose, responses of the test structure occupied by TS A sitting at TP 7 were used (B16 - B20). In particular, accelerations of the occupied structure at TP 7 to a burst random excitation at TP 7 were employed.

The measured accelerations contained contributions of several modes of vibration of the test structure. However, Human Models A and B, that shall here be verified further, correspond to the first or the second mode of the test structure only. Therefore, responses at frequencies around the first or second mode of the test structure were extracted by filtering using MATLAB (1999) routines. Responses of the corresponding 2-DOF human-structure models were computed to the same excitation. For this purpose, the empty test structure was represented by a SDOF model defined by the mean modal properties identified in experiments A17 - A21 (Tables E.1 to E.4).

Figures 6.10 and 6.11 demonstrate that the filtered experimental and computed response time histories are similar. Most importantly, the peak responses of experimentally and analytically estimated responses are very similar. This observation further confirms the validity of the identified SDOF human occupant model to represent not only groups of five but also single human occupants.

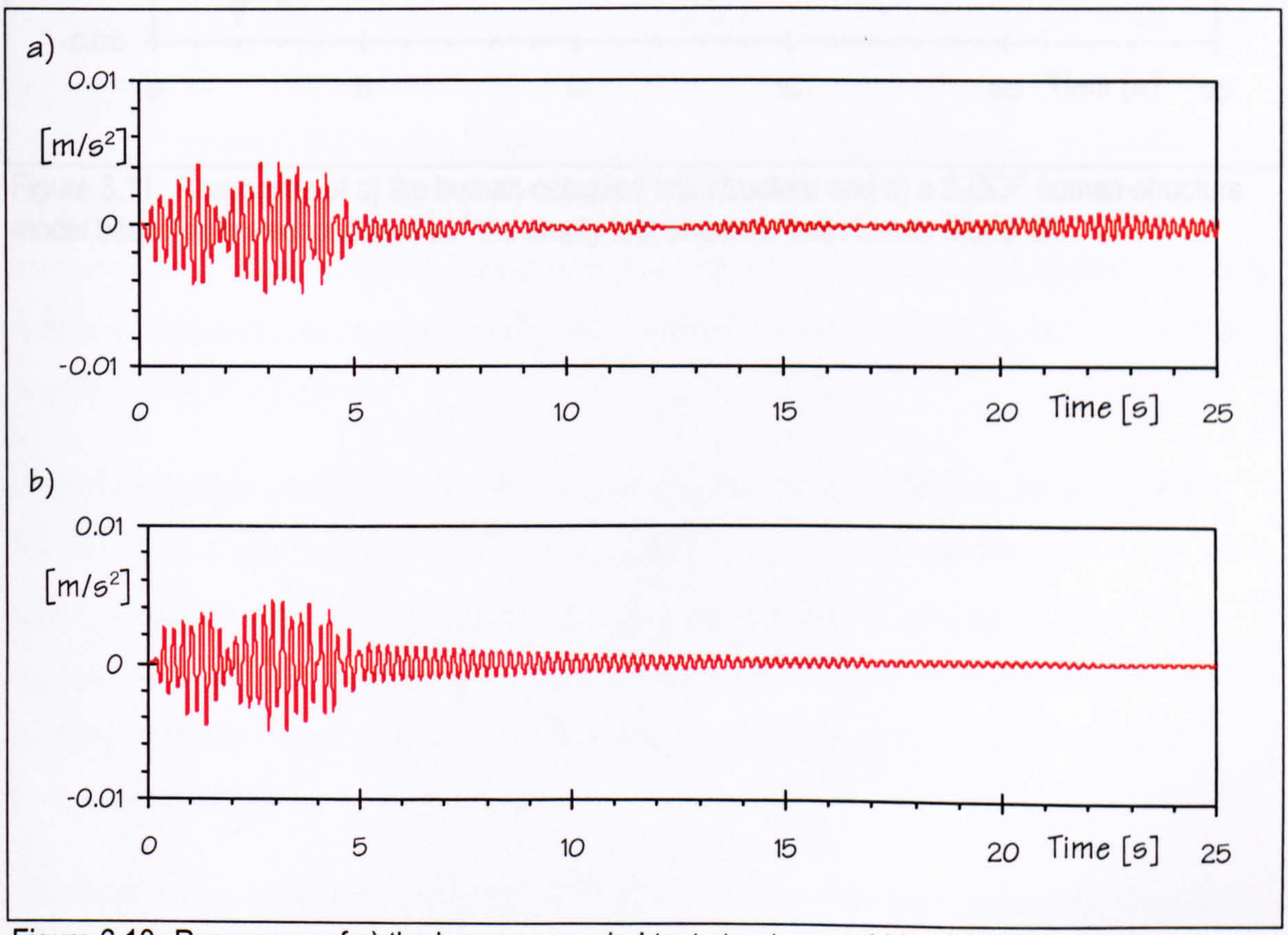

Figure 6.10: Responses of a) the human-occupied test structure and b) a 2-DOF human-structure model based on the first mode of the empty test structure and Human Model A*.

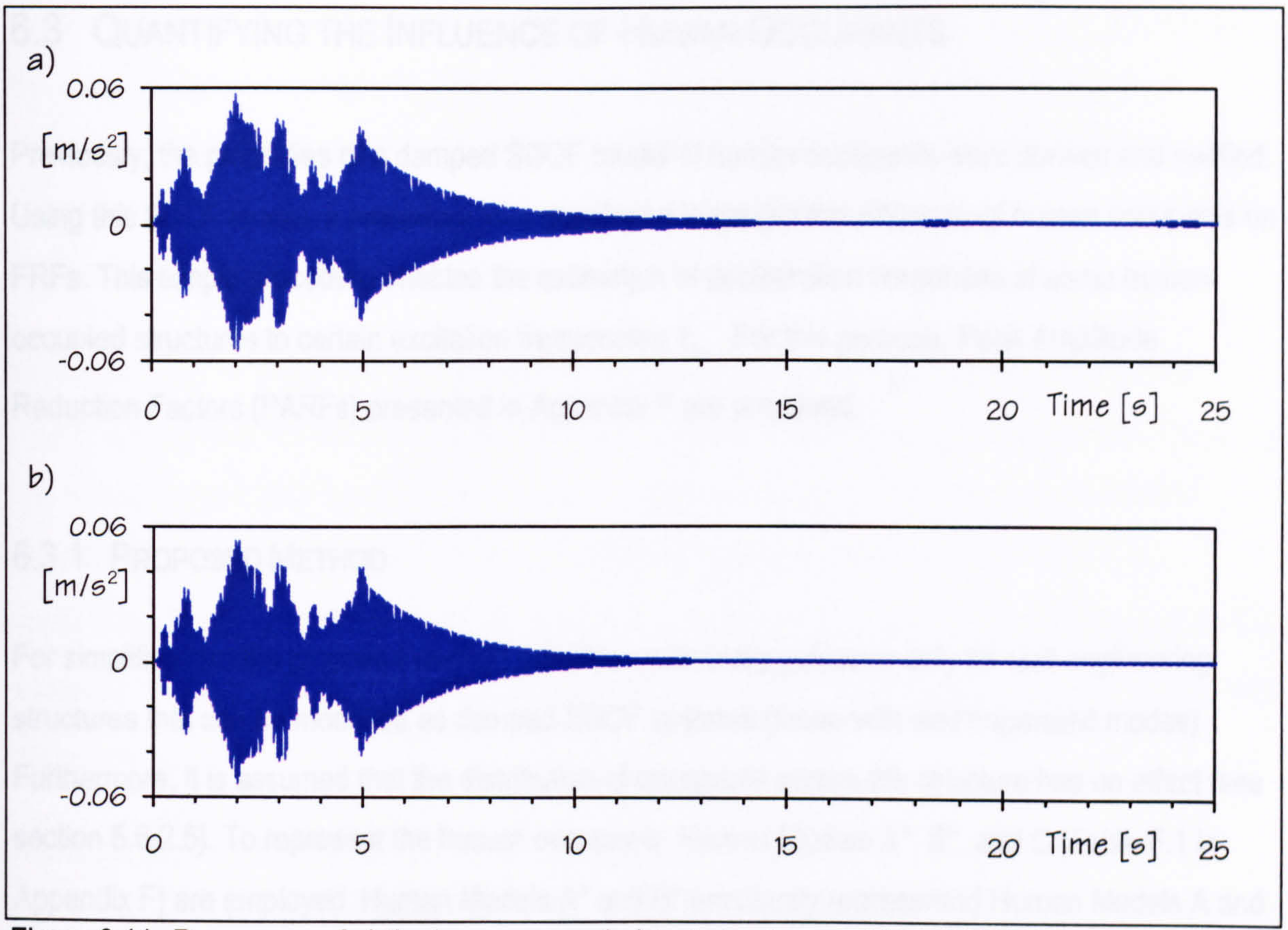

Figure 6.11: Responses of a) the human-occupied test structure and b) a 2-DOF human-structure model based on the second mode of the empty test structure and Human Model B*.

6.3 QUANTIFYING THE INFLUENCE OF HUMAN OCCUPANTS

Previously, the properties of a damped SDOF model of human occupants were derived and verified. Using this SDOF model, a procedure was developed to predict the influence of human occupants on FRFs. This simple procedure enables the estimation of acceleration responses of some human-occupied structures to certain excitation frequencies f_{EX}. For this purpose, Peak Amplitude Reduction Factors (PARFs) presented in Appendix F are proposed.

6.3.1 PROPOSED METHOD

For simplification, the proposed method provides preliminary guidance only for civil engineering structures that can be modelled as damped SDOF systems (those with well separated modes). Furthermore, it is assumed that the distribution of occupants across the structure has no effect (see section 5.6.2.5). To represent the human occupants, Human Models A*, B*, and C (Table F.1 in Appendix F) are employed. Human Models A* and B* previously represented Human Models A and B for illustration purposes only. However, PARFs (used in the proposed design procedure) computed using different sets of properties of Human Models A and B (Tables 6.3 and 6.4) are very similar across various sets of properties for Human Models A and B. Therefore, using only Human Models A* and B* is justified.

All these simplifications allow the human-occupied structure to be modelled as damped 2-DOF human-structure system (Figure 3.2b). The structural FRFs $A_{ss}(f)$ of this model and $A_s(f)$ of the SDOF structure model (sections 3.1.3.2 and 3.1.3.3) are employed to quantify the influence of human occupants. More specifically, the effect of human occupants on the magnitudes of the FRFs only is considered. For this purpose, the PARF (Peak Amplitude Reduction Factor) has been introduced and defined.

The PARF relates the magnitude $|A_{ss}(f_{EX})|$ of a 2-DOF model of the human-occupied structure to the magnitude $|A_s(f_s)|$ of a SDOF model of the empty structure:

$$PARF = \frac{|A_{ss}(f_{EX})|}{|A_s(f_s)|} = \frac{|A_{ss}(f_{EX})|}{a_s}. \qquad (6.2)$$

PARFs depend on the properties of the SDOF structure model. Furthermore, they are affected by the mass of human occupants in relation to the mass of the structure (α). Additionally, the properties of the human occupant model play a significant role. Appendix F presents PARFs corresponding to 36 different configurations. Half of these cases correspond to SDOF models of an empty structure with realistic damping ratios ζ_s = 1% and the other half to ζ_s = 2%.

An example will be presented here illustrating the identification of PARF. Figure 6.12 presents PARFs for cases of human occupation in which human occupants have only a small influence on the structure (α = 1%). Therefore, in this case, PARFs are close to unity (red) if the excitation frequency f_{EX} and the natural frequency f_s of the empty structure are similiar (Figure 6.12). Importantly, small (blue) PARFs indicate pairs of frequencies (f_{EX}, f_s) for which the response of the occupied structure at frequencies f_{EX} is lower than the response of the empty structure at its natural frequency f_s.

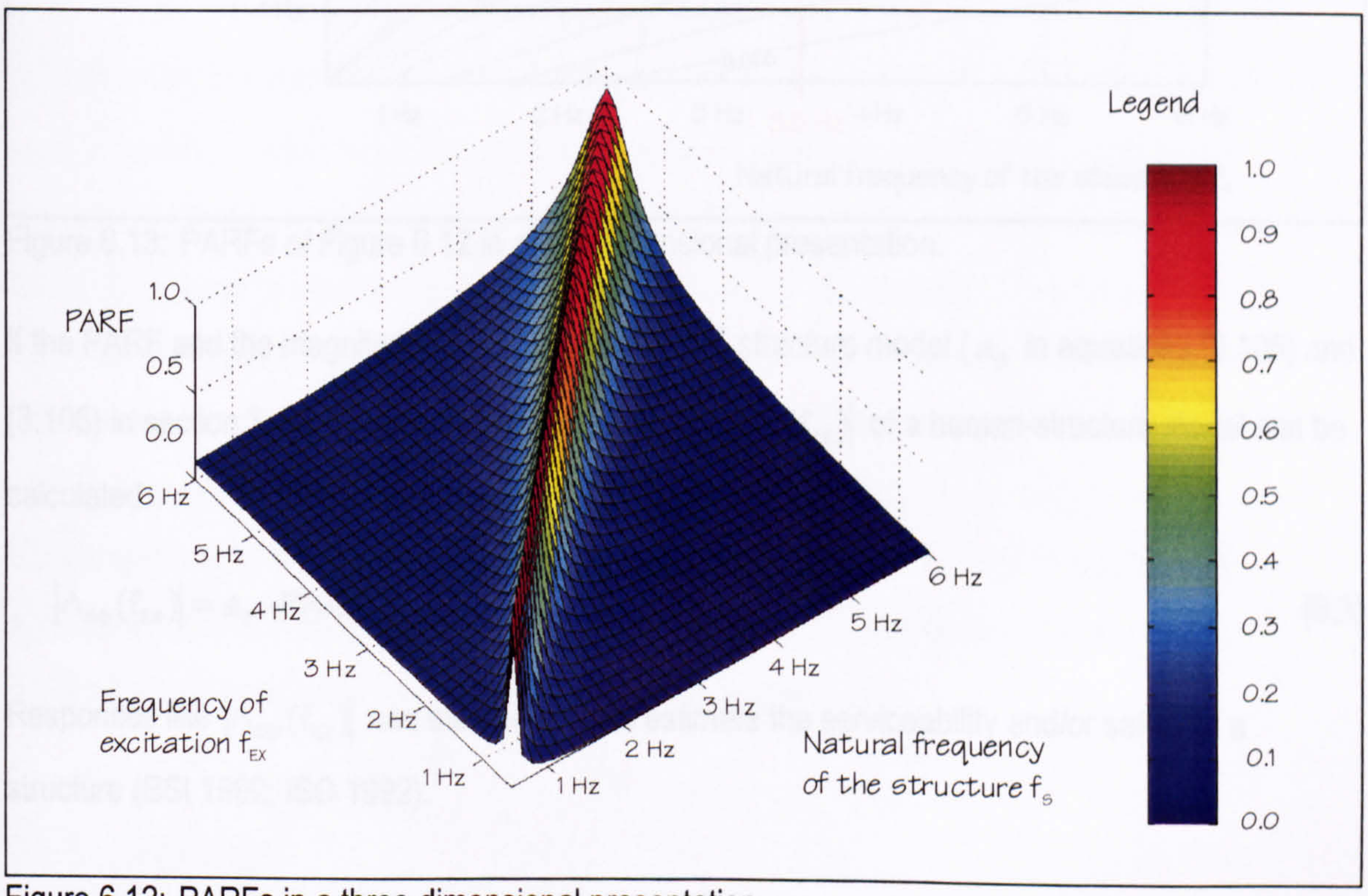

Figure 6.12: PARFs in a three-dimensional presentation.

Appendix F contains figures similar to Figure 6.13, which presents the same data as Figure 6.12, but only in the (f_{EX}, f_s) plane. To illustrate the proposed procedure, Figure 6.13 is used to extract a PARF. As an example, it was assumed that the empty structure has a natural frequency f_s of about

3.5 Hz and excitation frequencies f_{EX} range from 2.0 to 2.5 Hz. In this case, PARFs range from 0.05 to slightly above 0.1 (Figure 6.13).

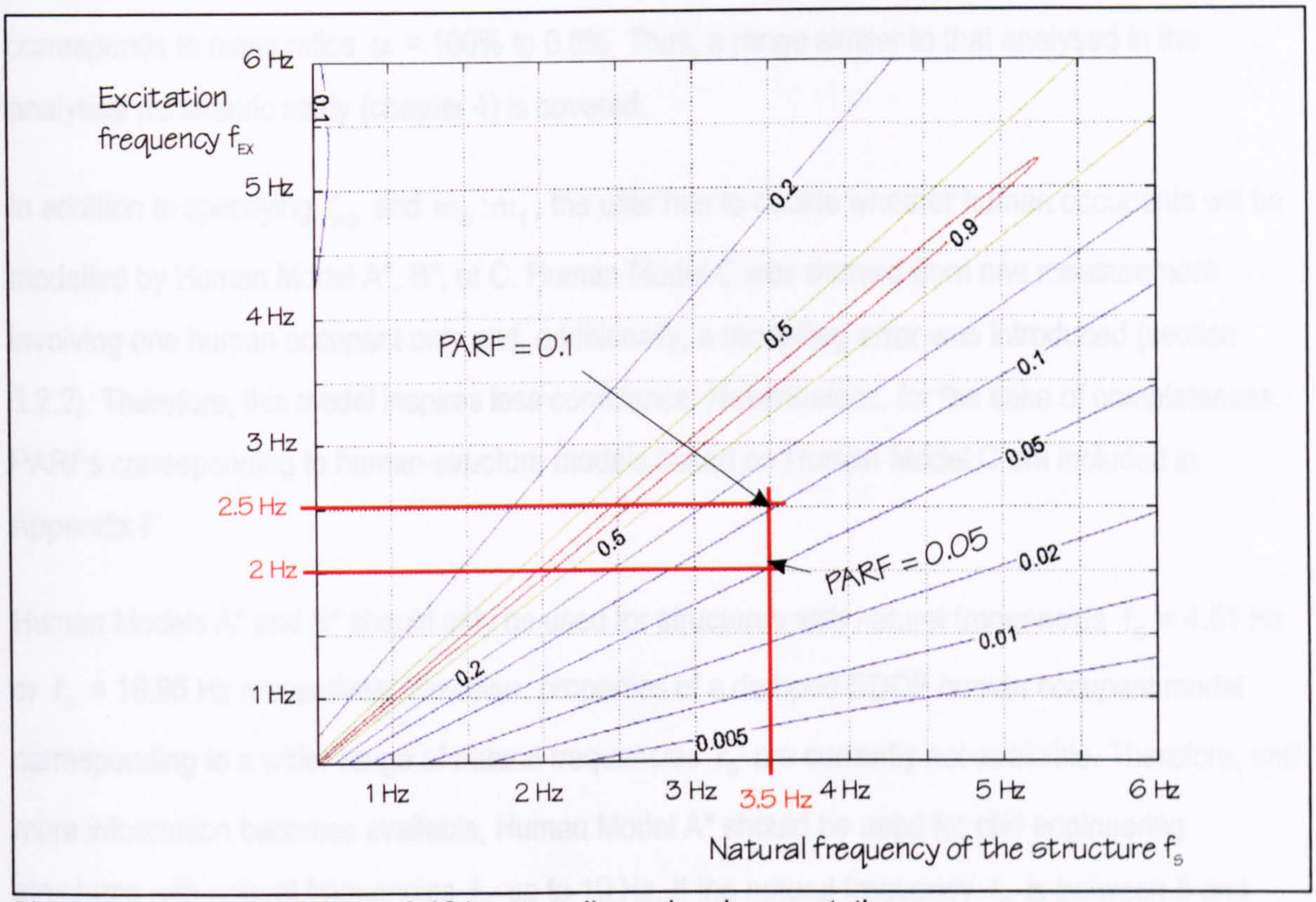

Figure 6.13: PARFs of Figure 6.12 in a two-dimensional presentation.

If the PARF and the magnitude $|A_s(f_s)|$ of the SDOF structure model (a_s in equations (3.105) and (3.106) in section 3.1.3.2) are known, the magnitude $|A_{ss}(f_{EX})|$ of a human-structure model can be calculated:

$$|A_{ss}(f_{EX})| = a_s \cdot PARF. \tag{6.3}$$

Responses like $|A_{ss}(f_{EX})|$ can then be used to estimate the serviceability and/or safety of a structure (BSI 1992; ISO 1992).

6.3.2 Implementation and Application

In Appendix F, different numbers of human occupants are studied. In particular $m_s : m_T$ ratios ranging from 1:1 to 100:1 were employed. The $m_s : m_T$ ratio relates the modal mass of the empty structure (m_s) to the total mass of the modelled occupants (m_T). In the experiments with five TSs

or one TS (at an antinode of the first, second, or third mode of the test structure) performed here, $m_S : m_T$ ratios ranged from about 20:1 to 120:1. Thus, the range employed in Appendix F (1:1 to 100:1) seems appropriate. Furthermore, it is noted that this range $m_S : m_T$ = 1:1 to 100:1 corresponds to mass ratios α = 100% to 0.8%. Thus, a range similar to that analysed in the analytical parametric study (chapter 4) is covered.

In addition to specifying ζ_S and $m_S : m_T$, the user has to decide whether human occupants will be modelled by Human Model A*, B*, or C. Human Model C was derived from one measurement involving one human occupant only and, additionally, a modelling error was introduced (section 6.2.2). Therefore, this model inspires less confidence. Nevertheless, for the sake of completeness, PARFs corresponding to human-structure models based on Human Model C are included in Appendix F.

Human Models A* and B* should only be used for structures with natural frequencies f_S = 4.51 Hz or f_S = 16.95 Hz respectively. However, properties of a damped SDOF human occupant model corresponding to a wider range of natural frequencies f_S are currently not available. Therefore, until more information becomes available, Human Model A* should be used for civil engineering structures with natural frequencies f_S up to 10 Hz. If the natural frequency f_S is between 8 and 10 Hz, it is recommended to use PARFs based on both Human Models A* and B* and investigate the possible differences produced by the application of the two occupant models. If the natural frequency f_S exceeds 10 Hz, only PARFs corresponding to Human Model B* should be used. Although structures with such high fundamental natural frequencies are unlikely to have relevant vibrations resulting from human-induced forces, human occupants can lead to a potentially significant lower 'additional' mode (Figure 2.1 and section 6.4). Therefore, Appendix F presents PARFs for structures with natural frequencies f_S as high as 20 Hz.

6.3.3 Discussion

In this section, the effects of (1) the natural frequency f_S of the SDOF model of the empty structure, (2) the properties of the human occupant model, and (3) the amount of human occupants on PARFs (and responses of the human-occupied structure) are discussed. For this purpose, Figure 6.14 is used.

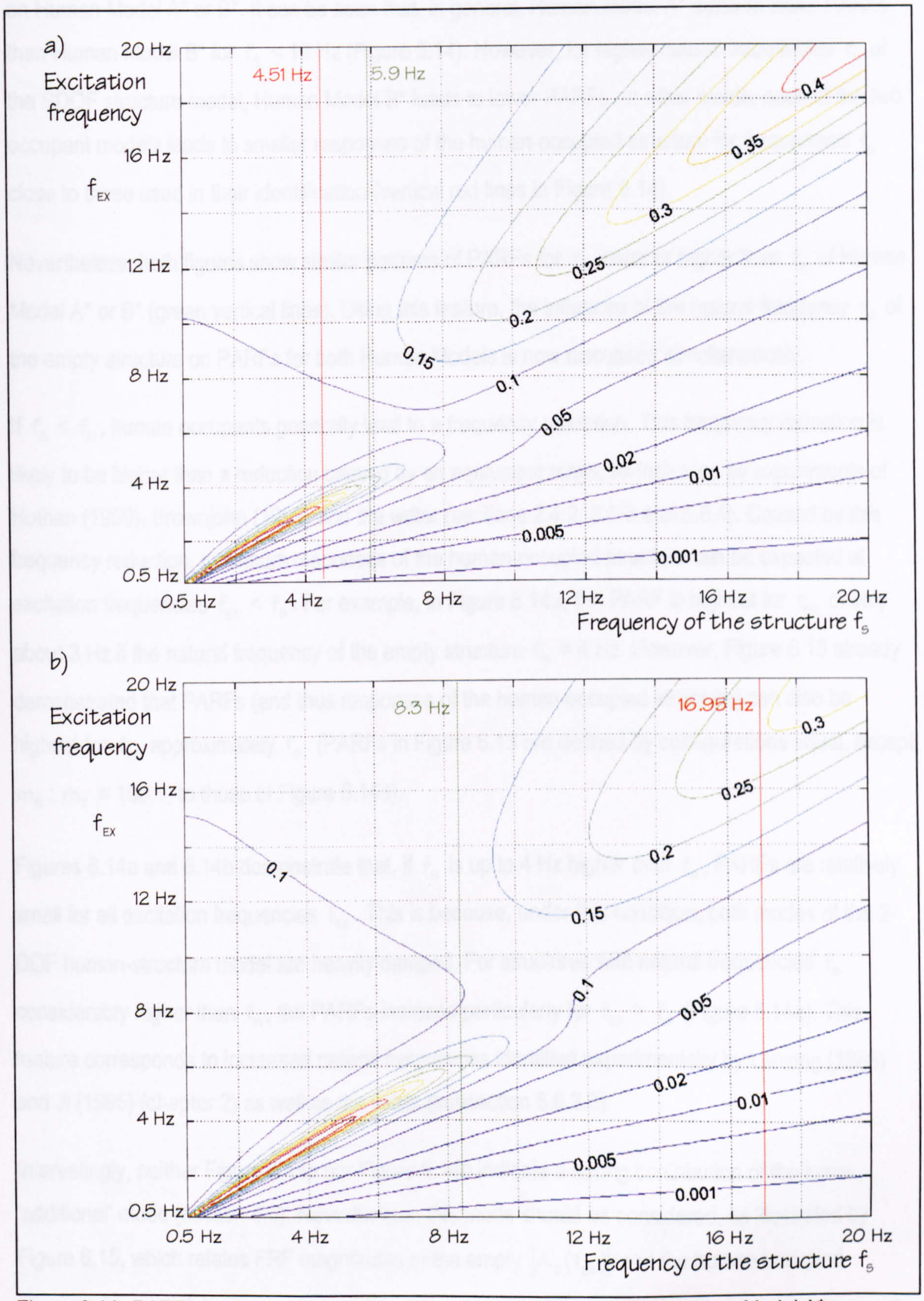

Figure 6.14: PARFs corresponding to $\zeta_s = 5\%$, $m_s : m_T = 1.5{:}1$, and a) Human Model A* (maximum PARF = 0.77) or b) Human Model B* (maximum PARF = 0.79). Legend as in Figure 6.12.

Figures 6.14a and 6.14b present PARFs corresponding to 2-DOF human-structures models based on Human Model A* or B*. It can be seen that, in general, Human Model A* leads to lower PARFs than Human Model B* for f_S < 10 Hz (Figure 6.14). However, for higher natural frequencies f_S of the SDOF structure model, Human Model B* leads to lower PARFs. In other words, each of the two occupant models leads to smaller responses of the human-occupied structure for frequencies f_S close to those used in their identification (vertical red lines in Figure 6.14).

Nevertheless, both figures show similar patterns of PARFs for f_S lower or higher than f_H of Human Model A* or B* (green vertical lines). Using this feature, the influence of the natural frequency f_S of the empty structure on PARFs for both Human Models is now discussed simultaneously.

If $f_S < f_H$, human occupants generally lead to a frequency reduction. This frequency reduction is likely to be higher than a reduction caused by an equivalent mass, as indicated by experiments of Hothan (1999), Brownjohn (1999) and the writer (sections 2.4.2, 2.4.3 and 5.6.4). Caused by this frequency reduction, maximum responses of the human-occupied structure can be expected at excitation frequencies $f_{EX} < f_S$. For example, in Figure 6.14a, the PARF is highest for f_{EX} of only about 3 Hz if the natural frequency of the empty structure f_S = 4 Hz. However, Figure 6.13 already demonstrated that PARFs (and thus responses of the human-occupied structure) can also be highest for f_{EX} approximately f_S. (PARFs in Figure 6.13 are defined by configurations equal, except $m_S : m_T$ = 100:1, to those of Figure 6.14a).

Figures 6.14a and 6.14b demonstrate that, if f_S is up to 4 Hz higher than f_H, PARFs are relatively small for all excitation frequencies f_{EX}. This is because, under this condition, both modes of the 2-DOF human-structure model are heavily damped. For structures with natural frequencies f_S considerably higher than f_H, the PARFs increase particularly for $f_{EX} > f_S$ (Figure 6.14a). This feature corresponds to increased natural frequencies identified experimentally by Lenzing (1988) and Ji (1995) (chapter 2) as well as the writer (subsection 5.6.3.3).

Interestingly, neither Figure 6.14a nor Figure 6.14b indicate a strong contribution of the lower 'additional' mode (section 4.6). Nevertheless, this mode should be considered, as illustrated by Figure 6.15, which relates FRF magnitudes of the empty $|A_S(f_{EX})|$ and the human-occupied structure $|A_{SS}(f_{EX})|$ for the same frequency f_{EX}. Figure 6.15 demonstrates that, for a structure with

a natural frequency f_s = 10 Hz, the magnitude of the human occupied structure $|A_{ss}(4\,Hz)|$ is 1.2 times the magnitude of the empty structure $|A_s(4\,Hz)|$ at the same frequency. This increase of the magnitude of the FRF due to human occupation corresponds to research by Folz and Foschi (1991), Ellis and Ji (1997), and Hothan (1999), who found that the lower 'additional' mode of the human-structure system can determine the response of the structure. Moreover, Figure 6.15, which corresponds to PARFs presented in Figure 6.14a, emphasises that human occupation can increase the response of a structure for frequencies f_{EX} below the natural frequency of the structure f_s.

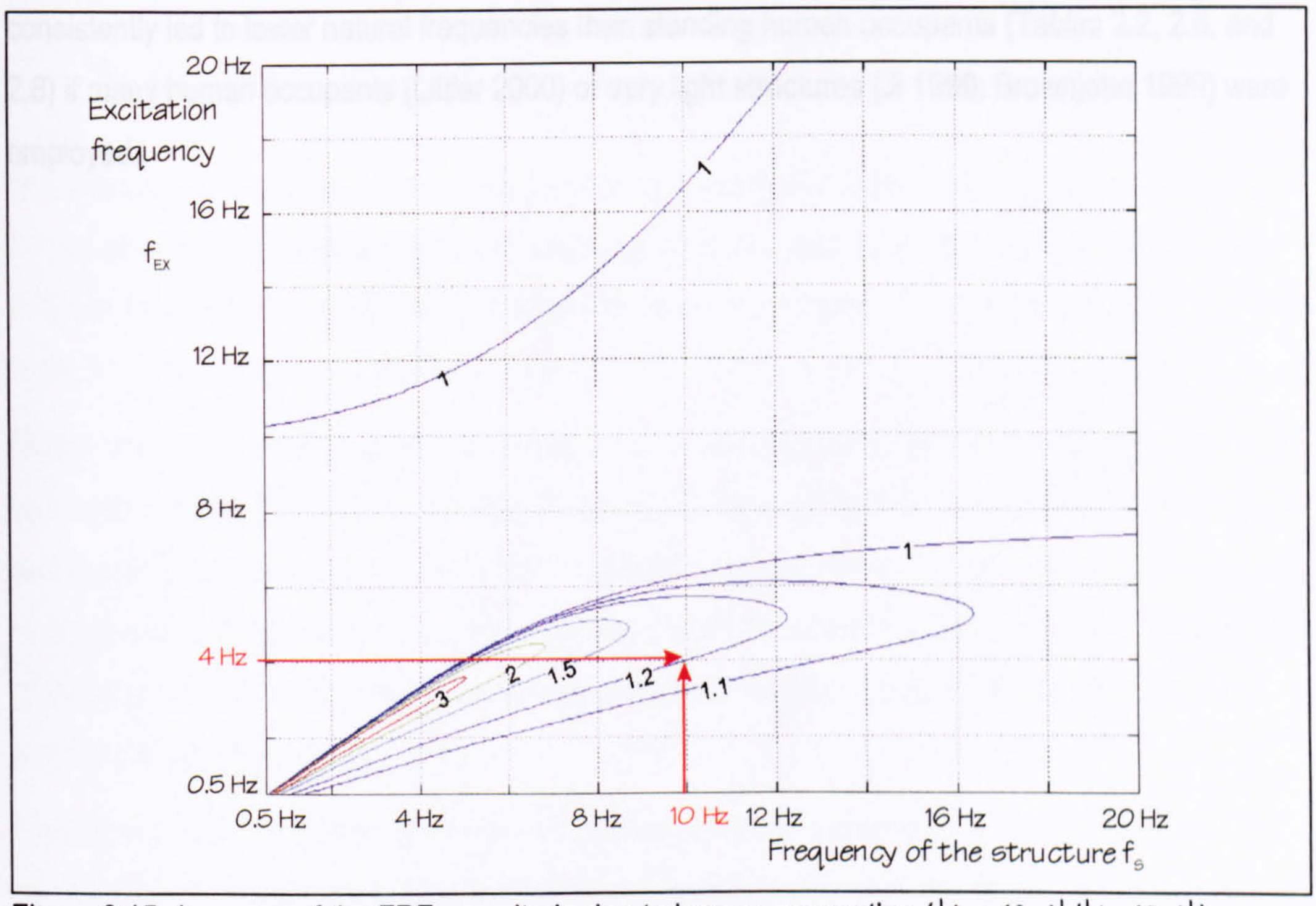

Figure 6.15: Increase of the FRF magnitude due to human occupation ($|A_{ss}(f_{EX})| / |A_s(f_{EX})|$).

6.3.4 Remarks

Current design guidelines request a dynamic analysis only if a structure has a natural frequency below 6 Hz (Department of National Heritage, Scottish Office 1997; IStructE 2001) or 8.4 Hz (BSI 1996). These values were defined by the ability of humans to excite structures with such low natural frequencies to vibrations that are serviceability or even safety issues.

In this context, it should be noted that, according to Kasperski (1996, p. 457), "an economic design in accordance to EC 1 will lead to natural frequencies between 2.5 to 3 Hz." If this is the case, newly built structures are likely to experience strong human-induced vibrations.

Finally, it has to be noted that there is a wide range of possible influence factors on the effect of human occupants. The posture of human occupants, for instance, can be a significant factor. Here, only properties of SDOF models of sitting human occupants were employed. However, if human occupants are standing, PARFs are likely to be higher as indicated by measurements of Brownjohn (1999) (section 2.4.3) and the writer (section 5.6.2.3). Furthermore, sitting human occupants consistently led to lower natural frequencies than standing human occupants (Tables 2.2, 2.6, and 2.8) if many human occupants (Littler 2000) or very light structures (Ji 1999; Brownjohn 1999) were employed.

7. CONCLUSIONS

This section presents conclusions drawn from the experimental research. It also informs about a derived human model and the influence of human occupants on civil engineering structures in general. It concludes with an approach proposed to account for the influence of human occupants in the design of human-occupied civil engineering structures.

7.1 EXPERIMENTAL RESEARCH

The influence of one to five human occupants on three vertical bending modes (4.5 Hz, 17 Hz, and 38 Hz) of a lightly damped test structure weighing 15 tonnes was estimated. For this purpose, nine FRFs of the empty and the human-occupied structure were acquired five times in nominally identical tests.

Modal properties (mode shapes, natural frequencies, damping ratios, and modal masses) were extracted from the FRFs by curve-fitting. This analysis revealed that mode shapes were almost real and identical for the empty and the human-occupied structure. However, human occupants noticeably affected modal masses, damping ratios, and natural frequencies. In general, the variability of these properties was higher for the human-occupied than for the empty test structure. This was most significant for damping ratios.

The experimental data demonstrated that the influence of human occupants increased with their number. It is also important to note that the influence of human occupants decreased with increasing natural frequency of the structure. Furthermore, it was found that the influence of human occupants increased with the mode shape amplitude at their location on the structure.

The influence of different postures (sitting and standing) of a human occupant on the modal properties of the human-occupied test structure were investigated. Although there seemed to be a systematic difference (indicated by damping ratios of the human-occupied structure), the experiments performed here did not confirm the significant effect of postures on natural frequencies of the occupied structure found by Littler (2000). Additionally, an effect of the studied small levels of vibration, as found in biomechanical research for higher levels of vibration, was not identified.

7.2 Modelling Human Occupants

Based on the experimental data, the properties of a damped SDOF model of sitting human occupants were identified. This SDOF model of an arbitrary number of occupants is characterised by a lumped mass m_H (as proportion of the total mass m_T of human occupants), a natural frequency f_H, and a damping ratio ζ_H. Importantly, these three parameters depend on the frequency f_s of the structural mode (4.51 or 16.95 Hz) the occupant model was related to. It was found that the mass m_H decreases with increasing frequency f_s. Also, the natural frequency f_H and the damping ratio ζ_H increase with increasing f_s. However, for natural frequencies $f_s \leq 16.95$ Hz, the approximate bands for the three key human modelling parameters are $m_H > 0.6\ m_T$, $f_H < 9$ Hz and $\zeta_H < 40\%$, approximately.

7.3 Influence of Human Occupants

Modelling the human-occupied structure as a damped 2-DOF human-structure system explained the influence of human occupants on natural frequencies, damping ratios and FRFs, and the responses of the human-occupied structure observed in this and all other research known to the writer.

In general, if only a few people occupy a civil engineering structure, they have little effect on natural frequencies of the structure but can increase damping significantly. Therefore, including their influence leads to a more realistic and economic design. However, although increasing damping, crowds can reduce fundamental frequencies significantly which could make structures more responsive to human-induced vibrations. Therefore, the influence of crowds on slender structures should be included into the design against human-induced vibrations. This might be necessary for structures with natural frequencies as high as 20 Hz if lively crowds are involved.

7.4 Preliminary Design Guideline

An analytical parametric study demonstrated that FRFs provide better information of the influence of human occupants on the structure than modal properties. This feature was employed to propose a procedure to quantify the influence of human occupants. The proposed procedure is limited to point-accelerances of structures with well-separated modes. Despite this and other limitations, the procedure is a valuable and relatively simple method for assessing the possible influence of human occupants particularly on assembly structures.

8. RECOMMENDATIONS FOR FUTURE WORK

It is recognised that the whole area of human-induced vibrations requires further research to enable a better understanding and more realistic and economical design. Concentrating on the influence of human occupants on civil engineering structure as one aspect of human-structure interaction, four major areas requiring further research are highlighted:

(1) Well documented high-quality investigations of the dynamic behaviour of real-life civil engineering structures, particularly assembly structures, are required. Such investigations should include high- and low-frequency assembly structures alike. Thereby, the influence of human occupants should be quantified and attention should be paid not only to vertical but also to horizontal modes. Furthermore, the day-to-day performance of human-occupied structures under human-induced vibrations should be monitored and evaluated. This procedure will help to identify actually occurring issues.

(2) The human body is a complex heavily damped dynamic system. Establishing the relevance of factors influencing the properties of human occupants for practical civil engineering applications requires further research. In particular, differences between a wider range of individuals should be evaluated and the effect of posture should be investigated further. Furthermore, the influence of the type, duration, and level of vibration require further investigation.

(3) In this research, the properties of a damped SDOF model of sitting human occupants corresponding to vertical structural modes with natural frequencies of about 4.5 Hz and 17 Hz was identified. However, a significantly wider range of experiments on structures with other natural frequencies is required to confirm and identify further properties of the damped SDOF occupant model and, possibly, extend it into a more realistic MDOF model.

(4) Combining experimental and analytical research, the use of SDOF occupant models in context with complex FE-models and detailed dynamic design of civil engineering structures should be explored.

REFERENCES

Al-Foqaha'a, A.A. (1997). *Design criterion for wood floor vibrations via finite element and reliability analyses.* Thesis (PhD). Washington State University, Pullman, USA.

Allen, D.L. (1974). Vibrational behaviour of long-span floor slabs. *Canadian Journal of Civil Engineering*, 1 (1), 108-115.

Allen, D.E. and Rainer, J.H. (1975). *Floor vibration.* Ottawa, Canada: Division of Building Research, NRCC. Canadian Building Digest (CBD) 173.

Allen, D.E., Onysko, D.M., and Murray, T.M. (1999). *ATC Design guide 1: Minimizing floor vibration.* Redwood City, Canada: Applied Technology Council (ATC).

Allen, G. (1978). Part II: A critical look at biodynamic modelling in relation to specifications for human tolerance of vibration and shock. In: *AGARD Conference Proceedings.* A25-5 to A25-15.

Anonymous (2001). News: Wobbly bridge syndrome is not new, says Arup. *New Civil Engineer (Institution of Civil Engineers (ICE))*, 7 June, 2001, 6.

APS Dynamics (1996a). *Instruction manual: Dual-Mode Model 114-EP Amplifier.* Carlsbad, California, USA: APS Dynamics, Incorporation.

APS Dynamics (1996b). *Instruction manual: Electro-Seis Model 113 Shaker.* Carlsbad, California, USA: APS Dynamics, Incorporation.

Argyris, J. and Mlejnek, H.-P. (1991). *Dynamics of structures.* Amsterdam, The Netherlands: Elsevier Science.

ASA (1932). Horizontal forces produced by movements of the occupants of a grandstand. *American Standards Association (ASA) Bulletin*, 123-126.

Bachmann, H. (1992). Vibration upgrading of gymnasia, dance halls, and footbridges. *Structural Engineering International (International Association for Bridge and Structural Engineering (IABSE))*, 2 (2), 118-124.

Bachmann, H., Ammann, W.J., Deischl, F., Eisenmann, J., Floegl, I., Hirsch, G.H., Klein, G.K., Lande, G.J., Marenholtz, O., Natke, H.G., Nussbaumer, H., Pretlove, A.J., Rainer, J.H.,

Saemann, E.-U., and Steinbeisser, L. (1995). *Vibration problems in structures: Practical guidelines*. Basel, Switzerland: Birkhäuser Verlag.

Batista, R.C. and Magluta, C. (1993). Spectator-induced vibration of Maracanã stadium. In: Moan, T., et al. (eds.). *Eurodyn'93, Trondheim, Norway, 21-23 June, 1993*. Rotterdam, The Netherlands: A.A. Balkema. Vol. 2, 985-992.

Baumann, K. and Bachmann, H. (1988). *Durch Menschen verursachte dynamische Lasten und deren Auswirkungen auf Balkentragwerke (Man-induced dynamic loads and their influence on beam structures)*. Zürich, Switzerland: Institute of Structural Engineering (IBK), Swiss Federal Institute of Technology (ETH). Report No. 7501-3. (in German)

Bendat, J.S. and Piersol, A.G. (1993). *Engineering applications of correlation and spectral analysis*. Second edition. New York, USA: John Wiley and Sons.

Bennett, R.M. and Swensson, K. (1997). Spectator live loads during football games. *Journal of Structural Engineering (American Society of Civil Engineers (ASCE))*, 123 (11), 1545-1547.

Beranek, L.L. (1988). *Noise and vibration contol*. Washington D.C., USA: Institute of Noise Control Engineering.

Beyer, K., Luz, E., and Klein, E. (1995). Schwingungsfragen bei der Seerheinbrücke Konstanz (Dynamic problems of the Seerhein bridge in Constance). *Bauingenieur*, 70, 443-446. (in German)

Bishop, N.W.M., Willford, M., and Pumphrey, R. (1993). Multi-person excitation of modern slender staircases. In: Smith, R.A. and Dickie, J.F. (eds.). *Engineering for crowd safety, London, UK, 17-18 March, 1993*. Amsterdam, The Netherlands: Elsevier Science. 399-408.

Boileau, P.-É. and Rakheja, S. (1998). Whole-body vertical biodynamic response characteristics of the seated vehicle driver: Measurement and model development. *International Journal of Industrial Ergonomics*, 22 (6), 449-472.

Boileau, P.-É., Wu, X., and Rakheja, S. (1998). Definition of a range of idealized values to characterize seated body dynamic response under vertical vibration. *Journal of Sound and Vibration*, 215 (4), 841-862.

Boileau, P.- É., Rakheja, S., Yang, X., and Stiharu, I. (1996). Comparison of biodynamic response characteristics of various human body models as applied to seated vehicle drivers. In: *UK Informal Group Meeting on Human Response to Vibration, Nuneaton, UK, 18-20 September, 1996.*

Bronstein, I.N., Semendjajew, K.A., and Grosche, G. (1996). *Teubner-Taschenbuch der Mathematik, Teil 1*. Zeidler, E. (ed.). Stuttgart, Germany: Teubner. (Handbook of Mathematics, Part I.) (in German)

Brownjohn, J.M.W. (1999). Energy dissipation in one-way slabs with human participation. In: *Proceedings of the Asia-Pacific Vibration Conference '99, Nanyang Technological University, Singapore, 11-13 December, 1999*. Vol. 1, 155-160.

Brownjohn, J.M.W. (2001). Energy dissipation from vibrating floor slabs due to human-structure interaction. *Shock and Vibration*, 8 (6), 315-323.

BSI (1987). BS 6841:1987. *British Standard guide to measurement and evaluation of human exposure to whole-body mechanical vibration and repeated shock.* Milton Keynes, UK: BSI.

BSI (1992). BS 6472:1992. *Guide to evaluation of human exposure to vibrations in buildings (1 Hz to 80 Hz).* London, UK: BSI.

BSI (1996). BS 6399: Part 1: 1996. *Loading for buildings. Part 1: Code of practice for dead and imposed loads.* London, UK: BSI.

Canisius, T.D.G. (2000). Towards a statistical human body model for determining jump dynamic forces. In: Virdi, K.S., et al. (eds.). *Abnormal loading on structures*. London, UK: E & FN Spon.

Canisius, T.D.G., Bougard, A.J., and Ellis, B.R. (1998). Performance of timber scaffold boards under human jump loads. *Proceedings of the ICE: Structures and Buildings*, 128 (4), 332-341.

Clark, R.L., Wicks, A., and Becker, W.J. (1989). Effects of an exponential window on the damping coefficient. In: *7th International Modal Analysis Conference (IMAC), Las Vegas, USA, 30 January - 2 February, 1989*. Vol. 1, 83-68.

Clough, R.W. and Penzien, J. (1993). *Dynamics of structures*. Second edition. New York, USA: McGraw-Hill.

Coermann, R.R. (1962). The mechanical impedance of the human body in sitting and standing position at low frequencies. *Human factors*, (4), 227-253.

Curtis, J. (2001). Letter: Pedestrians can contribute to lock-in. *New Civil Engineer (ICE)*, 8 March, 2001, 18.

Dallard, P., Fitzpatrick, T., Flint, A., Low, A., Ridsill-Smith, R., and Willford, M. (2000). Technical update: Pedestrian induced vibration of footbridges. *The Structural Engineer (IStructE)*, 78 (23/24), 13-15.

Dally, J.W. (1993). Statistical analysis of experimental data. In: Kobayashi, A.S. (ed.). *Handbook on experimental mechanics*. Englewood Cliffs, New Jersey, USA: Prentice-Hall.

Data Physics (1998). *Making measurements with SignalCalc 430*. DP430Win-42 Rev. 2.0. San Jose, California, USA: Data Physics Corporation.

Data Physics (1999). *SignalCalc 430 Dynamic signal analyser: Getting started*. DP430Win-42A Rev. 1.0. San Jose, California, USA: Data Physics Corporation.

Department of National Heritage, Scottish Office (1997). *Guide to safety at sports grounds (Green Guide)*. Fourth edition. London: The Stationary Office.

DTA (1993). *Handbook on guidelines to best practice, Vol. 1 - Instrumentation*. Cranfield, UK: Dynamic Testing Agency (DTA).

Ebrahimpour, A. and Fitts, L.L. (1996). Measuring coherency of human-induced rhythmic loads using force plates. *Journal of Structural Engineering (ASCE)*, 122 (7), 829-831.

Ebrahimpour, A. and Sack, R.L. (1992). Design live loads for coherent crowd harmonic movements. *Journal of Structural Engineering (ASCE)*, 118 (4), 1121-1136.

Ebrahimpour, A., Sack, R.L., and van Kleek, P.D. (1989). Computing crowd loads using a nonlinear equation of motion. In: *Proceeding of the 4th International Conference on Civil and Structural Engineering*. Vol. 2, 47-52.

Eibl, J. and Rösch, R. (1990). Schwingungsprobleme in einem Fußballstadion (Vibrational problems in a sports arena). *Bauingenieur*, 65, 307-311. (in German)

Ellis, B.R. and Ji, T. (1997). Human-structure interaction in vertical vibrations. *Proceedings of the ICE: Structures and Buildings*, 122 (1), 1-9.

Ellis, B.R., Ji, T., and Littler, J.D. (1994a). Crowd actions and grandstands. In: *Symposium: Places of Assembly and Long-Span Building Structures, Birmingham, UK, 7-9 September, 1994*. Zürich, Switzerland: IABSE. IABSE Report 71, 277-282.

Ellis, B.R., Ji, T., and Littler, J.D. (1994b). The response of grandstands to dynamic forces induced by crowds. *Australasian Structural Engineering Conference, Sydney, Australia, 21-23 September, 1994.*

Endevco (1996). *Instruction manual Model 2793 16-channel ISOTRON signal conditioner.* San Juan Capistrano, California, USA: Endevco Corporation.

Eriksson, P.-E. (1994). *Vibration of low-frequency floors - dynamic forces and response reduction.* Thesis (PhD). Chalmers University of Technology, Gothenburg, Sweden.

Ewins, D.J. (2000). *Modal testing: Theory and practice*. Second edition. Baldock, UK: Research Studies Press.

Eyre and Cullington (1985). *Human tolerance levels for bridge vibration*. Harmondsworth, UK: Ministry of Transport, Department of Transport and Road Research Laboratory (TRRL), Road Research Laboratory. Report No. 18.

Fairley, T.E. and Griffin, M.J. (1989). The apparent mass of the seated human body: Vertical vibration. *Journal of Biomechanics*, 22 (2), 81-94.

Fairley, T.E. and Griffin, M.J. (1990). The apparent mass of the seated human body in the fore-and-aft and lateral directions. *Journal of Sound and Vibration*, 139 (2), 299-306.

Falati, S. (1999). *The contribution of non-structural components to the overall dynamic behaviour of concrete floor slabs*. Thesis (PhD). University of Oxford, Oxford, UK.

Farah, A. (1977). *Human response: A criterion for the assessment of structural serviceability.* Thesis (PhD). University of Waterloo, Ontario, Canada.

Fitzpatrick, T. (2001). *Linking London: The Millennium Bridge*. London, UK: Royal Academy of Engineering.

Fladung, W. and Rost, R. (1997). Application and correction of the exponential window for frequency response functions. *Mechanical Systems and Signal Processing*, 11 (1), 23-36.

Folz, B. and Foschi, R.O. (1991). Coupled vibrational response of floor systems with occupants. *Journal of Engineering Mechanics (ASCE)*, 117 (4), 872-892.

Foschi, R.O. and Gupta, A. (1987). Reliability of floors under impact vibration. *Canadian Journal of Civil Engineering*, 14 (5), 683-689.

Foschi, R.O., Neumann, G.A., Yao, F., and Folz, B. (1995). Floor vibration due to occupant and reliability-based design guidelines. *Canadian Journal of Civil Engineering*, 22 (3), 471-479.

Friswell, M.I. and Mottershead, J.E. (1995). *Finite element model updating in structural dynamics.* Dordrecht, The Netherlands: Kluwer Academic Publishers.

Fujino, Y., Pacheo, B.M., Nakamura, S.-I., and Warnitchai, P. (1993). Synchronisation of human walking observed during lateral vibration of a congested pedestrian bridge. *Earthquake Engineering and Structural Dynamics*, 22 (9), 741-758.

Galbraith, F.W. and Barton, M.V. (1970). Ground loading from footsteps. *Journal of the Acoustic Society of America*, 48 (5, part 2), 1288-1292.

Gerasch, W.-J. (1990). Reduzierung von beim Tanzen erzeugten Bauwerksschwingungen durch Schwingungstilger (Vibration absorbers for the reduction of human induced vibrations). *Bauingenieur*, 65, 313-318. (in German)

Ginsberg, J.H. (2001). *Mechanical and structural vibrations: Theory and applications*. New York, USA: Wiley and Sons.

Griffin, M.J. (1990). *Handbook of human vibration*. London, UK: Academic Press.

Grundmann, H. and Schneider, M. (1990). Stochastic representation of footbridge vibrations taking into account feedback effects. In: Krätzig. W.B., et al. (eds.). *Eurodyn'90, Bochum, Germany, 5-7 June, 1990*. Rotterdam, The Netherlands: A.A. Balkema. Vol. 2, 623-630.

Grundmann, H., Kreuzinger, H. and Schneider, M. (1993). Schwingungsuntersuchungen für Fußgängerbrücken (Dynamic calculations of footbridges). *Bauingenieur*, 68, 215-225. (in German)

Hamam, A.S. (1994). *Measuring and modeling dynamic loads imposed by moving crowds*. Thesis (PhD). University of Oklahoma, Norman, USA.

Harte, R. and Meskouris, H. (1991). Menscheninduzierte Schwingungen im Gelsenkirchener Parkstadion: Messungen und Tragfähigkeitsanalyse. In: *Vibrationen: Ursachen, Messung, Analyse und Maßnahmen*. Zürich, Switzerland: Swiss Society of Engineers and Architects (SIA). Document D079, 19-24. (Human-induced vibrations at Gelsenkirchen Parkstadion: Measurements and stability analysis.) (in German)

Hinz, B. and Seidel, H. (1987). The non-linearity of the human body's dynamic response during sinusoidal whole body vibration. *Industrial Health*, 25 (4), 169-181.

Holmlund, P. (1999). Absorbed power and mechanical impedance of the seated human measured within a real vehicle environment compared with single axis laboratory data. *Journal of Low Frequency Noise, Vibration and Active Control*, 18 (3), 97-110.

Holmlund, P., and Lundström, R. (1998). Mechanical impedance of the human body in the horizontal direction. *Journal of Sound and Vibration*, 215 (4), 801-812.

Holmlund, P., Lundström, R., and Lindberg, L. (1995). Whole-body vibration: Mechanical impedance of human body in the vertical direction. In: *UK Informal Group Meeting on Human Response to Vibration, Silsoe, UK, 18-20 September, 1995.*

Holmlund, P., Lundström, R., and Lindberg, L. (2000). Mechanical impedance of the human body in vertical direction. *Applied Ergonomics*, 31 (4), 415-422.

Hothan, S. (1999). *Einfluß der Verkehrslast – Mensch – auf das Eigenschwingungsverhalten von Fußgängerbrücken und die Auslegung linearer Tilger.* Thesis (Dipl.-Ing.). Universität Hannover, Hanover, Germany. (The influence of man on free vibration properties of footbridges and the design of linear tuned mass dampers.) (in German)

Hunt, J.B. (1979). *Dynamic vibration absorbers.* London, United Kingdom: Mechanical Engineering Publications.

ICATS (2000a). *MODENT suite: A guided tour.* London, UK: ICATS.

ICATS (2000b). *MODENT, MODESH, MESHGEN, MODPLAN users guide*. London, UK: ICATS.

Inman, D.J. (2001). *Engineering vibration*. Second edition. Upper Saddle River, New Jersey, USA: Prentice-Hall.

ISO (1981). ISO 5982:1981. *Vibration and shock - Mechanical driving point impedance of the human body*. Geneva, Switzerland: International Organization for Standardization (ISO).

ISO (1987). ISO 7962:1987 (E). *Mechanical vibration and shock – Mechanical transmissibility of the human body in the z direction.* Geneva, Switzerland: ISO.

ISO (1989). ISO 2631-2:1989 (E). *Mechanical vibration and shock – Evaluation of human exposure to whole-body vibration - Part 2: Vibration in buildings (1 Hz to 80 Hz).* Geneva, Switzerland: ISO.

ISO (1992). ISO 10137. *Basis for the design of structures - Serviceability of buildings against vibration.* Geneva, Switzerland: ISO.

ISO (2001). ISO 5982:2001 (E). *Mechanical vibration and shock – Range of idealized values to characterize seated-body biodynamic response under vertical vibration.* Geneva, Switzerland: ISO.

IStructE (2001). *Dynamic performance requirements for permanent grandstands subjected to crowd action: Interim guidance for assessment and design*. London, UK: IStructE/DTLR/ Department

of Culture, Media and Sport (DCMS) Working Group on Dynamic Performance and Design of Stadia Structures and Seating Decks.

James, G., Burley, D., Clements, D., Dyke, P., Searl, J., and Wright, J. (1999). *Advanced modern engineering mathematics*. Second edition. Harlow, UK: Addison-Wesley.

Ji, T. (1995). A continuous model for the vertical vibration of the human body in a standing position. In: *UK Informal Group Meeting on Human Response to Vibration, Silsoe, UK, 18-20 September, 1995.*

Ji, T. (2000). On the combination of structural dynamics and biodynamics methods in the study of human-structure interaction. In: *UK Informal Group Meeting on Human Response to Vibration, Southampton, UK, 13-15 September, 2000*. 183-194.

Ji, T. and Ellis, B.R. (1994). People - A passive vibration control mechanism? In: Housner, G.W., Masri, S.F., and Chassiakos, A.G. (eds.). *The First World Conference on Structural Control. Los Angeles, USA, 3-5 August, 1994*. Los Angeles, California, USA: International Association for Structural Control. Vol. 3, FA2-63 to FA2-72.

Ji, T. and Ellis, B.R. (1995). Human actions on structures. *The Society for Earthquake Engineering and Civil Engineering Dynamics (SECED) Newsletter (ICE)*, Autumn, 4-5.

Ji, T. and Ellis, B.R. (1997). Floor vibrations induced by human movements in buildings. In: Lee, P.K.K. (ed.). *Structures in the new millennium: Proceedings of the 4th International Kerensky Conference, Hong Kong, 3-5 September, 1997*. Rotterdam, The Netherlands: A.A. Balkema Publishers. 213-219.

Ji, T. and Ellis, B.R. (1999). Human whole-body models in structural vibration. *The 13th ASCE Engineering Mechanics Conference, Baltimore, USA, 13-16 June, 1999.*

Kasperski, M. (1996). Actual problems with stand structures due to spectator-induced vibrations. In: Augusti, G., et al. (eds.). *Eurodyn'96, Florence, Italy, 5-8 June, 1996*. Rotterdam, The Netherlands: A.A. Balkema Publishers. 455-461.

Kasperski, M. (2001). Menschenerregte Schwingungen in Sportstadien (Men-induced vibrations in sport stadiums). *Bauingenieur*, 76, 575-581. (in German)

Kasperski, M. and Niemann, H.J. (1993). Man induced vibrations of a stand structure. In: Moan, T., et al. (eds.). *Eurodyn'93, Trondheim, Norway, 21-23 June, 1993*. Rotterdam, The Netherlands: A.A. Balkema Publishers. 977-983.

Kerr, S.C. (1998). *Human induced loading on staircases*. Thesis (PhD). University College London, London, UK.

Korenev, B.G. and Reznikov, L.M. (1993). *Dynamic vibration absorbers: Theory and technical applications*. Chichester, UK: John Wiley and Sons.

Lee, R.A. and Pradko, F. (1968). Analytical analysis of human vibration. In: *Automotive Engineering Congress, Detroit, Michigan, USA, 8-12 January, 1968*. Society of Automotive Engineers. Paper 680091.

Lenzen, K.H. (1966). Vibration of steel joist-concrete slab floors. *American Institute of Steel Construction (AISC) Engineering Journal*, 3 (July), 133-136.

Lenzing, H. (1988). *Durch Menschen induzierte Schwingungen*. Thesis (Dipl.-Ing.). Universität Hannover, Hanover, Germany. (Human-induced vibrations.) (in German)

Littler, J.D. (1998). Full-scale testing of large cantilever grandstands to determine their dynamic response. In: Thompson, P.D., Tolloczko, J.J.A. and Clarke, J.N. (eds.). *Stadia, arenas and grandstands*. London: E and FN Spon. 123-134.

Littler, J.D. (2000). *Retractable grandstands: Dynamic response*. Watford, UK: Building Research Establishment (BRE). Information Paper 4/00.

Lundström, R. and Holmlund, P. (1998). Absorption of energy during exposure to whole-body vibration exposure. *Journal of Sound and Vibration*, 214 (4), 789-799.

Lundström, R., Holmlund, P., and Lindberg, L. (1995). Absorption of energy during exposure to whole-body vibration. In: *UK Informal Group Meeting on Human Response to Vibration, Silsoe, UK, 18-20 September, 1995.*

Lundström, R., Holmlund, P., and Lindberg, L. (1998). Absorption of energy during vertical whole-body vibration exposure. *Journal of Biomechanics*, 31 (4), 317-326.

Luza, G. (1997). *Personeninduzierte Schwingungen von biege- und torsionssteifen, gedämpften Brücken (Human- induced vibrations of damped bridges that are stiff in bending and torsion).* Thesis (PhD). Technische Universität Wien, Vienna, Austria. (in German)

Maia, M.M., Silva, J.M.M., He, J., Lieven, N.A.J., Lin, R.M., Skingle, G.W., To, W.-M., and Urgueira, A.P.V. (1997). *Theoretical and experimental modal analysis*. Baldock, UK: Research Studies Press.

Manheim, D. and Honeck, W. (1987). A case study of spectator induced vibrations. In: Hall, J.R. (ed.). *Use of vibration measurements in structural evaluation, Atlantic City, New Jersey, USA, 29 April, 1987*. New York, USA: ASCE. 1-15.

Mann, W. (1979). Stoßkräfte aus fallenden Lasten und Personen und dadurch verursachter Bruch eines Gerüstes. *Die Bautechnik*, 56 (5), 169-171. (Impact forces from falling loads and people and the resulting failure of scaffolding.) (in German)

Mansfield, N.J. (1996). A study of the effect of vibration duration on the apparent mass of the seated human body. In: *UK Informal Group Meeting on Human Response to Vibration, Nuneaton, UK, 18-20 September, 1996.*

Mansfield, N.J. and Griffin, M.J. (1998). Effect of magnitude of vertical whole-body vibration on absorbed power for the seated human body. *Journal of Sound and Vibration*, 215 (4), 813-825.

Mansfield, N.J. and Griffin, M.J. (2000). Non-linearities in apparent mass and transmissibility during exposure to whole-body vertical vibration. *Journal of Biomechanics*, 33 (8), 933-941.

Mansfield, N.J. and Lundström, R. (1999a). The apparent mass of the human body exposed to non-orthogonal horizontal vibration. *Journal of Biomechanics*, 32 (12), 1269-1278.

Mansfield, N.J. and Lundström, R. (1999b). Models of the apparent mass of the seated human body exposed to horizontal whole-body vibration. *Aviation, Space, and Environmental Medicine*, 70 (12), 1166-1172.

Mansfield, N.J., Holmlund, P., and Lundström, R. (2000). Comparison of subjective responses to vibration and shock with standard analysis methods and absorbed power. *Journal of Sound and Vibration*, 230 (3), 477-491.

MATLAB (1999). *Matlab Version 5.3.1.* Natick, Massachusetts, USA: The MathWorks Incorporation.

Matsumoto, Y. (1996). The influence of posture on the apparent mass of standing subjects exposed to vertical vibration. In: *UK Informal Group Meeting on Human Response to Vibration, Nuneaton, UK, 18-20 September, 1996.*

Matsumoto, Y. and Griffin, M.J. (1998). Dynamic response of the standing human body exposed to vertical vibration: Influence of posture and vibration magnitude. *Journal of Sound and Vibration*, 212 (1), 85-107.

Matsumoto, Y. and Griffin, M.J. (2000). Comparison of biodynamic responses in standing and seated human bodies. *Journal of Sound and Vibration*, 238 (4), 691-704.

McConnell, K.G. (1995). *Vibration testing: Theory and practice.* New York, USA: John Wiley and Sons.

Meirovitch, L. (1986). *Elements of vibration analysis.* Second edition. New York, USA: McGraw-Hill.

Montgomery, D.C. and Runger, G.C. (1999). *Applied statistics and probability for engineers.* Second edition. New York, USA: John Wiley and Sons.

Morehead, J.C. (1991). The utilization of magnetic tape recording for modal data acquisition. In: *Proceedings of the 9th IMAC, Florence, Italy, 15 - 18 April, 1991.* Bethel, Connecticut, USA: Society of Experimental Mechanics (SEM). Vol. 1, 233-238.

Mouring, S.E. and Ellingwood, B.R. (1994). Guidelines to minimise floor vibrations from building occupants. *Journal of Structural Engineering (ASCE)*, 120 (2), 507-526.

Newland, D.E. (1993). *An introduction to random vibrations and spectral analysis.* Third edition. Harlow, UK: Longman.

Nigam, S.P. and Malik, M (1987). A study on a vibratory model of a human body. *Journal of Biomechanical Engineering*, 109 (2), 148-153.

Nilsson, L. (1976). *Impact loads produced by human motion. Part 1: Document D13:1976.* Stockholm, Sweden: Swedish Council for Building Research.

NRCC (1985). *Supplement to the National Building Code of Canada (NBC) 1985. Commentaries on Part 4, Commentary A: Serviceability criteria for deflections and vibrations.* Ottawa, Canada: NRCC.

NRCC (1995). *Users guide National Building Code of Canada (NBC) 1995. Commentary A: Serviceability criteria for deflections and vibrations.* Ottawa, Canada: NRCC.

Ohlsson, S. (1982). *Floor vibrations and human discomfort.* Thesis (PhD). Chalmers University of Technology, Gothenburg, Sweden.

Parker, D. (2000c). News feature: Marching to a new tune. *New Civil Engineer (ICE)*, 23 November, 2000, 12-13.

Pavic, A., Waldron, P., Reynolds, P., and Wright, J. (1999). *EPSRC research grant application: Dynamic crowd loading on flexible stadium structures.* University of Sheffield, Sheffield, UK.

Pimentel, R.L. (1997). *Vibration performance of pedestrian bridges due to human-induced loads.* Thesis (PhD). University of Sheffield, Sheffield, UK.

Pimentel, R.L. and Waldron, P. (1996). Validation of the numerical analysis of a pedestrian bridge for vibration serviceability applications. In: Friswell, M.I. and Mottershead, J.E. (eds.). *Identification in Engineering Systems, Swansea, UK, 27-29 March, 1996.* Trowbridge, UK: Cromwell Press. 648-657.

Pernica, G. (1990). Dynamic load factors for pedestrian movements and rhythmic exercises. *Canadian Acoustics*, 18 (2), 3-18.

Petersen, C. (1972). Theorie der Zufallsschwingungen (Randomschwingungstheorie) mit Anwendungen. In: *Arbeitsberichte zur Sicherheitstheorie der Bauwerke*. Munich, Germany: Laboratorium für den konstruktiven Ingenieurbau, Technische Universität München. Heft 2, 44-70. (Theory of random vibrations with applications.) (in German)

Polensek, A. (1975). Damping capacity of nailed wood-joist floors. *Wood Science*, 8 (2), 141-151.

Pradko, F. and Lee, R.A. (1966). Vibration comfort criteria. In: *Automotive Engineering Congress, Detroit, Michigan, 10-14 January, 1966.* Society of Automotive Engineers. Paper 660139.

Pradko, F., Lee, R.A., and Greene, J.D. (1967). Human vibration-response theory. *Biomechanics Monographs*, 205-222.

Prosig (1998). *DATS for Windows, Version 4.2. Spreadsheet signal processing for Microsoft Windows*. Fareham, UK: Prosig.

Qassem, W., Othman, M.O., and Abdul-Majeed, S. (1994). The effects of vertical and horizontal vibrations on the human body. *Medical Engineering and Physics*, 16 (2), 151-161.

Quast, U. (1993). Schwingungsverhalten der Tribünen des Volksparkstadions Hamburg (Vibration behaviour of the grand-stands in the Volksparkstadium at Hamburg). *Beton- und Stahlbetonbau*, 88 (9), 233-236. (in German)

Rainer, J.H. and Pernica, G. (1981). Damping of a floor sample. In: Hart, G. (ed.). *The Second Speciality Conference on Dynamic Response of Structures: Experimentation, Observation, Prediction and Control, Atlanta, Georgia, USA, 15-16 January, 1981.* 859-873.

Rainer, J.H. and Pernica, G. (1985). *Vibration characteristics of a floor sample.* Ottawa, Canada: NRCC, Division of Building Research. NRCC-24298.

Randall, R.B. (1987). *Frequency analysis*. Naerum, Denmark: Brüel and Kjær.

Randall, J.M. and Peng, C. (1995). Vibrating beam method for measuring animal natural frequencies. *Journal of Low Frequency Noise and Vibration*, 14 (3), 119-133.

Randall, J.M., Matthews R.T., and Stiles, M.A. (1997). Resonant frequencies of standing humans. *Ergonomics*, 40 (9), 879-886.

Rees, D.G. (1995). *Essential statistics*. Third edition. London, UK: Chapman and Hall.

Reid, W.M., Dickie, J.F., and Wright, J. (1997). Stadium structures: are they excited? *The Structural Engineer (IStructE)*, 75 (22), 383-388 and 76 (13), 258-261.

Reynolds, P. (2000). *The effects of raised access flooring on the vibrational performance of long-span concrete floors* .Thesis (PhD). University of Sheffield, Sheffield, UK.

Sample, I. (2001). The bridge of sways. *New Scientist*, 31 March, 2001, 38-41.

Schneider, M. (1991). *Ein Beitrag zu fußgängerinduzierten Brückenschwingungen*. Thesis (PhD). Technische Universität München, Munich, Germany. (Contribution to pedestrian induced vibrations of bridges.) (in German)

Schulze, H. (1980). *Fußgängerbrücken: Dynamische Einflüsse aus Verkehrslast: Richtline Ri-FB Dyn*. Berlin, German Democratic Republic (GDR): Kammer der Technik (KdT), Ministerium für Verkehr der DDR. (Footbridges: Dynamic influences of live loads: Guideline Ri-FB Dyn) (in German)

Setareh, M. and Hanson, R.D. (1992). Tuned mass dampers for balcony vibration control. *Journal of Structural Engineering (ASCE)*, 118 (3), 723-740.

Slavik, M. (1985). Beitrag zur dynamischen Berechnung von Fußgängerbrücken. *Die Straße*, 25 (12), 378-383. (Contribution to the dynamic design of footbridges.) (in German)

Stevenson, R. (1821). Description of bridges of suspension. *Edinburgh Philosophical Journal*, 5 (10), 237-256.

Struck, W. (1976). *Die stoßartige Beanspruchung leichter, nichttragender Bauteile durch einen mit der Schulter gegenprallenden Menschen; Vorschlag für ein Prüfverfahren*. Berlin, West-Germany: Bundsanstalt für Materialforschung und -prüfung (BAM). Bericht Nr. 37. (Impact loading of light-weight, non-structural elements due to a shouldering human.) (in German)

Struck, W. and Limberger, E. (1981). Die stoßartige Beanspruchung horizontaler Bauteile durch einen mit den Füßen aufprallenden Menschen. *Die Bautechnik*, 58 (10), 347-351. (Impact-like loading of horizontal elements by a person landing on its feet.) (in German)

Suggs, C.W., Abrams, C.F., and Stikeleather, L.F. (1969). Equipment note: Application of a damped spring-mass human vibration simulator in vibration testing of vehicle seats. *Ergonomics*, 12 (1), 79-90.

Taber, R.C., Brown, D.L., Vold, H., and Rocklin, G.T. (1985). Exponential window for burst random excitation. In: *Proceedings of the 3rd IMAC, Orlando, Florida, USA, 28-31 January, 1985*. 840-844.

Thorburn, S. (1997). Presidential address. The challenge of structural engineering: Safety, with economy and harmony. *The Structural Engineer (IStructE)*, 75 (20), 349-354.

Tilden, C.J. (1913). Kinetic effects of crowds. *Proceedings of the ASCE: Journal of the Structural Division*, 39 (3), 325-340.

Timoshenko, S., Young, D.H., and Weaver jr., W. (1974). *Vibration problems in engineering*. Fourth edition. New York, USA: John Wiley and Sons.

Tuan, C.Y. and Saul, W.E. (1985). Forces due to spectator movements. *Journal of Structural Engineering (ASCE)*, 111 (2), 418-434.

van Staalduinen, P. and Courage, W. (1994). Dynamic loading of Feyenoord stadium during pop concerts. In: *Symposium: Places of Assembly and Long-Span Building Structures, Birmingham, UK, 7-9 September, 1994*. Zürich, Switzerland: IABSE. IABSE Report 71, 283-288.

Vogel, C. (1983). *Beitrag zur Beurteilung des dynamischen Verhaltens der Überbauten von Fußgängerbrücken infolge Verkehrsbeanspruchung*. Thesis (PhD). Hochschule für Architektur und Bauwesen, Weimar, Germany. (Assessment of vibrations of footbridges due to traffic.) (in German)

Walley, F. (1959). St James's Park Bridge. *Proceedings of the ICE*, 12 (No. 6297), 217-222.

Wei, L. and Griffin, M.J. (1995). A method of predicting seat transmissibility. In: *UK Informal Group Meeting on Human Response to Vibration, Silsoe, UK, 18-20 September, 1995.*

Wei, L. and Griffin, M.J. (1998). Mathematical models for the apparent mass of the seated human body exposed to vertical vibration. *Journal of Sound and Vibration*, 212 (5), 855-874.

Weisstein, E.W. (1999). *Concise encyclopedia of mathematics*. Boca Raton, Florida, USA: Chapman and Hall/CRCnetBase (CD-ROM).

Williams, C., Rafiq, M.Y., and Carter, A. (1999). Human structure interaction: The development of an analytical model of the human body. In: *Vibration, Noise and Structural Dynamics. Venice, Italy, 28-30 April,* 1999. Staffordshire, UK: Staffordshire University Press. 32-39.

Wright, C.P. (1995). *Applied measurement engineering: How to design effective mechanical measurement systems.* Englewood Cliffs, New Jersey, USA: Prentice-Hall.

Wu, X., Rakheja, S., and Boileau, P.-É. (1999). Analyses of relationships between biodynamic response functions. *Journal of Sound and Vibration*, 226 (3), 595-606.

Wyatt, T.A. (1985). Short communication: Floor excitation by rhythmic vertical jumping. *Engineering Structures*, 7, 208-210.

BIBLIOGRAPHY

Abe, T., Hiromatsu, T., and Kushida, H. (1990). Study on estimation methods of floor structure vibration - vibrational characteristics of orthogonal anisotropic floor structures. In: *Proceedings of the 8th IMAC, Orlando, Kissimmee, Florida, USA, 29 January - 1 February, 1990.* Bethel, Connecticut, USA: SEM. Vol. 1, 645-651.

Al-Foqaha'a, A.A., Cofer, W.F., and Fridley, K.J. (1999). Vibration design criterion for wood floors exposed to normal human activities. *Journal of Structural Engineering (ASCE)*, 125 (12), 1401-1406.

Al-Foqaha'a, A.A., Cofer, W.F., and Fridley, K.J. (2001). Vibration design criterion for wood floors exposed to normal human activities: Closure. *Journal of Structural Engineering (ASCE)*, 127 (1), 99.

Allen, D.E. (1990). Floor vibrations from aerobics. *Canadian Journal of Civil Engineering*, 17 (5), 771-779.

Allen, D.E. and Pernica, G. (1984). A simple absorber for walking vibrations. *Canadian Journal of Civil Engineering*, 11 (1), 112-117.

Allen, D.E., Rainer J.H., and Pernica, G. (1985). Vibration criteria for assembly occupancies. *Canadian Journal of Civil Engineering*, 12 (3), 617-623.

Almeida, P.A.O. and Rodrigues, J.F.S. (1998). Investigation of the vibrations induced by people in soccer stadiums. In: *1998 SEM Spring Conference and Exhibition, Houston, Texas, USA, 1-3 June, 1998.* Bethel, Connecticut, USA: SEM. 271-274.

Almeida, P.A.O. and Rodrigues, J.F.S. (1999). Modal analysis of the structure of a soccer stadium. In: *Proceedings of the 17th IMAC, Orlando, Florida, USA, 8-11 February, 1999.* Bethel, Connecticut, USA: SEM. Vol. 2, 1417-1422.

Alves, N.K.C., Roitman, N., and Magluta, C. (1999). Dynamic response under human movements. *Materials and Structures (RILEM)*, 32 (215), 31-37.

Anonymous (1990). Police to limit Roebling pedestrians. *Cincinnati Enquirer*, 22 November, 1990, C1.

Anonymous (2000a). News: Universities to investigate pedestrian forces on bridge. *New Civil Engineer (ICE)*, 29 June, 2000, 8.

Anonymous (2000b). News: Cambridge launches its own Millennium bridge investigation. *New Civil Engineer (ICE)*, 20 July, 2000, 11.

Bachmann, H. (1983). Durch Menschen verursachte Bauwerksschwingungen - am Beispiel einer Turnhalle. *Schweizer Ingenieur und Architekt*, 101 (6), 104-110. (Human-induced vibrations of building - the example of a gymnasium.) (in German)

Bachmann, H. (1987a). Dynamische Bemessung von Turn- und Sporthallen. *Die Bautechnik*, 64 (11), 386-392. (Dynamic design of gymnasia.) (in German)

Bachmann, H. (1987b). Massnahmen gegen menscheninduzierte Bauwerksschwingungen. *Schweizer Ingenieur und Architekt*, 105 (12), 292-295. (Measures against human-induced vibrations of buildings.) (in German)

Bachmann, H. (1988a). Schwingungsprobleme bei Fußgängerbauwerken (Vibrational problems of pedestrian structures). *Bauingenieur*, 63, 67-75. (in German)

Bachmann, H. (1988b). Praktische Bauwerksdynamik am Beispiel der menschenerregten Schwingungen (Structural dynamics in applied engineering as illustrated in the example of man-induced vibrations). *Beton- und Stahlbetonbau*, 83 (9), 244-250. (in German)

Bachmann, H. (1991a). Schwingungssanierung einer Turnhalle (Improving of the dynamic properties of a gymnasium floor). *Stahlbau*, 60 (1), 1-4. (in German)

Bachmann, H. (1991b). Dynamische Einwirkungen und Schwingungsverhalten teilweise vorgespannter Fußgängerbrückenträger und Turnhallenträger (Dynamic actions and vibration behaviour of partially prestressed footbridge and gymnasium beams). *Beton- und Stahlbetonbau*, 86 (4), 86-90. (in German)

Bachmann, H. (1992). Case studies of structures with man-induced vibrations. *Journal of Structural Engineering (ASCE)*, 118 (3), 631-647.

Bachmann, H. and Ammann, W. (eds.) (1987). *Vibrations in structures: Induced by man and machines*. Zürich, Switzerland: IABSE. Structural Engineering Document (SED) 3.

Batista, R.C., Roitman, N., and Magluta, C. (1993). Structural dynamic analysis of Maracanã stadium. In: *Structural dynamics modelling: Test, analysis and correlation, Cranfield, UK, 7-8*

July, 1993. East Kilbride, UK: National Agency for Finite Element Methods and Standards (NAFEMS). 119-128.

Bishop, N.W.M., Willford, M., and Pumphrey, R. (1995). Human induced loading of flexible staircases. *Safety Science*, 18 (4), 261-276.

Blanchard, J., Davies, B.L., and Smith, J.W. (1977). Design criteria and analysis for dynamic loading of footbridges. In: *Symposium on dynamic behaviour of bridges, Crowthrone, UK, 19 May, 1977*. London, UK: Department of the Environment (DoE) and Department of Transport (DoT), Department of Transport and Road Research Laboratory (TRRL). 90-106.

Bodare, A. and Erlingsson, S. (1993). Rock music induced damage and vibration at Nya Ullevi Stadium. In: Prakash, S. (ed.). *Proceedings of Third International Conference on Case Histories in Geotechnical Engineering, St Louis, Missouri, USA, 1-4 June, 1993*. Rolla, Missouri, USA: University of Missouri-Rolla (UMR). 671-675.

Bolton, A. (1992). News: Fatal mix caused stand fall. *New Civil Engineer (ICE)*, 14 May, 1992. 5-6.

Boué, P. (1974). Aufgaben, Ausbildung und Schwingungsverhalten von Fußgängerbrücken aus Stahl. In: *Festschrift Otto Steinhardt zum 65. Geburtstag*. Karlsruhe, Germany: Universität Karlsruhe. 173-182. (Function, design and vibration behaviour of steel footbridges.) (in German)

Building Research Establishment (1997). *The response of structures to dynamic crowd loads*. Watford, UK: BRE. Digest 426.

Cantieni, R. (1988). Floor vibrations - two case studies. In*: Symposium/Workshop on Serviceability of Buildings (Movements, Deformations, Vibrations), 16-18 May, 1988, Ottawa, Canada*. Vol. 2, 29-40.

Caverson, R.G., Waldron, P., and Williams, M.S. (1994). Review of vibration guidelines for suspended concrete slabs. *Canadian Journal of Civil Engineering*, 21 (6), 931-938.

Chopra, A.K. (1995). *Dynamics of structures: Theory and applications to earthquake engineering*. Upper Saddle River, New Jersey, USA: Prentice-Hall.

Chui, Y.H. and Smith, I. (1989). Reliability of floors under impact vibration: Discussion. *Canadian Journal of Civil Engineering*, 16 (1), 97-98.

Dallard, P., Flint, A., le Bourva, S., Low, A., Ridshill, R.M., and Willford. M. (2001). Evening meeting: The London Millennium Footbridge. *The Structural Engineer (IStructE)*, 79 (22), 17-35.

de Andrade, C.F. and de Andrade, J.C. (2000). Preventing annoying wood floor vibrations: Discussion. *Journal of Structural Engineering (ASCE)*, 126 (3), 425-426.

de Andrade, C.F., de Andrade Filho, J.C., and de Andrade, J.C. (2001). Vibration design criterion for wood floors exposed to normal human activities: Discussion. *Journal of Structural Engineering (ASCE)*, 127 (1), 98-99.

de Andrade, J.C. (1985). Structural serviceability: Floor vibrations (Discussion). *Journal of Structural Engineering (ASCE)*, 111 (5), 1158-1160.

de Andrade, J.C. and de Andrade C.F. (1998). Measuring and modelling dynamic loads imposed by moving crowds: Discussion. *Journal of Structural Engineering (ASCE)*, 124 (9), 1088-1089.

Dieckmann, D. (1958). A study of the influence of vibration on man. *Ergonomics*, 4 (1), 347-355.

Dolan, J.D. and Murray, T.M. (2000). Preventing annoying wood floor vibrations: Closure. *Journal of Structural Engineering (ASCE)*, 126 (3), 426.

Dolan, J.D., Murray, T.M., Johnson, J.R., Runte, D., and Shue, B.C. (1999). Preventing annoying wood floor vibrations. *Journal of Structural Engineering (ASCE)*, 125 (1), 19-24 and 125 (4), 473.

Donkervoort, D.R., Hoenderkamp, J.C.D., and van Oosterhout, G.P.C. (1999). Floor vibrations due to walking loads. In: *Proceedings of the Second Conference on Steel Structures Eurosteel '99. Praha, Czech Republic, 26-29 May, 1999*. Vol. 1, 203-206.

DTA (1995). *Handbook on guidelines to best practice, Vol. 3 - Modal testing*. Cranfield, UK: DTA.

DTA (1996). *Handbook on guidelines to best practice, Vol. 2 - Signal processing*. Cranfield, UK: DTA.

Ebrahimpour, A. (1987). *Modeling spectator induced dynamic loads*. Thesis (PhD). University of Idaho, Moscow, USA.

Ebrahimpour, A., Hamam, A., Sack, R.L., and Patten, W.N. (1996). Measuring and modelling dynamic loads imposed by moving crowds. *Journal of Structural Engineering (ASCE)*, 122 (12), 1468-1474.

Ebrahimpour, A., Hamam, A., Sack, R.L., and Patten, W.N. (1998). Measuring and modelling dynamic loads imposed by moving crowds: Closure. *Journal of Structural Engineering (ASCE)*, 124 (9), 1089-1090.

Ebrahimpour, A., Patten, W.N., Sack R.L., Hancock, K., and Hamam, A. (1993). Defining occupant loads and mitigating associated vibrations. In: *International Colloquium: Structural Serviceability of Buildings, Gothenburg, Sweden, 9-11 June, 1993*. Zürich, Switzerland: IABSE. IABSE Report 69, 157-146.

Ebrahimpour, A. and Sack, R.L. (1989). Modeling dynamic occupant loads. *Journal of Structural Engineering (ASCE)*, 115 (6), 1476-1496.

Ebrahimpour, A. and Sack, R.L. (1996). Design live forces for crowds in motion. In: Ghosh, S.K. and Mohammadi, J. (eds.). *Building an International Community of Structural Engineers: Proceedings of Structures Congress XIV, Chicago, Illinois, USA, 15-18 April, 1996*. Reston, Virginia, USA: ASCE. Vol. 1, 420-427.

Ebrahimpour, A., Sack, R.L., Saul, W.E., and Thinness, G.L. (1986). Measuring dynamic occupant loads by microcomputer. In: *Proceedings of the 9th Conference on Electronic Computation, Birmingham, Alabama, USA, 23-26 February, 1986*. ASCE. 328-338.

Ebrahimpour, A., Sack, R.L., and Hamam, A. (1993). Loads imposed by crowds. In: Smith, R.A. and Dickie, J.F. (eds.). *Engineering for crowd safety, London, UK, 17-18 March, 1993*. Amsterdam, The Netherlands: Elsevier Science. 379-388.

Ebrahimpour A., Sack, R.L., Patten, W.N., and Hamam, A. (1994). Experimental measurements of dynamic loads imposed by moving crowds. In: Baker, N.C. and Loodno, B.J. (eds.). *Structures Congress XII, Atlanta, Georgia, USA, 24-28 April, 1994*. ASCE. 1385-1390.

Ellingwood, B.R. (1996). Structural serviceability: Review and standard implementation. In: Ghosh, S.K. and Mohammadi, J. (eds.). *Building an International Community of Structural Engineers: Proceedings of Structures Congress XIV, Chicago, Illinois, USA, 15-18 April, 1996*. Reston, Virginia, USA: ASCE. Vol. 1, 436-443.

Ellingwood, B. and Tallin, A. (1984). Structural serviceability: Floor vibrations. *Journal of Structural Engineering (ASCE)*, 110 (2), 401-418.

Ellingwood, B. and Tallin, A. (1985). Structural serviceability: Floor vibrations (Closure). *Journal of Structural Engineering (ASCE)*, 111 (5), 1160-1161.

Ellis, B.R. (2000). On the response of long-span floors to walking loads generated by individuals and crowds. *The Structural Engineer (IStructE)*, 78 (10), 17-25.

Ellis, B.R. and Ji, T. (1994). Floor vibration induced by dance-type loads: Verification. *The Structural Engineer (IStructE)*, 72 (3), 45-50.

Ellis, B.R., Ji, T., and Littler, J.D. (2000). The response of grandstands to dynamic crowd loads. *Proceedings of the ICE: Structures and Buildings*, 140 (4), 355-365.

Ellis, B.R., Kerridge, B., and Osborne, K. (1993). Vibration characteristics of shallow floor structures. In: *International Colloquium: Structural Serviceability of Buildings, Gothenburg, Sweden, 9-11 June, 1993*. Zürich, Switzerland: IABSE. IABSE Report 69, 303-308.

Endevco (1979). *Instruction manual for piezoelectric accelerometers.* San Juan Capistrano, California, USA: Endevco Corporation.

Engineering News (1916). Loads from moving crowds. *Engineering News*, 75 (16), 756-757.

Eriksson, P.-E. (1993). Low-frequency forces caused by people: Design force models. In: *International Colloquium: Structural Serviceability of Buildings, Gothenburg, Sweden, 9-11 June, 1993*. Zürich, Switzerland: IABSE. IABSE Report 69, 149-156.

Eriksson, P.-E. (1996). Dynamic service actions for floor systems - human activity. In: Ghosh, S.K. and Mohammadi, J. (eds.). *Building an International Community of Structural Engineers: Proceedings of Structures Congress XIV, Chicago, Illinois, USA, 15-18 April, 1996.* Reston, Virginia, USA: ASCE. Vol. 1, 413-419.

Eriksson, P.- E. and Ohlsson, S. (1988). Dynamic footfall forcing from groups of walking people. In: *Symposium/Workshop on Serviceability of Buildings (Movements, Deformations, Vibrations), Ottawa, Canada, 16-18 May, 1988*. 497-511.

Foschi, R.O. and Gupta, A. (1989). Reliability of floors under impact vibration: Reply. *Canadian Journal of Civil Engineering*, 16 (1), 98-99.

Foschi, R.O., Neumann, G.A., Yao, F., and Folz, B. (1996). Floor vibration due to occupant and reliability-based design guidelines: Reply. *Canadian Journal of Civil Engineering*, 23 (2), 572.

Ginty, D., Derwent, J.M., and Ji, T. (2001). The frequency ranges of dance-type loads. *The Structural Engineer (IStructE)*, 79 (6), 27-31.

Greimann, L.F. and Klaiber, F.W. (1978). Dynamic forces induced by spectators. *Proceedings of the ASCE: Journal of the Structural Division*, 104 (2), 348-351.

Hartley, M.J., Pavic, A., and Waldron, P. (1999). Investigation of pedestrian walking loads on a cable stayed footbridge using modal testing and FE model updating. In: *Proceedings of the 17th IMAC, Orlando, Florida, USA, 8-11 February, 1999*. Bethel, Connecticut, USA: SEM. Vol. 1, 7-13.

Herterich, J. and Schnauber, H. (1992). The effect of vertical mechanical vibration on standing man. *Journal of Low Frequency Noise and Vibration*, 11 (2), 52-60.

Hill, T. and Palmer, M. (2001). Predicting the response of slender steel staircases. *The Structural Engineer (IStructE)*, 79 (7), 16-18.

ISO (1999). Second ISO/CD 2631-2:1999. *Mechanical vibration and shock – Evaluation of human exposure to whole-body vibration - Part 2: Vibration in buildings (1 Hz to 80 Hz).* Geneva, Switzerland: ISO, Technical Committee (TC) 108, Subcommittee (SC) 4, Working Group (WG) 2.

Jacobs, N. (1996). Excursus. Temporary demountable structures: The need for guidance. *The Structural Engineer (IStructE)*, 74 (5), 84.

Janeway, R.N. (1975). Human vibration tolerance criteria and application to ride evaluation. *Automotive Engineering Congress*. Society of Automotive Engineers. Paper 680091.

Ji, T. (1997). The use of structural dynamics methods in the study of biodynamic properties of the human whole-body. In: *UK Informal Group Meeting on Human Response to Vibration, Southampton, UK, 17-19 September, 1997*. 209-219.

Ji, T. and Ellis, B.R. (1993). Evaluation of dynamic crowd effects for dance type loads. In: *International Colloquium: Structural Serviceability of Buildings, Gothenburg, Sweden, 9-11 June, 1993*. Zürich, Switzerland: IABSE. IABSE Report 69, 165-172.

Ji, T. and Ellis, B.R. (1994). Floor vibration induced by dance-type loads: Theory. *The Structural Engineer (IStructE)*, 72 (3), 37-44.

Ji, T. and Ellis, B.R. (1999). The evaluation of sports stadia grandstands for dynamic crowd loads at pop concerts in the United Kingdom. In: Fryba, L. and Naprstek, J. (eds.). *Eurodyn'99, Prague, Czech Republic, 7-10 June, 1999*. Rotterdam, The Netherlands: A.A. Balkema Publishers. 937-942.

Kazakevych, M. and Kulyabko, V.V. (1995). Stabilization of a cable-stayed footbridge. In: *Symposium: Extending the Lifespan of Structures, San Francisco, USA, August, 1995*. Zürich, Switzerland: IABSE. IABSE Report 73 (2), 1099-1104.

Kerr, S.C. and Bishop, N.W.M. (1997). Human induced loading of flexible staircases. In: Topping, B.H.V and Leeming, M.B. (eds.). *Innovation in Civil and Structural Engineering: Proceedings of The Mouchel Centenary Conference on Innovation in Civil and Structural Engineering, Cambridge, UK, 19-21 August, 1997*. Edinburgh, UK: Civil-Comp Press. 311-317.

Kerr, S.C. and Bishop, N.W.M. (2001). Human induced loading on flexible staircases. *Engineering Structures*, 23 (1), 37-45.

Kim, G.-C., Ahn, S.-K., and Lee, D.-G. (2001). Application of equivalent walking loads for vibration analysis of building structures. *The East Asia-Pacific Vibration Conference on Structural Engineering and Construction, Nanyang Technological University, Singapore, 5-7 December, 2001.*

Kobori, T. and Kajikawa, Y. (1974). Ergonomic evaluation methods for bridge vibrations. *Transactions of the Japanese Society of Civil Engineers (JSCE)*, 6, 40-41.

Kramer, H. (1998). Dynamische Belastung durch Fußgänger (Dynamic pedestrian loading). *Bauingenieur*, 73, 342-346. (in German)

Kremling, L. (1983). Kommentar zur SBA-Vorschrift 123/82. *Signal und Schiene*, 27 (4), 171-173. (Commentary to Staatliche Bauaufsicht (SBA)-Guideline 123/82.) (in German)

Krone, M., Klähne, T., and Kovacs, I. (1997). Die Südbrücke Oberhavel – Entwurf, Ausschreibung und Vergabe (The South Bridge Oberhavel – design tender and award of contracts). *Stahlbau*, 66 (4), 181-190. (in German)

Lang, G.F. and Snyder, D. (2001). Understanding the physics of electrodynamic shaker performance. *Sound and Vibration*, October, 2001.

Lawson, C.L. and Hanson, R.J. (1995). *Solving least squares problems*. Philadelphia, USA: Society for Industrial and Applied Mathematics (SIAM).

Leisi, R. and Szczesiak, T. (1996). Schwingungsprobleme bei einer Fuß- und Radwegbrücke. In: *Dynamische Probleme bei Bücken- und Hochbauten.* Zürich, Switzerland: SIA. Document D0138. (Vibration problems of a foot and cycle bridge.) (in German)

Leonard, D.R. (1966). *Human tolerance levels for bridge vibration*. Harmondsworth, UK: Ministry of Transport, Department of Transport and Road Research Laboratory (TRRL), Road Research Laboratory. Report No. 34.

Limberger, E. and Struck, W. (1972). Stoßartige Beanspruchung von Bauteilen und ihre rechnerische Simulation an mechanischen Modellen. *Die Bautechnik*, 49 (11), 384-388. (Impact loads of structural elements and simulation with mechanical models.) (in German)

Lissner, H.R. (1967). Biomechanics - What is it? In: *Biomechanics Monograph.* New York, USA: American Society of Mechanical Engineers (ASME). 1-11.

Littler, J.D. (1996). Measuring the dynamic response of temporary grandstands. In: Augusti, G., et al. (eds.). *Eurodyn'96, Florence, Italy, June 5 - 8, 1996.* Rotterdam, The Netherlands: A.A. Balkema Publishers. 907-913.

Littler, J.D. (1999). The dynamic response of a three tier cantilever grandstand. In: Fryba, L. and Naprstek, J. (eds.). *Eurodyn'99, Prague, Czech Republic, 7-10 June, 1999.* Rotterdam, The Netherlands: A.A. Balkema Publishers. Vol. 2, 623-628.

Littler, J.D. (2000a). *Temporary demountable grandstands: Dynamic response*. Watford, UK: BRE. Information Paper 3/00.

Littler, J.D. (2000b). *Permanent cantilever grandstands: Dynamic response*. Watford, UK: BRE. Information Paper 5/00.

Luza, G. (1998). Menscheninduzierte Einwirkungen für dynamische Berechnungen. *Zeitschrift für angewandte Mathematik und Mechanik (ZAMM)*, 78 (S2), 601-602. (Men-induced loads in dynamic calculations.) (in German)

Macduff, J.N. (1971). Vibrational characteristics of man. *Earth Moving Industry Conference, Peoria, Illinois, USA, 5-7 April, 1971.* Paper 710514.

Matsumoto, Y., Nishioka, T., Shiojiri, H., and Matsuzaki, K. (1978). Dynamic design of footbridges. In: *IABSE Proceedings*, P17-87, 1-15.

Matsumoto, Y., Sato, S., Nishioka, T., and Shiojiri, H. (1972). A study on dynamic design of pedestrian over-bridges. *Transactions of the Japanese Society of Civil Engineering (JSCE)*, 4, 50-51.

McConnell, K.G. and Varoto, P.S. (1995). The effects of window function and trigger levels on FRF estimations from impact tests In: *Proceedings of the 13th IMAC, Nashville, Tennessee, USA, 13-16 February, 1995.* Vol. 1, 798-807.

McConnell, K.G. and Varoto, P.S. (1995). The effect of windowing on FRF estimations for closely spaced peaks and valleys. In: *Proceedings of the 13th IMAC, Nashville, Tennessee, USA, 13-16 February, 1995.* Vol. 1, 769 - 775.

Meek, J.M. (1996). Schwingungstilger für Fußgängerbrücken (Tuned-mass dampers for footbridges). *Die Bautechnik*, 73 (6), 348-359. (in German)

Metcalfe, A.V. (1997). *Arnold applications of statistics series: Statistics in civil engineering*. London, UK: Arnold.

Miyamori, Y., Obata, T., Hayashikawa, T., and Sato, K. (2001). Study on identification of human walking model based on dynamic response characteristics of pedestrian bridges. *The East Asia-Pacific Vibration Conference on Structural Engineering and Construction, Nanyang Technological University, Singapore, 5-7 December, 2001.*

Montgomery, D.C. and Runger, G.C. (1999). *Applied statistics and probability for engineers.* Second edition. New York, USA: John Wiley and Sons.

Moreland, R. (1905). The weight of a crowd. *Engineering*, 28 April, 1905, 551.

Mouring, S.E. (1993). *Dynamic response of floor systems to building occupant activities.* Thesis (PhD). Johns Hopkins University, Baltimore, Maryland, USA.

Mouring, S.E. and Ellingwood, B.R. (1993). Minimizing floor vibration caused by building occupants. In: *International Colloquium: Structural Serviceability of Buildings, Gothenburg, Sweden, 9-11 June, 1993.* Zürich, Switzerland: IABSE. IABSE Report 69, 125-132.

Mouring, S.E. and Ellingwood, B.R. (1996). Minimizing floor vibrations from occupant activities. In: Ghosh, S.K. and Mohammadi, J. (eds.). *Building an International Community of Structural Engineers: Proceedings of Structures Congress XIV, Chicago, Illinois, USA, 15-18 April, 1996.* Reston, Virginia, USA: ASCE. Vol. 1, 405-412.

Murray, F.V. (2000). Croke Park redevelopment - stadium design in an urban context. *Proceedings of the ICE: Structures and Buildings*, 140 (4), 345-353.

Murray, T.M. (1999). Floor vibrations: The human tolerance side of the equation. In: *Proceedings of the 17th IMAC, Orlando, Florida, USA, 8-11 February, 1999.* Bethel, Connecticut, USA: SEM. Vol. 1, 1-6.

Murray, T.M. and Allen, D.E. (1993). Floor vibrations: A new design approach. In: *International Colloquium: Structural Serviceability of Buildings, Gothenburg, Sweden, 9-11 June, 1993.* Zürich, Switzerland: IABSE. IABSE Report 69, 119-124.

Neda, Z., Ravasz, E., Brechet, Y., Vicsek, T., and Barabasi, A.-L. (2000). Self-organizing processes: The sound of many hands clapping. *Nature*, 403, 849-850.

Nilsson, L. (1980). *Impact loads produced by human motion. Part 2: Document D20:1980.* Stockholm, Sweden: Swedish Council for Building Research.

Obata, T., Hayashikawa, T., and Sato, K. (1995). Experimental and analytical study of human vibration sensibility on pedestrian bridges. In: Loo, Y.C. (ed.). *Fifth East Asia-Pacific*

Conference on Structural Engineering and Construction: Building for the 21st Century, Gold Coast, Australia, 25-27 July, 1995. Nathan, Australia: Griffith University. Vol. 2, 1225-1230.

Onysko, D.M. (1996). Floor vibration due to occupant and reliability-based design guidelines: Discussion. *Canadian Journal of Civil Engineering*, 23 (2), 571-572.

Pan, T.-C. (1992). Vibration of pedestrian overpass. *Journal of Performance of Constructed Facilities*, 6 (1), 34-45.

Parker, D. (2000a). News: Arup pulls out all the stops for Millennium bridge probe. *New Civil Engineer (ICE)*, 6 July, 2000, 12.

Parker, D. (2000b). News: Vandals are biggest threat to footbridges. *New Civil Engineer (ICE)*, 31 August, 2000, 6.

Parker, D. (2001). Jerusalem collapse prompts floor reinforcement probe. *New Civil Engineer (ICE)*, 31 May, 2001, 6-7.

Pernica, G. (1983). Dynamic live forces at a rock concert. *Canadian Journal of Civil Engineering*, 10 (2), 185-191.

Petersen, C. (1996). *Dynamik der Baukonstruktionen*. Braunschweig, Germany: Vieweg. (Dynamic of civil engineering structures.) (in German)

Pimentel, R.L., Pavic, A., and Waldron, P. (2001). Evaluation of design requirements for footbridges excited by vertical forces from walking. *Canadian Journal of Civil Engineering*, 28 (5), 769-777.

Polensek, A. (1988). Structural dynamics and its effects on human response to floor vibrations. In: *International Conference on Timber Engineering, Madison, Wisconsin*. Forest Products Research Society. 746-755.

RACAL (1993). *RACAL Store Plus VL*. Southampton, UK: RACAL Instruments.

Rainer, J.H. (1984). *Dynamic response of a gymnasium floor*. Ottawa, Canada: NRCC, Division of Building Research. Building Research Note No. 213.

Rainer, J.H. (1984). *Vibrations in buildings*. Ottawa, Canada: NRCC, Division of Building Research. CBD 232.

Rainer, J.H. and Pernica, G. (1986). Vertical dynamic forces from footsteps. *Canadian Acoustics*, 14 (2), 12-21.

Rainer, J.H. and Swallow, J.C. (1986). Dynamic behaviour of a gymnasium floor. *Canadian Journal of Civil Engineering*, 13 (3), 270-277.

Rainer, J.H., Pernica, G., and Allen, D.E. (1988). Dynamic loading and response of footbridges. *Canadian Journal of Civil Engineering*, 15 (1), 66-71.

Rebelo, C. (1992). *Stochastische Modellierung menschenerzeugter Schwingungen*. Thesis (PhD). Technische Hochschule Karlsruhe, Karlsruhe, Germany. (Stochastic modelling of human-induced vibrations.) (in German)

Rebelo, C. and Scherer, R.J. (1993). Reduction factor for human loads in dancing halls. In: *International Colloquium: Structural Serviceability of Buildings, Gothenburg, Sweden, 9-11 June, 1993*. Zürich, Switzerland: IABSE. IABSE Report 69, 173-178.

Rebelo, C. and Scherer, R.J. (1994). A stochastic model for human induced rhythmic loads. In: Schuëller, G.I., Shinozuka, M., and Yao, J.T.P. (eds.). *Structural safety and reliability: Proceedings of the 6th International Conference on Structural Safety and Reliability, ICOSSAR '93, Innsbruck, 9-13 August, 1993*. Rotterdam, The Netherlands: A.A. Balkema Publishers. Vol. 2, 1473-1478.

Rebelo, C., Scherer, R.J., and Eibl, J. (1990). Statistical modelling of dynamic loads imposed by occupancies. In: Krätzig. W.B., et al. (eds.). *Eurodyn'90, Bochum, Germany, 5-7 June, 1990*. Rotterdam, The Netherlands: A.A. Balkema Publishers. Vol. 2, 645-651.

Reynolds, P. and Pavic, A. (2000). Structural Testing Series, Part 8: Quality assurance procedures for the modal testing of building floor structures. *Experimental Techniques (SEM)*, 24 (4), 36-41.

Sack, R.L. and Ebrahimpour, A. (1987). Simulating dynamic spectator loads. In: *Proceeding of the Third International Conference on Civil and Structural Engineering Computing*. Edinburgh, UK: Civil-Comp Press. Vol. 1, 215-122.

Sample, I. (2000). This week: Bad vibrations. *New Scientist*, 8 July, 2000, 14.

Saul, W.E. and Tuan, C.Y. (1986). Review of live loads due to human movements. *Journal of Structural Engineering (ASCE)*, 112 (5), 995-1004.

Saul, W.E., Tuan C.Y.-B., and McDonald, B. (1985). Loads due to human movements. In: Yao, J.T.P. and Corotis, R. (eds.). *Structural Safety Studies, Denver, Colorado, USA, 1-2 May, 1985*. ASCE. 107-119.

SBA (1982). SBA 123/82. *Brücken im Verkehrsbau, Fußgängerbrücken, Schwingungstechnische Untersuchungen.* Berlin, GDR: Ministerrat der DDR, Ministerium für Verkehrswesen, SBA. (Traffic bridges, footbridges, investigations of vibrations.) (in German)

SBA (1986). *Berichtigung zur SBA-Vorschrift 123/82 vom 1.7.1982.* Berlin, GDR: Ministerrat der DDR, Ministerium für Verkehrswesen, SBA. (Correction of SBA-Guideline 123/82.) (in German)

Schulze, H. (1980a). Dynamische Einflüsse der Verkehrslast auf Fußgängerbrücken. *Signal und Schiene*, 24 (2) 91-93 and 24 (3) 143 - 147. (Dynamic influences of live loads on footbridges.) (in German)

Schulze, H. (1980b). *Fußgängerbrücken: Dynamische Einflüsse aus Verkehrslast: Übersicht.* Berlin, GDR: Kammer der Technik (KdT), Ministerium für Verkehr der DDR. (Footbridges: Dynamic influences of live loads: Overview.) (in German)

SCOSS (2001). *Structural safety 2000-01: Thirteenth Report of the Standing Committee on Structural Safety (SCOSS).* London, UK: IStructE.

Scott, W.G. (1981). Concert loading is a special case. *New Civil Engineer (ICE)*, 7 May, 1981, 58.

Setareh, M. and Hanson, R.D. (1992). Tuned mass dampers to control floor vibration from humans. *Journal of Structural Engineering (ASCE)*, 118 (3), 741-762.

Smith, J.W. (1969). *The vibration of highway bridges and the effects on human comfort.* Thesis (PhD). University of Bristol, Bristol, UK.

Snœbjörnsson, J.T. and Sigbjörnsson, R. (1999). Footbridge dynamics and pedestrian induced vibrations - A case study. In: Fryba, L. and Naprstek, J. (eds.). *Eurodyn'99, Prague, Czech Republic, 7-10 June, 1999.* Rotterdam, The Netherlands: A.A. Balkema Publishers. Vol. 2, 789-794.

Soedel, W. and Dhar, M. (1978). Difficulties in finding modes experimentally when several contribute to a resonance. *Journal of Sound and Vibration*, 58 (1), 27-38.

Struck, W. (1977). Massestoß auf leichte Bauteile im Hochbau: Hinweise auf neue Beurteilungsmöglichkeiten. *Die Bautechnik*, 54 (2), 55-60. (Impact of light-weight elements in structural engineering: Guidelines of new evaluation techniques.) (in German)

Strum, R.D. and Kirk, D.E. (1989). *First principles of discrete systems and digital signal processing.* Reading, Massachusetts, USA: Addison-Wesly.

Sun, C.T. and Bai, J.M. (1995). Vibration of multi-degree-of-freedom systems with non-proportional viscous damping. *International Journal of Mechanical Sciences*, 37 (4), 441-455.

Thorburn, S. (1999). Safety at sports ground in the UK. *Structural Engineering International (IABSE)*, 9 (3), 156-188.

Tilly, G.P., Cullington, D.W., and Eyre, R. (1984). Dynamic behavior of footbridges. *IABSE surveys*, S-26/84, 13-24.

Tuan, Y.-B. (1983). *Loads due to human movements on assembly structures*. Thesis (PhD). University of Wisconsin-Madison, Madison, USA.

Wade, S. (1981). Loading code too low for Who. *New Civil Engineer (ICE)*, 26 March, 1981, 18.

Weaver, W., Timoshenko, S.P., and Young, D.H. (1990). *Vibration problems in engineering*. New York, USA: John Wiley and Sons.

Wei, L. and Griffin, M.J. (1998). The prediction of seat transmissibility from measures of seat impedance. *Journal of Sound and Vibration*, 214 (1), 121-137.

Wheeler, J.E. (1979). *Pedestrian-induced vibrations in footbridges*. Western Australia: Main Roads Department. Technical Report No. 15.

Wheeler, J.E. (1980). Pedestrian-induced vibrations in footbridges. In: *Tenth Australian Road Research Board (ARRB) Conference, Sydney, Australia, 25-29 August, 1980*. Vol. 10. Part 3, 21-35.

Wheeler, J.E. (1981). *Crowd loading on footbridges*. Western Australia: Main Roads Department. Technical Report No. 23.

Wheeler, J.E. (1982). Prediction and control of pedestrian-induced vibration in footbridges. *Proceedings of the ASCE: Journal of the Structural Division*, 108 (ST9), 2045-2065.

Wilkinson, E.R. and Coombe, J.P. (1991). University of Illinois Memorial Stadium: Investigation and rehabilitation. *Journal of Performance of Constructed Facilities*, 5 (1), 2-14.

Willford, M. (2001). An investigation into crowd-induced vertical dynamic loads using available measurements. *The Structural Engineer (IStructE)*, 79 (12), 21-25.

Williams, M. (2001). Vibrations of the Millennium Bridge. *The Society for Earthquake Engineering and Civil Engineering Dynamics (SECED) Newsletter (ICE)*, 15 (3), 1-3.

Williams, M.S. and Falati, S. (1999). Modal testing of a post-tensioned concrete model floor slab. In: *Proceedings of the 17th IMAC, Orlando, Florida, USA, 8-11 February, 1999*. Bethel, Connecticut, USA: SEM. Vol. 1, 14-20.

Williams, M.S. and Waldron, P. (1994). Evaluation of methods for predicting occupant-induced vibrations in concrete floors. *The Structural Engineer (IStructE)*, 72 (20), 334-340.

Wyatt, T.A. (1989). *Design guide on the vibration of floors. SCI Publication 076.* Ascot, UK: The Steel Construction Institute (SCI).

Zang, C., Grafe, H., and Imregun, M. (2001). Frequency-domain criteria for correlating and updating dynamic finite element models. *Mechanical Systems and Signal Processing*, 15 (1), 139-155.

APPENDIX A

The eigenproblem of the damped 2-DOF system (Figure 3.2) is a fourth order polynomial (see equation (3.81) in section 3.1.2.3). Solving such a fourth order polynomial (A.1) analytically was first presented by Geronimo Cardano (1501 - 1576) in the "Ars Magna". This procedure is outlined here based on a presentation by Bronstein et al. (1996, p. 648ff):

$$x^4 + a \cdot x^3 + b \cdot x^2 + c \cdot x + d = 0, \tag{A.1}$$

whereby the real terms a, b, c, and d are defined by the properties of the damped 2-DOF system (equations (A.2), (A.3), (A.4), and (A.5)).

$$a = \frac{m_s \cdot c_H + m_H \cdot c_H + m_H \cdot c_s}{m_s \cdot m_H} \tag{A.2}$$

$$b = \frac{m_s \cdot k_H + c_s \cdot c_H + m_H \cdot k_H + m_H \cdot k_s}{m_s \cdot m_H} \tag{A.3}$$

$$c = \frac{c_s \cdot k_H + c_H \cdot k_s}{m_s \cdot m_H} \tag{A.4}$$

$$d = \frac{k_s \cdot k_H}{m_s \cdot m_H} \tag{A.5}$$

Solving equation (A.1) for x involves transferring the fourth order polynomial into a third order (cubic) polynomial, whose solutions n_1, n_2, and n_3 specify the solutions of the fourth order polynomial.

First, the unknown x in the fourth order polynomial (A.1) is substituted according to equation (A.6).

$$y = x + \frac{a}{4} \tag{A.6}$$

This substitution transforms (A.1) into a polynomial with no cubic term (A.7) defined by terms p, q, and r specified in equations (A.8), (A.9), and (A.10).

$$y^4 + p \cdot y^2 + q \cdot y + r = 0 \tag{A.7}$$

$$p = b - \frac{3 \cdot a^2}{8} \tag{A.8}$$

$$q = \frac{a^3}{8} - \frac{a \cdot b}{2} + c \tag{A.9}$$

$$r = \frac{a^2 \cdot b}{16} - \frac{3 \cdot a^4}{256} - \frac{a \cdot c}{4} + d \tag{A.10}$$

The solutions y of the polynomial (A.7) can be calculated from the three solutions z_1, z_2, and z_3 of a third order polynomial (A.11) using equations (A.12), (A.13), (A.14), and (A.15).

$$z^3 + 2 \cdot p \cdot z^2 + (p^2 - 4 \cdot r) \cdot z - q^2 = 0 \tag{A.11}$$

$$y_1 = \frac{1}{2} \cdot (\sqrt{z_1} + \sqrt{z_2} - \sqrt{z_3}) \tag{A.12}$$

$$y_2 = \frac{1}{2} \cdot (\sqrt{z_1} - \sqrt{z_2} + \sqrt{z_3}) \tag{A.13}$$

$$y_3 = \frac{1}{2} \cdot (-\sqrt{z_1} + \sqrt{z_2} + \sqrt{z_3}) \tag{A.14}$$

$$y_4 = \frac{1}{2} \cdot (-\sqrt{z_1} - \sqrt{z_2} - \sqrt{z_3}) \tag{A.15}$$

These solutions y_1, y_2, y_3, and y_4 can be re-substituted into equation (A.6) and lead to the solutions x_1, x_2, x_3, and x_4 of the initial problem (A.1).

It remains to solve equation (A.11). This is done by transforming equation (A.11) into a form without a square term by substituting z with n according to equation (A.16).

$$n = z + \frac{2 \cdot p}{3} \tag{A.16}$$

This substitution transfers equation (A.11) into (A.17) with parameters k and m defined by equations (A.18) and (A.19).

$$n^3 + 3 \cdot m \cdot n + 2 \cdot k = 0 \tag{A.17}$$

$$k = -\frac{p^3}{27} + \frac{4 \cdot r \cdot p}{3} - \frac{q^2}{2} \tag{A.18}$$

$$m = -\frac{p^2}{9} - \frac{4 \cdot r}{3} \tag{A.19}$$

Equation (A.17) has three solutions n_1, n_2, and n_3 given by equations (A.20), (A.21), and (A.22).

$$n_1 = \sqrt[3]{\sqrt{m^3 + k^2} - k} + \sqrt[3]{-\sqrt{m^3 + k^2} - k} \tag{A.20}$$

$$n_2 = \frac{1}{2} \cdot \left(-1 + i \cdot \sqrt{3}\right) \cdot \sqrt[3]{\sqrt{m^3 + k^2} - k} + \frac{1}{2} \cdot \left(-1 - i \cdot \sqrt{3}\right) \cdot \sqrt[3]{-\sqrt{m^3 + k^2} - k} \tag{A.21}$$

$$n_3 = \frac{1}{2} \cdot \left(-1 - i \cdot \sqrt{3}\right) \cdot \sqrt[3]{\sqrt{m^3 + k^2} - k} + \frac{1}{2} \cdot \left(-1 + i \cdot \sqrt{3}\right) \cdot \sqrt[3]{-\sqrt{m^3 + k^2} - k} \tag{A.22}$$

The solutions n_1, n_2, and n_3 can be (Bronstein et al. 1996, p. 648):

(1) one real (n_1) and two complex conjugate (n_2 and n_3) values,

(2) three real numbers (n_1, n_2, and n_3),

(3) two real values with one repeated (n_1 and $n_2 = n_3$), or

(4) three repeated real values ($n_1 = n_2 = n_3$).

Based on the three solutions n_1, n_2, and n_3, the three solutions z_1, z_2, and z_3 can be found (A.16). They specify the four solutions y_1, y_2, y_3, and y_4 of equation (A.7) and thus the solutions x_1, x_2, x_3, and x_4 of the fourth order polynomial (A.1).

APPENDIX B

Estimating the natural frequencies $f_1^{(UM)}$ and $f_2^{(UM)}$ of an undamped 2-DOF human-structure system (Figure 4.1b) is straightforward (equation (3.83) in section 3.1.2.3). Here, this equation (3.83) is derived from the eigenproblem (equation (3.81)):

$$O = m_S \cdot m_H \cdot \lambda_r^4 + (m_H \cdot k_S + m_H \cdot k_H + m_S \cdot k_H) \cdot \lambda_r^2 + k_S \cdot k_H . \tag{B.1}$$

Rewriting equation (B.1) as:

$$O = \lambda_r^4 + \frac{k_S \cdot m_H}{m_S \cdot m_H} \cdot \lambda_r^2 + \frac{k_H \cdot m_H}{m_S \cdot m_H} \cdot \lambda_r^2 + \frac{m_S \cdot k_H}{m_S \cdot m_H} \cdot \lambda_r^2 + \frac{k_S \cdot k_H}{m_S \cdot m_H} \tag{B.2}$$

and introducing the circular natural frequencies of the undamped SDOF systems of the human (ω_H) and the structure (ω_S) leads to equation (B.3).

$$O = \lambda_r^4 + \left(\omega_S^2 + \frac{m_H}{m_S} \cdot \omega_H^2 + \omega_H^2 \right) \cdot \lambda_r^2 + \omega_H^2 \cdot \omega_S^2 \tag{B.3}$$

Equation (B.3) is a fourth order polynomial in λ_r but also a second order polynomial in λ_r^2.

Therefore, the pair of solutions λ_r^2 can be calculated from:

$$\lambda_r^2 = -\frac{1}{2} \cdot \left(\omega_S^2 + \frac{m_H}{m_S} \cdot \omega_H^2 + \omega_H^2 \right) \pm \sqrt{\left(\frac{1}{2} \cdot \left(\omega_S^2 + \frac{m_H}{m_S} \cdot \omega_H^2 + \omega_H^2 \right) \right)^2 - \omega_S^2 \cdot \omega_H^2} . \tag{B.4}$$

Using the fact that the complex eigenvalues λ_r specify the circular natural frequencies ω_r (equation (3.82) in section 3.1.2.3), the two circular natural frequencies ω_1 and ω_2 of an undamped 2-DOF system can be expressed as in equation (B.5):

$$\omega_{1,2}^2 = \frac{1}{2} \cdot \left(\omega_S^2 + \frac{m_H}{m_S} \cdot \omega_H^2 + \omega_H^2 \right) \mp \sqrt{\left(\frac{1}{2} \cdot \left(\omega_S^2 + \frac{m_H}{m_S} \cdot \omega_H^2 + \omega_H^2 \right) \right)^2 - \omega_S^2 \cdot \omega_H^2} \tag{B.5}$$

or, after taking a square root, by:

$$\omega_{1,2} = \sqrt{\frac{1}{2} \cdot \left(\omega_S^2 + \frac{m_H}{m_S} \cdot \omega_H^2 + \omega_H^2 \right) \mp \sqrt{\left(\frac{1}{2} \cdot \left(\omega_S^2 + \frac{m_H}{m_S} \cdot \omega_H^2 + \omega_H^2 \right) \right)^2 - \omega_S^2 \cdot \omega_H^2}} . \tag{B.6}$$

Equation (B.6) is unnecessary complex and a more convenient definition of the frequencies ω_1 and ω_2 can be derived. The first step in this approach is rewriting equation (B.5) as:

$$\omega_{1,2}^2 = \frac{1}{2}\cdot\left(\omega_H^2 + \frac{m_H}{m_S}\cdot\omega_H^2 + \omega_S^2\right) \mp \frac{1}{2}\cdot\sqrt{\left(\omega_H^2 + \frac{m_H}{m_S}\cdot\omega_H^2 + \omega_S^2\right)^2 - 4\cdot\omega_H^2\cdot\omega_S^2}\,. \tag{B.7}$$

The next step is rewriting the term under the root in (B.7). To simplify, this term is defined as a (B.8). It is rearranged as shown in equations (B.9) to (B.15) into the form presented in (B.16).

$$a = \left(\omega_H^2 + \frac{m_H}{m_S}\cdot\omega_H^2 + \omega_S^2\right)^2 - 4\cdot\omega_H^2\cdot\omega_S^2 \tag{B.8}$$

$$a = \left(\omega_H^4 + 2\cdot\frac{m_H}{m_S}\cdot\omega_H^4 + 2\cdot\omega_S^2\cdot\omega_H^2 + \left(\frac{m_H}{m_S}\right)^2\cdot\omega_H^4 + 2\cdot\frac{m_H}{m_S}\cdot\omega_H^2\cdot\omega_S^2 + \omega_S^4\right) - 4\cdot\omega_H^2\cdot\omega_S^2 \tag{B.9}$$

$$a = \omega_H^4 + 2\cdot\frac{m_H}{m_S}\cdot\omega_H^4 - 2\cdot\omega_S^2\cdot\omega_H^2 + \left(\frac{m_H}{m_S}\right)^2\cdot\omega_H^4 + 2\cdot\frac{m_H}{m_S}\cdot\omega_S^2\cdot\omega_H^2 + \omega_S^4 \tag{B.10}$$

$$a = \left(\omega_H^4 - 2\cdot\omega_S^2\cdot\omega_H^2 + \omega_S^4\right) + \left[\left(2\cdot\frac{m_H}{m_S}\cdot\omega_S^2\cdot\omega_H^2\right) + \left(2\cdot\frac{m_H}{m_S}\cdot\omega_H^4\right)\right] + \left(\left(\frac{m_H}{m_S}\right)^2\cdot\omega_H^4\right) \tag{B.11}$$

$$a = \left(\omega_H^2 - 2\cdot\omega_S\cdot\omega_H + \omega_e^2\right)\cdot\left(\omega_H^2 + 2\cdot\omega_S\cdot\omega_H + \omega_e^2\right) + \left[\frac{m_H}{m_S}\cdot\omega_H^2\cdot\left(2\cdot\omega_S^2 + 2\cdot\omega_H^2\right)\right] + \left(\frac{m_H}{m_S}\cdot\omega_H^2\right) \tag{B.12}$$

$$a = \left(\omega_H + \omega_S\right)^2\cdot\left(\omega_H - \omega_S\right)^2 + \left[\frac{m_H}{m_S}\cdot\omega_H^2\cdot\left(\left(\omega_S^2 + 2\cdot\omega_S\cdot\omega_H + \omega_H^2\right)\cdot\left(\omega_S^2 - 2\cdot\omega_S\cdot\omega_H + \omega_H^2\right)\right)\right] + \left(\frac{m_H}{m_S}\cdot\omega_H^2\right)^2 \tag{B.13}$$

$$a = (\omega_H + \omega_S)^2 \cdot (\omega_H - \omega_S)^2 + \left[\frac{m_H}{m_S} \cdot \omega_H^2 \cdot \left((\omega_S + \omega_H)^2 + (\omega_S - \omega_H)^2\right)\right] + \left(\frac{m_H}{m_S} \cdot \omega_H^2\right)^2 \tag{B.14}$$

$$a = (\omega_H + \omega_S)^2 \cdot (\omega_H - \omega_S)^2 + (\omega_S + \omega_H)^2 \cdot \frac{m_H}{m_S} \cdot \omega_H^2 + \frac{m_H}{m_S} \cdot \omega_H^2 \cdot (\omega_S - \omega_H)^2 + \left(\frac{m_H}{m_S} \cdot \omega_H^2\right)^2 \tag{B.15}$$

$$a = \left((\omega_H + \omega_S)^2 + \frac{m_H}{m_S} \cdot \omega_H^2\right) \cdot \left((\omega_H - \omega_S)^2 + \frac{m_H}{m_S} \cdot \omega_H^2\right) \tag{B.16}$$

Employing the expression provided in (B.16), equation (B.7) can be rewritten as equation (B.17).

$$\omega_{1,2}^2 = \frac{1}{2} \cdot \left(\omega_H^2 + \frac{m_H}{m_S} \cdot \omega_H^2 + \omega_S^2\right) \mp \frac{1}{2} \cdot \sqrt{\left((\omega_H + \omega_S)^2 + \frac{m_H}{m_S} \cdot \omega_H^2\right) \cdot \left((\omega_H - \omega_S)^2 + \frac{m_H}{m_S} \cdot \omega_H^2\right)} \tag{B.17}$$

Rearranging of this equation (B.17) leads to equation (B.18) and further to equation (B.19).

$$\omega_{1,2}^2 = \frac{1}{4} \cdot \left(\omega_H^2 + \frac{m_H}{m_S} \cdot \omega_H^2 + \omega_S^2\right) \mp \frac{1}{2} \cdot \sqrt{(\omega_H + \omega_S)^2 + \frac{m_H}{m_S} \cdot \omega_H^2} \cdot \sqrt{(\omega_H - \omega_S)^2 + \frac{m_H}{m_S} \cdot \omega_H^2} + \frac{1}{4} \cdot \left(\omega_H^2 + \frac{m_H}{m_S} \cdot \omega_H^2 + \omega_S^2\right) \tag{B.18}$$

$$\omega_{1,2}^2 = \left[\frac{1}{2} \cdot \sqrt{\left((\omega_H + \omega_S)^2 + \frac{m_H}{m_S} \cdot \omega_H^2\right)} \mp \frac{1}{2} \cdot \sqrt{\left((\omega_H - \omega_S)^2 + \frac{m_H}{m_S} \cdot \omega_H^2\right)}\right]^2 \tag{B.19}$$

Finally, taking the root of the binomial presented in equation (B.19), the circular natural frequencies ω_1 and ω_2 of the undamped 2-DOF human-structure system (Figure 4.1b) are presented in the form of equation (B.20).

$$\omega_{1,2} = \frac{1}{2} \cdot \sqrt{(\omega_H + \omega_S)^2 + \frac{m_H}{m_S} \cdot \omega_H^2} \mp \frac{1}{2} \cdot \sqrt{(\omega_H - \omega_S)^2 + \frac{m_H}{m_S} \cdot \omega_H^2} \tag{B.20}$$

Replacing the circular natural frequencies ω_H, ω_S, ω_1, and ω_2 by the natural frequencies f_S, f_H, $f_1^{(UM)}$, and $f_2^{(UM)}$ results in:

$$f_{1,2}^{(UM)} = \frac{1}{2} \cdot \sqrt{(f_H + f_S)^2 + \frac{m_H}{m_S} \cdot f_H^2} \mp \frac{1}{2} \cdot \sqrt{(f_H - f_S)^2 + \frac{m_H}{m_S} \cdot f_H^2} \,. \tag{B.21}$$

This equation (B.21) is stated by Randall and Peng (1995) and presented as equation (3.83) in section 3.1.2.3.

APPENDIX C

A MATLAB script is listed in this appendix. This routine calculates the natural frequencies and damping ratios of a damped 2-DOF human structure system based on the natural frequency, the mass, and the damping ratio of the two DOFs representing the structure and the human DOF. Additionally, it plots the structural accelerance FRFs $A_s(f)$ of the empty structure and the FRFs $A_{ss}(f)$ of the human-structure system (Figure C.1).

```
%%%%%%%%%%%%%%%%%%%%%%%%%%%%%%%%%%%%%%%%%%%%%%%%%%%%%%%
%                                                                                   %
%        Estimation of structural accelerance FRFs As and Ass                       %
%        of damped 2-DOF human-structure systems                                    %
%                                                                                   %
%%%%%%%%%%%%%%%%%%%%%%%%%%%%%%%%%%%%%%%%%%%%%%%%%%%%%%%

clear;

% ask for parameters of human-structure system
        fs = input('\n\n Please input\n\n  Frequency of the structure [Hz]      ');
        ms = input('\n  Modal mass of the structure [kg]   ');
        zs = input('\n  Damping ratio of the structure [%] ');
        fh = input('\n  Frequency of the human [Hz]        ');
        mh = input('\n  Modal mass of the human [kg]       ');
        zh = input('\n  Damping ratio of the human [%]     ');

% calculate stiffness
        ks = ms*(2*pi*fs)^2;
        kh = mh*(2*pi*fh)^2;

% calculate viscous damping
        cs = 2*zs/100*sqrt(ks*ms);
        ch = 2*zh/100*sqrt(kh*mh);

% define mass matrix, damping matrix, and stiffness matrix
        M = [ ms 0; 0  mh];
        C = [ cs+ch -ch; -ch  ch];
        K = [ ks+kh -kh; -kh  kh ];

% eigen analysis
        [evector,evalue] = polyeig(K, C, M);
```

```
% calculate modal parameters
        f1 = abs(min(evalue))/2/pi;
        f2 = abs(max(evalue))/2/pi;
        z1 = -real(min(evalue))/abs(min(evalue));
        z2 = -real(max(evalue))/abs(max(evalue));

% calculate FRF
        % specify frequency range of FRF
        w = 2*pi*linspace(1e-3,f2*2,10000);

        % calculate the FRF of empty structure
        SDOF = -w.^2./(ks-w.^2.*ms+i*w.*cs);

        % calculate structural FRF of the 2-DOF human-structure system
        nominator = (kh - w.^2*mh + i*w.*ch);
        denominator = ((ks+kh-w.^2.*ms+i*w.*(cs+ch)).*(kh-w.^2.*mh+i*w.*ch)-(-kh-i*w.*ch).^2);
        Ass =  -w.^2 .* nominator ./ denominator;

% peak amplitude of the structural FRF of the 2-DOF human-structure system
        [aDM fp_index] = max(abs(Ass));
        aS = 1/2/ms/(zs/100);

% plot FRFs
        figure(1); set(gcf,'Name','Structural accelerances');

        subplot(2,1,1)
        plot(w/2/pi,abs(SDOF),'k-',w/2/pi,abs(Ass),'b-');
        axis([0 f2*2 0 1.1*aS]);
        xlabel('Frequency [Hz]'); ylabel('Modulus [(m/s2)/N]');
        legend ('empty structure','occupied structure')

        subplot(2,1,2)
        plot(w/2/pi,angle(SDOF)*180/pi,'k-',w/2/pi,angle(Ass)*180/pi,'b-');
        axis([0 f2*2 -200 200]);
        xlabel('Frequency [Hz]'); ylabel('Phase [degree]');

% characteristics of the human-structure system
        fprintf('\n\n\t==========================================')
        fprintf('\n\n\tProperties of the human structure system\n')

        f_text = fprintf('\n\tNatural frequencies:  %.1f Hz and %.1f Hz',f1,f2);
        z_text = fprintf('\n\tDamping ratios:       %.1f%% and %.1f%%',z1*100,z2*100);
        fp_text = fprintf('\n\tPeak amplitude of the occupied structure at %.1f Hz.', w(fp_index)/2/pi);
        fprintf('\n\n\t==========================================\n')
```

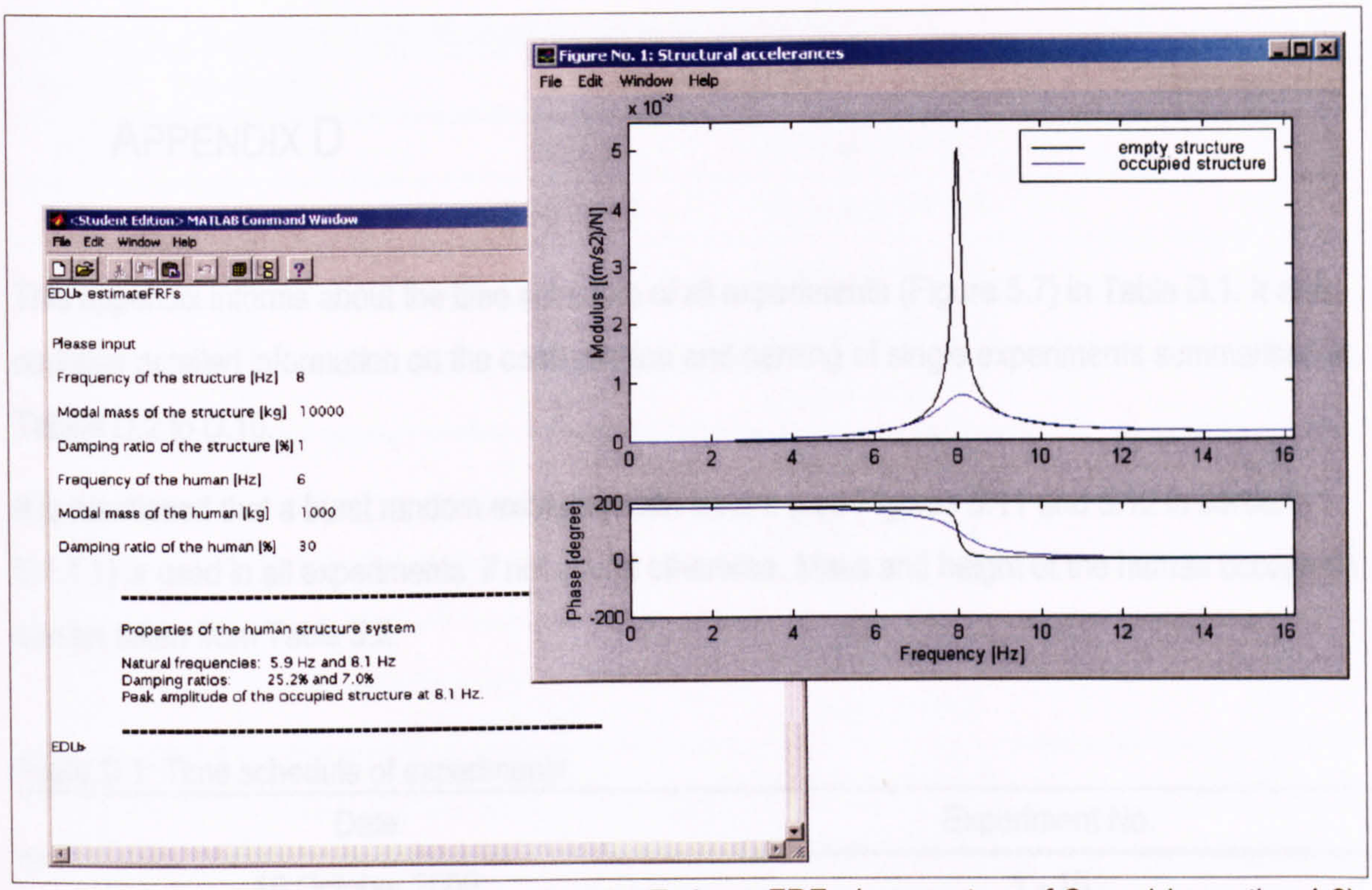

Figure C.1: Screenshot running MATLAB script EstimateFRFs (parameters of Case 1 in section 4.6).

APPENDIX D

This appendix informs about the time schedule of all experiments (Figure 5.7) in Table D.1. It also contains detailed information on the configuration and naming of single experiments summarised in Tables D.2 to D.10.

It is mentioned that a burst random excitation with level 2 (see Figures 5.11 and 5.12 in section 5.4.1.1) is used in all experiments, if not stated otherwise. Mass and height of the human occupants can be taken from Table 5.2.

Table D.1: Time schedule of experiments.

Date	Experiment No.
16 October 2000	1 - 15
20 October 2000	16 - 30
26 October 2000	31 - 52
1 November 2000	53 - 62
2 November 2000	63 - 72
8 November 2000	73 - 82
10 November 2000	79 - 81
14 November 2000	82 - 110
15 November 2000	111 - 141
16 November 2000	142 - 146
24 November 2000	147 - 172

Table D.2: Layout of experiments involving the empty structure.

Test ID	File Group	Test Condition	Experiment No.
A01	A	shaker at TP 5 [2)]	1
A02	B	shaker at TP 5 [2)]	2
A03	C	shaker at TP 5 [2)]	3
A04	D	shaker at TP 5 [2)]	4
A05	E	shaker at TP 5 [2)]	5
A06	F	shaker at TP 5	6
A07	G	shaker at TP 5	7
A08	H	shaker at TP 5	8
A09	I	shaker at TP 5	9
A11	L	shaker at TP 5	10
A12	M	shaker at TP 5 [1)]	11
A13	N	shaker at TP 5 [1)]	12
A14	O	shaker at TP 5 [1)]	13
A15	P	shaker at TP 5 [1)]	14
A16	Q	shaker at TP 5 [1)]	15
A17	R	shaker at TP 7	16
A18	S	shaker at TP 7	17
A19	T	shaker at TP 7	18
A20	U	shaker at TP 7	19
A21	V	shaker at TP 7	20
A22	W	shaker at TP 7	111
A23	X	shaker at TP 7	112
A24	Y	shaker at TP 7	113
A25	Z	shaker at TP 7	114
A26	J	shaker at TP 7	115

[1)] Excitation level 1 (see Figure 5.12 in section 5.4.1.1)
[2)] Excitation level 3 (see Figure 5.12 in section 5.4.1.1)

Table D.3: Layout of experiments involving one sitting occupant.

Test ID	File Group	Test Condition	Experiment No.
B01	A	shaker at TP 7; person A sitting at TP 5	21
B02	B	shaker at TP 7; person A sitting at TP 5	22
B03	C	shaker at TP 7; person A sitting at TP 5	23
B04	D	shaker at TP 7; person A sitting at TP 5	24
B05	E	shaker at TP 7; person A sitting at TP 5	25
B06	Z	shaker at TP 7 [2]; person A sitting at TP 5	36
B07	V	shaker at TP 7 [2]; person A sitting at TP 5	37
B08	W	shaker at TP 7 [2]; person A sitting at TP 5	38
B09	X	shaker at TP 7 [2]; person A sitting at TP 5	39
B10	Y	shaker at TP 7 [2]; person A sitting at TP 5	40
B11	Q	shaker at TP 7 [1]; person A sitting at TP 5	41
B12	R	shaker at TP 7 [1]; person A sitting at TP 5	42
B13	S	shaker at TP 7 [1]; person A sitting at TP 5	43
B14	T	shaker at TP 7 [1]; person A sitting at TP 5	44
B15	U	shaker at TP 7 [1]; person A sitting at TP 5	45
B16	F	shaker at TP 7; person A sitting at TP 7	26
B17	G	shaker at TP 7; person A sitting at TP 7	27
B18	H	shaker at TP 7; person A sitting at TP 7	28
B19	I	shaker at TP 7; person A sitting at TP 7	29
B20	K	shaker at TP 7; person A sitting at TP 7	30
B21	L	shaker at TP 7; person A sitting at TP 9	31
B22	M	shaker at TP 7; person A sitting at TP 9	32
B23	N	shaker at TP 7; person A sitting at TP 9	33
B24	O	shaker at TP 7; person A sitting at TP 9	34
B25	P	shaker at TP 7; person A sitting at TP 9	35
B26	J	shaker at TP 5; person A sitting at TP 5	46*

[1] Excitation level 1 (see Figure 5.12 in section 5.4.1.1)
[2] Excitation level 3 (see Figure 5.12 in section 5.4.1.1)

Table D.4: Layout of experiments involving one standing occupant.

Test ID	File Group	Test Condition	Experiment No.
C01	A	shaker at TP 7; person A standing at TP 5	48
C02	B	shaker at TP 7; person A standing at TP 5	49
C03	C	shaker at TP 7; person A standing at TP 5	50
C04	D	shaker at TP 7; person A standing at TP 5	51
C05	E	shaker at TP 7; person A standing at TP 5	52
C06	F	shaker at TP 7; person A standing at TP 7	53
C07	G	shaker at TP 7; person A standing at TP 7	54
C08	H	shaker at TP 7; person A standing at TP 7	55
C09	I	shaker at TP 7; person A standing at TP 7	56
C10	K	shaker at TP 7; person A standing at TP 7	57
C11	L	shaker at TP 7; person A standing at TP 9	58
C12	M	shaker at TP 7; person A standing at TP 9	59
C13	N	shaker at TP 7; person A standing at TP 9	60
C14	O	shaker at TP 7; person A standing at TP 9	61
C15	P	shaker at TP 7; person A standing at TP 9	62
C16	Q	shaker at TP 7 [2]; person A standing at TP 5	63
C17	R	shaker at TP 7 [2]; person A standing at TP 5	64
C18	S	shaker at TP 7 [2]; person A standing at TP 5	65
C19	T	shaker at TP 7 [2]; person A standing at TP 5	66
C20	U	shaker at TP 7 [2]; person A standing at TP 5	67
C21	V	shaker at TP 7 [1]; person A standing at TP 5	68
C22	W	shaker at TP 7 [1]; person A standing at TP 5	69
C23	X	shaker at TP 7 [1]; person A standing at TP 5	70
C24	Y	shaker at TP 7 [1]; person A standing at TP 5	71
C25	Z	shaker at TP 7 [1]; person A standing at TP 5	72
C26	J	shaker at TP 5; person A standing at TP 5	47

[1] Excitation level 1 (see Figure 5.12 in section 5.4.1.1)
[2] Excitation level 3 (see Figure 5.12 in section 5.4.1.1)

Table D.5: Layout of experiments involving five individuals.

Test ID	File Group	Test Condition	Experiment No.
E01	A	shaker at TP 7; person A sitting at TP 5	82
E02	B	shaker at TP 7; person A sitting at TP 5	83
E03	C	shaker at TP 7; person A sitting at TP 5	84
E04	D	shaker at TP 7; person A sitting at TP 5	85
E05	E	shaker at TP 7; person A sitting at TP 5	86
E06	F	shaker at TP 7; person B sitting at TP 5	87
E07	G	shaker at TP 7; person B sitting at TP 5	88
E08	H	shaker at TP 7; person B sitting at TP 5	89
E09	I	shaker at TP 7; person B sitting at TP 5	90
E10	J	shaker at TP 7; person B sitting at TP 5	91
E11	K	shaker at TP 7; person C sitting at TP 5	92
E12	L	shaker at TP 7; person C sitting at TP 5	93
E13	M	shaker at TP 7; person C sitting at TP 5	94
E14	N	shaker at TP 7; person C sitting at TP 5	95
E15	O	shaker at TP 7; person C sitting at TP 5	133
E16	P	shaker at TP 7; person D sitting at TP 5	106
E17	Q	shaker at TP 7; person D sitting at TP 5	107
E18	R	shaker at TP 7; person D sitting at TP 5	108
E19	S	shaker at TP 7; person D sitting at TP 5	109
E20	T	shaker at TP 7; person D sitting at TP 5	110
E21	U	shaker at TP 7; person E sitting at TP 5	121
E22	V	shaker at TP 7; person E sitting at TP 5	122
E23	W	shaker at TP 7; person E sitting at TP 5	134
E24	X	shaker at TP 7; person E sitting at TP 5	135
E25	Y	shaker at TP 7; person E sitting at TP 5	136

Table D.6: Layout of experiments involving groups of up to five occupants.

Test ID	File Group	Test Condition	Experiment No.
F01	A	shaker at TP 7; person A and B sitting at TP 5	116
F02	B	shaker at TP 7; person A and B sitting at TP 5	117
F03	C	shaker at TP 7; person A and B sitting at TP 5	118
F04	D	shaker at TP 7; person A and B sitting at TP 5	119
F05	E	shaker at TP 7; person A and B sitting at TP 5	120
F06	F	shaker at TP 7; person A, B, and C sitting at TP 5	96
F07	G	shaker at TP 7; person A, B, and C sitting at TP 5	97
F08	H	shaker at TP 7; person A, B, and C sitting at TP 5	98
F09	I	shaker at TP 7; person A, B, and C sitting at TP 5	99
F10	J	shaker at TP 7; person A, B, and C sitting at TP 5	100
F11	K	shaker at TP 7; person A, B, C, and D sitting at TP 5	101
F12	L	shaker at TP 7; person A, B, C, and D sitting at TP 5	102
F13	M	shaker at TP 7; person A, B, C, and D sitting at TP 5	103
F14	N	shaker at TP 7; person A, B, C, and D sitting at TP 5	104
F15	O	shaker at TP 7; person A, B, C, and D sitting at TP 5	105
F16	P	shaker at TP 7; person A, B, C, D, and E sitting at TP 5	123
F17	Q	shaker at TP 7; person A, B, C, D, and E sitting at TP 5	124
F18	R	shaker at TP 7; person A, B, C, D, and E sitting at TP 5	125
F19	S	shaker at TP 7; person A, B, C, D, and E sitting at TP 5	126
F20	T	shaker at TP 7; person A, B, C, D, and E sitting at TP 5	127
F21	U	shaker at TP 7; person C and E sitting at TP 3; person A, B, and D sitting at TP 7	128
F22	V	shaker at TP 7; person C and E sitting at TP 3; person A, B, and D sitting at TP 7	129
F23	W	shaker at TP 7; person C and E sitting at TP 3; person A, B, and D sitting at TP 7	130
F24	X	shaker at TP 7; person C and E sitting at TP 3; person A, B, and D sitting at TP 7	131
F25	Y	shaker at TP 7; person C and E sitting at TP 3; person A, B, and D sitting at TP 7	132

Table D.7: Layout of experiments analysing the influence of a static load.

Test ID	File Group	Test Condition	Experiment No.
G01	A	shaker at TP 7; mass of 408 kg at TP 5	137
G02	B	shaker at TP 7; mass of 408 kg at TP 5	138
G03	C	shaker at TP 7; mass of 408 kg at TP 5	139
G04	D	shaker at TP 7; mass of 408 kg at TP 5	140
G05	E	shaker at TP 7; mass of 408 kg at TP 5	141
G06	F	shaker at TP 7; mass of 168 kg at TP 3 and mass of 240 kg at TP 7	142
G07	G	shaker at TP 7; mass of 168 kg at TP 3 and mass of 240 kg at TP 7	143
G08	H	shaker at TP 7; mass of 168 kg at TP 3 and mass of 240 kg at TP 7	144
G09	I	shaker at TP 7; mass of 168 kg at TP 3 and mass of 240 kg at TP 7	145
G10	J	shaker at TP 7; mass of 168 kg at TP 3 and mass of 240 kg at TP 7	146

Table D.8: Layout of experiments investigating repeatability.

Test ID	File Group	Test Condition	Experiment No.
R01	A	shaker at TP 7; person A sitting at TP 5	73
R02	B	shaker at TP 7; person A sitting at TP 5	74
R03	C	shaker at TP 7; person A sitting at TP 5	75
R04	D	shaker at TP 7; person A sitting at TP 5	76
R06	F	shaker at TP 7; person A sitting at TP 5	77

Table D.9: Layout of experiments investigating the influence of a walking occupant.

Test ID	File Group	Test Condition	Experiment No.
D01	A	shaker at TP 7; continuous random excitation; person A walking at 1.5 Hz	79
D02	B	shaker at TP 7; continuous random excitation; person A walking at 1.8 Hz	80
D03	C	shaker at TP 7; continuous random excitation	81

Table D.10: Layout of experiments investigating the influence of the posture of a single occupant.

Test ID	File Group	Test Condition	Experiment No.
P01	P	shaker at TP 7; person A standing at TP 5 with bent knees	147
P02	V	shaker at TP 7; person A standing normally at TP 5	148
P03	F	shaker at TP 7; person A sitting at TP 5	149
P04	K	shaker at TP 7; person A standing at TP 5 with locked knees	150
P05	A	shaker at TP 7	151
P06	Q	shaker at TP 7; person A standing at TP 5 with bent knees	152
P07	W	shaker at TP 7; person A standing normally at TP 5	153
P08	G	shaker at TP 7; person A sitting at TP 5	154
P09	L	shaker at TP 7; person A standing at TP 5 with locked knees	155
P10	B	shaker at TP 7	156
P11	R	shaker at TP 7; person A standing at TP 5 with bent knees	157
P12	X	shaker at TP 7; person A standing normally at TP 5	158
P13	H	shaker at TP 7; person A sitting at TP 5	159
P14	M	shaker at TP 7; person A standing at TP 5 with locked knees	160
P15	C	shaker at TP 7	161
P16	S	shaker at TP 7; person A standing at TP 5 with bent knees	162
P17	Y	shaker at TP 7; person A standing normally at TP 5	163
P18	I	shaker at TP 7; person A sitting at TP 5	164
P19	N	shaker at TP 7; person A standing at TP 5 with locked knees	165
P20	D	shaker at TP 7	166
P21	T	shaker at TP 7; person A standing at TP 5 with bent knees	167
P22	Z	shaker at TP 7; person A standing normally at TP 5	168
P23	J	shaker at TP 7; person A sitting at TP 5	169
P24	O	shaker at TP 7; person A standing at TP 5 with locked knees	170
P25	E	shaker at TP 7	171
P26	U	shaker at TP 7; person A standing at TP 5 with bent knees	172

APPENDIX E

A wide range of experiments was performed to analyse the influence of human occupant on a test structure (Appendix D). Natural frequencies, damping ratios and modal masses determined from these modal tests by curve-fitting of FRFs are summarised here. They are provided by mean values and standard deviations of (always five) nominally identical tests.

E.1 EMPTY TEST STRUCTURE

Modal properties of the empty test structure are listed in Tables E.1 to E.3. Note that properties of the second mode of vibration are not provided for experiments A01 - A05, A06 - A09, A11, A12 - A16. In these cases, the excitation was applied at TP 5 (Table D.2 in Appendix D), a nodal point of the second mode (Figure 5.34a), and, therefore, properties of the second mode could not be identified.

Table E.1: Natural frequencies f_1, f_2, and f_3 of the empty test structure.

Test ID (No.)	f_1 [Hz]	f_2 [Hz]	f_3 [Hz]
A01 - A05 (1 - 5)	4.54 ± 0.00	-	37.86 ± 0.02
A06 - A09, A11 (6 - 10)	4.54 ± 0.00	-	37.85 ± 0.01
A12 - A16 (11 - 15)	4.54 ± 0.00	-	37.88 ± 0.02
A17 - A21 (16 - 20)	4.53 ± 0.00	16.93 ± 0.00	37.84 ± 0.00
A22 - A26 (111 - 115)	4.51 ± 0.00	16.95 ± 0.00	37.73 ± 0.00
P05, P10, P15, P20, and P25 (151, 156, 166, 168, and 171)	4.50 ± 0.00	16.98 ± 0.00	37.59 ± 0.01

Table E.2: Damping ratios ζ_1, ζ_2, and ζ_3 of the empty test structure.

Test ID (No.)	ζ_1 [%]	ζ_2 [%]	ζ_3 [%]
A01 - A05 (1 - 5)	0.32 ± 0.00	-	0.93 ± 0.02
A06 - A09, A11 (6 - 10)	0.34 ± 0.00	-	0.95 ± 0.04
A12 - A16 (11 - 15)	0.34 ± 0.01	-	0.92 ± 0.04
A17 - A21 (16 - 20)	0.35 ± 0.00	0.35 ± 0.00	0.93 ± 0.01
A22 - A26 (111 - 115)	0.32 ± 0.01	0.35 ± 0.00	0.94 ± 0.01
P05, P10, P15, P20, and P25 (151, 156, 166, 168, and 171)	0.37 ± 0.02	0.34 ± 0.00	1.00 ± 0.02

Table E.3: Modal masses m_1, m_2, and m_3 of the empty test structure.

Test ID (No.)	m_1 [kg]	m_2 [kg]	m_3 [kg]
A01 - A05 (1 - 5)	7260 ± 90	-	7760 ± 330
A06 - A09, A11 (6 - 10)	7030 ± 50	-	7660 ± 410
A12 - A16 (11 - 15)	6970 ± 110	-	7670 ± 160
A17 - A21 (16 - 20)	7010 ± 60	7420 ± 90	7760 ± 60
A22 - A26 (111 - 115)	7040 ± 160	7370 ± 30	7880 ± 110
P05, P10, P15, P20, P25 (151, 156, 166, 168, 171)	7090 ± 350	7340 ± 120	7980 ± 170

Table E.6: Modal masses m_1, m_2, and m_3 of the test structure occupied by TS A sitting at different locations, subjected to different excitation levels, and at different days.

Test ID (No.)	m_1 [kg]	m_2 [kg]	m_3 [kg]
B01 - B05 (21 - 25)	6880 ± 220	7400 ± 60	7710 ±130
B06 - B10 (36 - 40)	7250 ±350	7380 ± 30	7760 ±130
B11 - B15 (41 - 45)	7910 ± 620	7370 ± 20	7770 ± 100
B16 - B20 (26 - 30)	6950 ± 200	7420 ± 20	7790 ± 90
B21 - B25 (31 - 35)	6950 ± 30	7430 ± 80	7750 ± 110
R01 - R04, R06 (73 - 77)	7070 ± 300	7380 ± 60	7730 ± 60

Table E.7: Natural frequencies f_1, f_2, and f_3 of the test structure occupied by TS A standing at various points and under varying levels of excitation.

Test ID (No.)	f_1 [Hz]	f_2 [Hz]	f_3 [Hz]
C01 - C05 (45 - 52)	4.50 ± 0.00	16.95 ± 0.00	37.78 ± 0.00
C06 - C10 (53 - 57)	4.51 ± 0.00	16.96 ± 0.00	37.74 ± 0.00
C11 - C15 (58 - 62)	4.52 ± 0.00	16.95 ± 0.00	37.74 ± 0.00
C16 - C20 (63 -67)	4.49 ± 0.00	16.95 ± 0.00	37.77 ± 0.00
C21 - C25 (68 -72)	4.50 ± 0.00	16.96 ± 0.00	37.78 ± 0.00

Table E.8: Damping ratios ζ_1, ζ_2, and ζ_3 of the test structure occupied by TS A standing at various points and under varying levels of excitation.

Test ID (No.)	ζ_1 [%]	ζ_2 [%]	ζ_3 [%]
C01 - C05 (45 - 52)	0.54 ± 0.06	0.35 ± 0.01	0.98 ± 0.01
C06 - C10 (53 - 57)	0.42 ± 0.03	0.56 ± 0.00	1.00 ± 0.01
C11 - C15 (58 - 62)	0.34 ± 0.02	0.34 ± 0.01	1.00 ± 0.01
C16 - C20 (63 -67)	0.45 ± 0.02	0.34 ± 0.00	1.00 ± 0.01
C21 - C25 (68 -72)	0.52 ± 0.13	0.34 ± 0.01	1.00 ± 0.02

E.2 One Stationary Occupant

The influence of a single human occupant on the modal properties of the test structure was determined in Tests B, C, E, R, and P (Tables D.3 to D.5, D.8, and D.10). The resulting natural frequencies, damping ratios, and modal masses are listed in Tables E.4 to E.15.

Table E.4: Natural frequencies f_1, f_2, and f_3 of the test structure occupied by TS A sitting at different locations, subjected to different excitation levels, and at different days.

Test ID (No.)	f_1 [Hz]	f_2 [Hz]	f_3 [Hz]
B01 - B05 (21 - 25)	4.50 ± 0.00	16.93 ± 0.00	37.86 ± 0.00
B06 - B10 (36 - 40)	4.49 ± 0.00	16.95 ± 0.00	37.77 ± 0.01
B11 - B15 (41 - 45)	4.49 ± 0.00	16.95 ± 0.00	37.78 ± 0.02
B16 - B20 (26 - 30)	4.52 ± 0.00	16.94 ± 0.00	37.85 ± 0.01
B21 - B25 (31 - 35)	4.52 ± 0.00	16.96 ± 0.00	37.77 ± 0.00
R01 - R04, R06 (73 - 77)	4.49 ± 0.00	16.96 ± 0.00	37.74 ± 0.01

Table E.5: Damping ratios ζ_1, ζ_2, and ζ_3 of the test structure occupied by TS A sitting at different locations, subjected to different excitation levels, and at different days.

Test ID (No.)	ζ_1 [%]	ζ_2 [%]	ζ_3 [%]
B01 - B05 (21 - 25)	0.55 ± 0.06	0.36 ± 0.01	0.98 ± 0.01
B06 - B10 (36 - 40)	0.51 ± 0.09	0.35 ± 0.00	1.01 ± 0.02
B11 - B15 (41 - 45)	0.47 ± 0.02	0.35 ± 0.01	1.00 ± 0.05
B16 - B20 (26 - 30)	0.43 ± 0.03	0.47 ± 0.05	0.94 ± 0.00
B21 - B25 (31 - 35)	0.35 ± 0.01	0.35 ± 0.00	0.97 ± 0.01
R01 - R04, R06 (73 - 77)	0.57 ± 0.14	0.35 ± 0.00	1.06 ± 0.01

Table E.9: Modal masses m_1, m_2, and m_3 of the test structure occupied by TS A standing at various points and under varying levels of excitation.

Test ID (No.)	m_1 [kg]	m_2 [kg]	m_3 [kg]
C01 - C05 (45 - 52)	6900 ± 290	7330 ± 80	7830 ± 130
C06 - C10 (53 - 57)	7260 ± 230	7370 ± 60	7760 ± 90
C11 - C15 (58 - 62)	7000 ± 80	7410 ± 170	7670 ± 70
C16 - C20 (63 -67)	7360 ± 310	7410 ± 80	7730 ± 120
C21 - C25 (68 -72)	7180 ± 312	7390 ±150	7730 ± 210

Table E.10: Natural frequencies f_1, f_2, and f_3 of the test structure occupied by TS A, B, C, D, or E.

Test ID (No.)	f_1 [Hz]	f_2 [Hz]	f_3 [Hz]
E01 - E05 (82 - 86)	4.48 ± 0.01	16.96 ± 0.00	37.76 ± 0.00
E06 - E10 (87 - 91)	4.46 ± 0.00	16.95 ± 0.00	37.78 ± 0.00
E11 - E15 (92 - 95, 133)	4.47 ± 0.00	16.95 ± 0.00	37.76 ± 0.02
E16 - E20 (106 -110)	4.47 ± 0.01	16.95 ± 0.00	37.75 ± 0.01
E21 - E25 (121, 122, 134 - 136)	4.46 ± 0.00	16.95 ± 0.00	37.73 ± 0.00

Table E.11: Damping ratios ζ_1, ζ_2, and ζ_3 of the test structure occupied by TS A, B, C, D, or E.

Test ID (No.)	ζ_1 [%]	ζ_2 [%]	ζ_3 [%]
E01 - E05 (82 - 86)	0.64 ± 0.16	0.34 ± 0.01	0.97 ± 0.01
E06 - E10 (87 - 91)	0.60 ± 0.05	0.35 ± 0.00	0.99 ± 0.01
E11 - E15 (92 - 95, 133)	0.61 ± 0.08	0.35 ± 0.01	1.00 ± 0.02
E16 - E20 (106 -110)	0.54 ± 0.13	0.36 ± 0.01	1.01 ± 0.01
E21 - E25 (121, 122, 134 - 136)	0.58 ± 0.09	0.36 ± 0.00	1.03 ± 0.01

Table E.12: Damping ratios ζ_1, ζ_2, and ζ_3 of the test structure occupied by TS A, B, C, D, or E.

Test ID (No.)	ζ_1 [%]	ζ_2 [%]	ζ_3 [%]
E01 - E05 (82 - 86)	0.64 ± 0.16	0.34 ± 0.01	0.97 ± 0.01
E06 - E10 (87 - 91)	0.60 ± 0.05	0.35 ± 0.00	0.99 ± 0.01
E11 - E15 (92 - 95, 133)	0.61 ± 0.08	0.35 ± 0.01	1.00 ± 0.02
E16 - E20 (106 -110)	0.54 ± 0.13	0.36 ± 0.01	1.01 ± 0.01
E21 - E25 (121, 122, 134 - 136)	0.58 ± 0.09	0.36 ± 0.00	1.03 ± 0.01

Table E.13: Natural frequencies f_1, f_2, and f_3 of the test structure occupied by TS A in different postures.

Test ID (No.)	f_1 [Hz]	f_2 [Hz]	f_3 [Hz]
P03, P08, P13, P18, and P23 [1] (149, 154, 159, 164, 169)	4.47 ± 0.00	16.98 ± 0.00	37.62 ± 0.01
P02, P07, P12, P17, and P22 [2] (148, 153, 158, 163, 168)	4.48 ± 0.00	16.98 ± 0.00	37.62 ± 0.01
P04, P09, P14, P19, and P24 [3] (150, 155, 160, 165, 170)	4.47 ± 0.00	16.98 ± 0.00	37.63 ± 0.01

[1] Sitting at TP 5.
[2] Standing with locked knees at TP 5.
[3] Standing normally at TP 5.

Table E.14: Damping ratios ζ_1, ζ_2, and ζ_3 of the test structure occupied by TS A in different postures.

Test ID (No.)	ζ_1 [%]	ζ_2 [%]	ζ_3 [%]
P03, P08, P13, P18, and P23 (149, 154, 159, 164, 169)	0.57 ± 0.09	0.35 ± 0.00	1.04 ± 0.01
P02, P07, P12, P17, and P22 (148, 153, 158, 163, 168)	0.69 ± 0.07	0.35 ± 0.01	1.04 ± 0.02
P04, P09, P14, P19, and P24 (150, 155, 160, 165, 170)	0.51 ± 0.05	0.35 ± 0.01	1.03 ± 0.01

Table E.15: Modal masses m_1, m_2, and m_3 of the test structure occupied by TS A in different postures.

Test ID (No.)	m_1 [kg]	m_2 [kg]	m_3 [kg]
P03, P08, P13, P18, and P23 (149, 154, 159, 164, 169)	7120 ± 220	7290 ± 50	7860 ± 80
P02, P07, P12, P17, and P22 (148, 153, 158, 163, 168)	7210 ± 280	7330 ± 70	7870 ± 60
P04, P09, P14, P19, and P24 (150, 155, 160, 165, 170)	7130 ± 670	7350 ± 110	7830 ± 70

E.3 Groups of Sitting Occupants

Tables E.16 to E.18 list the natural frequencies, damping ratios, and modal masses determined for the test structure occupied by two (F01 - F05), three (F06 - F10), four (F11 - F15), or five people (F16 - F20 and F21 - F25) as outlined in Table D.6. The test subjects (Table 5.2) were usually sitting close to TP 5 and only in tests F21 - F25 at TPs 3 and 7 (Figure 5.9).

Table E.16: Natural frequencies f_1, f_2, and f_3 of the test structure occupied by a group of sitting people.

Test ID (No.)	f_1 [Hz]	f_2 [Hz]	f_3 [Hz]
F01 - F05 (116 - 120)	4.43 ± 0.00	16.95 ± 0.00	37.76 ± 0.01
F06 - F10 (96 - 100)	4.41 ± 0.01	16.95 ± 0.00	37.81 ± 0.01
F11 - F15 (101 - 105)	4.38 ± 0.01	16.95 ± 0.00	37.84 ± 0.01
F16 - F20 (123 - 127)	4.34 ± 0.02	16.94 ± 0.00	37.83 ± 0.01
F21 - F25 (128 - 132)	4.42 ± 0.01	16.98 ± 0.01	37.78 ± 0.00

Table E.17: Damping ratios ζ_1, ζ_2, and ζ_3 of the test structure occupied by a group of sitting people.

Test ID (No.)	ζ_1 [%]	ζ_2 [%]	ζ_3 [%]
F01 - F05 (116 - 120)	0.74 ± 0.09	0.36 ± 0.00	1.09 ± 0.03
F06 - F10 (96 - 100)	0.88 ± 0.07	0.36 ± 0.00	1.09 ± 0.02
F11 - F15 (101 - 105)	1.32 ± 0.20	0.38 ± 0.00	1.14 ± 0.01
F16 - F20 (123 - 127)	1.69 ± 0.67	0.41 ± 0.01	1.24 ± 0.01
F21 - F25 (128 - 132)	1.20 ± 0.27	1.40 ± 0.04	1.10 ± 0.01

Table E.18: Modal masses m_1, m_2, and m_3 of the test structure occupied by a group of sitting people.

Test ID (No.)	m_1 [kg]	m_2 [kg]	m_3 [kg]
F01 - F05 (116 - 120)	7470 ± 980	7440 ± 80	7720 ± 200
F06 - F10 (96 - 100)	7930 ± 1090	7430 ± 140	7980 ± 120
F11 - F15 (101 - 105)	7900 ± 540	7400 ± 90	7950 ± 90
F16 - F20 (123 - 127)	7940 ±1100	7420 ± 110	7720 ± 90
F21 - F25 (128 - 132)	7260 ± 560	7450 ± 40	7840 ± 110

E.4 Equivalent Mass

Natural frequencies, damping ratios, and modal masses of the test structure loaded with a mass equivalent to the overall mass of the five TSs are provided in Tables E.19 to E.21. The equivalent mass was applied at TP 5 in G01 - G05 or distributed to TPs 3 and 7 in G06 - G10.

Table E.19: Natural frequencies f_1, f_2, and f_3 of the test structure loaded with an equivalent mass.

Test ID (No.)	f_1 [Hz]	f_2 [Hz]	f_3 [Hz]
G01 - G05 (137 - 141)	4.39 ± 0.00	16.93 ± 0.00	38.45 ± 0.05
G06 - G10 (142 - 146)	4.44 ± 0.00	16.34 ± 0.00	37.84 ± 0.01

Table E.20: Damping ratios ζ_1, ζ_2, and ζ_3 of the test structure loaded with an equivalent mass.

Test ID (No.)	ζ_1 [%]	ζ_2 [%]	ζ_3 [%]
G01 - G05 (137 - 141)	0.33 ± 0.01	0.40 ± 0.01	1.92 ± 0.12
G06 - G10 (142 - 146)	0.34 ± 0.00	0.47 ± 0.01	1.76 ± 0.02

Table E.21: Modal masses m_1, m_2, and m_3 of the test structure loaded with an equivalent mass.

Test ID (No.)	m_1 [kg]	m_2 [kg]	m_3 [kg]
G01 - G05 (137 - 141)	7410 ± 160	7530 ± 180	8580 ± 260
G06 - G10 (142 - 146)	7190 ± 50	8020 ± 40	7870 ± 70

APPENDIX F

This appendix provides Peak Amplitude Reduction Factors (PARFs) for a range of 2-DOF human-structure models. As outlined in section 6.3, these values can be used to quantify the influence of human occupants on SDOF structure models.

The presented PARFs correspond to damped SDOF structure models with natural frequencies f_s between 0.5 and 20.0 Hz and damping ratios ζ_s of 1% or 2%. Human occupants are represented by the damped SDOF human occupant model A*, B*, or C (Table F.1). They cover excitation frequencies f_{EX} = 0.5 to 10.0 Hz and $m_s : m_T$ ratios of 1:1, 1.5:1, 3:1, 10:1, 50:1, and 100:1.

Table F.1: Properties of Human Models A*, B*, and C corresponding to SDOF structure models with natural frequencies of 4.51 Hz, 16.95 Hz, and 3.16 Hz respectively.

	Natural frequency f_H	Damping ratio ζ_H	Mass m_H
Human Model A*	5.9 Hz	33%	0.9 m_T
Human Model B*	8.3 Hz	35%	0.8 m_T
Human Model C	3.8 Hz	10%	1.0 m_T

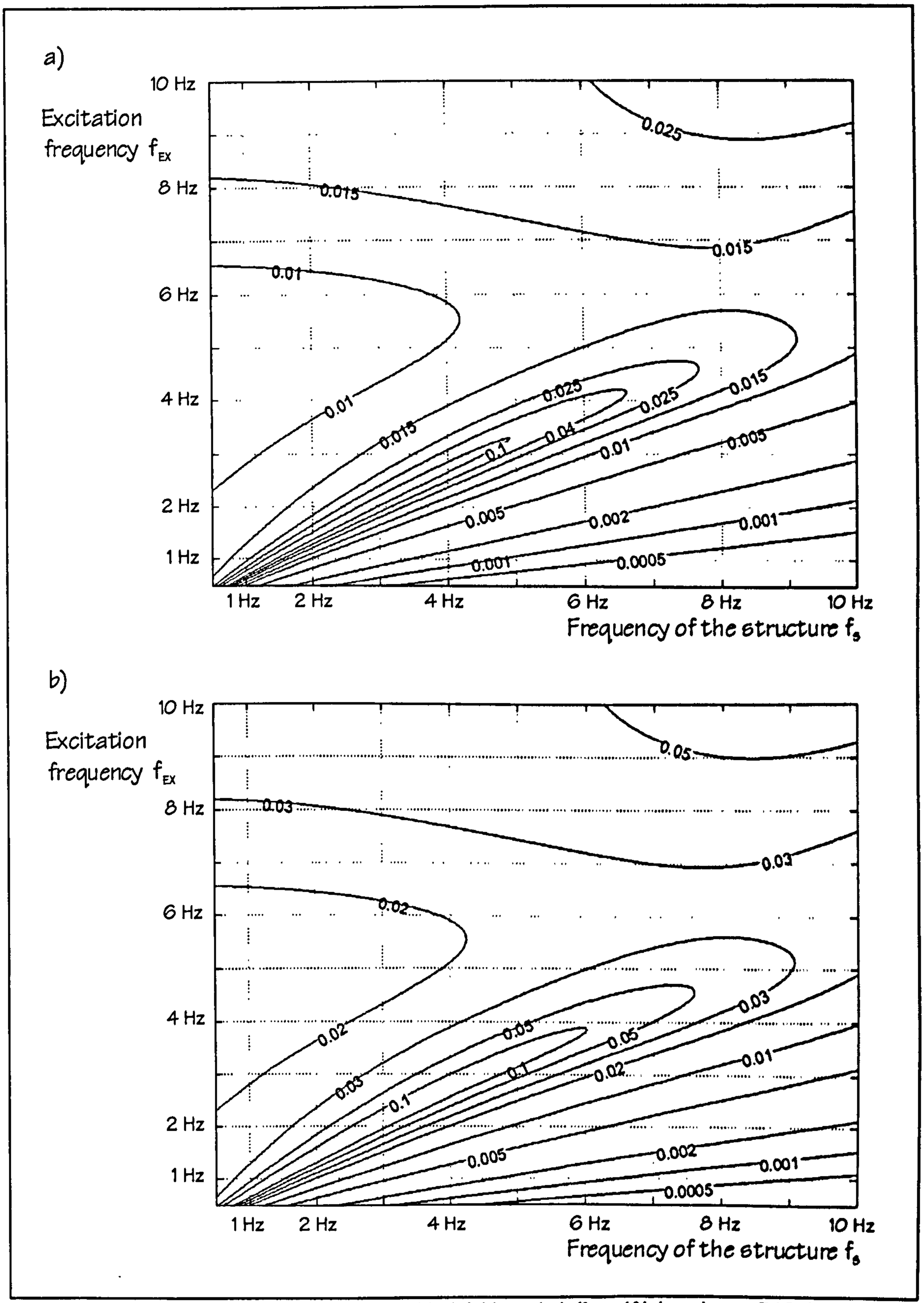

Figure F.1: PARF for $m_s : m_T$ = 1:1, Human Model A*, and a) ζ_s = 1% (maximum PARF = 0.8) or b) ζ_s = 2% (maximum PARF = 0.8).

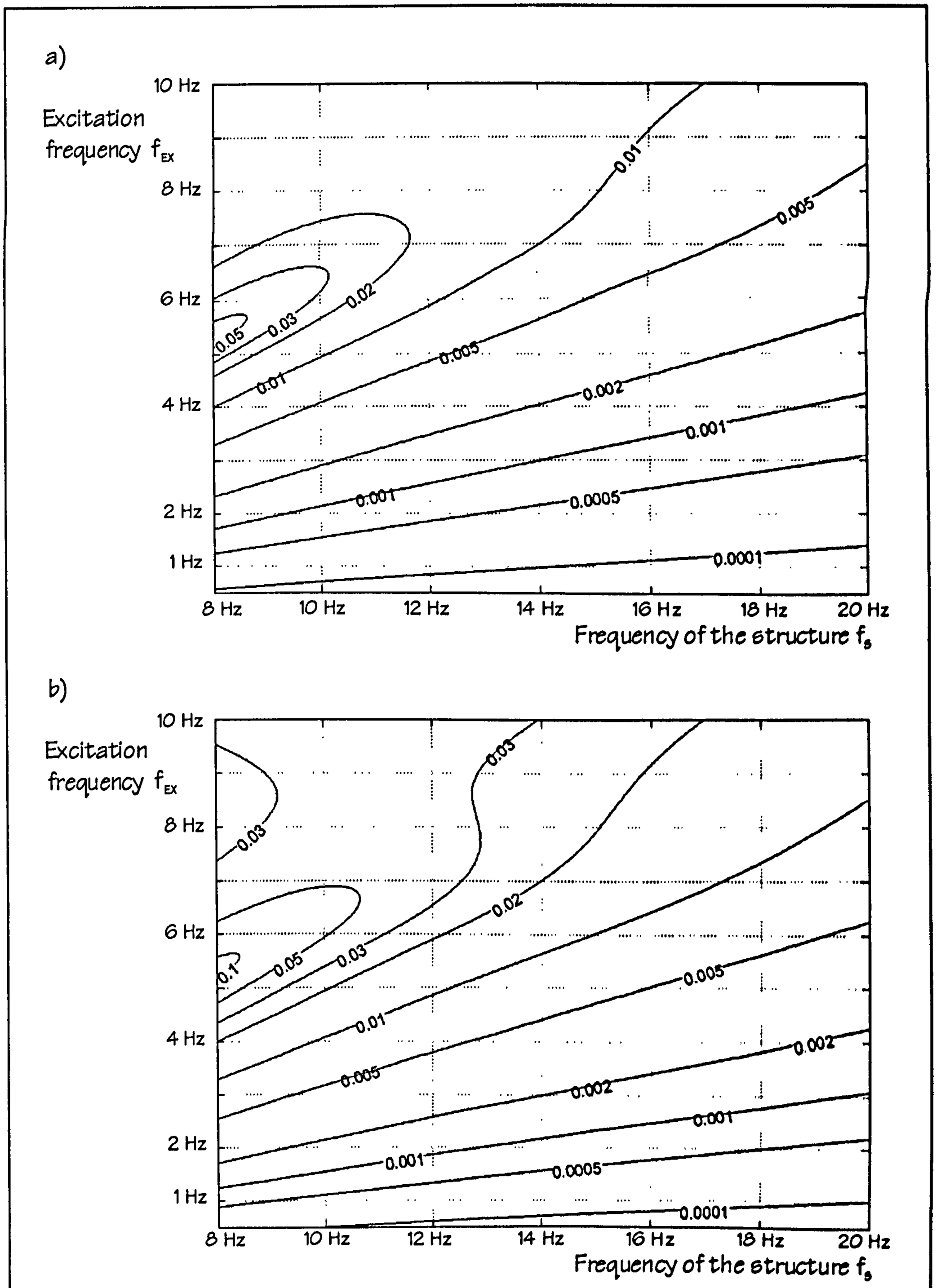

Figure F.2: PARF for $m_s : m_T$ = 1:1, Human Model B*, and a) ζ_s = 1% (maximum PARF = 0.1) or b) ζ_s = 2% (maximum PARF = 0.2).

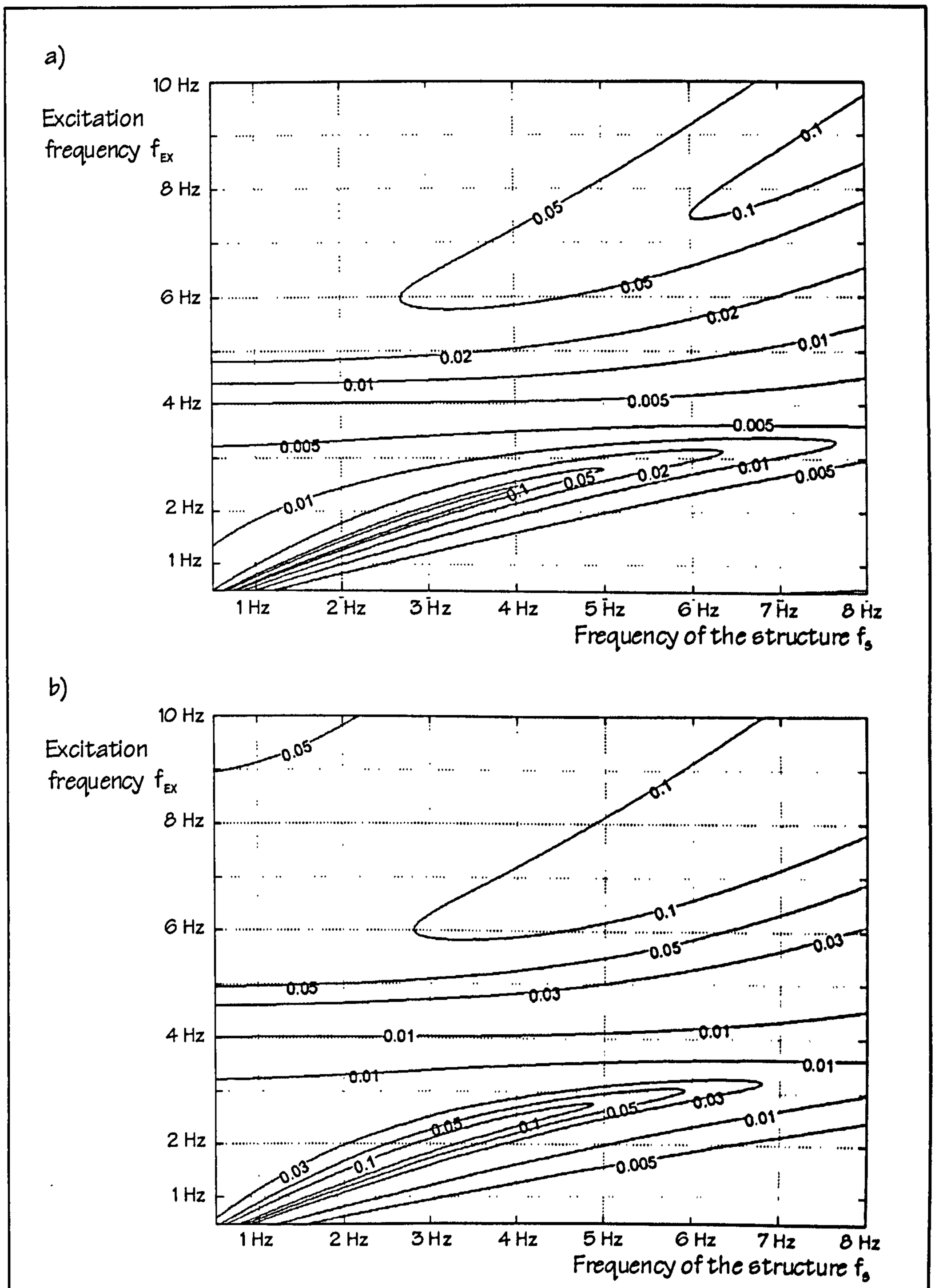

Figure F.3: PARF for $m_s : m_T$ = 1:1, Human Model C, and a) ζ_s = 1% (maximum PARF = 0.7) or b) ζ_s = 2% (maximum PARF = 0.7).

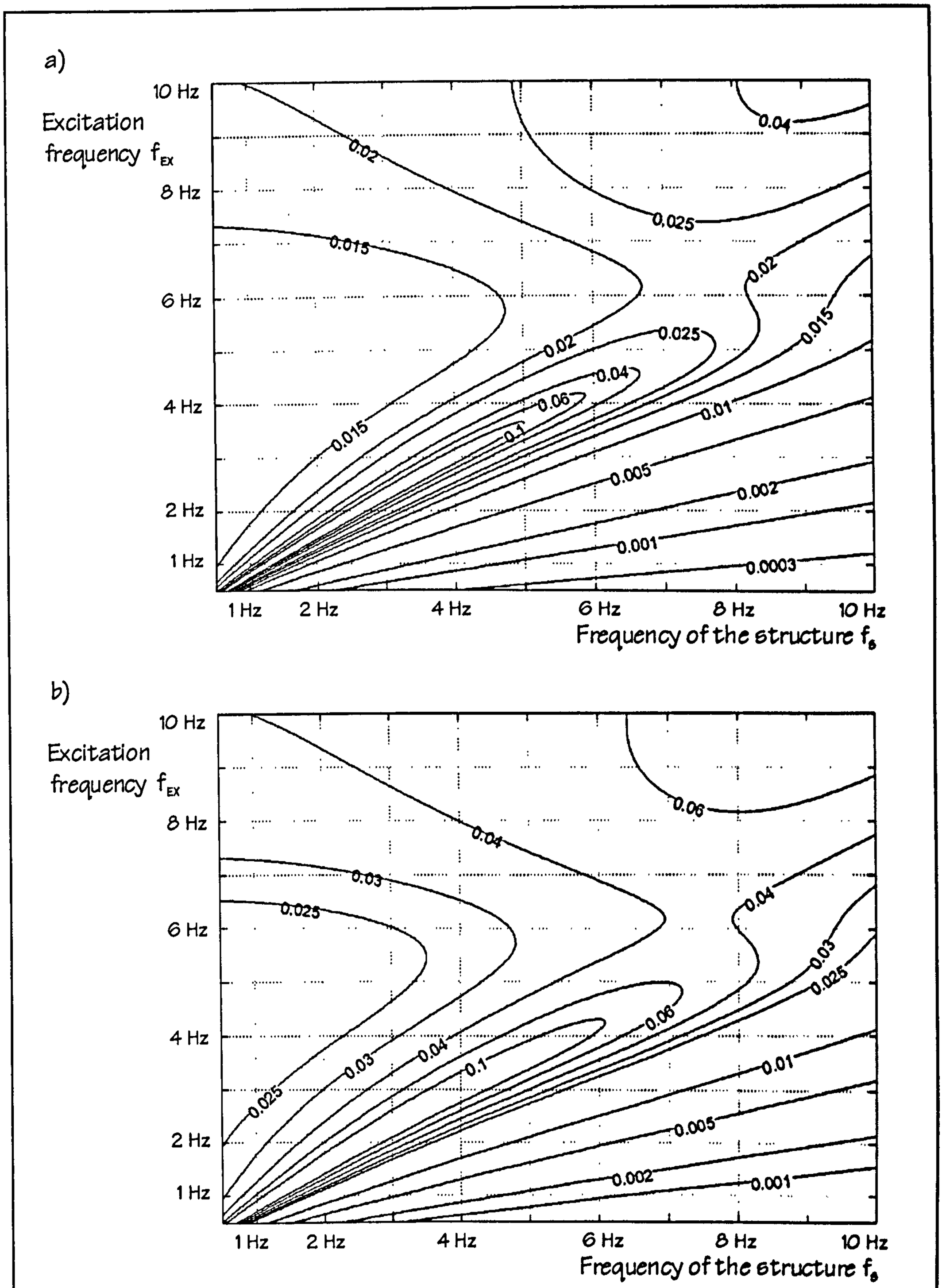

Figure F.4: PARF for $m_s : m_T$ = 1.5:1, Human Model A*, and a) ζ_s = 1% (maximum PARF = 0.8) or b) ζ_s = 2% (maximum PARF = 0.8).

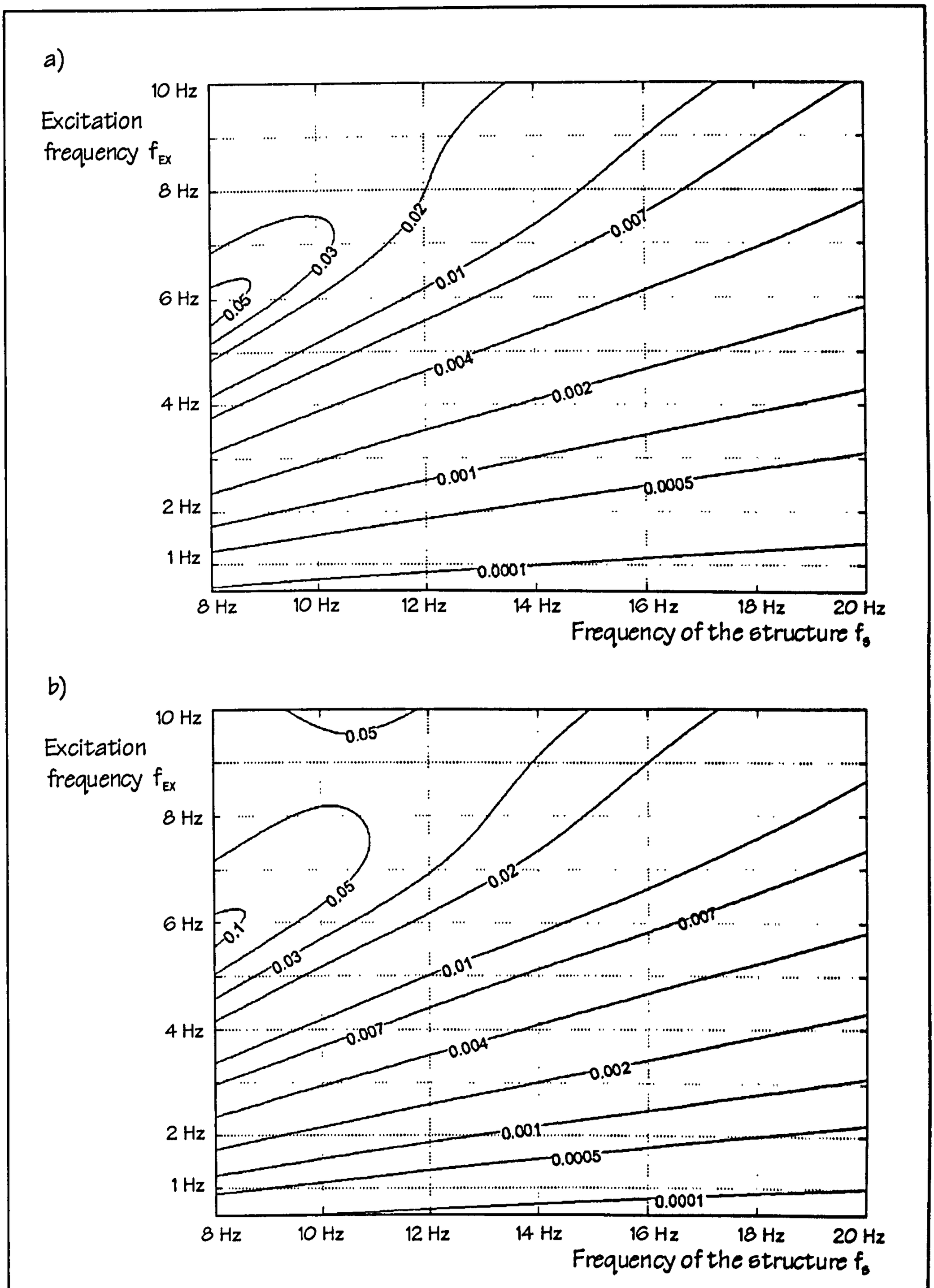

Figure F.5: PARF for $m_s : m_T$ = 1.5:1, Human Model B*, and a) ζ_s = 1% (maximum PARF = 0.1) or b) ζ_s = 2% (maximum PARF = 0.2).

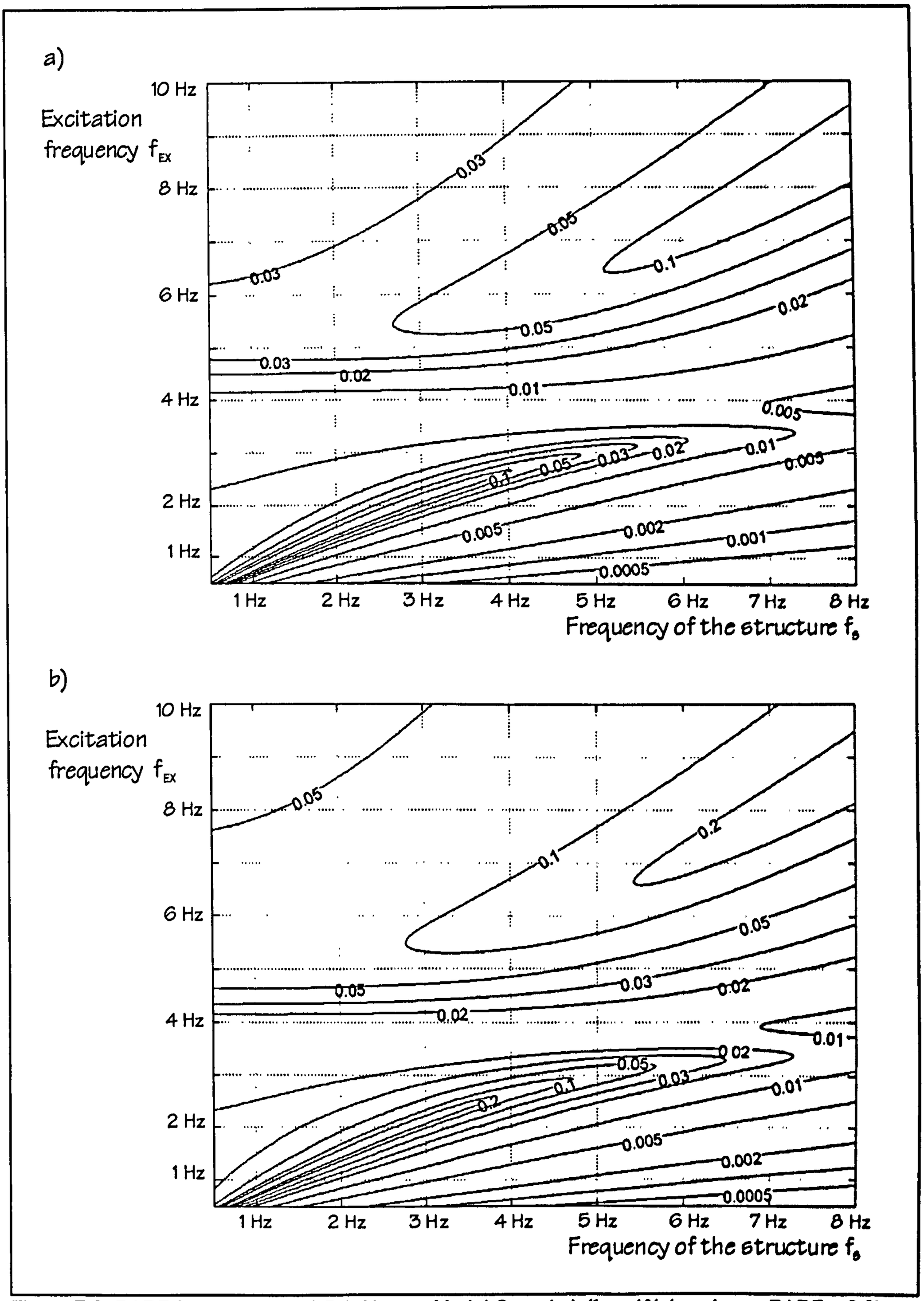

Figure F.6: PARF for $m_s : m_T$ = 1.5:1, Human Model C, and a) ζ_s = 1% (maximum PARF = 0.8) or b) ζ_s = 2% (maximum PARF = 0.8).

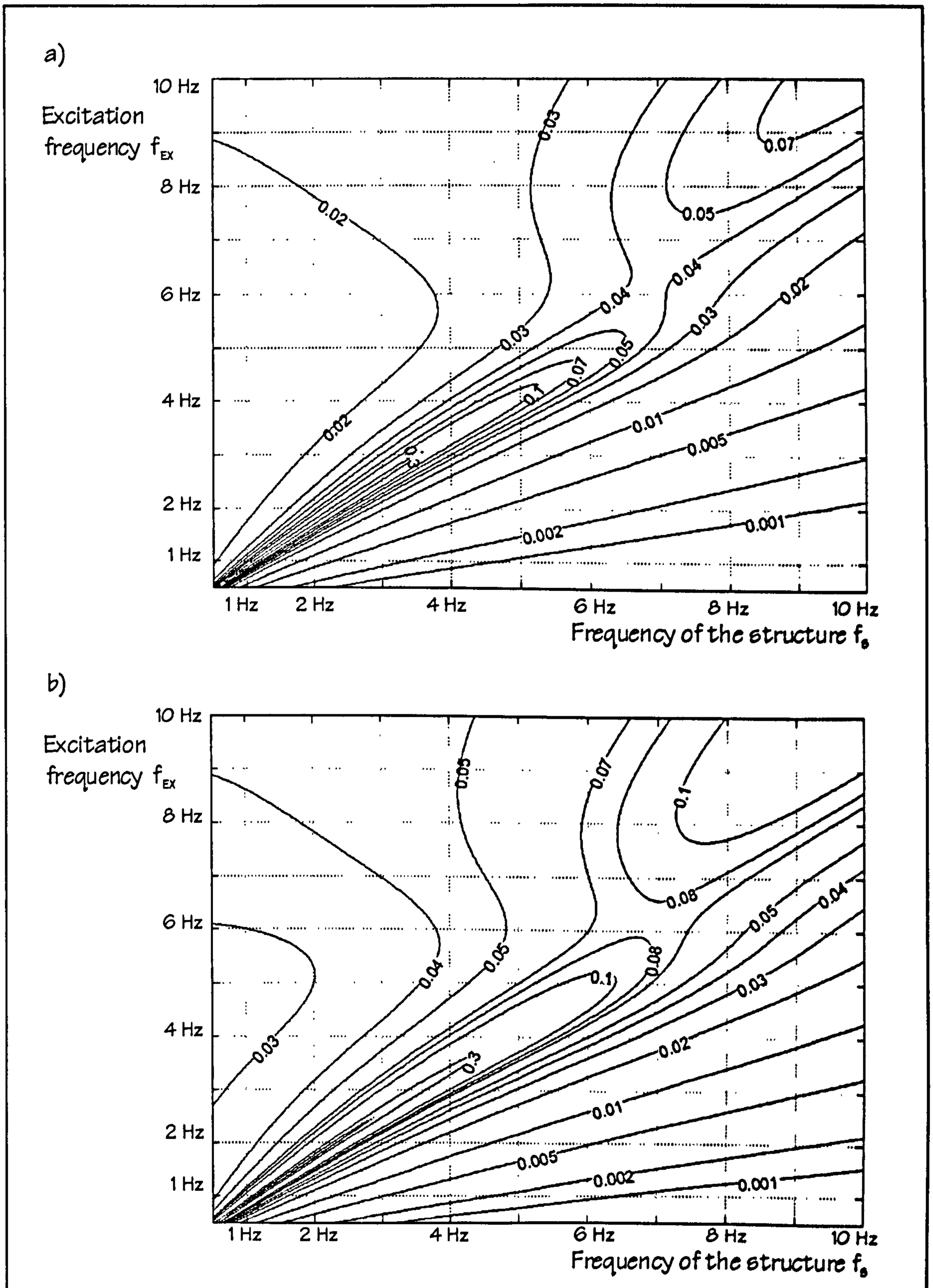

Figure F.7: PARF for $m_s : m_T$ = 3:1, Human Model A*, and a) ζ_s = 1% (maximum PARF = 0.9) or b) ζ_s = 2% (maximum PARF = 0.9).

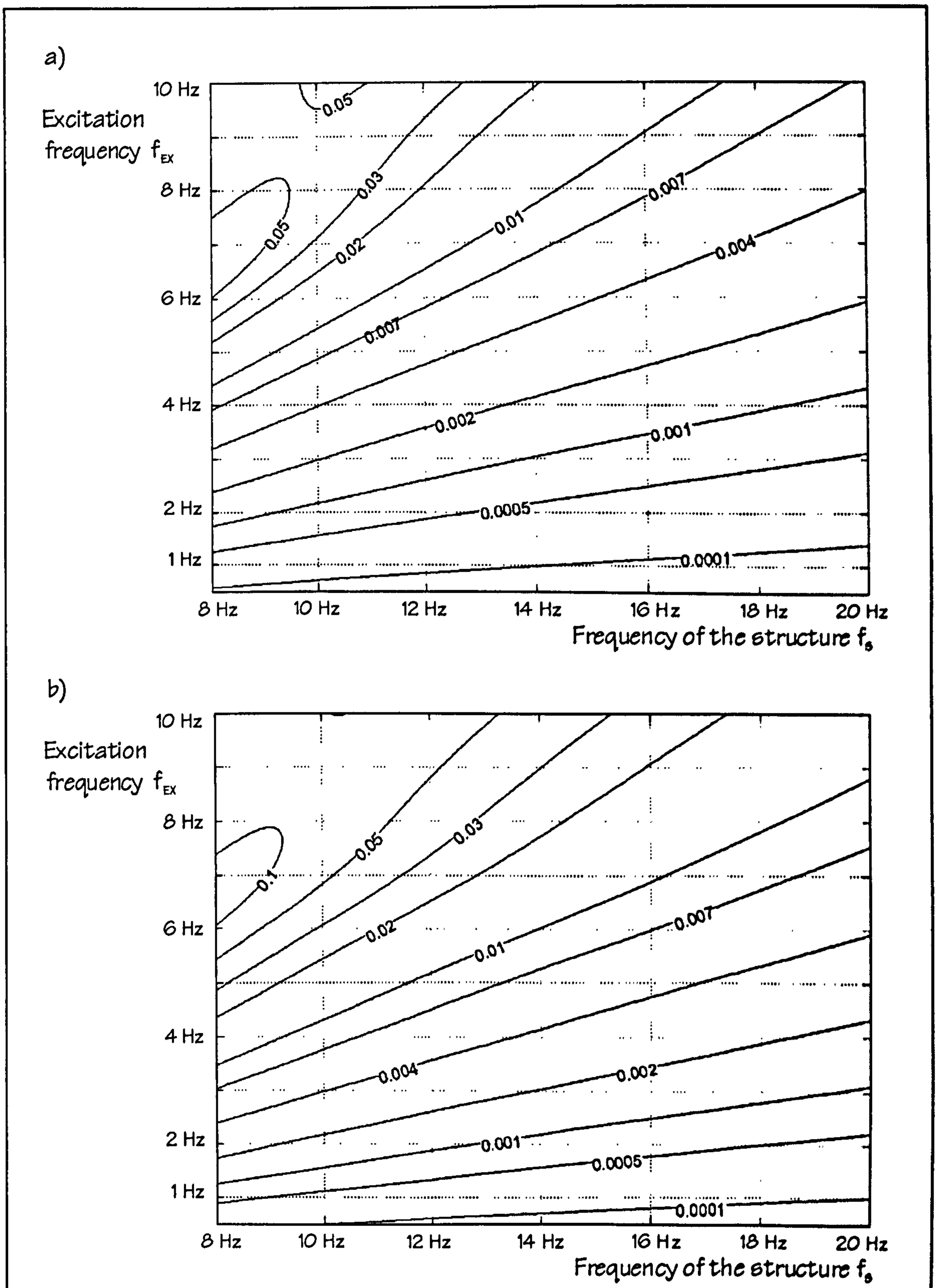

Figure F.8: PARF for $m_s : m_T$ = 3:1, Human Model B*, and a) ζ_s = 1% (maximum PARF = 0.1) or b) ζ_s = 2% (maximum PARF = 0.2).

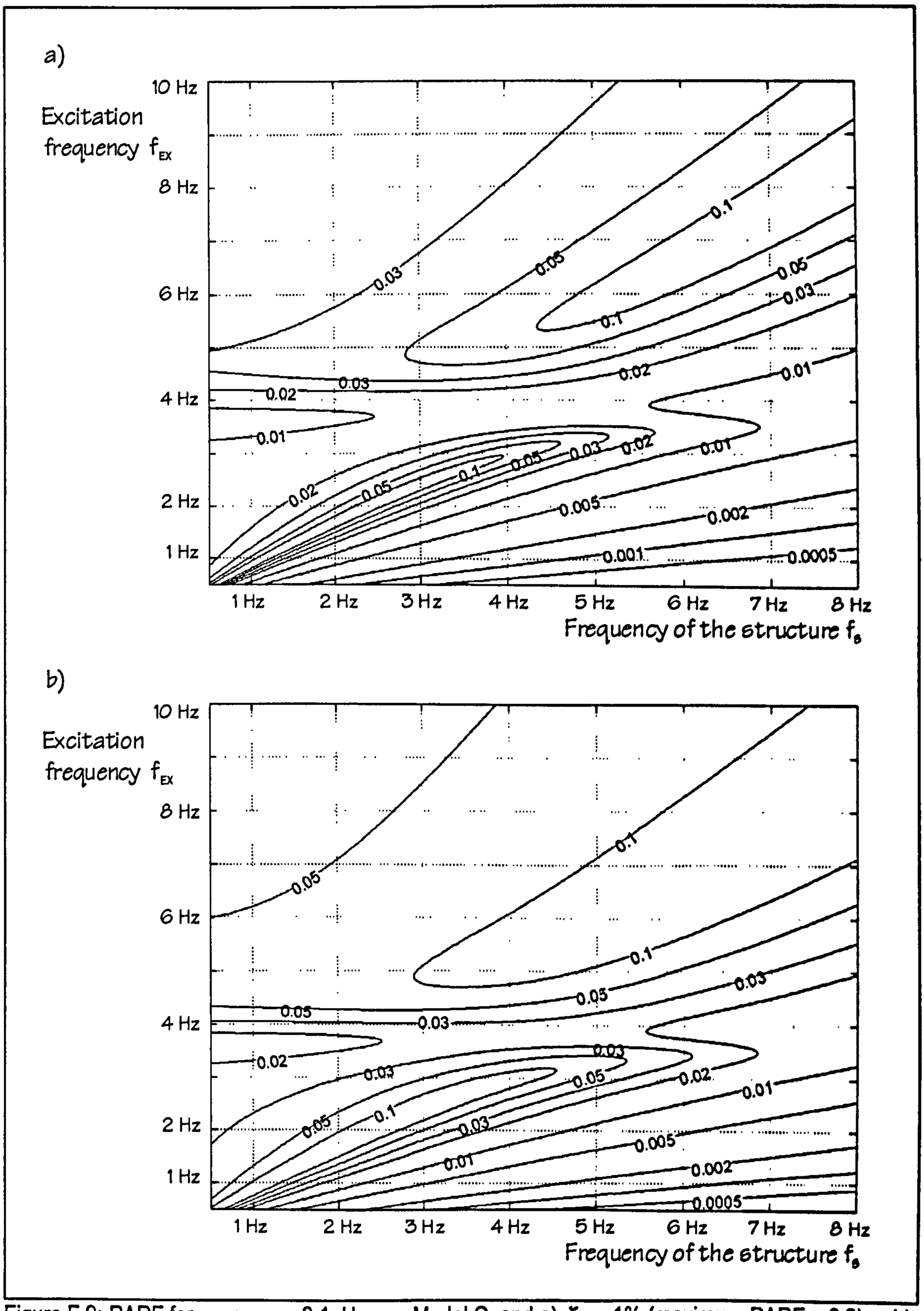

Figure F.9: PARF for $m_s : m_T$ = 3:1, Human Model C, and a) ζ_s = 1% (maximum PARF = 0.9) or b) ζ_s = 2% (maximum PARF = 0.9).

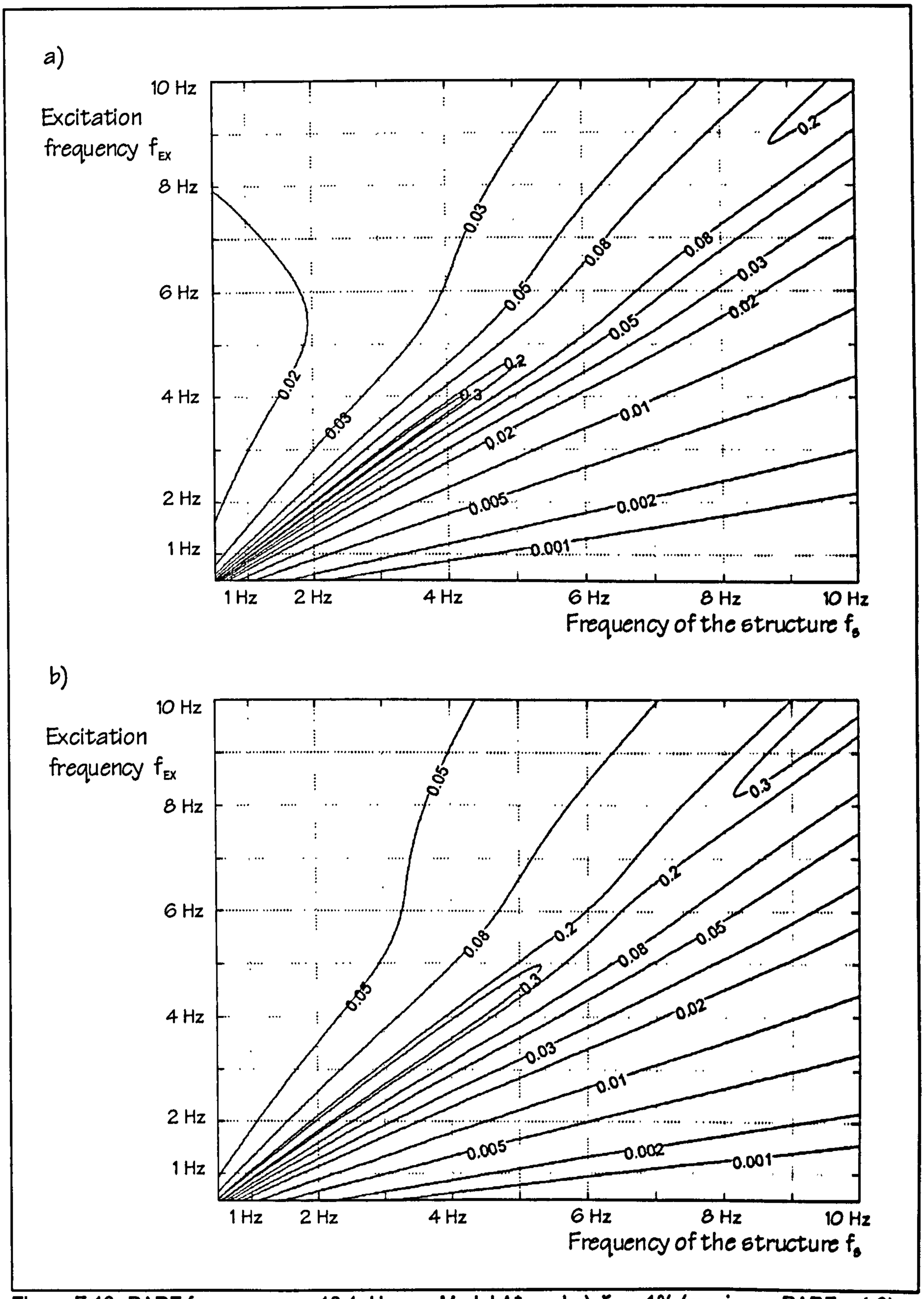

Figure F.10: PARF for $m_s : m_T$ = 10:1, Human Model A*, and a) ζ_s = 1% (maximum PARF = 1.0) or b) ζ_s = 2% (maximum PARF = 1.0).

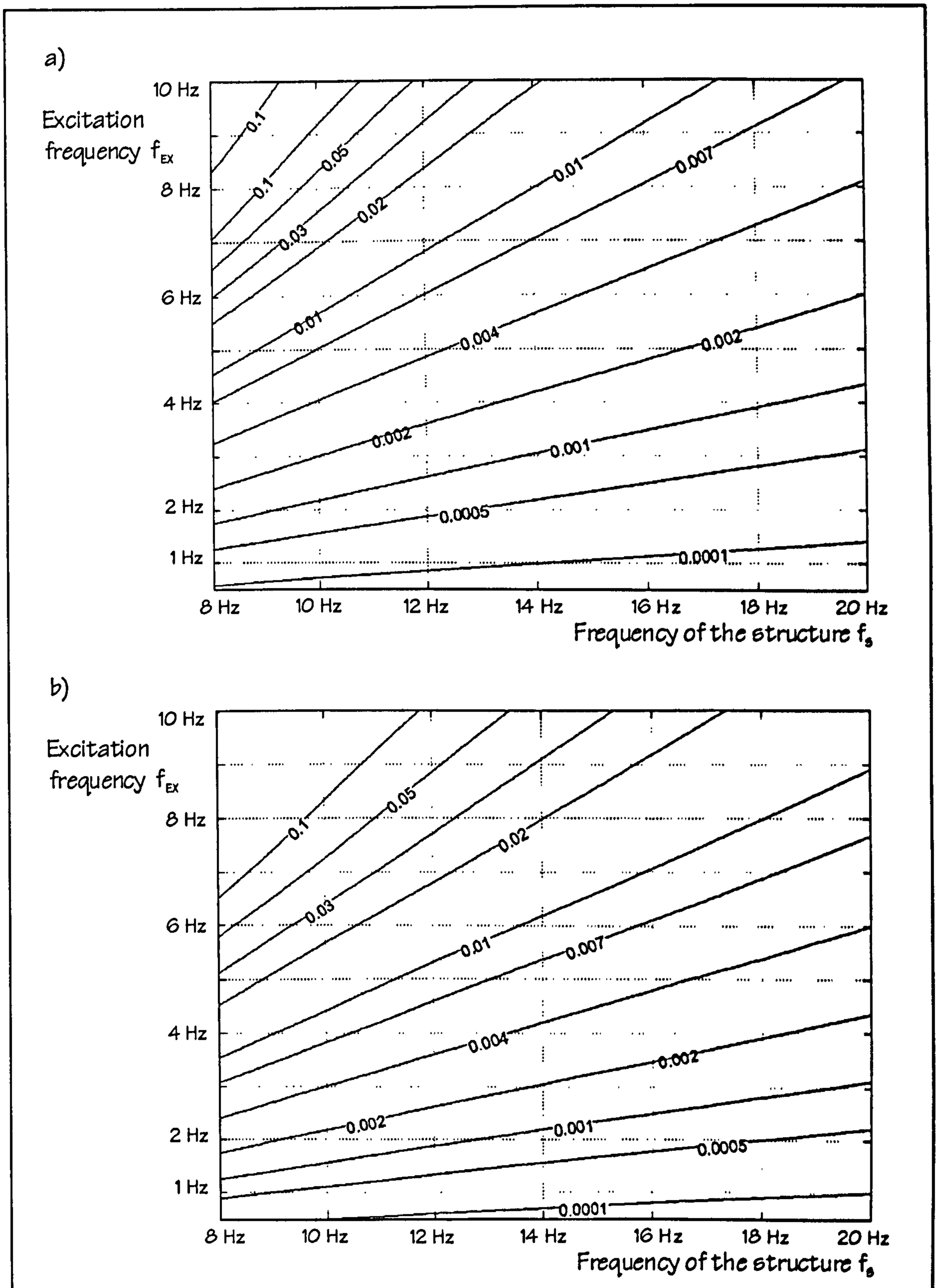

Figure F.11: PARF for $m_s : m_T$ = 10:1, Human Model B*, and a) ζ_s = 1% (maximum PARF = 0.2) or b) ζ_s = 2% (maximum PARF = 0.3).

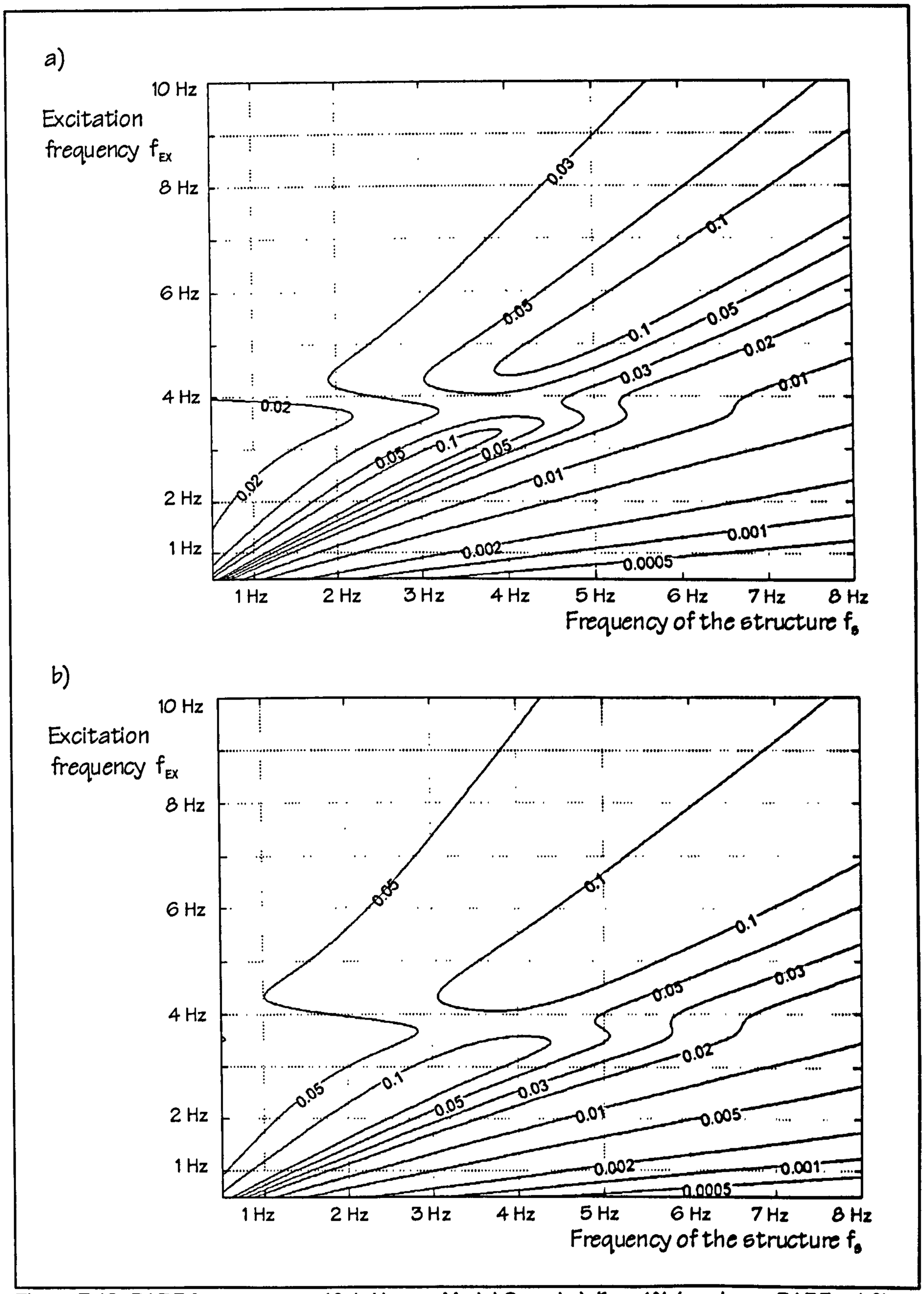

Figure F.12: PARF for $m_s : m_T$ = 10:1, Human Model C, and a) ζ_s = 1% (maximum PARF = 1.0) or b) ζ_s = 2% (maximum PARF = 1.0).

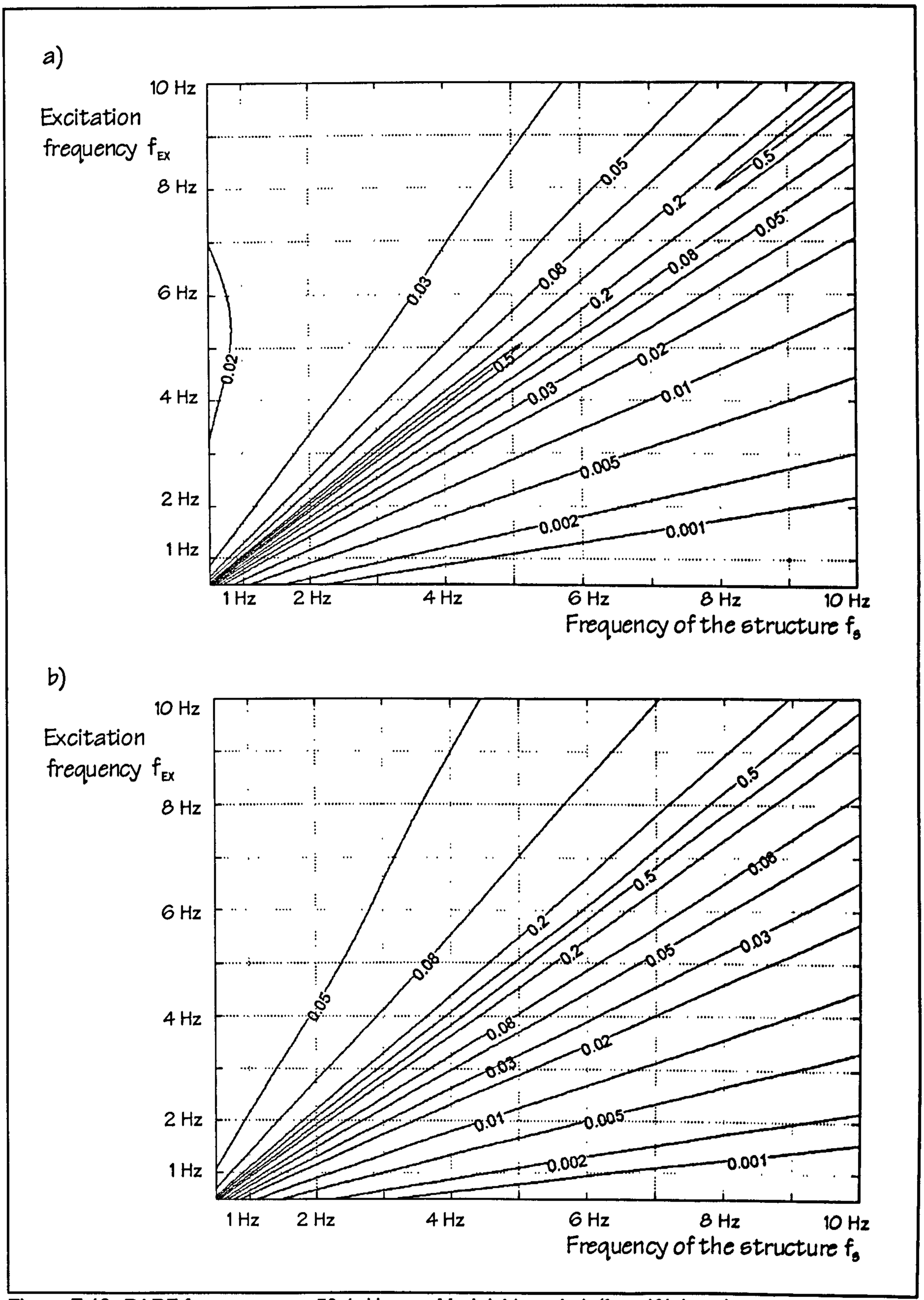

Figure F.13: PARF for $m_s : m_T$ = 50:1, Human Model A*, and a) ζ_s = 1% (maximum PARF = 1.0) or b) ζ_s = 2% (maximum PARF = 1.0).

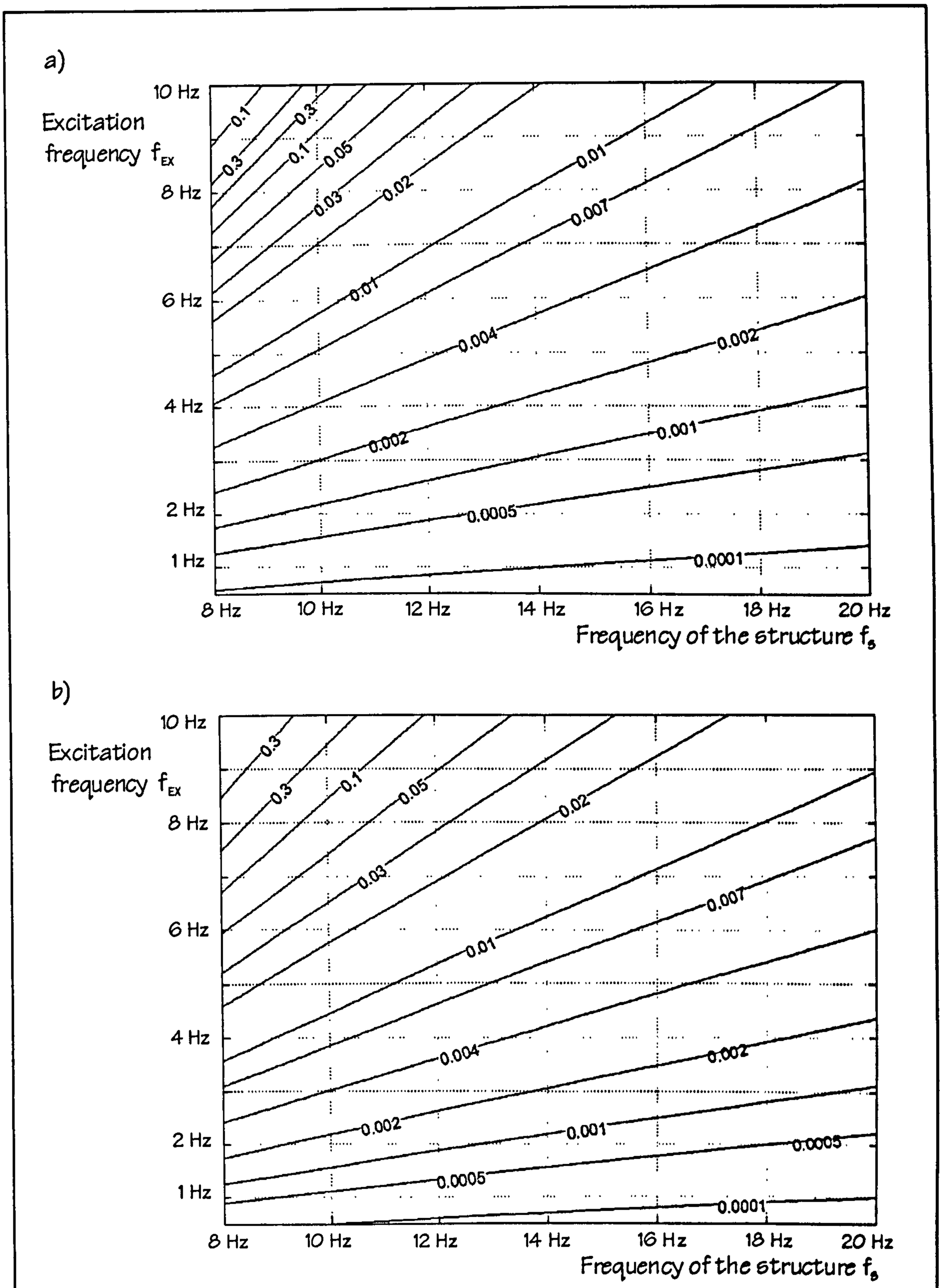

Figure F.14: PARF for $m_s : m_T$ = 50:1, Human Model B*, and a) ζ_s = 1% (maximum PARF = 0.5) or b) ζ_s = 2% (maximum PARF = 0.7).

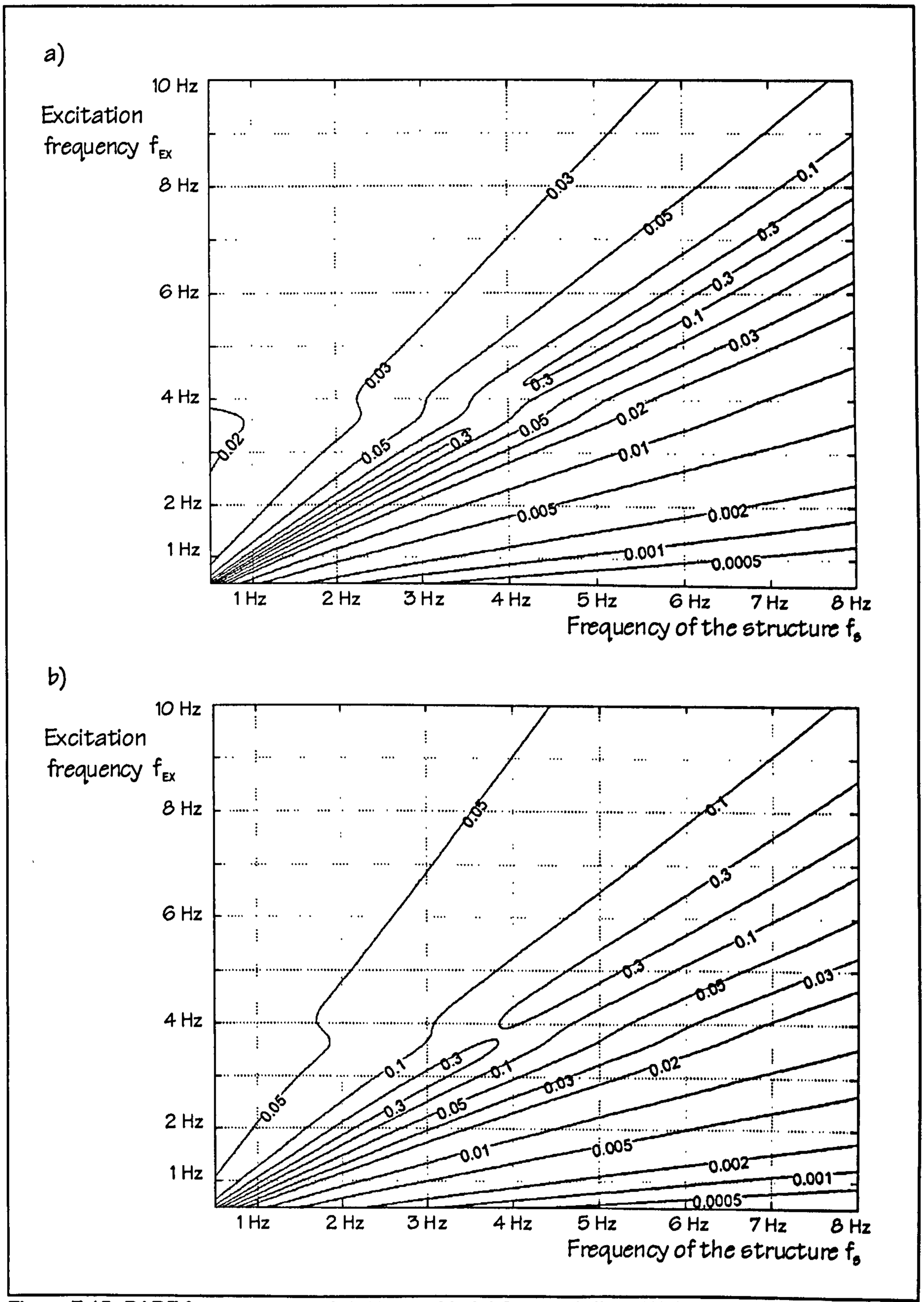

Figure F.15: PARF for $m_s : m_T$ = 50:1, Human Model C, and a) ζ_s = 1% (maximum PARF = 1.0) or b) ζ_s = 2% (maximum PARF = 1.0).

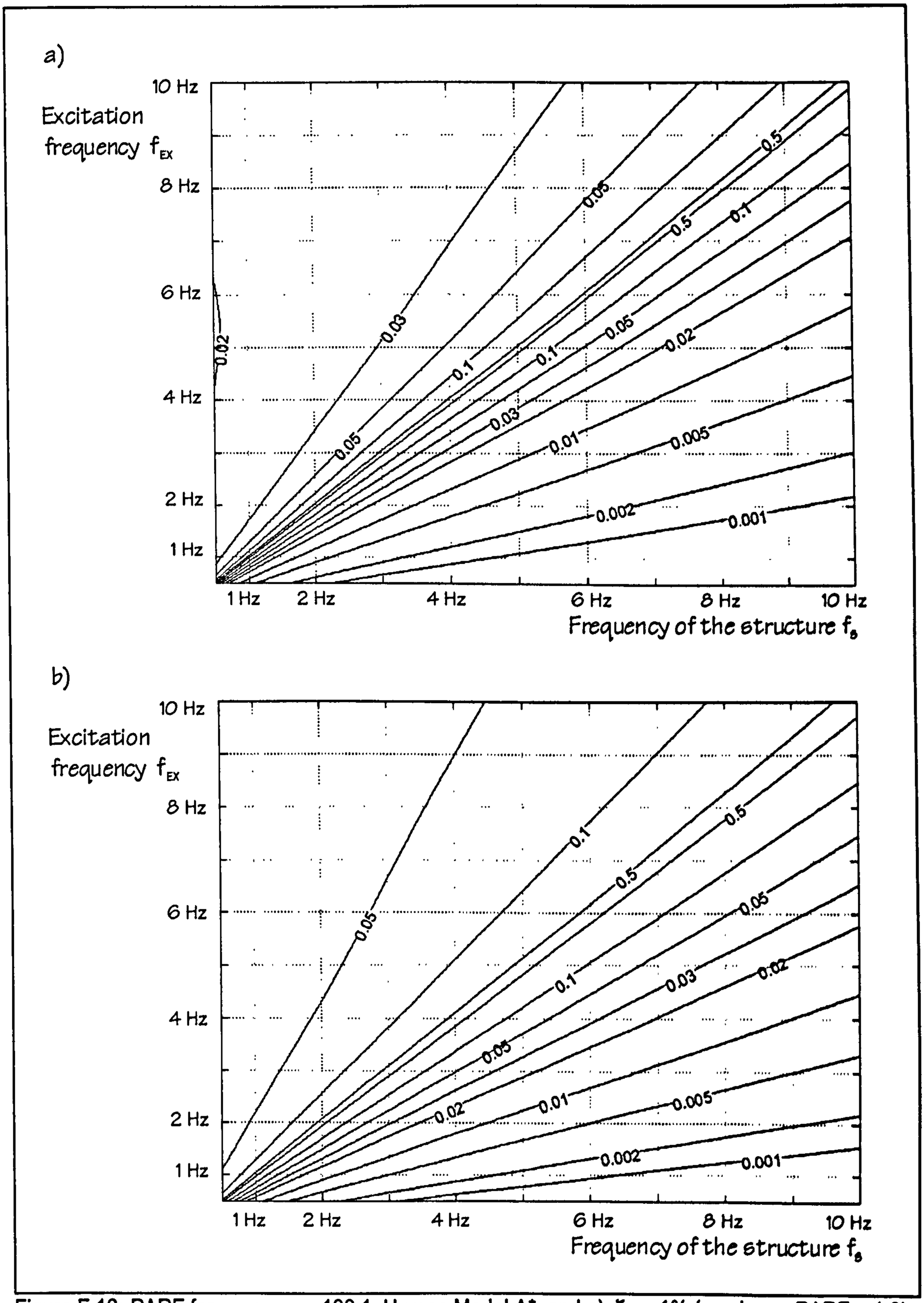

Figure F.16: PARF for $m_s : m_T$ = 100:1, Human Model A*, and a) ζ_s = 1% (maximum PARF = 1.0) or b) ζ_s = 2% (maximum PARF = 1.0).

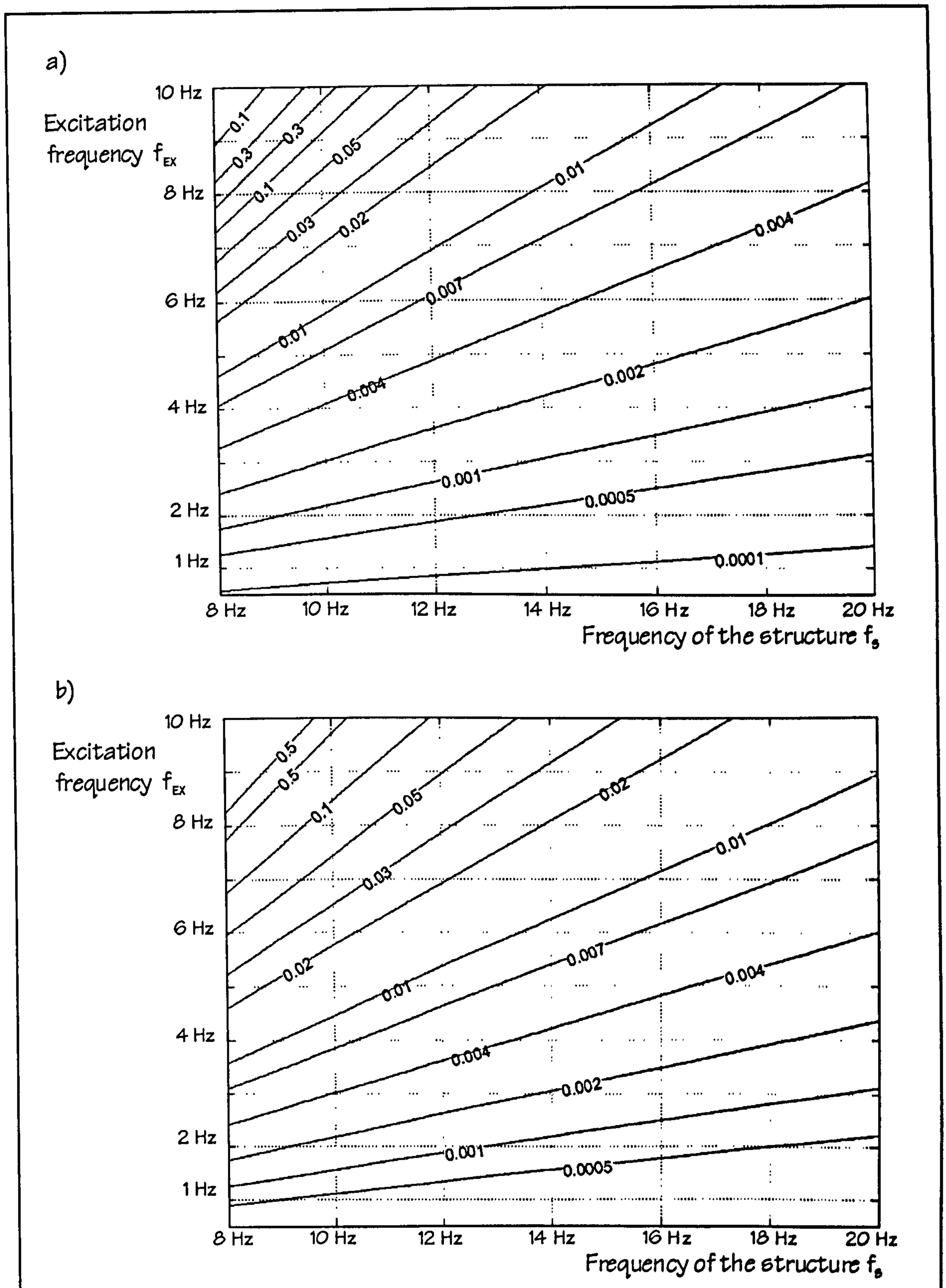

Figure F.17: PARF for $m_s : m_T$ = 100:1, Human Model B*, and a) ζ_s = 1% (maximum PARF = 0.7) or b) ζ_s = 2% (maximum PARF = 0.8).

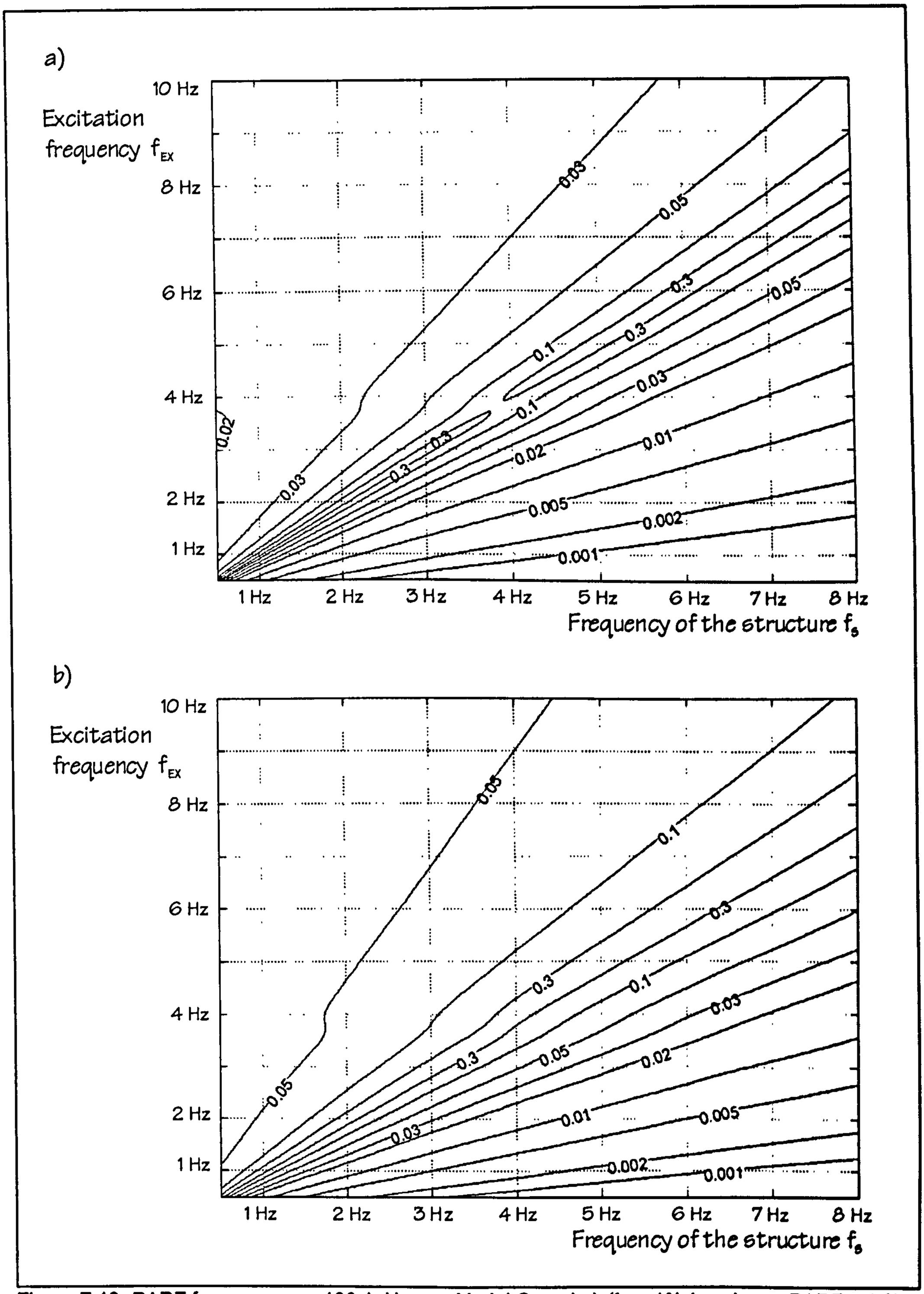

Figure F.18: PARF for $m_s : m_T$ = 100:1, Human Model C, and a) ζ_s = 1% (maximum PARF = 1.0) or b) ζ_s = 2% (maximum PARF = 1.0).